Report on the PHT Scientific Validation for OLP Version 9.0

Ulrich Klaas, Karsten Wilke, Csaba Kiss and Mario Radovich
(PHTNDC at MPIA)

and

Phil Richards
(CCLRC, RAL)

with contributions by:
Huw Morris (CCLRC, RAL)
Rene Laureijs, Bernhard Schulz, Carlos Gabriel (IDC Vilspa)
José Acosta Pulido (IAC)
Peter Ábrahám, Simone Bianchi, Martin Haas
and Manfred Stickel (PHTNDC at MPIA)

SAI/2000–014/Rp

Version 2.0

December 19, 2000

Max-Planck-Institut für Astronomie, Heidelberg

Contents

Chapter 1

Results and Achievements by PHT OLP V9.0 Scientific Validation

1.1 Calibration Upgrades from OLP8 to OLP9

In Table 1.1 we list the major calibration upgrades which were implemented for OLP9 and describe which AOTs or AOT submodes were affected by the individual upgrades. There are two calibration upgrades which are part of the formal OLP/CALG delivery, but which are standalone and are not used by the OLP processing. They are or can be used in the Interactive Analysis environment.

Table 1.1: Calibration upgrades from OLP 8.4 to OLP 9.0 and impact on the different AOT modes

	calibration upgrade	**affects AOT**
1)	refinement of flux dependent signal linearization	all AOTs, except PHT40
2)	refinement of FCS characterisation	all AOTs, except PHT40
3)	refinement of signal correction of chopped measurements	PHT03, PHT22 in chopped mode
4)	sparse maps with different calibration filters for start and end modules	PHT17/18/19 and PHT37/38/39
5)	dynamic spectral response function for staring PHT-S measurements	PHT40 point & extended sources in staring mode
6)	complementary flux units for point and extended source products	all AOTs, except PHT40
7)	color correction tables PCCMBBONE and PCMBBTWO	(color correction factors for modified black bodies)

1.1.1 Dynamic spectral response function correction for staring PHT-S measurements

The previous spectral response function calibration of staring ISOPHOT-S measurements was limited in accuracy by transient effects which could not be corrected for using the static average spectral response function as stored in CalG file PSPECAL.
The main idea behind the dynamic spectral response calibration is that a standard star spectrum of similar brightness as the target spectrum suffers the same transient effects. By taking into account the same temporal evolution of the signals for both standard and target spectrum, the transient effects cancel out by dividing the target spectrum by the standard spectrum, without having to derive "infinite values" with a sophisticated transient correction. Since target and standard spectrum can be quite different in shape, a library of standard stars is necessary to calibrate each PHT-S pixel individually in this way. For the automatic approach in the OLP, the transient behaviour with time for the different flux (signal) regimes was characterized by surfaces stored in the new CalG file PSDYNAMIC constructed from the library of standard stars. The software will determine for each ramp the appropriate transient dependent correction factor.
There are new SPD products, PSSD and PSLD, containing the dark measurements, which precede each sky measurement.
Due to the calibration scheme, which determines directly the flux in Jy, the units of the main SPD products, PSSS and PSLS, changed from V/s to Jy. In order to have consistent data products for all PHT40 submodes, the processing for chopped observations (implemented with OLP 8.4) and raster observations (still using the default RSRF in CalG PSPECAL) had to be adapted, too.

1.1.2 Refinement of flux dependent signal linearization

The signal linearization tables P%%SLINR, introduced with OLP V8.4 have been upgraded with regard to the following aspects:

a) the new linearisation tables have been re-normalised with respect to the median responsivity per bandpass to avoid filter-to-filter corrections at the signal level.

b) the shape of the curves among the pixels in the C100 and C200 arrays for a given filter has been homogenized. The curves of the individual pixels have now similar shape based on fine-tuning by eye.

c) the curves of responsivity as a function of signal smoothly become constant in the extrapolations to very small and very strong signals where no calibration observations are available.

Due to the re-normalization also the default responsivity values in files P*RESP_01 and P*RESP_02 have been updated.

1.1.3 Refinement of FCS characterization

The CALG files P%%ILLUM, P%%FCSPOW, P%%FLAT, PPFTOF and PFLUXCONV have been upgraded to reflect the introduction of the new signal linearization corrections (P%%SLINR, see item 2 above). The physical FCS model was refined to give a better relation between the electrical FCS heating power and the FCS/TRS temperature and this was used to determine the extrapolated FCS powers outside the calibrated range.

1.1.4 Refinement of signal correction of chopped photometry measurements

Several deficiencies in the CalG files P%%CHOPSIG installed with OLP V8.4 were closed:

a) signal loss correction for P2 detector;

b) chopper offset (residual signal difference for zero flux difference in both beams) corrections for all detectors;

c) the signal loss corrections were re-derived with the updated signal linearization calibration as described above under item 2.

Chopped observations with the read-out data reduction flag being set are properly processed now. Refinements were also achieved in the chopped pattern processing and a bug omitting the filter-to-filter correction for chopped measurements was fixed.

1.1.5 Consistent handling of different calibration filters for start and end modules of sparse maps

So far it was assumed in the OLP processing that the FCS measurements of the start and end modules of sparse maps are done in the same filter. This needs, however not to be the case. This led to a mismatch of the responsivity values for the sparse map modules which are interpolated values in time between the two responsivity values from the bracketting FCS measurements. With the new version the correct filter information for the evaluation of both FCS measurements is used.

1.1.6 Complementary flux units for point and extended source products

Depending on the original observer definition whether the target was a point (P) or extended (E) source, different PHT photometry AAR products are generated, e.g. PPAP and PPAE for PHT-P or PCAP and PCAE for PHT-C pointed observations. P-type products are in unit Jy, E-Type products in unit MJy sr^{-1}. The comparison between both products, needed e.g. for background subtraction, where the on-source measurement may be in Jy while the off-source measurement is in MJy sr^{-1}, is not straight forward, since a conversion using the wavelength dependent effective solid angles and point spread function factors is necessary.
For these products now complementary flux information in the respective units is provided, i.e. for P-type products in addition the surface brightness in MJy sr^{-1} and for E-type products the flux in Jy/pixel. The same is true for the scan products PPAS and PCAS.
For the OLP 9 version this additional information is restricted to the data records, corresponding information in the headers has to be postponed to a later version. This made it necessary to define new keyword fields for the AAR products.

1.1.7 Color correction tables PCCMBBONE and PCCMBBTWO

In the "What's New" note from 23 December 1999 "Wrong colour correction Cal-G tables for ISOPHOT" observers were warned about faulty contents of the CALG files PCCMBBONE and PCCMBBTWO providing the color correction factors for modified blackbodies. From this time to now the correct files were only available via the PIA homepage. The correct files are now available in the IDA with the OLP 9 delivery.

1.2 Photometric Accuracies of Staring Modes

Global calibration accuracies have been estimated from the investigation of the test cases and the comparison with published reference photometry. (for a dependence on flux, see Table 1.2 below). They can be applied, if not one of the caveats on photometry applies, cf. Sect. 2.
The terms **absolute accuracy**, **relative accuracy** and **reproducibility** have been defined in the following context:

- **absolute accuracy** is the accuracy achieved w.r.t. the reference photometry, if the filter measurement had a corresponding FCS transfer measurement in the same filter. Hence, the quality of the FCS calibration against celestial standards is directly verified. Note that no calibration accuracy of the reference photometry (models, IRAS) has been taken into account, as this is beyond the scope of this report. A typical order of the absolute accuracy of the reference photometry is 2 – 10%. Table 1.2 lists the achieved values per detector and flux range.

- **relative (filter-to-filter) accuracy** is the accuracy achieved w.r.t. the reference photometry, if the filter measurement was not performed in the filter in which the FCS calibration was done. Currently, assumptions about the constancy of the responsivity over the full flux range and for all filters, and, related to that relative filter-to-filter correction factors, apply. It has been proven that this is in general not correct, and it is considered that in future OLP versions corrections for non-linearities of the responsivity with the in-band power will be applied. Hence, the relative uncertainty can be much larger than the absolute one in multi-filter measurements with certain source SEDs. Table 1.2 lists the achieved values per detector and flux range. The number of suitable test cases performed in multi-filter mode is much smaller than the number of test cases in any of the absolute measurement modes (i.e. with an FCS measurement in the respective filter). The relative filter-to-filter accuracy could only be established for a minor subset.

- absolute and relative accuracy are assumed to add to the total photometric uncertainty. In multi-filter measurements with one FCS measurement the absolute measurement uncertainty is subtracted from all measurements in non-FCS filters in order to derive the relative measurement accuracy.

- **reproducibility** is the relative consistency of measurements repeated several times with the same measurement set-up. It is a measure of the internal stability of the instrument and describes also the current limitations in signal processing. Table 1.3 lists the achieved values per detector both for a bright secondary standard and a faint source. These values were obtained from special calibration monitoring programs performed during ISO's Routine Phase [18].

In summary, the following calibration accuracies have been achieved per detector for staring mode observations in multi-filter and absolute photometry mode (cf. Tables 1.2 and 1.3 for details):

1) ISOPHOT-P1:
10 % absolute accuracy and 20 % relative accuracy for bright sources (> 30 Jy). For fainter sources (> 0.1 Jy) the absolute accuracy was within 40 % for OLP 8.4 (no P1 nodding observation was examined for this version of the report). The relative reproducibility accuracy is 5 % for bright sources and 10 % for faint sources.

2) ISOPHOT-P2:
Better than 10 % absolute accuracy and 5 % relative accuracy for bright sources (> 10 Jy). For fainter sources (> 0.5 Jy) the absolute accuracy was within 10 % for OLP 8.4 (no P2 nodding observation was examined for this version of the report). The relative reproducibility accuracy is 2 % for bright sources and 12 % for faint sources.

3) ISOPHOT-P3:
5 % absolute accuracy and 10 % relative accuracy for bright sources (> 5 Jy). For fainter sources (> 0.2 Jy) the absolute accuracy was within 20 %. for OLP 8.4 (no P3 nodding observation was examined for this version of the report). The relative reproducibility accuracy is 7 % for bright sources and 7 % for faint sources. Under extreme Space Weather conditions and for the very end of the science window the achieved accuracy for faint sources is poorer.

4) ISOPHOT-C100:
20 % absolute accuracy and 25 % relative accuracy down to $\sim$ 5 Jy. The absolute accuracy of nodding photometry in the flux range below 1 Jy was 40 % for OLP 8.4 (no C100 nodding observation was examined for this version of the report). The absolute accuracy in mini-map mode is < 25 % for the full flux range, using the PCAS products (cf. Table 1.6). The relative reproducibility accuracy is 3 % for bright sources and 20 % for faint sources.

5) ISOPHOT-C200:
10 % absolute accuracy for fluxes > 0.5 Jy. At the lowest flux level only absolute photometry and nodding mode achieve this accuracy. The accuracy achieved in mini-map mode is < 20 % for the full flux range, using the PCAS products (cf. Table 1.6). The multi-filter test case of α Boo indicates a relative accuracy better than 20 % down to fluxes of a few Jy, limited by the accuracy to subtract the then 4 times brighter background. The relative reproducibility accuarcy is around 10 % both for bright and faint sources.

6) ISOPHOT-S:
Due to the implementation of the dynamic spectral reponse function calibration method the performance numbers for staring mode observations have been significantly improved: better than 10 % absolute and better than 20 % relative, in the flux range 1 - 6000 Jy for SS and 0.3 - 1500 Jy for SL.
Thanks to a calibration method with spectral response functions specific for chopped mode and adjusted to the detector behaviour for a certain flux modulation, 10 % absolute accuracy and 10 % relative accuracy are achieved for chopped point source observations, in the flux range 0.5 to about 500 Jy with the SS detector, and in the flux range 0.2 to about 200 Jy with the SL detector.

Table 1.2: Absolute and relative (filter-to-filter) calibration accuracies per detector achieved for various flux ranges in multi-filter mode with OLP V9.0. Bold values indicate a significant improvement w.r.t. OLP V8.4. Improved PHT-S accuracies in staring mode were established with this version.

detector	**AOT mode**	**flux range** [Jy]	**abs. accuracy** [%]	**rel. accuracy** [%]	**standard**
P1	P03 off & on	300 - 6000	$\leq$ **5**	15	α Boo
P1	P03, P05 off & on	70 - 1250	10	25	γ Dra
P1	P03 off & on	50 - 1000	10	**5**	Sirius
P1	P05 off & on	50 - 1000	**5**	–	Sirius
P1	P05 off & on	35 - 600	< **10**	–	α Ari
P2	P03 off & on	100 - 200	$\leq$ 5	5	α Boo
P2	P03, P05 off & on	25 - 40	< **5**	5	γ Dra
P2	P05 off & on	$\sim$ 25	**5**	–	Sirius
P2	P05 off & on	13 - 20	< **10**	–	α Ari
P3	P03 off & on	10 - 25	$\leq$ **5**	10	α Boo
P3	P17 off & P19 on	2.5 - 8	$\leq$ **5**	10	HR 337
P3	P03, P05 off & on	$\sim$ 5	**5**	–	γ Dra
C100	P22 off & on	6 - 25	5	10	α Boo
C100	P37 off & P39 on	2.5 - 8	25	**25**	HR 337
C100	P22, P25 off & on	$\sim$ 5	20	**25**	γ Dra
C200	P25 off & on	500 - 900	**10**	–	Uranus
C200	P25 off & on	40 - 120	**10**	–	Ceres
C200	P22 off & on	2 - 5	10	**20**	α Boo
C200	P25 off & on	$\sim$ 0.5	10	–	γ Dra
SS	P40 off & on	1 - 6000	< **10**	< **20**	
SL	P40 off & on	0.3 - 1500	< **10**	< **20**	

Table 1.3: Relative Calibration Reproducibility Accuracy per Detector for Bright and Faint Fluxes from Monitoring Programs.

detector	target	**flux** [Jy]	**relative accuracy** **1** σ [%]
P1	NGC 6543	8	5
P1	HD 172323	0.085	10
P2	NGC 6543	100	2
P2	HR 5986	0.67	12
P3	NGC 6543	100	7
P3	HR 7310	0.67	7
C100	NGC 6543	50	3
C100	HR 7310	0.21	20
C200	NGC 6543	11	10
C200	HR 6705	0.67	7

1.3 Re-validation of Staring Mode Photometry and Spectroscopy

1.3.1 Flux Dependent Signal Linearization

This general calibration feature was successfully revalidated. A prerequisite for this was a consistent treatment of a significant fraction of the PHT calibration files which were provided for this OLP version.

1.3.2 Multi-filter Staring Modes

The PHT staring photometric modes PHT03 and PHT22 OLP processing was successfully re-validated. This includes extended source photometry with PHT-C (PHT22), cf. Table 1.4. For bright sources in general both the absolute and relative calibration are slightly improved by this OLP version, see Sect. 1.2 above. We noted however that for some filters and some flux ranges the photometry is less reliable. This has been flagged in the Caveat Sect. 2.14.

1.3.3 Absolute Photometric Modes

The PHT absolute photometric modes PHT05 and PHT25 OLP processing was successfully re-validated. The absolute calibration of PHT-P is slightly improved for this version, see Sect. 1.2 above.

1.3.4 PHT22 Raster Maps

The PHT-C staring mode raster map PHT22 OLP processing was successfully revalidated with regard to point source photometry from mini-maps. The accuracy of this photometric mode can be improved considerably when using the PCAS product and applying an evaluation method as outlined in Sect. 8.5.3, see Table 1.6 below. Using the PGAI products and aperture photometry gives an accuracy of only 30 % for point sources above 1 Jy for C100 and only 50 % for the full flux range of C200. The reason for this behaviour is not yet completely understood. Tests of the flat-field accuracies confirm similar values as found for V8.4) (cf. Table 1.5) and residual flat-field patterns can be seen in maps with no pixel overlap.

1.3.5 Spectroscopy in Staring Mode on Point Sources

The PHT OLP processing of the spectroscopic mode PHT40 staring on point sources was successfully re-validated. Due to the new dynamic spectral response function calibration both absolute and relative calibration accuracy have been significantly improved, see Sect. 1.2 above.

1.3.6 Spectroscopy in Staring Mode on Extended Sources

The PHT OLP processing of the spectroscopic mode PHT40 staring on extended sources was successfully re-validated. Due to the new dynamic spectral response function calibration both absolute and relative calibration accuracy have been significantly improved, see Sect. 1.4.

1.3.7 Spectroscopy in Chopped Mode

The PHT OLP processing of the spectroscopic mode PHT40 OLP chopping was successfully re-validated.

Table 1.4: Calibration Accuracy per Detector for Extended Sources for Various Flux Ranges with OLP V8.4/9.0. The range for which both absolute and relative accuracies can be given is covered for PHT-C by multi-filter background measurements, while the larger range is covered by raster maps. For PHT-S the relative accuracy is a measure of the relative spectral shape. The absolute accuracy depends highly on the exposure time, it can be as good as 10 %.

detector	**flux range** [MJy sr^{-1}]	**absolute accuracy** [%]	**relative accuracy** [%]	**standard**
C100	5 - 15	< 25	20	COBE/DIRBE
	5 - 400	< 25	–	COBE/DIRBE
C200	4 - 10	< 25	20	COBE/DIRBE
	3 - 600	< 25	–	COBE/DIRBE
SL	3 - 20	10 - < 50	20	COBE/DIRBE

Table 1.5: Flat-field (ff) accuracies for ISOPHOT-C P22 raster maps. The ff accuracies are determined as ratio of the standard deviation of the mean background surface brightness to the mean surface brightness value for a flat sky background field with no sources. They are filter independent. There is some trend that for the same set of raster parameters the ff accuracy improves with increasing absolute surface brightness. For C100 the ff accuracy can vary over the map area.

detector	**flat-field accuracy**	
	no pixel overlap (%)	**with pixel overlap** (%)
C100	8 - 20	4 - 12
C200	7 - 15	3 - 5

Table 1.6: Absolute calibration accuracies achieved for various flux ranges in mini-map mode using the PCAS data products and PCAS evaluation method (described in this report).

detector	**flux range** [Jy]	**abs. accuracy** [%]	**standard**
C100	1 – 5	**<5**	Sirius
C100	∼ 1	**<5**	HD 187612
C100	0.4 - 1.2	**<10**	HR 7980
C100	0.1 - 0.5	**<20**	HD 203280, HD 12311
			HD 180711, HD 157325
			HR 7310
C100	0.05 - 0.1	**<25**	HD 142373, HD 185395
			HD 185144, HD 1581
C200	500 – 900	**10**	Uranus
C200	40 – 120	**<20**	Ceres
C200	0.6	**<20**	γ Dra
C200	0.4	**<15**	HR 1654
C200	0.15 - 0.3	**<25**	HR 7980

Table 1.7: Results from comparison of sets of P22 raster maps with different raster step size (OLP 8.4). Internal consistency is derived as the ratio of half of the difference in flux to the average flux for a pair of maps on the same target.

target name	**filter** (μm)	**raster parameters** **MxN**	**dMxdN** (arcsec)	**flux** (Jy)	**internal consistency** (%)
C100 detector					
BD+31 643	60	11 x 11	69 x 69	325.757	+1.0
BD+31 643	60	9 x 9	15 x 15	319.498	-1.0
HR 1457	100	9 x 3	69 x 69	5.464	-13.6
HR 1457	100	7 x 7	15 x 15	7.189	+13.6
C200 detector					
HR 2020	170	2 x 2	90 x 90	2.389	-14.3
HR 2020	170	3 x 3	46 x 46	3.187	+14.3
NGC 6543	170	4 x 4	92 x 92	20.884	-16.0
NGC 6543	170	10 x 10	46 x 46	28.817	+16.0
NGC 6503	170	4 x 4	92 x 92	42.828	-5.6
NGC 6503	170	10 x 10	46 x 46	47.932	+5.6
IC 1228	170	4 x 4	92 x 92	8.421	-25.7
IC 1228	170	10 x 10	46 x 46	14.236	+25.7

1.4 Validation

1.4.1 Chopped Photometry

A new information with OLP 9 is the assessment of the chopped photometry reproducibility deduced from a set of monitoring measurement. For each detector the measurement was repeated 6 times (except for P2: for technical reasons only 3 repeated measurements could be acquired). In summary, the following calibration accuracies have been achieved per detector and flux range (cf. Table 1.8 for details):

1) **ISOPHOT-P1:**
   Better than 25 % absolute over the full flux range 0.06 - 10 Jy. One open issue is the relative filter calibration for some test cases. The relative reproducibility accuracy is 15 %.

2) **ISOPHOT-P2:**
   A signal correction is now applied. The majority of test cases shows overcorrected fluxes (+50 - +80 %). There is however a strong discrepancy between OLP and PIA results, the latter ones being more accurate. Examinations of the codes are ongoing. The relative reproducibility accuracy is < 10 %.

3) **ISOPHOT-P3:**
   In general fluxes are too low by 40 - 70 %. The relative reproducibility accuracy is < 10 %.

4) **ISOPHOT-C100:**
   Better than 30 % absolute in the flux range 0.1 - 2 Jy. Below 0.1 relative flux accuracies become significantly higher (in absolute terms there is only a few mJy difference between measured flux and reference flux. Multi-filter measurements often display oblique SED shapes w.r.t. the reference SED. The relative reproducibility accuracy is 15 %.

5) **ISOPHOT-C200:**
   Suitable test cases are hard to find. The contamination by cirrus confusion is highest and noticable. This has also an impact on the reproducibility where a strong trend was found for the test case when the chopper angle was rotating w.r.t. the sky.

Based on the results per detector listed above, chopped photometry with ISOPHOT-P and -C can not be declared as scientifically valid because of the too severe restrictions and caveats. These are:

1) **Except for P1 and partially for C100 the general accuracy is not better than 40 - 50 %.**

2) **For P2 very often an overestimation of the expected flux value (+50 - +80 %) is observed, for P3 an underestimation (-40 - -70 %).**

3) **For C200 no statistically meaningful assessment could be performed yet.**

For C100 and in particular C200 for fluxes < 0.1 and < 1 Jy, respectively, achievable accuracies may be in general limited by sky background gradients and fluctuations which cannot be assessed by the limited number of off-positions. More statistics will be built up in future versions of the report.

Table 1.8: Absolute and relative (filter-to-filter) calibration accuracies per detector for chopped photometry achieved for various flux ranges in multi-filter mode with OLP V9.0.

detector	**AOT**	**flux range** [Jy]	**abs. accuracy** [%]	**rel. accuracy** [%]	**standard**
P1	P03	2 - 10	$<$ 10	–	HR 6817
P1	P03	1 - 2.6	$<$ **5**	**80**	BS 5062
P1	P03	2.2	$<$ **10**	–	HR 5986
P1	P03	0.06	$<$ **25**	–	HD 172323(6×)
P2	P03	0.2 - 6	in general fluxes 50 - 80 % too high		
P3	P03	7 - 19	**20**	–	HR 1457
P3	P03	0.15 - 1	in general fluxes 40 - 70 % too low		
C100	P22	1.5 - 2	$<$ **25**	$<$ **15**	HR 6705
C100	P22	0.2	$<$ **30**	–	HR 7310(6×)
C100	P22	0.15	$<$ **5**	–	HR 5981
C100	P22	0.08	$<$ **70**	–	IRC+60228
C200	P22	2 - 5	40	**60**	HR 5340
C200	P22	$<$ 1	strong cirrus contamination		
SS	P40	0.1 - 20	**10**	$<$ **10**	
SL	P40	0.1 - 10	**10**	$<$ **10**	

1.5 General Accuracy Limitations of OLP Processing

The previous sections provided an overview of the currently achievable average calibration accuracy using OLP products and Sect. 2 lists the conditions of limitations due to yet incomplete corrections or calibrations.
There are, however, a few general accuracy limitations which should be taken into account when using ISOPHOT data products:

- **Accuracy Limitations of Celestial Standards**
During the course of the ISO project considerable improvements for certain classes of standard sources have been achieved by new observational programmes and refined modelling. One specific case from which ISOPHOT calibration benefited a lot were the new thermophysical models of asteroids [31]. On the other hand, it has to be noted that in the FIR range the stellar spectra a very often extrapolations of measured SEDs up to at most $35\,\mu$m. In particular for faint standard stars (< 1 Jy) not much is known about the true SED in the FIR. There are indications that some standard stars do not have good flux predictions. Those will have to be identified by cross-calibration with other stars.

- **Measurement beyond Sensitivity Limit**
There are measurements in the data base which did not apply the most optimal observing strategy (cf. [27], [28]). Then even the best reduction does not achieve a satisfying result. Sensitivity limits and the corresponding minimum exposure times are given in the above cited reference documents, which have been derived from actual ISOPHOT observations.

- **Confusion by Sky Background Structure**
In the FIR the sky shows a significant structure, mainly due to IR cirrus (see [32] for a discussion on actual data). This sky confusion limits the ability to adequately determine a sky background and to derive accurate fluxes of faint sources. It can be partly circumvented by an optimized observing strategy (cf. [27], [28]) and by determining the sky background as close as possible to the source.

- **Processing Items which Require User Interaction**
There are several processing steps from the raw data to the final data products for which interactive processing can provide much better results due to visual inspection of the intermediate data products and optimizing the processing parameters or due to interactive input by the user with regard to special properties of the source (extension, structure, etc.).

1.6 Areas of Improved Processing by Interactive Data Analysis

The provision of a percentage number characterizing which improvements in calibration accuracy can be obtained by careful interactive processing is currently not possible, since so far no comprehensive systematic investigation was performed. Interactive Analysis uses the same set of general calibration files (cal-G) as OLP. The limitations due to photometric bias, e.g. the accuracy of the standard source fluxes, fully apply to interactive calibration, too. One can expect, however, to achieve a higher accuracy with IA for the following cases (cf. [33] for a tutorial):

1) measurements with signal transients which do not stabilise during the measurement time, but which are long enough to perform a reasonable transient fit.

    a) PIA provides several transient correction tools. The most efficient ones are the ones for ISOPHOT-S based on the Fouks-Schubert model (full drift modelling and initial signal jump) and the empirical solution for FIR detectors (P3, C100, and C200) based on exponential functions.

    b) PIA allows to view the transient fitting and to accept or reject it.

2) flat-fielding of maps, depending on the sampling mode and the dynamic range.

   a) In case of pixel overlap the redundancy information in the individual "pixel" maps can be used to do a flat-field correction using the sky measurement itself.

   b) For maps with large areas of flat sky background systematic flat-field residuals can be removed to a certain degree by determining the average and the relative flat-field residual pattern, even for maps with no pixel overlap. The average surface brightness is quite consistent with COBE/DIRBE photometry (cf. Table 1.4).

   c) In case of a sufficient dynamic range in surface brightness a statistical flat-field method can be applied establishing the correlations of the surface brightness per pixel with regard to a reference pixel. This method allows also to correct for additive offsets among the pixels.

3) correction of non-linear signal drifts in maps.

   a) The time sequence of the signals can be interactively inspected and non-linear baseline fits be applied in order to flatten the map.

4) detection of faint sources by refined deglitching and filtering.

   a) PIA offers more refined deglitching methods, like the two-threshold algorithm.

   b) Individual ramps or signal sequences can be inspected by eye and can be deselected or corrected manually.

1.7 Status of Scientific Validation of PHT AOTs

With the finalisation of the OLP9.0 validation the current validation status per AOT submode is given in Table 1.9. The table also provides an overview of the next steps to further upgrade both validated and non-validated modes for the final OLP version 10.0 which will produce the ISO Post Operations Phase Legacy Archive.
In Table 1.10 we list the validated modes per detector sub-system. For completeness we have added the polarisation modes which can only be evaluated interactively using PIA and special FORTRAN routines.

Table 1.9: Scientific Validation of OLP AOT Processing, July 2000. non-lin R/FCS: refinement of flux dependent signal linearization and FCS power files; beam: comparison with COBE/DIRBE photometry and empirical determination of effective solid angle; chop: chopper signal correction, including correction of chopped FCS measurement; flat-field: improvement of flat-field correction using actual sky measurement; map cal: assessment of accuracy of photometry from maps; deglitch: improved deglitching method; norm. source flux: normalized source flux relative to 180 arcsec aperture to determine relative source profile.

AOT	**submode**	**scientifically valid since**	**next upgrades**	**foreseen in OLP Vx.y**
PHT03	staring point source	V6	non-lin R/FCS	10.0
	staring extended source	no	non-lin R/FCS	10.0
			beam	10.0
	nodding	V6	non-lin R/FCS	10.0
	chopped point source	no	chop & non-lin R/FCS	10.0
	raster map	no	map cal	10.0
PHT04	staring point source	no	non-lin R/FCS	10.0
			beam	10.0
			norm. source flux	10.0
	staring extended source	no	non-lin R/FCS	10.0
			beam	10.0
			norm. source flux	10.0
	chopped point source	no	chop & non-lin R/FCS	10.0
PHT05	staring point source	V6	non-lin R/FCS	10.0
	staring extended source	no	non-lin R/FCS	10.0
			beam	10.0
PHT17/9	staring point source	V6	non-lin R/FCS	10.0
	staring extended source	no	non-lin R/FCS	10.0
			beam	10.0
PHT22	staring point source	V7	non-lin R/FCS	10.0
	staring extended source	V7	non-lin R/FCS	10.0
	nodding	V7	non-lin R/FCS	10.0
	chopped point source	no	chop & non-lin R/FCS	10.0
	raster map	V8.4	flat-field	10.0
PHT25	staring point source	V7	non-lin R/FCS	10.0
	staring extended source	V7	non-lin R/FCS	10.0
PHT32	chopped mapping	no	map cal	10.0
			deglitch & flat-field	10.0
PHT37/9	staring point source	V7	non-lin R/FCS	10.0
	staring extended source	V7	non-lin R/FCS	10.0
PHT40	staring point source	V5		
	staring extended source	V6		
	chopped point source	V6		
	raster map	V6		

Table 1.10: Scientifically Validated Observing Modes per Detector, July 2000

detector	**scientifically validated mode**	**AOT**
P1	absolute photometry point sources	PHT05
	staring multi-filter photometry point sources	PHT03
	faint source multi-filter nodding	PHT03
	multi-filter sparse map	PHT17/18/19
P2	absolute photometry point sources	PHT05
	staring multi-filter photometry point sources	PHT03
	faint source multi-filter nodding	PHT03
	multi-filter sparse map	PHT17/18/19
	polarimetry (PIA)	PHT50
P3	absolute photometry point sources	PHT05
	staring multi-filter photometry point sources	PHT03
	faint source multi-filter nodding	PHT03
	multi-filter sparse map	PHT17/18/19
C100	absolute photometry point sources	PHT25
	absolute photometry extended sources	PHT25
	staring multi-filter photometry point sources	PHT22
	staring multi-filter extended sources	PHT22
	faint source multi-filter nodding	PHT22
	staring multi-filter raster maps	PHT22
	multi-filter sparse map	PHT37/38/39
C200	absolute photometry point sources	PHT25
	absolute photometry extended sources	PHT25
	staring multi-filter photometry point sources	PHT22
	staring multi-filter extended sources	PHT22
	faint source multi-filter nodding	PHT22
	staring multi-filter raster maps	PHT22
	multi-filter sparse map	PHT37/38/39
	polarimetry (PIA)	PHT51
SS/SL	staring point source spectroscopy	PHT40
	extended source spectroscopy	PHT40
	chopped point source spectroscopy	PHT40

Chapter 2

Known Limitations and Caveats

This section addresses the limitations and caveats of the PHT calibration file Version 6.0 and the OLP implementation 9.0 which have been identified during the scientific pipeline validation process. It addresses also which caveats from calibration file Version 5.4 and OLP version 8.4 have been closed out by this latest version.

2.1 Validity Ranges of FCS Calibration Files

OLP 8.4 contained the following caveats concerning the validity ranges of the FCS calibration files (cf. Report on the Scientific Validation for PHT OLP 8.4 [1]):

1 *OLP 8.4 Caveat:* A poorer calibration accuracy can be expected for observations for which the headers of the PHT data products indicate that the FCS power settings were outside the validity range given in the header of the P*FCSPOW*.FITS CAL-G files. The deviation is larger for extrapolations further away from the validity range.

2 *OLP 8.4 Caveat:* The FCS calibration for P3, C100 and C200 before revolution 94 is less well sampled with standard calibration observations, than after revolution 94. Therefore, the quality of the FCS calibration of observations before revolution 94 can be poorer as compared to observations taken later in the mission. This also applies for the FCS flat-field calibration for the C100 and C200 detectors.

For OLP 9.0 the FCS calibration files were derived once more, now based on a refined set of signal linearization corrections. Table 2.1 lists the limits used for OLP V8.4 and OLP V9.0. The limits for the validity of the FCS ranges are included in the headers of the relevant FCS calibration files. Only a warning is written to the product file headers indicating the limit violation and possible degradation in calibration. To derive responsivities for the full range of electrical FCS powers used in the AOTs the lower and upper ends of the calibrated ranges were extrapolated using a model of the FCS (grey body). This model has been refined for the current set of calibration files.
Therefore, both OLP V8.4 caveats remain for OLP Version 9.0:

Caveat 1: A poorer calibration accuracy can be expected for observations for which the headers of the PHT data products indicate that the FCS power settings were outside the validity range given in the header of the P*FCSPOW*.FITS CAL-G files. The deviation is larger for extrapolations further away from the validity range.

Due to a change in the illumination characteristics of the long wavelength section of the FCS in the beginning of revolution 94, the FCS power files for the FIR detectors P3, C100, and C200 are time dependent. Before revolution 94 the coverage of the calibration curves by standard sources is less good than for the rest of the mission. This affects only a small number of Routine Phase observations (from rev. 79 to rev. 93):

Caveat 2: The FCS calibration for P3, C100 and C200 before revolution 94 is less well sampled with standard calibration observations, than after revolution 94. Therefore, the quality of the FCS calibration of observations before revolution 94 can be poorer as compared to observations taken later in the mission. This also applies for the FCS flat-field calibration for the C100 and C200 detectors.

Table 2.1 compares the valid ranges of the main FCS, FCS1, for OLP V8.4 and OLP V9.0 (in mW of electrical FCS power). In general the ranges are identical, since from OLP V8.4 onwards the full calibration data sets has been used, some extension to lower FCS powers has been achieved for filters P_4.85 and P_11.5, and C_200. Note that strictly speaking for PHT-P the power range is associated with the corresponding standard aperture (cf. Sect. 2.2 for a table of the standard apertures per PHT-P filter and additional caveat).

Table 2.1: Validity Ranges of FCS Tables (for FCS1 only). The validity range is given by the calibrated electrical heating power range (in mW) for each filter.

	up to revolution 93				**after revolution 93**			
	OLP V8.4		**OLP V9.0**		**OLP V8.4**		**OLP V9.0**	
Filter	**min**	**max**	**min**	**max**	**min**	**max**	**min**	**max**
P_3.29	17.48	50.00	17.48	50.00	17.48	50.00	17.48	50.00
P_3.6	9.49	50.01	9.49	50.01	9.49	50.01	9.49	50.01
P_4.85	15.01	35.34	12.36	35.34	15.01	35.34	12.36	35.34
P_7.3	7.48	22.13	7.48	22.13	7.48	22.13	7.48	22.13
P_7.7	8.59	24.41	8.58	24.41	8.59	24.41	8.58	24.41
P_10	5.45	11.49	5.45	11.49	5.45	11.49	5.45	11.49
P_11.3	4.81	11.78	4.81	11.78	4.81	11.78	4.81	11.78
P_11.5	3.73	9.68	3.50	9.68	3.73	9.68	3.50	9.68
P_12.8	3.65	7.63	3.65	7.63	3.65	7.63	3.65	7.63
P_16	2.66	6.58	2.66	6.58	2.66	6.58	2.66	6.58
P_20	1.72	4.00	1.72	4.00	1.72	4.00	1.72	4.00
P_25	1.40	3.61	1.40	3.61	1.40	3.61	1.40	3.61
P_60	1.05	2.98	1.05	2.98	0.42	2.13	0.42	2.13
P_100	0.42	1.84	0.42	1.84	0.27	1.84	0.27	1.84
C_50	1.03	4.23	1.03	4.23	0.59	5.27	0.59	5.27
C_60	1.09	3.88	1.09	3.88	0.39	6.39	0.39	6.39
C_70	0.74	4.03	0.74	4.03	0.43	3.15	0.43	3.15
C_90	0.46	1.93	0.46	1.93	0.29	4.40	0.29	4.40
C_100	0.46	2.03	0.46	2.03	0.20	3.79	0.20	3.79
C_105	0.40	2.22	0.40	2.22	0.20	5.84	0.20	5.84
C_120	0.31	1.86	0.31	1.86	0.24	3.47	0.24	3.47
C_135	0.27	1.34	0.27	1.34	0.17	2.60	0.17	2.60
C_160	0.22	1.16	0.22	1.16	0.07	2.45	0.07	2.45
C_180	0.27	1.90	0.27	1.90	0.12	2.88	0.12	2.88
C_200	0.22	0.81	0.22	0.81	0.16	5.78	0.13	5.78

2.2 Inhomogeneous FCS Illumination of PHT-P Apertures

The illumination of the both the PHT-P apertures and the PHT-C arrays by the internal Fine Calibration Source (FCS) is not flat. As a result the illumination of the detector does not scale with the area of the aperture. This effect is corrected for in the case of PHT-C by the so-called illumination matrix (PC1ILLUM and PC2ILLUM cal-G files). Currently, for PHT-P linearity with the aperture area is assumed and the corresponding PHT-P CAL-G files (PP1FCSAP, PP2FCSAP and PP3FCSAP) only contain correction factors of 1 (i.e. they do not imply any correction).

Table 2.2: ISOPHOT Standard Calibration Apertures

Filter	**Standard Aperture**
P_3.29	23"
P_3.6	23"
P_4.85	23"
P_7.3	23"
P_7.7	23"
P_10	52"
P_11.3	52"
P_11.5	52"
P_12.8	52"
P_16	52"
P_20	79"
P_25	79"
P_60	180"
P_100	180"

Therefore the following caveat remains in place:

Caveat 3: In case the FCS calibration of an observation is performed in a non-standard aperture of this filter (cf. Table 1) strong deviations (factor $\simeq 2$) of the correct responsivity and thus the derived fluxes can occur. The deviations are strongest for the usage of the largest apertures in combination with P1 filters.

2.3 Non-geometric Aperture Beam Size Scaling

By evaluation of multi-aperture measurements on flat backgrounds it has been found that in some filters strong non-linear behaviour w.r.t. the geometrical aperture area occurs (in particular for the largest apertures, $\geq$ 120", of the 11.5 micron filter). This means, that, if observations are performed in apertures deviating strongly from the ones used in calibration (cf. Table 2.2), deviations from the correct flux can occur. This is especially of importance for multi-aperture measurements, because often background measurements are performed in different (larger) apertures than the related source observations and are scaled to the corresponding on-source aperture size.
The extended source calibration and the correction for non-geometric beam size effects of ISOPHOT-P is not yet finalized. Currently, the s/w uses the geometrical beam sizes only. Therefore the following caveat still applies:

Caveat 4: If observations are performed in apertures, which are different in diameter from the ones used in standard calibration, deviations from the correct flux calibration can occur. This implies especially for extended source or background observations using the largest apertures with P1 and P2.

2.4 Non-linearity of Detector Responsivity with Flux

It has been a major calibration project for OLP V8.4 to characterize the non-linearity of the detector systems with incident flux. New calibration files PP1SLINR, PP2SLINR, PP3SLINR, PC1SLINR, PC2SLINR have been established which provide a linearization of the detector signals so that the responsivity becomes homogeneous for the full applicable flux range. Further refinement of the calibration files has been done for OLP V9.0.

With the successful implementation of this correction, the OLP 7.0 caveat:

1 *OLP 7.0 Caveat* Measurements with inband powers far away ($\geq$ factor 10) from the ones used for the related FCS measurement(s) have poorer calibration accuracy.

is no longer applicable for OLP versions 8.4 and 9.0. Note however, that the linearity calibration is only valid for certain signal ranges. Table 2.3 lists the lower and upper signal limits as given in the headers of the calibration files PP1SLINR, PP2SLINR, PP3SLINR, PC1SLINR, PC2SLINR. The polynomial approximations to the non-linearity curves are not extrapolated beyond the calibrated signal ranges but are kept at the level of the boundary. In different filters different relative signal ranges may be covered so that in some cases with signals at the boundaries of the calibrated ranges some unsteadiness may be introduced.

Table 2.3: Calibrated Signal Ranges of Non-linearity Correction Tables

Detector	**Filter**	**Lower Limit** [V/s]	**Upper Limit** [V/s]
P1	3.3	0.000	55.4
P1	3.6	0.000	166.1
P1	4.8	0.000	126.8
P1	7.3	0.000	95.5
P1	7.7	0.000	27.1
P1	10.0	0.000	23.5
P1	11.3	0.000	2.9
P1	12.0	0.021	35.7
P1	12.8	0.031	11.4
P1	15.0	0.019	3.7
P2	20.0	0.075	9.5
P2	25.0	0.100	10.9
P3	60.0	0.248	56.3
P3	100.0	0.267	68.1
C100	60.0	0.000	55.4
C100	65.0	0.000	45.2
C100	80.0	0.202	32.2
C100	90.0	0.000	45.1
C100	100.0	0.000	36.5
C100	105.0	0.000	34.6
C200	120.0	0.000	25.2
C200	150.0	0.000	33.4
C200	170.0	0.000	23.9
C200	180.0	0.000	21.1
C200	200.0	0.000	7.3

2.5 Detector Signal Transients

PHT OLP does not use physical (Fouks) or empirical (exponential, signal jump) signal transient correction functions, as they are available in the PIA, because those require still a highly interactive mode. Currently OLP detects detector transients by statistical trend analysis methods and discards parts of a measurement found to be affected by drifts. This method works reasonably well, if a given measurement reaches stability, i.e. for bright sources and for very long observations. The condition that stability is achieved is that the variation of the signals during the considered time interval is less than 5%. Then the signals within the stability period are used to derive the final signal per chopper plateau. In case this criterium is not met, OLP uses the weighted mean of the last 8 signals.
For ISOPHOT-S measurements there is, however, an intrinsic transient correction by the calibration method, both for staring and chopped measurements. In particular for the staring

measurements the temporal behaviour of the transient is corrected for by considering the standard star measurement at the same time suffering the same transient effect due to the selection of a standard star or, in case of faint sources, sky background close in flux. Only in case of ISOPHOT-S raster maps a static spectral response function is applied, so that transient effects play a role. Therefore, for the majority of ISOPHOT-S measurements the following caveat does not apply any more.

Caveat 5: The transient correction only works satisfactory for ISOPHOT-P and -C measurements longer than the detector transient time constant at a given illumination. The transients are very often the limiting factor for the achieved accuracy. Measurements flagged by the OLP software as *"plateau data affected by residual drift"* can show strong deviations (residual drift is greater than 5%) from the correct result.

Note: The quality of an observation, w.r.t. drift and other criteria is coded into the SPD field **PxxSFLAG** where xx identifies the detectors as follows: C1, C2, P1, P2, P3, SS and SL. The flags are given for each chopper plateau individually and are defined in the OLP include file SPP_PIX_FLAGS_PAR.INC. The following table gives an overview:

Table 2.4: Quality flags for PHT SPD Data

Flag	**Description**
0	normal
1	calibration measurement saturated
2	part of plateau data affected by drifts
3	all ramps on plateau rejected
4	plateau data affected by residual drift
5	zero standard deviation
7	zero signal for plateau

2.6 Long Term Detector Drifts

For single pointing measurements with one FCS measurement per detector no attempt is made by PHT OLP software to correct for long term detector responsivity drifts, i.e. stability of the detector responsivity during the execution time of an AOT is assumed. For raster pointing observations and sparse maps OLP does a linear interpolation with time of the responsivity values derived from the two bracketing FCS measurements. Detailed investigation of PHT-C maps has shown that the detector long term drift is not linear, but very often shows an exponential behaviour due to switch-on effects. Therefore, models of the detector behaviour or baseline fits would be required for optimum results.

Caveat 6: PHT OLP does not correct (in case of single pointings) or correct only with a linear interpolation (in case of maps) for long term detector drifts within an AOT.

2.7 Error Calculation and Propagation

Uncertainties provided by OLP 9.0 are still pure statistical errors from signal evaluation. In order to assess all other uncertainties it is necessary to refer to the related documentation on PHT calibration in combination with the OLP products. (cf. documents ISOPHOT Handbook [2] and ISOPHOT Error Budgets [3]).

Caveat 7: The PHT OLP software does only provide an uncertainty from the statistical signal evaluation. It does not give any estimates of the systematic uncertainties of all performed calibration steps. Therefore, OLP 9.0 uncertainties are **minimal** errors. It is essential to refer to special documentation which provide an overview of the uncertainties introduced step by step. These depend on the exact observing conditions and evaluation steps which may even not be completed inside OLP (e.g. background subtraction in maps or from independent staring measurements).

2.8 Limitations in Use of PHT Color Correction Factors

Color correction factors are in general not applied by PHT OLP, the quoted fluxes in the data products always refer to the standard SED $F_\nu \cdot \nu$ = constant. Color correction can be performed inside PIA. The color correction factors have been calculated from the bandpass transmission files currently available, which have typically about 300 data points equally spaced in wavelength. Two different interpolation and integration methods have been used to derive the color correction factors and they give equal results except for the cases where steep Wien branches are convolved with the bandpass transmission numbers. Furthermore, the bandpass transmission files used are centred on the main throughput range. All wavelengths for which the transmission was below 10^{-4} have been excluded. Taking into account the latest available data sets of all transmission components (filter transmission, field lens transmission, blocking material transmission, spectral detector responses) the bandpass transmission of some filters (in particular P1 filters) need some update and refinement, because they show minor credible transmission peaks outside the main range. In case of extreme source SEDs these "leaks" can make a significant contribution to the resulting inband power and hence alter the corresponding color correction factor considerably.
For CALG V6.0 there was no re-determination of color correction factors. Therefore, the following caveats still apply for CAL-G V6.0 color correction factors:

Caveat 8: For the establishment of the color correction factors provided by CAL-G Version 6.0 not yet final PHT filter bandpass data including a wide wavelength range outside the nominal bandpass have been used. For some filters and in the case of extremely rising or falling SEDs this can mean an underestimate by out-of-band contributions. Color correction factors above 2 should be considered as less accurate and factors above 4 only as an indication of the order of the correction, as they clearly depend on the integration and interpolation method used. This applies in particular for SEDs of cold sources in combination with the P1 filters which fall onto the steep Wien branch of these SEDs. In these cases it is recommended to contact the ISO Data Centres for the most recent bandpass transmission and establish the color correction factor yourself.

From CAL-G V5.4 onwards the relative spectral system responses of all ISOPHOT-P and -C bandpasses (the same ones on which the tabulated color correction factors are based) are provided in the two CAL-G files PPFILTRAN.FITS and PCFILTRAN.FITS. This enables observers to calculate color correction factors for any SED shape not covered by the dedicated color correction CAL-G files.

2.9 Incomplete Raster Map Appearance in Case of Zero Signal Flag

For PHT-P raster maps the following caveat applies:

Caveat 9: In case the total flux on the detector is very small, resulting in close to zero or even negative signals at the end of the DERIVE_SPD processing stage, OLP sets the "zero signal flag" for the corresponding plateaux times and does not continue to process these data sections in DERIVE_AAR (cf. description of SPD product types, coding of pixel status flag PPxSFLAG; a listing of the quality flags is given in Table 2.4). This leads then to incomplete appearing map products PGAI. The most likely cases are for the short wavelength filters of PHT-P1, where the sky background (Zodiacal Light) shows a minimum, in particular in combination with small aperture sizes.

2.10 Application of Point Spread Function Fraction Factors to AAR Data Products

It should be noted that:

Caveat 10: The point spread function fraction correction factors are applied to all data products associated to point source photometry, like PPAP and PCAP, regardless whether a background subtraction was performed or not. For staring mode observations without background subtration this has to be accounted for when subtracting the separate background measurement.

The background measurement can be either a point source photometry (in Jy), of type PPAP or PCAP, too:

$\mathrm{F_{src+back}} = \mathrm{F_{on}} \;/\; \mathrm{f_{psf}}$
$\mathrm{F_{back}} = \mathrm{F_{off}} \;/\; \mathrm{f_{psf}}$
$\rightarrow \mathrm{F_{src}} = \mathrm{F_{src+back}}$ - $\mathrm{F_{back}} = (\mathrm{F_{on}}$ - $\mathrm{F_{off}}) \;/\; \mathrm{f_{psf}}$

or an extended source measurement of type PPAE or PCAE (in MJy sr^{-1}; for the conversion of in-band power to surface brightness, cf. chapter 8.4.10 in [2]):

$\mathrm{F_{src+back}} = \mathrm{F_{on}} \;/\; \mathrm{f_{psf}}$
$\mathrm{B_{back}} = (\mathrm{F_{off\_pix}} \;/\; ((1\text{-}\varepsilon^2) \cdot \Omega)$
$\rightarrow \mathrm{F_{src}} = \mathrm{F_{src+back}}$ - $\mathrm{F_{back}} = (\mathrm{F_{on}}$ - $\mathrm{n_{pix}} \cdot (\mathrm{B_{back}} \cdot (1\text{-}\varepsilon^2) \cdot \Omega)) \;/\; \mathrm{f_{psf}}$

$\mathrm{F_{on}}$, $\mathrm{F_{off}}$, $\mathrm{F_{off\_pix}}$ are fluxes in the aperture uncorrected for point source function effects (the latter one for one single pixel of the array). $\mathrm{B_{back}}$ is the surface brightness of the background.

Please note the following definitions with regard to application of $\mathrm{f_{psf}}$-factors to header keywords :

1) For PPAP and PPAE:
$\mathrm{f_{psf}} = \mathrm{f_{psf}^{\mathit{aperture}}}$
$\mathrm{n_{pix}} = 1$

2) For PCAP and PCAE staring modes:
total flux of the array is used!
$\mathrm{f_{psf}} = \mathrm{f_{psf}^{\mathit{array}}}$
converted flux from surface brightness has to be multiplied with number of pixels, because the solid angle Ω is defined per pixel!
$\mathrm{n_{pix}} = 9$ for C100, $\mathrm{n_{pix}} = 4$ for C200

3) For C100 PCAP and PCAE chopped mode (PHT22):
$\mathrm{f_{psf}} = \mathrm{f_{psf}^{\mathit{pixel}}}$
because only the central pixel is used!
$\mathrm{n_{pix}} = 1$
Note that $\mathrm{f_{psf}^{\mathit{array}}}$ is applied to the data fields PCAPSRCE for consistency with the

staring mode!

4) For C200 PCAP and PCAE chopped mode (PHT22):
$f_{psf} = f_{psf}^{array}$
$n_{pix} = 4$

2.11 Failure of Chopped Signal Pattern Generator in Case of Data Reduction

Since OLP 8.4 a signal pattern of the chopped measurement is generated for a more robust determination of the difference signal. This pattern consists of 4 points each for the on-source and the off-source cycle, regardless of how many ramps per chopper plateau are actually performed (however, the minimum number of ramps is four per chopper plateau).

With the successful implementation of the fix for SPR-3209 "zero on-off differences for chopped observations", the OLP 8.4 caveat:

1 *OLP 8.4 Caveat* In case of the data reduction factor being greater than 1 (i.e. for bright sources with very fast read-outs) the generation of the chopped signal pattern fails due to a timing jitter. The pattern will be zero and the resulting flux will be zero, too.

is no longer applicable for OLP version 9.0.

2.12 Residual Flat-field Structures in PHT22 Raster Maps

As part of the scientific validation of PHT22 raster maps for OLP V8.4 the flat-field accuracies for maps having a wide range of selected raster parameters, with and without pixel overlap, and a wide range of sky background brightness have been assessed. It is found that in case of no pixel overlap flat field accuracies both for C100 and C200 are in general worse than 8 % (standard deviation of the mean sky bakground versus mean sky background). This limit is due to systematic flat-field residuals of the arrays and can be recognized as systematically repeated patterns in most of the maps. In addition, for C100 maps, temporal variations of these flat-field structures are found. This is linked to non-linear detector drifts as flagged in Sect. 2.6. Therefore, for OLP 8.4 the following caveat was imposed on mapping products PGAI:

Caveat 11: Systematic flat-field residuals in maps with no pixel overlap which account to between 10 and 20 % as well as temporal variations of the flat-field in case of C100 maps limit the ability of faint source detections and photometry on low sky background levels.

This caveat is still applicable for OLP 9.0.

2.13 Point Source Photometry from Staring Mode Raster Mini-Maps

A deeper investigation of photometric accuracies for point source fluxes measured on mini-maps (staring raster maps with restricted grid size, typical 3×3 for C100 or 2×2 for C200 yielded the following results:

Caveat 12: Aperture photometry on PGAI map products gives reliable fluxes only for a rather limited flux range. These products should mainly be used for a check what can be seen in the maps (source detected, structures around ...). For reliable photometry over a wide flux range the PCAS products (photometry per raster point) should be used applying an evaluation method as outlined in Sect. 8.5.3.

2.14 Filters with Less Reliable Photometry

The investigation of mainly the staring mode photometry test cases has shown several systematic artifacts in the resulting SEDs which shall be flagged here:

Caveat 13: Several filters display systematic flux offsets in multi-filter SEDs. Since in most cases they do not show up over the full flux range, most of the artifacts may be related to a poor linearisation correction for this filter. The filters and the flux levels for which these artifacts were found are listed below.

1) P1 12.8 μm filter: positive flux offset from +15 % at flux level 100 Jy to factor of 3 at background level.
2) P1 3.3 and 11.3 μm filters.
3) P2 20 μm filter: -40 % at background level.
4) C100 65 and 80 μm filters: +20 - +40 % at background level (restricted to multi-filter cases?).

2.15 Limitations of PHT-S Dynamic Spectral Response Calibration

The nature of the PHT-S dynamic spectral response calibration implies the following two restrictions:

Caveat 14: The transient behaviour of the PHT-S detectors is temperature dependent. The calibration was established for a certain temperature range in which the calibration standard measurements are located. Since PHT-S was not actively temperature controlled fluctuations of the detector temperature outside the calibrated range (2.7 K $<$ T $<$ 3.1 K) can occur. In this case absolute and relative spectral shape accuracies are worse than the quoted one due to different signal transient behaviour. These observations are flagged by a warning message in the PSSS and/or PSLS product headers.

The warning message is the following:

```
COMMENT ****************************************************
COMMENT !!!WARNING!!!
COMMENT Detector temperature outside valid range
COMMENT *************************************************
```

Caveat 15: For certain wavelength ranges fluxes of some targets can be outside the range covered by standard stars. In this case a worsening of the relative spectral shape accuracy is possible. These observations are flagged by a warning message in the PSSS and/or PSLS product headers.

The warning message is the following:

```
COMMENT *****************************************************
COMMENT !!!WARNING!!!
COMMENT Flux for pixel i out of cal range
COMMENT **************************************************
```

From the scientific validation assessment performed in this report the following two general caveats have been derived:

Caveat 16: The Zodical Light level is below the sensitivity limit of PHT-SS (short wavelength array). (The Zodiacal Light intensity is less than $1\,\mathrm{MJy\,sr^{-1}}$ for 2.5 to $4.9\,\mu$m).

Caveat 17: Quoted absolute accuracies are only valid for Zodiacal Light level in the PHT-SL range (Zodiacal Light intensity $\sim$ 5 - 2O $\mathrm{MJy\,sr^{-1}}$ for 5.8 to $11.6\,\mu$m), if the exposure time is greater equal 1024 seconds.

Chapter 3

Prerequisites for OLP Scientific Validation

The scientific validation of the PHT pipeline follows the guidelines as out-lined in the e-mail by the ISO Project Scientist Martin Kessler, "Scope of OLP Scientific Validation - IDT AI #8/16" from 18-JUL-1995. The major goals of the scientific validation process according to this note are to:

- confirm that the applied processing has had the expected effect(s) on the data;
- establish that sufficient processing has been applied to the data so that the products are usable by the observer;
- demonstrate that the processing is reliable, stable and repeatable;
- establish the level of accuracy of the calibration;
- document any known caveats or concerns with the processing and/or calibration;
- demonstrate that, with the aid of the relevant ISO Data Users Manual (IDUM, now part of the ISO Handbooks), observers can further process products to a publish-able form.

The scientific validation process is restricted to PHT Standard Processed Data (SPD) and Auto-Analysis Products. Edited Raw Data (ERD) were declared scientifically valid for data products generated with OLP version 4.0 or higher, during the "OLP V4.0 AND BEYOND REVIEW MEETING" on the 24th of April 1996. Therefore, all tests outlined here assume the correctness of all ERD data.
All test data sets were processed with the IDC test pipeline version 9.0beta. Re-processing with a delta version of 9.0beta at RAL was performed as necessary in order to validate OLP modules which have been improved during the validation process.
The report refers to several sets of data products. In the following we provide an overview:

Table 3.1: Usage of data sets during OLP 9 scientific validation

data set	**used in period and purpose**
OLP 9.0b3	main set during SVP1
OLP 9.0b6	main set during SVP2
OLP 9.0b10	end of SVP2 for confirmation of SPRs 3373 & 3374 fix
OLP 9.01	OLP 9 patch and for confirmation of SPR 3382 fix

OLP 9.01 products were also obtained by on-the-fly re-processing after official release of the OLP 9 software.

Chapter 4

Overview of Results from SVP1

During the first period of the PHT OLP 9.0 Scientific Validation the following results were achieved:

- The changes for chopped PHT-S processing imposed by SCREW-425 were correctly implemented and the results of OLP 8.4 were reproduced.
- The actual SCREW-425 implementation, namely the dynamic response method for PHT-S staring measurements failed due to two software problems as outlined in Table 4.1 below.
- The upgrade of the signal linearization files P%%SLINR (SPR-3214) failed due to wrong ordering of filters in the CALG files (with increasing wavelength instead of change wheel position). This prohibited quantitative assessment and derivation of accuracy parameters of both staring mode and chopped mode photometry.
- A check of SPD product headers revealed two problems with absolute photometry products, see Table 4.1 below.

By the end of SVP1 the following software problem reports for updates had been recorded:

Table 4.1: Problems found during OLP 9.0 Scientific Validation Period 1

Problem	**CI**	**SPR**
Wrong filter ordering in CalG files P%%SLINR	CALG	3259
Refinement of CalG files PSDYNAMIC.FITS	CALG	3260
High fluxes in PHT-SS Spectra	OLP	3267
Zero FCS powers in SPD header for AOTs P05/P25	OLP	3268
Inappropriate error messages related to signal linearization in PHT SPD	OLP	3269
Low PHT-SS SPD fluxes compared to model spectra for Vega and Sirius	OLP	3270
Match of default responsivity calibration with new signal linearization scheme	CALG	3291
Browse products generation fails using OLP9.0 products	BPG_PHT	3241

Chapter 5

Revalidation Tests during SVP1

5.1 Dynamic Spectral Response Function for ISOPHOT-S Staring Measurements of Point Sources

An overview of the test cases is outlined in Ref. [4], chapter 3.1.1.

5.1.1 References to Calibration Analysis and Software Change Documentation

- calibration report:
  - Dynamic Calibration for ISOPHOT-S [5]
- Software Change Requests: SCREW 425

5.1.2 Summary of Results

Two major implementation problems were encountered which prohibited a quantitative assessment of the dynamic spectral response calibration during SVP1:

- In the PHT-SS range fluxes close or at the background level turned out to be a factor $\sim$ 100 greater than expected $\rightarrow$ SPR-3267.
- The resulting fluxes of bright calibration standards in the PHT-SS range came out too low and the spectra were bent w.r.t. the model reference $\rightarrow$ SPR-3270.

We therefore restrict the analysis in this section to the self-consistency checks with calibration standards and refer the reader to Sect. 8.1 for a final assessment of this calibration.

5.1.3 Consistency Check of PHT-S Dynamic Response Calibration on Calibration Stars

- authors: K. Wilke, U. Klaas
- date: 29-March-2000
- SVP period 2

Motivation

We process on-source and off-source measurements of two calibration stars (HR 7001 = Vega and HR 2491 = Sirius) which were used to establish the dynamic relative spectral reponse function surfaces of CALG file PSDYNAMIC and check whether the input model SED is reproduced.

Method

We compare the stellar SEDs with the flux models by Cohen. For the accompanying background measurements we compare the background SED with COBE/DIRBE photometry (in this range the background is dominated by the smooth Zodiacal Light and hence should not be dependent on the beam size).

Results

Fig. 5.1 shows the background subtracted spectra of both Vega and Sirius using the new calibration method. The spectra show strong bents with regard to the flux models. Comparison with the on-source spectrum without any background subtraction ensures that this feature is not introduced by the background subtraction (the background level is far too low).
Fig. 5.2 shows the spectra of the off-source position (calibrated in MJy sr^{-1}) versus COBE/DIRBE photometry. In the case of Vega the background is far too high in both channels, while for the Sirius background the long-wavelength channel SL looks relatively okay. Although we should not expect to detect the Zodiacal Light level in the SS channel the resulting noise level is far too high.
The detailed source code analysis has shown several implementation problems which are documented in SPRs 3267 and 3270. We refer the reader to Sect. 8.1.3 for a final assessment of the cases.

Conclusions

- The validation of the PHT-S dynamic response calibration failed for OLP 9.0b3 (SVP1) due to several implementation problems which could be tracked with the help of the test case results. The problems are documented in SPRs 3267 and 3270.

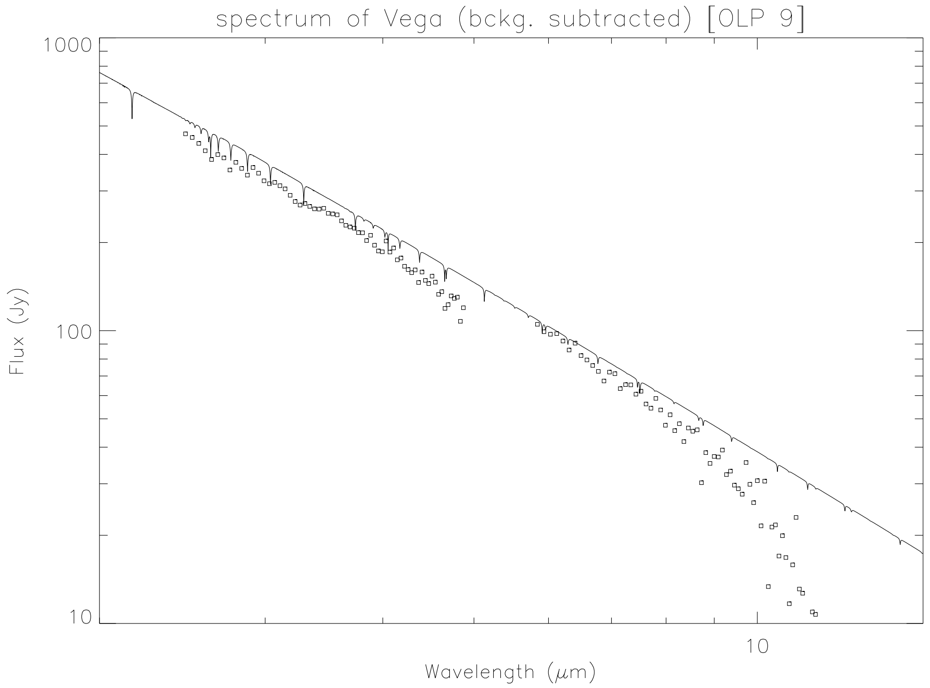

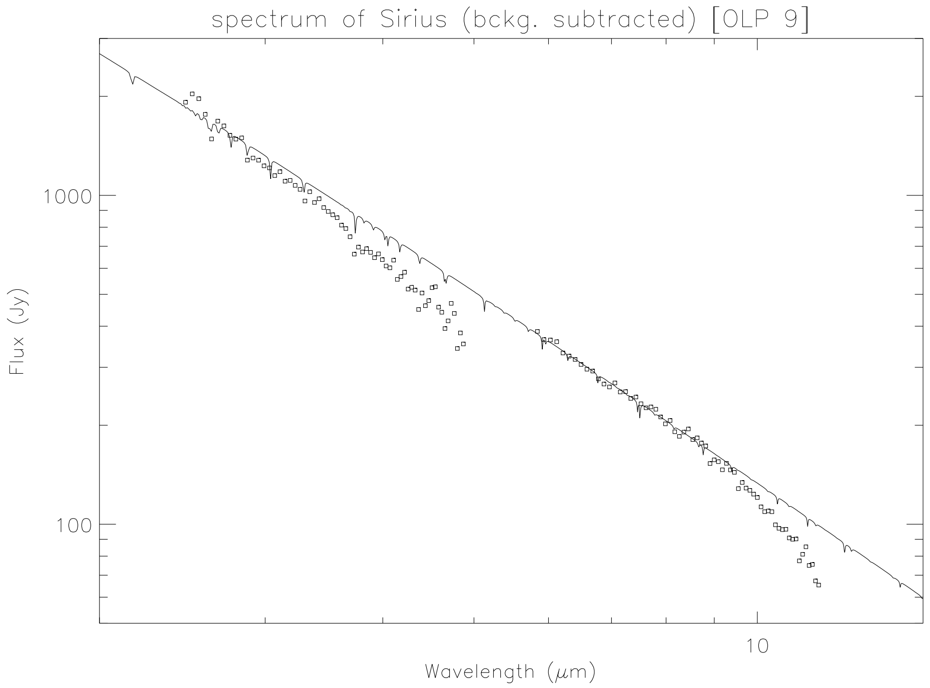

Figure 5.1: Comparison of the spectra of the stars HR 7001 (Vega) and HR 2491 (Sirius) obtained with dynamic response calibration for OLP9.0b3 with the flux models by Cohen.

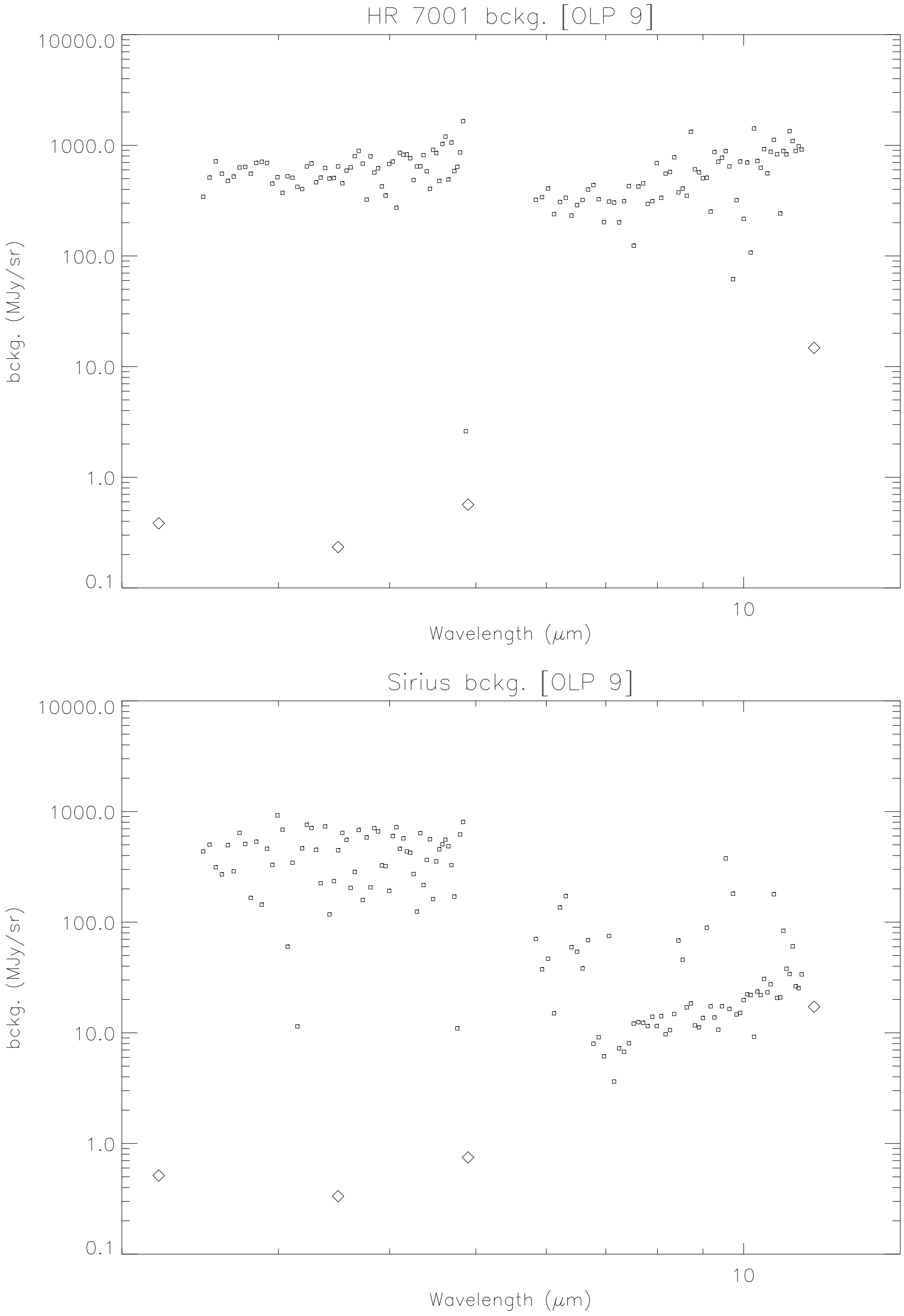

Figure 5.2: Comparison of the spectra of the background positions of HR 7001 (Vega) and HR 2491 (Sirius) obtained with dynamic response calibration for OLP9.0b3 with COBE/DIRBE photometry.

5.2 Dynamic Spectral Response Function for ISOPHOT-S Staring Measurements of Extended Sources

An overview of the test cases is outlined in Ref. [4], chapter 3.1.2.

5.2.1 References to Calibration Analysis and Software Change Documentation

- calibration report:
  - Dynamic Calibration for ISOPHOT-S [5]
- Software Change Requests: SCREW 425

5.2.2 Summary of Results

The analysis of extended source spectroscopy using the dynamic spectral response method was restricted during SVP1 to the analysis of background spectra as performed in Sect. 5.1.3. As concluded in Sect. 5.1 summary several software problems prohibited a quantitative assessment; the reader is therefore referred to Sect. 8.2.

5.3 Verification of no Impact on Chopped PHT-S Measurement Processing by SCREW 425 Implementation

An overview of the test cases is outlined in Ref. [4], chapter 3.1.3. The main purpose of this re-validation is that chopped PHT-S data reduction remains unchanged results. Due to the implementation of the dynamic response function for staring PHT-S measurements also some re-structering of code of the chopped measurement processing, which uses however a different calibration method, was necessary.

5.3.1 References to Calibration Analysis and Software Change Documentation

- calibration report:
  - Calibration of ISOPHOT-S Chopped Measurements [9]
- Software Change Request: SCREW 425

5.3.2 Summary of Results

- The changes to PHT-S chopped mode processing necessary in the context of SCREW 425 for implementation of the dynamic reponse calibration for staring mode measurements (due to the commonality of product types) have been correctly implemented.
- The PHT-S chopped mode remains scientifically valid with the accuracies established for OLP 8 (cf. Scientific Validation Report for this version [1]).

5.3.3 Consistency Check of Chopped PHT-S Relative Spectral Response Function on Calibration Stars

- authors: K. Wilke, U. Klaas
- date: 24-March-2000
- SVP period 1

Motivation

We process measurements of two calibration stars (HR 6817 and HR 6847) which were used to establish the Relative Spectral Response Function (RSRF) for chopped PHT-S measurements and check whether the input model SED is reproduced. Both calibration stars were measured both in rectangular chopped and triangular chopped mode. This allows to assess the consistency of the processing of the two chopper modes.

Method

We compare the results of both OLP 8.6b1 and OLP 9.0b3 with the flux models by Hammersley et al. 1998 [11].

Results

In Figs. 5.3 to 5.6 we perform an individual comparison of both OLP versions with the flux model. One can see that the results are absolutely identical.

Conclusions

- The two OLP versions give identical results. SCREW 425 is successfully implemented with regrad to chopped PHT-S observation processing.
- The changes applied to the processing have not altered the validation and the achieved calibration accuracy.

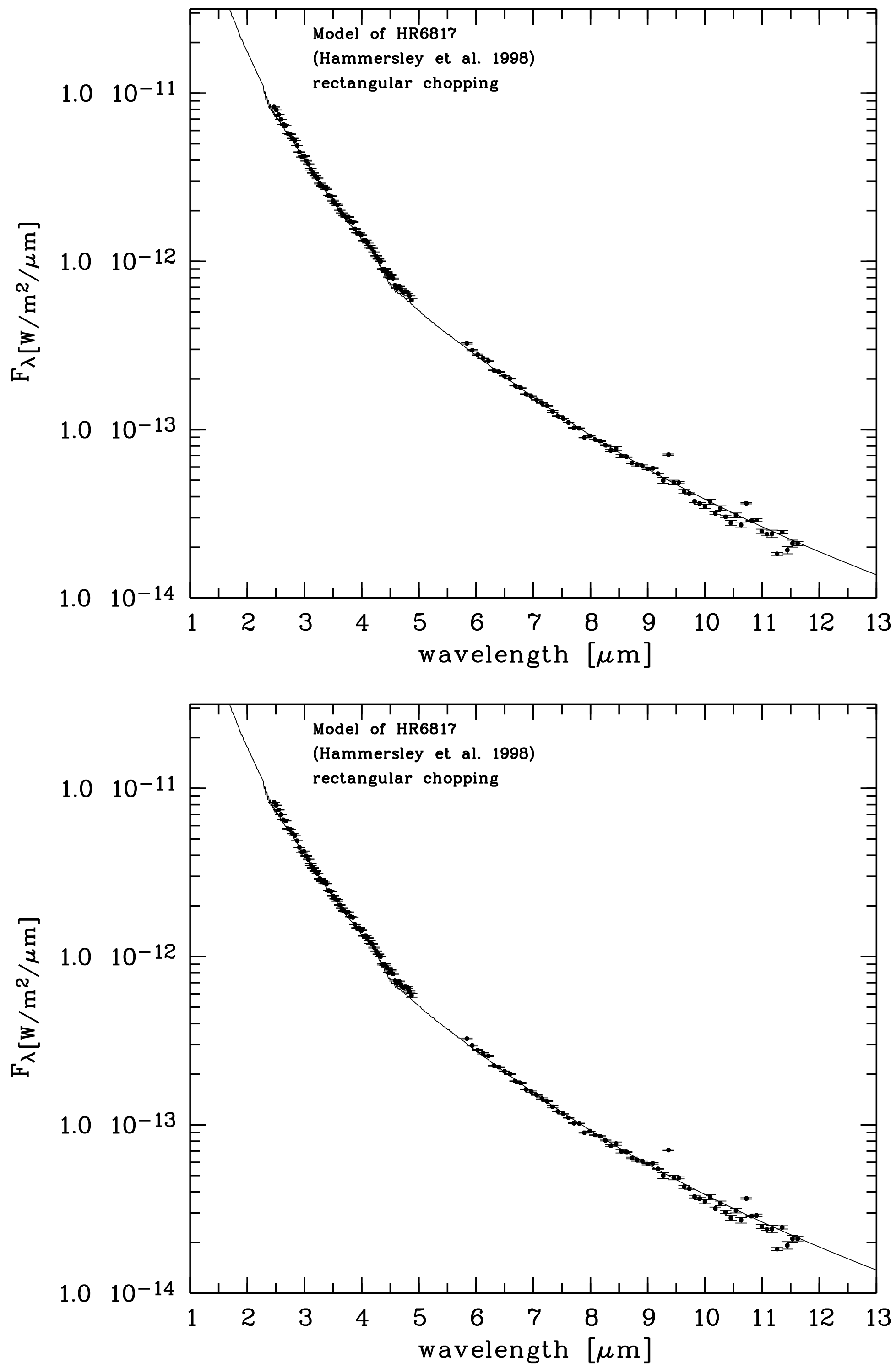

Figure 5.3: Comparison of the spectrum of HR 6817 obtained in PHT-S rectangular chopped mode for both OLP 8.6b1 (upper panel) and OLP 9.0b3 (lower panel) with the flux model by Hammersley et al. 1998.

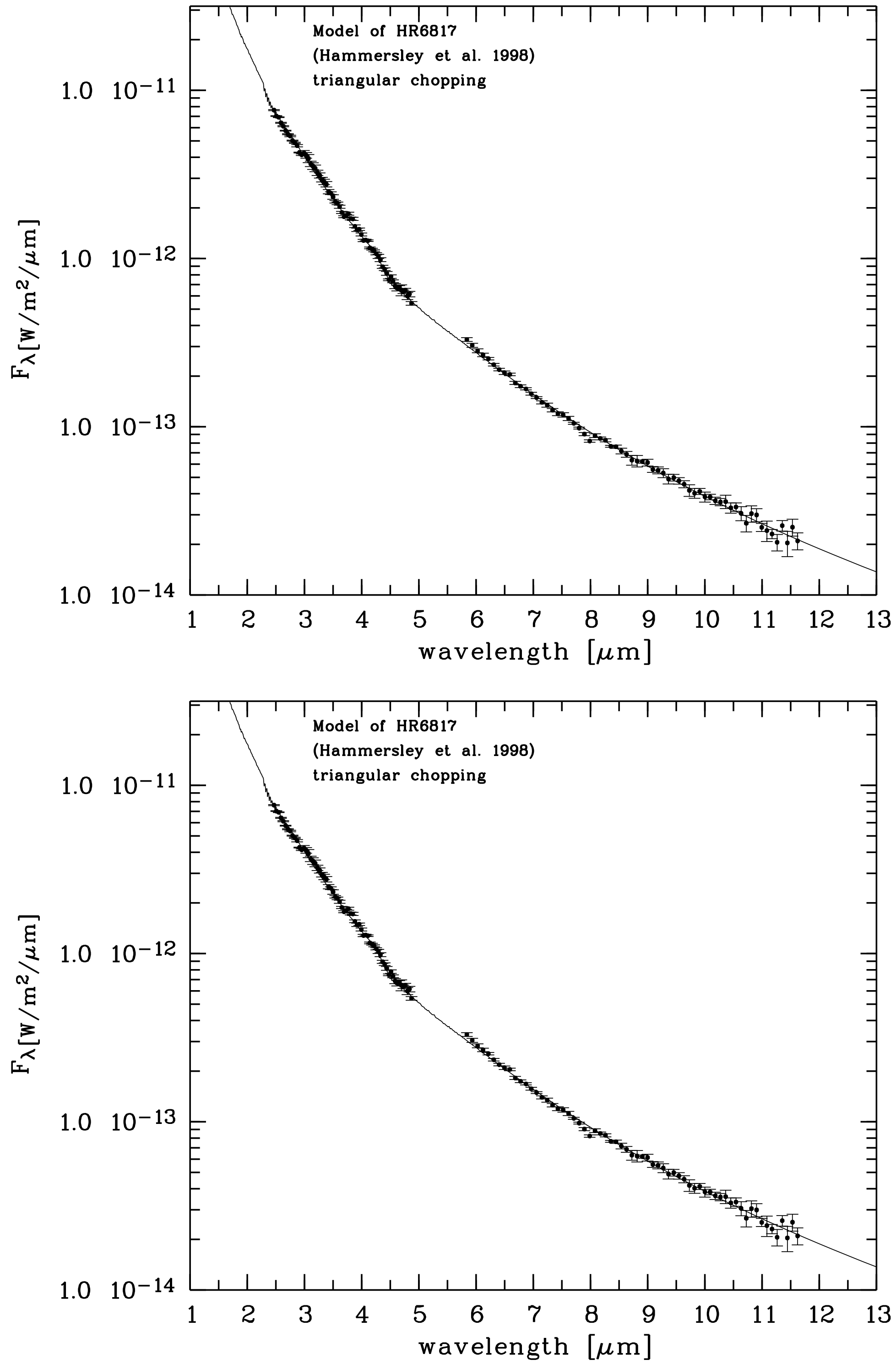

Figure 5.4: Comparison of the spectrum of HR 6817 obtained in PHT-S triangular chopped mode for both OLP 8.6b1 (upper panel) and OLP 9.0b3 (lower panel) with the flux model by Hammersley et al. 1998.

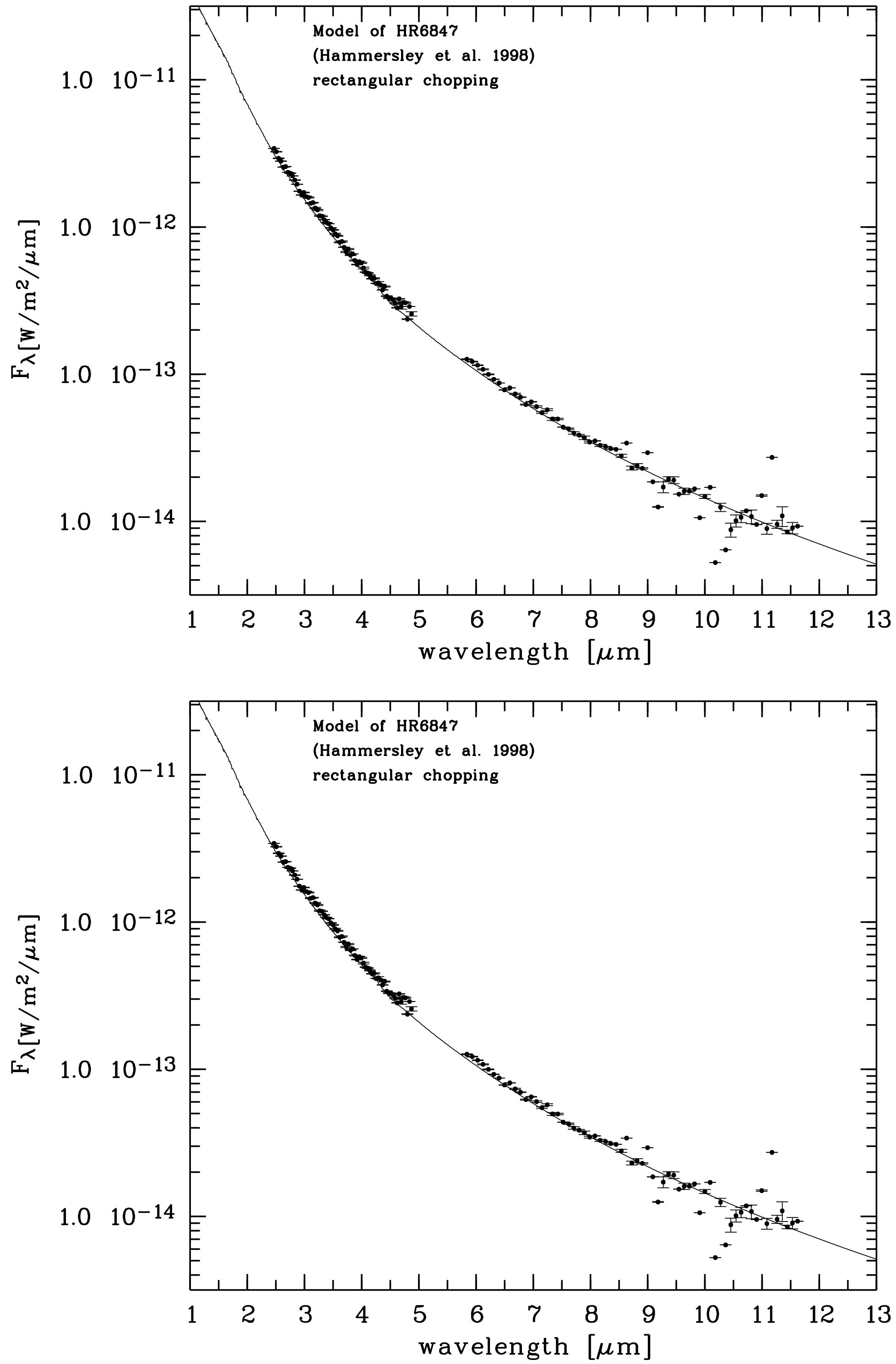

Figure 5.5: Comparison of the spectrum of HR 6847 obtained in PHT-S rectangular chopped mode for both OLP 8.6b1 (upper panel) and OLP 9.0b3 (lower panel) with the flux model by Hammersley et al. 1998.

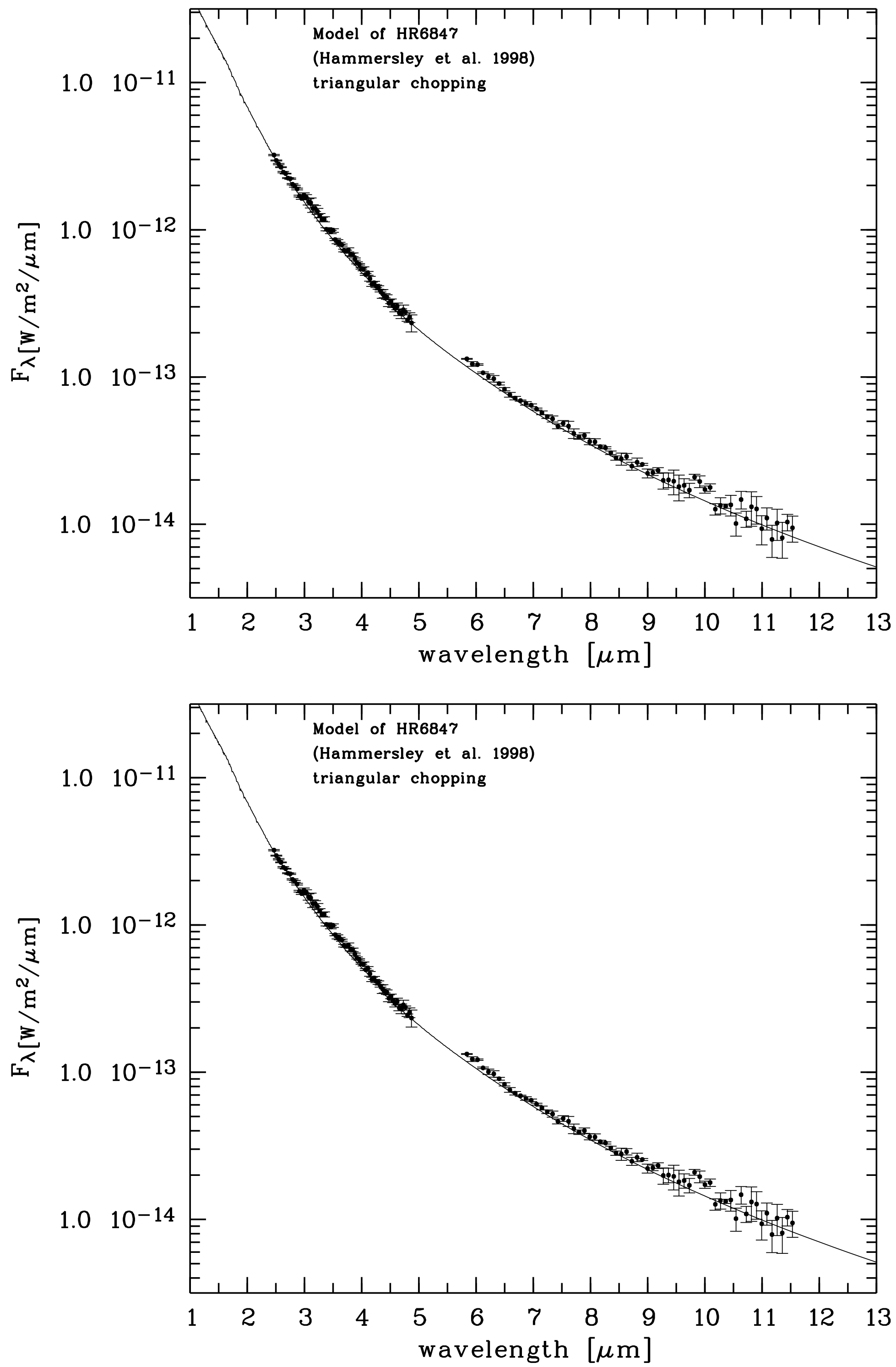

Figure 5.6: Comparison of the spectrum of HR 6847 obtained in PHT-S triangular chopped mode for both OLP 8.6b1 (upper panel) and OLP 9.0b3 (lower panel) with the flux model by Hammersley et al. 1998.

5.4 Revalidation of Staring Mode Photometry

An overview of the test cases is outlined in Ref. [4], chapter 3.2.

5.4.1 References to Calibration Analysis and Software Change Documentation

- calibration reports:
  - Linearization of ISOPHOT-P and -C detector signals in OLP8 [30]
- Software Problem Reports: SPRs 3214, 3215

5.4.2 Summary of Results

- This section reflects the status of the OLP 9.0 staring mode photometry performance after scientific validation period 1 obtained with the highest priority test cases. The wrong ordering of the filters in the signal linearization files PP1SLINR, PC1SLINR and PC2SLINR (with increasing central wavelength instead of change wheel position) as documented in SPR-3259 different deficiencies with Cal-G prohibited a calibration accuracy assessment at this stage. The reader is therefore referred to Sect. 8.4 for a final assessment of calibration accuracies for staring mode photometry.
- The file headers of absolute photometry SPD products were not properly written. This was documented in SPRs 3268 and 3269.

5.4.3 General Re-validation of PHT03 and PHT22 Staring Mode: The SED of α Bootes (HR 5340)

- authors: U. Klaas
- date: 19-March-2000
- SVP period 1

Motivation

TDTs 45200201(background, PHT-P), 45200202(α Boo, PHT-P), 45200203(background, PHT-C), 45200204(α Boo, PHT-C) is one of the key OLP validation cases [1]. The staring mode AOTs PHT-03 and PHT-22 use all available PHT filters (but the 3.6 and 4.85 μm filters had to be excluded from the analysis, because the source saturates the measurement) on a stellar (declining) SED. α Bootes is one of the most important stellar PHT calibration standards and there are detailed models available from M. Cohen (composite spectrum from 1 to 35 μm and extrapolations to 300 μm). This test case is very suitable for a test of both the absolute calibration and the relative filter-to-filter calibration. It should be noted that this multi-filter measurement was not used for the establishment of the FCS calibration curve.

Method

We compare the background subtracted, color corrected flux values of both OLP V8.6b1 and OLP V9.0b3 results against the model prediction.

Results

Figs. 5.7 and 5.8 show a comparison between OLP9 and OLP 8 results both for the source and the background flux. In particular for the background fluxes and the faint part of the source flux at long wavelengths we see a noticable degradance of the OLP 9 product. The problem could be traced back to a wrong ordering of the filters in the CALG files P%%SLINR and was documented in SPR-3259.
Therefore, no quantitative assessment of calibration accuracies is performed here, instead we refer to Sect. 8.4.3.

Conclusions

- OLP 9.0b3 data products are affected by a wrong filter ordering in the signal linearization CALG files P%%SLINR $\rightarrow$ SPR-3259.

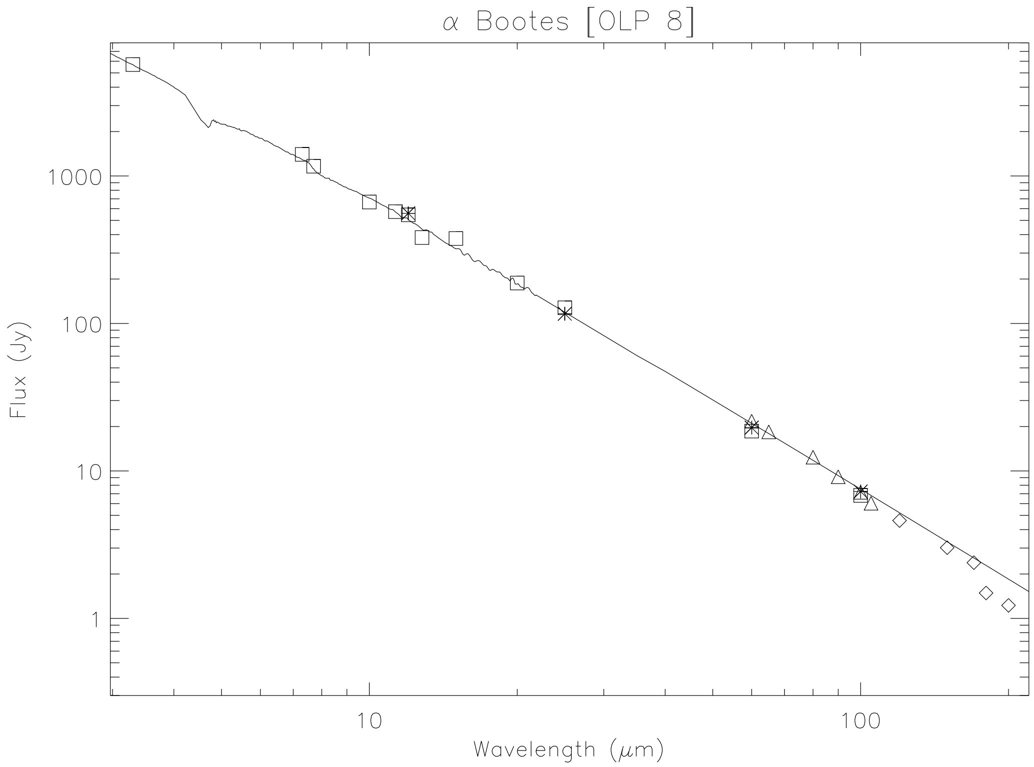

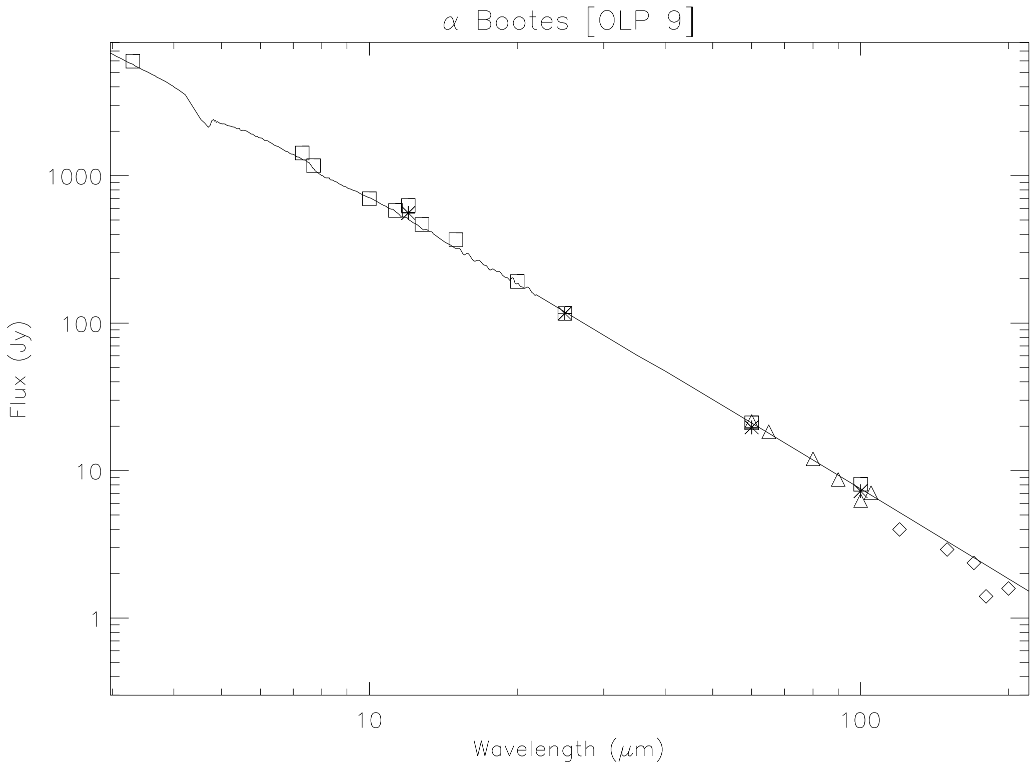

Figure 5.7: Comparison of PHT-P and PHT-C photometry, using the full ISOPHOT filter set, with the composite spectrum and out to 300 μm extrapolated SED of α Boo (HR 5340) provided by M. Cohen and with IRAS photometry for OLP 8.6b1 (upper panel) and OLP 9.0b3 (lower panel). All photometric points are color corrected for a 4000 K BB. The meaning of the symbols is the following: solid line: model, asterisk: IRAS, square: PHT-P (P03 AOT), triangle: C100 (P22 AOT), diamond: C200 (P22 AOT).

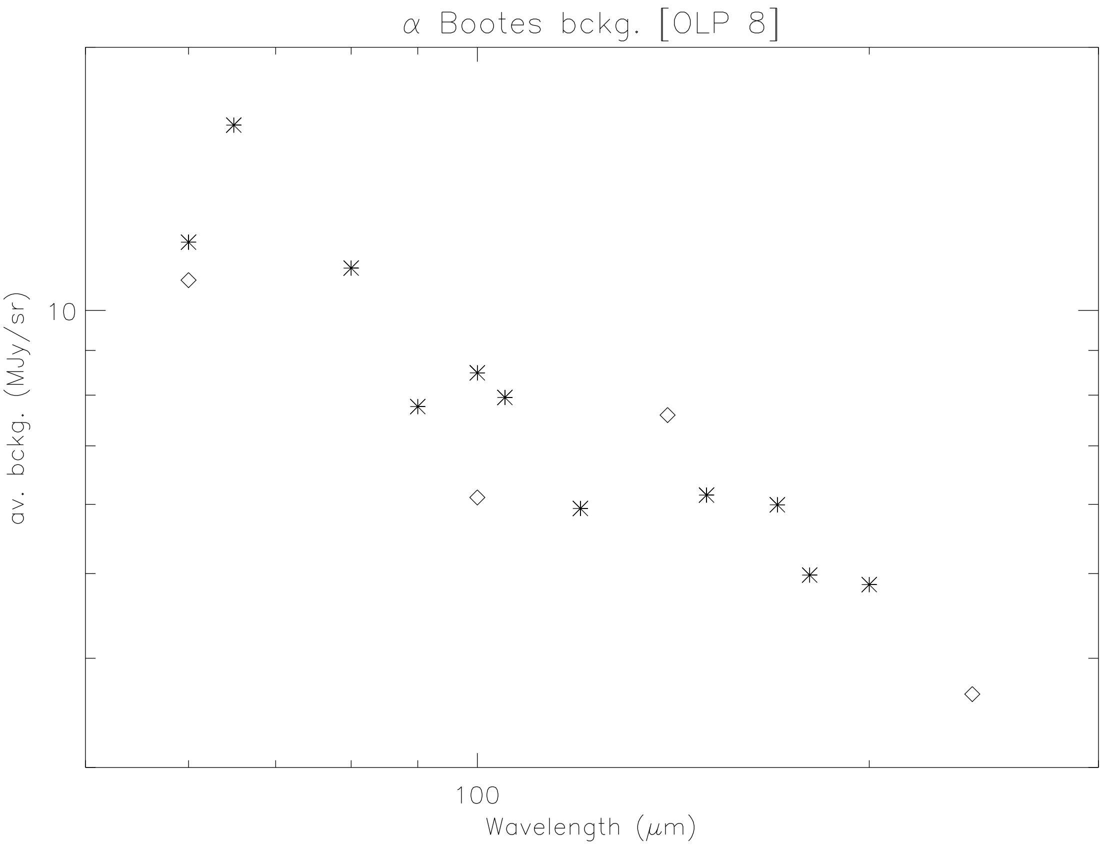

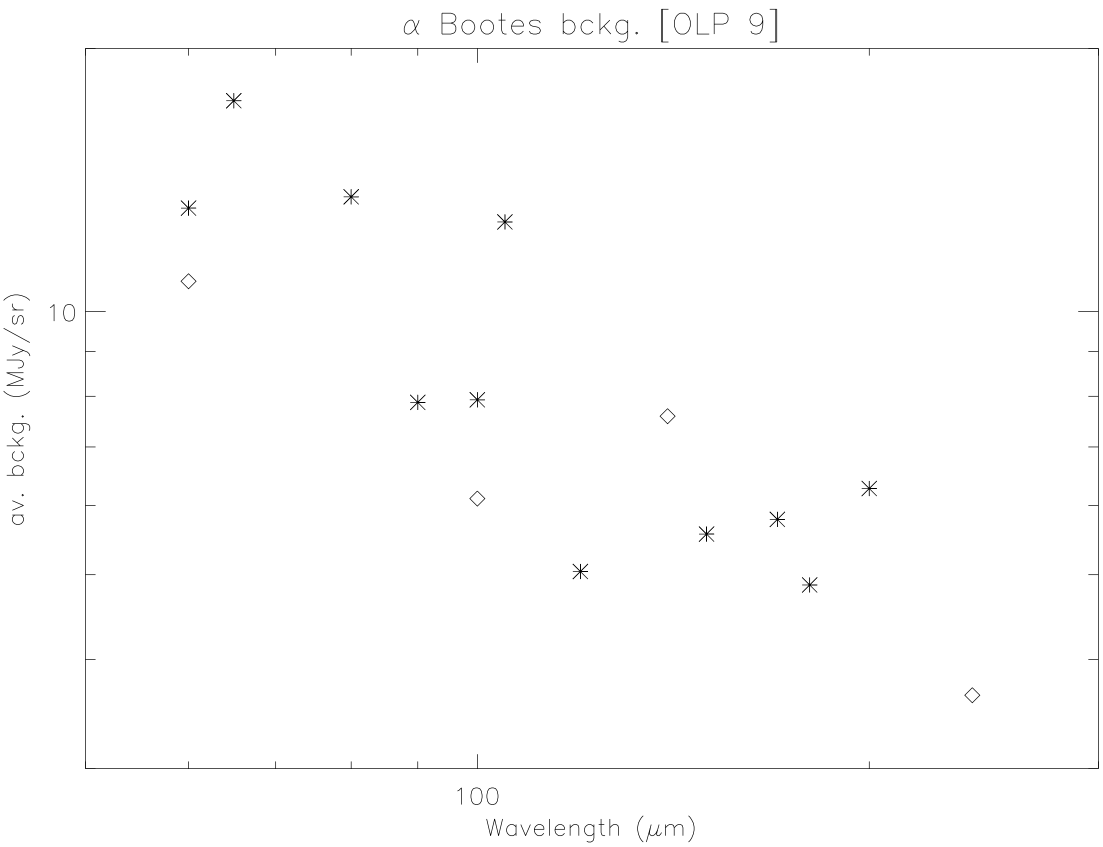

Figure 5.8: Comparison of OLP V8.6b1 and OLP V9.0b3 surface brightness (asterisk) with COBE annual map fluxes (diamond).

Evaluation Log

1) Point source photometry for Alpha Bootes in comparison with IRAS and Cohen model. Fluxes are in Jy.

Measurements:
PHT-P: ppap45200202 (src+back)
ppae45200201 (back)
PHT-C: pcap45200204 (src+back)
pcae45200203 (back)

Colour correction: black body, T = 4000 K

Model: Cohen

Det	cwl (μm)	OLP 8	OLP 9	IRAS	Model	Δ (OLP 8)	Δ (OLP 9)
P1	3.3	5695.854	5968.594		5695.470	0.01	4.80
P1	7.3	1400.773	1423.773		1291.496	8.46	10.24
P1	7.7	1165.112	1169.081		1116.581	4.35	4.70
P1	10.0	665.884	697.696		708.004	-5.95	-1.46
P1	11.3	572.895	580.845		570.349	0.45	1.84
P1	12.0	545.015	627.175	558.500	507.360	7.42	23.62
P1	12.8	382.347	466.127		435.541	-12.21	7.02
P1	15.0	376.618	368.284		320.700	17.44	14.84
P2	20.0	187.989	191.659		185.467	1.36	3.34
P2	25.0	127.784	116.274	116.400	119.146	7.25	-2.41
P3	60.0	18.614	21.082	19.650	21.030	-11.49	0.25
C1	60.0	21.747	21.559	19.650	21.030	3.41	2.52
C1	65.0	18.395	18.354		17.910	2.71	2.48
C1	80.0	12.390	12.020		11.800	5.00	1.86
C1	90.0	9.127	8.704		9.303	-1.90	-6.43
P3	100.0	6.825	8.077	7.250	7.521	-9.25	7.40
C1	100.0	7.160	6.265	7.250	7.521	-4.80	-16.69
C1	105.0	6.036	7.075		6.814	-11.42	3.84
C2	120.0	4.607	3.991		5.201	-11.42	-23.27
C2	150.0	3.018	2.915		3.310	-8.83	-11.92
C2	170.0	2.387	2.365		2.568	-7.03	-7.91
C2	180.0	1.487	1.403		2.286	-34.94	-38.64
C2	200.0	1.225	1.588		1.845	-33.59	-13.94

2) surface brightness photometry of Alpha Bootes background

λ	OLP8 (MJy/sr)	OLP9 (MJy/sr)	COBE (MJy/sr)
60.0	11.97	13.13	10.83
65.0	16.29	17.42	
80.0	11.18	13.53	
90.0	7.76	7.87	
100.0	8.48	7.93	6.11
105.0	7.95	12.66	
120.0	5.94	5.04	
150.0	6.15	5.56	7.59
170.0	5.99	5.78	
180.0	4.98	4.87	
200.0	4.86	6.27	3.64

λ	background flux (Jy)	expected source flux (Jy)	Source/background
60.0	8.80	21.03	2.39
65.0	11.62	17.91	1.54
80.0	8.76	11.80	1.35
90.0	5.36	9.30	1.74
100.0	6.01	7.52	1.25
105.0	10.15	6.81	0.67
120.0	9.77	5.20	0.53
150.0	9.82	3.31	0.34
170.0	10.87	2.57	0.24
180.0	8.58	2.29	0.27
200.0	9.76	1.85	0.19

5.4.4 General Re-validation of Multi-filter Staring Mode (PHT03/PHT22) and Absolute Photometry (PHT05/PHT25): The SED of γ Draconis (HR 6705)

- authors: U. Klaas
- date: 20-March-2000
- SVP period 1

Motivation

The star γ Draconis (HR 6705) is one of the most important calibration stars for ISOPHOT. Also several AOT commissioning observations were performed on this star. The set of observations comprises multi-filter photometry, TDTs 35602101 (background, PHT-P), 35602102 (γ Dra, PHT-P), 35602203, 39802002 (background PHT-C), 35602204, 39802003 (γ Dra, PHT-C), absolute photometry, TDTs 35300301...35300306 (PHT-P) and 35300308...35300312 (PHT-C), multi-filter PHT-C100 photometry with different reset interval settings, cf. [4] for more details. It is one of the key OLP validation cases [1]. The staring mode AOTs PHT-03 and PHT-22 use all available PHT filters out to 200 μm complementing the α Bootes observations towards the fainter flux end. There are detailed models available from M. Cohen (composite spectrum from 1 to 35 μm and extrapolations to 300 μm). This test case is very suitable for a test of both the absolute calibration and the relative filter-to-filter calibration. Furthermore, the last C100 measurements of TDT 35602204, including the C100 FCS measurement failed due to a R/T problem (therefore repetition by TDT 39802003). The available C100 measurements of TDT 35602204 are calibrated with the C100 default responsivities.

Method

We compare the background subtracted, color corrected flux values of both OLP V8.6b1 and OLP V9.0b3 results against the model prediction.

Results

Figs. 5.9 to 5.13 show a comparison between OLP9 and OLP 8 results both for the source and the background flux. In particular for the multi-filter background fluxes and the faint part of the multi-filter source flux SED at long wavelengths we see a noticable degradance of the OLP 9 product. The problem could be traced back to a wrong ordering of the filters in the CALG files P%%SLINR and was documented in SPR-3259.
Therefore, no quantitative assessment of calibration accuracies is performed here, instead we refer to Sect. 8.4.4.
When inspecting the SPD product file headers for the absolute photometry measurements (TDTs 35300301 ... 12) an incorrect TRS number, zero values of the selected and measured FCS powers and zero optical powers for the FCS calibration were found, although the data products reflected reasonable photometric results. Furthermore the warning message:

```
**************************************************
The selected FCS power was outside the calibrated range
**************************************************
```

had been prompted, not reflecting the true situation → SPR-3268.
Also in absolute photometry SPD products including a cold FCS measurement the inappropriate error message:

```
**************************************************
Filter unknown during vignetting correction
**************************************************
```

was found → SPR-3269.

Conclusions

- OLP 9.0b3 data products are affected by a wrong filter ordering in the signal linearization CALG files P%%SLINR → SPR-3259.

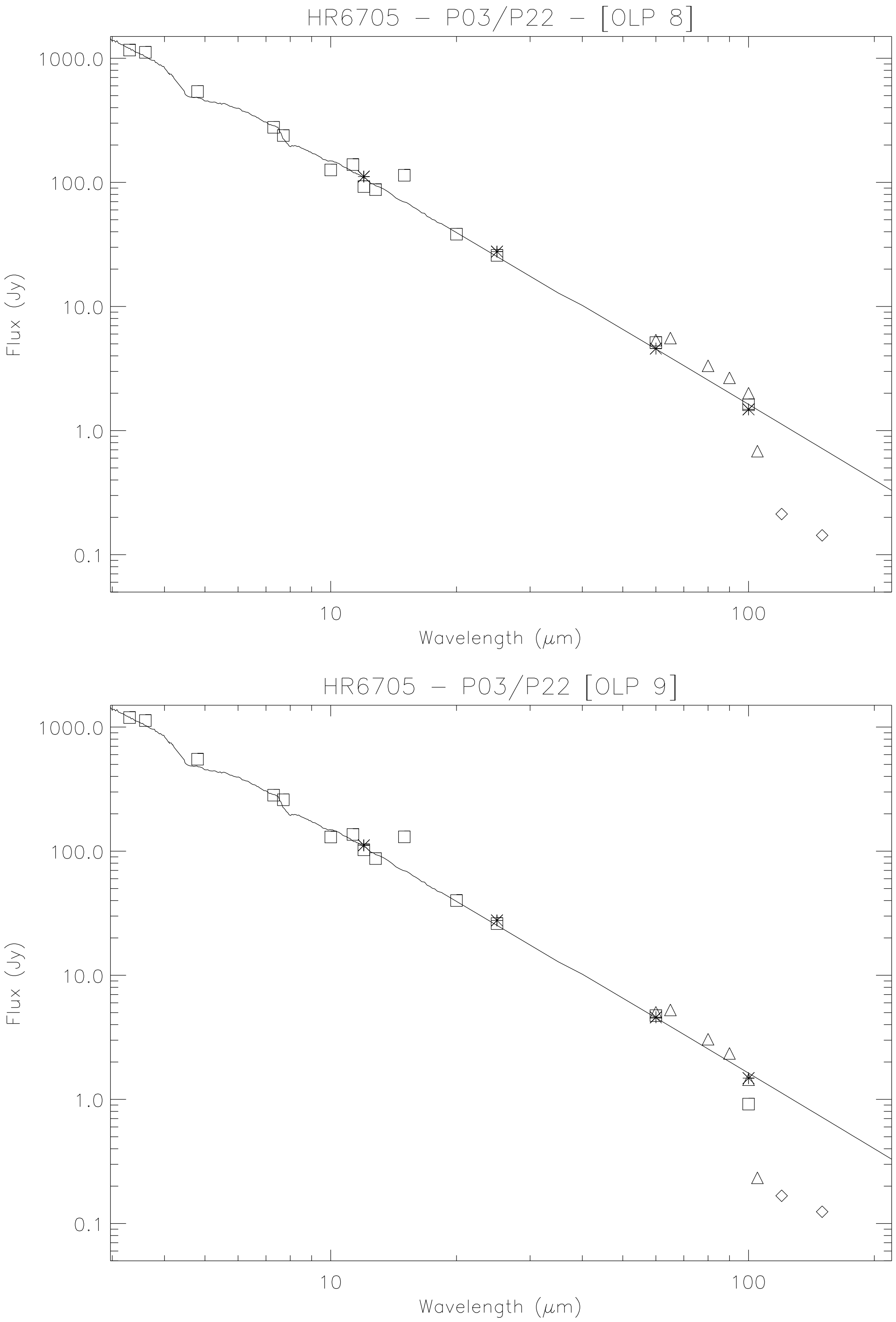

Figure 5.9: Comparison of PHT-P and PHT-C multi-filter photometry (P03/P22), using the full ISOPHOT filter set, with the composite spectrum and out to 300 μm extrapolated SED of γ Dra (HR 6705) provided by M. Cohen and with IRAS photometry for OLP 8.6b1 (upper panel) and OLP 9.0b3 (lower panel). All photometric points are color corrected for a 4000 K BB. The meaning of the symbols is the following: solid line: model, asterisk: IRAS, square: PHT-P (P03 AOT), triangle: C100 (P22 AOT), diamond: C200 (P22 AOT).

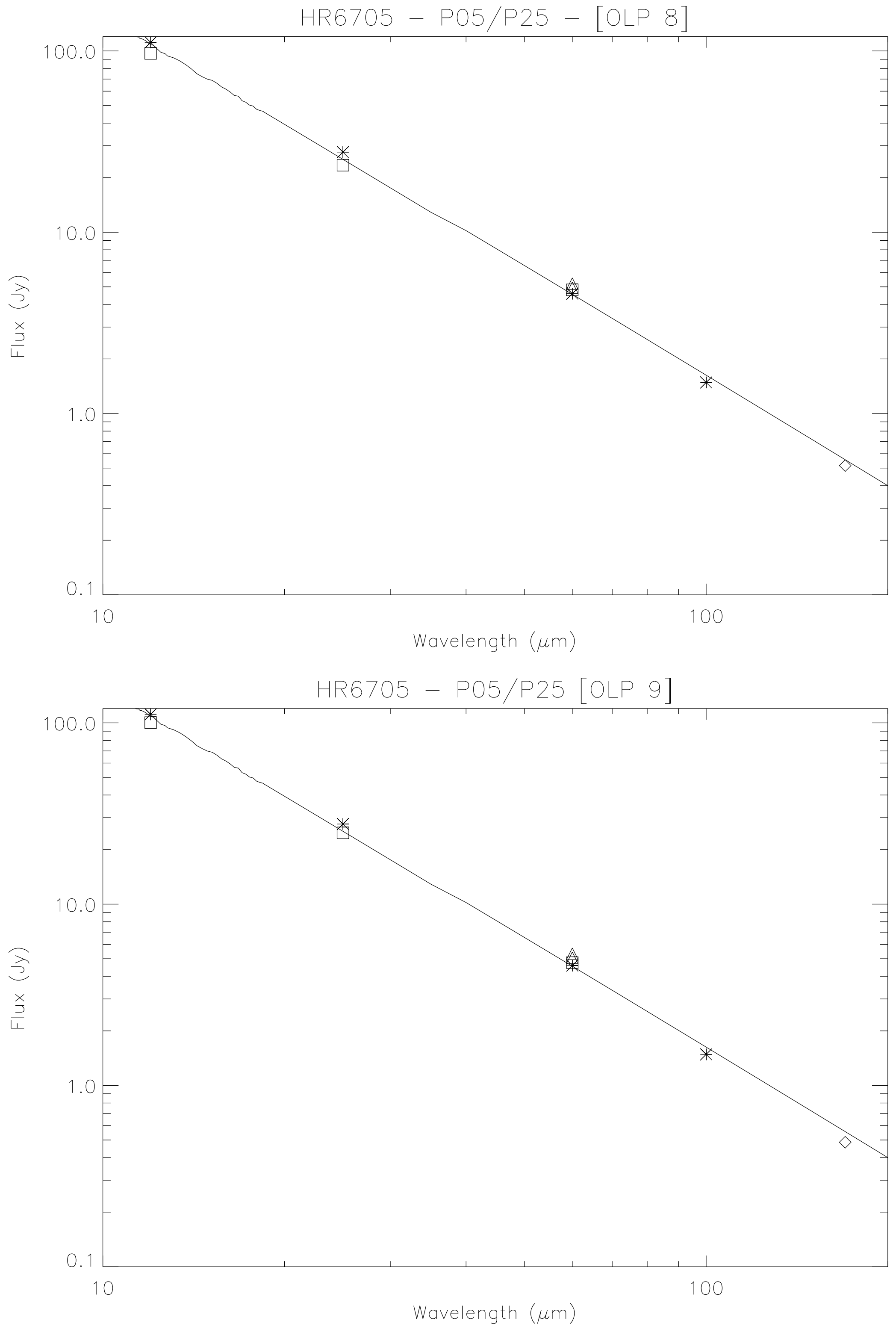

Figure 5.10: Comparison of PHT-P and PHT-C absolute photometry (P05/P25), with the composite spectrum and out to 300 μm extrapolated SED of γ Dra (HR 6705) provided by M. Cohen and with IRAS photometry for OLP 8.6b1 (upper panel) and OLP 9.0b3 (lower panel). All photometric points are color corrected for a 4000 K BB. The meaning of the symbols is the following: solid line: model, asterisk: IRAS, square: PHT-P (P05 AOT), triangle: C100 (P25 AOT), diamond: C200 (P25 AOT).

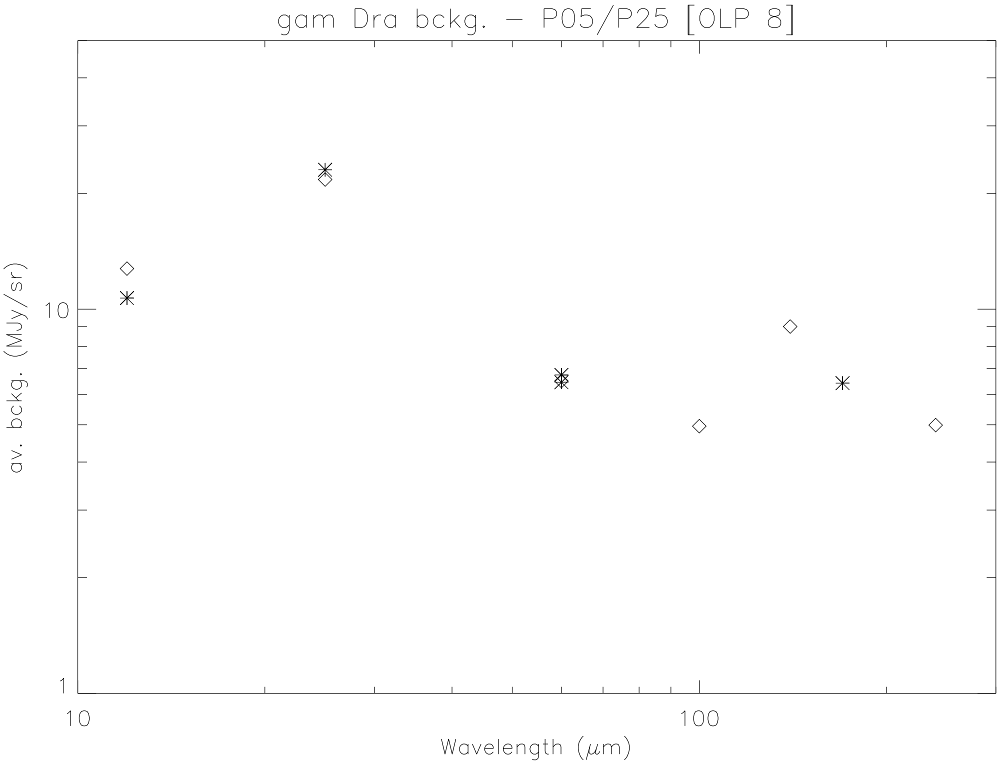

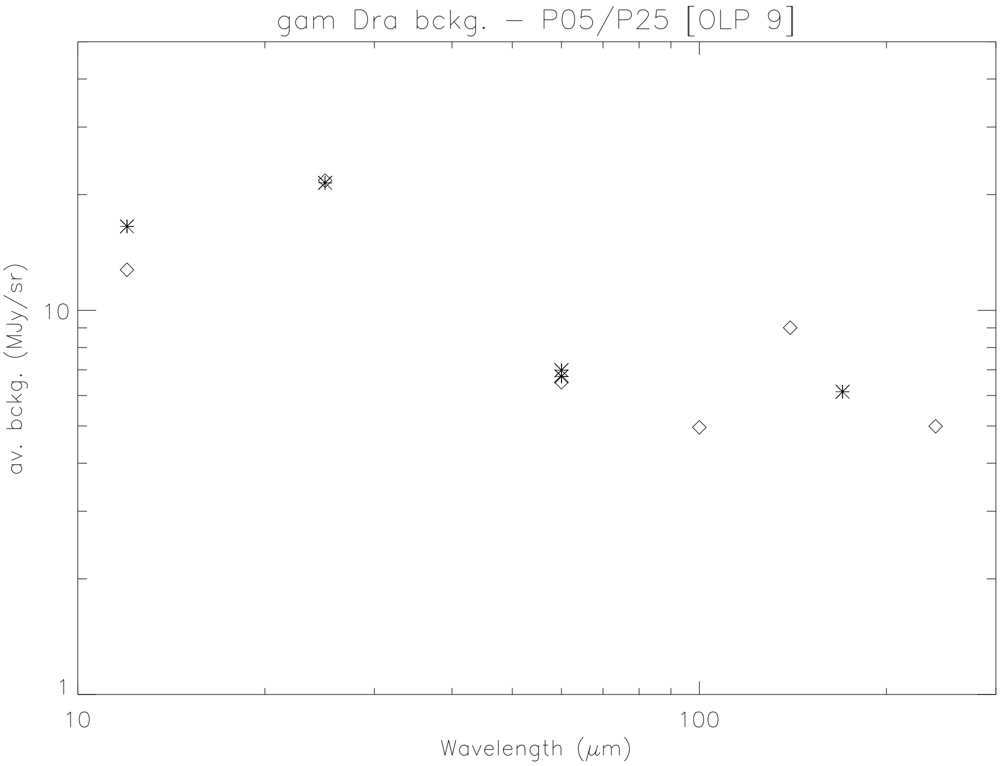

Figure 5.11: Comparison of OLP V8.6b1 and OLP V9.0b3 surface brightness, determined with the absolute photometry mode P05/P25 (asterisk) on revolution 353, with COBE annual map fluxes (diamond).

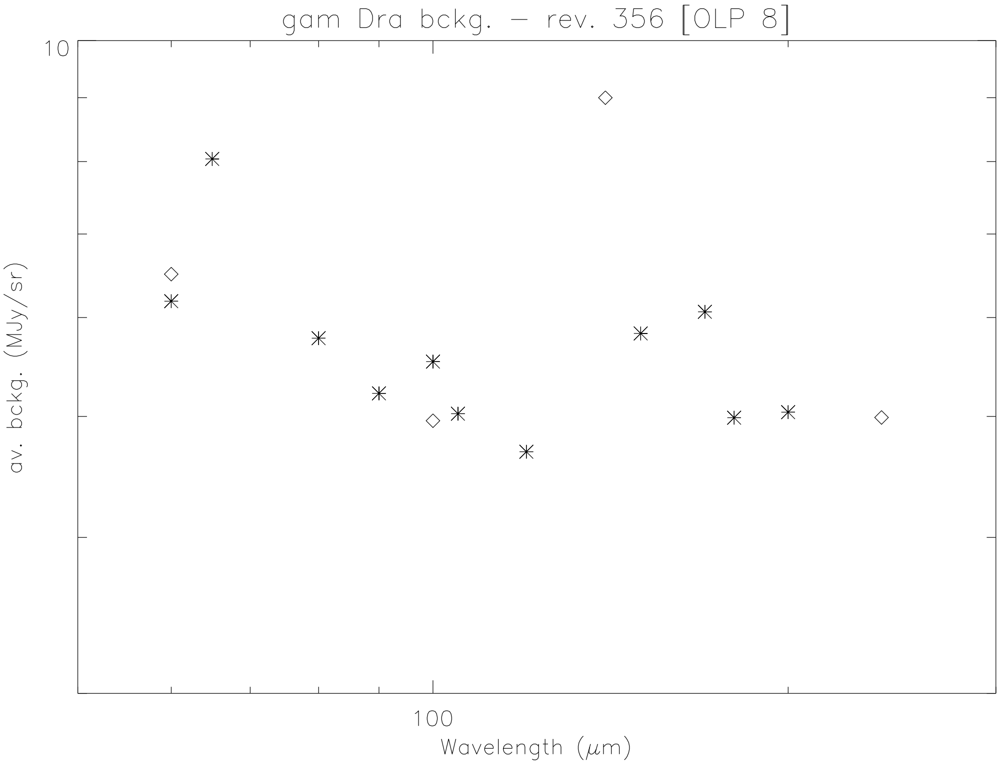

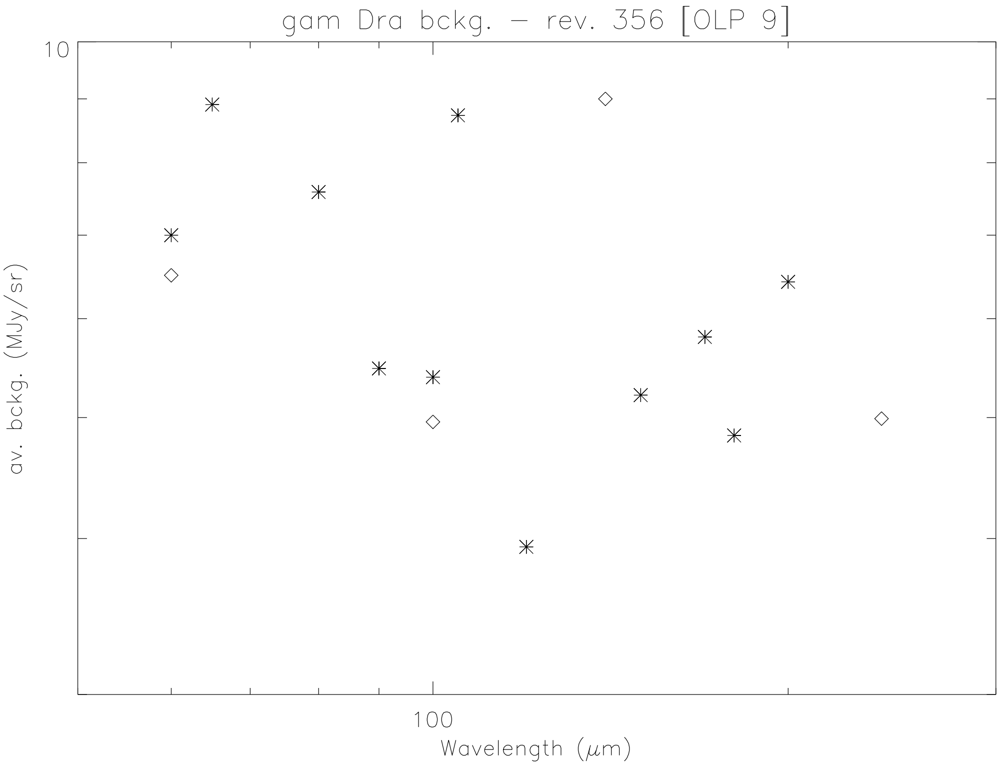

Figure 5.12: Comparison of OLP V8.6b1 and OLP V9.0b3 C100 and C200 surface brightness, determined with the multi-filter photometry mode P22 (asterisk) on revolution 356, with COBE annual map fluxes (diamond).

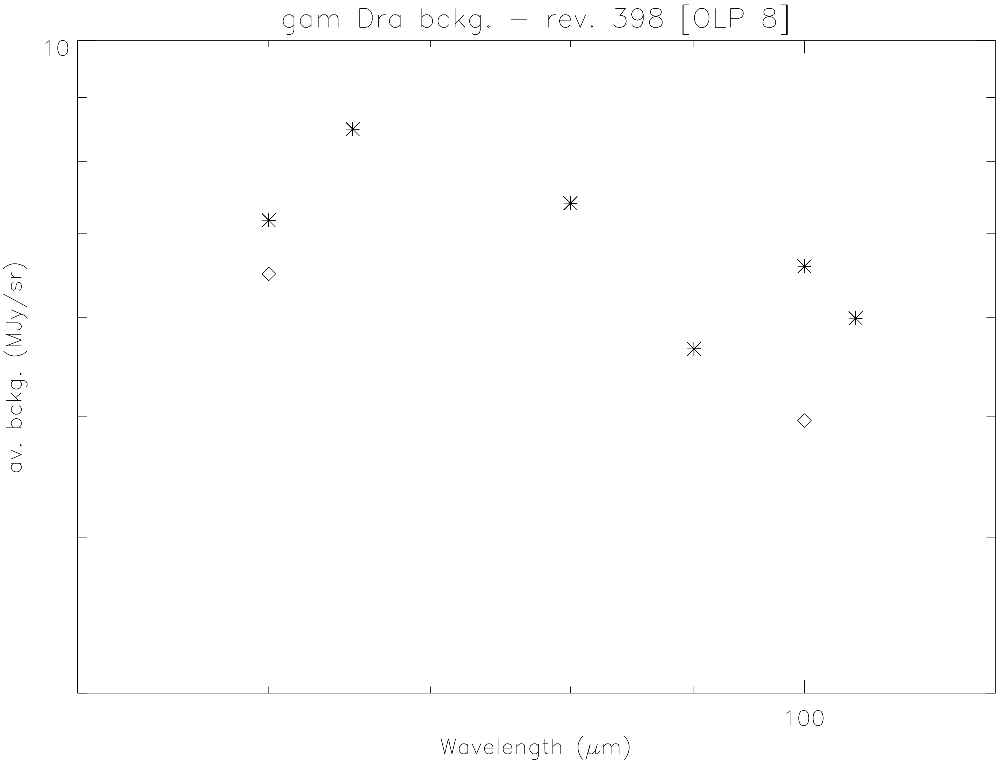

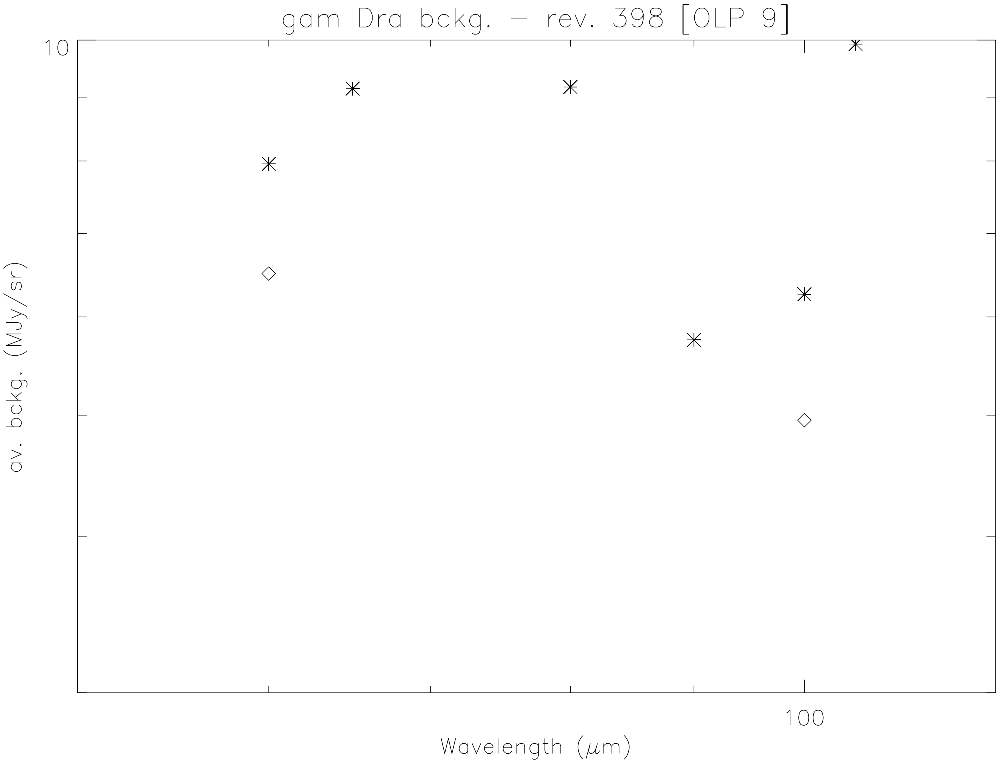

Figure 5.13: Comparison of OLP V8.6b1 and OLP V9.0b3 C100 surface brightness, determined with the multi-filter photometry mode P22 (asterisk) on revolution 398, with COBE annual map fluxes (diamond).

Evaluation Log

1) P03 and P22 multi-filter photometry

Measurements:

PHT-P:	ppap35602102 (src+back)	FCS = 15, 20, 60 um
	ppae35602101 (back)	FCS = 3.3, 20, 100 um
PHT-C1:	pcap39802003 (src+back)	FCS = 60 um
	pcae39802002 (back)	FCS = 90 um
PHT-C2:	pcap35602204 (src+back)	FCS = 170 um
	pcae35602203 (back)	FCS = 170 um

Colour correction: black body, T = 4000 K

Model: Cohen

Det	cwl (μm)	OLP 8	OLP 9	IRAS	Model	Δ (OLP 8)	Δ (OLP 9)
P1	3.3	1164.273	1192.724		1203.159	-3.23	-0.87
P1	3.6	1117.075	1128.214		1030.575	8.39	9.47
P1	4.8	539.840	550.865		482.322	11.93	14.21
P1	7.3	277.822	282.670		285.925	-2.83	-1.14
P1	7.7	238.588	259.432		224.074	6.48	15.78
P1	10.0	126.034	130.056		149.024	-15.43	-12.73
P1	11.3	139.136	136.504		120.822	15.16	12.98
P1	12.0	92.502	102.617	111.479	108.718	-14.92	-5.61
P1	12.8	87.453	87.192		93.877	-6.84	-7.12
P1	15.0	114.088	130.469		69.510	64.13	87.70
P2	20.0	38.263	39.997		39.387	-2.85	1.55
P2	25.0	25.813	26.089	27.671	25.229	2.32	3.41
P3	60.0	5.119	4.729	4.583	4.545	12.64	4.05
C1	60.0	5.358	5.028	4.583	4.545	17.89	10.64
C1	65.0	5.567	5.253		3.872	43.76	35.68
C1	80.0	3.329	3.051		2.550	30.54	19.64
C1	90.0	2.662	2.345		2.012	32.28	16.55
P3	100.0	1.614	0.916	1.483	1.627	-0.77	-43.71
C1	100.0	1.999	1.440	1.483	1.627	22.85	-11.47
C1	105.0	0.683	0.233		1.474	-53.69	-84.18
C2	120.0	0.213	0.167		1.126	-81.11	-85.15
C2	150.0	0.143	0.124		0.717	-80.01	-82.66
C2	170.0	-0.331	-0.325		0.556	-159.50	-158.45
C2	180.0	-1.046	-1.021		0.495	-311.14	-306.19
C2	200.0	-0.174	-0.203		0.400	-143.50	-150.81

TDT: ppap39801901 (OLP 9, colour corrected, no background subtraction):

3.6 μm 1130.693 Jy

15 μm 107.328 Jy

2) P05 and P25 absolute photometry

Measurements:	
PHT-P1:	ppap35300302 (src+back)
	ppae35300301 (back)
PHT-P2:	ppap35300304 (src+back)
	ppae35300303 (back)
PHT-P3:	ppap35300306 (src+back)
	ppae35300305 (back)
PHT-C1:	pcap35300309 (src+back)
	pcae35300310 (src+back, b)
	pcae35300308 (back)
PHT-C2:	pcap35300312 (src+back)
	pcae35300311 (back)

Colour correction: black body, T = 4000 K

Model: Cohen

Det	cwl (μm)	OLP 8	OLP 9	IRAS	Model	Δ (OLP 8)	Δ (OLP 9)
P1	12.0	96.917	100.369	111.479	108.718	-10.86	-7.68
P2	25.0	23.440	24.748	27.671	25.229	-7.09	-1.91
P3	60.0	4.812	4.759	4.583	4.545	5.88	4.71
C1	60.0	5.201	5.323	4.583	4.545	14.43	17.11
C1b	60.0	4.941	5.056	4.583	4.545	8.71	11.25
C2	170.0	0.516	0.486		0.556	-7.21	-12.67

3) Surface brightness on background positions:

a) absolute photometry on revolution 353

λ	OLP8 (MJy/sr)	OLP9 (MJy/sr)	COBE (MJy/sr)
12.0	10.69	16.54	12.75
25.0	23.06	21.47	21.75
60.0	6.45	6.99	6.50
60.0	6.74	6.73	6.50
170.0	6.42	6.14	

b) multi-filter C100 and C200 photometry on revolution 356

λ	OLP8 (MJy/sr)	OLP9 (MJy/sr)	COBE (MJy/sr)
60.0	6.18	7.00	6.50
65.0	8.04	8.91	
80.0	5.78	7.58	
90.0	5.22	5.47	
100.0	5.53	5.39	4.96
105.0	5.02	8.73	
120.0	4.68	3.94	
150.0	5.83	5.21	9.00
170.0	6.06	5.80	
180.0	4.99	4.84	
200.0	5.04	6.42	4.99

c) multi-filter C100 photometry on revolution 398

λ	OLP8 (MJy/sr)	OLP9 (MJy/sr)	COBE (MJy/sr)
60.0	7.18	7.96	6.50
65.0	8.49	9.14	
80.0	7.41	9.17	
90.0	5.66	5.75	
100.0	6.59	6.26	4.96
105.0	5.99	9.93	

5.4.5 General Re-validation of PHT03 and PHT05 Staring Mode: The SED of Sirius (HR 2491)

- authors: U. Klaas
- date: 19-March-2000
- SVP period 1

Motivation

Beside Vega (HR 7001), Sirius is the main primary stellar standard with a model provided by M. Cohen (1-300 μm, R = 4000 up to 35 μm, delivered 12-Jan-1996). Therefore, a dedicated cross-calibration program was performed on this star using absolute photometry complemented by multi-filter photometry out to 25 μm.

Method

We compare the background subtracted, color corrected flux values of both OLP V8.6b1 and OLP V9.0b3 results against the model prediction.

Results

Fig. 5.14 shows a comparison between OLP9 and OLP 8 results. In particular for the 15 μm filter we see a noticable quality degradance of the OLP 9 product. The problem could be traced back to a wrong ordering of the filters in the CALG files P%%SLINR and was documented in SPR-3259.
Therefore, no quantitative assessment of calibration accuracies is performed here, instead we refer to Sect. 8.4.5

Conclusions

- OLP 9.0b3 data products are affected by a wrong filter ordering in the signal linearization CALG files P%%SLINR $\rightarrow$ SPR-3259.

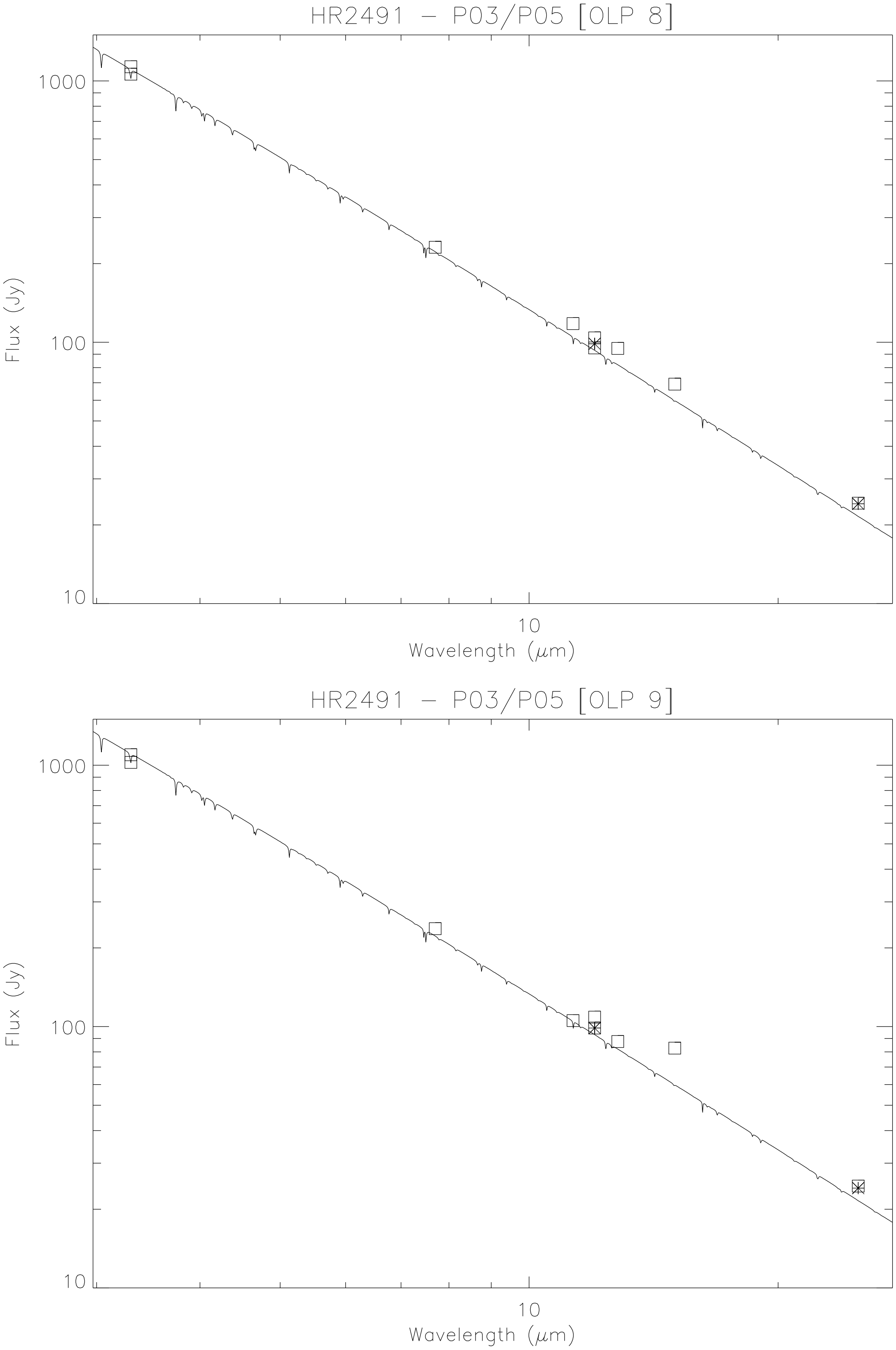

Figure 5.14: Comparison of PHT-P absolute and multi-filter photometry with the composite spectrum of Sirius (HR 2491) provided by M. Cohen and with IRAS photometry for OLP 8.6b1 (upper panel) and OLP 9.0b3 (lower panel). All photometric points are color corrected for a 10000 K BB. The meaning of the symbols is the following: solid line: model, asterisk: IRAS, square: PHT-P (P03 and P05 AOTs).

Evaluation Log

1) P03 multi-filter and P05 absolute photometry

Measurements:

PHT-P1:	ppap70705302 (src+back)	FCS = 3.3 um
	ppap70705301 (src+back)	FCS = 12.8 um
	ppap70705310 (src+back)	P05
	ppap70705313 (src+back)	P05
PHT-P2:	ppap70705307 (src+back)	P05

Colour correction: black body, T = 10000 K

Model: Cohen

Det	cwl (μm)	OLP 8	OLP 9	IRAS	Model	Δ (OLP 8)	Δ (OLP 9)
ppap70705301:							
P1	11.3	117.881	105.407		100.654	17.11	4.72
P1	12.8	94.729	87.628		82.001	15.52	6.86
P1	15.0	69.134	82.676		59.566	16.06	38.80
ppap70705302:							
P1	3.3	1133.059	1096.323		1021.900	10.88	7.28
P1	7.7	230.947	236.889		222.038	4.01	6.69
P1	12.0	103.930	108.627	98.690	93.157	11.56	16.61
ppap70705310:							
P1b	3.3	1061.453	1025.462		1021.900	3.87	0.35
ppap70705313:							
P1b	12.0	95.136	98.703	98.690	93.157	2.12	5.95
ppap70705707:							
P2	25.0	24.229	24.531	24.092	21.541	12.48	13.88

5.4.6 General Re-validation of PHT03 Staring Mode: Photometric Reproducibility Aspects in the Case of the SED of Vega (HR 7001)

- authors: U. Klaas
- date: 19-March-2000
- SVP period 1

Motivation

We investigate here the photometric accuracy of PHT-P multi-filter aperture photometry for an observation of Vega from a general observer program which was repeated several times as part of a variability monitoring project. From 3.3 to 100 μm it used the typical exposure time of 32 s per filter and non-standard apertures. The absolute calibration via the FCS of the on-source measurement was performed in the 3.6, 20, and 100 μm filter, respectively. The absolute calibration of the off-source measurement was performed in the 7.3, 25, and 100 μm filter, respectively. We selected 3 measurements out of this program from rev. 85 (TDT 08500106; before rev. 94 FCS change!), rev. 558 (TDT 55800419) and rev. 865 (TDT 86500706). The used apertures w.r.t. the standard apertures for point source calibration are listed in the following Table 5.1:

Table 5.1: Apertures used in the Vega variability monitoring program versus standard apertures

filter	**program aperture** ["]	**standard aperture** ["]
P1_3P29_UM	18	23
P1_3P6_UM	18	23
P1_4P85_UM	18	23
P1_7P3_UM	18	23
P1_10_UM	18	52
P1_11P5_UM	18	52
P1_12P8_UM	18	52
P1_16P0_UM	18	52
P2_20_UM	52	79
P2_25_UM	52	79
P3_60_UM	120	180
P3_100_UM	120	180

Method

Vega is one of the primary photometric stellar standards. However, due to its IR excess, the photospheric models, e.g. by Cohen, are valid only out to approximately 15 μm. Beyond 15 μm we solely compare with the available IRAS photometry.
The color correction was dependent on the relative contribution by the stellar photosphere and the IR disc, and hence on the wavelength. We followed the description as given in Ref.[14]:

- from 3.3 to 16 μm the SED behaves like a 10000 K Black Body,
- from 60 to 100 μm the SED behaves like an 80 K modified BB, $\varepsilon \propto \nu$
- from 20 to 25 μm the SED is a mixture of a 10000 K BB and an 80 K modified BB with a ratio 2:1.

Results

Figs. 5.15 to 5.17 show a comparison between OLP9 and OLP 8 results. In particular for 15 μm filter we see a noticable degradance of the OLP 9 product. The problem could be traced back to a wrong ordering of the filters in the CALG files P%%SLINR and was documented in SPR-3259.
Therefore, no quantitative assessment of calibration accuracies is performed here, instead we refer to Sect. 8.4.7.

Conclusions

- OLP 9.0b3 data products are affected by a wrong filter ordering in the signal linearization CALG files P%%SLINR $\rightarrow$ SPR-3259.

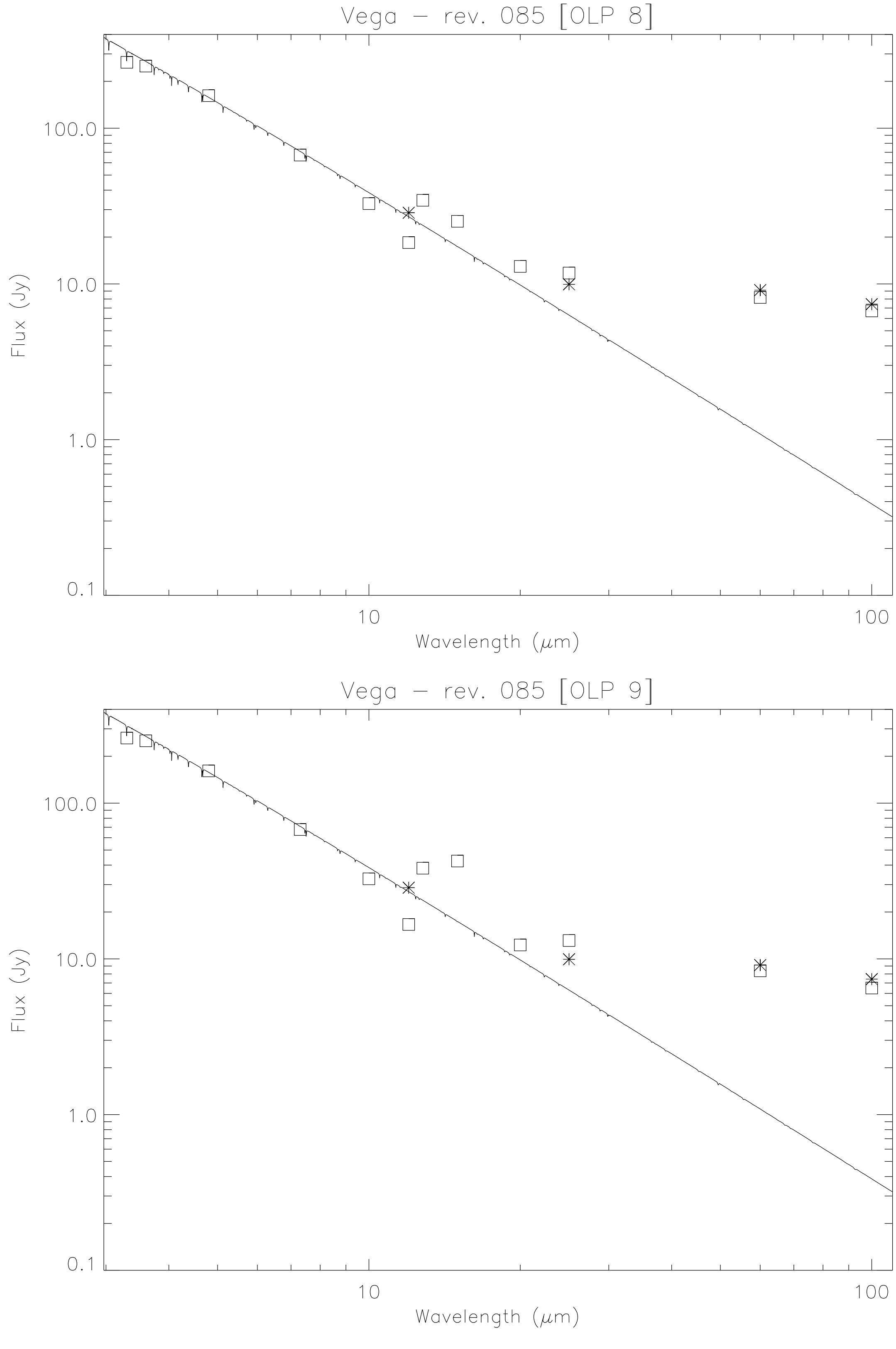

Figure 5.15: Comparison of PHT-P multi-filter photometry of Vega (HR 7001) on revolution 085 with the composite spectrum provided by M. Cohen out to 15 μm and with IRAS photometry beyond 15 μm for OLP 8.6b1 (upper panel) and OLP 9.0b3 (lower panel). A description of the applied color correction factors is given in the text. The meaning of the symbols is the following: solid line: model, asterisk: IRAS, square: PHT-P.

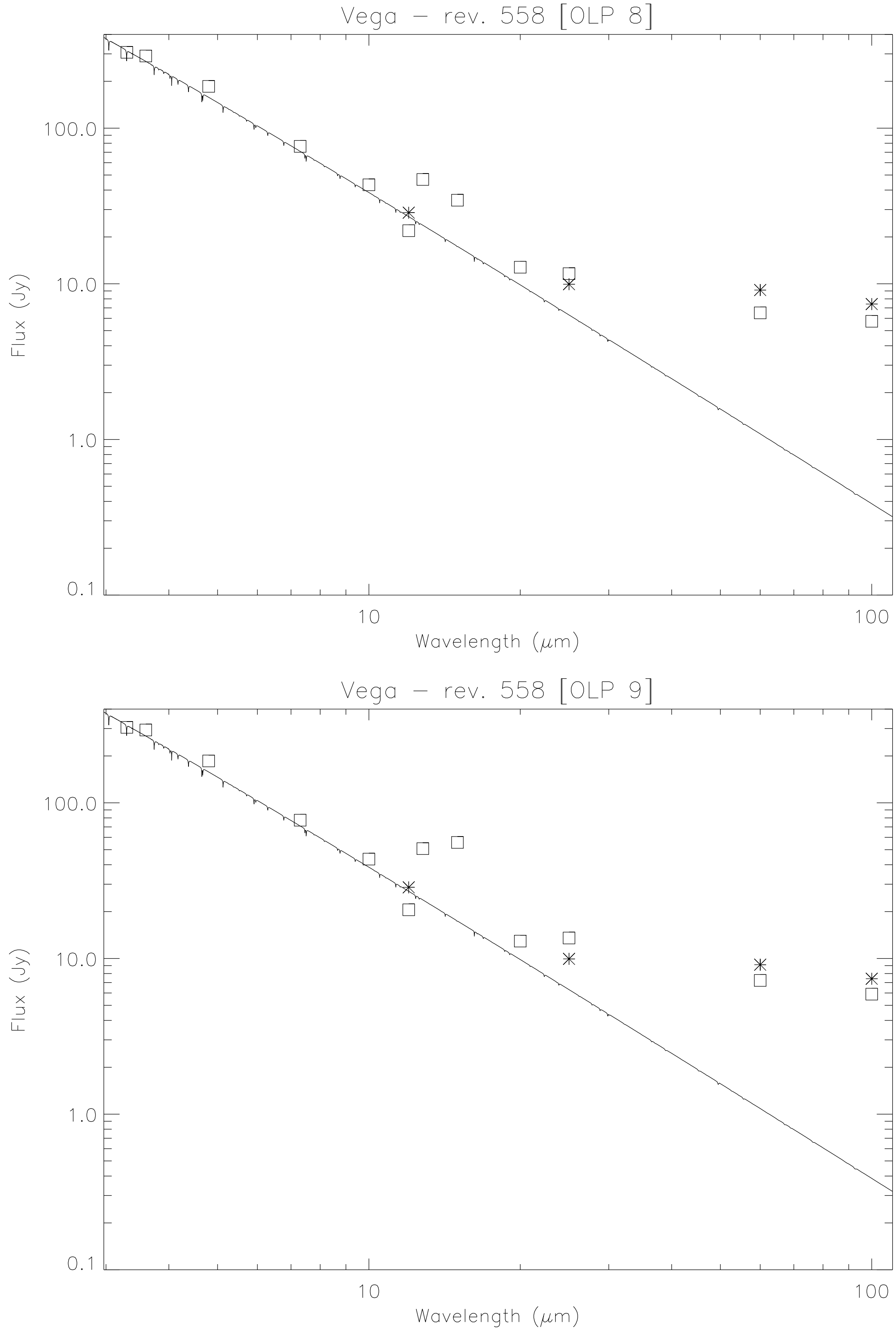

Figure 5.16: Comparison of PHT-P multi-filter photometry of Vega (HR 7001) on revolution 558 with the composite spectrum provided by M. Cohen out to $15\,\mu$m and with IRAS photometry beyond $15\,\mu$m for OLP 8.6b1 (upper panel) and OLP 9.0b3 (lower panel). A description of the applied color correction factors is given in the text. The meaning of the symbols is the following: solid line: model, asterisk: IRAS, square: PHT-P.

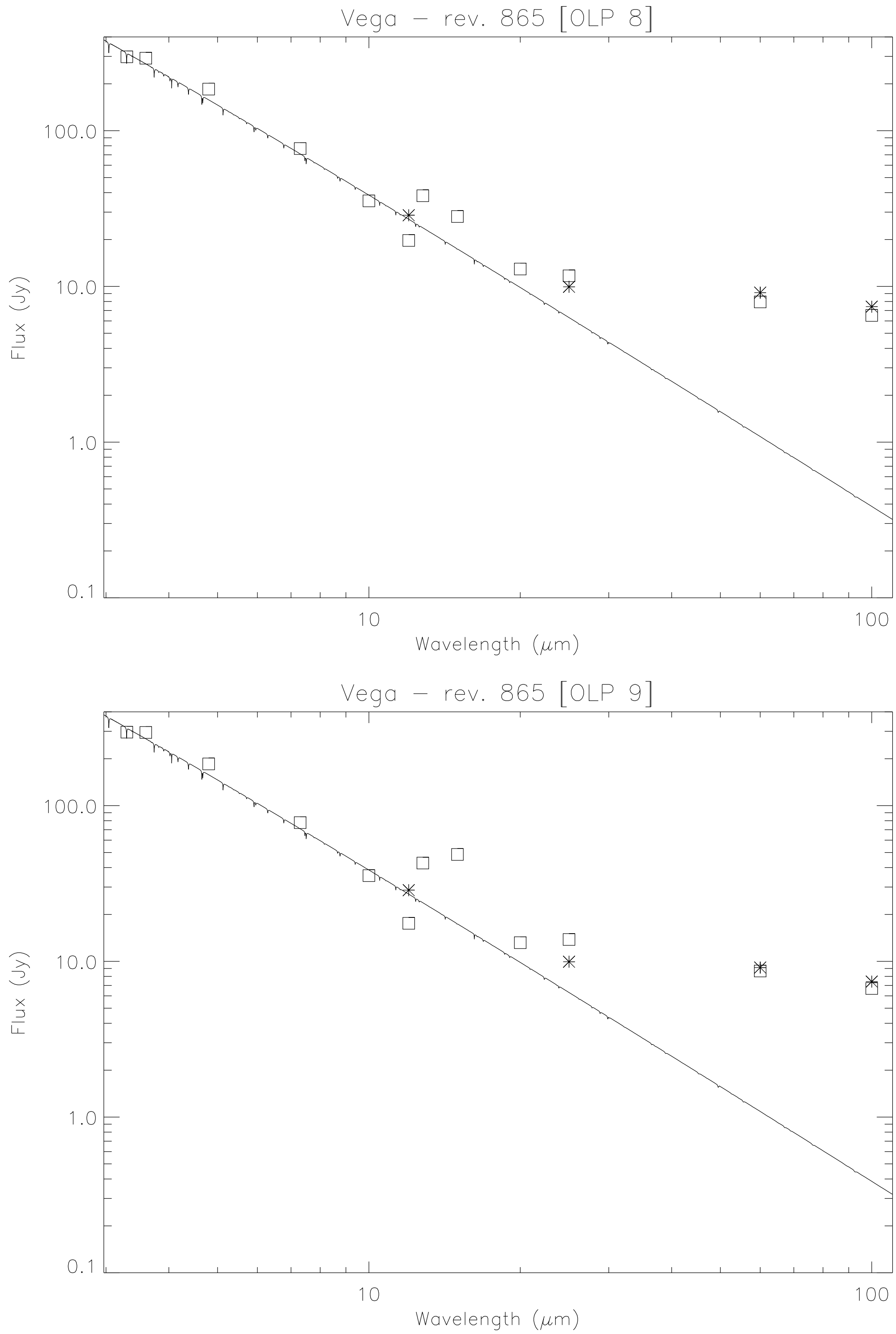

Figure 5.17: Comparison of PHT-P multi-filter photometry of Vega (HR 7001) on revolution 865 with the composite spectrum provided by M. Cohen out to 15 μm and with IRAS photometry beyond 15 μm for OLP 8.6b1 (upper panel) and OLP 9.0b3 (lower panel). A description of the applied color correction factors is given in the text. The meaning of the symbols is the following: solid line: model, asterisk: IRAS, square: PHT-P.

Evaluation Log

1) Vega PHT-P aperture photometry from 3.3 to 100 um on revolution 085

Measurements:
PHT-P: ppap08500106 (src+back) FCS = 3.6, 20, 100 um
ppap08500105 (back) FCS = 7.3, 25, 100 um

Colour correction: mixture of 10000 K BB & 80 K modified (em.=1) BB
see text for details

Model: Cohen

Det	cwl (μm)	OLP 8	OLP 9	IRAS	Model	Δ (OLP 8)	Δ (OLP 9)
P1	3.3	264.977	261.889		293.430	-9.70	-10.75
P1	3.6	250.343	251.442		268.410	-6.73	-6.32
P1	4.8	161.699	161.140		157.795	2.47	2.12
P1	7.3	67.196	67.677		70.934	-5.27	-4.59
P1	10.0	32.763	32.666		38.570	-15.06	-15.31
P1	12.0	18.429	16.625	28.640	26.997	-31.74	-38.42
P1	12.8	34.425	38.199		23.779	44.77	60.64
P1	15.0	25.240	42.482		17.356	45.43	144.77
P2	20.0	12.951	12.276		9.838	31.65	24.78
P2	25.0	11.742	13.119	9.938	6.301	86.36	108.22
P3	60.0	8.182	8.377	9.121	1.087	652.97	670.98
P3	100.0	6.706	6.496	7.408	0.387	1634.99	1580.76

2) Vega PHT-P aperture photometry from 3.3 to 100 um on revolution 558

Measurements:
PHT-P: ppap55800420 (src+back) FCS = 3.6, 20, 100 um
ppap55800419 (back) FCS = 7.3, 25, 100 um

Colour correction: mixture of 10000 K BB & 80 K modified (em.=1) BB
see text for details

Model: Cohen

Det	cwl (μm)	OLP 8	OLP 9	IRAS	Model	Δ (OLP 8)	Δ (OLP 9)
P1	3.3	306.993	305.309		293.430	4.62	4.05
P1	3.6	290.779	293.634		268.410	8.33	9.40
P1	4.8	185.415	185.711		157.795	17.50	17.69
P1	7.3	76.357	77.331		70.934	7.65	9.02
P1	10.0	43.227	43.473		38.570	12.07	12.71
P1	12.0	21.938	20.547	28.640	26.997	-18.74	-23.89
P1	12.8	46.791	50.754		23.779	96.78	113.44
P1	15.0	34.429	55.651		17.356	98.37	220.65
P2	20.0	12.775	12.934		9.838	29.86	31.47
P2	25.0	11.613	13.534	9.938	6.301	84.31	114.81
P3	60.0	6.507	7.224	9.121	1.087	498.84	564.85
P3	100.0	5.745	5.898	7.408	0.387	1386.31	1425.91

3) Vega PHT-P aperture photometry from 3.3 to 100 um on revolution 865

Measurements:		
PHT-P:	ppap86500706 (src+back)	FCS = 3.6, 20, 100 um
	ppap86500705 (back)	FCS = 7.3, 25, 100 um

Colour correction: mixture of 10000 K BB & 80 K modified (em.=1) BB
see text for details

Model: Cohen

Det	cwl (μm)	OLP 8	OLP 9	IRAS	Model	Δ (OLP 8)	Δ (OLP 9)
P1	3.3	298.270	296.416		293.430	1.65	1.02
P1	3.6	292.034	294.906		268.410	8.80	9.87
P1	4.8	184.949	185.244		157.795	17.21	17.40
P1	7.3	76.780	77.766		70.934	8.24	9.63
P1	10.0	35.400	35.489		38.570	-8.22	-7.99
P1	12.0	19.727	17.541	28.640	26.997	-26.93	-35.02
P1	12.8	38.202	42.767		23.779	60.66	79.86
P1	15.0	28.111	48.547		17.356	61.97	179.72
P2	20.0	12.934	13.179		9.838	31.48	33.96
P2	25.0	11.689	13.815	9.938	6.301	85.52	119.27
P3	60.0	7.947	8.664	9.121	1.087	631.38	697.37
P3	100.0	6.511	6.693	7.408	0.387	1584.59	1631.64

5.4.7 General Re-validation of PHT03 and PHT22 Staring Mode: The SED of Arp 220

- authors: U. Klaas
- date: 19-March-2000
- SVP period 1

Motivation

TDTs 47600413(background, PHT-P), 47600414(Arp 220, PHT-P), 47600415(background, PHT-C), 47600416(Arp 220, PHT-C) is one of the key OLP validation cases [1]. The staring mode AOTs PHT-03 and PHT-22 in all PHT filters measure a galaxy SED which is steeply rising between 10 and 60 μm and gradually declining beyond 100 μm, hence has a very different shape than a stellar atmosphere SED. It can therefore be used for a check of the robustness of the relative filter-to-filter calibration and the color correction factors applied to modified Black Bodies in the temperature range 50 – 120 K. Arp 220 is significantly bright over the full wavelength range from 3.3 to 200 μm. Its photometric properties are discussed in detail in "Infrared spectral energy distributions of the interacting galaxies Arp 244, NGC 6240 and Arp 220" [15].

Method

We compare the background subtracted flux values of both OLP V8.6b1 and OLP V9.0b3 results against the IRAS photometry and a model fit based on the OLP V6.x calibration.

Results

Figs. 5.18 to 5.20 show a comparison between OLP9 and OLP 8 results both for the source and the background flux. In particular for the multi-filter background fluxes and the P1 12.8 and 15 μm filters we see a noticable degradance of the OLP 9 product. The problem could be traced back to a wrong ordering of the filters in the CALG files P%%SLINR and was documented in SPR-3259.
Therefore, no quantitative assessment of calibration accuracies is performed here, instead we refer to Sect. 8.4.8.

Conclusions

- OLP 9.0b3 data products are affected by a wrong filter ordering in the signal linearization CALG files P%%SLINR $\rightarrow$ SPR-3259.

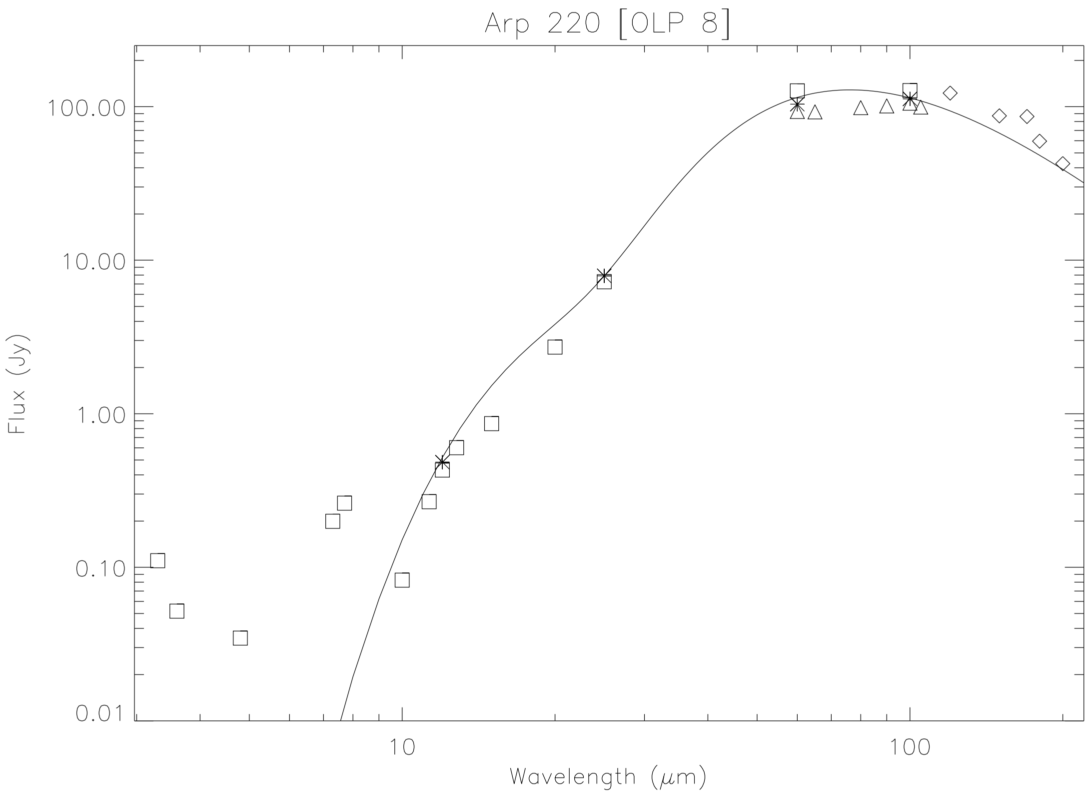

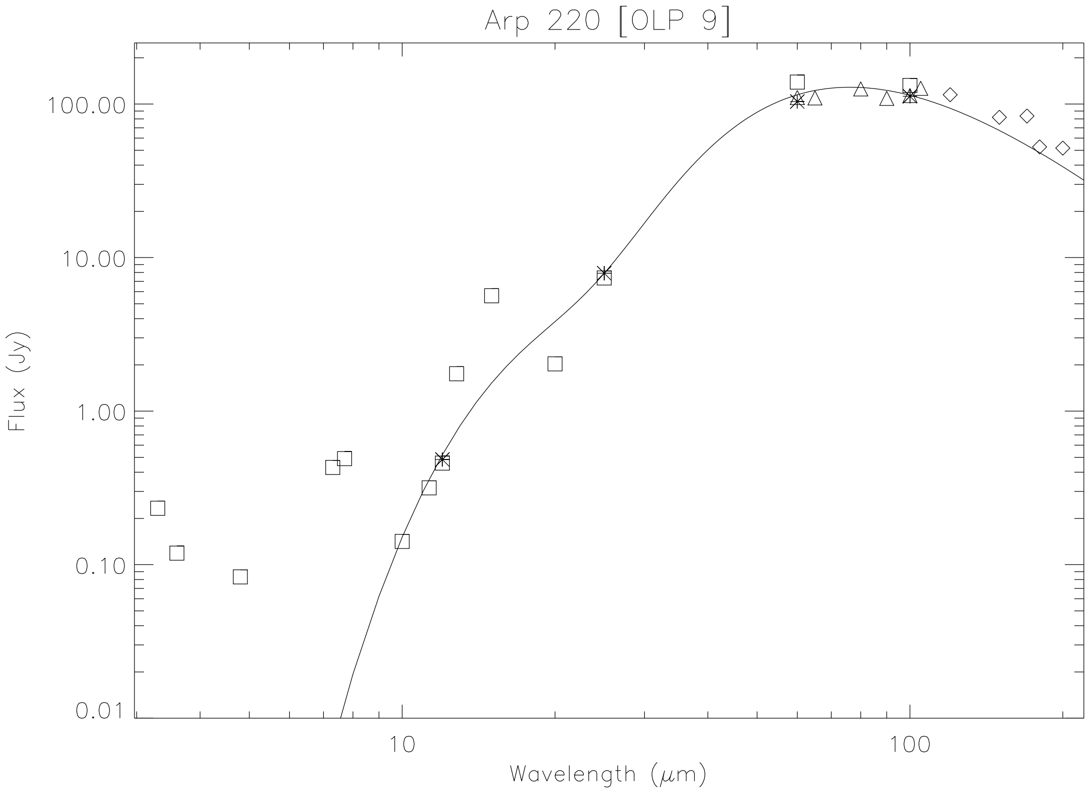

Figure 5.18: Comparison of PHT-P and PHT-C photometry, using the full ISOPHOT filter set, with IRAS photometry and the model fit as described in [15]. Note that this model fit only serves as a guide for the eye to recognize more easily the changes between the two versions. It is not an absolute photometric reference. No color correction has been applied. The meaning of the symbols is the following: solid line: model, asterisk: IRAS, square: PHT-P (P03 AOT), triangle: C100 (P22 AOT), diamond: C200 (P22 AOT).

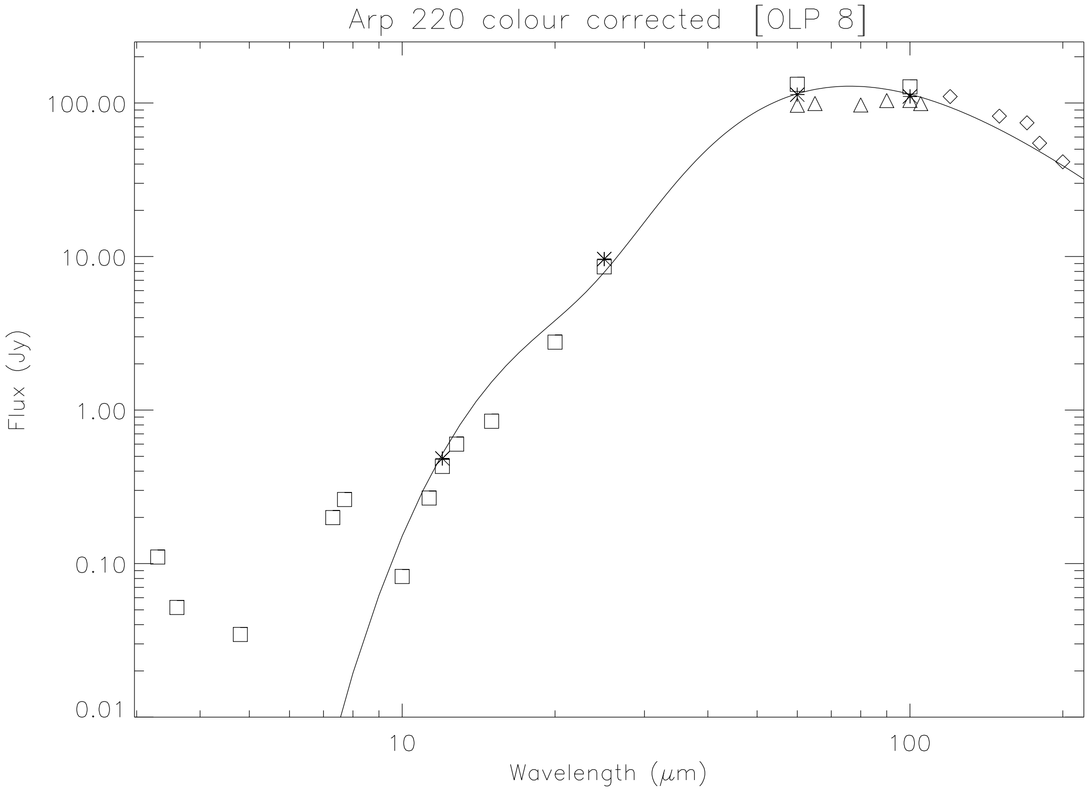

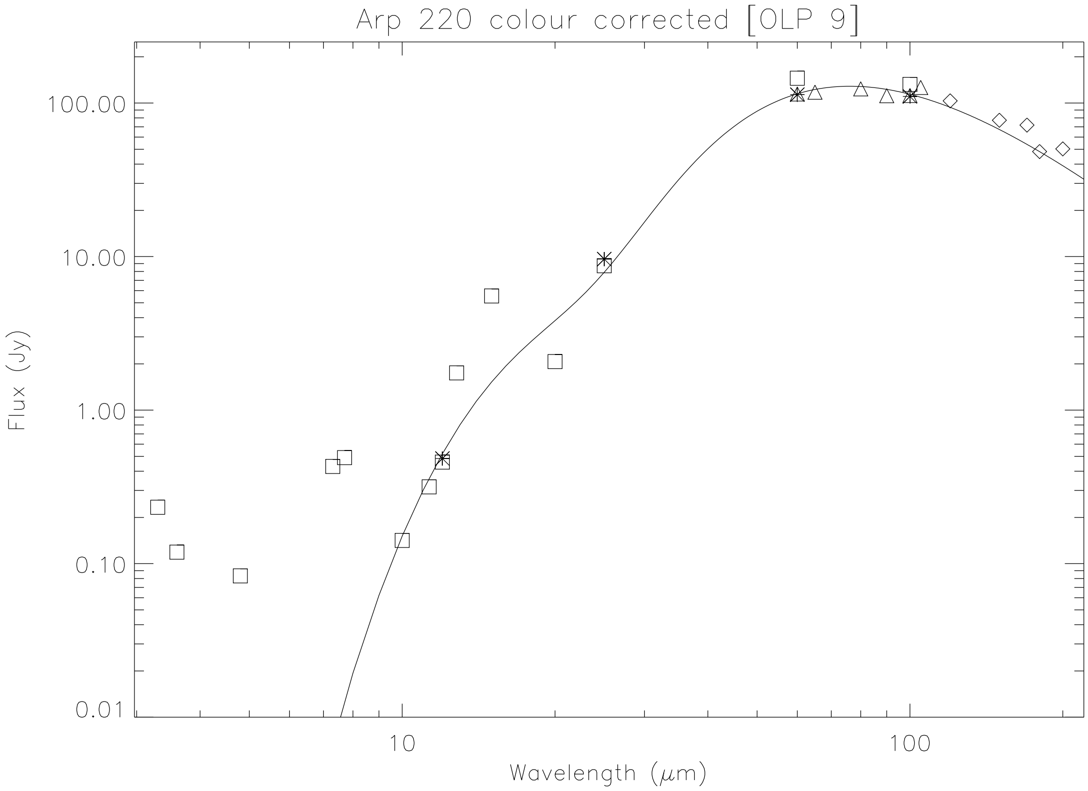

Figure 5.19: Comparison of PHT-P and PHT-C photometry, using the full ISOPHOT filter set, with IRAS photometry and the model fit as described in [15]. Note that this model fit only serves as a guide for the eye to recognize more easily the changes between the two versions. It is not an absolute photometric reference. Color correction according to the model parameters, modified BBs $\propto \lambda^{-1}$ with T1 = 120 K and T2 = 47 K, has been applied . The meaning of the symbols is the following: solid line: model, asterisk: IRAS, square: PHT-P (P03 AOT), triangle: C100 (P22 AOT), diamond: C200 (P22 AOT).

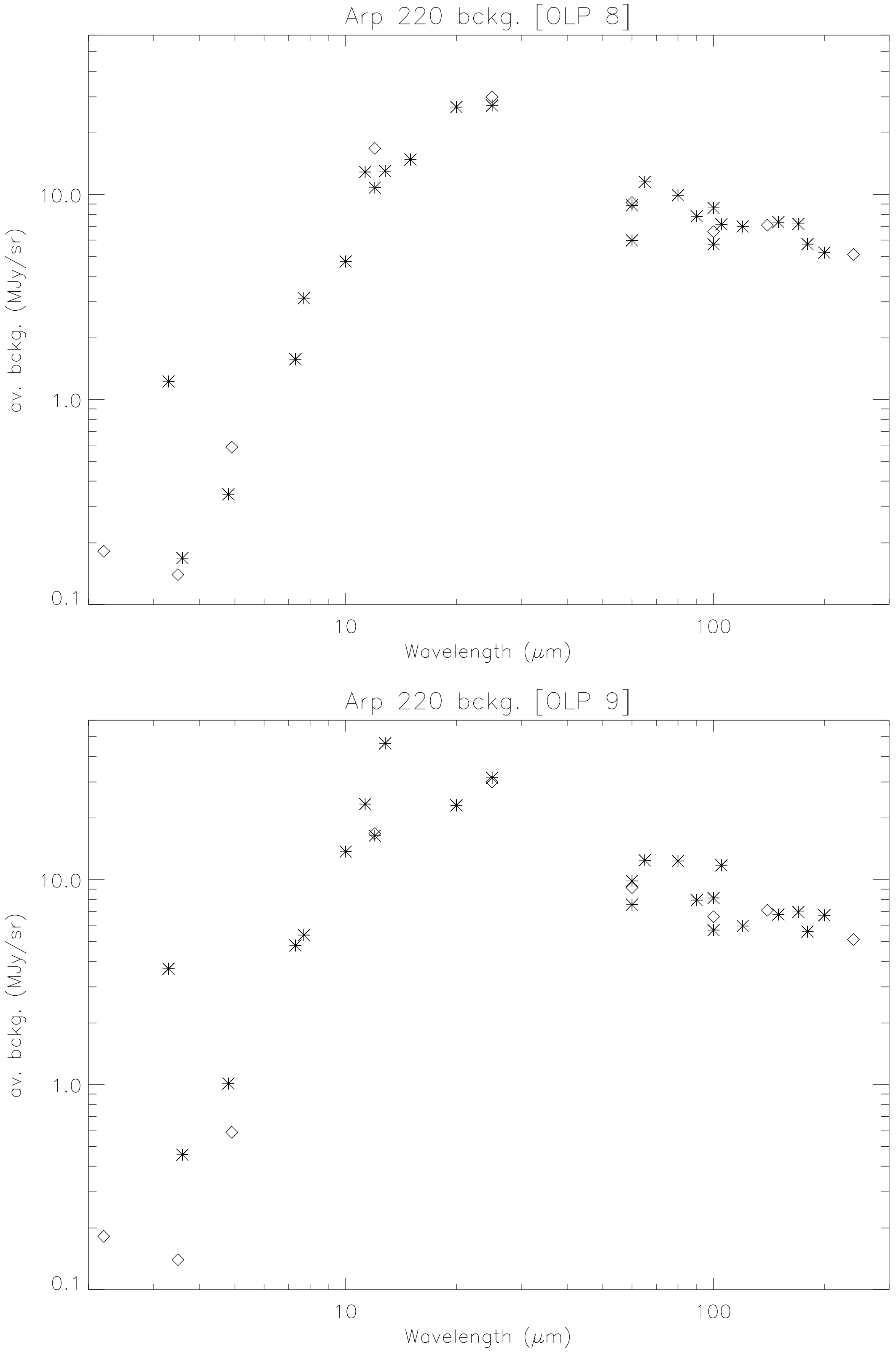

Figure 5.20: Comparison of PHT surface brightness photometry with COBE, both for OLP 8.6b1 and OLP 9.0b3. Asterisk: PHT-P and PHT-C photometry, diamond: COBE.

Evaluation Log

1) point source photometry of Arp 220 (not colour corrected)

Measurements:		
PHT-P:	ppap47600414 (src+back)	FCS = 3.3, 25, 100 um
	ppae47600413 (back)	FCS = 3.3, 20, 100 um
PHT-C:	pcap47600416 (src+back)	FCS = 90, 170 um
	pcae47600415 (back)	FCS = 90, 170 um

Model: Sum of 2 modified bb, em. $\propto \lambda^{-1}$, T1 = 120 K, T2 = 47 K

Det	cwl (μm)	OLP 8	OLP 9	IRAS	Model	Δ (OLP 8)	Δ (OLP 9)
P1	3.3	0.110	0.233		-0.001	-15475.22	-32526.85
P1	3.6	0.052	0.119		-0.001	-8905.31	-20304.14
P1	4.8	0.035	0.083		-0.000	-50776.99	-122075.57
P1	7.3	0.199	0.430		0.009	2208.56	4874.34
P1	7.7	0.262	0.490		0.015	1669.48	3217.88
P1	10.0	0.082	0.142		0.151	-45.43	-6.21
P1	11.3	0.268	0.316		0.367	-27.05	-13.73
P1	12.0	0.430	0.459	0.484	0.519	-17.26	-11.69
P1	12.8	0.601	1.751		0.746	-19.44	134.61
P1	15.0	0.862	5.643		1.525	-43.48	270.07
P2	20.0	2.717	2.031		3.827	-29.02	-46.93
P2	25.0	7.242	7.365	7.910	7.902	-8.35	-6.80
P3	60.0	126.798	138.928	103.800	114.880	10.37	20.93
C1	60.0	93.042	110.211	103.800	114.880	-19.01	-4.06
C1	65.0	92.523	109.608		122.541	-24.50	-10.55
C1	80.0	98.543	125.489		128.115	-23.08	-2.05
C1	90.0	101.134	108.875		122.723	-17.59	-11.28
P3	100.0	127.305	132.026	112.400	113.981	11.69	15.83
C1	100.0	105.380	113.547	112.400	113.981	-7.55	-0.38
C1	105.0	99.406	126.631		109.033	-8.83	16.14
C2	120.0	122.571	115.018		93.777	30.70	22.65
C2	150.0	87.091	81.967		67.225	29.55	21.93
C2	170.0	86.342	83.531		53.793	60.51	55.28
C2	180.0	59.597	52.598		48.236	23.56	9.04
C2	200.0	42.555	51.657		39.038	9.01	32.32

2) point source photometry of Arp 220 (colour corrected from 10 to 200 = μm)

Measurements:

PHT-P:	ppap47600414 (src+back)	FCS = 12, 25, 100 um
	ppae47600413 (back)	FCS = 12, 20, 100 um
PHT-C:	pcap47600416 (src+back)	FCS = 90, 170 um
	pcae47600415 (back)	FCS = 90, 170 um

Colour correction: according to model

Model: Sum of 2 modified bb, em. $\propto \lambda^{-1}$, T1 = 120 K, T2 = 47 K

Det	cwl (μm)	OLP 8	OLP 9	IRAS	Model	Δ (OLP 8)	Δ (OLP 9)
P1	3.3	0.110	0.233		-0.001	-15475.22	-32526.85
P1	3.6	0.052	0.119		-0.001	-8905.31	-20304.14
P1	4.8	0.035	0.083		-0.000	-50776.99	-122075.57
P1	7.3	0.199	0.430		0.009	2208.56	4874.34
P1	7.7	0.262	0.490		0.015	1669.48	3217.88
P1	10.0	0.082	0.142		0.151	-45.43	-6.21
P1	11.3	0.268	0.316		0.367	-27.05	-13.73
P1	12.0	0.430	0.459	0.484	0.519	-17.26	-11.69
P1	12.8	0.600	1.748		0.746	-19.60	134.14
P1	15.0	0.846	5.538		1.525	-44.54	263.17
P2	20.0	2.769	2.070		3.827	-27.64	-45.90
P2	25.0	8.570	8.716	9.631	7.902	8.46	10.30
P3	60.0	132.357	145.019	113.300	114.880	15.21	26.23
C1	60.0	96.717	114.565	113.300	114.880	-15.81	-0.27
C1	65.0	99.273	117.605		122.541	-18.99	-4.03
C1	80.0	97.087	123.635		128.115	-24.22	-3.50
C1	90.0	103.727	111.667		122.723	-15.48	-9.01
P3	100.0	127.432	132.159	110.400	113.981	11.80	15.95
C1	100.0	103.925	111.979	110.400	113.981	-8.82	-1.76
C1	105.0	99.109	126.252		109.033	-9.10	15.79
C2	120.0	110.127	103.340		93.777	17.43	10.20
C2	150.0	82.084	77.254		67.225	22.10	14.92
C2	170.0	74.241	71.823		53.793	38.01	33.52
C2	180.0	54.727	48.300		48.236	13.46	0.13
C2	200.0	41.395	50.250		39.038	6.04	28.72

3) Surface brightness photometry of Arp 220 background

λ	OLP8 (MJy/sr)	OLP9 (MJy/sr)	COBE (MJy/sr)
3.3	1.23	3.68	
3.6	0.17	0.46	
4.8	0.35	1.01	
7.3	1.57	4.77	
7.7	3.12	5.37	
10.0	4.72	13.71	
11.3	12.89	23.38	
12.0	10.81	16.40	16.81
12.8	13.04	46.31	
15.0	14.83	152.14	
20.0	26.76	23.06	
25.0	27.21	31.44	29.99
60.0	5.98	7.56	9.15
100.0	5.73	5.68	6.60
60.0	8.87	9.87	9.15
65.0	11.54	12.43	
80.0	9.93	12.34	
90.0	7.84	7.95	
100.0	8.61	8.14	6.60
105.0	7.17	11.76	
120.0	6.99	5.95	
150.0	7.34	6.77	7.10
170.0	7.19	6.96	
180.0	5.74	5.58	
200.0	5.21	6.71	5.11

5.4.8 General Re-validation of PHT03 and PHT22 Staring Mode: The SED of NGC 6240

- authors: U. Klaas
- date: 19-March-2000
- SVP period 1

Motivation

TDTs 47600509(background, PHT-P), 47600510(NGC 6240, PHT-P), 47600511(background, PHT-C), 47600512(NGC 6240, PHT-C) is another one of the key OLP validation cases [1]. Like for Arp 220, the staring mode AOTs PHT-03 and PHT-22 in all PHT filters measure a galaxy SED which is steeply rising between 8 and 60 μm and gradually declining beyond 100 μm, hence has a very different shape than a stellar atmosphere SED. It can therefore be used for a check of the robustness of the relative filter-to-filter calibration and the color correction factors applied to modified Black Bodies in the temperature range 40 – 140 K. It is 3 times fainter than Arp 220 and does not reach possible upper boundary conditions with regard to the C100 fluxes like Arp 220. Its photometric properties are discussed in detail in "Infrared spectral energy distributions of the interacting galaxies Arp 244, NGC 6240 and Arp 220" [15].

Method

We compare the background subtracted flux values of both OLP V8.6b1 and OLP V9.0b3 results against the IRAS photometry and a model fit based on the OLP V6.x calibration.

Results

Figs. 5.21 to 5.23 show a comparison between OLP9 and OLP 8 results both for the source and the background flux. In particular for the multi-filter background fluxes and the P1, C100 105 μm and C200 filters of the source SED we see a noticable degradance of the OLP 9 product. The problem could be traced back to a wrong ordering of the filters in the CALG files P%%SLINR and was documented in SPR-3259.
Therefore, no quantitative assessment of calibration accuracies is performed here, instead we refer to Sect. 8.4.9.

Conclusions

- OLP 9.0b3 data products are affected by a wrong filter ordering in the signal linearization CALG files P%%SLINR $\rightarrow$ SPR-3259.

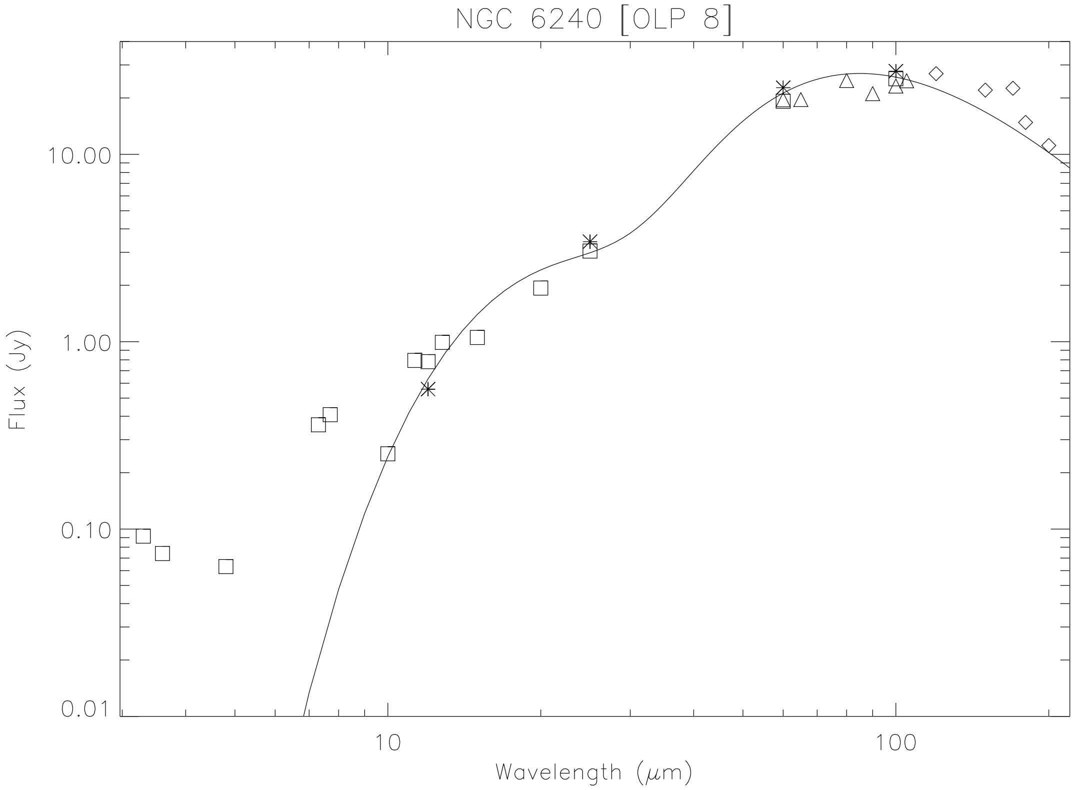

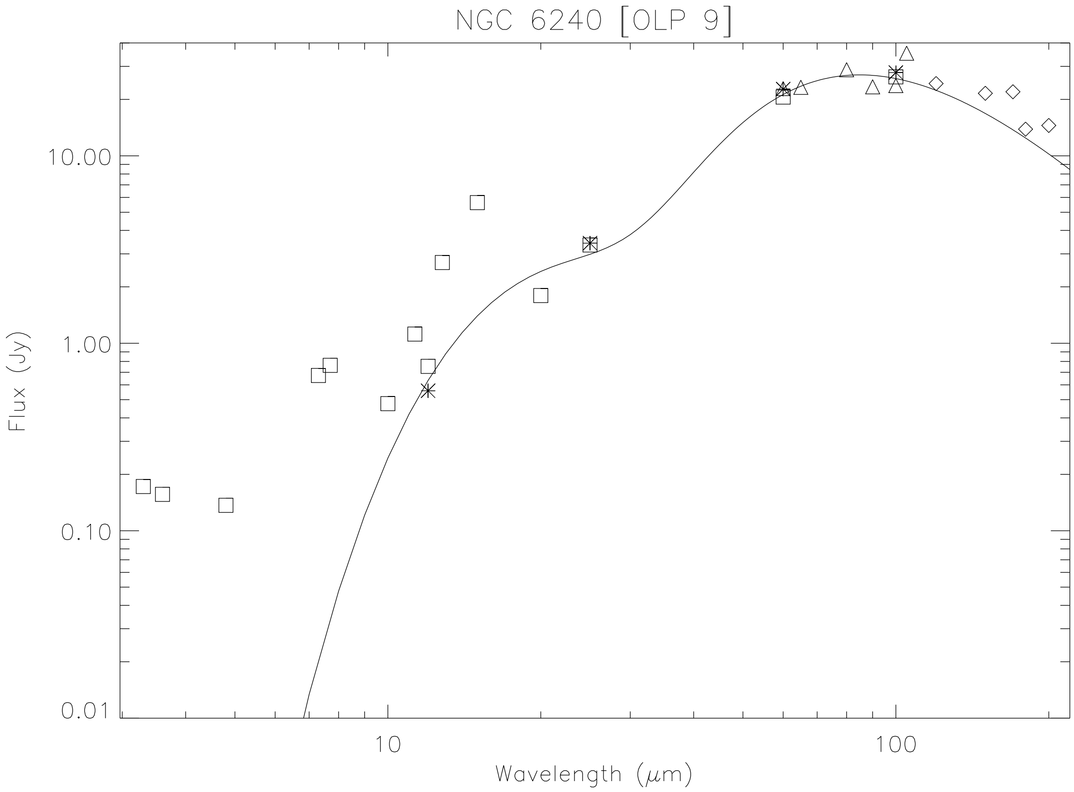

Figure 5.21: Comparison of PHT-P and PHT-C photometry, using the full ISOPHOT filter set, with IRAS photometry and the model fit as described in [15]. Note that this model fit only serves as a guide for the eye to recognize more easily the changes between the two versions. It is not an absolute photometric reference. No color correction has been applied. The meaning of the symbols is the following: solid line: model, asterisk: IRAS, square: PHT-P (P03 AOT), triangle: C100 (P22 AOT), diamond: C200 (P22 AOT).

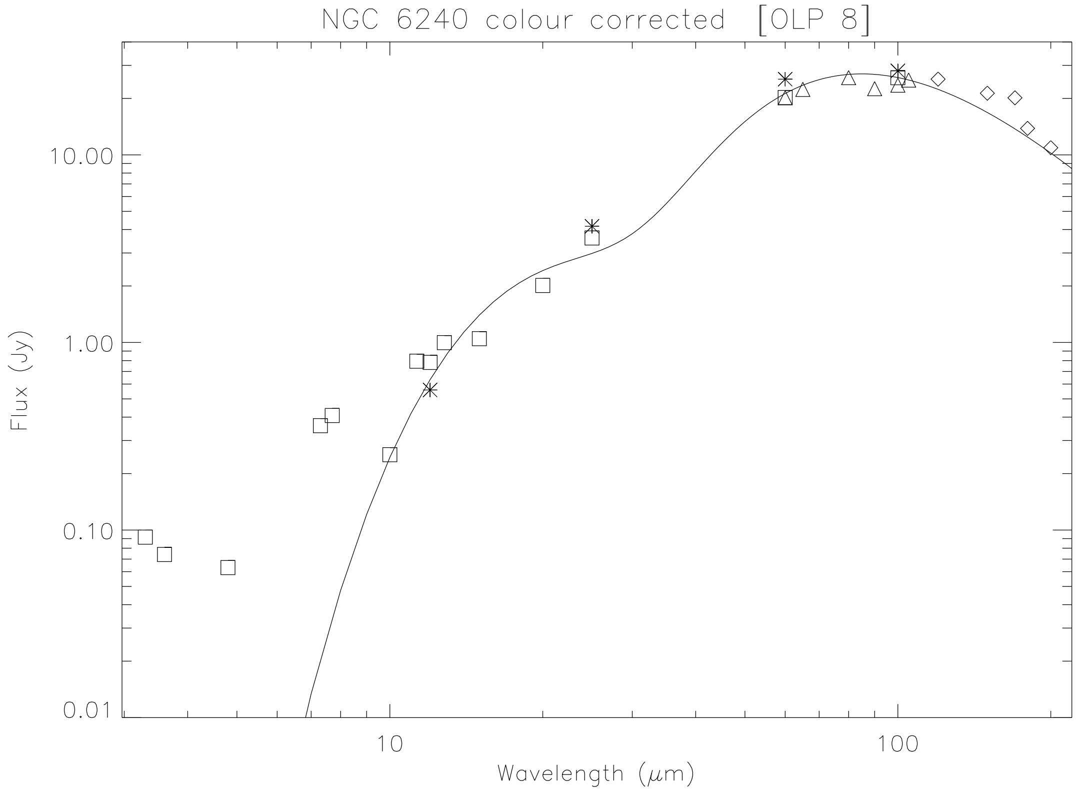

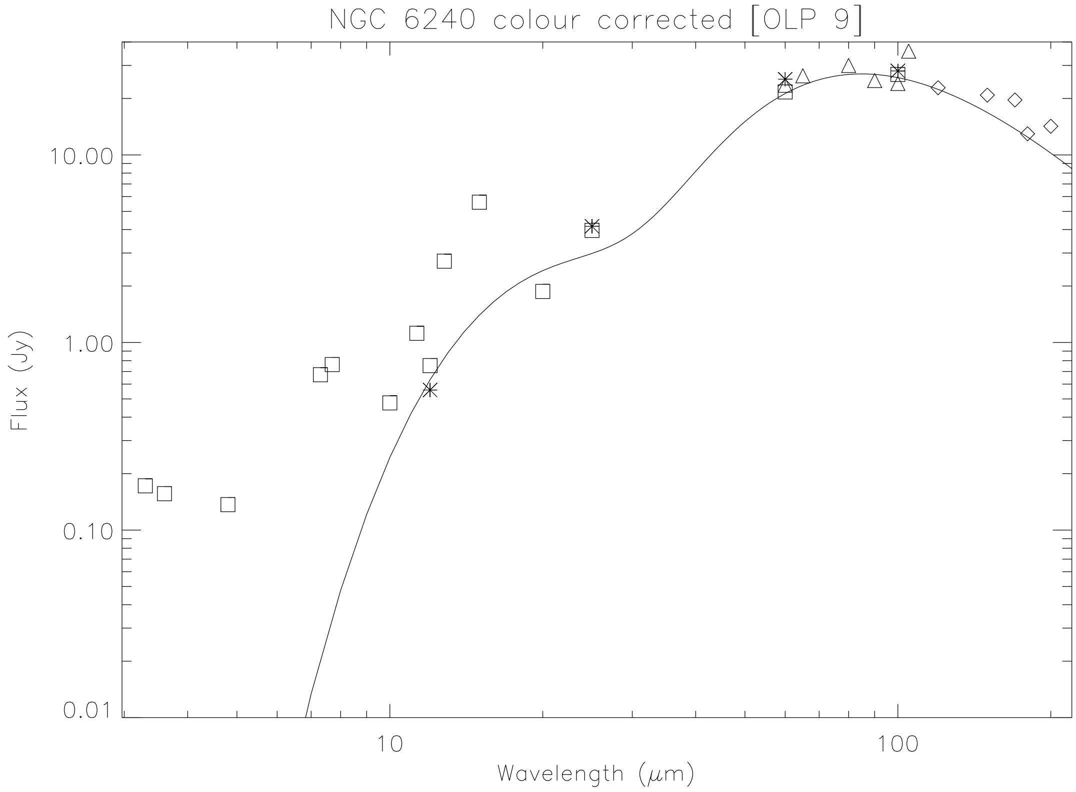

Figure 5.22: Comparison of PHT-P and PHT-C photometry, using the full ISOPHOT filter set, with IRAS photometry and the model fit as described in [15]. Note that this model fit only serves as a guide for the eye to recognize more easily the changes between the two versions. It is not an absolute photometric reference. Color correction according to the model parameters, modified BBs $\propto \lambda^{-1}$ with T1 = 140 K and T2 = 42 K, has been applied . The meaning of the symbols is the following: solid line: model, asterisk: IRAS, square: PHT-P (P03 AOT), triangle: C100 (P22 AOT), diamond: C200 (P22 AOT).

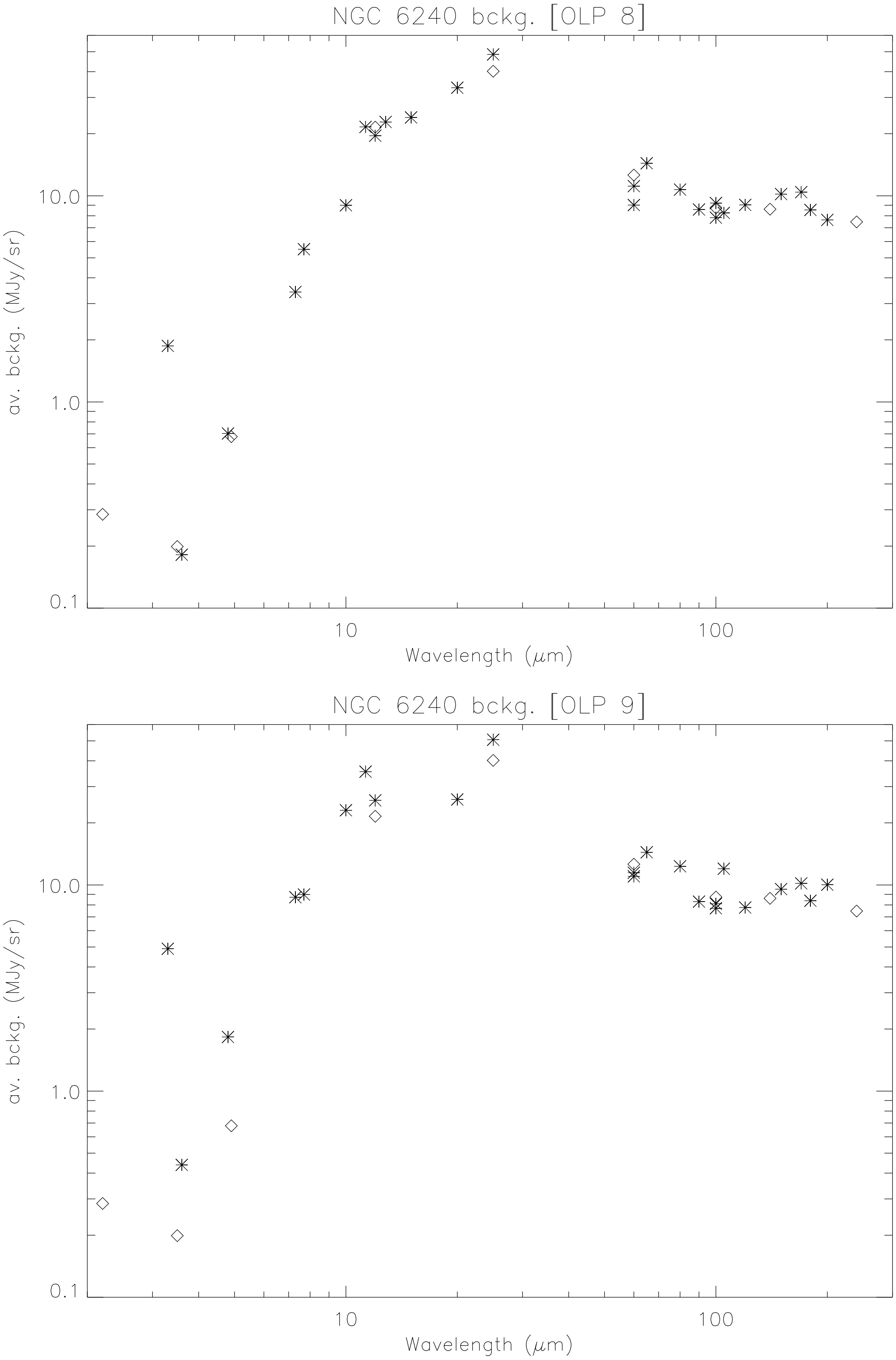

Figure 5.23: Comparison of PHT surface brightness photometry with COBE, both for OLP 8.6b1 and OLP 9.0b3. Asterisk: PHT-P and PHT-C photometry, diamond: COBE.

Evaluation Log

1) point source photometry of NGC 6240 (not colour corrected)

Measurements:		
PHT-P:	ppap47600510 (src+back)	FCS = 12, 25, 100 um
	ppae47600509 (back)	FCS = 12, 20, 100 um
PHT-C:	pcap47600512 (src+back)	FCS = 90, 170 um
	pcae47600511 (back)	FCS = 90, 170 um

Model: Sum of 2 modified bb, em. $\propto \lambda^{-1}$, T1 = 140 K, T2 = 42 K

Det	cwl (μm)	OLP 8	OLP 9	IRAS	Model	Δ (OLP 8)	Δ (OLP 9)
P1	3.3	0.092	0.172		-0.003	-2812.82	-5197.19
P1	3.6	0.074	0.156		-0.003	-2789.22	-5776.94
P1	4.8	0.063	0.137		-0.000	-24755.49	-53495.98
P1	7.3	0.360	0.674		0.024	1420.38	2743.17
P1	7.7	0.408	0.762		0.037	990.25	1938.36
P1	10.0	0.252	0.476		0.244	3.31	95.19
P1	11.3	0.794	1.119		0.482	64.69	132.02
P1	12.0	0.782	0.753	0.558	0.634	23.48	18.84
P1	12.8	0.991	2.696		0.830	19.43	224.85
P1	15.0	1.053	5.626		1.399	-24.70	302.22
P2	20.0	1.932	1.797		2.417	-20.05	-25.65
P2	25.0	3.046	3.345	3.417	2.983	2.13	12.15
P3	60.0	19.204	20.576	22.680	21.233	-9.56	-3.09
C1	60.0	19.560	22.834	22.680	21.233	-7.88	7.54
C1	65.0	19.604	23.186		23.504	-16.60	-1.35
C1	80.0	24.762	28.780		26.842	-7.75	7.22
C1	90.0	21.099	23.341		26.852	-21.43	-13.07
P3	100.0	25.313	26.358	27.780	25.814	-1.94	2.11
C1	100.0	23.156	23.683	27.780	25.814	-10.30	-8.26
C1	105.0	24.705	35.271		25.058	-1.41	40.76
C2	120.0	26.947	24.278		22.343	20.61	8.66
C2	150.0	22.025	21.539		16.814	30.99	28.10
C2	170.0	22.528	21.953		13.752	63.81	59.63
C2	180.0	14.806	13.867		12.442	19.00	11.46
C2	200.0	11.145	14.514		10.220	9.05	42.02

2) point source photometry of NGC 6240 (colour corrected from 12.8 to 200 μm)

Measurements:		
PHT-P:	ppap47600510 (src+back)	FCS = 12, 25, 100 um
	ppae47600509 (back)	FCS = 12, 20, 100 um
PHT-C:	pcap47600512 (src+back)	FCS = 90, 170 um
	pcae47600511 (back)	FCS = 90, 170 um

Colour correction: according to model

Model: Sum of 2 modified bb, em. $\propto \lambda^{-1}$, T1 = 140 K, T2 = 42 K

Det	cwl (μm)	OLP 8	OLP 9	IRAS	Model	Δ (OLP 8)	Δ (OLP 9)
P1	3.3	0.092	0.172		-0.003	-2812.82	-5197.19
P1	3.6	0.074	0.156		-0.003	-2789.22	-5776.94
P1	4.8	0.063	0.137		-0.000	-24755.49	-53495.98
P1	7.3	0.360	0.674		0.024	1420.38	2743.17
P1	7.7	0.408	0.762		0.037	990.25	1938.36
P1	10.0	0.252	0.476		0.244	3.31	95.19
P1	11.3	0.794	1.119		0.482	64.69	132.02
P1	12.0	0.782	0.753	0.558	0.634	23.48	18.84
P1	12.8	0.997	2.713		0.830	20.16	226.81
P1	15.0	1.047	5.593		1.399	-25.15	299.82
P2	20.0	2.013	1.872		2.417	-16.72	-22.55
P2	25.0	3.605	3.958	4.162	2.983	20.86	32.72
P3	60.0	20.215	21.659	25.310	21.233	-4.80	2.01
C1	60.0	20.144	23.516	25.310	21.233	-5.13	10.75
C1	65.0	22.328	26.408		23.504	-5.01	12.35
C1	80.0	25.794	29.979		26.842	-3.91	11.69
C1	90.0	22.517	24.911		26.852	-16.14	-7.23
P3	100.0	25.777	26.841	28.030	25.814	-0.14	3.98
C1	100.0	23.509	24.043	28.030	25.814	-8.93	-6.86
C1	105.0	25.030	35.736		25.058	-0.11	42.61
C2	120.0	25.326	22.818		22.343	13.35	2.13
C2	150.0	21.301	20.831		16.814	26.69	23.89
C2	170.0	20.132	19.618		13.752	46.39	42.66
C2	180.0	13.837	12.960		12.442	11.22	4.17
C2	200.0	10.915	14.215		10.220	6.81	39.10

3) Surface brightness photometry of NGC 6240 background

λ	OLP8 (MJy/sr)	OLP9 (MJy/sr)	COBE (MJy/sr)
3.3	1.87	4.90	
3.6	0.18	0.44	
4.8	0.70	1.83	
7.3	3.41	8.71	
7.7	5.50	8.98	
10.0	8.99	23.03	
11.3	21.58	35.44	
12.0	19.56	25.73	21.54
12.8	22.81	73.59	
15.0	23.99	215.07	
20.0	33.44	25.98	
25.0	48.51	50.62	40.18
60.0	9.02	11.01	12.61
100.0	7.83	7.70	8.74
60.0	11.14	11.46	12.61
65.0	14.38	14.40	
80.0	10.72	12.32	
90.0	8.58	8.30	
100.0	9.22	8.10	8.74
105.0	8.26	11.98	
120.0	9.03	7.77	
150.0	10.19	9.54	8.61
170.0	10.42	10.17	
180.0	8.54	8.38	
200.0	7.64	10.03	7.47

5.4.9 General Re-validation of PHT17/19 and PHT37/39 Sparse Map On-Off Mode: The SED of Arp 244

- authors: U. Klaas
- date: 20-March-2000
- SVP period 1

Motivation

The observations of Arp 244 complement the evaluation of galaxy SEDs, since the measurements were performed in sparse map off-on mode (PHT17/PHT19 for PHT-P observations and PHT37/PHT39 for PHT-C observations, respectively; note that the 25 μm observations failed due to R/T problems). Furthermore, the observations were performed in the Performance Verification Phase, so that the pre-rev. 94 FCS calibration applies for the FIR detectors (C100 and C200). Since the object is extended, the 180 arcsec aperture was used for the PHT-P observations. This gives some feedback on the surface brightness calibration using the maximum aperture size with regard to the standard aperture for this filter. Also, the C200 sparse map elements have FCS calibrations in different filters so that they are test case for the check-out of SPR-3208 (sparse maps with different cal filters) implementation. The photometric properties of this object are discussed in detail in "Infrared spectral energy distributions of the interacting galaxies Arp 244, NGC 6240 and Arp 220" [15].

Method

We compare the background subtracted flux values of both OLP V8.6b1 and OLP V9.0b3 results against the IRAS photometry and a model fit based on the OLP V6.x calibration. As the source is extended, we do not use IRAS PSC or FSC photometry, but total fluxes as given in [29].

Results

Figs. 5.24 to 5.26 show a comparison between OLP9 and OLP 8 results both for the source and the background flux. In particular for the multi-filter background fluxes and the C100 and C200 photometry we see a noticable degradance of the OLP 9 product. The problem could be traced back, except for the C100 filters, to a wrong ordering of the filters in the CALG files P%%SLINR and was documented in SPR-3259.
Therefore, no quantitative assessment of calibration accuracies is performed here, instead we refer to Sect. 8.4.10.

Conclusions

- OLP 9.0b3 data products are affected by a wrong filter ordering in the signal linearization CALG files P%%SLINR $\rightarrow$ SPR-3259.

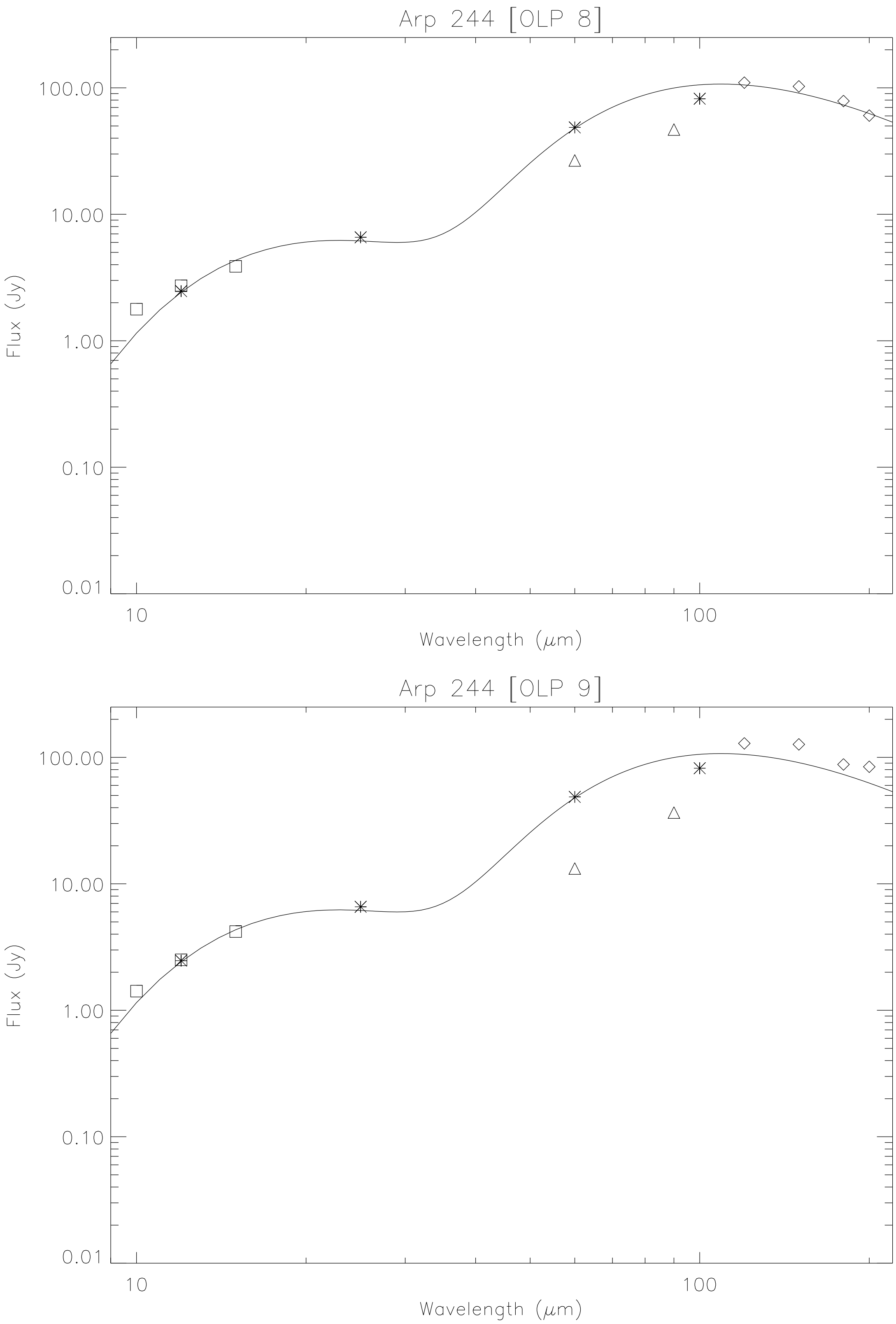

Figure 5.24: Comparison of PHT-P and PHT-C photometry with IRAS photometry and the model fit as described in [15]. Note that this model fit only serves as a guide for the eye to recognize more easily the changes between the two versions. It is not an absolute photometric reference. No color correction has been applied. The meaning of the symbols is the following: solid line: model, asterisk: IRAS, square: PHT-P (P03 AOT), triangle: C100 (P22 AOT), diamond: C200 (P22 AOT).

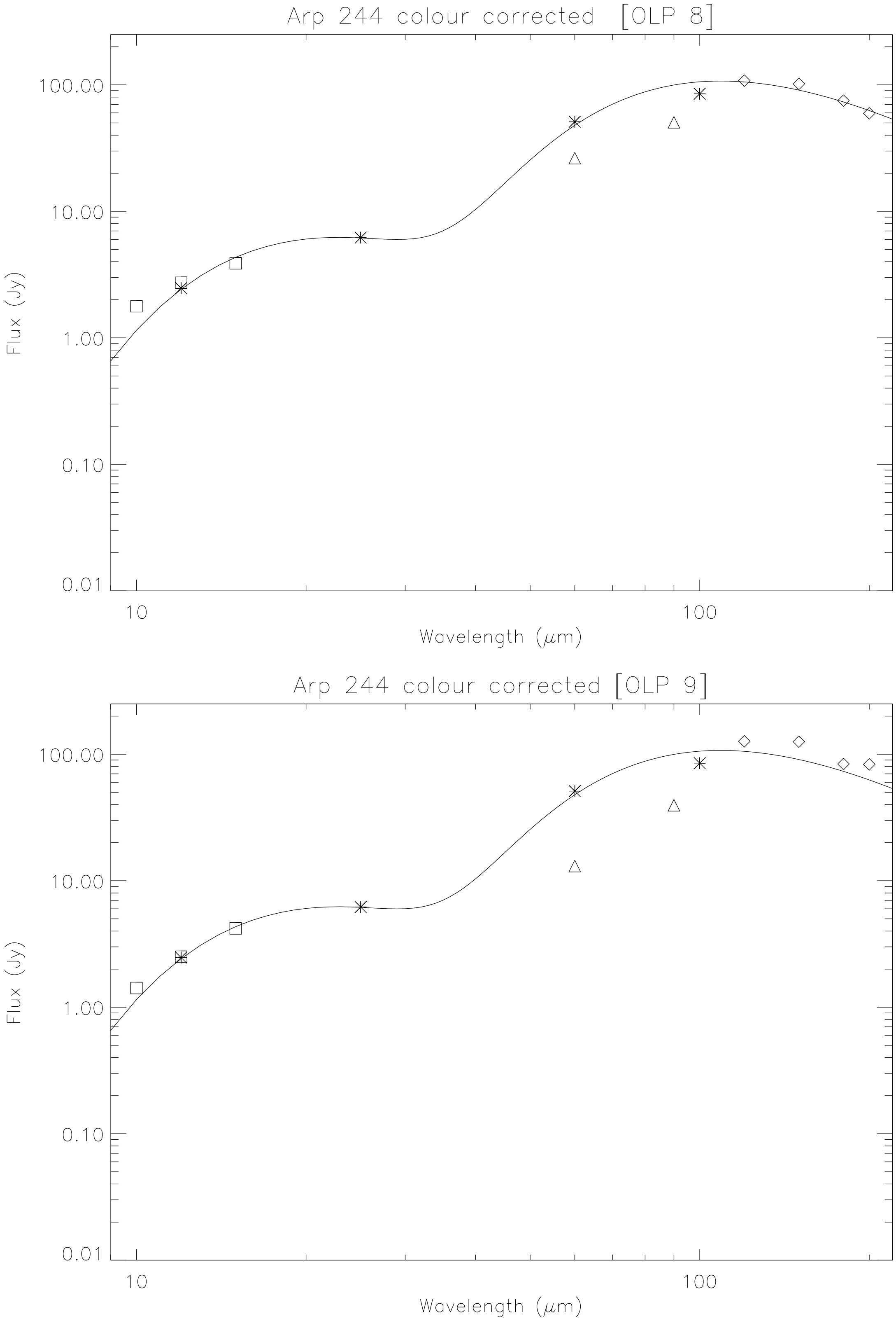

Figure 5.25: Comparison of PHT-P and PHT-C photometry with IRAS photometry and the model fit as described in [15]. Note that this model fit only serves as a guide for the eye to recognize more easily the changes between the two versions. It is not an absolute photometric reference. Color correction according to the model parameters, modified BBs $\propto \lambda^{-1}$ with T1 = 160 K and T2 = 33 K, has been applied. The meaning of the symbols is the following: solid line: model, asterisk: IRAS, square: PHT-P (P03 AOT), triangle: C100 (P22 AOT), diamond: C200 (P22 AOT).

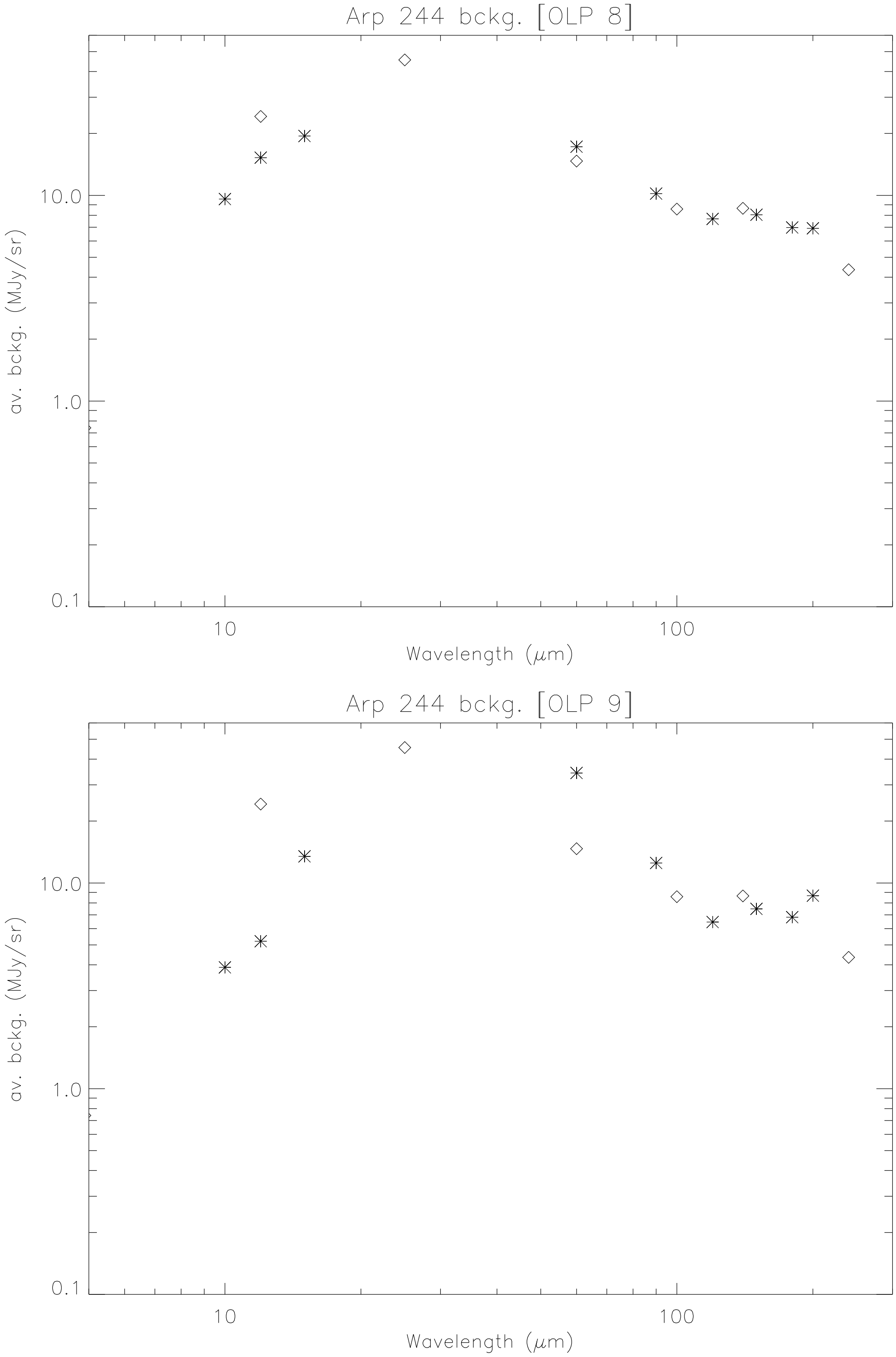

Figure 5.26: Comparison of PHT surface brightness photometry with COBE, both for OLP 8.6b1 and OLP 9.0b3. Asterisk: PHT-P and PHT-C photometry, diamond: COBE.

Evaluation Log

1) point source photometry of Arp 244 (not colour corrected)

Measurements:

PHT-P:	ppap06903802 (P19 src+back)	FCS = 15 um
	ppae06903801 (P17 back)	FCS = 15 um
PHT-C:	pcap06903806 (P39 C100 src+back)	FCS = 90 um
	pcae06903805 (P37 C100 back)	FCS = 90 um
	pcap06903808 (P39 C200 src+back)	FCS = 150 um
	pcae06903807 (P37 C200 back)	FCS = 180 um

Model: Sum of 2 modified bb, em. $\propto \lambda^{-1}$, T1 = 160 K, T2 = 33 K

Det	cwl (μm)	OLP 8	OLP 9	IRAS	Model	Δ (OLP 8)	Δ (OLP 9)
P1	10.0	1.778	1.418		1.150	54.60	23.30
P1	12.0	2.723	2.507	2.470	2.420	12.52	3.60
P1	15.0	3.878	4.196		4.334	-10.52	-3.18
C1	60.0	26.659	13.218	48.680	47.813	-44.24	-72.36
C1	90.0	46.857	36.606		99.706	-53.00	-63.29
C2	120.0	109.886	128.937		105.397	4.26	22.33
C2	150.0	102.676	126.644		90.809	13.07	39.46
C2	180.0	78.634	87.871		73.181	7.45	20.07
C2	200.0	60.329	84.269		62.622	-3.66	34.57

2) point source photometry of Arp 244 (colour corrected from 12.8 to 200 μm)

Measurements:

PHT-P:	ppap06903802 (P19 src+back)	FCS = 15 um
	ppae06903801 (P17 back)	FCS = 15 um
PHT-C:	pcap06903806 (P39 C100 src+back)	FCS = 90 um
	pcae06903805 (P37 C100 back)	FCS = 90 um
	pcap06903808 (P39 C200 src+back)	FCS = 150 um
	pcae06903807 (P37 C200 back)	FCS = 180 um

Colour correction: according to model

Model: Sum of 2 modified bb, em. $\propto \lambda^{-1}$, T1 = 160 K, T2 = 33 K

Det	cwl (μm)	OLP 8	OLP 9	IRAS	Model	Δ (OLP 8)	Δ (OLP 9)
P1	10.0	1.778	1.418		1.150	54.60	23.30
P1	12.0	2.723	2.507	2.470	2.420	12.52	3.60
P1	15.0	3.881	4.200		4.334	-10.43	-3.09
C1	60.0	26.317	13.048	51.081	47.813	-44.96	-72.71
C1	90.0	50.574	39.510		99.706	-49.28	-60.37
C2	120.0	107.964	126.682		105.397	2.44	20.20
C2	150.0	101.851	125.627		90.809	12.16	38.34
C2	180.0	74.961	83.766		73.181	2.43	14.46
C2	200.0	59.537	83.163		62.622	-4.93	32.80

3) Surface brightness photometry of Arp 244 background

λ	OLP8 (MJy/sr)	OLP9 (MJy/sr)	COBE (MJy/sr)
10.0	9.60	3.89	
12.0	15.25	5.21	24.20
15.0	19.43	13.47	
60.0	17.24	34.27	14.68
90.0	10.20	12.51	
120.0	7.68	6.46	
150.0	8.05	7.49	8.65
180.0	6.98	6.82	
200.0	6.92	8.67	4.35

5.4.10 Re-validation of C200 Absolute Photometry: The SEDs of Ceres and Uranus

- authors: U. Klaas
- date: 19-March-2000
- SVP period 1

Motivation

This is a check-out of the C200 absolute photometry mode for two bright sky standards, Ceres and Uranus.

Method

We compare the background subtracted, color corrected flux values of both OLP V8.6b1 and OLP V9.0b3 results against the model prediction by Lagerros for Ceres and Abbas for Uranus.

Results

Figs. 5.27 and 5.28 show a comparison between OLP9 and OLP 8 results. In particular for the Uranus photometry we see a noticable degradance of the OLP 9 product. The problem could be traced back to a wrong ordering of the filters in the CALG files P%%SLINR and was documented in SPR-3259.
Therefore, no quantitative assessment of calibration accuracies is performed here, instead we refer to Sect. 8.4.11.

Conclusions

- OLP 9.0b3 data products are affected by a wrong filter ordering in the signal linearization CALG files P%%SLINR → SPR-3259.

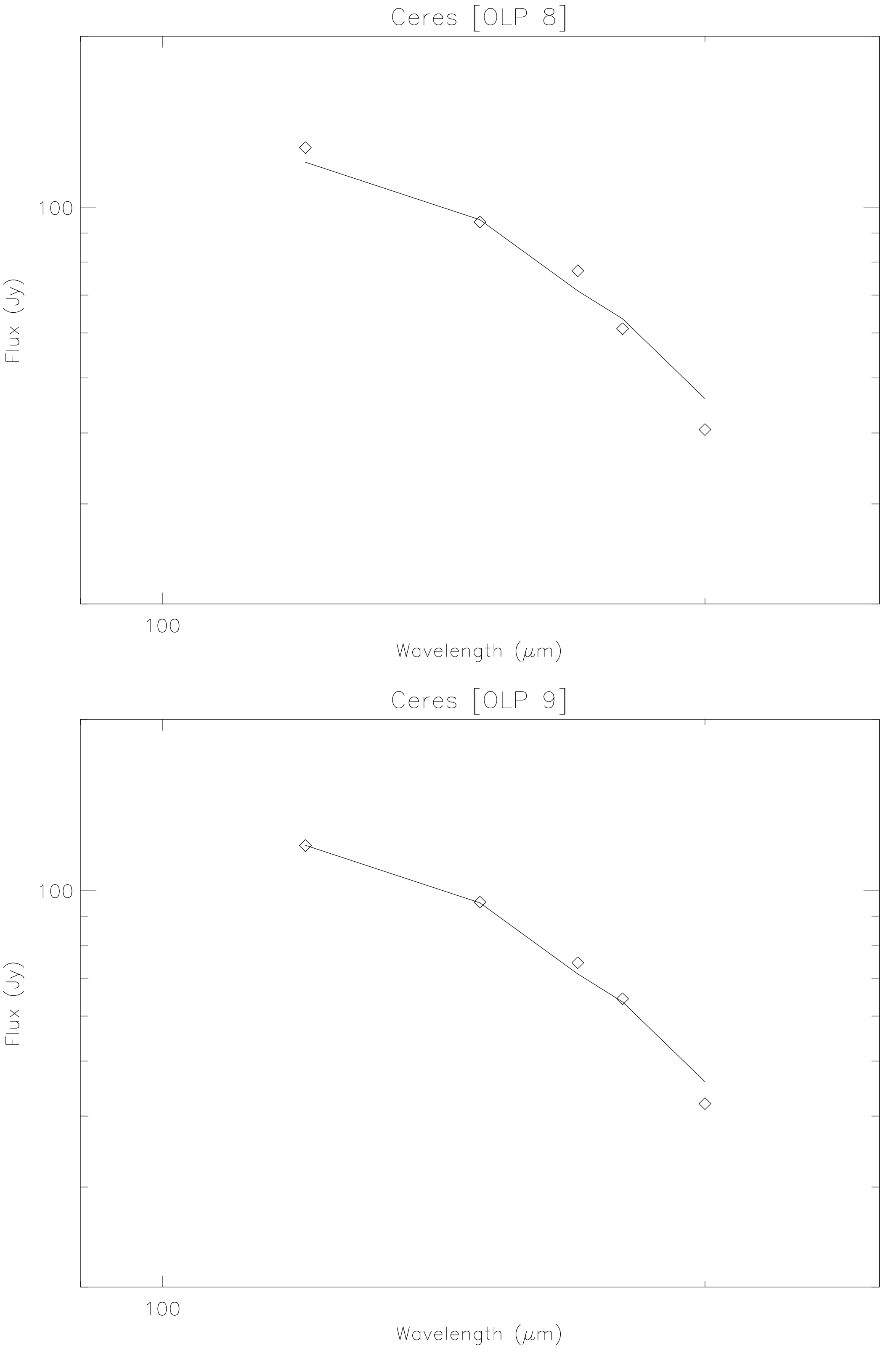

Figure 5.27: Comparison of C200 photometry of Ceres with the model thermophysical model by Lagerros for OLP 8.6b1 (upper panel) and OLP 9.0b3 (lower panel). All photometric points are color corrected for a 240 K BB. The meaning of the symbols is the following: solid line: Lagerros model, diamond: PHT-C200 (P25 AOT).

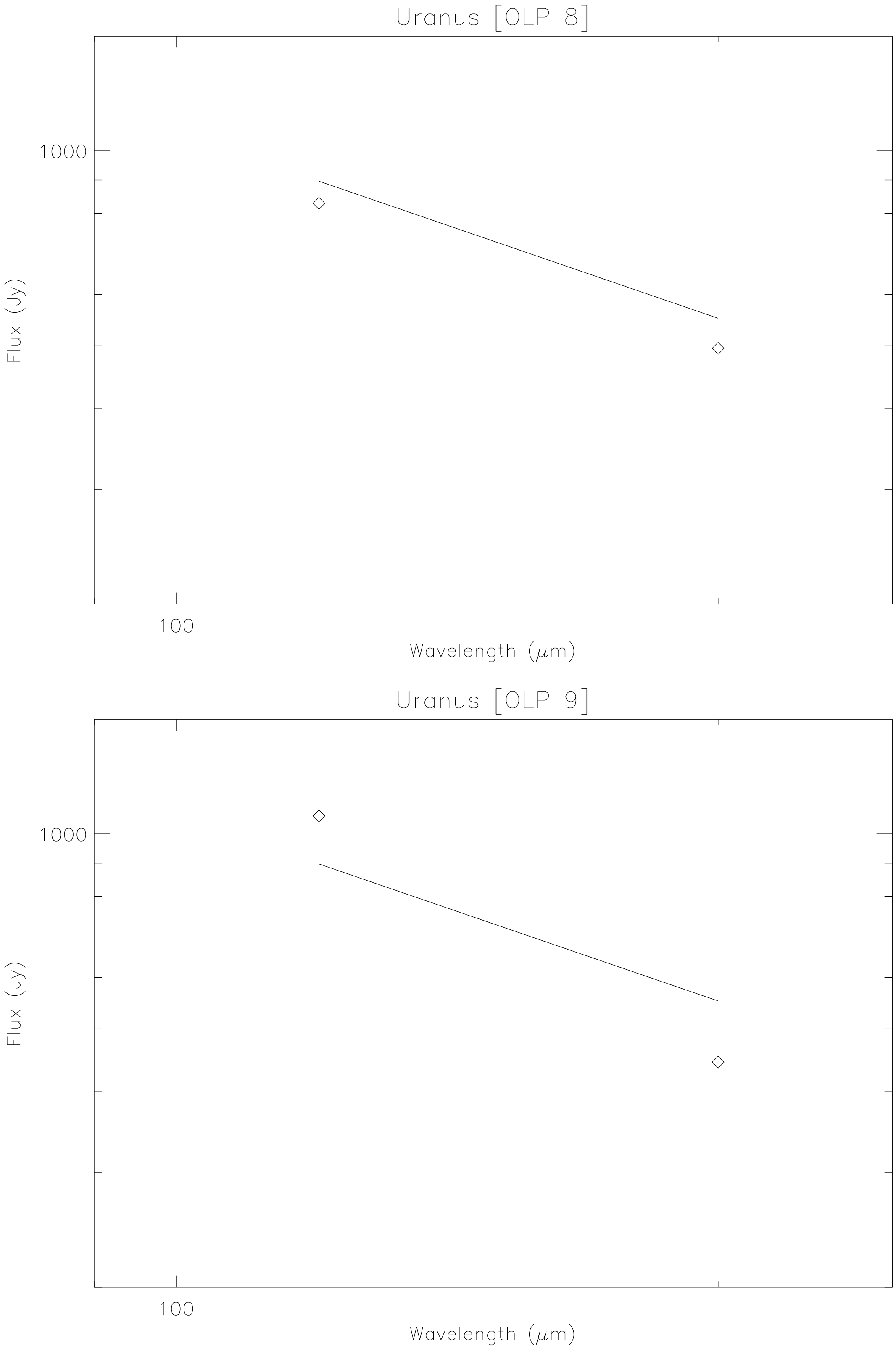

Figure 5.28: Comparison of C200 photometry of Uranus with the model provided by Abbas for OLP 8.6b1 (upper panel) and OLP 9.0b3 (lower panel). All photometric points are color corrected for a 60 K BB. The meaning of the symbols is the following: solid line: Abbas model, diamond: PHT-C200 (P25 AOT).

Evaluation Log

1) Absolute C200 Photometry of Ceres

Measurements:
PHT-C (120 um): pcap57901707 (src+back)
pcae57901606 (back)
PHT-C (170 um): pcap57902111 (src+back)
pcae57902010 (back)
PHT-C (200 um): pcap57901303 (src+back)
pcae57901302 (back)
PHT-C (150 um): pcap59402607 (src+back)
pcae59402506 (back)
PHT-C (180 um): pcap59402203 (src+back)
pcae59402102 (back)

Colour correction: black body, T = 240 K

Model: Lagerros

Det	cwl (μm)	OLP 8	OLP 9	Model	Δ (OLP 8)	Δ (OLP 9)
C2	120.0	127.281	119.841	119.960	6.10	-0.10
C2	150.0	94.105	95.241	95.000	-0.94	0.25
C2	170.0	77.252	74.522	71.180	8.53	4.70
C2	180.0	61.055	64.365	63.570	-3.96	1.25
C2	200.0	40.563	42.080	45.990	-11.80	-8.50

2) Absolute C200 Photometry of Uranus

Measurements:
PHT-C (120 um): pcap55204907 (src+back)
pcae55204906 (back)
PHT-C (200 um): pcap55204703 (src+back)
pcae55204702 (back)

Colour correction: black body, T = 60
Model: Abbas

Det	cwl (μm)	OLP 8	OLP 9	Model	Δ (OLP 8)	Δ (OLP 9)
C2	120.0	829.006	1064.417	897.600	-7.55	18.58
C2	200.0	495.406	444.260	552.000	-10.11	-19.52

Chapter 6

Validation of Chopped Photometry during SVP1

6.1 Validation of Chopped Photometry Test Cases with Quasi-simultaneous Staring Mode References and Reproducibility Checks

An overview of the test cases is outlined in Ref. [4], chapter 5.1.

6.1.1 References to Calibration Analysis and Software Change Documentation

- calibration reports:
  - Analysis of Chopped ISOPHOT Measurements [19]
- Software Change Requests: none
- Software Problem Reports: SPR 3213, 3216

6.1.2 Summary of Results

- The assessment of the quality of chopped photometry calibration during SVP1 is severly hampered by an underlying problem in the signal linearization calibration files (applicable both to staring and chopped photometry) as documented in SPR-3259. Therefore, we restrict the analysis to an overview of the general purpose multi-filter test case for the galaxy IRAS 03068-5346 which shows similar problems as the high priority staring mode photometry test cases shown in Sect. 5.4. We refer the reader to Sect. 9 for a quantitative assessment of chopped photometry.

6.1.3 Validation of PHT03 and PHT22 Chopped Mode: The SED of IRAS 03068-5346

- authors: U. Klaas
- date: 21-March-2000
- SVP period 1

Motivation

Like for validation of staring mode observations The measurements on the IR galaxy IRAS 03068-5346 were designed to check out the processing of multi-filter chopped mode for all PHT-P and PHT-C filters. For reference photometry in nodding mode was taken for some filters and IRAS photometry is available.

Method

We compare the background subtracted flux values of both OLP V8.6b1 and OLP V9.0b3 results against the IRAS photometry and the ISOPHOT nodding mode photometry. Furthermore, we compare the derived background surface brightness with COBE/DIRBE photometry.

Results

Figs. 6.1 and 6.2 show a comparison between OLP9 and OLP 8 results both for the source and the background flux. Due to the underlying problem of wrong filter sorting in the signal linearization CALG files P%%SLINR encountered during the staring mode photometry validation (cf. Sect. 5.4) and also noted here, in particular for the background fluxes, no assessment of the quality of chopped photometry with the new signal correction CALG files P%%CHOPSIG can be performed. We refer the reader therefore to Sect. 9.1.3 for a final assessment.

Conclusions

- Also chopped photometry OLP 9.0b3 data products are affected by a wrong filter ordering in the signal linearization CALG files P%%SLINR $\rightarrow$ SPR-3259.

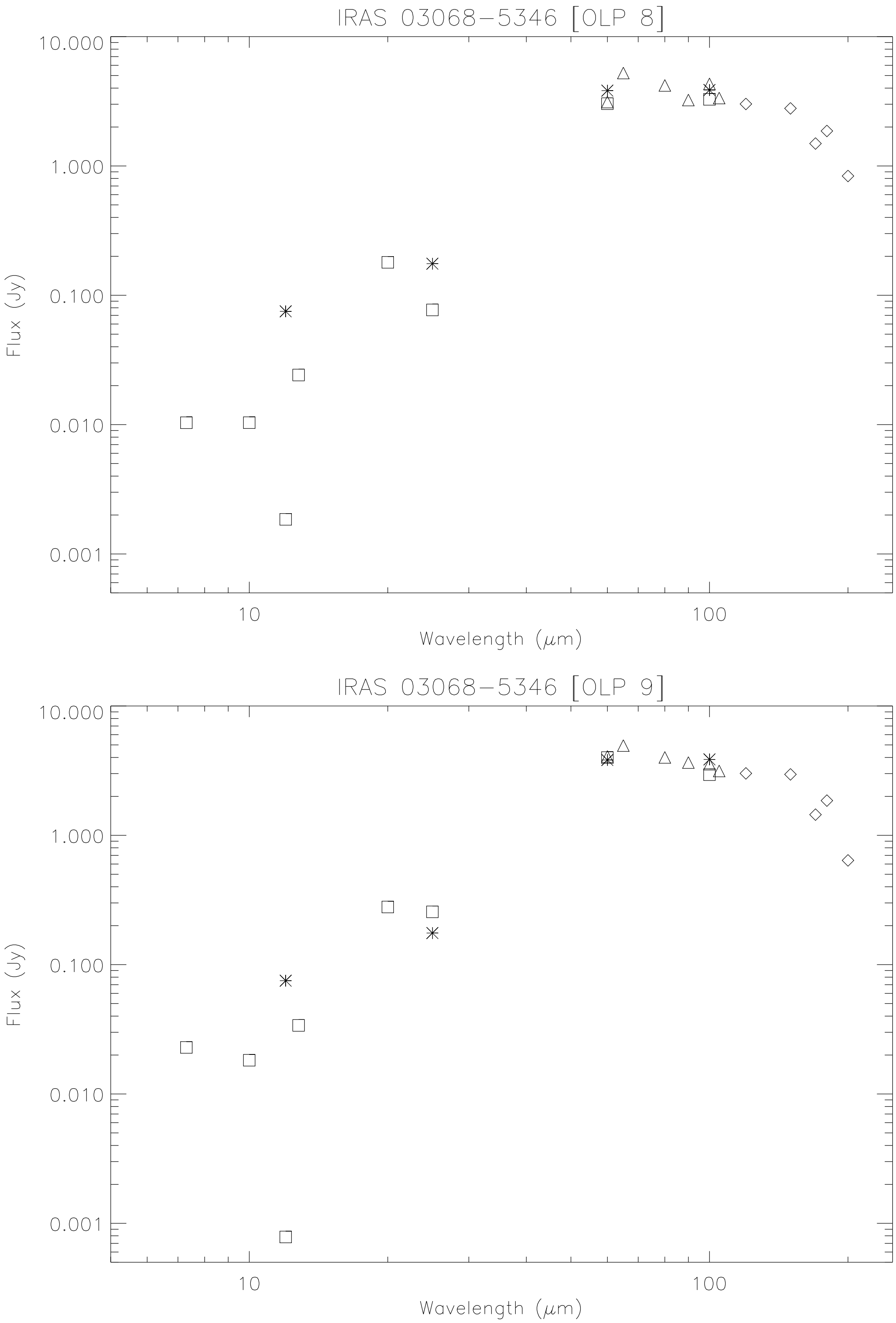

Figure 6.1: Comparison of PHT-P and PHT-C chopped photometry, using the full ISOPHOT filter set, with IRAS photometry both for OLP 8.6b1 (upper panel) and OLP 9.0b3 (lower panel). Color correction has been applied (modified BBs $\propto \lambda^{-2}$ with T1 = 140 K and T2 = 40 K). The meaning of the symbols is the following: asterisk: IRAS, square: PHT-P (P03 AOT), triangle: C100 (P22 AOT), diamond: C200 (P22 AOT).

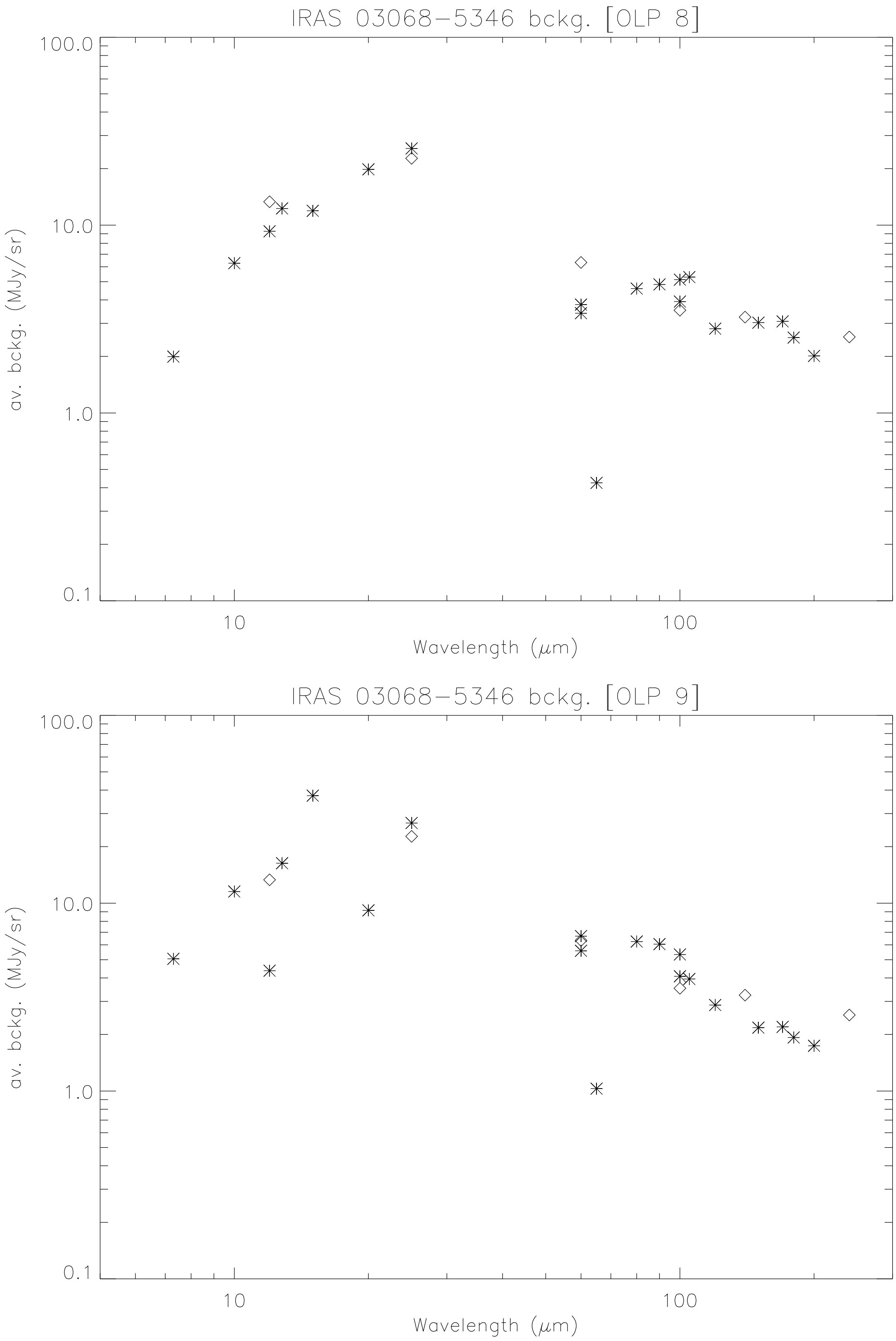

Figure 6.2: Comparison of surface brightness from chopped PHT photometry of the background beam for IRAS 03068-5346 with COBE, both for OLP 8.6b1 (upper panel) and OLP 9.0b3. Asterisk: PHT-P and PHT-C photometry, diamond: COBE.

Evaluation Log

1) Chopped Point Source Photometry

Measurements:
PHT-P1: ppap81101701: FCS = 12 um
PHT-P2: ppap81101701: FCS = 25 um
PHT-P3: ppap81101802: FCS = 100 um
PHT-C1: pcap81101906: FCS = 90 um
PHT-C2: pcap81102008: FCS = 170 um

Colour correction: mod. bb, em.=2, T1 = 140 K (P1, P2), T2 = 40 K (P3, C1, C2)

Det	cwl (μm)	OLP 8	OLP 9	IRAS
P1	7.3	0.010	0.023	
P1	10.0	0.010	0.018	
P1	12.0	0.002	0.001	0.075
P1	12.8	0.024	0.034	
P1	15.0	0.000	0.000	
P2	20.0	0.180	0.279	
P2	25.0	0.077	0.256	0.176
P3	60.0	3.031	3.991	3.822
C1	60.0	3.120	4.068	3.822
C1	65.0	5.231	4.940	
C1	80.0	4.195	4.001	
C1	90.0	3.234	3.650	
P3	100.0	3.273	2.944	3.862
C1	100.0	4.307	3.547	3.862
C1	105.0	3.351	3.145	
C2	120.0	3.014	3.013	
C2	150.0	2.788	2.959	
C2	170.0	1.490	1.446	
C2	180.0	1.864	1.855	
C2	200.0	0.836	0.640	

TDT: ppap54502911 (OLP 9)
10.0 um -0.008 Jy
12.0 um 0.014 Jy
15.0 um 0.045 Jy
25.0 um -0.246 Jy

2) Background photometry from off-source beam

Det	λ	OLP8 (MJy/sr)	OLP9 (MJy/sr)	COBE (MJy/sr)
P1	7.3	2.00	5.06	
P1	10.0	6.27	11.54	
P1	12.0	9.27	4.37	13.32
P1	12.8	12.26	16.32	
P1	15.0	11.92	37.36	
P2	20.0	19.81	9.16	
P2	25.0	25.60	26.72	22.69
P3	60.0	3.40	5.58	6.33
C1	60.0	3.78	6.68	6.33
C1	65.0	0.42	1.03	
C1	80.0	4.59	6.25	
C1	90.0	4.84	6.05	
P3	100.0	3.92	4.08	3.52
C1	100.0	5.12	5.33	3.52
C1	105.0	5.29	3.95	
C2	120.0	2.81	2.87	
C2	150.0	3.03	2.17	3.24
C2	170.0	3.07	2.19	
C2	180.0	2.52	1.93	
C2	200.0	2.01	1.74	2.54

Chapter 7

Overview of Results from SVP2

During the second period of the PHT OLP 9.0 Scientific Validation the following results were achieved:

- The dynamic spectral response function calibration for PHT-S staring observations (SCREW-425) has been successfully implemented. The performance of this mode w.r.t. achievable absolute and relative accuracies has been significantly improved. In general absolute accuracies of better than 10 % and relative accuracies (relative spectral shape) of better than 20 % are achieved now.

- The changes in the processing of PHT-S staring mode observations made also some changes in the processing of the chopped PHT-S observations necessary. These were successfully implemented and the good processing and calibration performance for this mode was maintained.

- The calibration updates for staring mode photometry, refined linearisation correction and FCS calibration files gave further improvement for the calibration of bright sources. For those absolute accuracies of better than 10 % are uniformly achieved now.

- Among the PHT-P filters a subset was identified which gives less reliable photometry, proven by systematic features showing up repeatedly in several test cases. The worst case is the 12.8 μm filter which shows positive flux deviations for all sources below 100 Jy; at the background level the flux can be by a fcator of 4 higher than for neighbouring filters. Further candidates for which possibilities for refinement have to be investigated are the 3.3, 11.3 and 20 μm filters. For C100 multi-filter background measurements a systematic pattern deviating from a smooth behaviour is observed. Some caution on this finding is applicable, since no proper color correction is performed yet, however, it appears unlikely that the positive excesses of the not so commonly used 65 and 80 μm filters are due to missing color correction. Therefore, these two filters are flagged, too.

- A comprehensive study of photometry from mini-maps was performed. It was found that aperture photometry from map products PGAI does not give accurate results. A method was developed to make use of the PCAS products (photometry per raster point) from which accurate photometry (better than 20 - 25 %) can be derived over a large flux range.

- The scientific validation assessment of chopped photometry was continued. Progress can be reported with regard to several technical and calibration aspects:
  - The pattern processing of observations with data reduction in the read-outs (very bright sources) was fixed.
  - A bug, the omission to apply the filter-to-filter correction for target measurements was identified and fixed. As an immediate consequence P1 chopped photometry gives accurate results (< 25 %) for the great majority of test cases.
  - Analysis of monitoring measurements has shown the good reproducibility ($<$ 15 %) of the chopped photometry processing. An exception was found for C200

which shows the problematics and limitations of this submode by small scale background gradients and fluctuations (cirrus confusion).

- In general a reasonably good consistency of the off-beam surface brightness with COBE/DIRBE photometry (within the limitations of the comparison, e.g. no color correction is performed yet) is found which indicates that the calibration measurement using the actual responsivity from the chopped FCS measurement is basically working. There is some correlation that worse point source photometry is found for cases where the consistency with COBE/DIRBE is not good either. However, this is not a firm relation, since other parameters than the absolute calibration can have an impact on the final result (e.g. chopper frequency dependent signal correction factors).

On the other hand there is a number of findings which prohibit currently to declare the chopped mode scientifically valid and require further investigations:

- In general an overcorrection is found for chopped P2 photometry (fluxes too high by 50 - 80 %). Here is also a clear discrepancy between OLP and PIA results which needs to be followed up.
- In general resulting P3 fluxes are too low.
- C100 multi-filter chopped photometry of faint sources yield an SED shape which oblique with regard to the reference SED. In most cases the 60 μm photometry comes now out less accurate (too high flux) than for OLP 8.
- C200 multi-filter photometry shows a relatively high scatter, while the off-beam surface brightness SEDs look considerably smoother.

By the end of SVP2 the following software problem reports for updates had been recorded:

Table 7.1: Problems found during OLP 9.0 Scientific Validation Period 2

Problem	**CI**	**SPR**
PHT-P1 flux discrepancies	OLP	3373
NDRs not rejected for chopped measurements	OLP	3374
Anomalous spikes in PHT-S spectrum of NGC 253	OLP	3382

Note, that in order to verify the proper implementation of the fixes several subsets of data products were re-processed with the fix implemented. The OLP version for verifying SPR-3373&3374 implementation is OLP 9.0b10 and for verifying SPR-3382 implementation is OLP9.01 (patch to OLP 9.0 final). Cf. Table 3.1 for an overview which OLP version products were used during the OLP 9 validation.

Chapter 8

Revalidation Tests during SVP2

8.1 Dynamic Spectral Response Function for ISOPHOT-S Staring Measurements of Point Sources

An overview of the test cases is outlined in Ref. [4], chapter 3.1.1.

8.1.1 References to Calibration Analysis and Software Change Documentation

- calibration report:
  - Dynamic Calibration for ISOPHOT-S [5]
- Software Change Requests: SCREW 425

8.1.2 Summary of Results

- Algorithms and CALG files according to SCREW-425 are correctly implemented.
- The new dynamic spectral response function for single pointing staring observations (note: not applicable to raster staring observations) provides considerable improvement with regard to the static default staring response function.
- We derive from stellar spectra a calibration accuracy for point sources of $< 10\,\%$ absolute and $< 20\,\%$ for relative spectral shape.

8.1.3 Consistency Check of PHT-S Dynamic Response Calibration on Calibration Stars

- authors: K. Wilke, U. Klaas
- date: 13-July-2000
- SVP period 2

Motivation

We process on-source and off-source measurements of several calibration stars of different brightness (HR 7001 = Vega, HR 2491 = Sirius, HR 5340, HR 7469, HR 7924, HR 8487) which were used to establish the dynamic relative spectral reponse function surfaces of CALG file PSDYNAMIC and check whether the input model SED is reproduced. We compare with OLP 8 products in order to find out the improvement with regard to the static default spectral response function. For the Vega and Sirius off-measurements we compare the resulting background SED with COBE/DIRBE photometry.

Method

We compare the stellar SEDs with the flux models by Cohen. For the accompanying background measurements we compare the background SED with COBE/DIRBE photometry (in this range the background is dominated by the smooth Zodiacal Light and hence should not be dependent on the beam size).

Results

Fig. 8.1 displays the spectra of both Vega and Sirius in the same way as for fig. 5.1 (the fluxes in Jy are now contained in the SPD product!). Although there is no perfect match with the flux model, in particular for Sirius, one sees that the bents seen in the OLP 9.0b3 products are gone and that the absolute level is okay. In fact for Vega and Sirius the least matching results are achieved. This is reproduced by interactive processing, too, so that it is not a specific feature of the OLP processing. For Sirius the explanation appears to be quite straight forward, since the following warning message is found both in the PSSS and the PSLS product headers:

```
COMMENT ****************************************************
COMMENT !!!WARNING!!!
COMMENT Detector temperature outside valid range
COMMENT *************************************************
```

This means that according to the caveat in Sect. 2.15 the detector temperature was outside the range $2.7\,\mathrm{K} < \mathrm{T} < 3.1\,\mathrm{K}$ and hence the transient behaviour of the detector signals was different from the ones of the calibration stars leading to a less good match by the dynamic spectral response calibration.
In figs. 8.2 to 8.7 we perform the comparison with OLP8. For all stars we can conclude that the spectra have become much smoother and more accurate. Some typical features introduced by the static response function for quite a range of flux levels are removed by the new method. In the case of HR 5340 which is so bright that parts of the spectrum are saturated some wavelength areas can be recovered now.
We conclude from this analysis that the absolute calibration accuracy is better than 10 % while the relative calibration accuracy (relative spectral shape) is better than 20 % which is a significant improvement with regard to the old calibration method.
Fig. 8.8 shows the comparison of the background spectra for Vega and Sirius off-positions like in fig. 5.2. We see that the unrealistically high background values found for OLP 9.0b3 are gone. It has to be clearly stated that in the SS range we cannot expect any detection of the background, even with the longest integration (what is not the case for the examples here). What we see in the SS range is not a calibration uncertainty of a factor of 10, but the detector noise level. For the Vega background position we find a good consistency with the

COBE/DIRBE 12 μm point, while for the Sirius background the consistency seems to be only within 50 %, but the slope towarsd the shorter wavelengths looks better here. Clearly, a better statistics is needed here before drawing quantitative conclusions (see also Sect. 8.2.4).

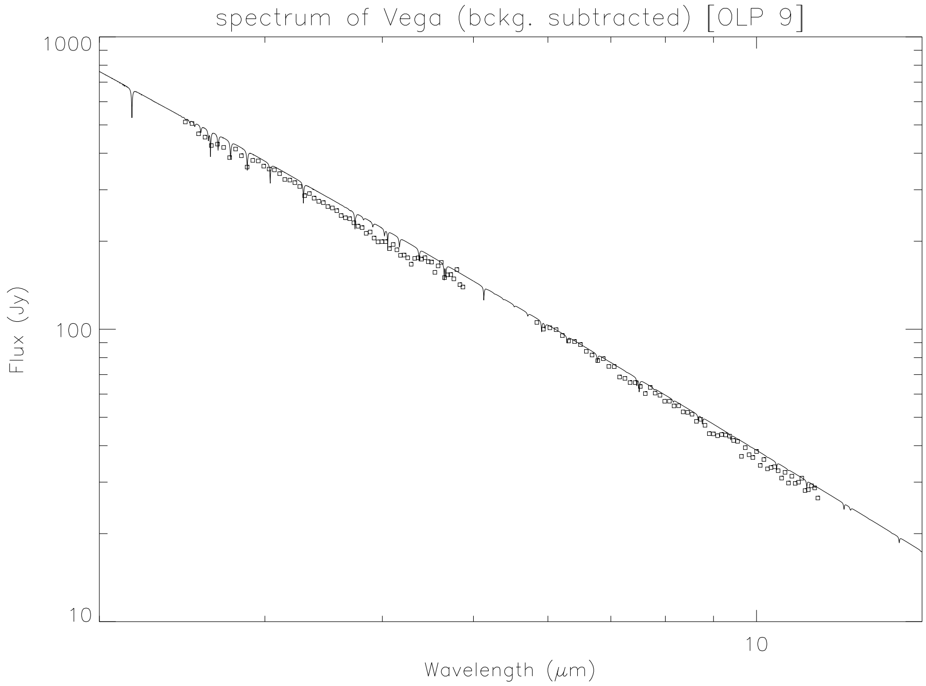

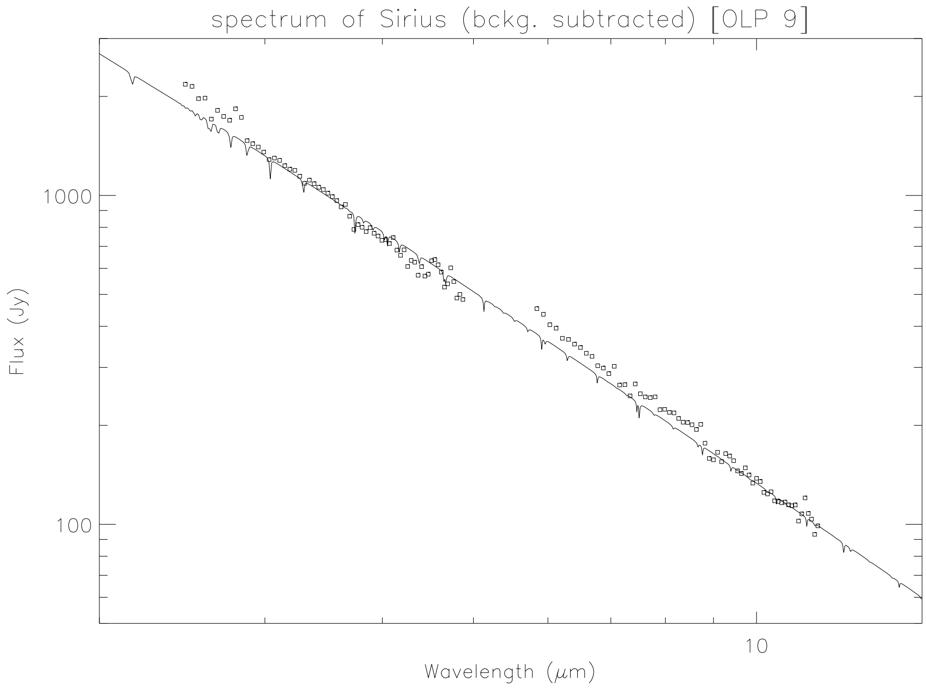

Figure 8.1: Comparison of the spectra of the stars HR 7001 (Vega) and HR 2491 (Sirius) obtained with dynamic response calibration for OLP9.01 with the flux models by Cohen.

Conclusions

- The implementation of SCREW-425 introducing the dynamic spectral response function into the PHT-S calibration was successful as verified by the self-consistency check on calibration standards. The method means a significant improvement with regard to the static default response function.

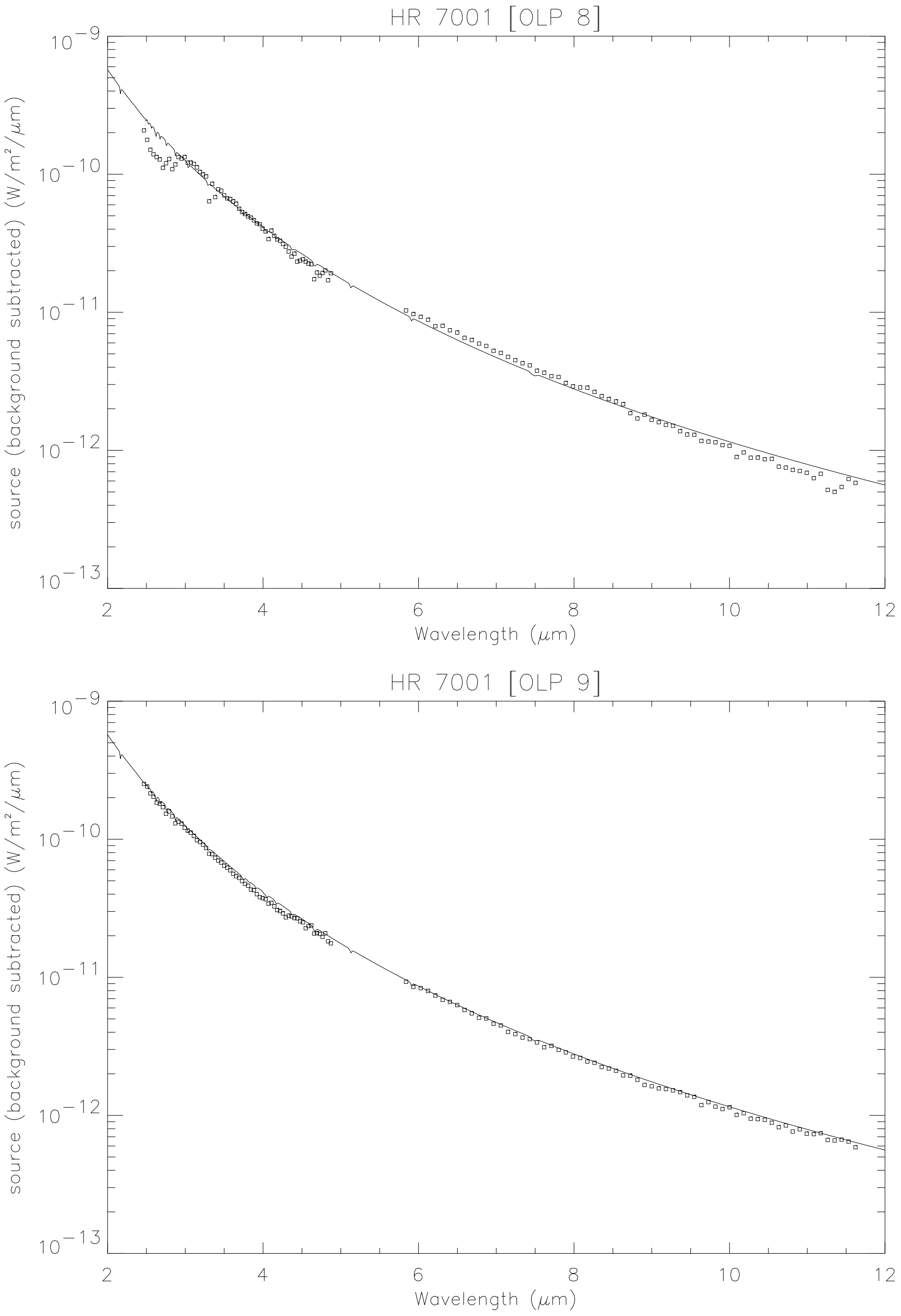

Figure 8.2: Comparison of the spectrum of HR 7001 (Vega) with the flux models by Cohen for OLP 8.6 (upper panel) and OLP 9.01 (lower panel). This time the display shows F_λ vs. λ which are the units of the AAR product.

- For some stars we get perfect agreement with the flux model, for other stars some discrepancies remain, but also for those stars the accuracy of the spectrum is improved. From all test cases we derive an absolute calibration accuracy of better than 10 %, the relative accuracy is somewhat worse, but always better than 20 %. This accuracy holds down to flux levels of 10^{-14} W m^{-2} μm^{-1} (corresponds to a flux density in frequency range of $\sim$ 300 mJy at 10 μm).
- The spectral shapes of background continua are reasonably well reproduced for the SL range (for the SS range the ZL background level is below the detection limit).

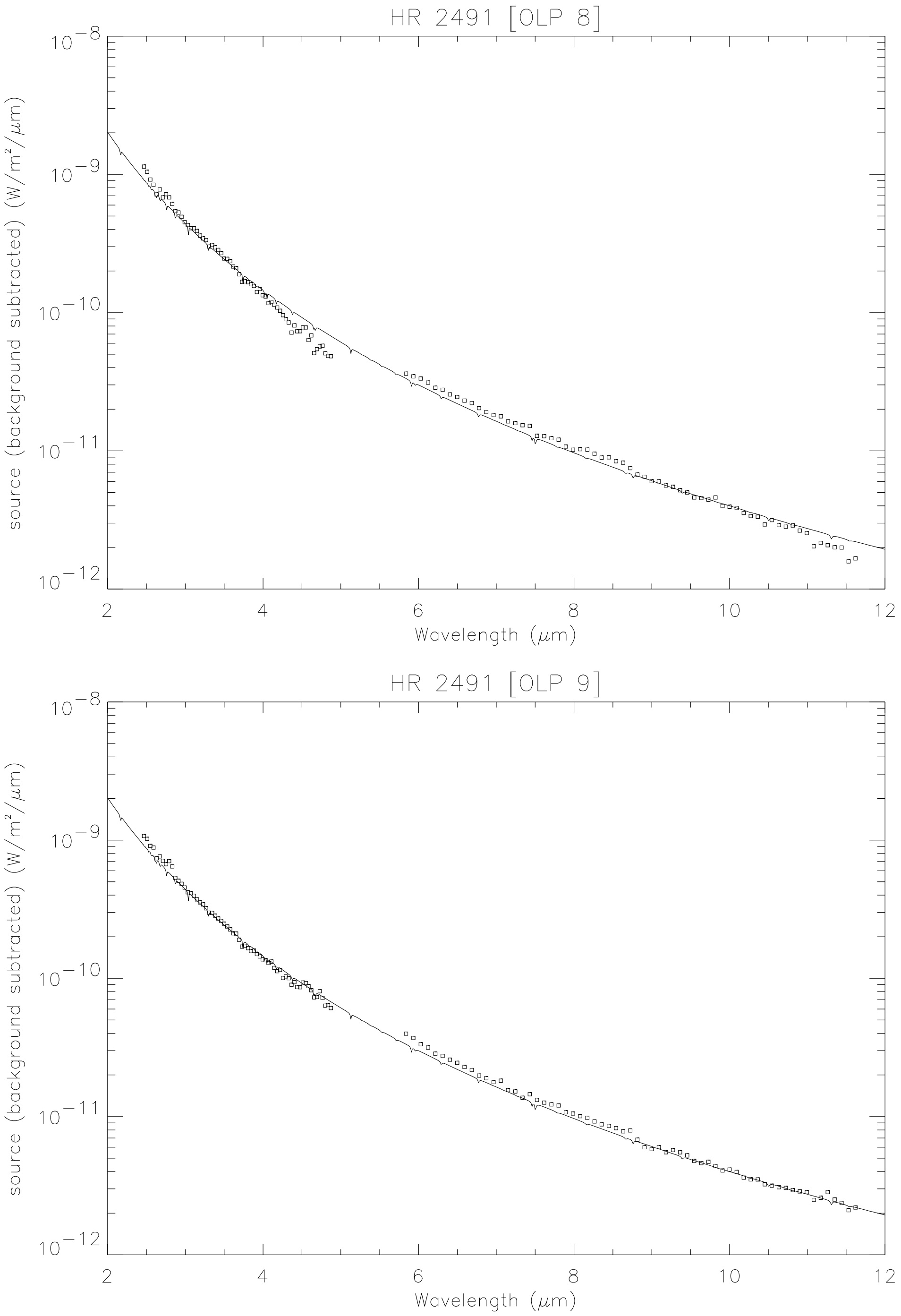

Figure 8.3: Comparison of the spectrum of HR 2491 (Sirius) with the flux models by Cohen for OLP 8.6 (upper panel) and OLP 9.01 (lower panel). This time the display shows F_λ vs. λ which are the units of the AAR product.

From the few test cases a consistency of better than 50 % with COBE/DIRBE 12 μm photometry is derived, but better statistics is needed here.

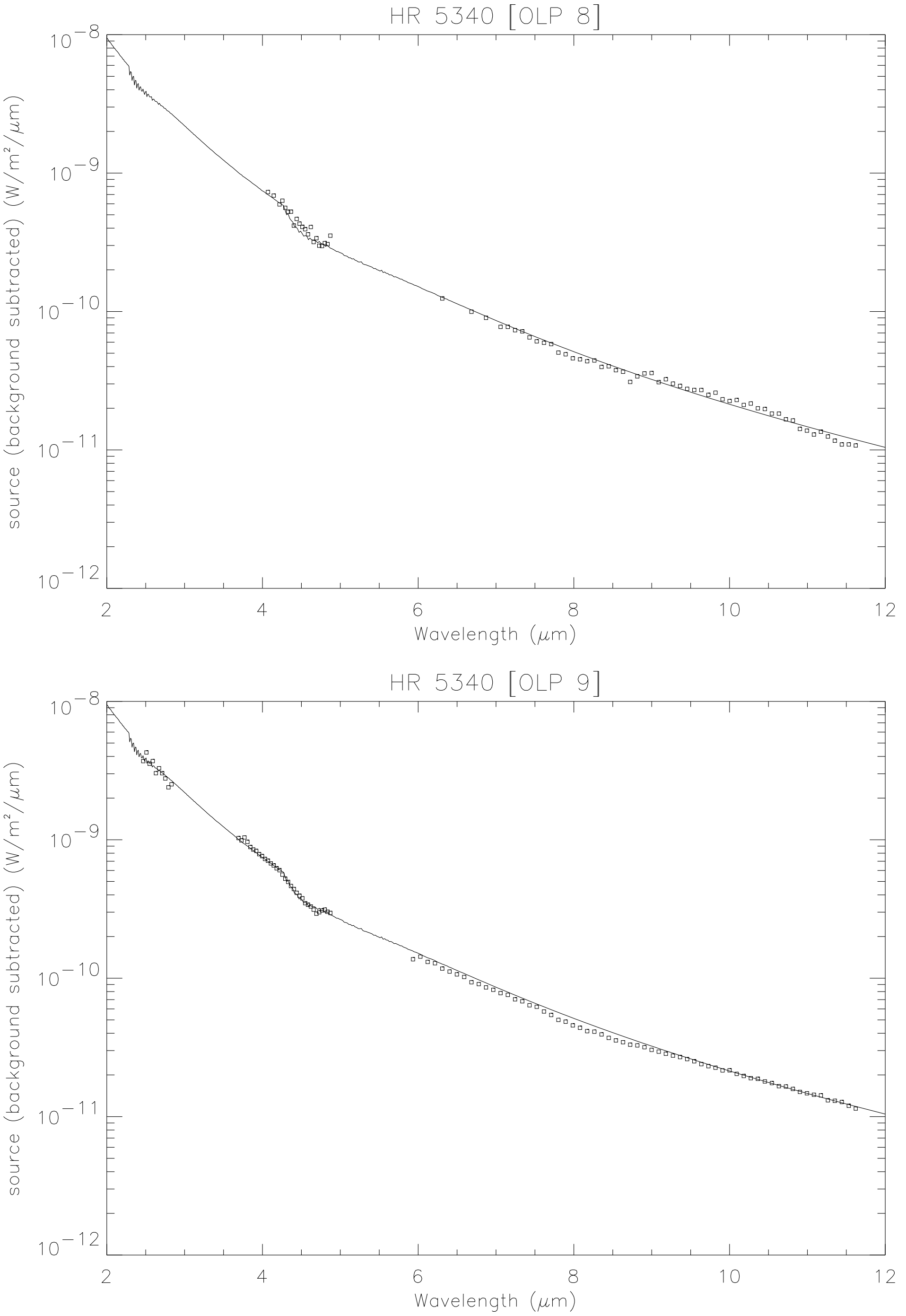

Figure 8.4: Comparison of the spectrum of HR 5340 (α Boo, background subtracted) with the flux model for OLP 8.6 (upper panel) and OLP 9.01 (lower panel).

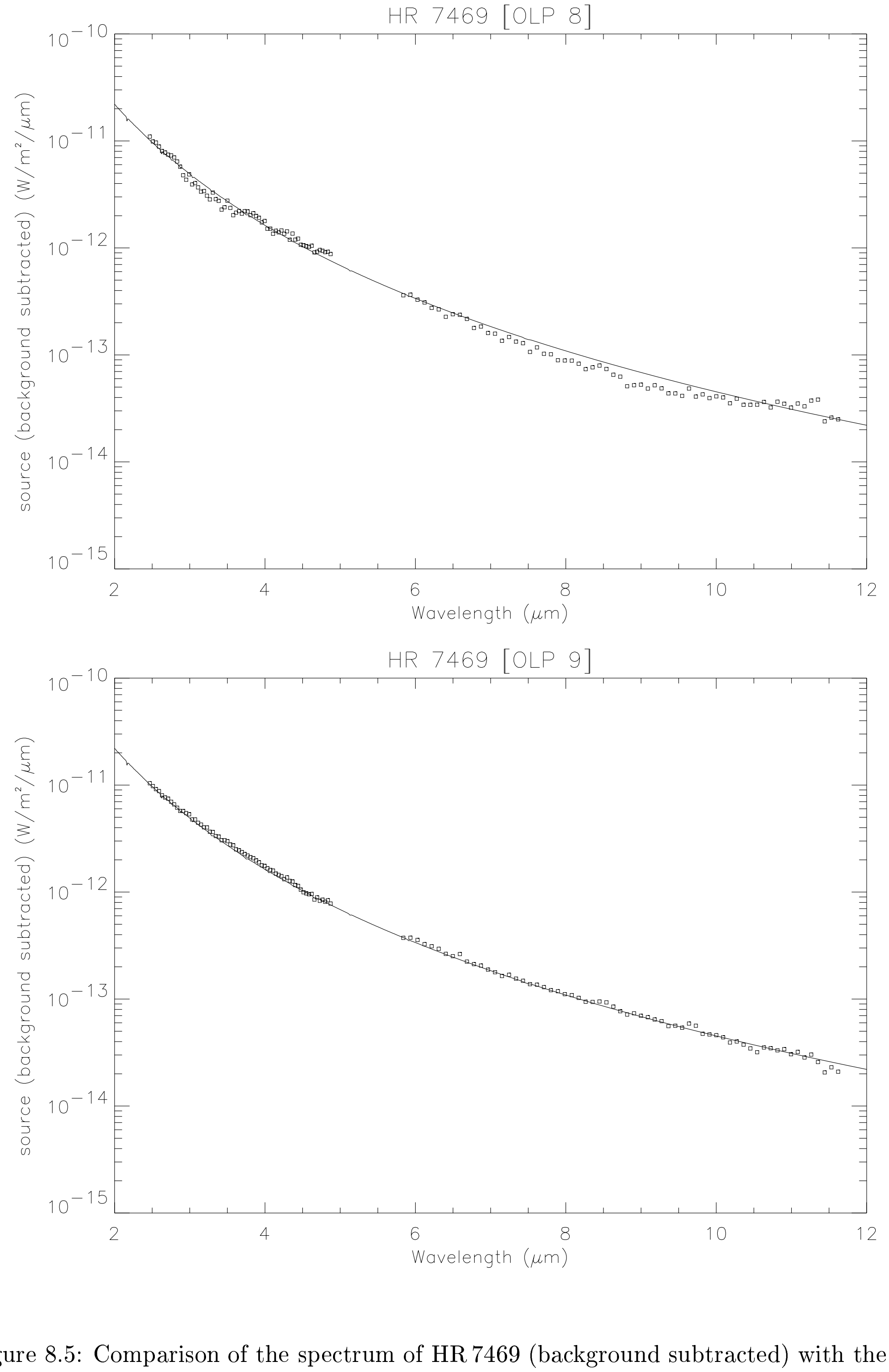

Figure 8.5: Comparison of the spectrum of HR 7469 (background subtracted) with the flux model for OLP 8.6 (upper panel) and OLP 9.01 (lower panel).

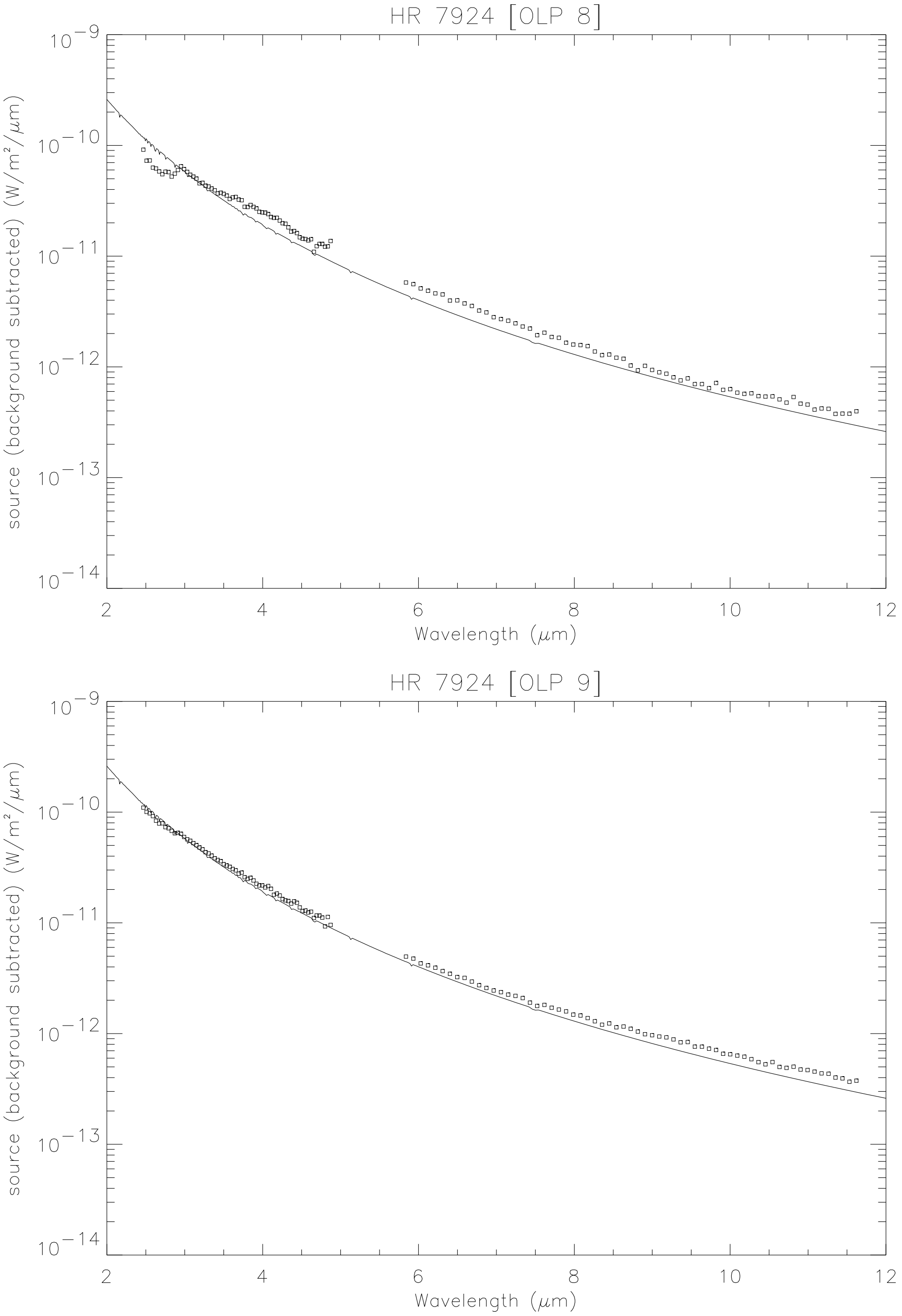

Figure 8.6: Comparison of the spectrum of HR 7924 (background subtracted) with the flux model for OLP 8.6 (upper panel) and OLP 9.01 (lower panel).

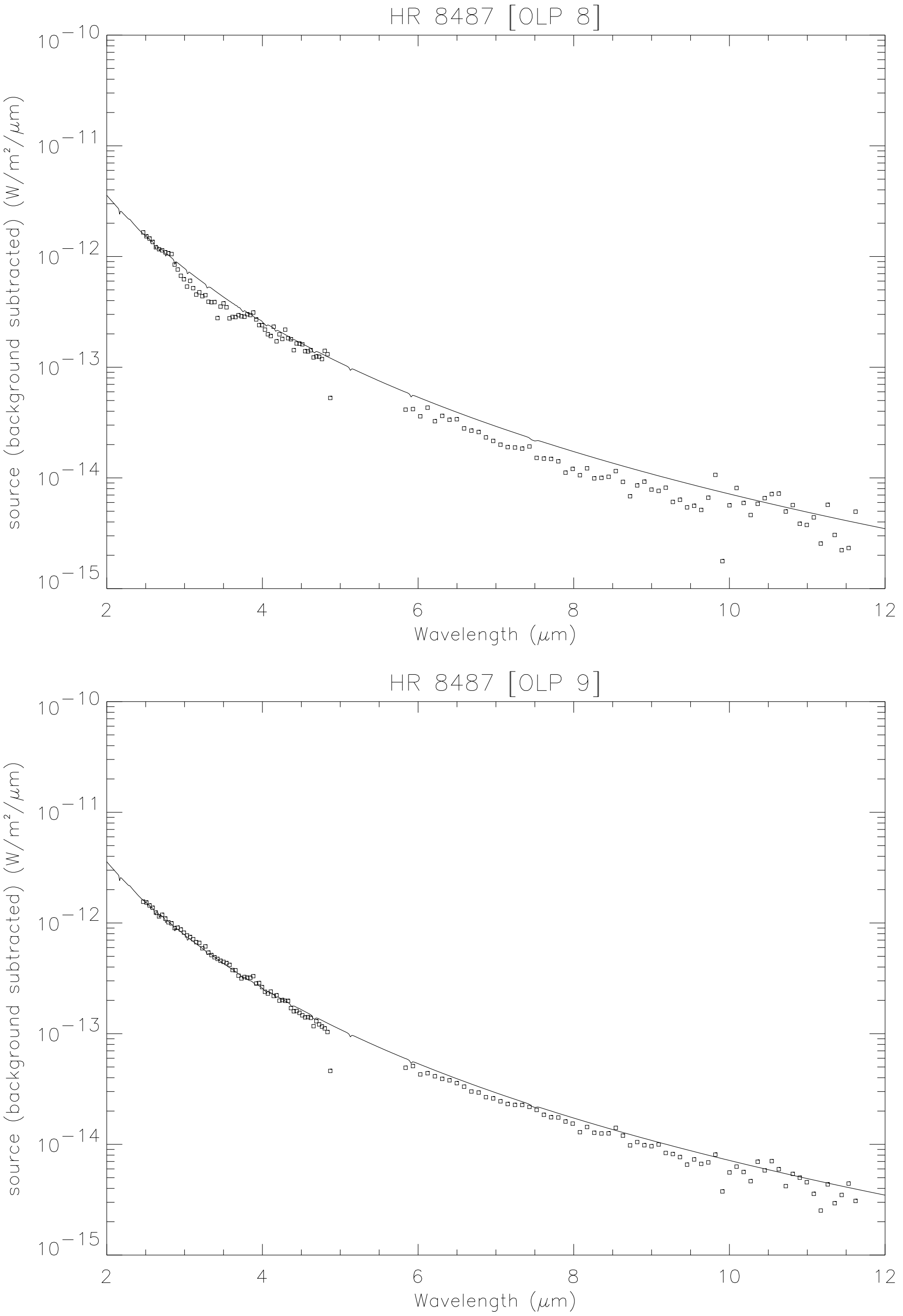

Figure 8.7: Comparison of the spectrum of HR 8487 (background subtracted) with the flux model for OLP 8.6 (upper panel) and OLP 9.01 (lower panel).

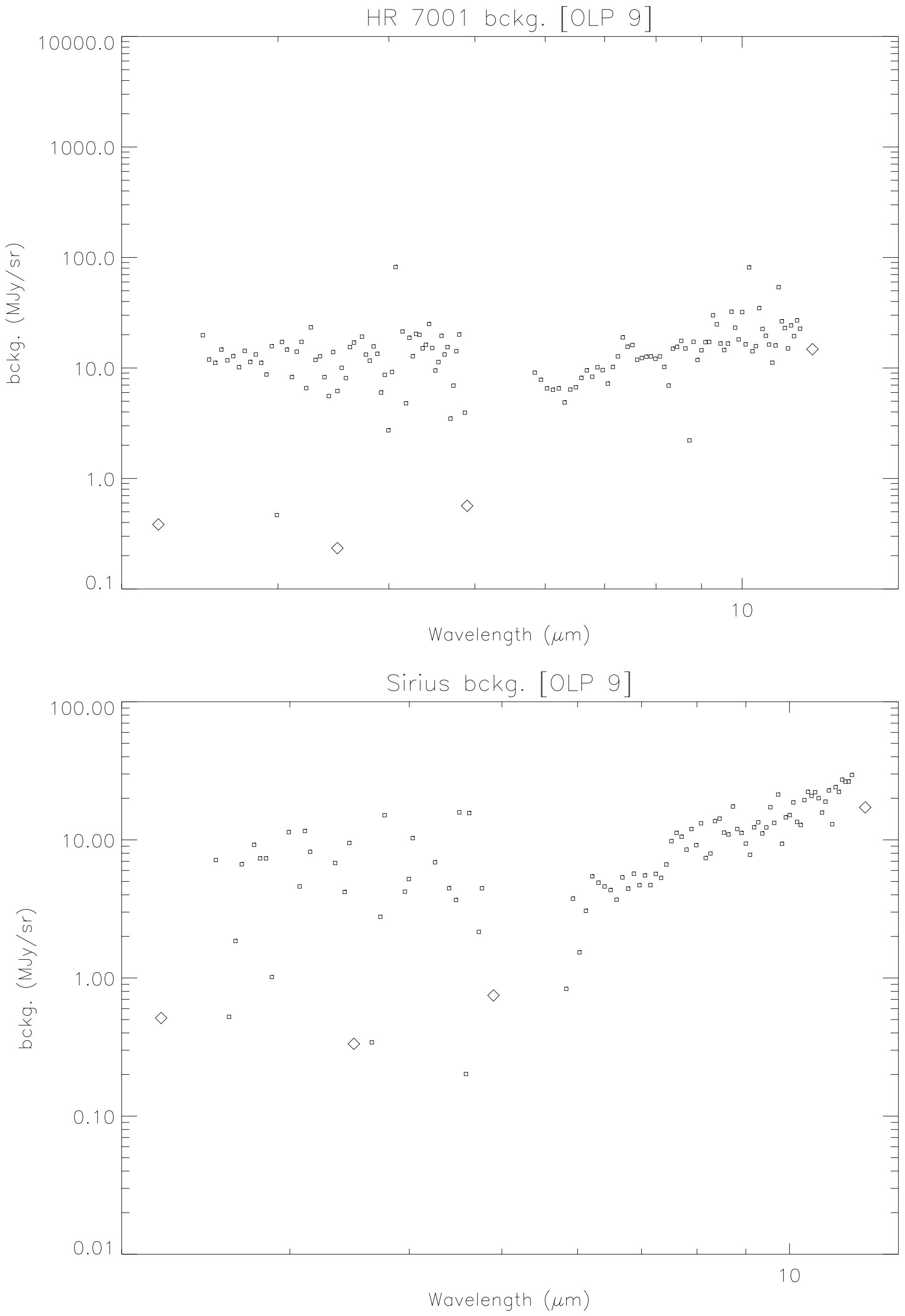

Figure 8.8: Comparison of the spectra of the background positions of HR 7001 (Vega) and HR 2491 (Sirius) obtained with dynamic response calibration for OLP9.01 with COBE/DIRBE photometry.

8.1.4 MIR Spectra of the Stars BS 8679 and BS 6056 from Staring On and Off PHT-S Measurements

- authors: K. Wilke, U. Klaas
- date: 13-July-2000
- SVP period 2

Motivation

We found two stars in the data base with similar spectral type as standard stars but different brightness. It is therefore possible to test absolute and relative accuracy of the new ISOPHOT-S dynamic calibration on different brightness levels than standard stars used to establish the calibration. The properties of the three stars are compiled in Table 8.1:

Table 8.1: Properties of stars used for verification of chopped ISOPHOT-S spectra

Name	**Spectral Type**	**Apparent Brightness** (mag)	**Reference Star**	**Spectral Type**	**Apparent Brightness** (mag)
BS 6056	M0.5III	$m_v = 2.74$	HD 25025 (=γ Eri)	M0.5III	$m_v = 2.931$
BS 8679	M0III	$m_v = 4.01$	HD 95578 (=61 Leo)	M0III	$m_v = 3.079$

Method

Scale the model spectra of HD 25025 and HD 95578 according to the apparent brightness ratio in the V band. Compare the absolute fluxes and relative shapes of the ISOPHOT-S spectra with the scaled model spectra.

Results

In figs. 8.9 and 8.10 we perform the comparison with OLP8. The results confirm the findings of the previous chapter that the spectra have become much smoother and more accurate and some typical features introduced by the static response function for quite a range of flux levels are removed by the new method.
We derive similar calibration accuracies as before, i.e. an absolute calibration accuracy of better than 10 % and a relative calibration accuracy (relative spectral shape) of better than 20 %.

Conclusions

- With the spectroscopy of non-calibration stars we confirm the improved quality of PHT-S staring mode products using the dynamic spectral response function method.
- We confirm the calibration accuracy being in the range better than 10 % for absolute calibration and better than 20 % for the relative shape of the SED.

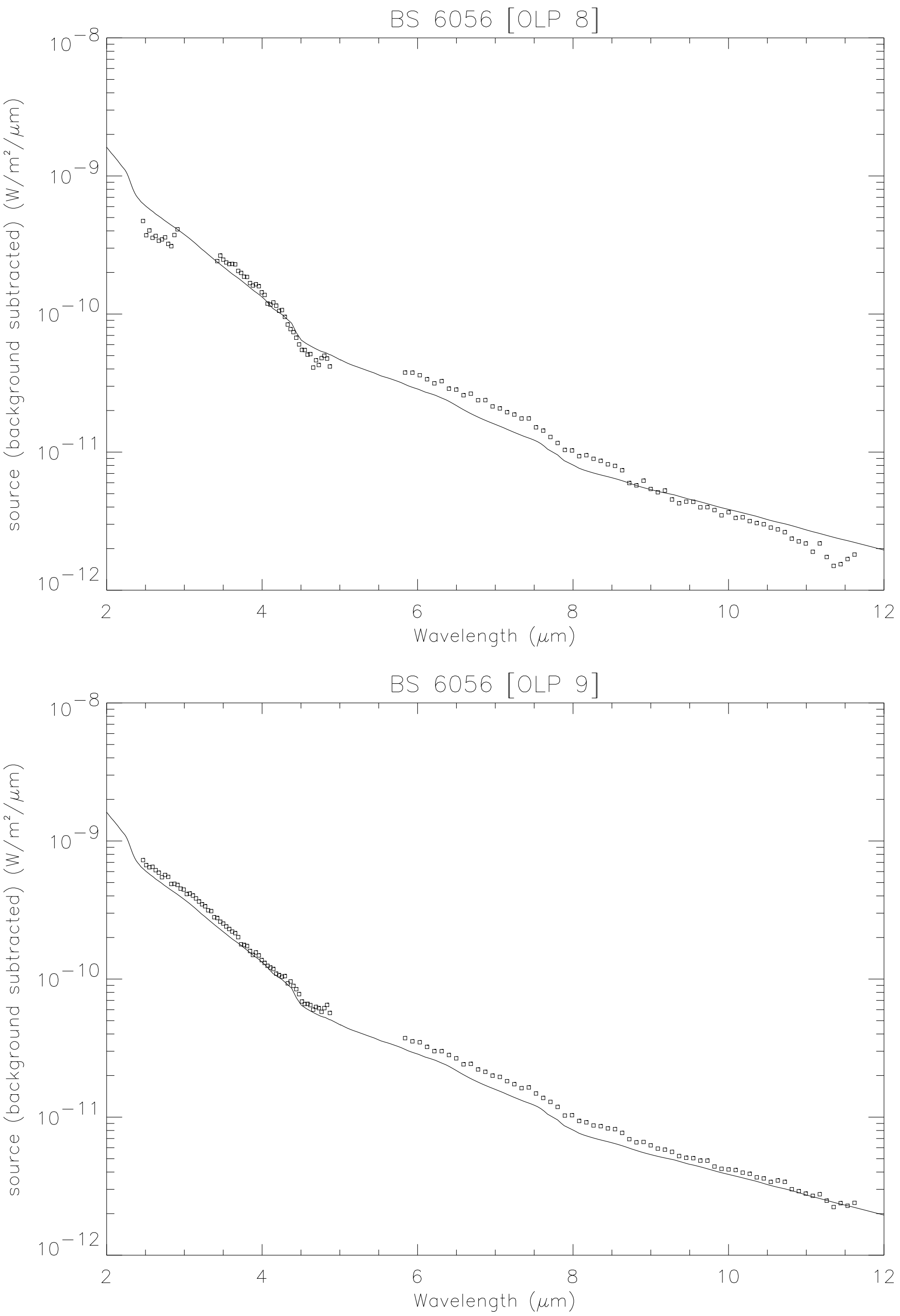

Figure 8.9: Comparison of the spectrum of BS 6056 (background subtracted) with the scaled flux model of HD 25025 for OLP 8.6 (upper panel) and OLP 9.01 (lower panel).

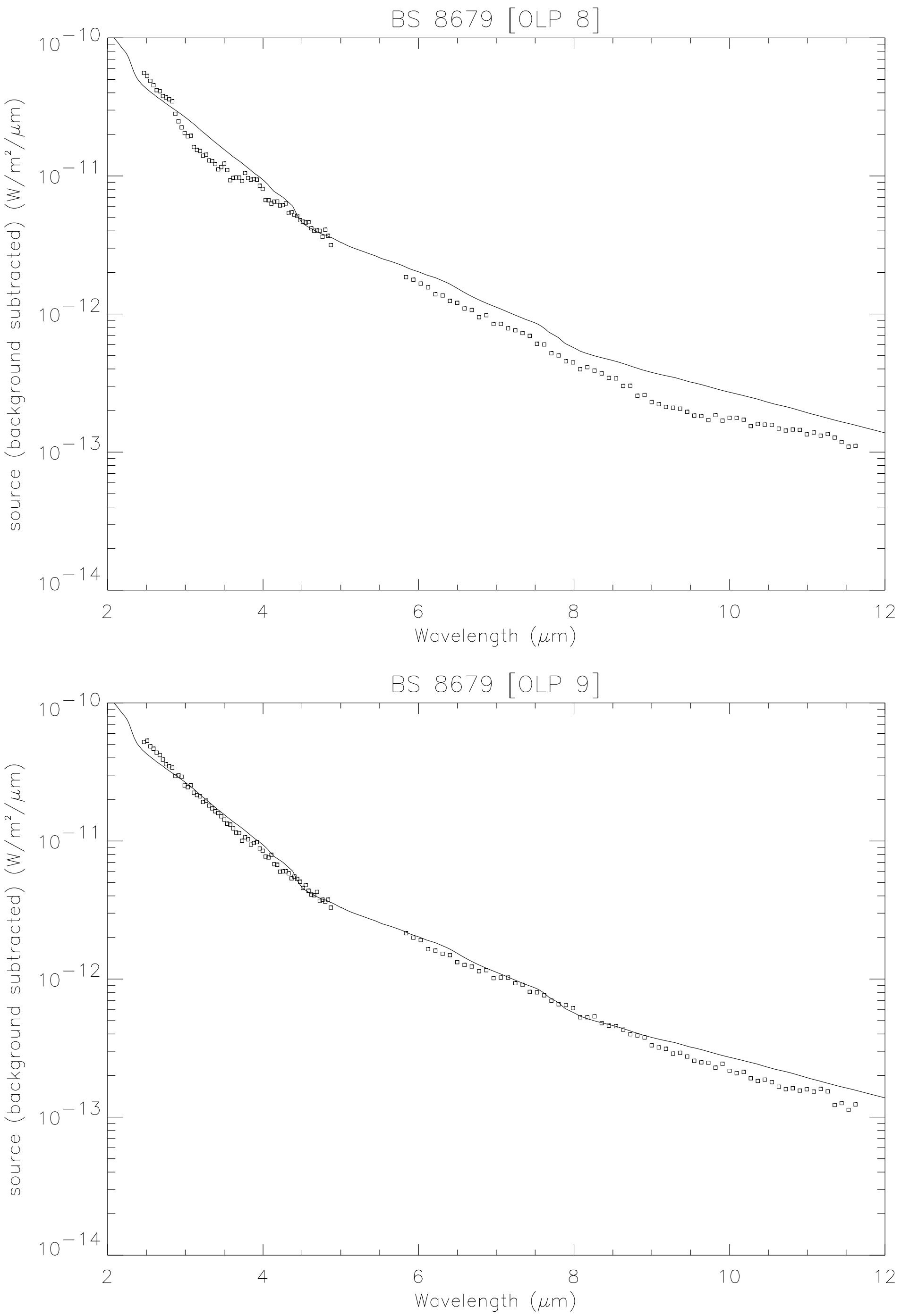

Figure 8.10: Comparison of the spectrum of BS 8679 (background subtracted) with the scaled flux model of HD 95578 for OLP 8.6 (upper panel) and OLP 9.01 (lower panel).

8.1.5 MIR Spectra of Galaxies from Staring PHT-S Measurements

- authors: K. Wilke, U. Klaas
- date: 13-July-2000
- SVP period 2

Motivation

We investigate here the spectra of the two galxies NGC 253 and Circinus. These galaxies have different SED shapes than the standard stars from which the dynamic PHT-S spectral response function was derived. There is groundbased 8 – 13 micron spectroscopy available (cf. Ref. [8]).

Method

We compare the absolute fluxes and relative shapes of the ISOPHOT-S spectra with the groundbased spectroscopy. Note that we compare an aperture size of $24 \times 24\,\mathrm{arcsec}^2$ for ISOPHOT-S with 5 arcsec aperture size of the groundbased measurements. We expect therefore, that the ISOPHOT-S flux is higher, since it contains a larger fraction of the galaxies. The galaxies are active galaxies with strong line emission. Due to the mixture of emission regions the relative line ratios may be different.

Results

Figs. 8.11 and 8.12 shows the comparison of the final OLP 9 product (OLP 9.01) with OLP 8 and OLP 9.0b6 displaying the software problem as documented in SPR-3382 which introduces strong glitch artifacts and which wass noticed when analyzing the spectra of these galaxies.
As expected, in the OLP 9 version the continuum level is higher than for the smaller aperture size groundbased spectrum. NGC 253, being a starburst galaxies shows PAH features already in the small groundbased aperture, which come more prominently out in the ISOPHOT-S aperture. Circinus, containing an AGN, displays only a featureless spectrum in the small aperture, but again prominent PAH features in the ISOPHOT-S aperture. With regard to OLP 8 results, the continuum level and the peak fluxes are slightly increased, being a consequence of the transient correction, for Circinus the spectral shape in the SS range changes considerably.
Due to the different beams no quanitative asessment of calibration accuracies is possible.

Conclusions

- The comparison of ISOPHOT-S spectra of galaxies with groundbased 8 - 13 micron spectroscopy shows reasonable consistency, having in mind the different beam sizes on these active galaxies providing different mixture of activity areas.
- These test cases demonstrate well the fix of SPR-3382.

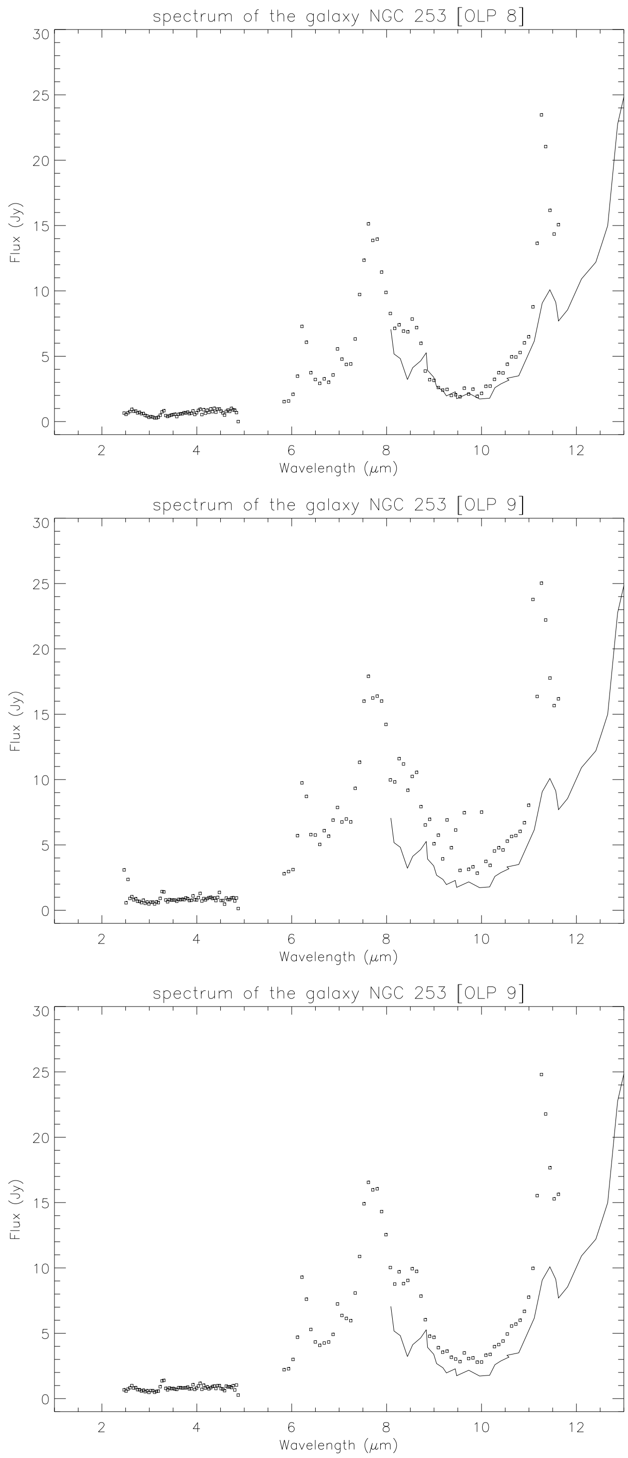

Figure 8.11: Comparison of the spectrum of NGC 253 with groundbased 8 - 13 micron spectroscopy for OLP 8.6 (upper panel), OLP 9.0b6 (middle panel) and OLP 9.01 (lower panel).

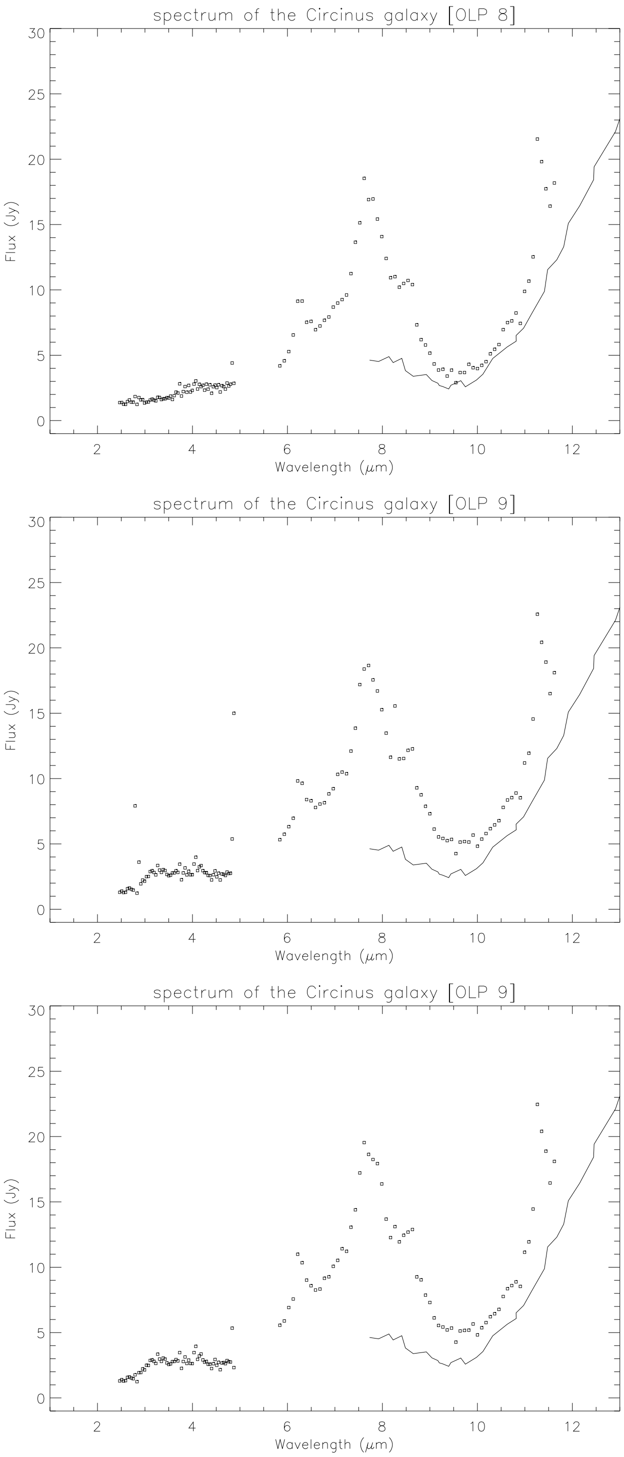

Figure 8.12: Comparison of the spectrum of the Circinus galaxy with groundbased 8 - 13 micron spectroscopy for OLP 8.6 (upper panel), OLP 9.0b6 (middle panel) and OLP 9.01 (lower panel).

8.1.6 MIR Spectra of Planetary Nebulae from Staring PHT-S Measurements

- authors: K. Wilke, U. Klaas
- date: 13-July-2000
- SVP period 2

Motivation

We investigate here the spectra of several Planetary Nebulae. These objects have different SED shapes than the standard stars from which the dynamic PHT-S spectral response function was derived. Some objects have very strong ionic lines, others show a pronounced continuum. The is groundbased 8 – 13 micron (cf. Refs. [34], [35], [36]) and IRAS LRS (cf. Ref. [37]) available.

Method

We compare the absolute fluxes and relative shapes of the ISOPHOT-S spectra with the groundbased spectroscopy. Note that we compare an aperture size of $24 \times 24\,\mathrm{arcsec}^2$ for ISOPHOT-S with 5 arcsec aperture size of the groundbased measurements. We expect therefore, that the ISOPHOT-S flux is higher, if the PN is not compact. We can also compare ratios of the line peak fluxes.

Results

Figs. 8.13 and 8.14 show two PNs with strong silicate emission features. The OLP 9 spectrum of HB 12 is now in good consistency with the groundbased spectrum with regard to continuum level and features. The same is true for VY 2-2 where now the relative shape in the $8 - 10\,\mu$m region looks more consistent with the reference spectra.
NGC 6572 (fig. 8.15) shows strong emission lines. The ratio of the [SIV]$10.51\,\mu$m / [ArIII]$8.99\,\mu$m lines is ~ 2.5 for both the groundbased and ISOPHOT-S OLP 9 spectrum. The raising continuum of the ISOPHOT-S spectrum, in line with the IRAS LRS spectrum indicates extended emission (then, in principle the point source calibration is not applicable).
For NGC 5315 (fig. 8.16) now the PAH features come out more clearly and the emission lines have become sharper. The read-out timing of the SS channel was not matched to the incoming flux, so that this part suffers from digitization noise and is not very reliable.
The match of the compact PN IC 4997 with the groundbased spectrum is now quite good, in particular the shape of the spectrum in the short wavelength part of SL has become shallower. The signals in the SS channel reflect detector noise.
For BD+30 3639 we have two spectra (figs. 8.18 and 8.19). The reproducibility of the continuum level and the peaks of the PAH features is quite good (the [ArII]$6.99\,\mu$m line shows a slightly larger discrepancy, but that may be due to the fact that the line is centered in one pixel for spectrum 2, but appears broader due to location inbetween 2 pixels in spectrum 1.). The source is clearly extended. Spectrum 2 had a less well matching of the read-out timing for the SS channel. Previously, in OLP 8, this resulted in negative signals and stop of processing (values set all to zero), while the new calibration method recovers this part of the spectrum, but somewhat more noise than for spectrum 1.

Conclusions

- The comparison of ISOPHOT-S spectra of galaxies with groundbased 8 - 13 micron spectroscopy shows reasonable consistency, having in mind the different beam sizes on these partly extended objects.

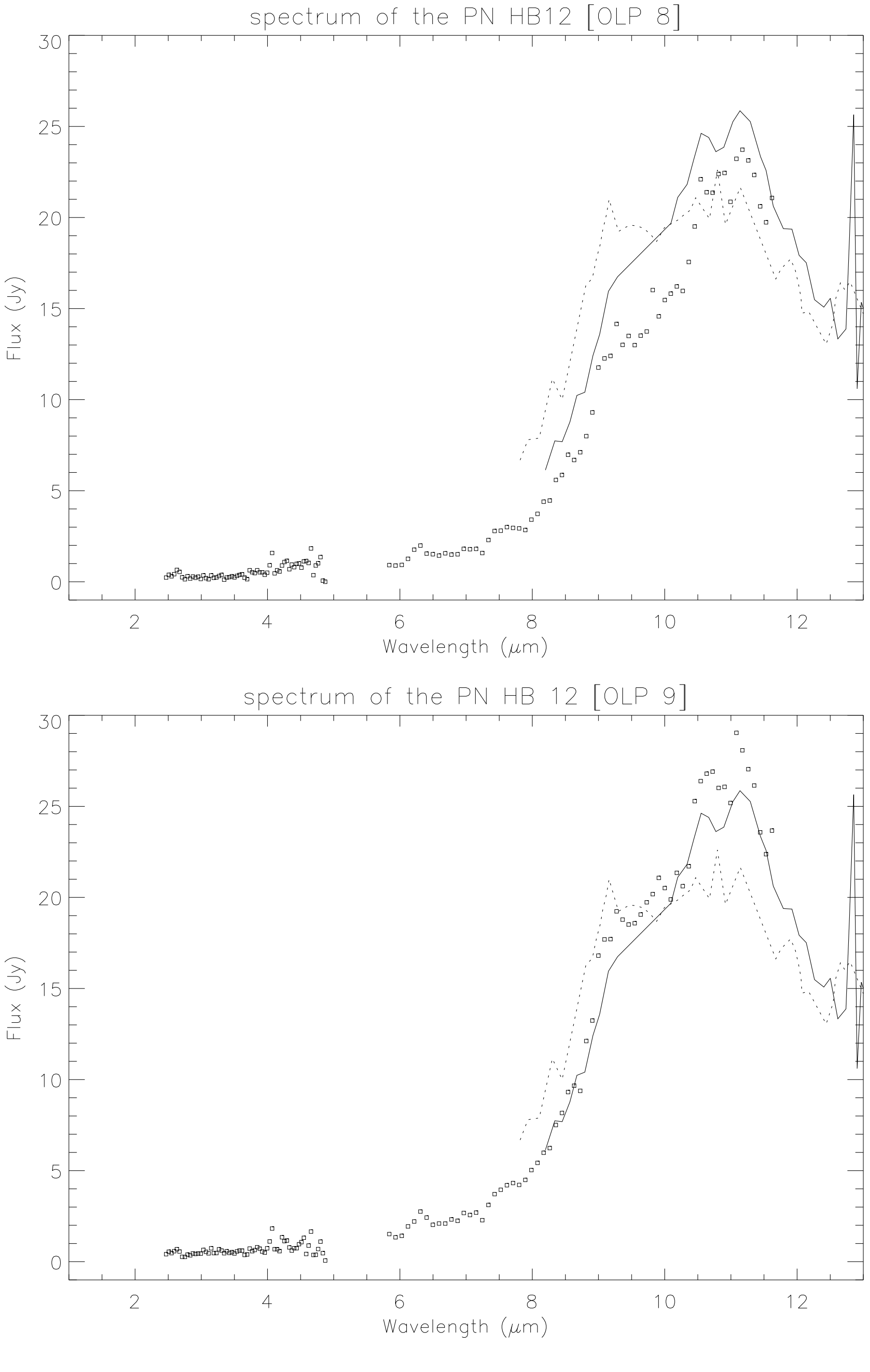

Figure 8.13: Comparison of the spectrum of HB 12 with groundbased 8 - 13 micron spectroscopy (solid line) and IRAS LRS spectroscopy (dashed line) for OLP 8.6 (upper panel) and OLP 9.01 (lower panel).

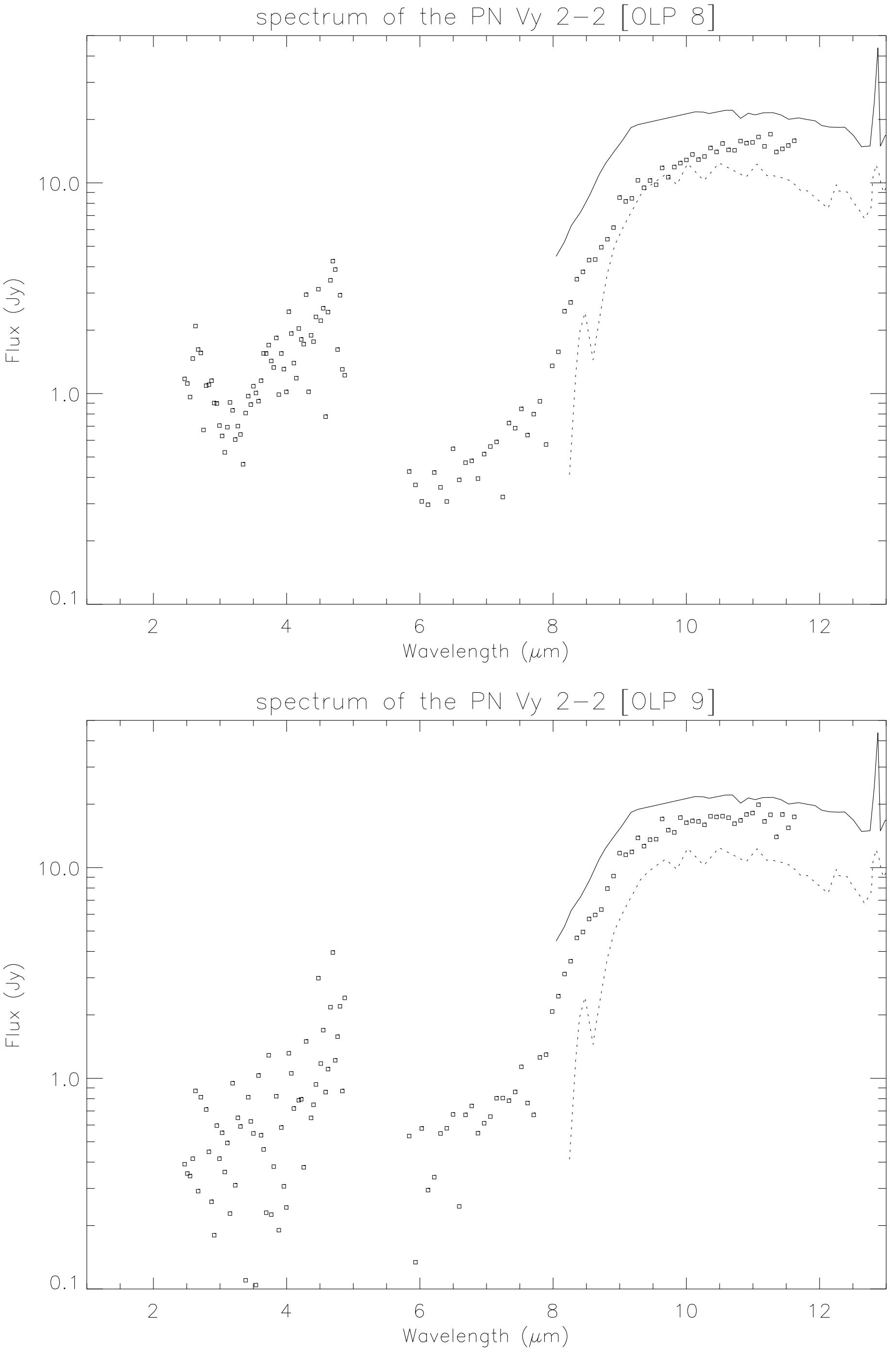

Figure 8.14: Comparison of the spectrum of VY 2-2 with groundbased 8 - 13 micron spectroscopy (solid line) and IRAS LRS spectroscopy (dashed line) for OLP 8.6 (upper panel) and OLP 9.01 (lower panel).

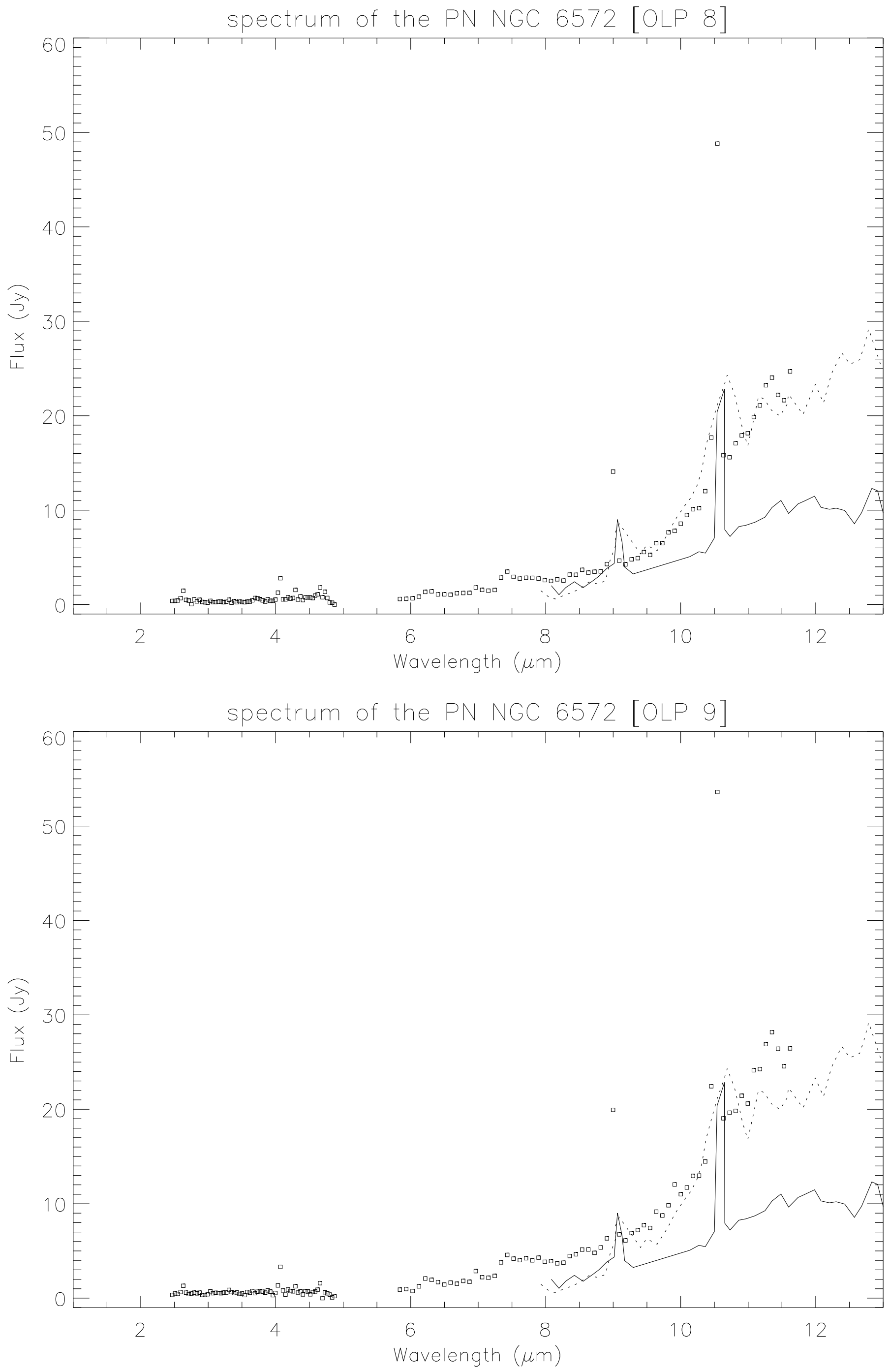

Figure 8.15: Comparison of the spectrum of NGC 6572 with groundbased 8 - 13 micron spectroscopy (solid line) and IRAS LRS spectroscopy (dashed line) for OLP 8.6 (upper panel) and OLP 9.01 (lower panel).

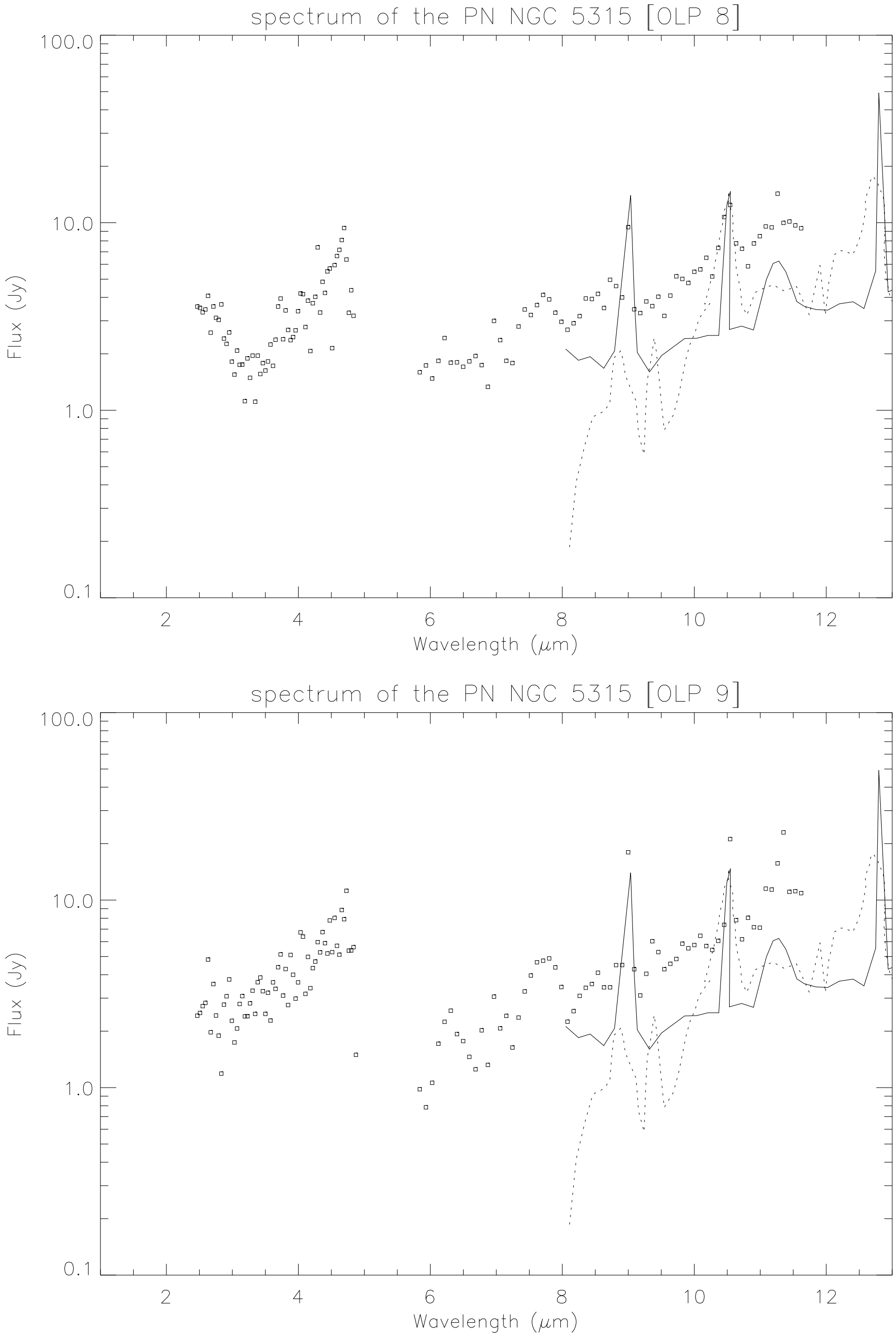

Figure 8.16: Comparison of the spectrum of NGC 5315 with groundbased 8 - 13 micron spectroscopy (solid line) and IRAS LRS spectroscopy (dashed line) for OLP 8.6 (upper panel) and OLP 9.01 (lower panel).

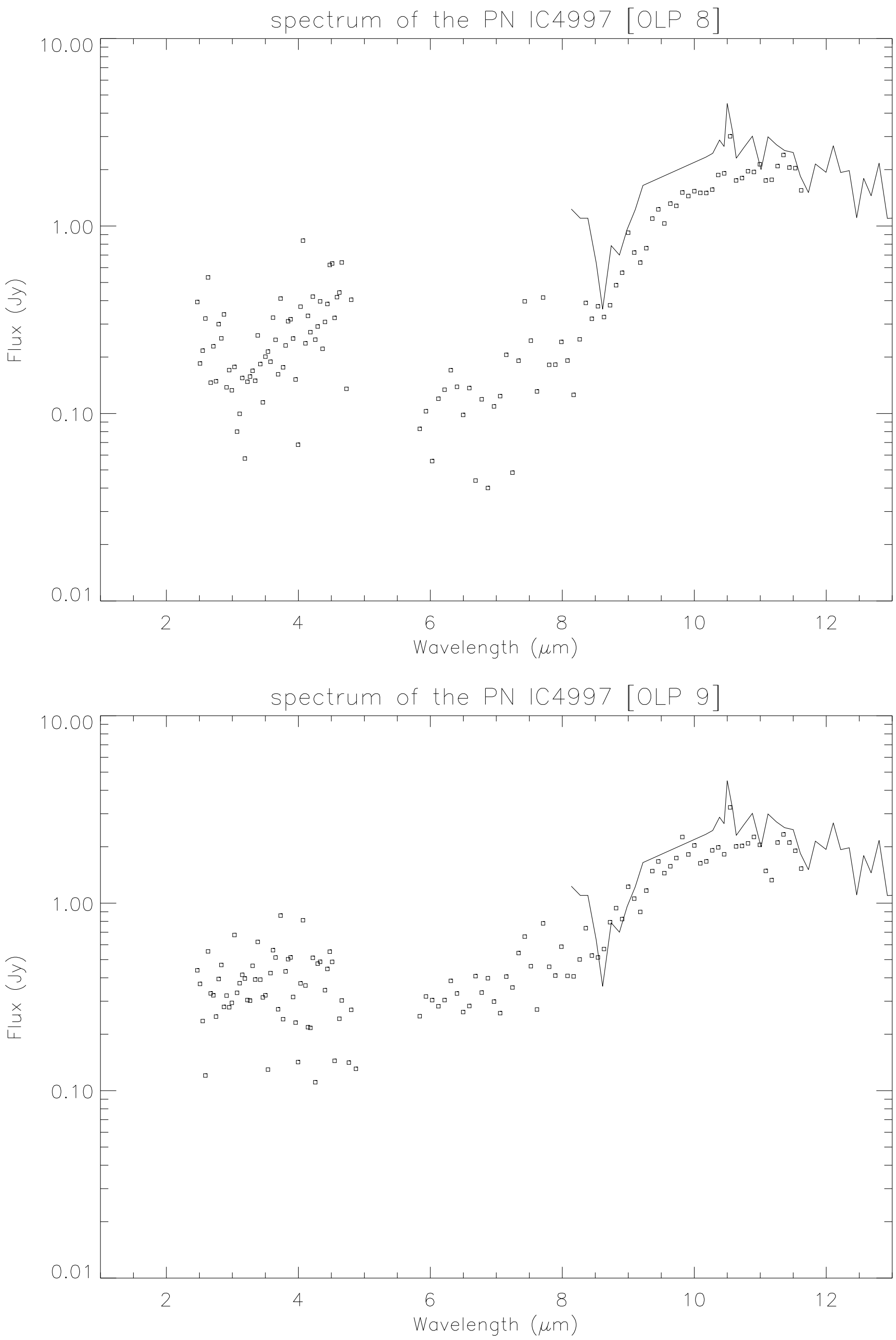

Figure 8.17: Comparison of the spectrum of IC 4997 with groundbased 8 - 13 micron spectroscopy (solid line) for OLP 8.6 (upper panel) and OLP 9.01 (lower panel).

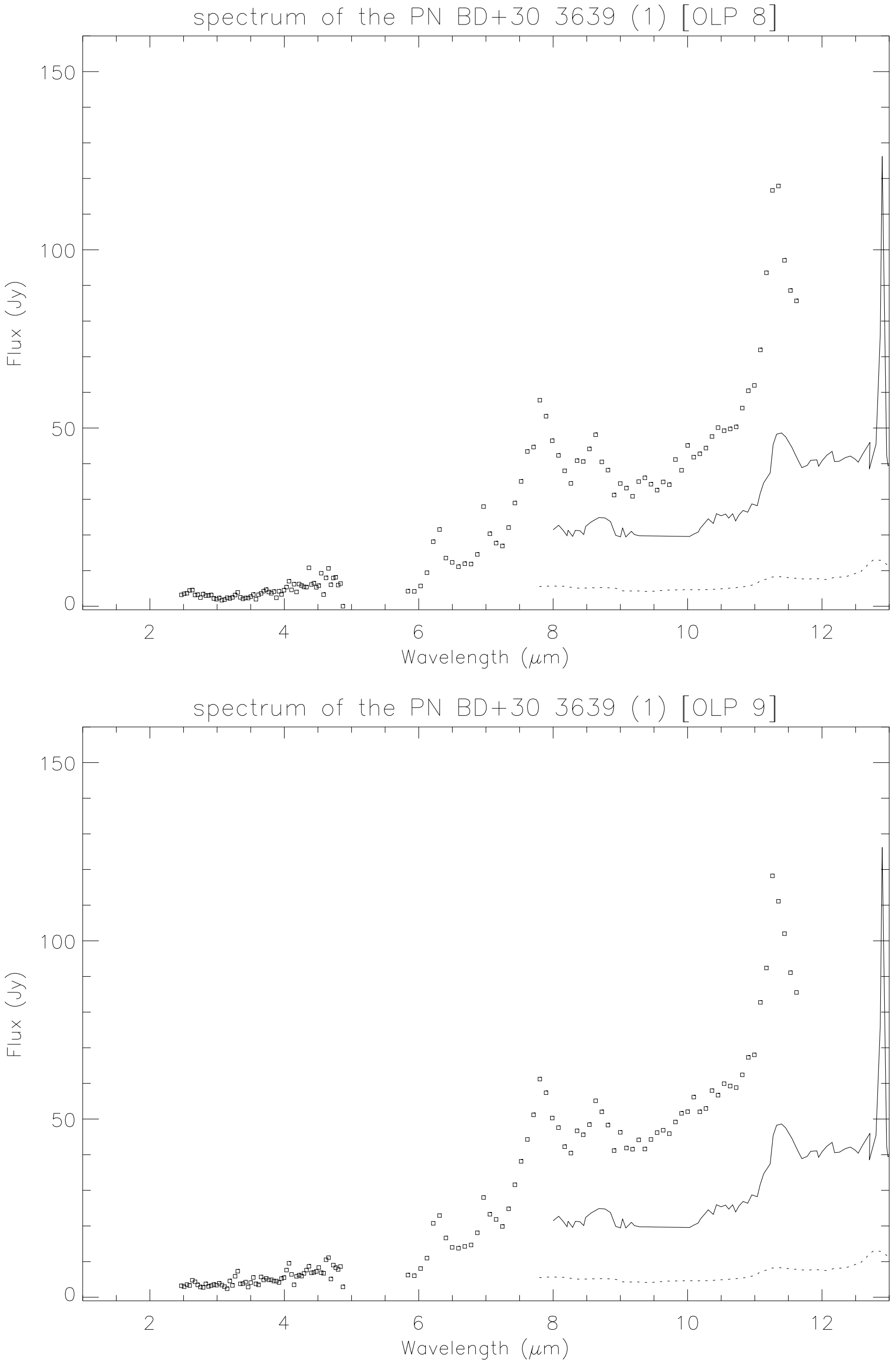

Figure 8.18: Comparison of the spectrum of BD+30 3639 (1) with groundbased 8 - 13 micron spectroscopy (solid line) and IRAS LRS spectroscopy (dashed line) for OLP 8.6 (upper panel) and OLP 9.01 (lower panel).

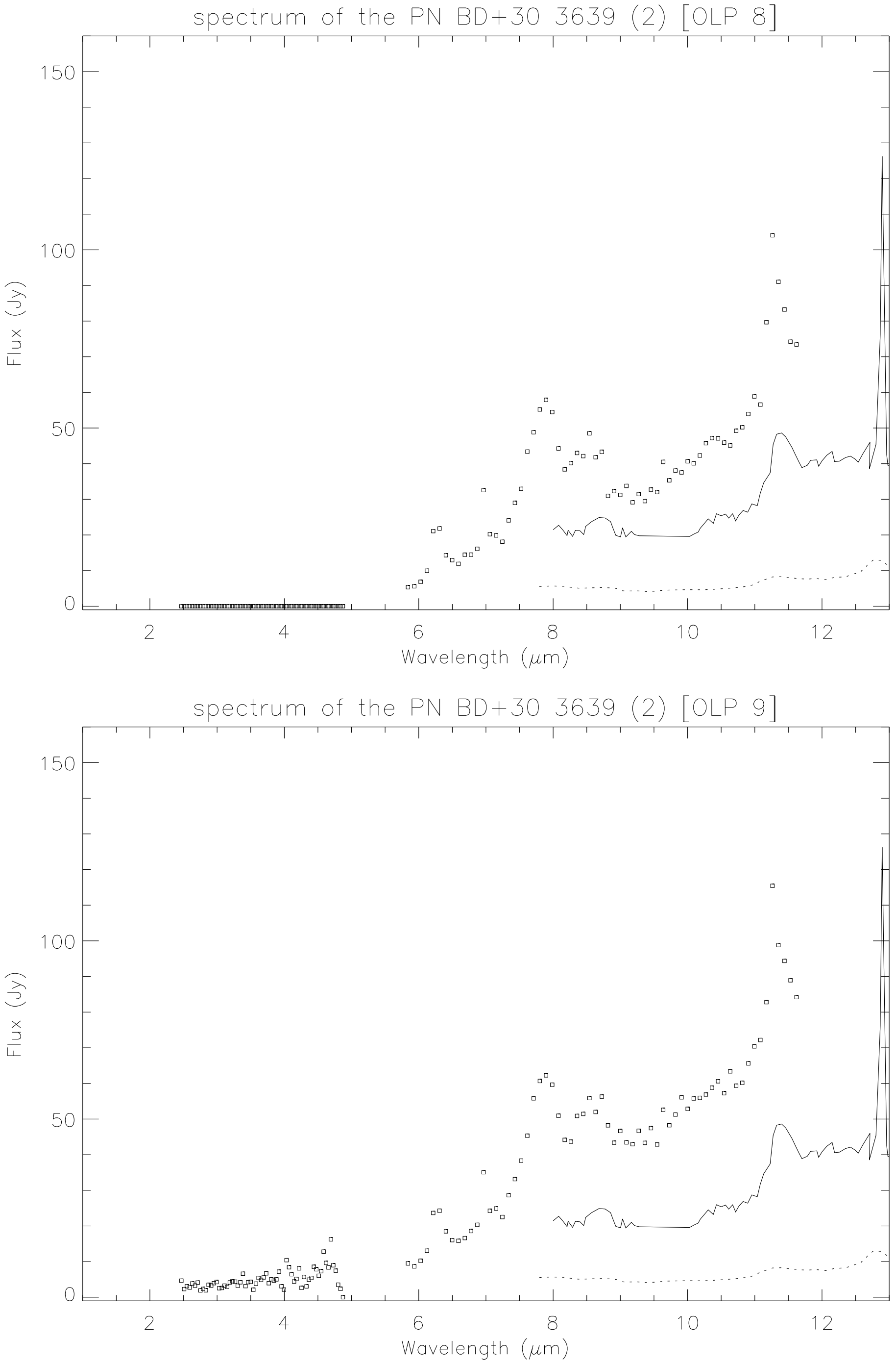

Figure 8.19: Comparison of the spectrum of BD+30 3639 (2) with groundbased 8 - 13 micron spectroscopy (solid line) and IRAS LRS spectroscopy (dashed line) for OLP 8.6 (upper panel) and OLP 9.01 (lower panel).

8.2 Dynamic Spectral Response Function for ISOPHOT-S Staring Measurements of Extended Sources

An overview of the test cases is outlined in Ref. [4], chapter 3.1.2.

8.2.1 References to Calibration Analysis and Software Change Documentation

- calibration report:
  - Dynamic Calibration for ISOPHOT-S [5]
- Software Change Requests: SCREW 425

8.2.2 Summary of Results

- The algorithms and CALG files for dynamic spectral response calibration are successfully implemented for extended sources, too.
- Comparison of spectra of the ZL background with COBE/DIRBE photometry suggest good absolute accuracy, however the statistics is still quite small. For a good S/N spectrum a good accuracy was achieved, suggesting that the 10 % absolute accuracy holds down to this low flux level. Spectra of less good S/N seem to achieve at least better than 50 %. This is valid only for the SL range. In the SS range the ZL is too faint (cosmological window!) to be detected, and it shows only detector noise for the ZL background spectra.
- The SCREW-425 implementation has maintained the processing of PHT-S raster maps. For these still the static default response function calibration applies, hence some transient related features like the "absorption feature" at $\sim 3\,\mu$m are still present. There is some difference between the OLP 8 and the OLP 9 spectra which is explained by the discarding of the first NDRs per ramp introduced for OLP 9 with the SPR-3270 fix.

8.2.3 ISOPHOT-S Spectroscopy of the Extended HII Region M17

- authors: K. Wilke, U. Klaas
- date: 13-July-2000
- SVP period 2

Motivation

M17, a bright HII region in combination with a Molecular Cloud, is a good example exhibiting pronounced PAH features in combination with narrow ionic lines. The extended source has been observed at several positions with ISO-SWS and been mapped by ISOCAM-CVF.

Method

We compare the ISOPHOT-S extended source spectrum of both OLP V8.6b1 and OLP V9.0b1 in $W/m^2/\mu m/sr$ with the ISO-SWS spectrum by Verstraete et al. [16], fig. 2 therein, and the ISOCAM-CVF spectra by Cesarsky et al. [17], fig. 2 therein, both converted to the above unit. It has to be emphasized that the position of the ISOPHOT-S spectrum does not coincide either with one of the positions along the scan as presenetd by Verstrate et al. nor with the three spectra displayed from the CAM-CVF map by Cesarsky et al. The position of the ISOPHOT-S spectrum lies somewhat south of the scan performed with SWS and south-east of the connecting line between positions 1 and 3 of the CAM-CVF spectra. It should, however, be possible to construct the spectrum from the CAM-CVF map at the ISOPHOT-S position. Therefore, the comparison of abolute levels and also relative feature strength is rather limited in such a complex object as M17 and we will restrict our analysis to qualitative comparison. It should be noted that no background subtraction was performed for the ISOPHOT-S measurement, as is the case for the other spectra.

Results

Figs. 8.20 to 8.25 show the comparison of the PHT-S spectrum with CAM and SWS spectra of various regions inside M17. There is not much difference between OLP 8 and OLP 9 results. The largest change appears in the $3\,\mu m$ area where the kink is not so pronounced any more. Furthermore the spectrum has become somewhat shallower.
As already pointed out in the previous report [1], it is difficult to intercompare the spectra due to different pointings and aperture sizes, hence resulting in a different mixture of HII region and molecular cloud areas, which can be seen from different strength of ionic lines, PAH features and continuum.

Conclusions

- The new calibration method maintains more or less the overall spectral shape and straightens it slightly.
- Due to different pointings and aperture sizes no quantitative assessment of calibration accuracies is possible for this highly heterogeneous object.

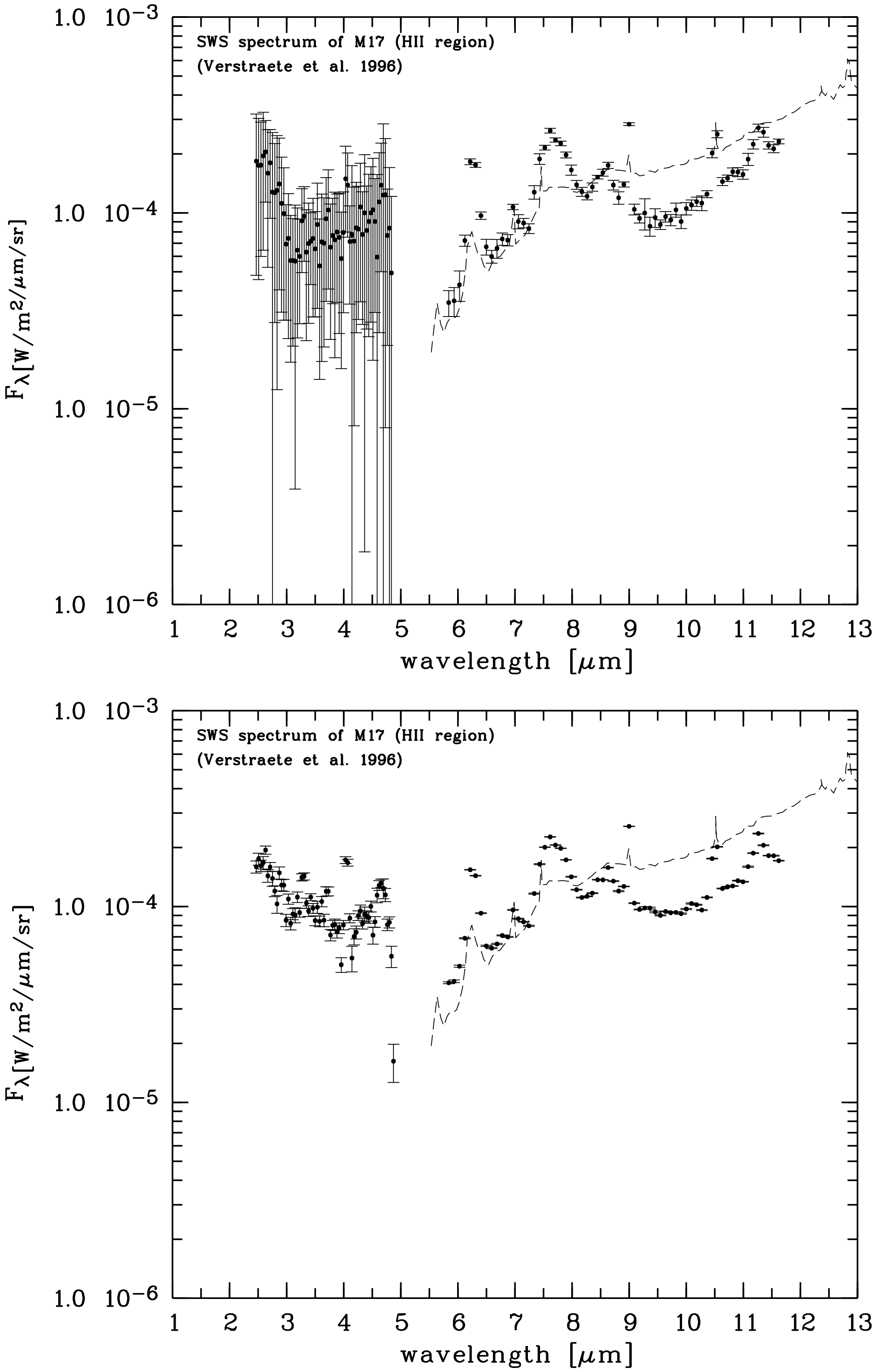

Figure 8.20: Comparison of the ISOPHOT-S spectrum of M17 for both OLP 8.6b1 (upper panel) and OLP 9.01 (lower panel) with the HII region spectrum obtained by Verstraete et al. 1996 (figure 2a therein).

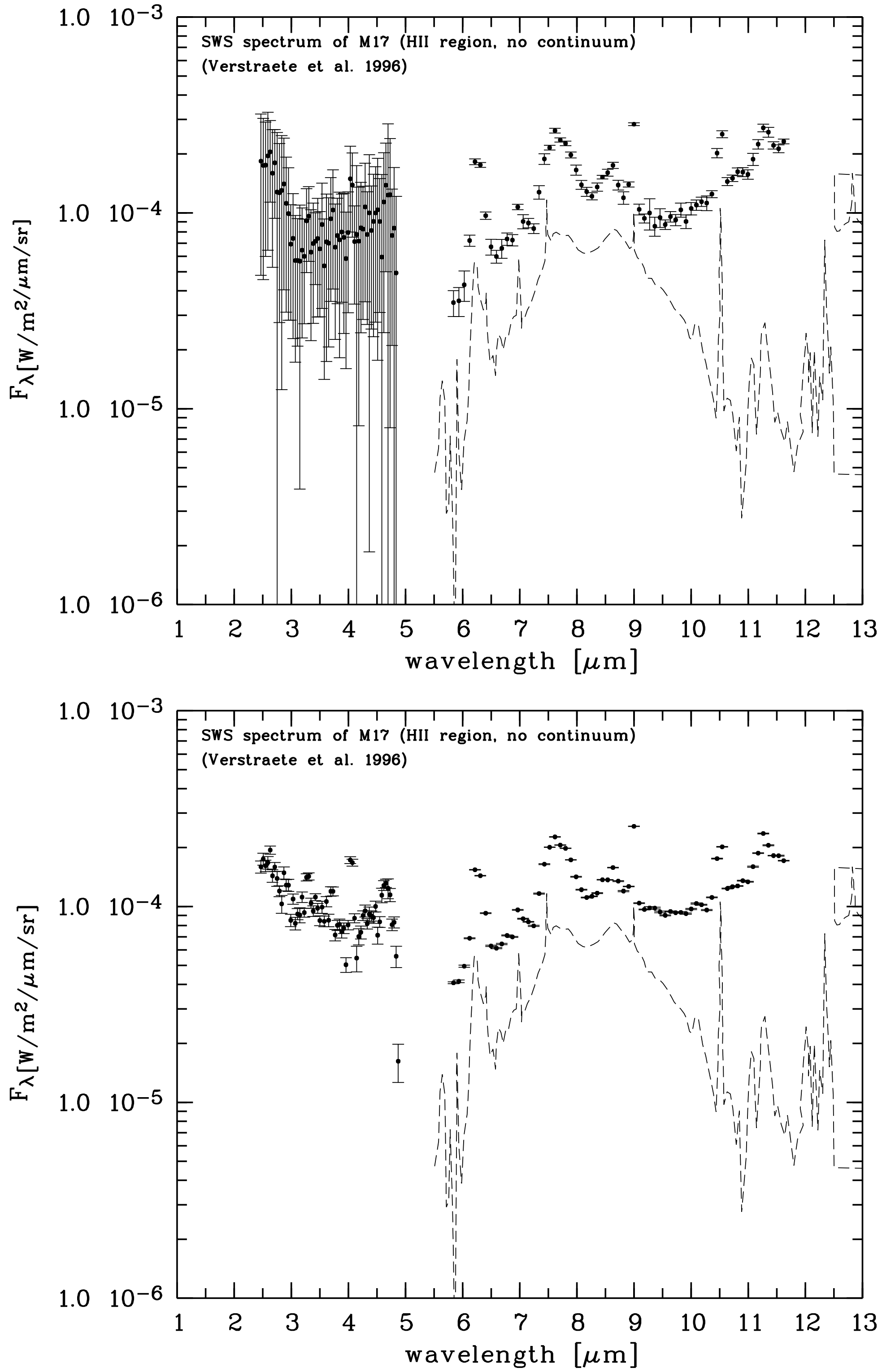

Figure 8.21: Comparison of the ISOPHOT-S spectrum of M17 for both OLP 8.6b1 (upper panel) and OLP 9.01 (lower panel) with the HII region spectrum with no continuum presented by Verstraete et al. 1996 (figure 2b therein).

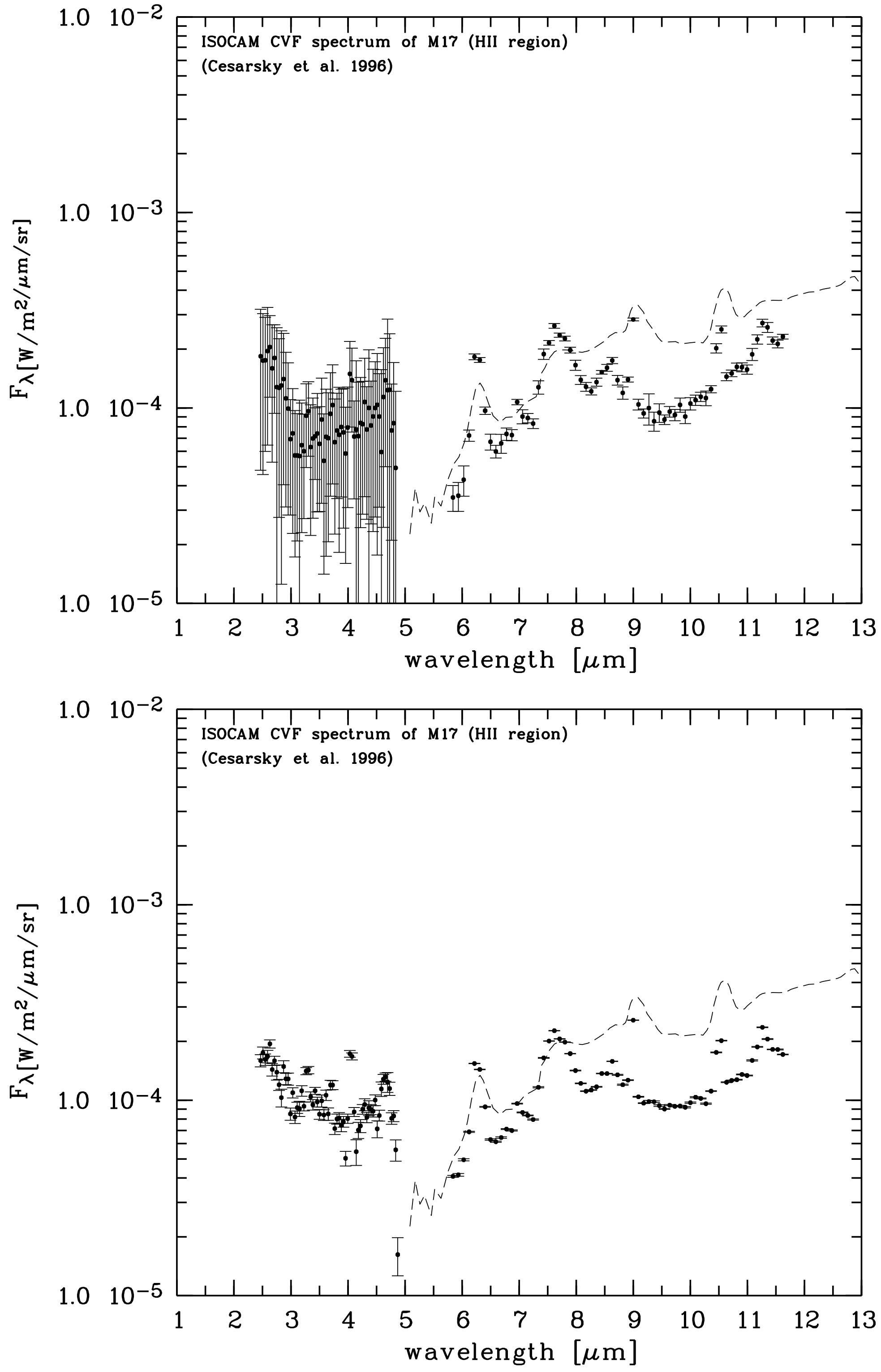

Figure 8.22: Comparison of the ISOPHOT-S spectrum of M17 for both OLP 8.6b1 (upper panel) and OLP 9.01 (lower panel) with the HII region spectrum obtained by Cesarsky et al. 1996 on position 1 (figure 2 therein).

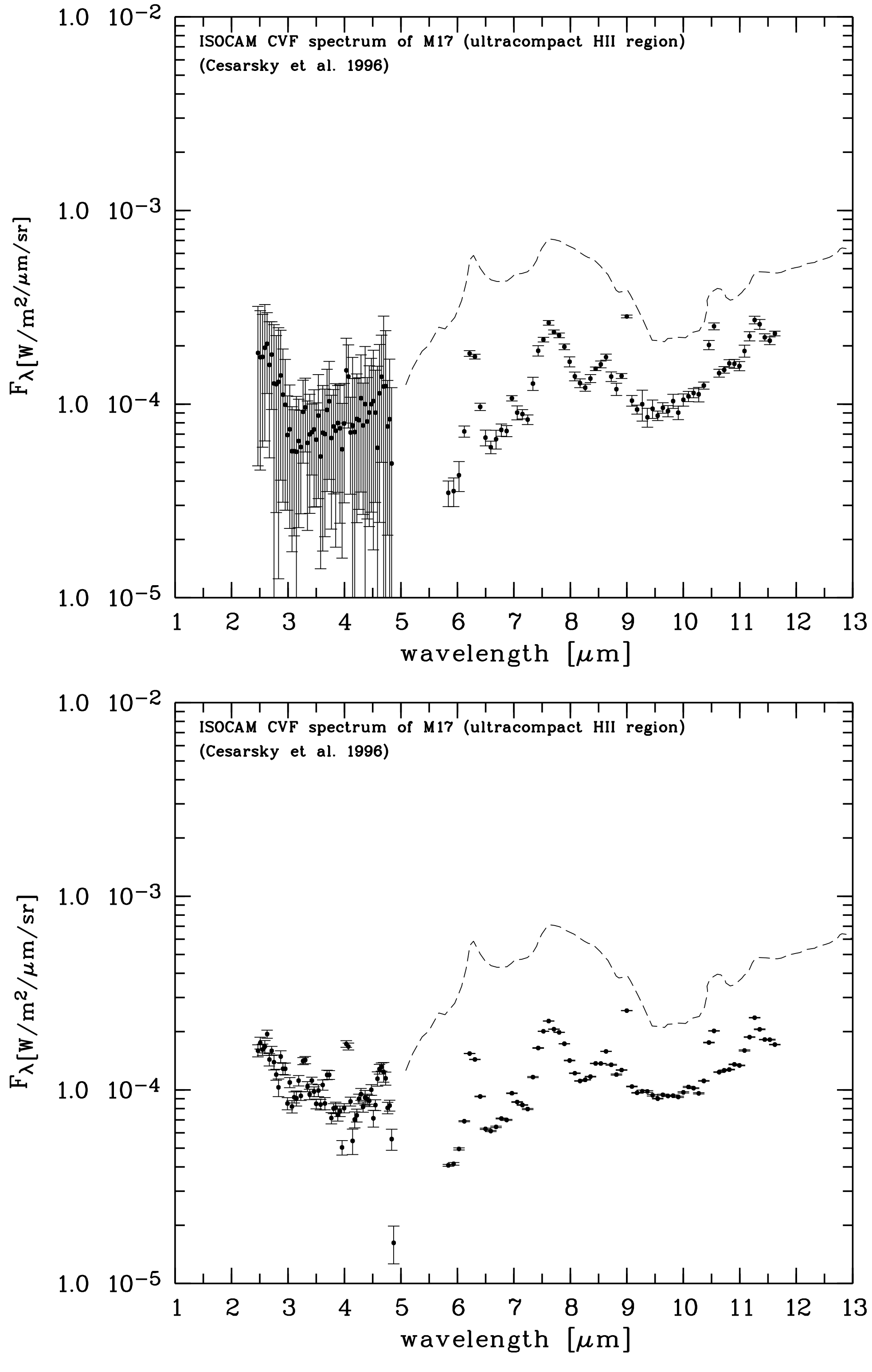

Figure 8.23: Comparison of the ISOPHOT-S spectrum of M17 for both OLP 8.6b1 (upper panel) and OLP 9.0b6 (lower panel) with the ultra-compact HII region spectrum obtained by Cesarsky et al. 1996 on position 2 (figure 2 therein).

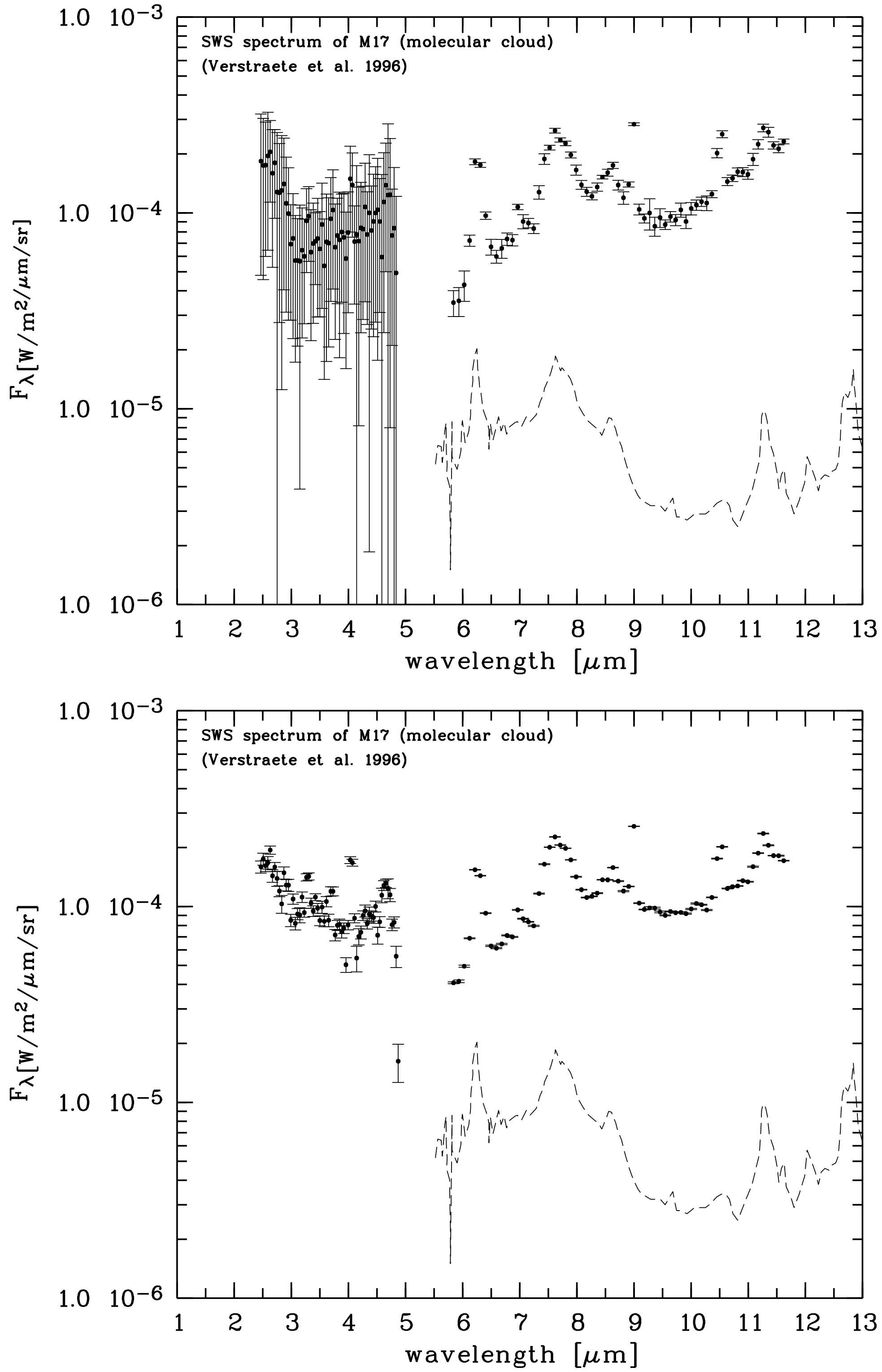

Figure 8.24: Comparison of the ISOPHOT-S spectrum of M17 for both OLP 8.6b1 (upper panel) and OLP 9.01 (lower panel) with the Molecular Cloud spectrum obtained by Verstraete et al. 1996 (figure 2d therein).

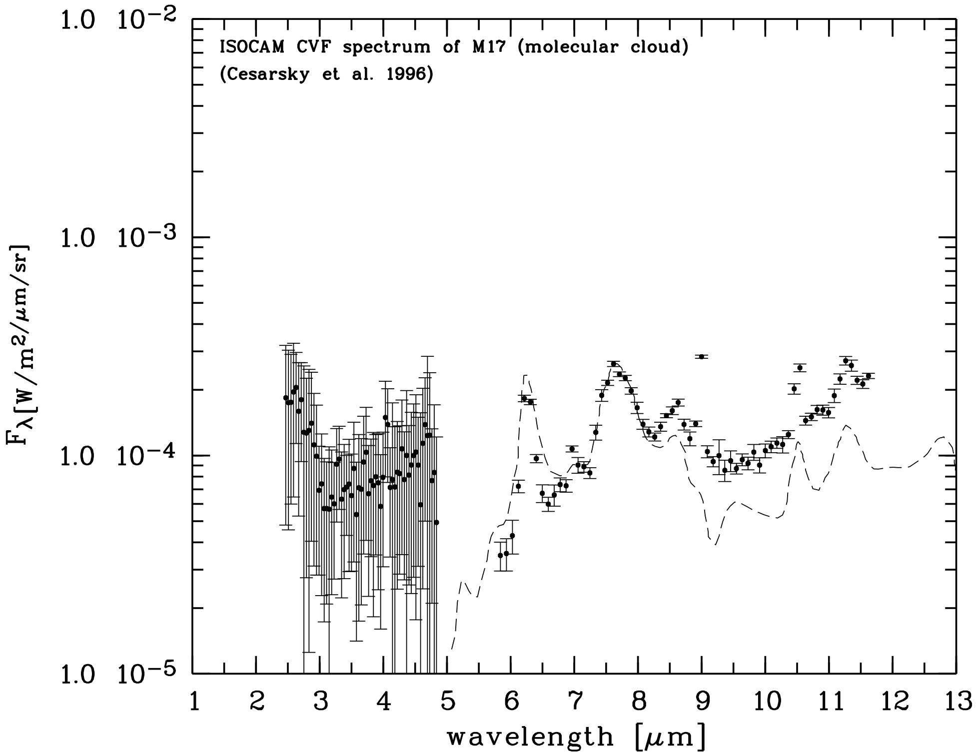

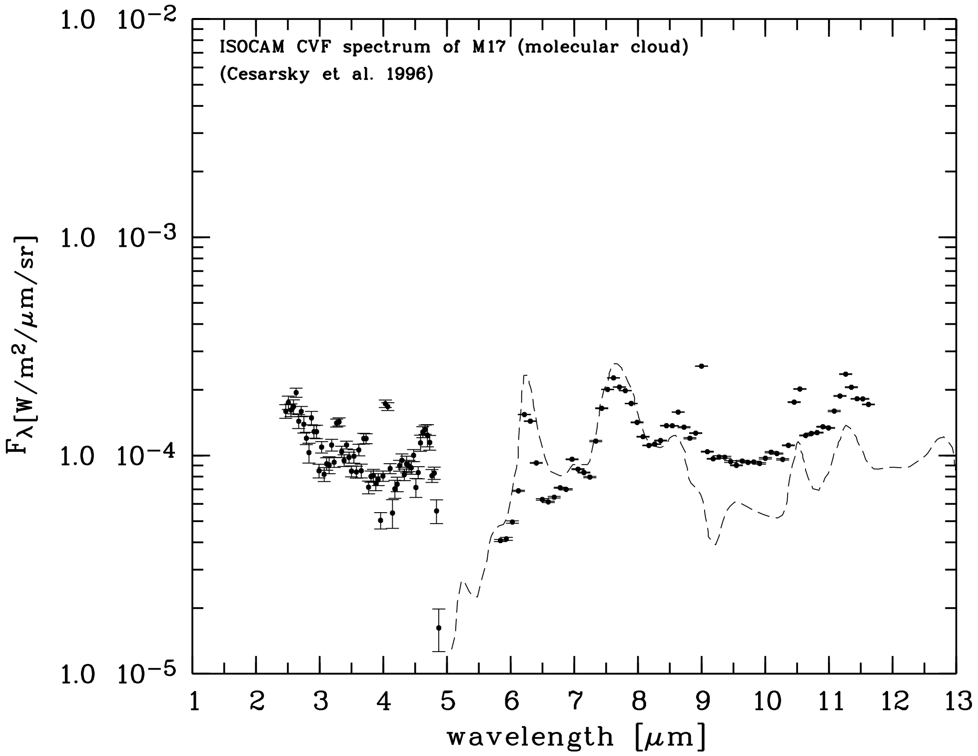

Figure 8.25: Comparison of the ISOPHOT-S spectrum of M17 for both OLP 8.6b1 (upper panel) and OLP 9.01 (lower panel) with the Molecular Cloud spectrum obtained by Cesarsky et al. 1996 on position 3 (figure 2 therein).

8.2.4 Absolute Surface Brightness Spectrum of the Zodiacal Light

- authors: K. Wilke, U. Klaas
- date: 13-July-2000
- SVP period 2

Motivation

The plain Zodiacal Light background can be compared to COBE/DIRBE absolute photometry, as there should be no impact by the very different beam sizes.

Method

We compare the ISOPHOT-S extended source spectrum of the Zodiacal Light from a position in the ecliptic plain at an ecliptic longitude of 66 degrees of both OLP V8.6b1 and OLP V9.01 with the COBE/DIRBE photometry from annnual maps.

Results

Fig. 8.26 shows the comparison of the OLP 8 and OLP 9 spectrum. The OLP 9 spectrum looks slightly smoother. Actually, both spectra fit inbetween the photometric points of COBE/DIRBE at 4.9 and 12 μm. However, the OLP 9 spectrum is flatter, indicating a higher colour temperature. We have still to fit the spectrum with a BB curve to find out the difference in colour temperature.

Conclusions

- For the high quality ZL spectrum a very good absolute calibration accuracy is derived from comparison with COBE/DIRBE photometry. Clarification is still needed with regard to the different colour temperatures derived from OLP 8 and OLP 9 product.

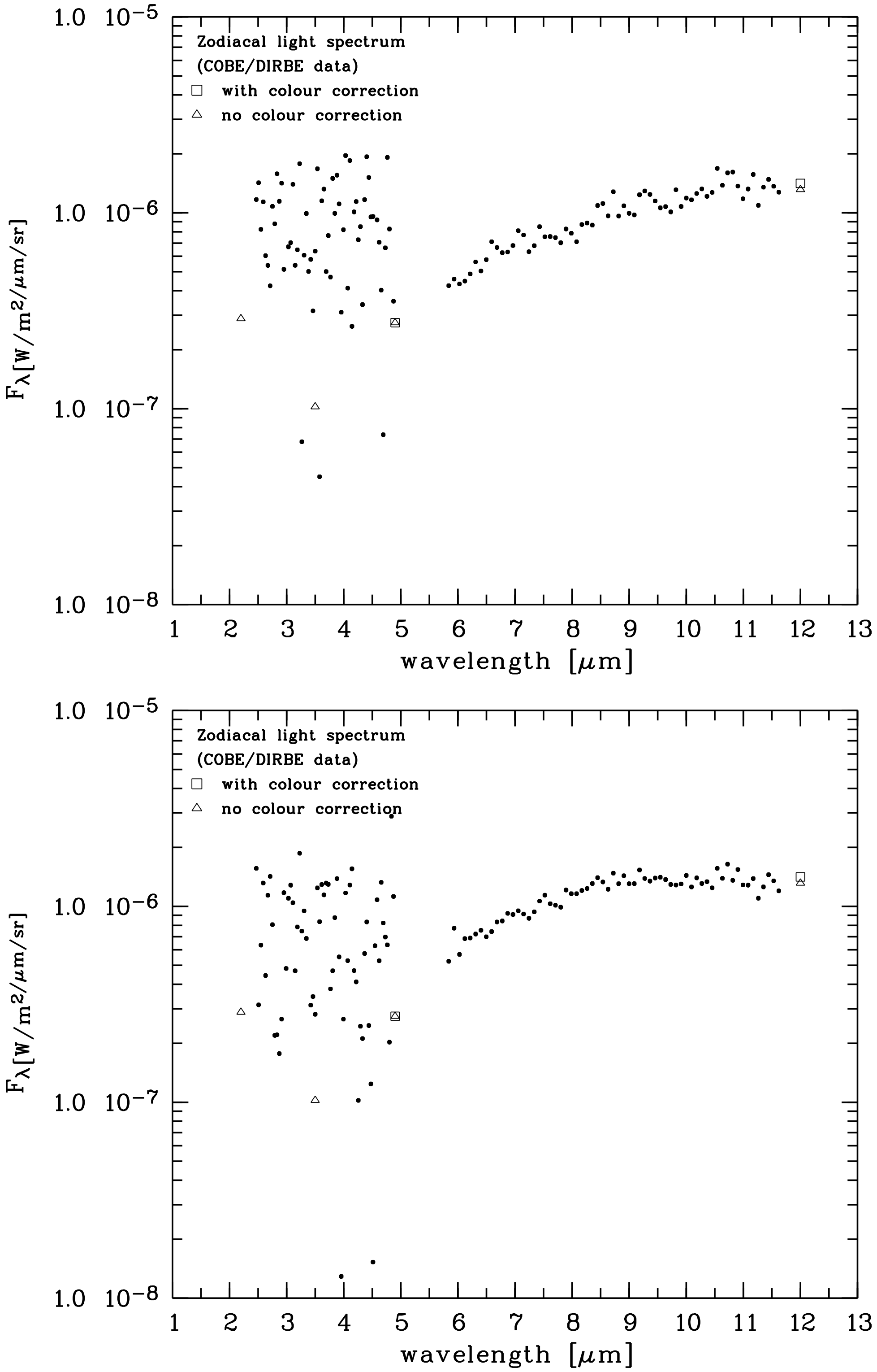

Figure 8.26: Comparison of the ISOPHOT-S spectrum of the Zodiacal Light on a position in the ecliptic plane at minimum ecliptic longitude (close to ISO Sun constraint) for both OLP 8.6b1 (upper panel) and OLP 9.01 (lower panel) with COBE/DIRBE photometry. For colour correction of the COBE/DIRBE data points a 260 K BB has been assumed.

8.2.5 Diffuse Emission of the Galactic Disk

- authors: K. Wilke, U. Klaas
- date: 29-May-2000
- SVP period 2

Motivation

As part of the Central Program spectrophotometry of the UIR bands was performed at various positions along the Galactic plane [23]. Also with IRTS/MIRS spectra of the UIR bands in the diffuse Galactic light were taken [24].

Method

We compare the ISOPHOT-S extended source spectrum of the diffuse Galactic light at the position l = 45 deg and b = 0 deg of both OLP V8.61b1 and OLP V9.0b6 with the IRTS/MIRS result at l = 50 deg (Fig. 1b in [24]).

Results

Fig. 8.27 displays the OLP 8 and OLP 9 results. In essence, nothing has changed, since the static default response function is still applied to this raster observation. There are changes in flux for some individual pixels due to SPR-3270 (w.r.t. discarding of non-destructive read-outs at the beginning of the ramp).
We can therefore not proceed to clarify the discrepancy with the IRTS/MIRS spectrum in the 9 - 11 μm wavelength range, noticed in the previous report (cf.[1]), with regard to checking whether transients in the PHT-S spectrum may play a role.

Conclusions

- The PHT-S raster map results are conserved by SCREW-425 implementation. Some minor modifications of the resulting spectra come from the SPR-3270 fix, now discarding the first NDRs of a ramp according to the requirements.
- No change in calibration accuracy took place, since PHT-S raster map processing has still to use the static default response function.

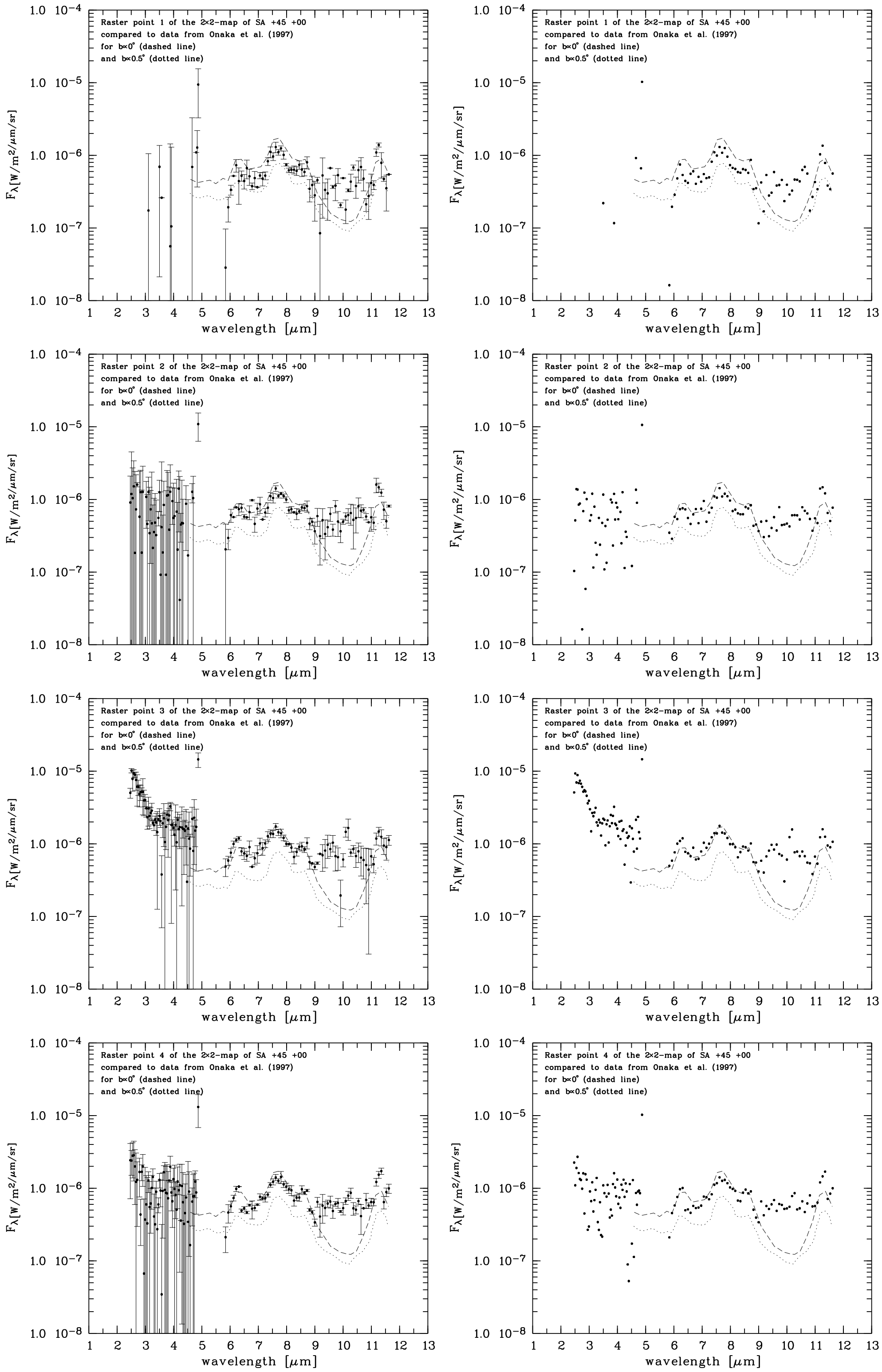

Figure 8.27: Comparison of the ISOPHOT-S spectrum of the diffuse Galactic light at the position l = 45 deg and b = 0 deg from 4 raster positions of a 2x2 raster, with 24 arcesc separation between the raster points (corresponding to the aperture size of ISOPHOT-S), for both OLP 8.6b1 (left panel) and OLP 9.0b6 (right panel) with IRTS/MIRS spectrum for l = 50 deg, b = 0 deg and b = 0.5 deg. Note: In the OLP 9 version uncertainties are not displayed.

8.2.6 Spectrum of the Galactic Centre Source Sgr A West

- authors: K. Wilke, U. Klaas
- date: 13-July-2000
- SVP period 2

Motivation

We compare here the spectra of the same source, namely the bright Galactic Centre source Sgr A West, first taken as single pointing spectrum and calibrated from OLP V9 onwards with the dynamic spectral response function, and secondly being the central position of a 7x7 raster which will be continued to be calibrated with the static default response function, since for rasters the pre-requisiste of a well defined illumination history is not fulfilled and therefore the dynamic response function calibration cannot be applied.

Method

We compare the single pointing spectrum with the raster position 4,4 of the 7x7 raster (25th raster point in the sequence) which coincides with the position of the single pointing. We also compare OLP V8.6 with OLP V9.0. For the single pointing spectrum the static default response function is still applied in OLP V8.6, hence the difference between the two calibration methods for this flux regime becomes visible. For the raster no change is expected between V8.6 and V9.0, since the calibration method remains unchanged here.

Results

Fig. 8.28 shows an intercomparison between single pointing and the central pointing of a raster map and between OLP 8 and OLP 9. The most remarkable change can bee seen in the SS range of the single pointing spectrum from OLP 8 to OLP 9. The deep absorption feature by a moderate ice feature, the spectrum is much flatter in OLP 9. There is a good match between SS and SL range for OLP 9. Also the silicate absorption feature at $10\,\mu$m is not as deep as in the OLP 8 product.
The raster map result shows that due to the preceding illumination the transient effects are not so drastic using the static default response function, the single pointing and the raster spectrum coincide within better than 40 %. Indeed, although the spectral response function calibration, is the same there is some difference between the OLP 8 and OLP 9 raster spectrum, in particular the silicate absorption trough is not so deep in the OLP 9 version. This must be a consequence of discarding the first NDRs of each ramp, introduced by the SPR-3270 fix.

Conclusions

- For the bright Galactic Centre source Sgr A West considerable improvement for the single pointing spectrum, in particular in the SS range, is achieved with the dynamic spectral response method.
- Although the spectral response calibration is unchanged for raster maps, the discarding of the first NDRs per ramp, fixed by the SPR-3270 implementation, noticably changes the shape of the spectrum. There is relatively good agreement of better than 40 % for the spectrum on the central raster point (here the 25th in a sequence guaranteeing an illumination of the detector sufficently in advance) and the dynamically calibrated single pointing spectrum.

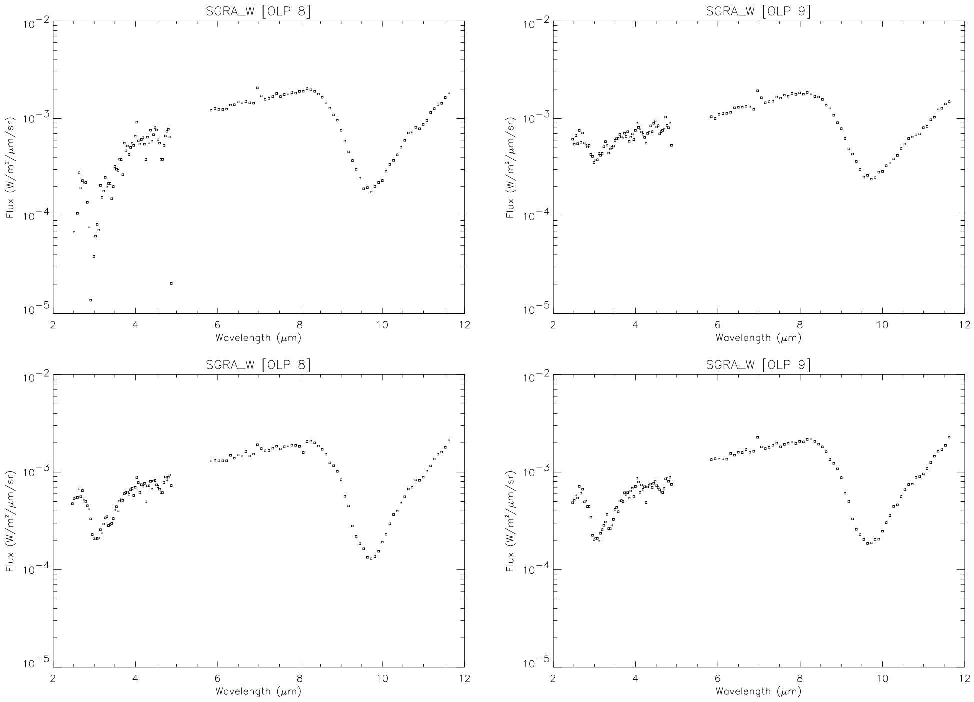

Figure 8.28: Comparison of the ISOPHOT-S spectrum of the Galactic Centre source Sgr A West taken as single pointing spectrum and calibrated with a dynamic spectral response function for OLP 9 (OLP 8 version is calibrated with the static default response function) with the ISOPHOT-S spectrum from a 7x7 raster, centred on the single pointing position (= raster position 4,4) and calibrated with the static default response function for both OLP 8 and 9 versions. Upper left: OLP 8.6b1 single pointing; upper right: OLP 9.01 single pointing; lower left: OLP 8.6b1 raster pointing; lower right: OLP 9.01 raster pointing.

8.3 Verification of no Impact on Chopped PHT-S Measurement Processing by SCREW 425 Implementation

An overview of the test cases is outlined in Ref. [4], chapter 3.1.3. The main purpose of this re-validation is that chopped PHT-S data reduction remains unchanged results. Due to the implementation of the dynamic response function for staring PHT-S measurements also some re-structering of code of the chopped measurement processing, which uses however a different calibration method, was necessary.

8.3.1 References to Calibration Analysis and Software Change Documentation

- calibration report:
  - Calibration of ISOPHOT-S Chopped Measurements [9]
- Software Change Request: SCREW 425

8.3.2 Summary of Results

- The changes to PHT-S chopped mode processing necessary in the context of SCREW 425 for implementation of the dynamic reponse calibration for staring mode measurements (due to the commonality of product types) have been correctly implemented.
- The PHT-S chopped mode remains scientifically valid with the accuracies established for OLP 8 (cf. Scientific Validation Report for this version [1]).

8.3.3 Consistency Check of Chopped PHT-S Relative Spectral Response Function on Calibration Stars

- authors: K. Wilke, U. Klaas
- date: 29-May-2000
- SVP period 2

Motivation

We process measurements of two calibration stars (HR 6817 and HR 6847) which were used to establish the Relative Spectral Response Function (RSRF) for chopped PHT-S measurements and check whether the input model SED is reproduced. Both calibration stars were measured both in rectangular chopped and triangular chopped mode. This allows to assess the consistency of the processing of the two chopper modes.

Method

We compare the results of both OLP 8.6b1 and OLP 9.0b6 with the flux models by Hammersley et al. 1998 [11].

Results

In Figs. 8.29 to 8.32 we perform an individual comparison of both OLP versions with the flux model. One can see that the results are practically identical. Some noticable differences for some pixels are a consequence of the SPR-3270 fix (discarding of first NDRs per ramp).

Conclusions

- The two OLP versions give very similar results; slight changes are expected by the discarding of the first NDRs per ramp according to the SPR-3270 fix. SCREW 425 is successfully implemented with regard to chopped PHT-S observation processing.
- The changes applied to the processing have not altered the validation and the achieved calibration accuracy.

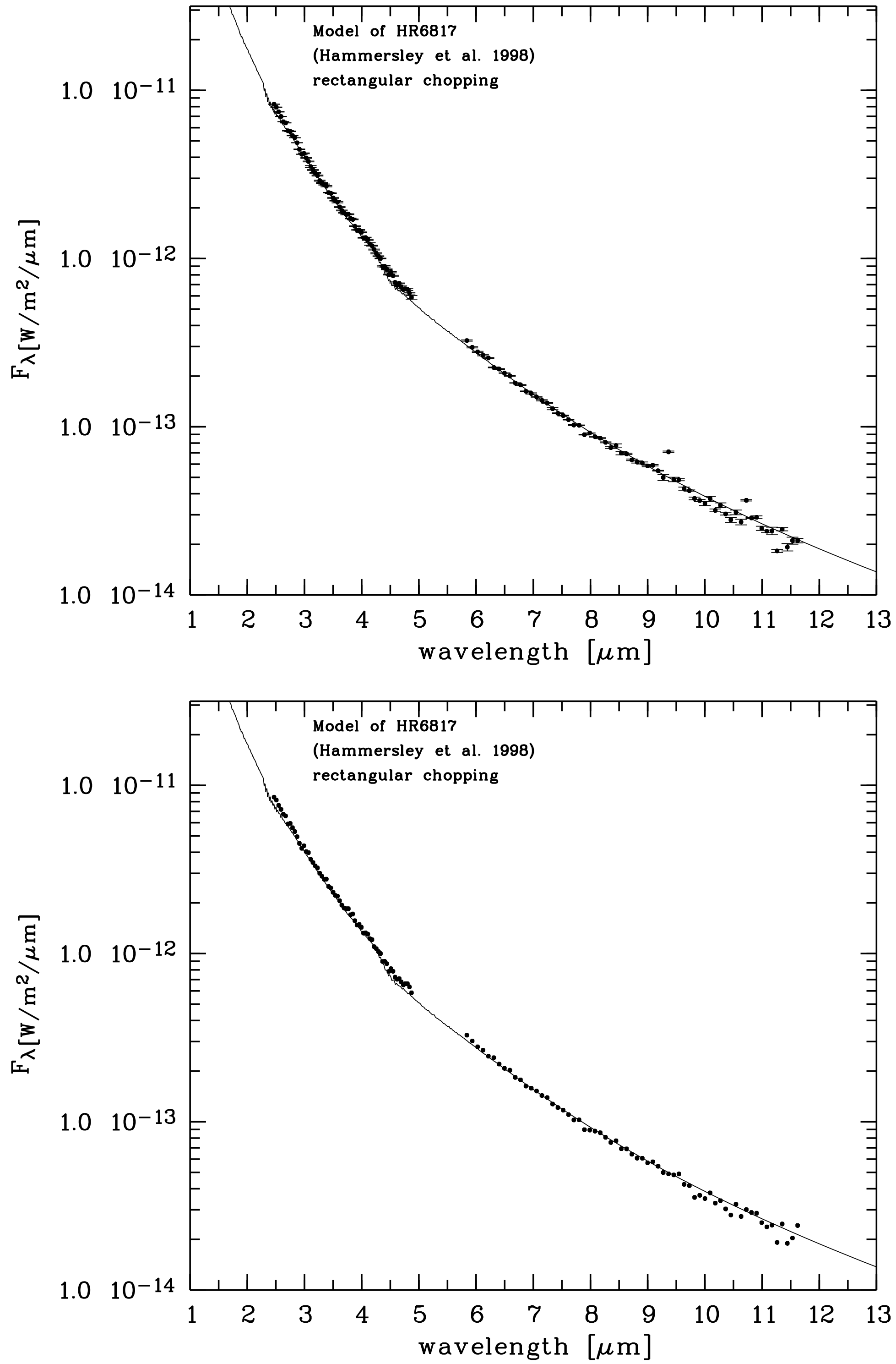

Figure 8.29: Comparison of the spectrum of HR 6817 obtained in PHT-S rectangular chopped mode for both OLP 8.6b1 (upper panel) and OLP 9.0b6 (lower panel) with the flux model by Hammersley et al. 1998.

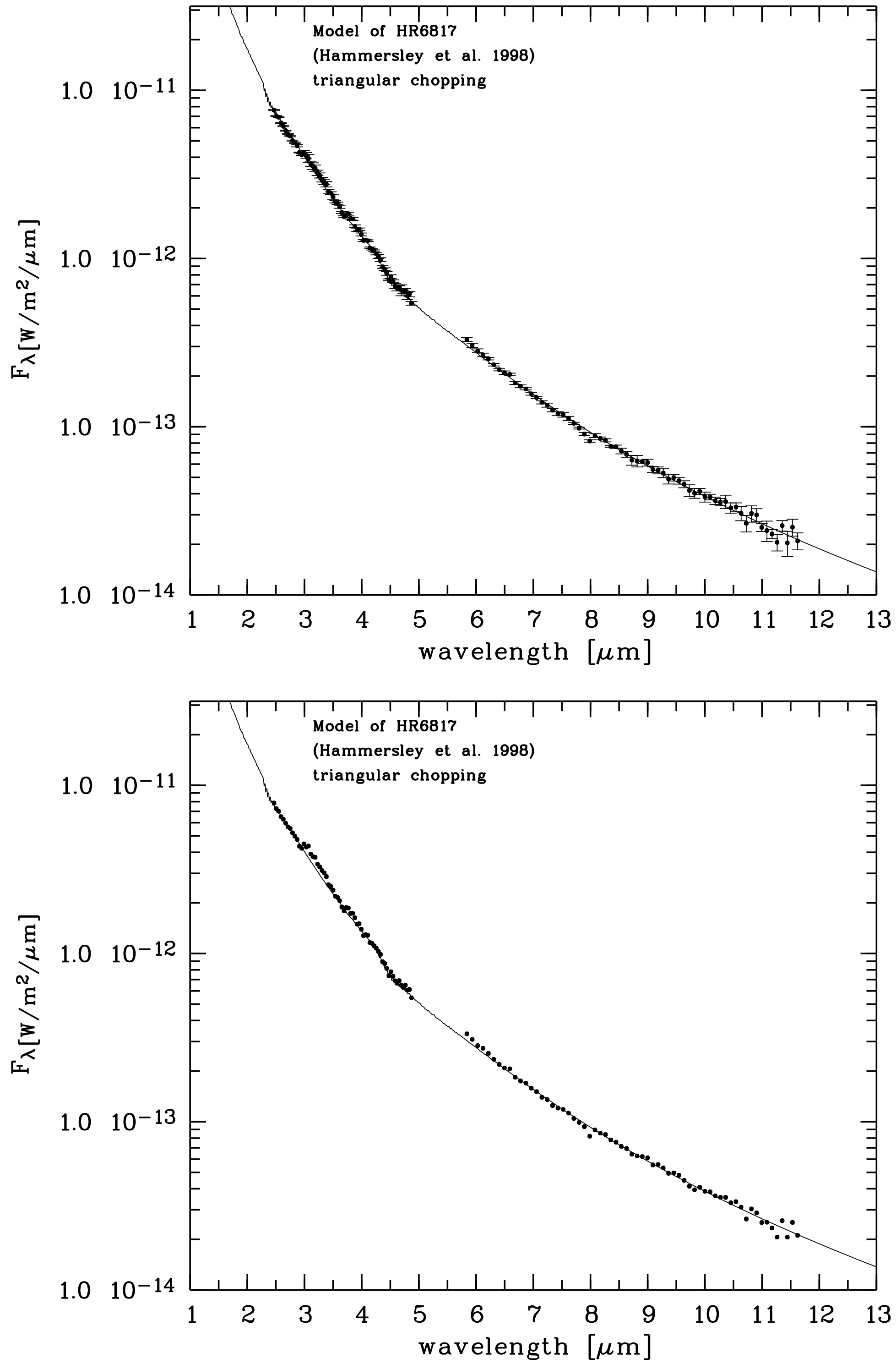

Figure 8.30: Comparison of the spectrum of HR 6817 obtained in PHT-S triangular chopped mode for both OLP 8.6b1 (upper panel) and OLP 9.0b6 (lower panel) with the flux model by Hammersley et al. 1998.

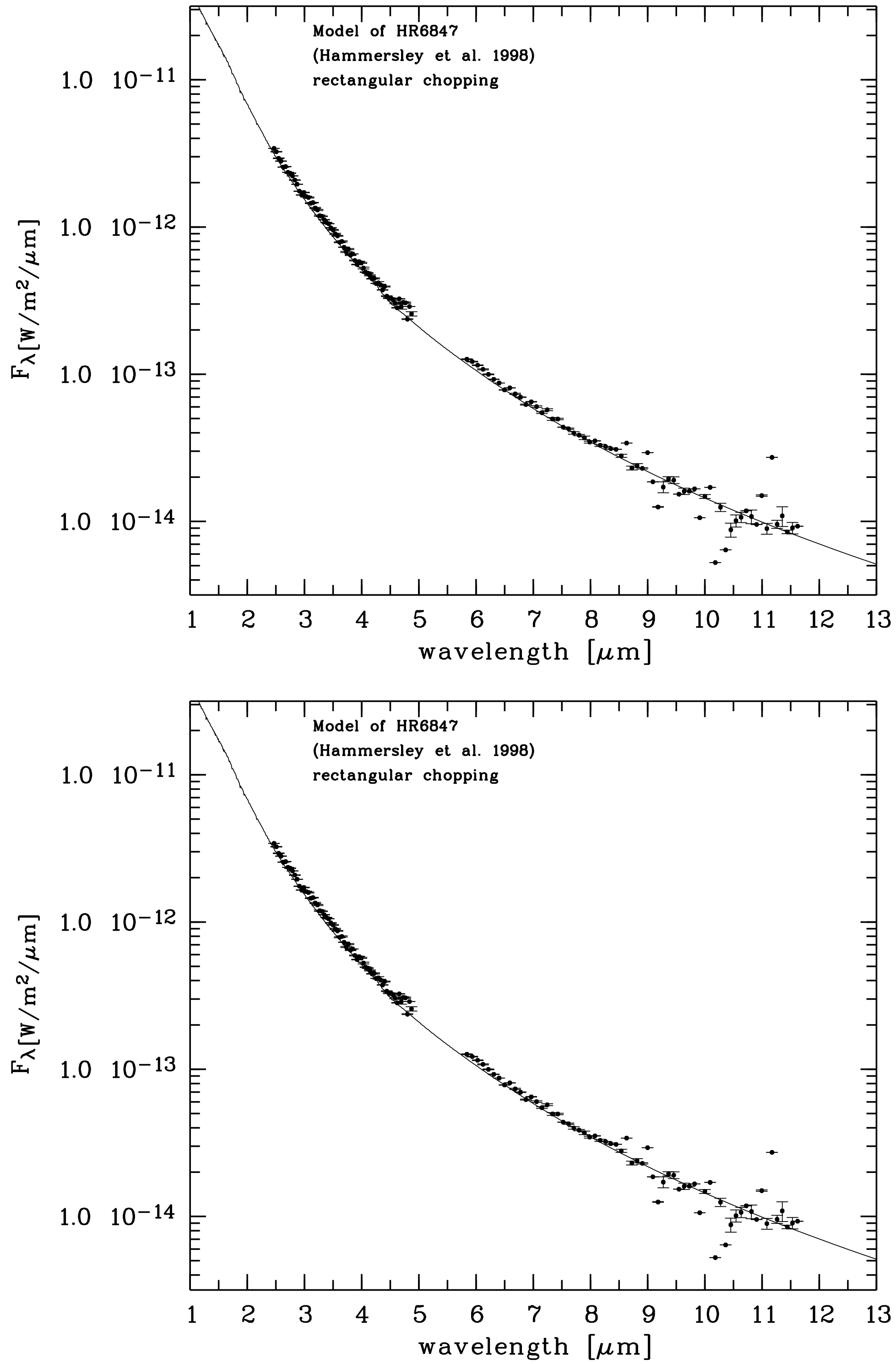

Figure 8.31: Comparison of the spectrum of HR 6847 obtained in PHT-S rectangular chopped mode for both OLP 8.6b1 (upper panel) and OLP 9.0b6 (lower panel) with the flux model by Hammersley et al. 1998.

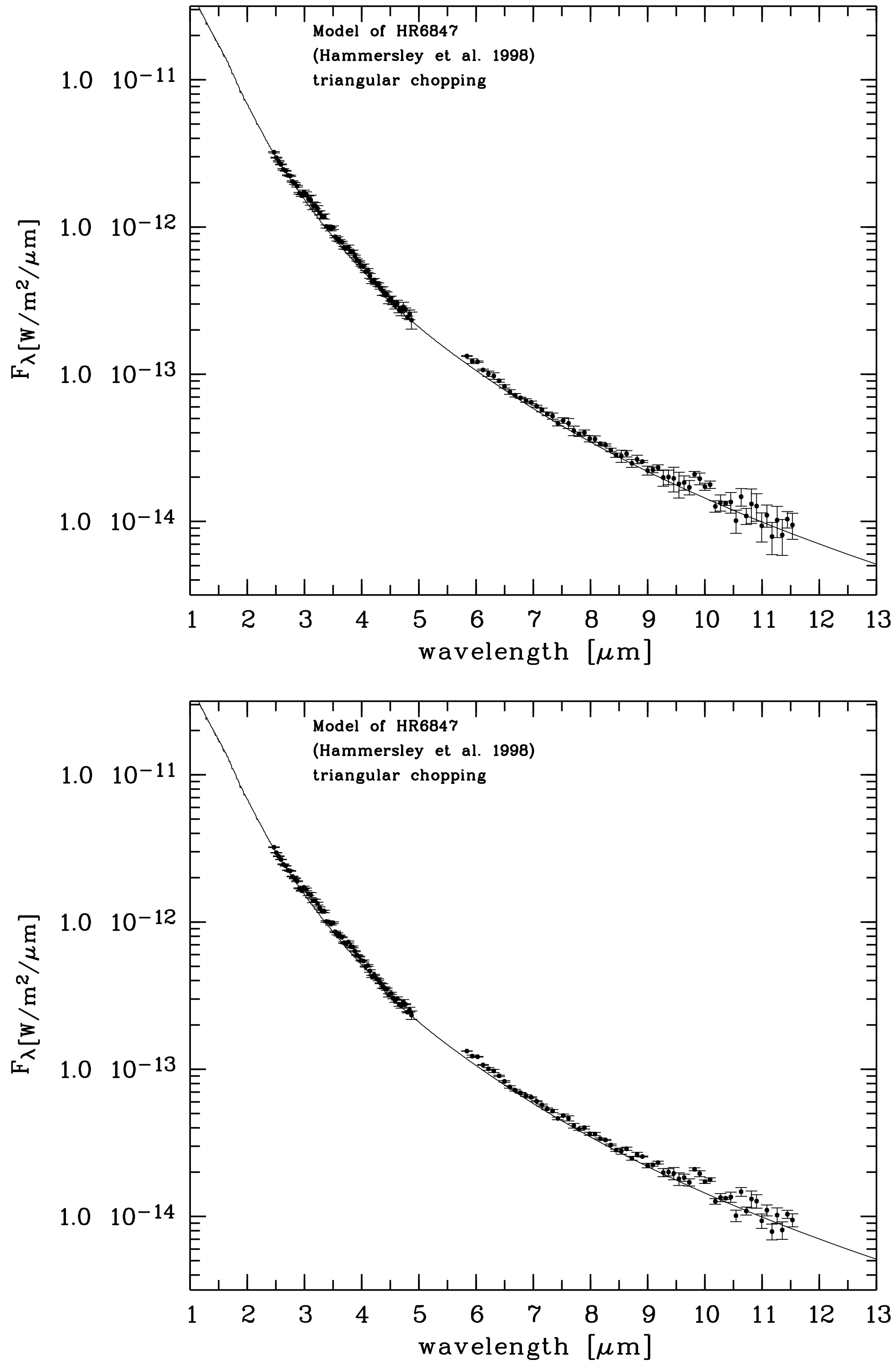

Figure 8.32: Comparison of the spectrum of HR 6847 obtained in PHT-S triangular chopped mode for both OLP 8.6b1 (upper panel) and OLP 9.0b6 (lower panel) with the flux model by Hammersley et al. 1998.

8.3.4 MIR Spectra of Galaxies from Chopped PHT-S Measurements

- authors: K. Wilke, U. Klaas
- date: 29-May-2000
- SVP period 2

Motivation

There is a set of chopped PHT-S measurements on galaxies 10^{-14} to 10^{-12} W/m^2/μm. These galaxies have different SED shapes than the standard stars from which the chopped PHT-S spectral response function was derived. There is groundbased $8-13$ micron spectroscopy available (cf. Ref. [8]). We selected a range of galaxies from featureless continuum to spectra with PAH features and strong 10 μm silicon absorption.

Method

We compare the absolute fluxes and relative shapes of the ISOPHOT-S spectra of both OLP 8.6b1 and OLP 9.0b6 with the groundbased spectroscopy. Note that we compare an aperture size of 24x24 arcsec^2 for ISOPHOT-S with 5 arcsec aperture size of the groundbased measurements.

Results

In Figs. 8.33 to 8.38 we perform an individual comparison of both OLP versions with the flux model. One can see that the results are practically identical. Some noticable differences for some pixels are a consequence of the SPR-3270 fix (discarding of first NDRs per ramp).

Conclusions

- The two OLP versions give very similar results; slight changes are expected by the discarding of the first NDRs per ramp according to the SPR-3270 fix. SCREW 425 is successfully implemented with regard to chopped PHT-S observation processing.
- The changes applied to the processing have not altered the validation and the achieved calibration accuracy.

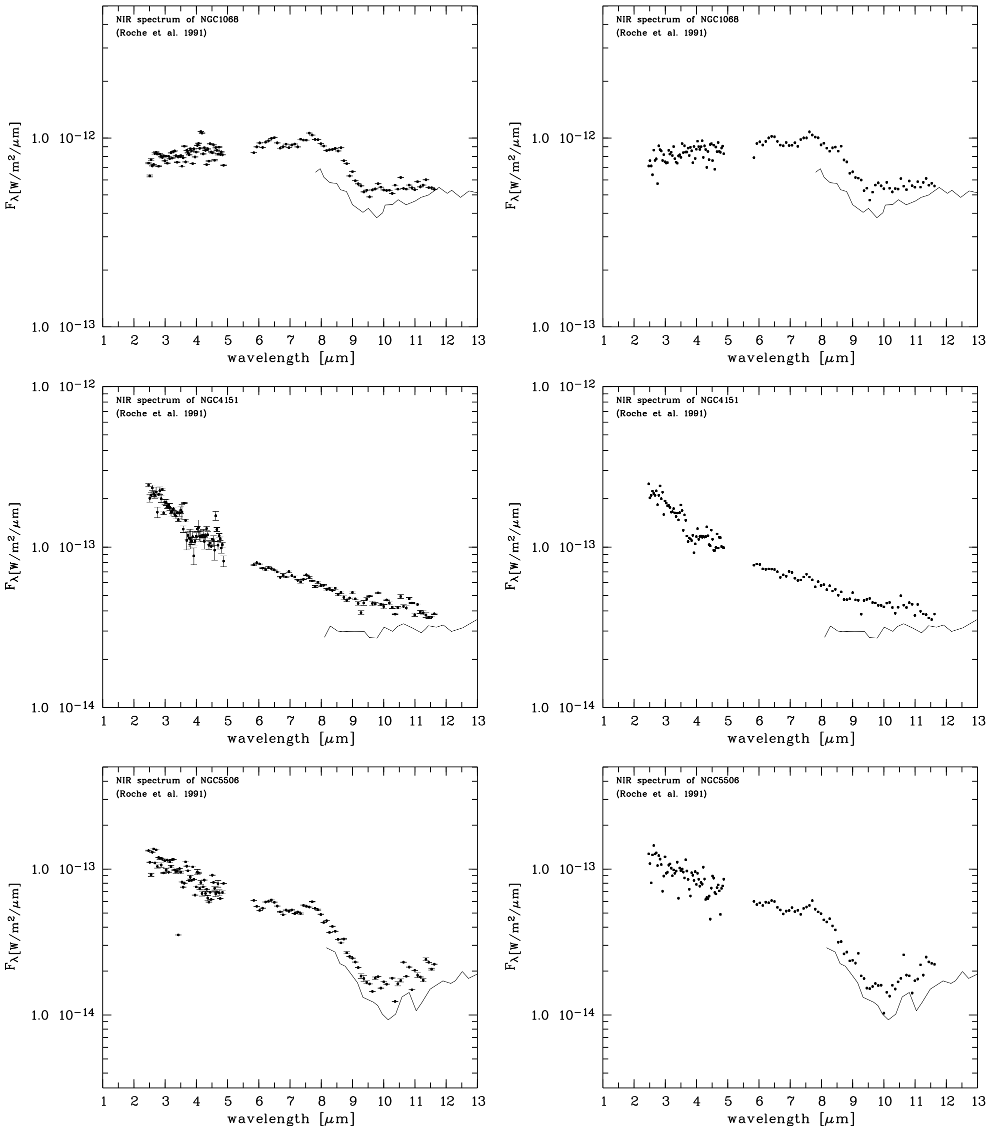

Figure 8.33: Comparison of ISOPHOT-S spectra of the 3 galaxies NGC 1068, NGC 4151 and NGC 5506 obtained in chopped mode (dots) for both OLP 8.6b1 (left panels) and OLP 9.0b6 (right panels) with groundbased 8 – 13 micron spectroscopy (solid line). Note: In the OLP 9 version uncertainties are not displayed.

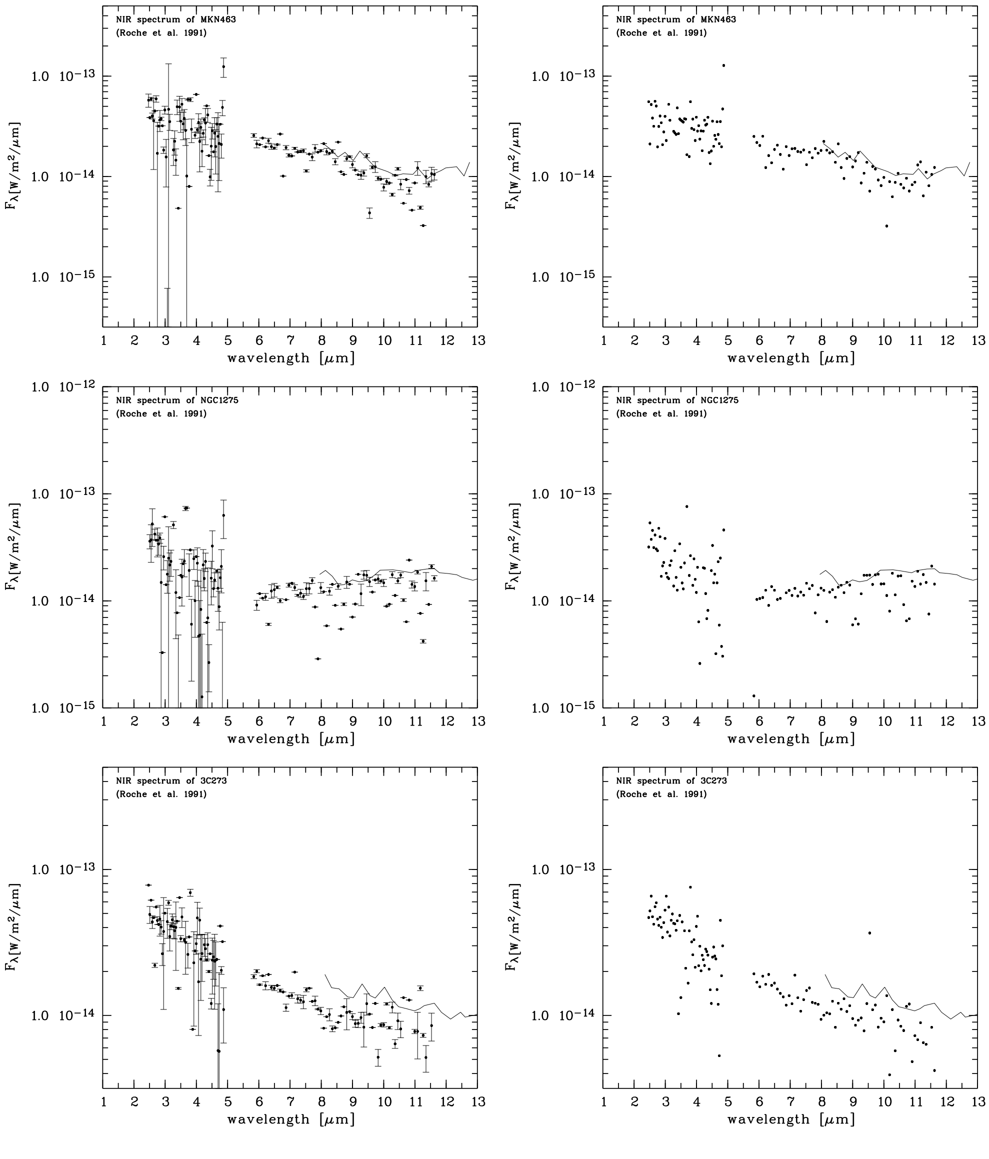

Figure 8.34: Comparison of ISOPHOT-S spectra of the 3 galaxies Mkn 463, NGC 1275 and 3C273 obtained in chopped mode (dots) for both OLP 8.6b1 (left panels) and OLP 9.0b6 (right panels) with groundbased 8 – 13 micron spectroscopy (solid line). Note: In the OLP 9 version uncertainties are not displayed.

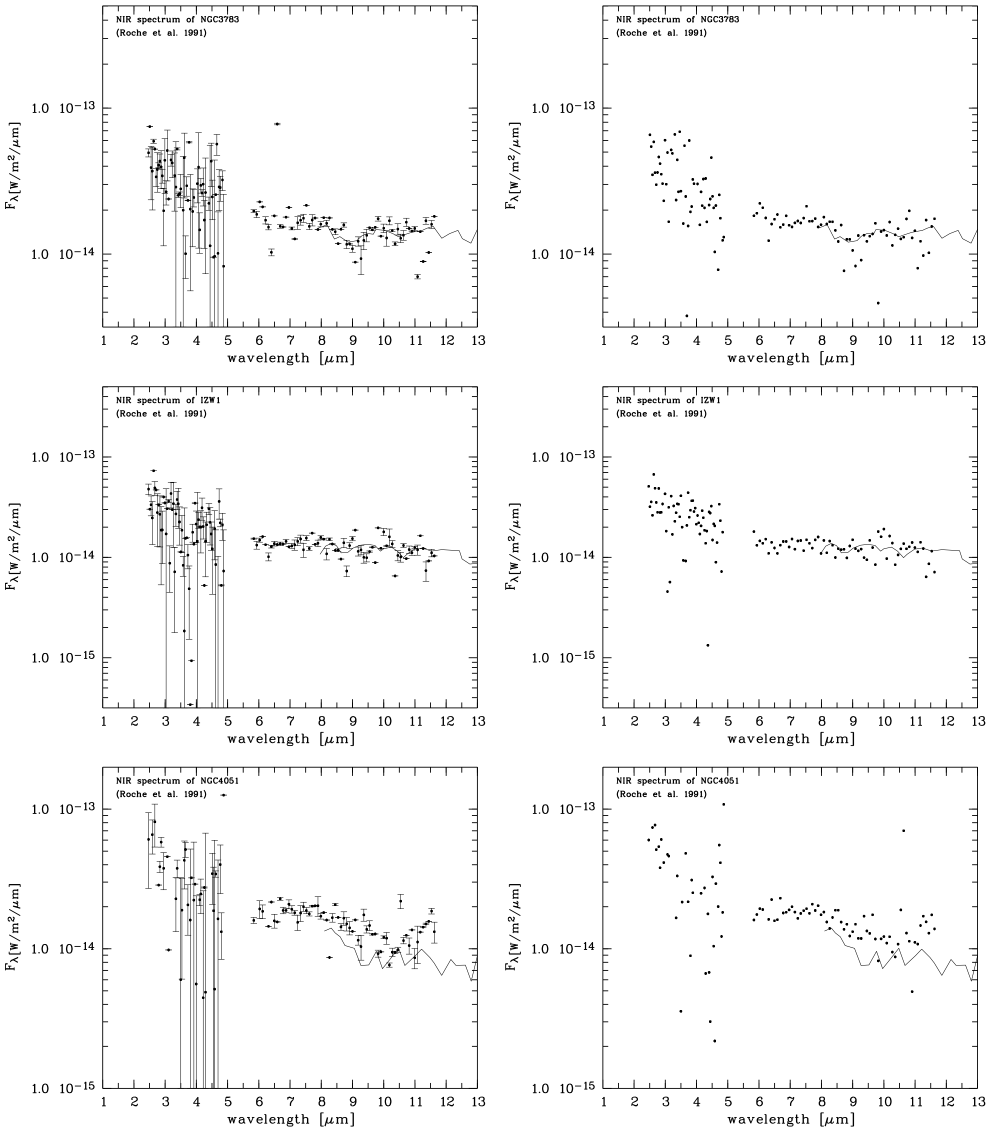

Figure 8.35: Comparison of ISOPHOT-S spectra of the 3 galaxies NGC 3783, IZw1 and NGC 4051 obtained in chopped mode (dots) for both OLP 8.6b1 (left panels) and OLP 9.0b6 (right panels) with groundbased 8 – 13 micron spectroscopy (solid line). Note: In the OLP 9 version uncertainties are not displayed.

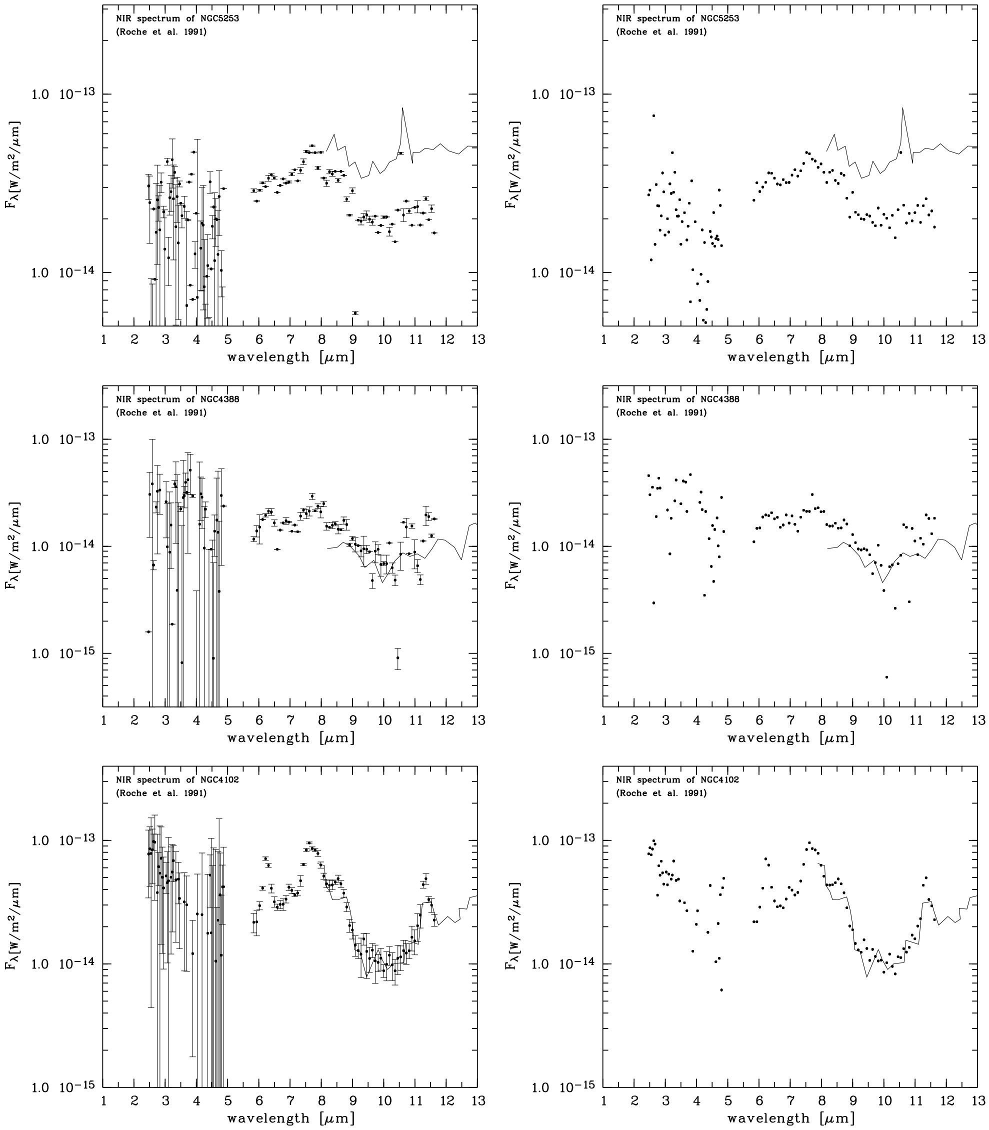

Figure 8.36: Comparison of ISOPHOT-S spectra of the 3 galaxies NGC 5253, NGC 4388 and NGC 4102 obtained in chopped mode (dots) for both OLP 8.6b1 (left panels) and OLP 9.0b6 (right panels) with groundbased 8 – 13 micron spectroscopy (solid line). Note: In the OLP 9 version uncertainties are not displayed.

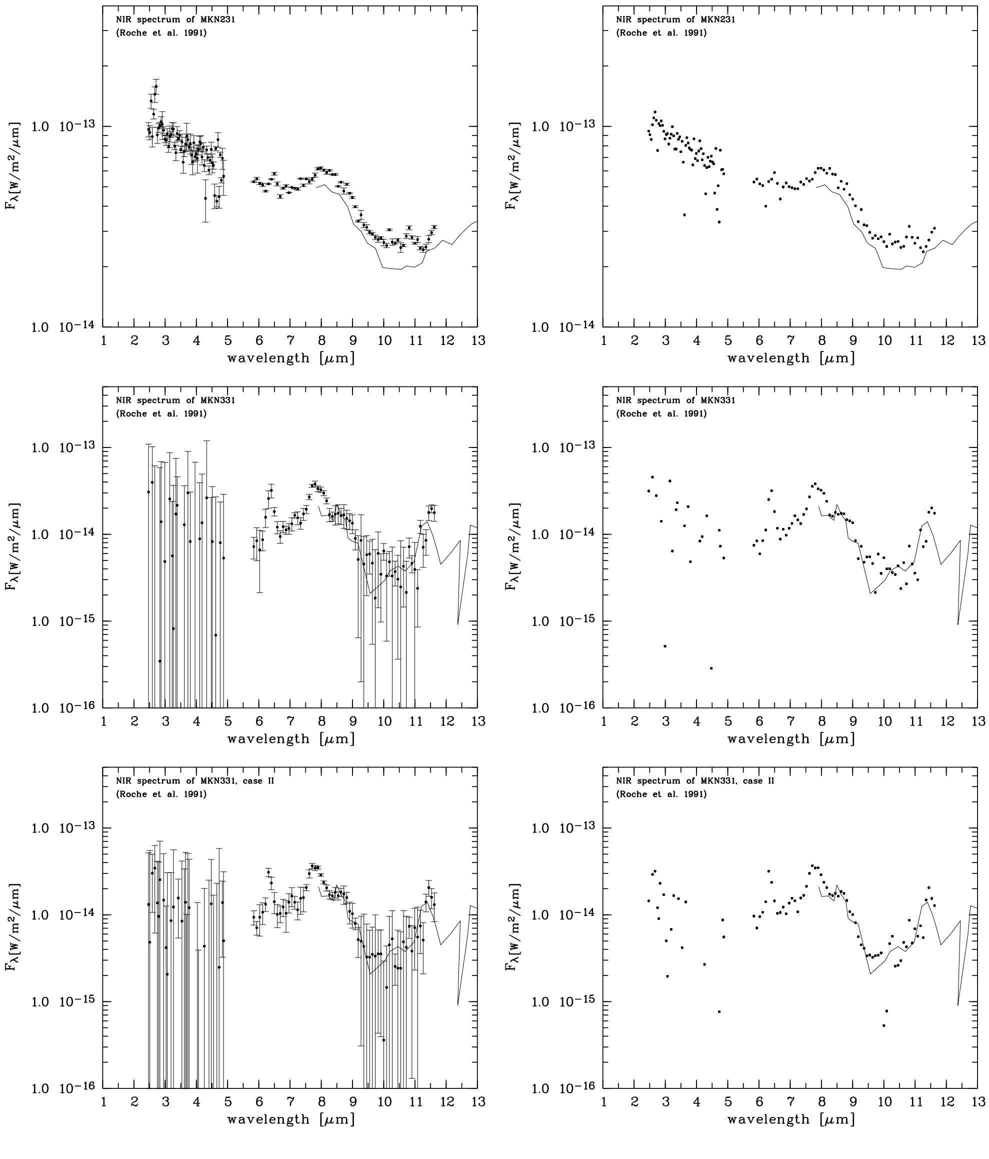

Figure 8.37: Comparison of ISOPHOT-S spectra of the 2 galaxies Mkn 231 and Mkn 331 (two spectra) obtained in chopped mode (dots) for both OLP 8.6b1 (left panels) and OLP 9.0b6 (right panels) with groundbased 8 – 13 micron spectroscopy (solid line). Note: In the OLP 9 version uncertainties are not displayed.

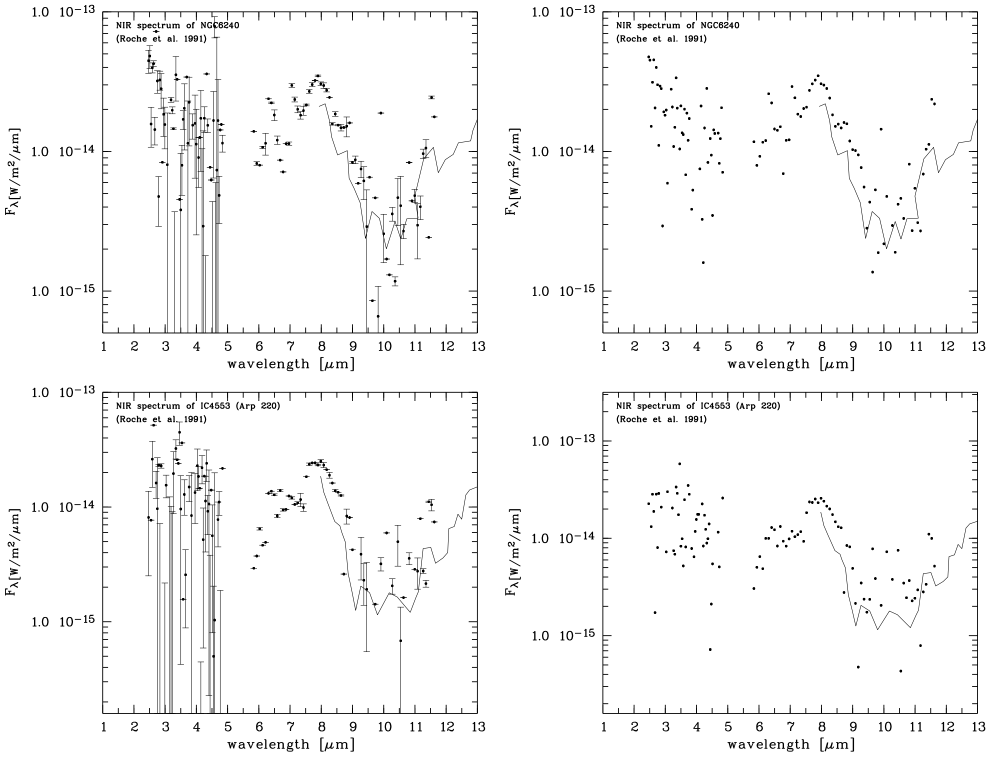

Figure 8.38: Comparison of ISOPHOT-S spectra of the 2 galaxies NGC 6240 and Arp220 obtained in chopped mode (dots) for both OLP 8.6b1 (left panels) and OLP 9.0b6 (right panels) with groundbased 8 – 13 micron spectroscopy (solid line). Note: In the OLP 9 version uncertainties are not displayed.

8.3.5 MIR Spectra of a Symbiotic Star and a Nova from Chopped PHT-S Measurements

- authors: K. Wilke, U. Klaas
- date: 29-May-2000
- SVP period 2

Motivation

In order to to increase the variety of object types for which PHT-S spectra are checked we included the spectrum of a symbiotic star, AG Peg, and the spectrum of a Nova, Nova Her91, in our test case list. For both targets groundbased 8 - 13 micron spectroscopy is available (cf. Refs. [12] and [13], respectively). The comparison for the Nova is of qualitative nature, as changes in the SED between the epoch of the groundbased measurement (1991, 67 days after the eruption) and the epoch of the ISOPHOT-S measurement (1996) are quite likely.

Method

We compare the absolute fluxes and relative shapes of the ISOPHOT-S spectra of both OLP 8.6b1 and OLP 9.0b6 with the groundbased spectroscopy. Note that we compare an aperture size of 24x24 arcsec^2 for ISOPHOT-S with 5 arcsec aperture size of the groundbased measurements.

Results

In Figs. 8.29 to 8.32 we perform an individual comparison of both OLP versions with the flux model. For AG Peg, both OLP versions show practically identical results. Due to the low flux level of Nova Her91, the measurement is at the detection limit of both PHT-S channels and hence very noisy. Therefore, the discarding of the first NDRs has an impact on all measurement points; within the scatter the resulting upper limits and trends remain the same.
One can see that the results are absolutely identical.

Conclusions

- The two OLP versions give very similar results. Changes are expected by the discarding of the first NDRs per ramp according to the SPR-3270 fix, in particular for the measurement of Nova Her91 which is close to the detection limit. SCREW 425 is successfully implemented with regard to chopped PHT-S observation processing.
- The changes applied to the processing have not altered the validation and the achieved calibration accuracy.

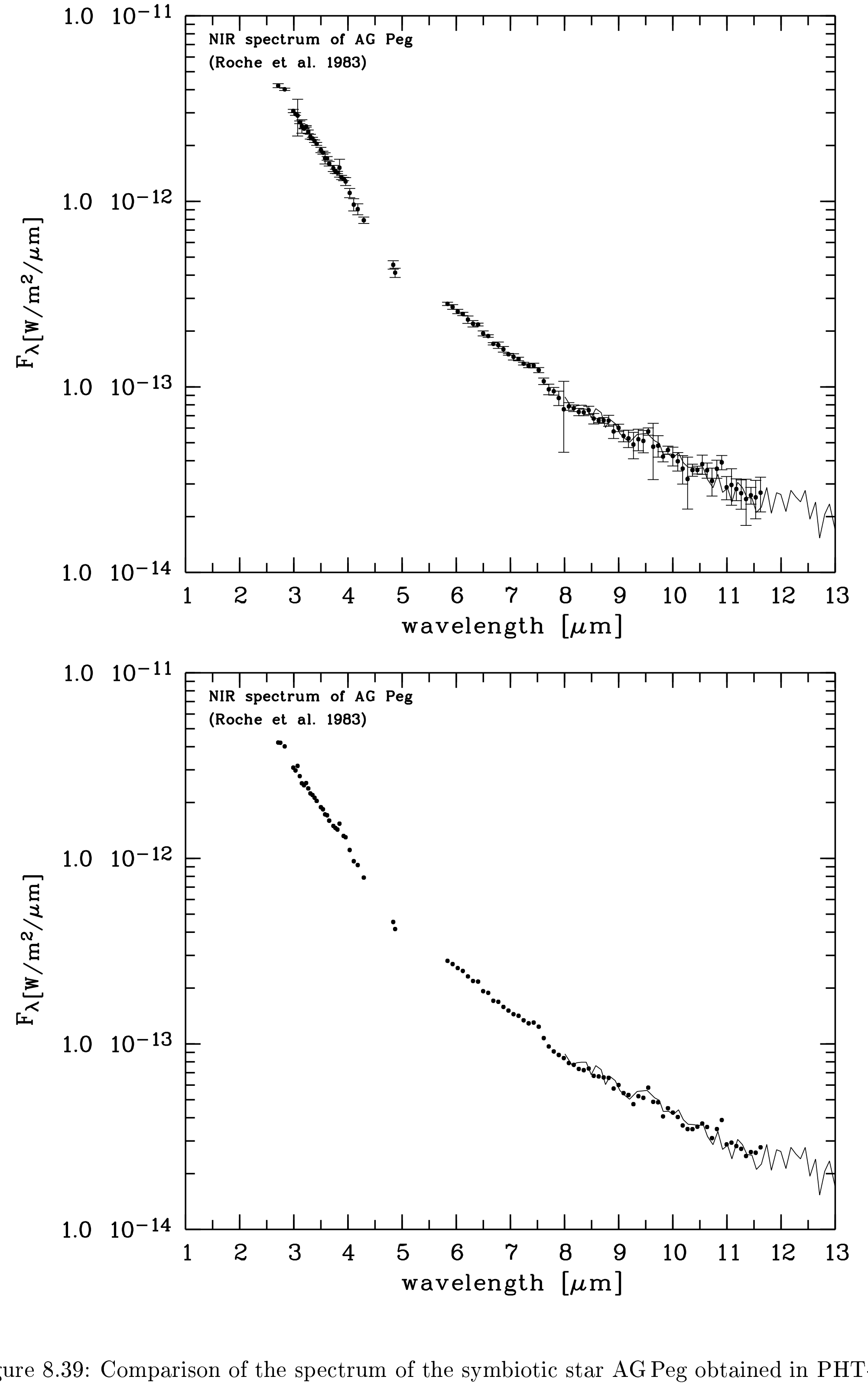

Figure 8.39: Comparison of the spectrum of the symbiotic star AG Peg obtained in PHT-S triangular chopped mode for both OLP 8.6b1 (upper panel) and OLP 9.0b6 (lower panel) with the groundbased 8 – 13 micron spectroscopy by Roche et al. 1983. Note: the OLP 9 version does not display any uncertainties.

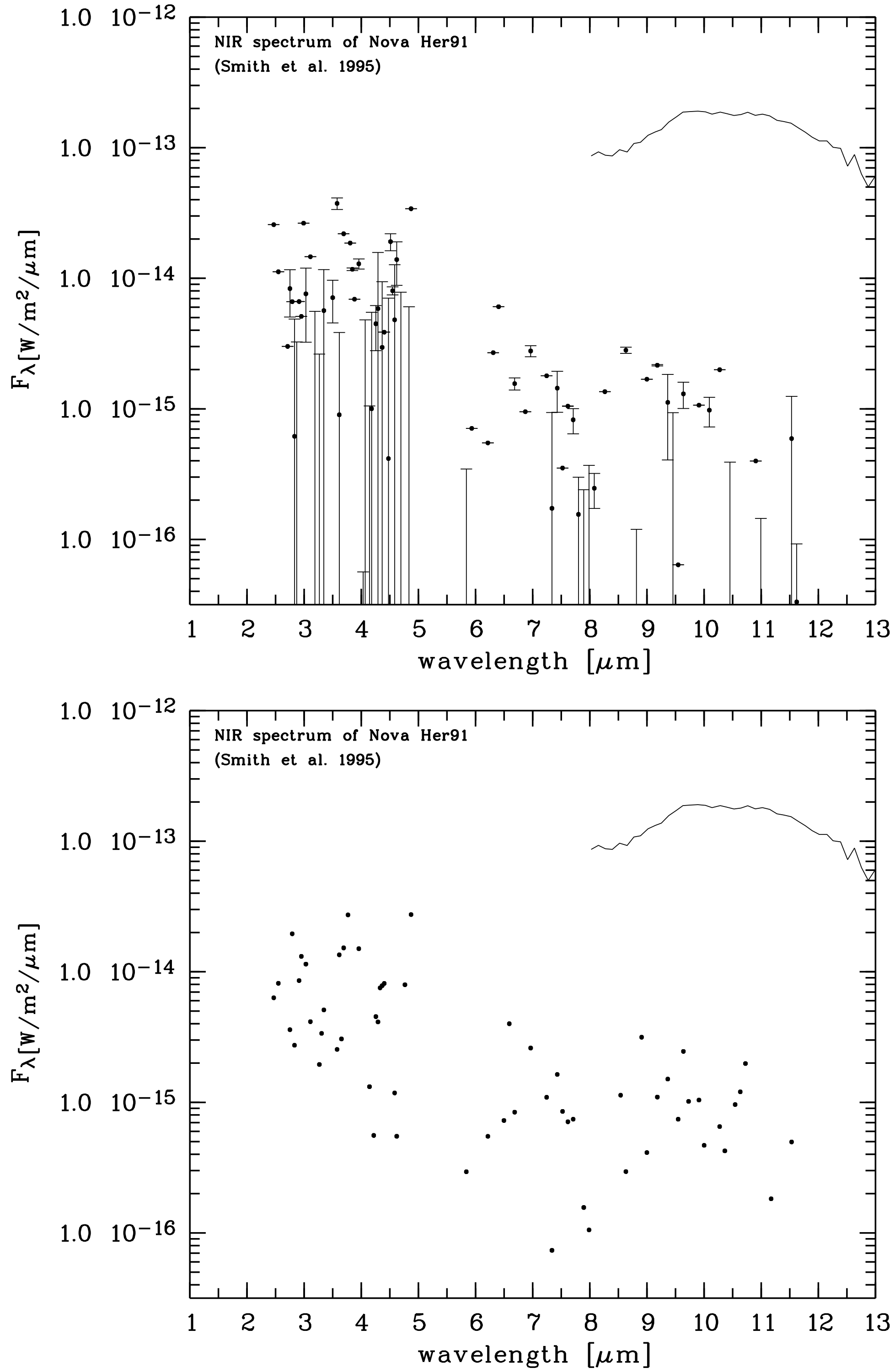

Figure 8.40: Comparison of the spectrum of Nova Her91 obtained in PHT-S rectangular chopped mode in 1996 for both OLP 8.6b1 (upper panel) and OLP 9.0b6 (lower panel) with the groundbased 8 – 13 micron spectroscopy by Smith et al. 1995, obtained in 1991, 67 days after its maximum. Note: the OLP 9 version does not display any uncertainties.

8.3.6 MIR Spectra of the Stars HD 23763, HR 7428 and HD 23441 from Chopped PHT-S Measurements

- authors: K. Wilke, U. Klaas
- date: 29-May-2000
- SVP period 2

Motivation

We found three star in the data base with similar spectral type as standard star but different brightness. It is therefore possible to test absolute and relative accuracy of the new ISOPHOT-S chopped calibration on differen brightness levels than standard stars used to establish the calibration. The properties of the three stars are compiled in Table 8.2:

Table 8.2: Properties of stars used for verification of chopped ISOPHOT-S spectra

Name	**Spectral Type**	**Apparent Brightness** (mag)	**Comment**	**Reference Star**	**Spectral Type**	**Apparent Brightness** (mag)
HD 23763	A1V	$m_k = 6.567$		Sirius (HR 2491)	A1V	m_k = -1.39
HR 7428 (HD 184398)	K2II-III+A0V Sp(IR) K2II-III Ca-	$m_v = 6.37$	RS CVn binary	HR 6688	K2III	$m_v = 3.747$
HD 23441	A0Vn	$m_v = 6.43$	Pleiades 859	Vega (HR 7001)	A0V	$m_v = 0.033$

For a reference of the spectral types of HR 7428, cf. [20], and of HD 23441, cf. [22]. HR 7428 has an IRAS 12 μm flux of 1.82 Jy, cf. [21] (=1.26 Jy for T=4000 K BB).

Method

Scale the model spectra of Sirius, HR 6688 and Vega according to the apparent brightness ratio in the K or V band. Compare the absolute fluxes and relative shapes of the ISOPHOT-S spectra of both OLP 8.6b1 and OLP 9.0b6 with the scaled model spectra.

Results

In Figs. 8.41 to 8.43 we perform an individual comparison of both OLP versions with the flux model. One can see that the results are practically identical. Some noticable differences for some pixels are a consequence of the SPR-3270 fix (discarding of first NDRs per ramp).

Conclusions

- The two OLP versions give very similar results; slight changes are expected by the discarding of the first NDRs per ramp according to the SPR-3270 fix. SCREW 425 is successfully implemented with regard to chopped PHT-S observation processing.
- The changes applied to the processing have not altered the validation and the achieved calibration accuracy.

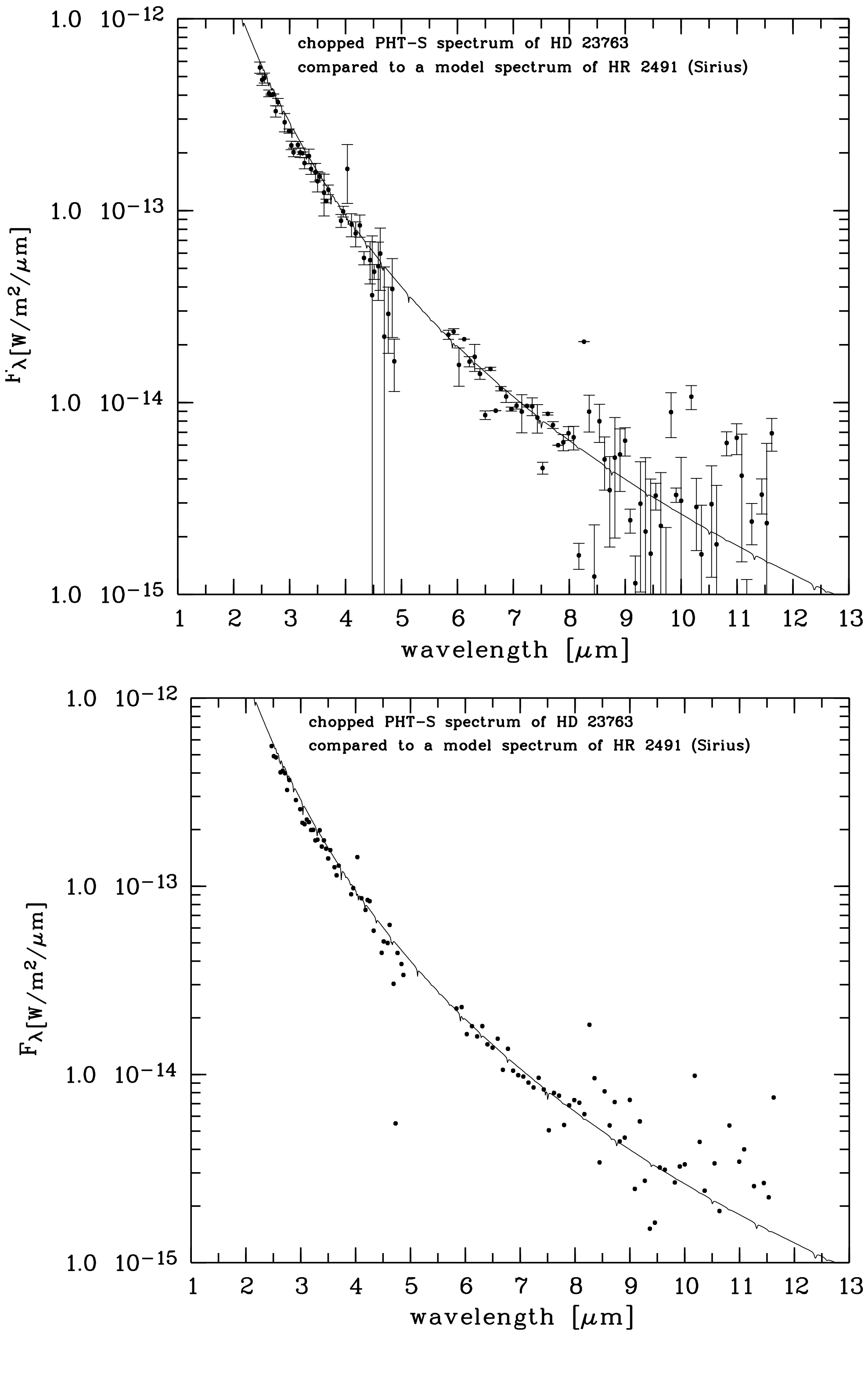

Figure 8.41: Comparison of the spectrum of the A1V star HD 23763 obtained in PHT-S sawtooth chopped mode for both OLP 8.6b1 (upper panel) and OLP 9.0b6 (lower panel) with the model of Sirius scaled with the K-magnitude ratio of (6.567 mag / -1.39 mag). Note: In the OLP 9 version uncertainties are not displayed.

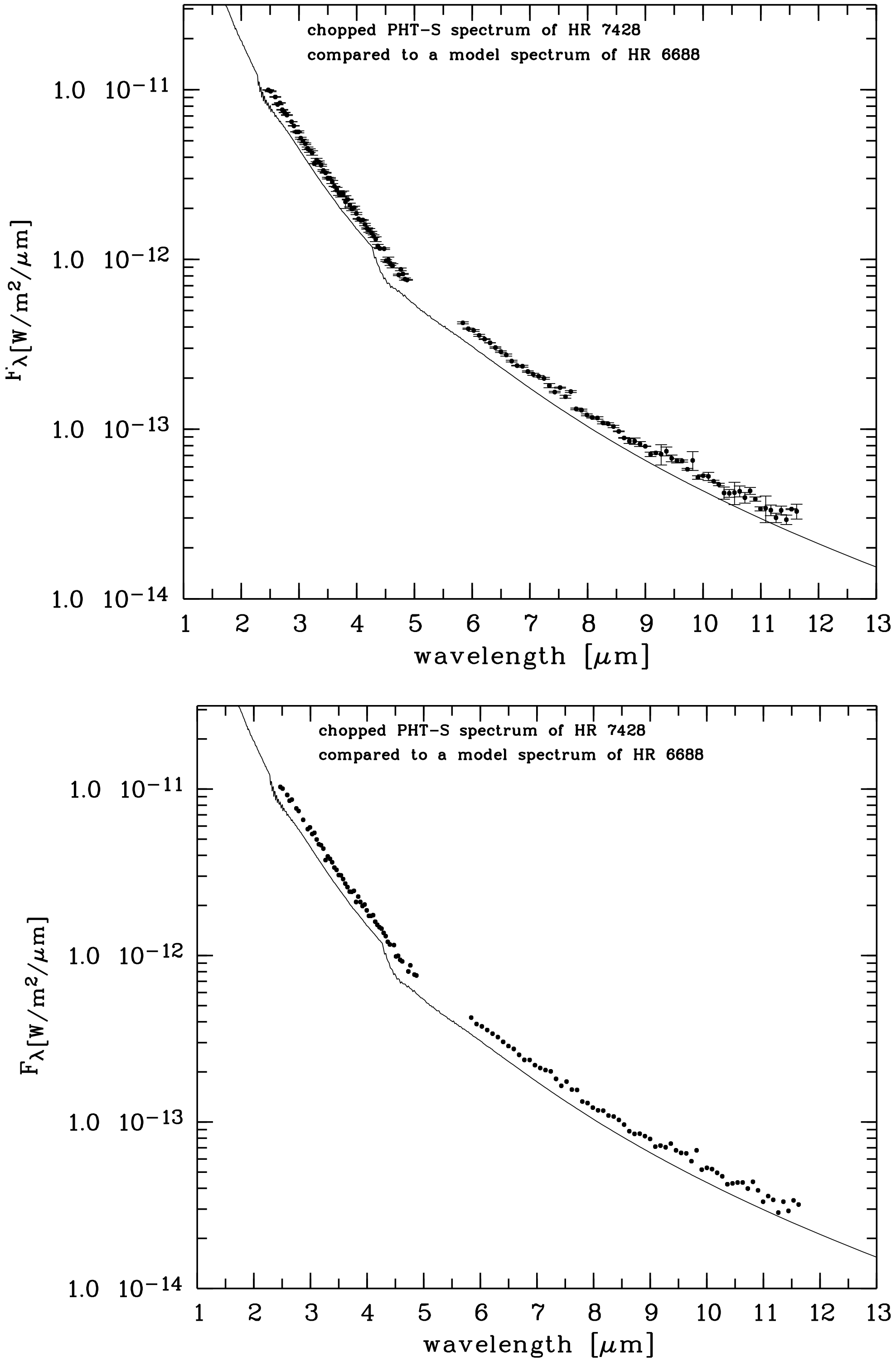

Figure 8.42: Comparison of the spectrum of the RS CVn binary HR 7428 (spectral type: K2II-III+A0V) obtained in PHT-S rectangular chopped mode for both OLP 8.6b1 (upper panel) and OLP 9.0b6 (lower panel) with the model of HR 6688 (spectral type: K2III) scaled with the V-magnitude ratio of (6.37 mag / 3.747 mag). Note: In the OLP 9 version uncertainties are not displayed.

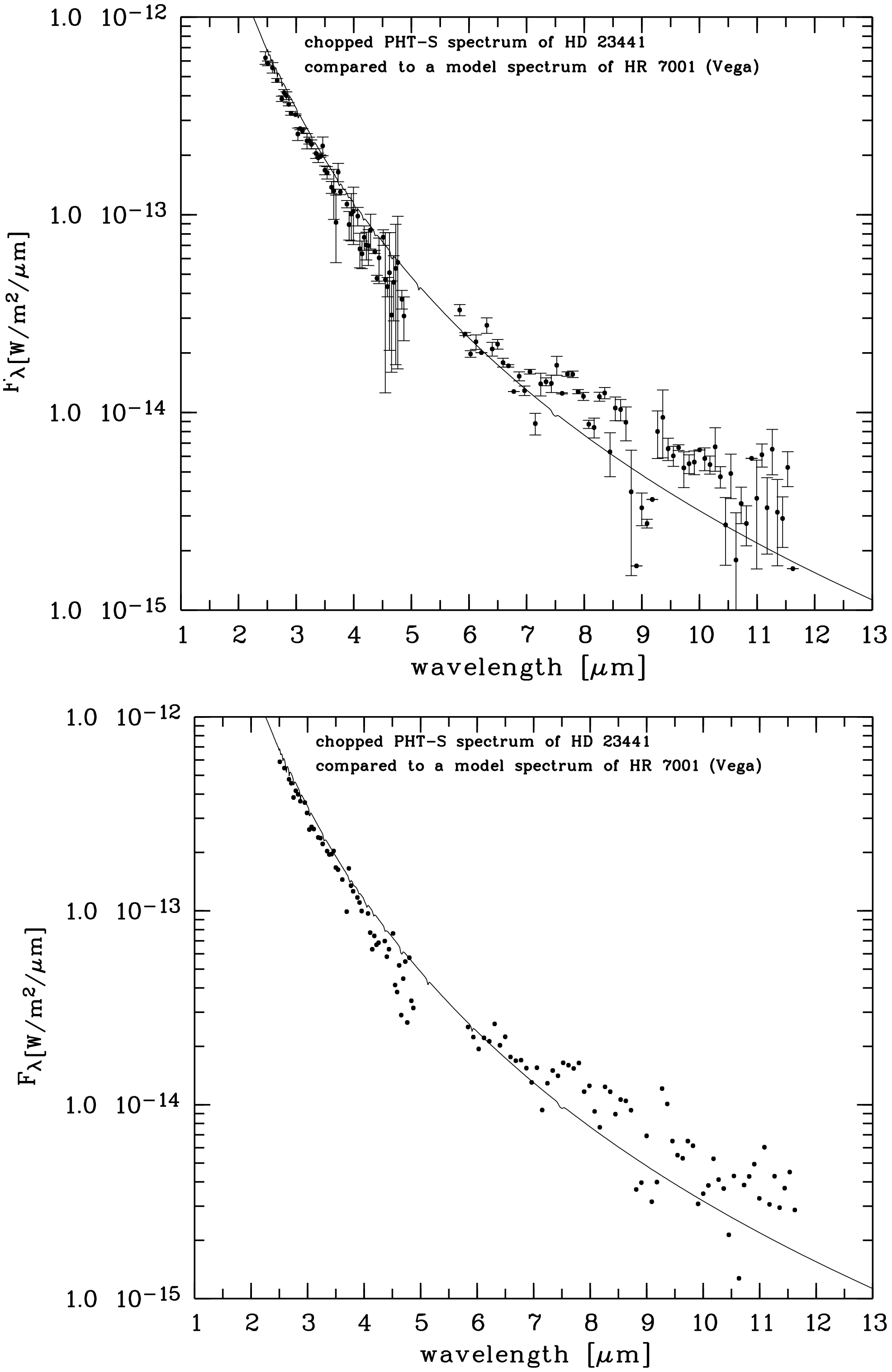

Figure 8.43: Comparison of the spectrum of the A0Vn star HD 23441 obtained in PHT-S sawtooth chopped mode for both OLP 8.6b1 (upper panel) and OLP 9.0b6 (lower panel) with the model of Vega scaled with the V-magnitude ratio of (6.43 mag / 0.033 mag). Note: In the OLP 9 version uncertainties are not displayed.

8.4 Revalidation of Staring Mode Photometry

An overview of the test cases is outlined in Ref. [4], chapter 3.2.

8.4.1 References to Calibration Analysis and Software Change Documentation

- calibration reports:
  - Linearization of ISOPHOT-P and -C detector signals in OLP8 [30]
- Software Problem Reports: SPRs 3214, 3215

8.4.2 Summary of Results

- In the second version of the CALG files the signal linearisation tables were ordered correctly allowing quantitative assessment of staring mode photometry. The linearisation scheme, including associated corrections, like filter-to-filter calibration or default responsivity calibration is consistently implemented.
- The calibration of bright sources has been further improved. In general absolute accuracies of better than 10 % are achieved now.
- There are still several cases, in particular the C200 photometry of γ Dra (in contrast to the excellent absolute photometry performance at 170 μm) where linearisation did not bring the expected effect matching multi-filter photometry on-source and off-source to give accurate fluxes. Since for these sources the background is already quite dominant, it has to be further investigated whether the discrepancies are due to limitations of the current calibration or due to a general limitation to achieve higher accuracy for the on-off mode.
- A few filters were identified which show systematically a worse accuracy than adjacent ones in wavelength. Since they exhibit offsets only for part of the flux range considered, this may be due to a non-perfect linearisation for this filter. The worst case is the 12.8 μm filter which shows flux deviations for sources below a flux level of 100 Jy. Other suspect cases are the narrow band filters at 3.3 μm and 11.3 μm for P1 and the 20 μm filter for P2. For C100 multi-filter surface brightness distributions a characteristic non-smooth pattern is observed with the 65 and 80 μm filters showing a strong surface brightness excess w.r.t. COBE/DIRBE photometry. This may include the 105 μm filter, too, affecting the accuracy of background subtraction. The relation to linearisation is less clear here and has to be investigated. On the other hand there may be some impact on the final calibration accuracy of other modes, like chopped photometry.
- One case of C100 pre-rev. 94 calibration (Arp 244) showed strong flux deficiencies w.r.t. the reference. The FCS electrical power applied is just outside the calibrated range. Methods to improve the calibration of this period with limited calibration data are under investigation.

8.4.3 General Re-validation of PHT03 and PHT22 Staring Mode: The SED of α Bootes (HR 5340) - Final Assessment

- authors: U. Klaas
- date: 10-May-2000
- SVP period 2

Motivation

TDTs 45200201(background, PHT-P), 45200202(α Boo, PHT-P), 45200203(background, PHT-C), 45200204(α Boo, PHT-C) is one of the key OLP validation cases [1]. The staring mode AOTs PHT-03 and PHT-22 use all available PHT filters (but the 3.6 and 4.85 μm filters had to be excluded from the analysis, because the source saturates the measurement) on a stellar (declining) SED. α Bootes is one of the most important stellar PHT calibration standards and there are detailed models available from M. Cohen (composite spectrum from 1 to 35 μm and extrapolations to 300 μm). This test case is very suitable for a test of both the absolute calibration and the relative filter-to-filter calibration. It should be noted that this multi-filter measurement was not used for the establishment of the FCS calibration curve.

Method

We compare the background subtracted, color corrected flux values of both OLP V8.6b1 and OLP V9.0b6 results against the model prediction.

Results

In the following Tab. 8.3 we compare the photometry from part 1 of the evaluation log section with the model. We estimate the absolute photometric accuracy per detector assembly for this target as the deviation from the model flux in the filter in which the FCS calibration was done, and the relative filter-to-filter accuracy as the peak-to-peak variation of the other filters around this offset. Note that for P1 the FCS calibration was actually done in the 3.6 μm filter, but for this filter the sky measurement is heavily saturated. The photometric accuracies are presented in Tab. 8.4. Fig. 8.44 shows the PHT photometric data points in comparison to the model and IRAS photometry (color corrected) from 3.3 to 200 μm for OLP 8.4 and OLP 9.0b6, respectively.
In the whole P1 range the offset of the SED is shifted up by 2 – 5 %. The P3 photometry has been improved. The offset of the SED from 105 – 200 μm has become smaller by 5 %, yet the fluxes in the two longest wavelength C200 filters are by 25 to 30 % too low. As already outlined in the previous report (cf. [1]) this flux fall-off seems to be related to the absolute level of the background (for source-to-background ratios see last table in evaluation log, item 2).
Part 2 of the evaluation log section and Fig. 8.45 provide the surface brightness photometry of the background position and the comparison with COBE. From Table 8.5 it can be seen that the consistency with COBE has somewhat degraded using the new signal linearization files. We notice systematic offsets in the 65, 80, 100 and 105 μm filters relative to the COBE reference. The relative filter-to-filter calibration for C200 looks improved; it is very smooth now, however the slope towards longer wavelengths appears to be too shallow with regard to COBE.

Conclusions

- PHT photometry gives a good representation of the SED from 3.3 to 170 μm; it is quite similar to the OLP 8.4 result.
- PHT-P3 photometry has been slightly improved.
- There is still a flux fall-off at the longest wavelengths, where the source flux makes up only 20 % of the background. A reason may be that the background flux is derived too high which is supported by the consistency check with COBE/DIRBE photometry.

Table 8.3: Consistency check of photometric results with HR 5340 model

Filter	**consistency w.r.t. model OLP V8.4** [%]	**consistency w.r.t. model OLP V9.0b6** [%]
3.3	+0.0	+4.8
7.3	+8.5	+10.2
7.7	+4.4	+4.7
10	-6.0	-1.5
11.3	+0.5	+1.8
12	+7.4	+12.1
12 IRAS	+10.1	+10.1
12.8	-12.2	-7.8
15	+17.4	+22.7
20	+1.4	+3.3
25	+7.3	-2.4
25 IRAS	-2.3	-2.3
60 PHT-P	-11.5	+0.3
60 PHT-C	+3.4	+5.2
60 IRAS	-6.6	-6.6
65	+2.7	+6.2
80	+5.0	+6.2
90	-1.9	-3.1
100 PHT-P	-9.3	+7.4
100 PHT-C	-4.8	+1.0
100 IRAS	-3.6	-3.6
105	-11.4	-4.2
120	-11.4	-2.4
150	-8.8	-5.6
170	-7.0	-10.8
180	-34.9	-27.7
200	-33.6	-28.2

Table 8.4: Absolute and relative calibration accuracies per detector achieved for HR 5340 observation with OLP V9.0b6

detector	**absolute accuracy** [%]	**relative accuracy** [%]
P1	<5 at 3.3 μm	17
P2	<4 at 20 μm	6
P3	<1 at 60 μm	7
C100	<4 at 90 μm	10
C200	11 at 170 μm	20
		<10 for $\lambda <170$ μm

- The consistency of the background photometry with COBE/DIRBE is somewhat degraded. There is a systematic positive offset found for the C100 65, 80, 100 and 105 μm filters. The relative filter-to-filter calibration for C200 looks very smooth now, however the background SED seems to be too shallow compared to COBE/DIRBE.

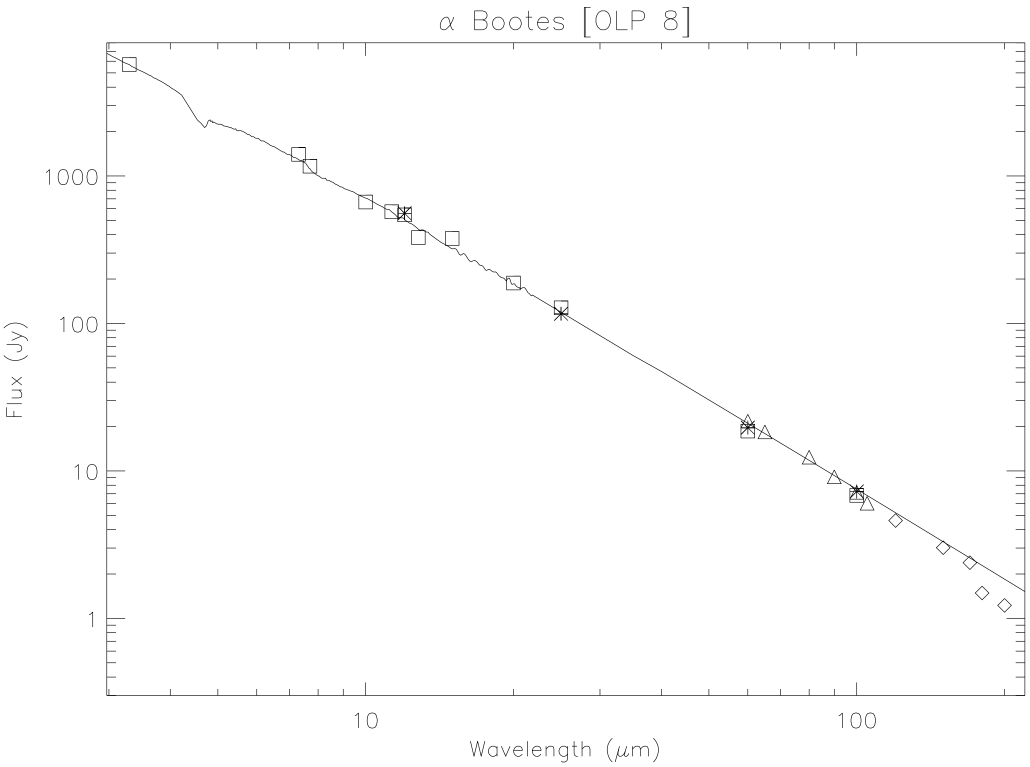

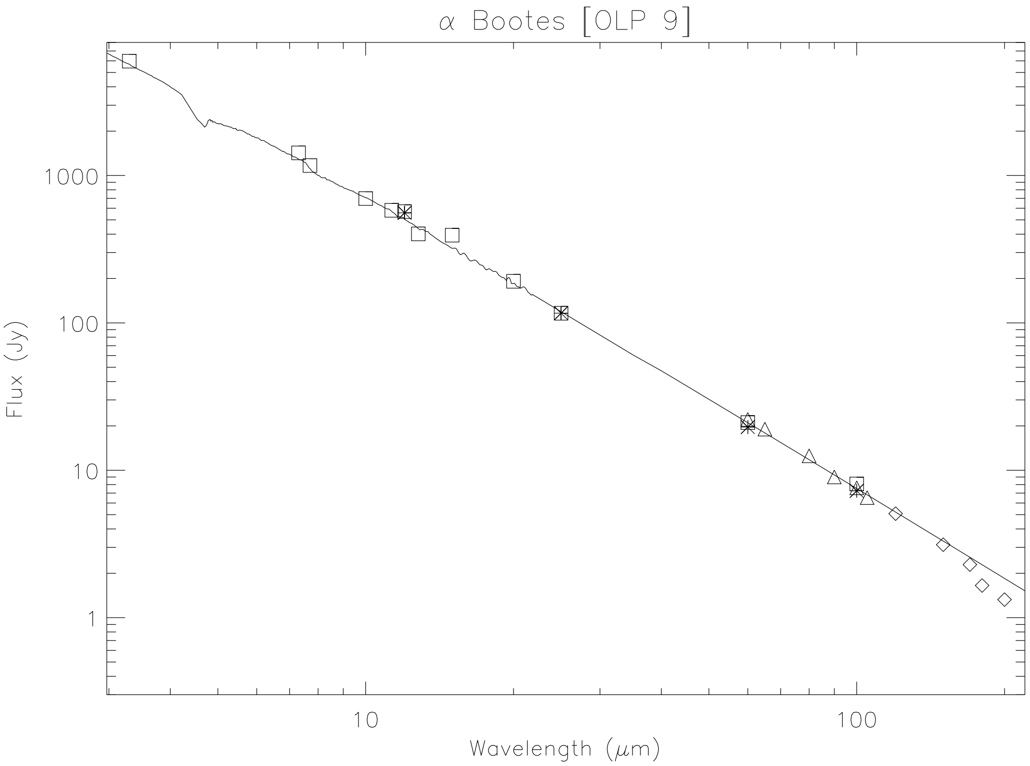

Figure 8.44: Comparison of PHT-P and PHT-C photometry, using the full ISOPHOT filter set, with the composite spectrum and out to 300 μm extrapolated SED of α Boo (HR 5340) provided by M. Cohen and with IRAS photometry for OLP 8.6b1 (upper panel) and OLP 9.0b6 (lower panel). All photometric points are color corrected for a 4000 K BB. The meaning of the symbols is the following: solid line: model, asterisk: IRAS, square: PHT-P (P03 AOT), triangle: C100 (P22 AOT), diamond: C200 (P22 AOT).

Table 8.5: Consistency check of α Boo background position surface brightness results with COBE/DIRBE annual maps.

wavelength μm	**consistency w.r.t. COBE OLP V8.4** [%]	**consistency w.r.t. COBE OLP V9.0b6** [%]
60	+10.5	+13.0
100	+38.8	+43.5
150	-19.0	-19.6
200	+33.5	+47.5

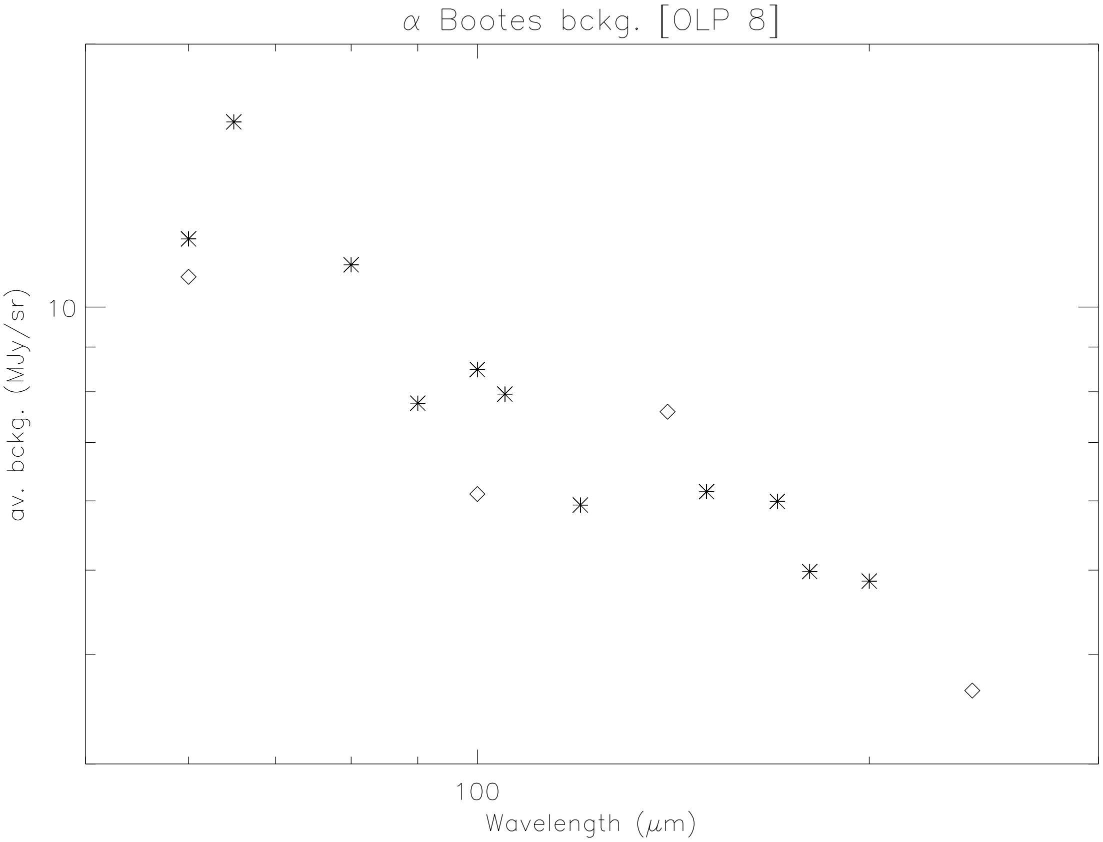

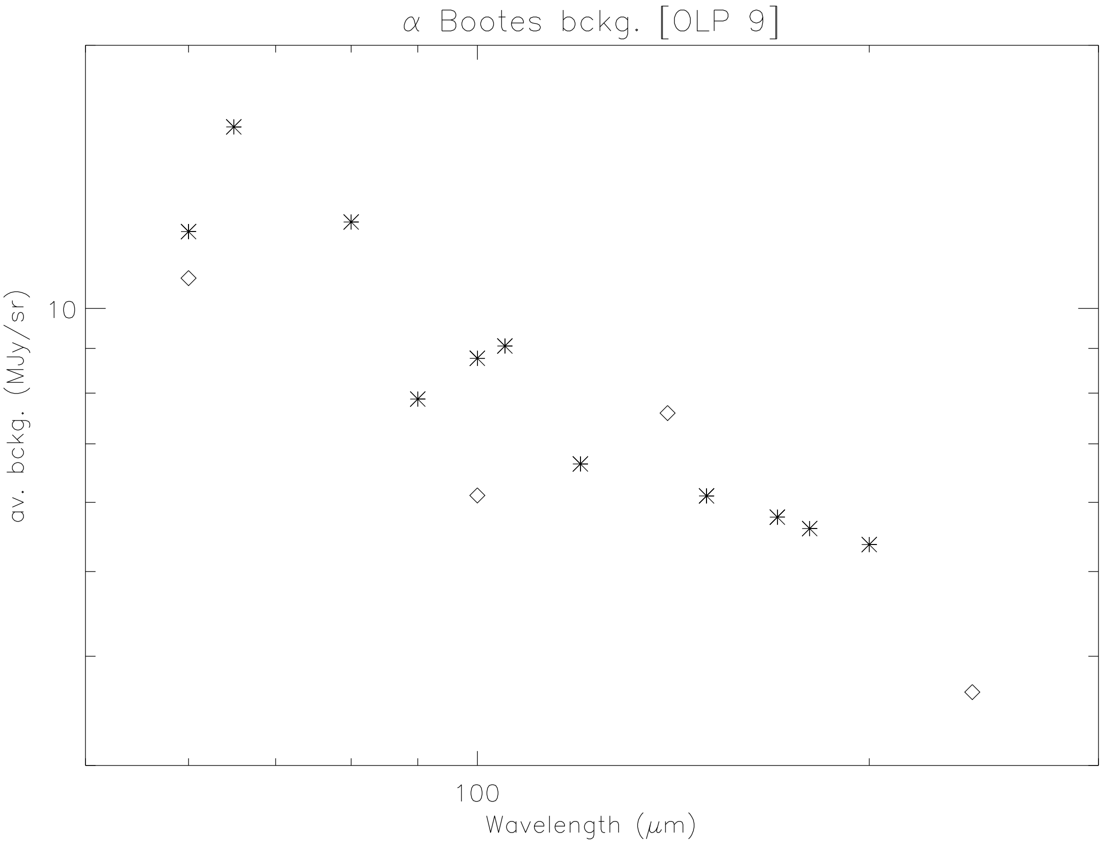

Figure 8.45: Comparison of OLP V8.6b1 and OLP V9.0b6 surface brightness (asterisk) with COBE annual map fluxes (diamond).

Evaluation Log

1) Point source photometry for Alpha Bootes in comparison with IRAS and Cohen model. Fluxes are in Jy.

Measurements:	
PHT-P:	ppap45200202 (src+back)
	ppae45200201 (back)
PHT-C:	pcap45200204 (src+back)
	pcae45200203 (back)
Colour correction:	black body, T = 4000 K
Model:	Cohen

Det	cwl (μm)	OLP 8	OLP 9	IRAS	Model	Δ (OLP 8)	Δ (OLP 9)
P1	3.3	5695.854	5968.594		5695.470	0.01	4.80
P1	7.3	1400.773	1423.773		1291.496	8.46	10.24
P1	7.7	1165.112	1169.081		1116.581	4.35	4.70
P1	10.0	665.884	697.696		708.004	-5.95	-1.46
P1	11.3	572.895	580.845		570.349	0.45	1.84
P1	12.0	545.015	568.950	558.500	507.360	7.42	12.14
P1	12.8	382.347	401.790		435.541	-12.21	-7.75
P1	15.0	376.618	393.588		320.700	17.44	22.73
P2	20.0	187.989	191.659		185.467	1.36	3.34
P2	25.0	127.784	116.274	116.400	119.146	7.25	-2.41
P3	60.0	18.614	21.082	19.650	21.030	-11.49	0.25
C1	60.0	21.747	22.120	19.650	21.030	3.41	5.18
C1	65.0	18.395	19.023		17.910	2.71	6.21
C1	80.0	12.390	12.532		11.800	5.00	6.20
C1	90.0	9.127	9.012		9.303	-1.90	-3.12
P3	100.0	6.825	8.077	7.250	7.521	-9.25	7.40
C1	100.0	7.160	7.596	7.250	7.521	-4.80	1.00
C1	105.0	6.036	6.529		6.814	-11.42	-4.19
C2	120.0	4.607	5.078		5.201	-11.42	-2.37
C2	150.0	3.018	3.126		3.310	-8.83	-5.55
C2	170.0	2.387	2.290		2.568	-7.03	-10.82
C2	180.0	1.487	1.654		2.286	-34.94	-27.66
C2	200.0	1.225	1.326		1.845	-33.59	-28.15

2) surface brightness photometry of Alpha Bootes background

λ	OLP8 (MJy/sr)	OLP9 (MJy/sr)	COBE (MJy/sr)
60.0	11.97	12.24	10.83
65.0	16.29	16.13	
80.0	11.18	12.56	
90.0	7.76	7.88	
100.0	8.48	8.77	6.11
105.0	7.95	9.06	
120.0	5.94	6.64	
150.0	6.15	6.10	7.59
170.0	5.99	5.77	
180.0	4.98	5.60	
200.0	4.86	5.37	3.64

λ	background flux (Jy)	expected source flux (Jy)	Source/background
60.0	8.21	21.03	2.56
65.0	10.76	17.91	1.66
80.0	8.13	11.80	1.45
90.0	5.36	9.30	1.73
100.0	6.65	7.52	1.13
105.0	7.26	6.81	0.94
120.0	12.86	5.20	0.40
150.0	10.77	3.31	0.31
170.0	10.85	2.57	0.24
180.0	9.87	2.29	0.23
200.0	8.35	1.85	0.22

8.4.4 General Re-validation of Multi-filter Staring Mode (PHT03/PHT22) and Absolute Photometry (PHT05/PHT25): The SED of γ Draconis (HR 6705) - Final Assessment

- authors: U. Klaas
- date: 15-May-2000
- SVP period 2

Motivation

The star γ Draconis (HR 6705) is one of the most important calibration stars for ISOPHOT. Also several AOT commissioning observations were performed on this star. The set of observations comprises multi-filter photometry, TDTs 35602101 (background, PHT-P), 35602102 (γ Dra, PHT-P), 35602203, 39802002 (background PHT-C), 35602204, 39802003 (γ Dra, PHT-C), absolute photometry, TDTs 35300301...35300306 (PHT-P) and 35300308...35300312 (PHT-C), multi-filter PHT-C100 photometry with different reset interval settings, cf. [4] for more details. It is one of the key OLP validation cases [1]. The staring mode AOTs PHT-03 and PHT-22 use all available PHT filters out to $200\,\mu$m complementing the α Bootes observations towards the fainter flux end. There are detailed models available from M. Cohen (composite spectrum from 1 to 35 μm and extrapolations to 300 μm). This test case is very suitable for a test of both the absolute calibration and the relative filter-to-filter calibration. Furthermore, the last C100 measurements of TDT 35602204, including the C100 FCS measurement failed due to a R/T problem (therefore repetition by TDT 39802003). The available C100 measurements of TDT 35602204 are calibrated with the C100 default responsivities.

Method

We compare the background subtracted, color corrected flux values of both OLP V8.6b1 and OLP V9.0b6 results against the model prediction.

Results

In the following Tab. 8.6 we compare the photometry from part 1 of the evaluation log section with the model. We estimate the absolute photometric accuracy per detector assembly for this target as the deviation from the model flux in the filter in which the FCS calibration was done, and the relative filter-to-filter accuracy as the peak-to-peak variation of the other filters around this offset. Figs. 8.46 and 8.47 show the PHT photometric data points in comparison to the model and IRAS photometry (color corrected) for OLP 8.6 and OLP 9.0b6, respectively. The absolute photometry results as shown in Fig. 8.47 are practically unchanged and the achieved absolute photometry is better than 15 % for all detectors. The multi-filter photometry results show some features which are quite similar for both OLP versions:

- The $15\,\mu$m flux shows a high excess of 70 % (OLP 9)with regard to the model. We could clarify that this to a large extent due to detector transients. The is a second measurement (TDT 39801901) which was only repeated at 3.6 and $15\,\mu$m, but with longer exposure times. While the $3.6\,\mu$m fluxes coincide within 0.2 %, the $15\,\mu$m flux of the longer exposure is only off by 23 %, so that at least 47 % of the flux excess of the first measurement can be accounted for by transients. This is one of the few examples we encountered during OLP scientific validation with such a high impact by transients.
- The C100 filters are systematically too high by 20 to 45 %, except the $105\,\mu$m filter which is significantly too low. Again, this filter was the first filter in the multi-filter sequence performed on rev. 398. It is hard to believe the the flux deficiency in the $105\,\mu$m filter is due to background features, since the adjacent $100\,\mu$m filter does not show this problem. Also cirrus confusion is very likely to be ruled out, as for the off position the well selected calibration measurement offset was chosen. This could,

however be caused by a too high surface brightness for the 105 μm filter as derived for the background measurement.

- Like the 105 μm filter for C100 the P3 100 μm filter shows now a similar drastic fall-off in flux.
- All C200 fluxes are too low and from 170 μm onwards are even negative. This is in contrast to the excellent absolute photometry performance at 170 μm.

Table 8.6: Consistency check of photometric results with HR 6705 model

Filter	**mode**	**consistency w.r.t. model OLP V8.6** [%]	**consistency w.r.t. model OLP V9.0b6** [%]
3.3	multf	-3.23	-0.86
3.6	multf	8.39	9.47
3.6	multf 2	8.62	9.71
4.8	multf	11.93	14.21
7.3	multf	-2.83	-1.13
7.7	multf	6.48	15.79
10.0	multf	-15.43	-12.55
11.3	multf	15.16	13.34
12.0	multf	-14.92	-13.29
12.0	abs	-10.86	-7.38
12.0 IRAS		-7.5	-7.5
12.8	multf	-6.84	-5.99
15.0	multf	64.13	69.70
15.0	multf 2	21.36	23.30
20.0	multf	-2.85	1.55
25.0	multf	2.32	3.41
25.0	abs	-7.09	-1.91
25.0 IRAS		7.1	7.1
60.0 PHT-P	multf	12.64	4.05
60.0 PHT-P	abs	5.88	4.71
60.0 PHT-C	multf	17.89	19.03
60.0 PHT-C(a)	abs	14.43	17.11
60.0 PHT-C(b)	abs	8.71	11.25
60.0 IRAS		-0.8	-0.8
65.0	multf	43.76	44.32
80.0	multf	30.54	35.06
90.0	multf	32.28	31.05
100.0 (PHT-P)	multf	-0.77	-43.71
100.0 (PHT-C)	multf	22.85	26.76
100.0 IRAS		+0.4	+0.4
105.0	multf	-53.69	-43.30
120.0	multf	-81.11	-76.90
150.0	multf	-80.01	-78.54
170.0	multf	-159.50	-158.84
170.0	abs	-7.21	-12.28
180.0	multf	-311.14	-338.70
200.0	multf	-143.50	-152.14

The photometric accuracies are presented in Tab. 8.7. The 15 μm, 100 μm (P3) and 105 μm (C100) results from the multi-filter measurements on revs. 356 and 398 have not been taken into account. Also the C200 multi-filter measurements from rev. 356 could not be used to establish quantitative numbers.

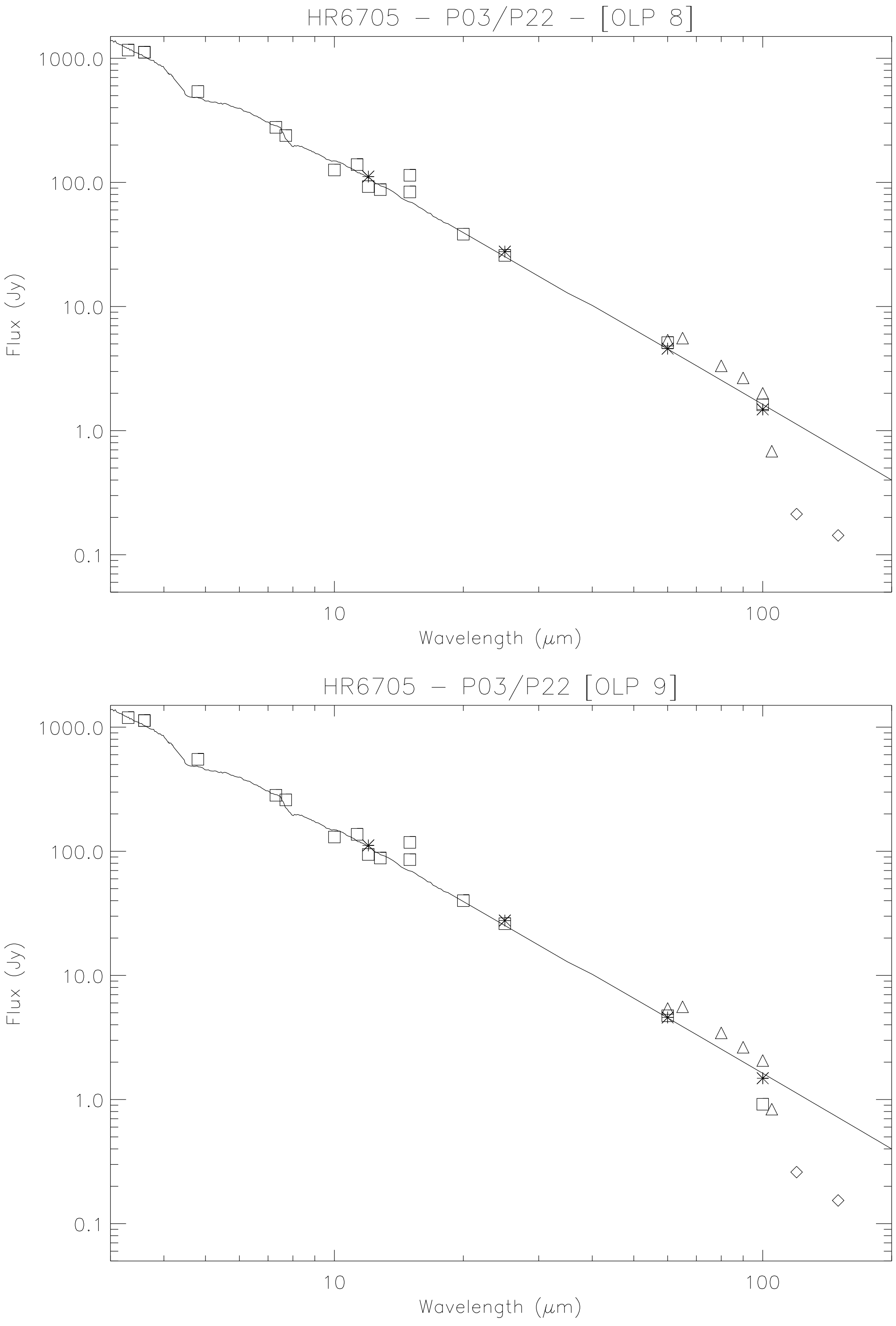

Figure 8.46: Comparison of PHT-P and PHT-C multi-filter photometry (P03/P22), using the full ISOPHOT filter set, with the composite spectrum and out to 300 μm extrapolated SED of γ Dra (HR 6705) provided by M. Cohen and with IRAS photometry for OLP 8.6b1 (upper panel) and OLP 9.0b6 (lower panel). All photometric points are color corrected for a 4000 K BB. The meaning of the symbols is the following: solid line: model, asterisk: IRAS, square: PHT-P (P03 AOT), triangle: C100 (P22 AOT), diamond: C200 (P22 AOT).

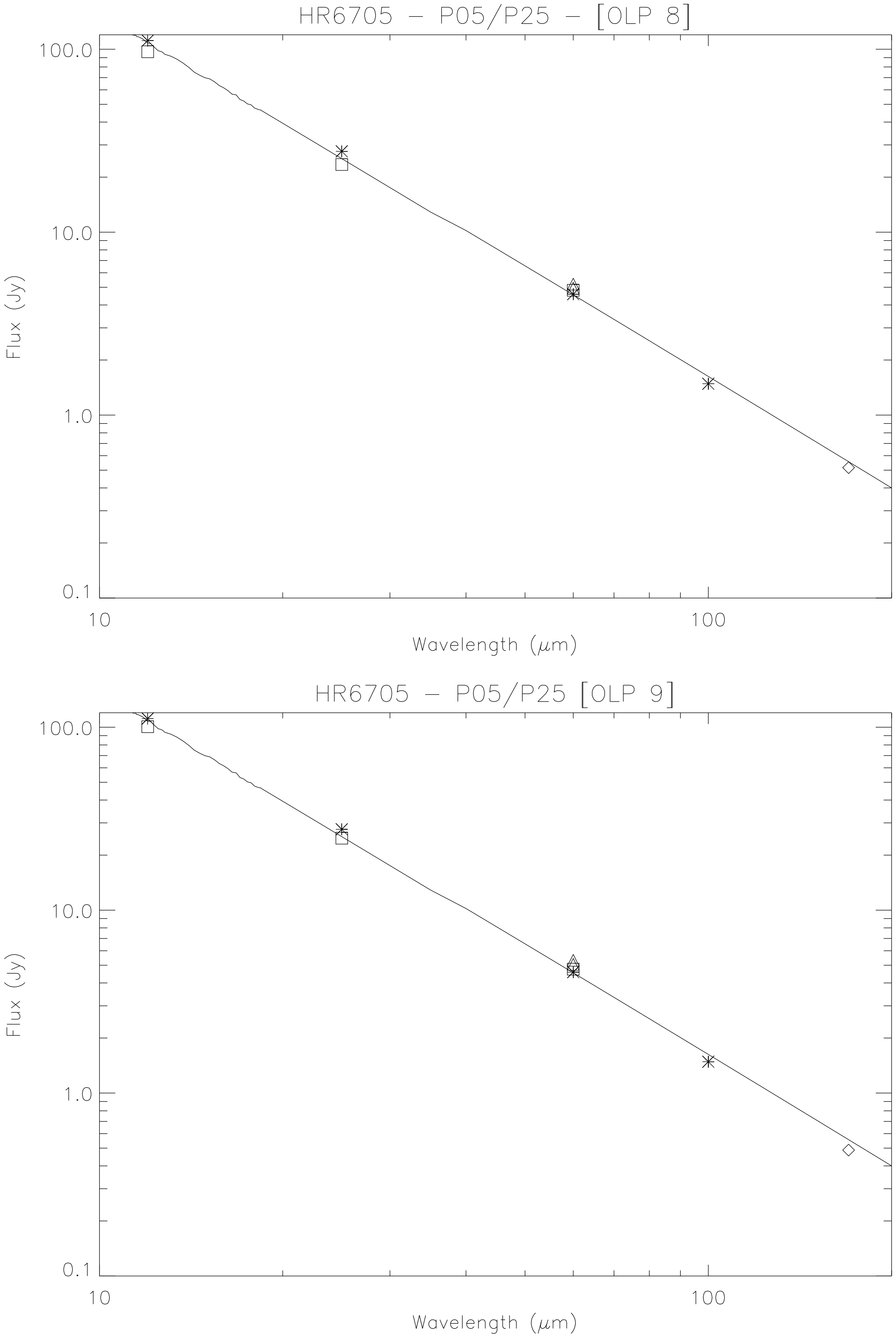

Figure 8.47: Comparison of PHT-P and PHT-C absolute photometry (P05/P25), with the composite spectrum and out to 300 μm extrapolated SED of γ Dra (HR 6705) provided by M. Cohen and with IRAS photometry for OLP 8.6b1 (upper panel) and OLP 9.0b6 (lower panel). All photometric points are color corrected for a 4000 K BB. The meaning of the symbols is the following: solid line: model, asterisk: IRAS, square: PHT-P (P05 AOT), triangle: C100 (P25 AOT), diamond: C200 (P25 AOT).

Table 8.7: Absolute and relative calibration accuracies per detector achieved for HR 6705 observation with OLP V9.0b6

detector	**mode**	**absolute accuracy** [%]	**relative accuracy** [%]
P1	multf	10 at 3.6 μm	25
P1	abs	8 at 12 μm	n/a
P2	multf	$<$ 2 at 20 μm	5
P2	abs	$<$ 2 at 25 μm	n/a
P3	multf	5 at 60 μm	–
P3	abs	5 at 60 μm	n/a
C100	multf	20 at 60 μm	25
C100	abs	$<$ 17 at 60 μm	n/a
C200	abs	12 at 170 μm	n/a

The first attempt to perform a C100 multi-filter sequence on γ Dra on rev. 356 failed due to a telemetry drop which caused non-execution of the three last filter measurements and the FCS calibration measurement. However, the first three filter measurements at 105, 90, and 65 μm are available and are calibrated using the orbit dependent default responsivity calibration. The background is subtracted using the associated background measurement from' rev. 356 which is calibrated using the actual responsivity of its FCS measurement. Fig. 8.48 displays the result. We can see that the 65 and 90 μm filter are reasonably well calibrated (they are 20 % below the model, while the corresponding measurements using the actual responsivity from rev. 398 yield a too high flux by 30 to 40 %). The 105 μm filter shows the same flux fall-off as the corresponding measurement from the complete sequence of rev. 398, which could be due to the derived background flux. From the consistency with the model in the 2 filters we conclude that the default responsivity calibration processing is consistently implemented.
Part 4 of the evaluation log section and Figs. 8.49 to 8.51 provide the surface brightness photometry of the background position and the comparison with COBE both for absolute and multi-filter photometry mode. From Table 8.8 it can be seen that at 25 and 60 μm the consistency of the measurements from the absolute photometry on rev. 353 and from the multi-filter photometry on the two revolutions 356 and 398 with COBE is very good. Looking on Figs. 8.50 and 8.51 we notice again the systematic positive offset in the C100 range for the filters 65, 80, 100 and 105 μm. In particular for the latter two the offset has increased from OLP 8 to OLP 9. The C200 filters yield again a very smooth background SED.

Conclusions

- In the P1 and P2 part of the SED we do not recognize significant changes from OLP 8 to OLP 9. There is a slight improvement of the P2 accuracy. The large offset of the 15 μm flux from the rev. 356 measurement can be attributed to 2/3 to transients, which is exceptional among the considered OLP test cases.
- For P3 the good relative filter-to-filter calibration reported last time is lost, presumably by a too high background value derived for the 100 μm filter.
- For C100 the positive offset in flux of 20 – 40 % for all filters remains. A default responsivity calibration for C100 gives reasonably accurate photometry, however the fluxes are lower than the model in contrary to the fluxes derived with actual responsivity calibration. An exception is the 105 μm filter which shows a strong flux fall-off both for actual and default responsivity calibration method. Very likely this is caused by the background subtraction.
- For C200 in multi-filter mode no useful results could be achieved. The fluxes are all too low or even negative.

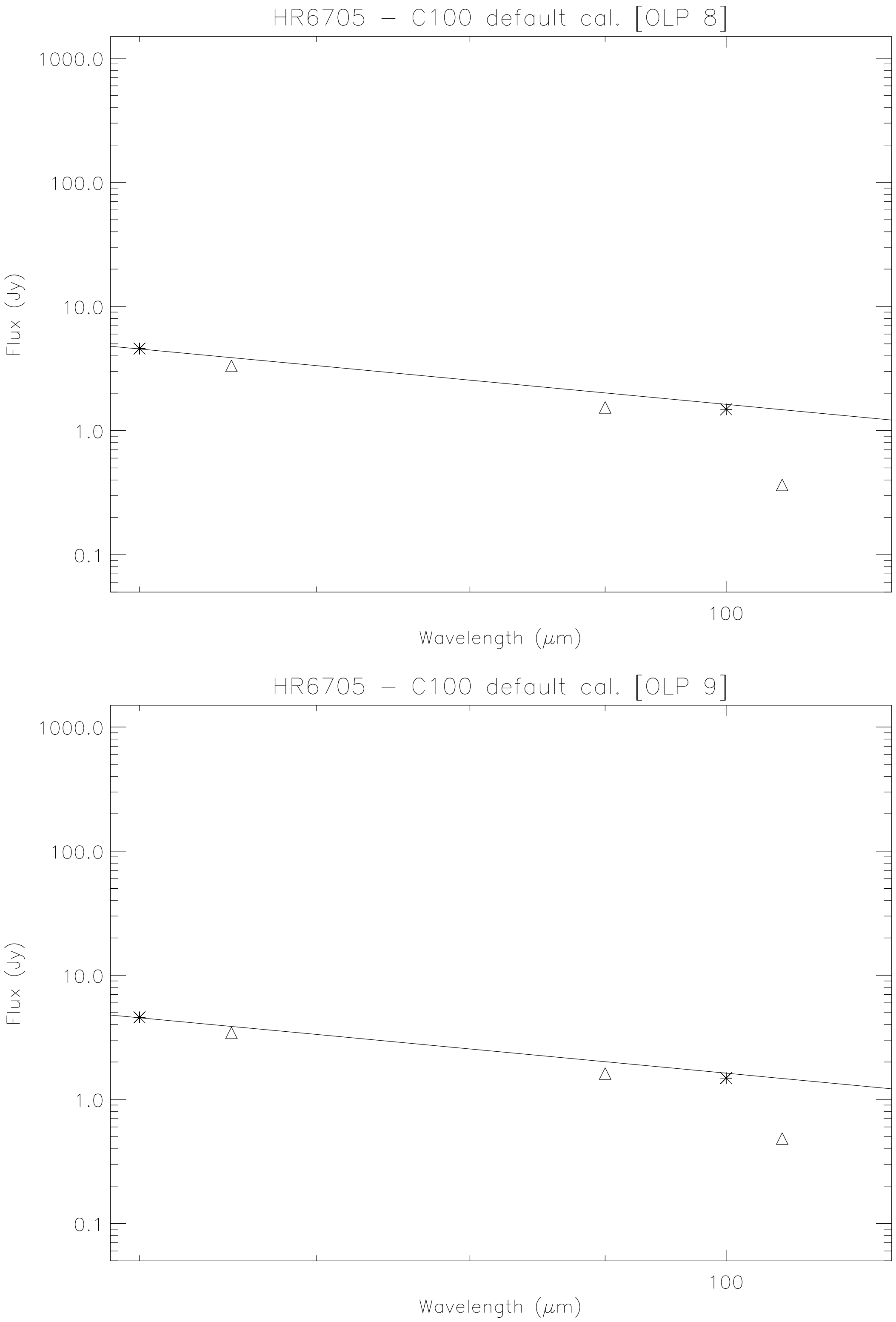

Figure 8.48: Comparison of the (incomplete due to telemetry drop) C100 PHT-C multi-filter photometry (P22) from rev. 356, using the default responsivity calibration (C100 FCS measurement failed due to the telemetry drop), with the out to 300 μm extrapolated SED of γ Dra (HR 6705) provided by M. Cohen and with IRAS photometry for OLP 8.6b1 (upper panel) and OLP 9.0b6 (lower panel). All photometric points are color corrected for a 4000 K BB. The meaning of the symbols is the following: solid line: model, asterisk: IRAS, triangle: C100 (P22 AOT).

Table 8.8: Consistency check of γ Dra background position surface brightness results with COBE/DIRBE annual maps. Rev. 353 results are from absolute photometry, revs. 356 and 398 results are from multi-filter photometry.

wavelength μm	**consistency w.r.t. COBE OLP V8.6** [%]	**consistency w.r.t. COBE OLP V9.0b6** [%]
12 (rev 353)	-16.1	+32.0
25 (rev 353)	+6.0	-1.3
60 (rev 353)	-0.8	+1.5
60 (rev 353)	+3.7	+3.5
60 (rev 356)	-4.9	-1.1
60 (rev 398)	+10.5	+13.1
100 (rev 356)	+11.5	+18.1
100 (rev 398)	+32.9	+38.1
150 (rev 356)	-35.2	-36.3
200 (rev 356)	+1.0	+11.2

- Absolute photometry gives an accuracy of better than 15 % for all detectors, even for the 170 μm filter of C200 in stark contrast to the multi-filter measurement.
- The consistency check of surface brightness photometry with COBE/DIRBE gives very good results for the 25 and 60 μm filters (for 60 μm also a good internal consistency is found). For the multi-filter mode we notice again like in may other cases the positive offsets of surface brightness w.r.t. COBE/DIRBE in the 65, 80, 100 and 105 μm filters. The C200 filters yield a smooth background SED pointing to a good relative filter-to-filter calibration.

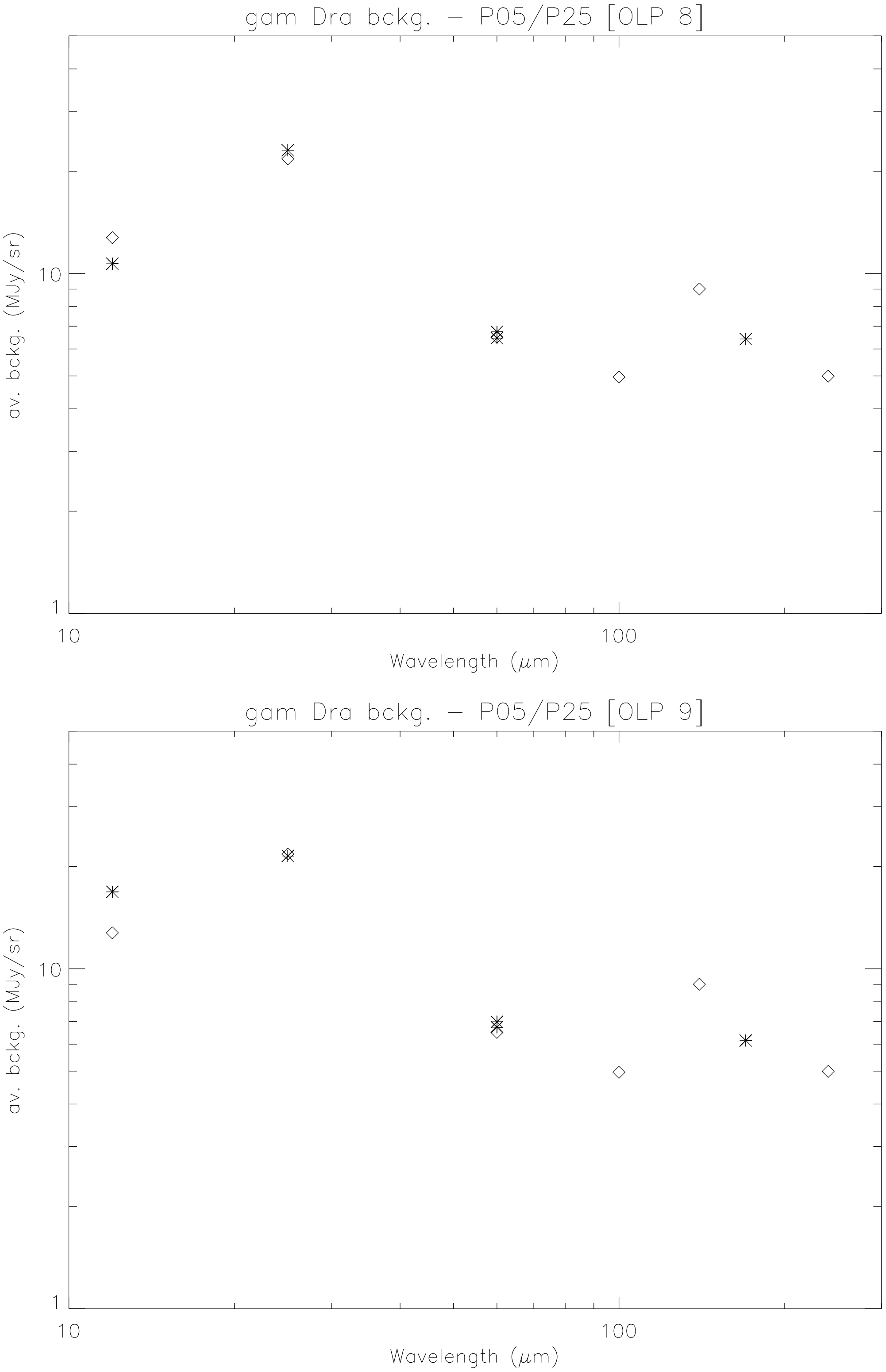

Figure 8.49: Comparison of OLP V8.6b1 and OLP V9.0b6 surface brightness, determined with the absolute photometry mode P05/P25 (asterisk) on revolution 353, with COBE annual map fluxes (diamond).

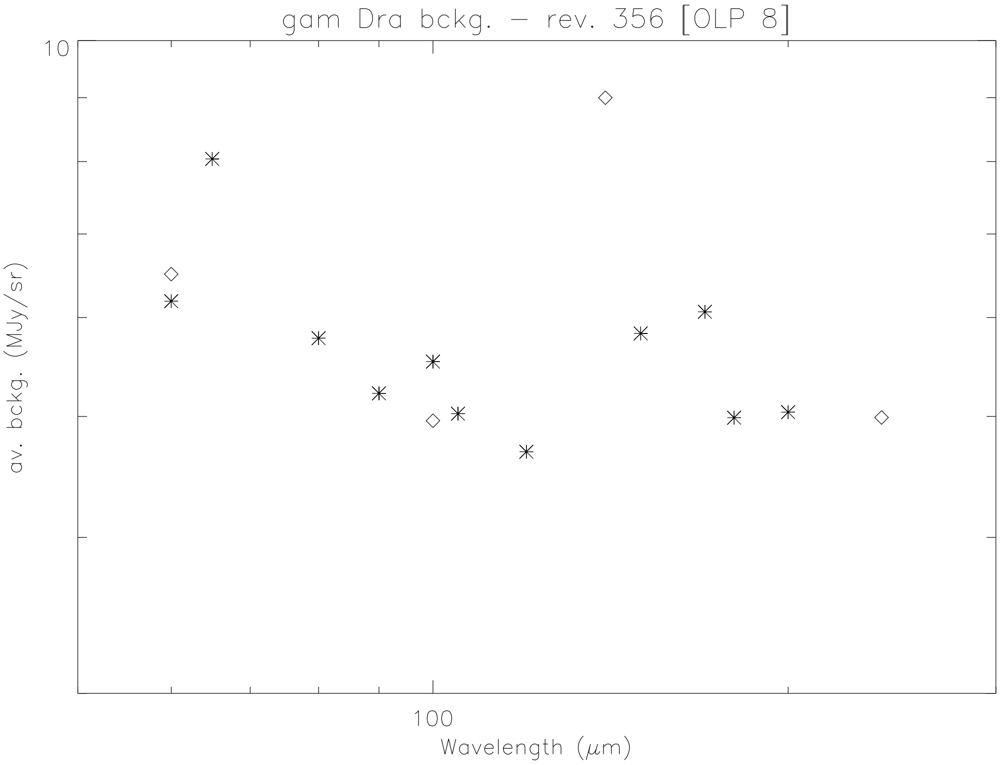

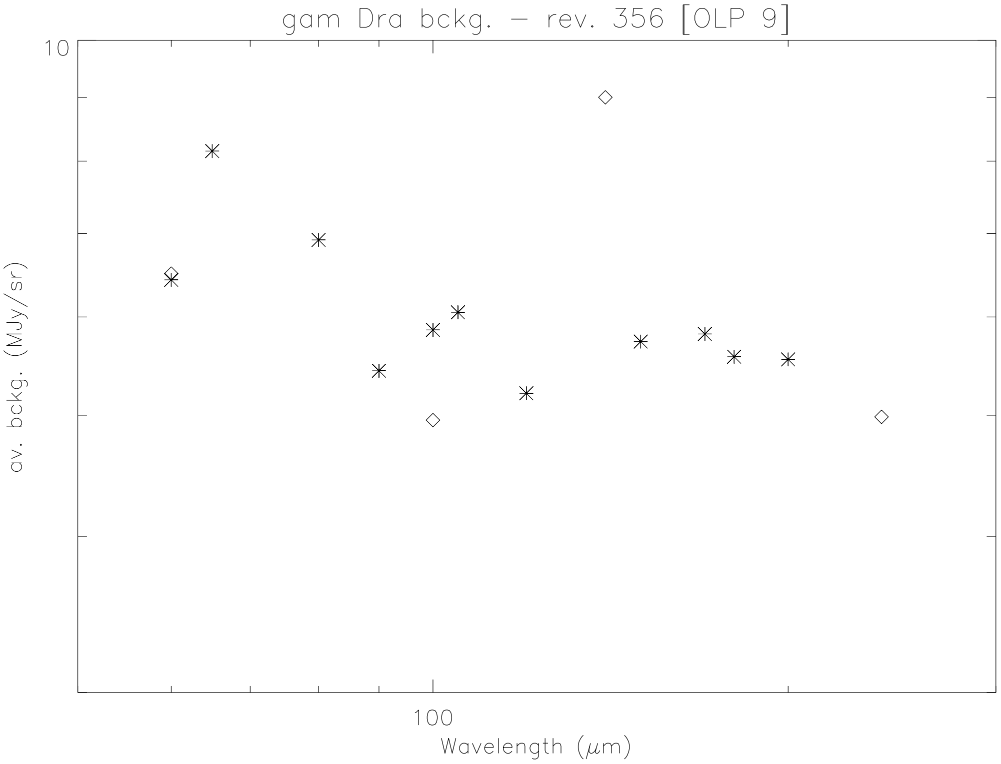

Figure 8.50: Comparison of OLP V8.6b1 and OLP V9.0b6 C100 and C200 surface brightness, determined with the multi-filter photometry mode P22 (asterisk) on revolution 356, with COBE annual map fluxes (diamond).

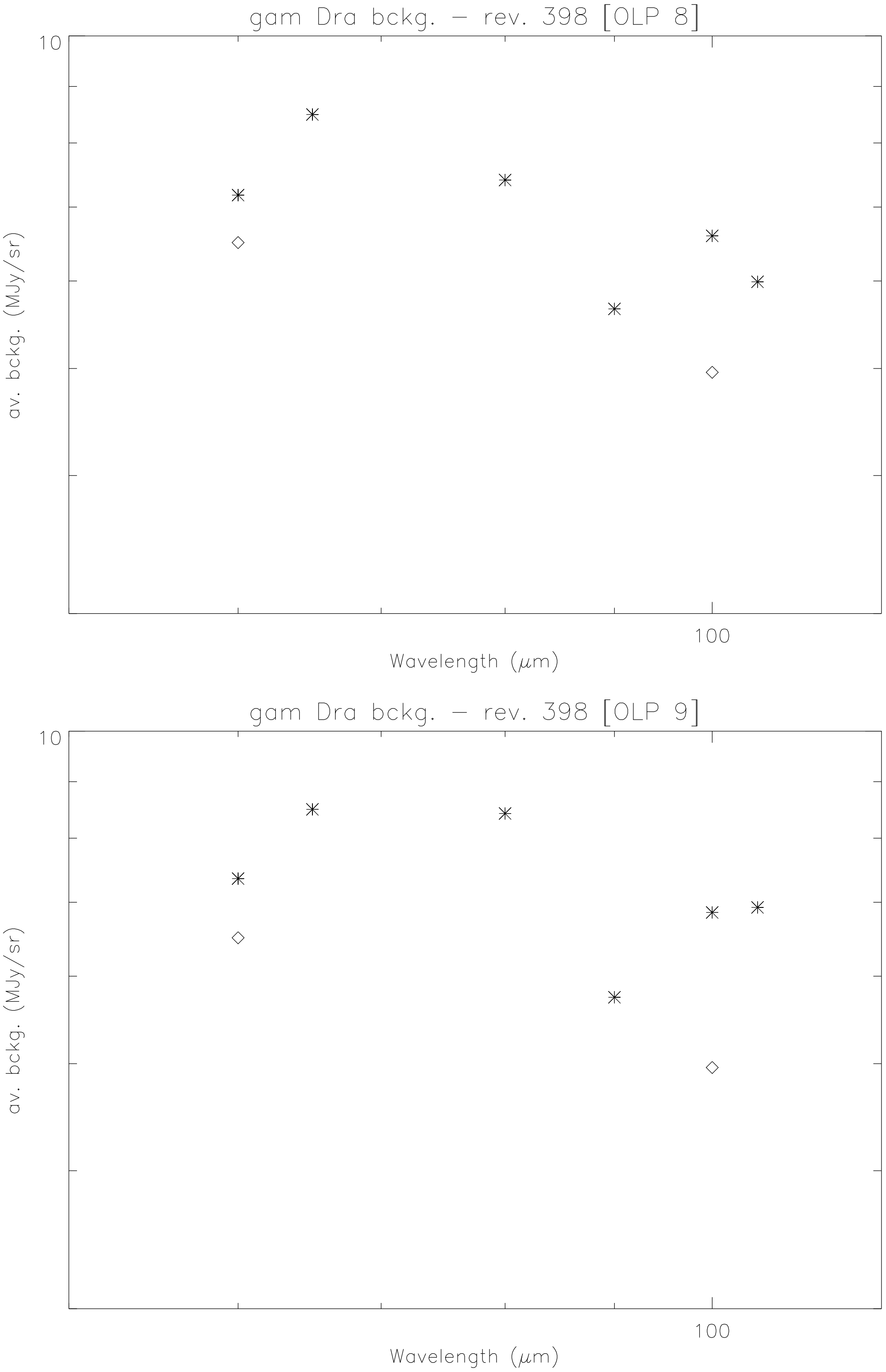

Figure 8.51: Comparison of OLP V8.6b1 and OLP V9.0b6 C100 surface brightness, determined with the multi-filter photometry mode P22 (asterisk) on revolution 398, with COBE annual map fluxes (diamond).

Evaluation Log

1) P03 and P22 multi-filter photometry

Measurements:		
PHT-P:	ppap35602102 (src+back)	FCS = 3.6, 20, 60 um
	ppap39801901 (src+back)	FCS = 3.6 um (3.6 & 15 um only)
	ppae35602101 (back)	FCS = 12, 20, 100 um
PHT-C1:	pcap39802003 (src+back)	FCS = 60 um
	pcae39802002 (back)	FCS = 90 um
PHT-C2:	pcap35602204 (src+back)	FCS = 170 um
	pcae35602203 (back)	FCS = 170 um

Colour correction: black body, T = 4000 K

Model: Cohen

Det	cwl (μm)	OLP 8	OLP 9	IRAS	Model	Δ (OLP 8)	Δ (OLP 9)
P1	3.3	1164.273	1192.860		1203.159	-3.23	-0.86
P1	3.6	1117.075	1128.218		1030.575	8.39	9.47
P1b	3.6	1119.436	1130.687		1030.575	8.62	9.71
P1	4.8	539.840	550.869		482.322	11.93	14.21
P1	7.3	277.822	282.687		285.925	-2.83	-1.13
P1	7.7	238.588	259.463		224.074	6.48	15.79
P1	10.0	126.034	130.315		149.024	-15.43	-12.55
P1	11.3	139.136	136.942		120.822	15.16	13.34
P1	12.0	92.502	94.265	111.479	108.718	-14.92	-13.29
P1	12.8	87.453	88.252		93.877	-6.84	-5.99
P1	15.0	114.088	117.956		69.510	64.13	69.70
P1b	15.0	83.790	85.706		69.510	20.54	23.30
P2	20.0	38.263	39.997		39.387	-2.85	1.55
P2	25.0	25.813	26.089	27.671	25.229	2.32	3.41
C1	60.0	5.358	5.410	4.583	4.545	17.89	19.03
P3	60.0	5.119	4.729	4.583	4.545	12.64	4.05
C1	65.0	5.567	5.588		3.872	43.76	44.32
C1	80.0	3.329	3.444		2.550	30.54	35.06
C1	90.0	2.662	2.637		2.012	32.28	31.05
C1	100.0	1.999	2.062	1.483	1.627	22.85	26.76
P3	100.0	1.614	0.916	1.483	1.627	-0.77	-43.71
C1	105.0	0.683	0.836		1.474	-53.69	-43.30
C2	120.0	0.213	0.260		1.126	-81.11	-76.90
C2	150.0	0.143	0.154		0.717	-80.01	-78.54
C2	170.0	-0.331	-0.327		0.556	-159.50	-158.84
C2	180.0	-1.046	-1.183		0.495	-311.14	-338.70
C2	200.0	-0.174	-0.209		0.400	-143.50	-152.14

2) P05 and P25 absolute photometry

Measurements:

PHT-P1:	ppap35300302 (src+back)
	ppae35300301 (back)
PHT-P2:	ppap35300304 (src+back)
	ppae35300303 (back)
PHT-P3:	ppap35300306 (src+back)
	ppae35300305 (back)
PHT-C1:	pcap35300309 (src+back)
	pcae35300310 (src+back, b)
	pcae35300308 (back)
PHT-C2:	pcap35300312 (src+back)
	pcae35300311 (back)

Colour correction: black body, T = 4000 K

Model: Cohen

Det	cwl (μm)	OLP 8	OLP 9	IRAS	Model	Δ (OLP 8)	Δ (OLP 9)
P1	12.0	96.917	100.697	111.479	108.718	-10.86	-7.38
P2	25.0	23.440	24.748	27.671	25.229	-7.09	-1.91
P3	60.0	4.812	4.759	4.583	4.545	5.88	4.71
C1	60.0	5.201	5.323	4.583	4.545	14.43	17.11
C1b	60.0	4.941	5.056	4.583	4.545	8.71	11.25
C2	170.0	0.516	0.488		0.556	-7.21	-12.28

3) C100 on-source default calibration

Measurements:

PHT-C1:	pcap35602204 (src+back)	no FCS (orbit dep. default R)
	pcae35602203 (back)	FCS = 90 um

Colour correction: black body, T = 4000 K

Model: Cohen

Det	cwl (μm)	OLP 8	OLP 9	IRAS	Model	Δ (OLP 8)	Δ (OLP 9)
C1	65.0	3.322	3.433		3.872	-14.21	-11.33
C1	90.0	1.537	1.614		2.012	-23.62	-19.76
C1	105.0	0.365	0.483		1.474	-75.26	-67.21

4) Surface brightness on background positions:

a) absolute photometry on revolution 353

λ	OLP8 (MJy/sr)	OLP9 (MJy/sr)	COBE (MJy/sr)
12.0	10.69	16.83	12.75
25.0	23.06	21.47	21.75
60.0	6.45	6.99	6.50
60.0	6.74	6.73	6.50
170.0	6.42	6.15	

b) multi-filter C100 and C200 photometry on revolution 356

λ	OLP8 (MJy/sr)	OLP9 (MJy/sr)	COBE (MJy/sr)
60.0	6.18	6.43	6.50
65.0	8.04	8.15	
80.0	5.78	6.92	
90.0	5.22	5.43	
100.0	5.53	5.86	4.96
105.0	5.02	6.05	
120.0	4.68	5.21	
150.0	5.83	5.73	9.00
170.0	6.06	5.81	
180.0	4.99	5.58	
200.0	5.04	5.55	4.99

c) multi-filter C100 photometry on revolution 398

λ	OLP8 (MJy/sr)	OLP9 (MJy/sr)	COBE (MJy/sr)
60.0	7.18	7.35	6.50
65.0	8.49	8.50	
80.0	7.41	8.42	
90.0	5.66	5.74	
100.0	6.59	6.85	4.96
105.0	5.99	6.93	

8.4.5 General Re-validation of PHT03 and PHT05 Staring Mode: The SED of Sirius (HR 2491) - Final Assessment

- authors: U. Klaas
- date: 15-May-2000
- SVP period 2

Motivation

Beside Vega (HR 7001), Sirius is the main primary stellar standard with a model provided by M. Cohen (1-300 μm, R = 4000 up to 35 μm, delivered 12-Jan-1996). Therefore, a dedicated cross-calibration program was performed on this star using absolute photometry complemented by multi-filter photometry out to 25 μm.

Method

We compare the color corrected flux values of both OLP V8.6 and OLP V9.0b6 results against the model prediction by Cohen and IRAS photometry.

Results

In the following Tab. 8.9 we compare the photometry from part 1 of the evaluation log section with the model. We estimate the absolute photometric accuracy per detector assembly for this target as the deviation from the model flux in the filter in which the FCS calibration was done, and the relative filter-to-filter accuracy as the peak-to-peak variation of the other filters around this offset. Two multi-filter sequences were performed, one from 3.3 to 12 μm with absolute calibration at 3.3 μm, and the other one from 11.3 to 15 μm with absolute calibration at 12.8 μm. The photometric accuracies are presented in Tab. 8.10. Fig. 8.52 shows the PHT photometric data points in comparison to the model and IRAS photometry (color corrected) for OLP 8.6 and OLP 9.0b6, respectively. The systematic offset beyond 10 μm is caused by the fact that no background measurement is available and hence the background, which is noticable here, is not subtracted. Therefore, the calibration accuracies for these wavelengths are actually better, since the background is estimated to account for nearly the whole offset.

Table 8.9: Consistency check of photometric results with Sirius model

Filter	**mode**	**consistency w.r.t. model OLP V8.6** [%]	**consistency w.r.t. model OLP V9.0b6** [%]
3.3	multf	10.88	7.28
3.3	abs	3.87	0.35
7.7	multf	4.01	6.69
11.3	multf	17.11	9.84
12.0	multf	11.56	7.41
12.0	abs	2.12	6.40
12.8	multf	15.52	14.83
15.0	multf	16.06	13.15
25.0	abs	12.48	13.88

Conclusions

- The accuracy of the absolute photometry on Sirius is better than 5 % (for P2 25 μm this is derived estimating the amount of the non-subtracted background due to lack of a measurement).

Table 8.10: Absolute and relative calibration accuracies per detector achieved for Sirius observation with OLP V9.0b6

detector	**mode**	**absolute accuracy** [%]	**relative accuracy** [%]
P1	multf	8 at 3.3 μm	1
P1	abs	4 at 3.3 μm	n/a
P1*	abs	< 6 at 12.0 μm	n/a
P1*	multf	< 15 at 12.8 μm	5
P2*	abs	< 14 at 25 μm	n/a

* no subtraction of ZL background performed!

- The accuracy of P1 multi-filter photometry is better than 10 % absolute and better than 5 % relative.

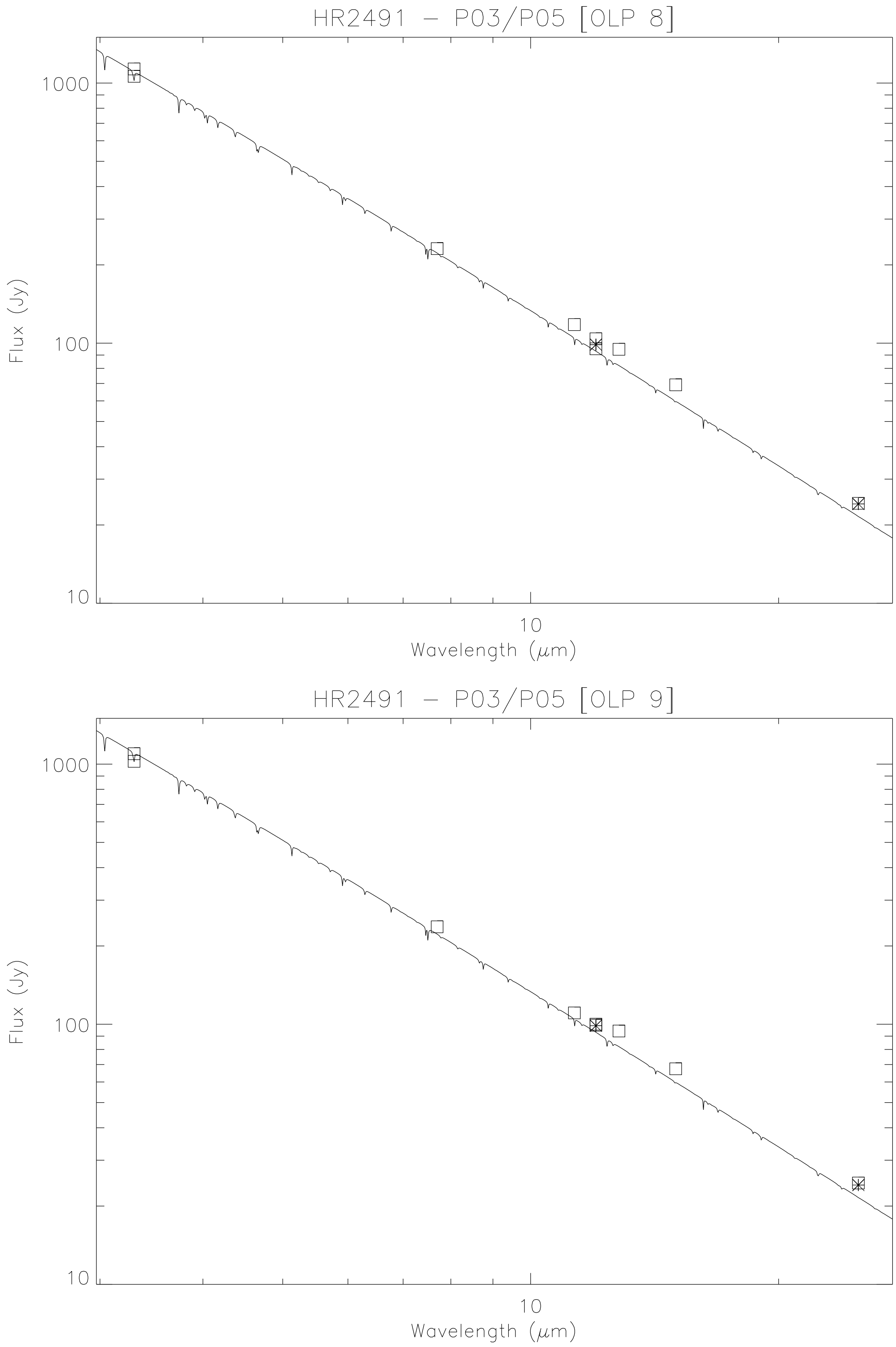

Figure 8.52: Comparison of PHT-P absolute and multi-filter photometry with the composite spectrum of Sirius (HR 2491) provided by M. Cohen and with IRAS photometry for OLP 8.6b1 (upper panel) and OLP 9.0b6 (lower panel). All photometric points are color corrected for a 10000 K BB. The meaning of the symbols is the following: solid line: model, asterisk: IRAS, square: PHT-P (P03 and P05 AOTs).

Evaluation Log

1) P03 multi-filter and P05 absolute photometry

Measurements:		
PHT-P1:	ppap70705302 (src+back)	FCS = 3.3 um
	ppap70705301 (src+back)	FCS = 12.8 um
	ppap70705310 (src+back)	P05
	ppap70705313 (src+back)	P05
PHT-P2:	ppap70705307 (src+back)	P05

Colour correction: black body, T = 10000 K

Model: Cohen

Det	cwl (μm)	OLP 8	OLP 9	IRAS	Model	Δ (OLP 8)	Δ (OLP 9)
ppap70705301:							
P1	11.3	117.881	110.563		100.654	17.11	9.84
P1	12.8	94.729	94.161		82.001	15.52	14.83
P1	15.0	69.134	67.398		59.566	16.06	13.15
ppap70705302:							
P1	3.3	1133.059	1096.323		1021.900	10.88	7.28
P1	7.7	230.947	236.889		222.038	4.01	6.69
P1	12.0	103.930	100.059	98.690	93.157	11.56	7.41
ppap70705310:							
P1b	3.3	1061.453	1025.462		1021.900	3.87	0.35
ppap70705313:							
P1b	12.0	95.136	99.117	98.690	93.157	2.12	6.40
ppap70705707:							
P2	25.0	24.229	24.531	24.092	21.541	12.48	13.88

8.4.6 General Re-validation of PHT05 Staring Mode: The SED of α Ari (HR 617) - Final Assessment

- authors: U. Klaas
- date: 30-July-2000
- SVP period 2

Motivation

For the star α Ari a complete suite of absolute photometry measurements was performed out to 100 μm. We can therefore test the absolute calibration accuracies of all PHT-P filters in the flux range covered by this star. The star is about half as bright as Sirius and γ Dra. In this version of the report we restrict the analysis to a wavelength up to 25 μm, since we do not perform any background subtraction and the contribution by the background becomes noticable from 20 μm onwards. The background measurements for the star a covered by nodding observations which will be analyzed in a later version of the report.

Method

We compare the color corrected flux values of OLP V9.01 results against the model prediction by Cohen and IRAS photometry.

Results

Fig. 8.53 shows the results of this comparison. For P1 we find very accurate absolute photometry of better than 10% for the 3.3, 3.6, 7.3, 7.7, 10, 12, and 15 μm filter. The plot shows that inside the 4.8 μm range there is a noticable absorption feature, so the color correction with a pure black body is not correct and the effect by the different SED needs to be investigated. The 11.3 and 12.8 μm filters show clear offsets, which are probably due to intrinsic calibration uncertainties. For the 12.8 mum filter we find a clear trend of increasing relative flux offset towards fainter sources for other test cases investigated in this section (e.g. 8.4.8 and 8.4.9). Therefore this filter has to be flagged as giving high photometric uncertainties for fluxes below 100 Jy. For P2 it becomes noticable that no background subtraction has been performed. From a background estimate at 25 μm using COBE/DIRBE fluxes, the contribution to the total flux is around 25 % which would give a final consistency with the model of 7 %. Therefore also the P2 absolute photometry is better than 10 % for the examined flux range.

Conclusions

- We find very accurate absolute photometry results with accuracies better than 10 % over the full P1 filter range. The 4.8 μm filter color correction appears to be not appropriate due to an underlying absorption feature. This will be investigated in more detail. The two filters 11.3 and 12.8 μm show a less good performance and in particular the 12.8 μm filter photometry has to be flagged as less reliable over a large flux range ($<$ 100 Jy) with the relative uncertainties becoming larger and larger for fainter total flux. This should be rectified with the next OLP version (10.0).
- The conclusions for P2 absolute photometry are currently restricted due to the not yet performed proper background subtraction; data on the background level are available from parallelly performed nodding observations. Estimations using COBE/DIRBE photomery at 25 μm lead to the conclusion, that the P2 absolute photometry is as accurate as 10 %, too.

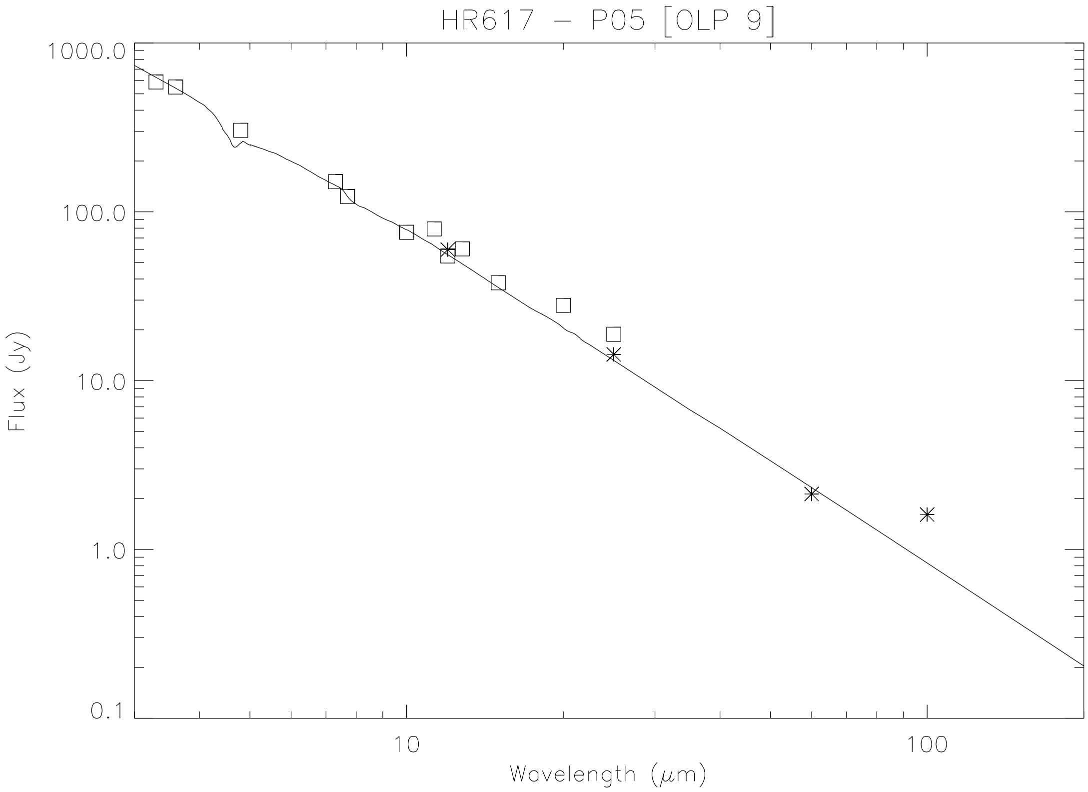

Figure 8.53: Comparison of PHT-P absolute photometry with the composite spectrum of α Ari (HR 617) plus extrapolation out to 300 μm provided by M. Cohen and with IRAS photometry for OLP 9.01 (lower panel). All photometric points are color corrected for a 4000 K BB. The meaning of the symbols is the following: solid line: model, asterisk: IRAS, square: PHT-P (P05).

Evaluation Log

1) P05 absolute photometry (no background subtraction yet!)

Measurements:		
PHT-P1:	ppap80400408 (src+back)	3.3 um
	ppap80400411 (src+back)	3.6 um
	ppap80400410 (src+back)	4.8 um
	ppap80400409 (src+back)	7.3 um
	ppap80400407 (src+back)	7.7 um
	ppap80400406 (src+back)	10 um
	ppap80400405 (src+back)	11.3 um
	ppap80400404 (src+back)	12 um
	ppap80400403 (src+back)	12.8 um
	ppap80400401 (src+back)	15 um
PHT-P2:	ppap79001603 (src+back)	20 um
	ppap79001601 (src+back)	25 um

Colour correction: black body, T = 4000 K

Model: Cohen

Det	cwl (μm)	OLP 8	OLP 9	IRAS	Model	Δ (OLP 8)	Δ (OLP 9)
P1	3.3	0.000	587.522		625.866	-100.00	-6.13
P1	3.6	0.000	548.872		540.252	-100.00	1.60
P1	4.8	0.000	303.946		255.084	-100.00	19.16
P1	7.3	0.000	150.938		143.409	-100.00	5.25
P1	7.7	0.000	123.353		123.240	-100.00	0.09
P1	10.0	0.000	75.639		78.282	-100.00	-3.38
P1	11.3	0.000	79.202		62.951	-100.00	25.82
P1	12.0	0.000	54.748	59.690	55.717	-100.00	-1.74
P1	12.8	0.000	60.326		49.125	-100.00	22.80
P1	15.0	0.000	37.969		35.649	-100.00	6.51
P2	20.0	0.000	27.906		20.520	-100.00	35.99
P2	25.0	0.000	18.821	14.293	13.180	-100.00	42.80

8.4.7 General Re-validation of PHT03 Staring Mode: Photometric Reproducibility Aspects in the Case of the SED of Vega (HR 7001) - Final Assessment

- authors: U. Klaas
- date: 15-May-2000
- SVP period 2

Motivation

We investigate here the photometric accuracy of PHT-P multi-filter aperture photometry for an observation of Vega from a general observer program which was repeated several times as part of a variability monitoring project. From 3.3 to 100 μm it used the typical exposure time of 32 s per filter and non-standard apertures. The absolute calibration via the FCS of the on-source measurement was performed in the 3.6, 20, and 100 μm filter, respectively. The absolute calibration of the off-source measurement was performed in the 7.3, 25, and 100 μm filter, respectively. We selected 3 measurements out of this program from rev. 85 (TDT 08500106; before rev. 94 FCS change!), rev. 558 (TDT 55800419) and rev. 865 (TDT 86500706). The used apertures w.r.t. the standard apertures for point source calibration are listed in the following Table 8.11:

Table 8.11: Apertures used in the Vega variability monitoring program versus standard apertures

filter	**program aperture** ["]	**standard aperture** ["]
P1_3P29_UM	18	23
P1_3P6_UM	18	23
P1_4P85_UM	18	23
P1_7P3_UM	18	23
P1_10_UM	18	52
P1_11P5_UM	18	52
P1_12P8_UM	18	52
P1_16P0_UM	18	52
P2_20_UM	52	79
P2_25_UM	52	79
P3_60_UM	120	180
P3_100_UM	120	180

Method

Vega is one of the primary photometric stellar standards. However, due to its IR excess, the photospheric models, e.g. by Cohen, are valid only out to approximately 15 μm. Beyond 15 μm we solely compare with the available IRAS photometry.
The color correction was dependent on the relative contribution by the stellar photosphere and the IR disc, and hence on the wavelength. We followed the description as given in Ref.[14]:

- from 3.3 to 16 μm the SED behaves like a 10000 K Black Body,
- from 60 to 100 μm the SED behaves like an 80 K modified BB, $\varepsilon \propto \nu$
- from 20 to 25 μm the SED is a mixture of a 10000 K BB and an 80 K modified BB with a ratio 2:1.

Results

In parts 1 to 3 of the evaluation log section we give the background subtracted and color corrected photometry for the three epochs. We notice that with regard to OLP V8.6 there are slight changes in the fluxes, namely

- the $25\,\mu$m flux is noticably higher for all three cases.
- there is a minor increase of the $60\,\mu$m flux for all three cases giving better consistency with the IRAS flux.

For illustration the resulting SEDs are plotted in Figs. 8.54 to 8.56. The excess of the $12.8\,\mu$m flux can be explained to a large extent by the general trend for this filter found for other test cases (see. e.g. Sect. 8.4.6, 8.4.8, 8.4.9) and hence due to the linearisation correction for this filter. This is supported by the fact that for OLP 7 with no linearisation correction the fluxes were closer to the model. The flux offset in the $15\,\mu$m filter seems to be due to a different nature. It is always the first filter in the P1 sequence and very likely most heavily affected by transients. An offset of this order is possible when comparing against a similar measurement sequence for the equally bright star γ Dra (cf. Sect. 8.4.4). Remarkable is also the relatively strong negative offset for the $12\,\mu$m flux for which there is currently no explanation.

Conclusions

- The relative spectral shapes derived from the repeated measurement sequence do not differ too much from those found for OLP 8.6 (cf. [1]). The P2 fluxes are in general noticably higher now being less consistent with IRAS (for the applied complex colour correction!). The P3 $60\,\mu$m fluxes are slightly increased and are more consistent with IRAS now (still there is the difference between measurements 1 & 3 and 2). Since measurement 1 was calibrated with the pre-rev. 94 calibration thsi shows the good consistency for the two sets of calibration files for P3 for this flux range.
- The absolute calibration accuracy of P1 is better than 10 %, the relative filter-to-filter calibration out to $10\,\mu$m is in the order of 10 %, too. The consistency with IRAS at $60\,\mu$m (with the maximum of the FIR excess) is around 10 %.
- The excess of the $12.8\,\mu$m filter flux fits into the general trend for a positive flux excess for other test cases and should be explained by an improper linearity correction.
- The excess of the $15\,\mu$m flux is however very likely due to transient effects, the measurement in this filter being the first one in a sequence with a large flux gradient up to the calibration filter at $3.6\,\mu$m.

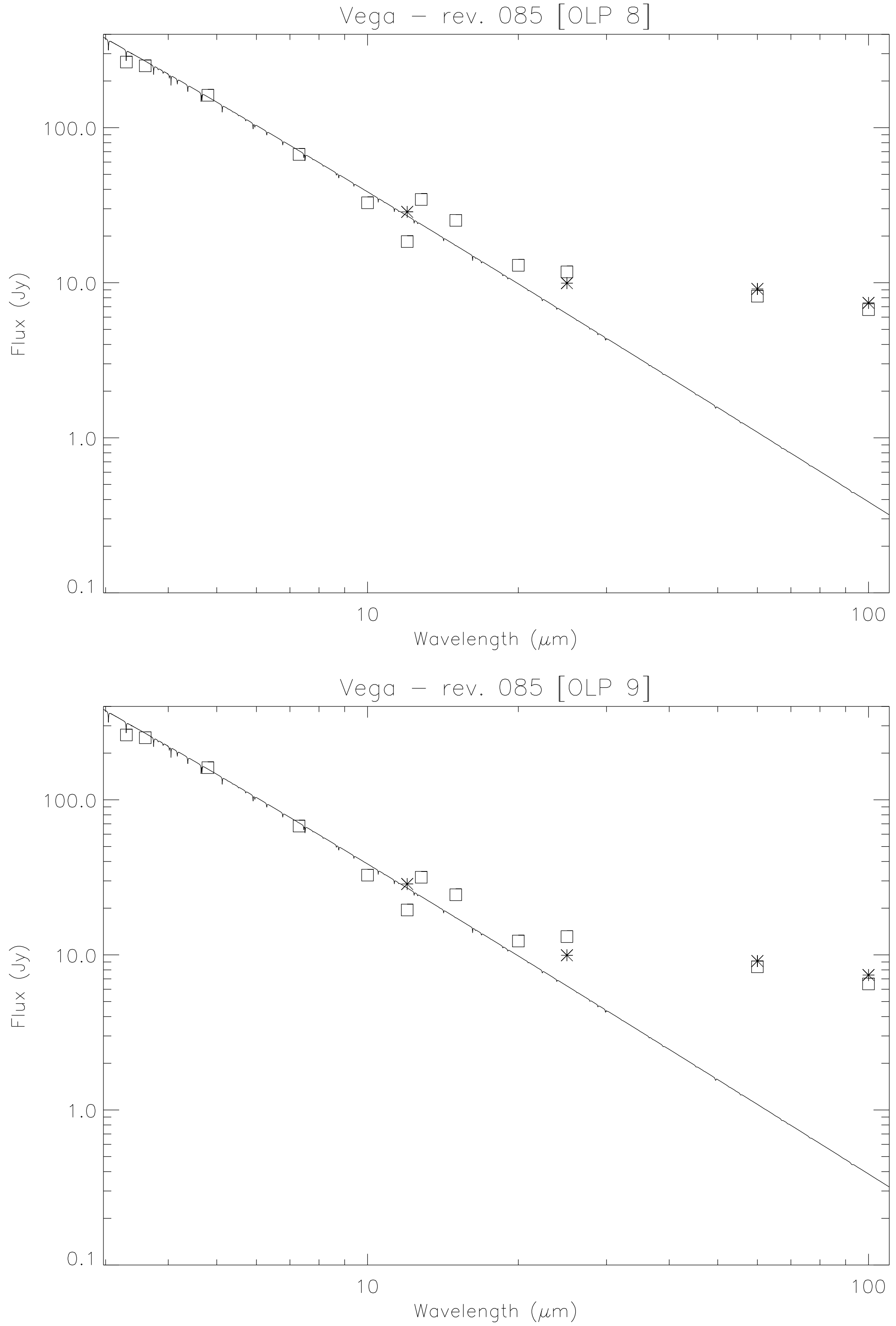

Figure 8.54: Comparison of PHT-P multi-filter photometry of Vega (HR 7001) on revolution 085 with the composite spectrum provided by M. Cohen out to $15\,\mu$m and with IRAS photometry beyond $15\,\mu$m for OLP 8.6b1 (upper panel) and OLP 9.0b6 (lower panel). A description of the applied color correction factors is given in the text. The meaning of the symbols is the following: solid line: model, asterisk: IRAS, square: PHT-P.

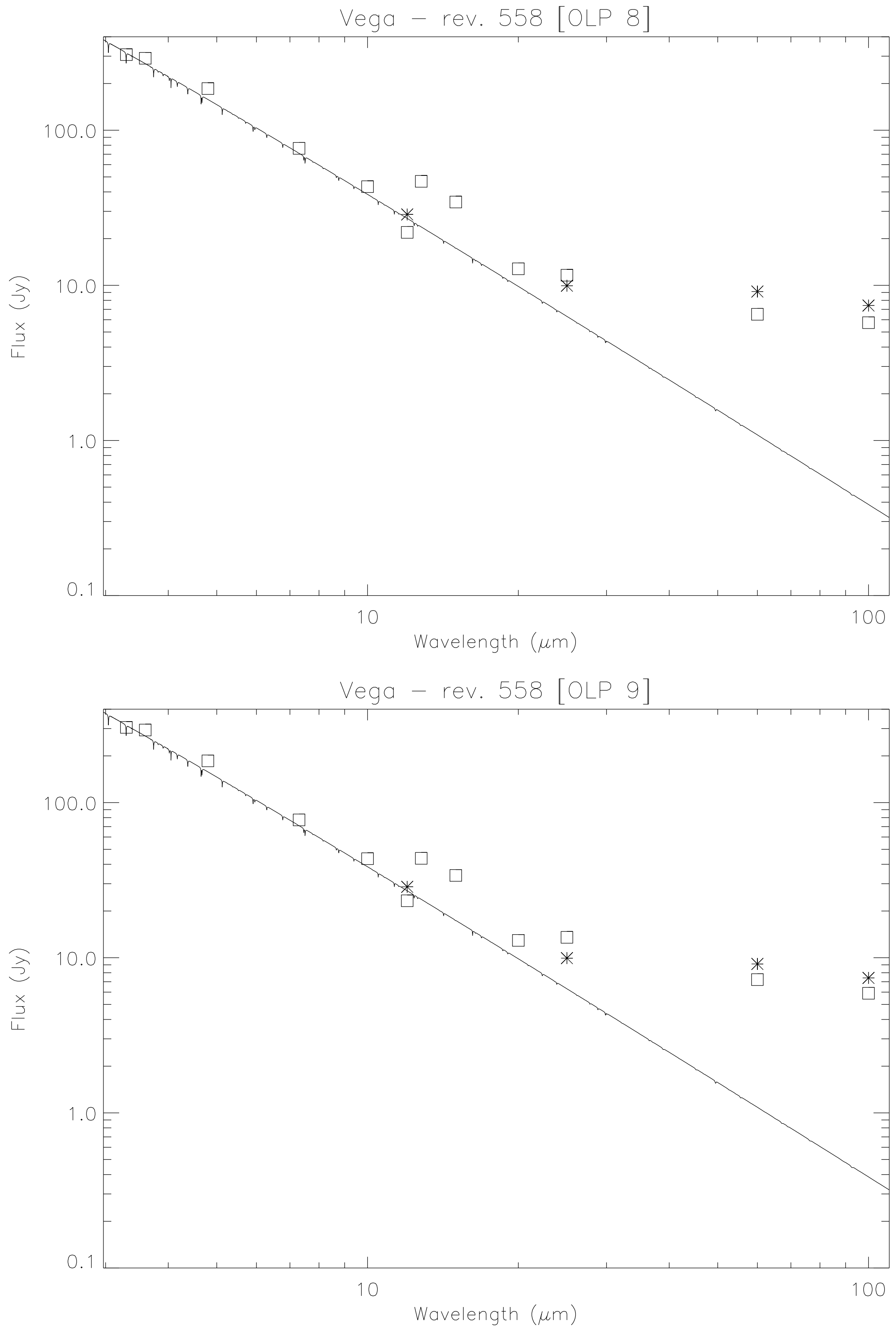

Figure 8.55: Comparison of PHT-P multi-filter photometry of Vega (HR 7001) on revolution 558 with the composite spectrum provided by M. Cohen out to 15 μm and with IRAS photometry beyond 15 μm for OLP 8.6b1 (upper panel) and OLP 9.0b6 (lower panel). A description of the applied color correction factors is given in the text. The meaning of the symbols is the following: solid line: model, asterisk: IRAS, square: PHT-P.

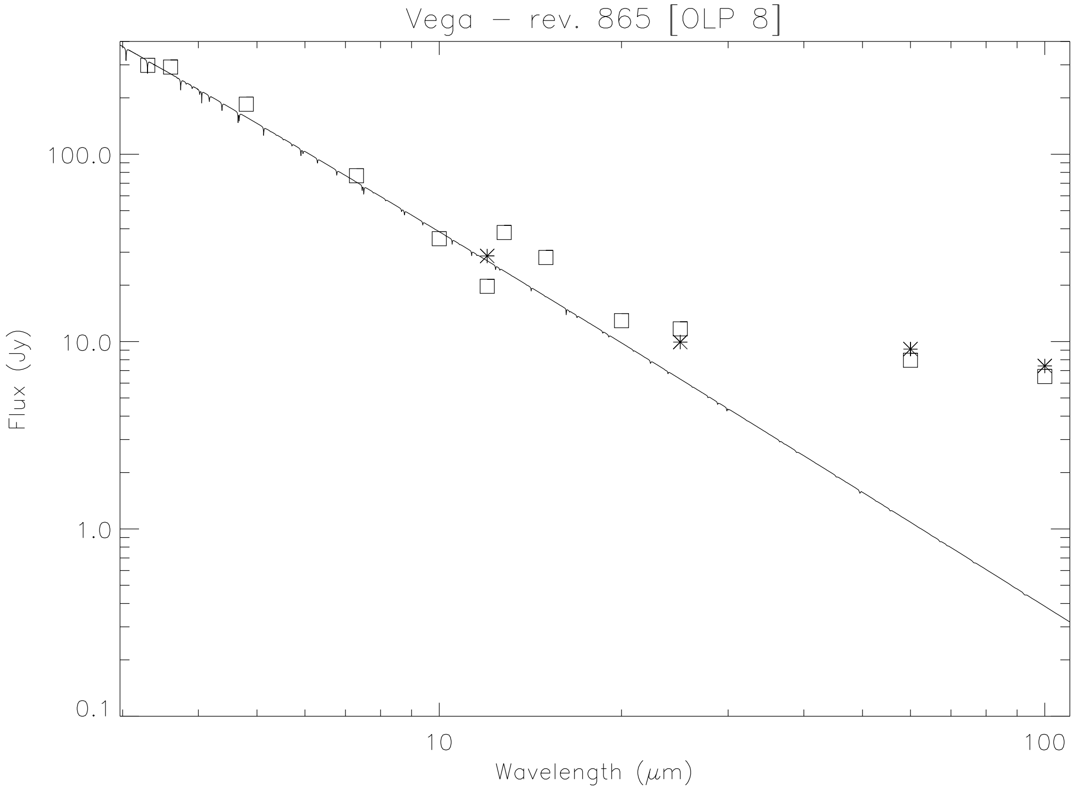

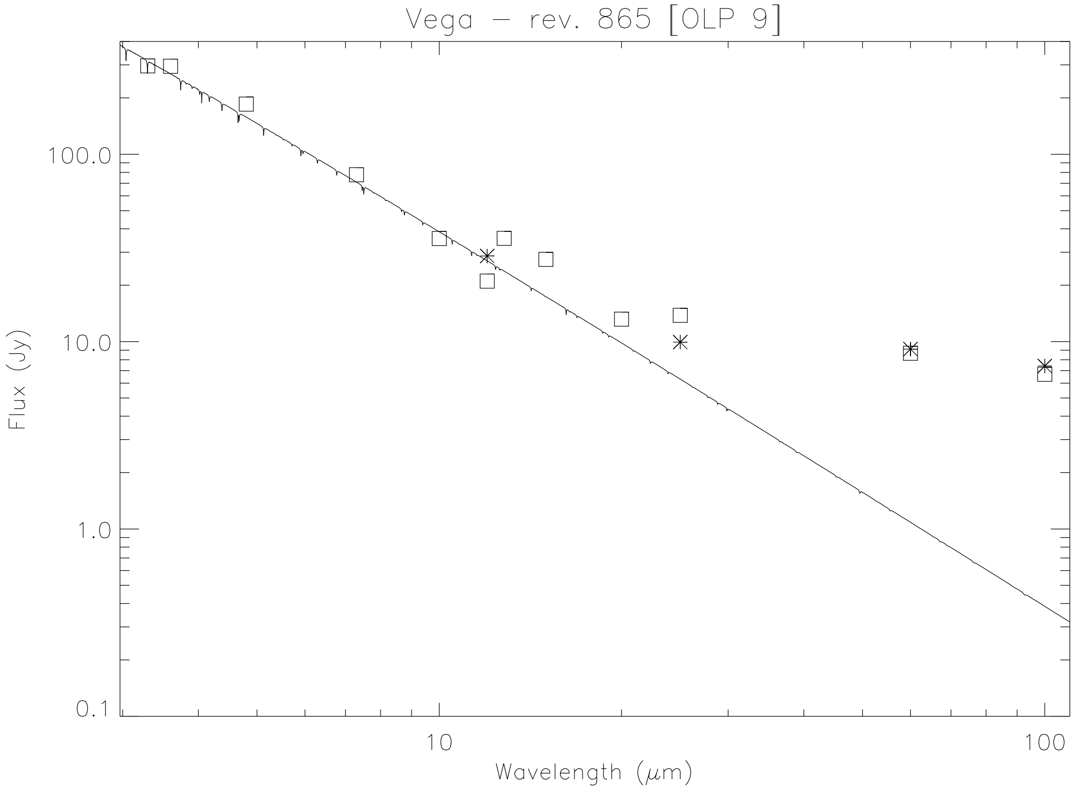

Figure 8.56: Comparison of PHT-P multi-filter photometry of Vega (HR 7001) on revolution 865 with the composite spectrum provided by M. Cohen out to 15 μm and with IRAS photometry beyond 15 μm for OLP 8.6b1 (upper panel) and OLP 9.0b6 (lower panel). A description of the applied color correction factors is given in the text. The meaning of the symbols is the following: solid line: model, asterisk: IRAS, square: PHT-P.

Evaluation Log

1) Vega PHT-P aperture photometry from 3.3 to 100 um on revolution 085

Measurements:

PHT-P:	ppap08500106 (src+back)	FCS = 3.6, 20, 100 um
	ppap08500105 (back)	FCS = 7.3, 25, 100 um

Colour correction: mixture of 10000 K BB & 80 K modified (em.=1) BB
see text for details

Model: Cohen

Det	cwl (μm)	OLP 8	OLP 9	IRAS	Model	Δ (OLP 8)	Δ (OLP 9)
P1	3.3	264.977	261.889		293.430	-9.70	-10.75
P1	3.6	250.343	251.442		268.410	-6.73	-6.32
P1	4.8	161.699	161.140		157.795	2.47	2.12
P1	7.3	67.196	67.677		70.934	-5.27	-4.59
P1	10.0	32.763	32.666		38.570	-15.06	-15.31
P1	12.0	18.429	19.469	28.640	26.997	-31.74	-27.88
P1	12.8	34.425	31.667		23.779	44.77	33.17
P1	15.0	25.240	24.407		17.356	45.43	40.63
P2	20.0	12.951	12.276		9.838	31.65	24.78
P2	25.0	11.742	13.119	9.938	6.301	86.36	108.22
P3	60.0	8.182	8.377	9.121	1.087	652.97	670.98
P3	100.0	6.706	6.496	7.408	0.387	1634.99	1580.76

2) Vega PHT-P aperture photometry from 3.3 to 100 um on revolution 558

Measurements:

PHT-P:	ppap55800420 (src+back)	FCS = 3.6, 20, 100 um
	ppap55800419 (back)	FCS = 7.3, 25, 100 um

Colour correction: mixture of 10000 K BB & 80 K modified (em.=1) BB
see text for details

Model: Cohen

Det	cwl (μm)	OLP 8	OLP 9	IRAS	Model	Δ (OLP 8)	Δ (OLP 9)
P1	3.3	306.993	305.309		293.430	4.62	4.05
P1	3.6	290.779	293.634		268.410	8.33	9.40
P1	4.8	185.415	185.711		157.795	17.50	17.69
P1	7.3	76.357	77.331		70.934	7.65	9.02
P1	10.0	43.227	43.473		38.570	12.07	12.71
P1	12.0	21.938	23.286	28.640	26.997	-18.74	-13.74
P1	12.8	46.791	43.719		23.779	96.78	83.86
P1	15.0	34.429	33.905		17.356	98.37	95.35
P2	20.0	12.775	12.934		9.838	29.86	31.47
P2	25.0	11.613	13.534	9.938	6.301	84.31	114.81
P3	60.0	6.507	7.224	9.121	1.087	498.84	564.85
P3	100.0	5.745	5.898	7.408	0.387	1386.31	1425.91

3) Vega PHT-P aperture photometry from 3.3 to 100 um on revolution 865

Measurements:
PHT-P: ppap86500706 (src+back) FCS = 3.6, 20, 100 um
ppap86500705 (back) FCS = 7.3, 25, 100 um

Colour correction: mixture of 10000 K BB & 80 K modified (em.=1) BB
see text for details

Model: Cohen

Det	cwl (μm)	OLP 8	OLP 9	IRAS	Model	Δ (OLP 8)	Δ (OLP 9)
P1	3.3	298.270	296.416		293.430	1.65	1.02
P1	3.6	292.034	294.906		268.410	8.80	9.87
P1	4.8	184.949	185.244		157.795	17.21	17.40
P1	7.3	76.780	77.766		70.934	8.24	9.63
P1	10.0	35.400	35.489		38.570	-8.22	-7.99
P1	12.0	19.727	21.031	28.640	26.997	-26.93	-22.10
P1	12.8	38.202	35.581		23.779	60.66	49.64
P1	15.0	28.111	27.462		17.356	61.97	58.23
P2	20.0	12.934	13.179		9.838	31.48	33.96
P2	25.0	11.689	13.815	9.938	6.301	85.52	119.27
P3	60.0	7.947	8.664	9.121	1.087	631.38	697.37
P3	100.0	6.511	6.693	7.408	0.387	1584.59	1631.64

8.4.8 General Re-validation of PHT03 and PHT22 Staring Mode: The SED of Arp 220 - Final Assessment

- authors: U. Klaas
- date: 10-May-2000
- SVP period 2

Motivation

TDTs 47600413(background, PHT-P), 47600414(Arp 220, PHT-P), 47600415(background, PHT-C), 47600416(Arp 220, PHT-C) is one of the key OLP validation cases [1]. The staring mode AOTs PHT-03 and PHT-22 in all PHT filters measure a galaxy SED which is steeply rising between 10 and 60 μm and gradually declining beyond 100 μm, hence has a very different shape than a stellar atmosphere SED. It can therefore be used for a check of the robustness of the relative filter-to-filter calibration and the color correction factors applied to modified Black Bodies in the temperature range 50 – 120 K. Arp 220 is significantly bright over the full wavelength range from 3.3 to 200 μm. Its photometric properties are discussed in detail in "Infrared spectral energy distributions of the interacting galaxies Arp 244, NGC 6240 and Arp 220" [15].

Method

We compare the background subtracted flux values of both OLP V8.6 and OLP V9.0b6 results against the IRAS photometry and a model fit based on the OLP V6.x calibration.

Results

Fig. 8.57 shows the derived SED for Arp 220. The model fit from [15] is plotted as a guide line to easier recognize the changes w.r.t. OLP V8.6. Note that this fit cannot serve as reference photometry.
We have color corrected the photometry w.r.t. modified blackbodies with emissivities $\propto \lambda^{-1}$ for the 12.8 to 200 μm range (for details, see part 2 of the evaluation log section). This color corrected SED is shown in Fig. 8.58.
We notice the following results:

- The dip in the SED in the C100 range is gone with the version 9. The C100 photometry is consistent with IRAS. The SED looks now very smooth from 60 to 200 μm.
- The P3 fluxes are still a bit too high, the discrepancy with IRAS is somewhat increased.
- In the P1 and P2 range, the calibration for some filters looks degraded. The most significant one is the 12.8 μm flux which is a factor of 2 too high. This is confirmed by the background photometry where the 12.8 μm is a factor of 4(!) too high. Another filter is the 20 μm filter and the 11.3 μm filter for which the fluxes appear, too low (for the 11.3 μm filter this is suggested by the PHT-S flux (cf. Fig. 8.38).

In Fig. 8.59 we plot the derived multi-filter surface brightness values in comparison with COBE photometry. The PHT-P surface brightness photometry looks further improved with the exception of the 12.8 μm and 20 μm filters which were already flagged above in the context of less good point source photometry performance (the 3.3 μm point has to be excluded from the discussion, because a fair photometry on the background in this narrow band filter cannot be performed with the selected aperture size). For C100 surface brightness photometry we notice the good match at 60 μm, but the positive excess for the 65, 80, 100 and 105 μm surface brightness, confirming the behaviour found for the previous test cases. We confirm the smoother behaviour of the C200 filter-to-filter calibration, the 120 mum surface brightness looks to be somewhat too high.

Conclusions

- The new version of the linearization files removes the dip in the maximum of the SED of Arp 220. The 60 to 200 μm SED looks now very smooth.
- Some PHT-P filters show a bad calibration performance for the lower flux levels (since it was not found for the stellar test cases). In particular the 12.8 μm filter has to be flagged here.
- Surface brightness photometry for PHT-P looks very good, except for the 12.8 μm and 20 μm filters which so also problems for the point source photometry.
- Surface brightness photometry for PHT-C confirms the systematic excess for the 65, 80, 100, and 105 μm fluxes. The surface brightness values for C200 give a very smooth SED now, indicating a good filter-to-filter calibration.

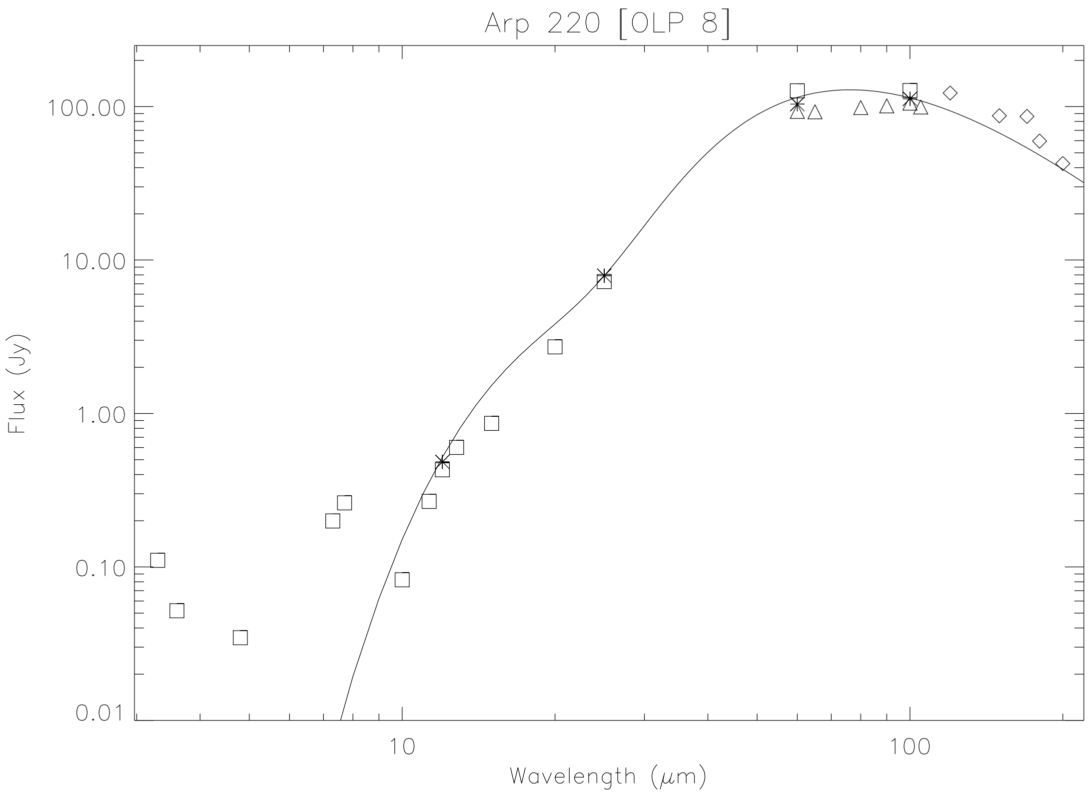

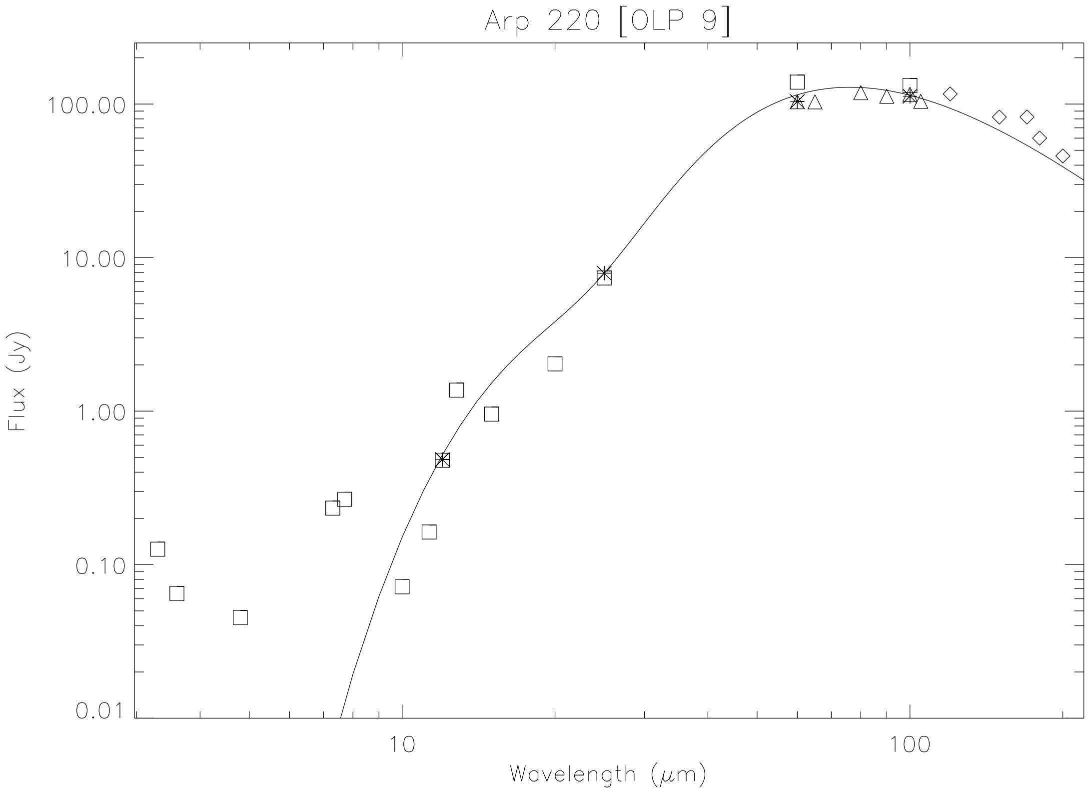

Figure 8.57: Comparison of PHT-P and PHT-C photometry, using the full ISOPHOT filter set, with IRAS photometry and the model fit as described in [15]. Note that this model fit only serves as a guide for the eye to recognize more easily the changes between the two versions. It is not an absolute photometric reference. No color correction has been applied. The meaning of the symbols is the following: solid line: model, asterisk: IRAS, square: PHT-P (P03 AOT), triangle: C100 (P22 AOT), diamond: C200 (P22 AOT).

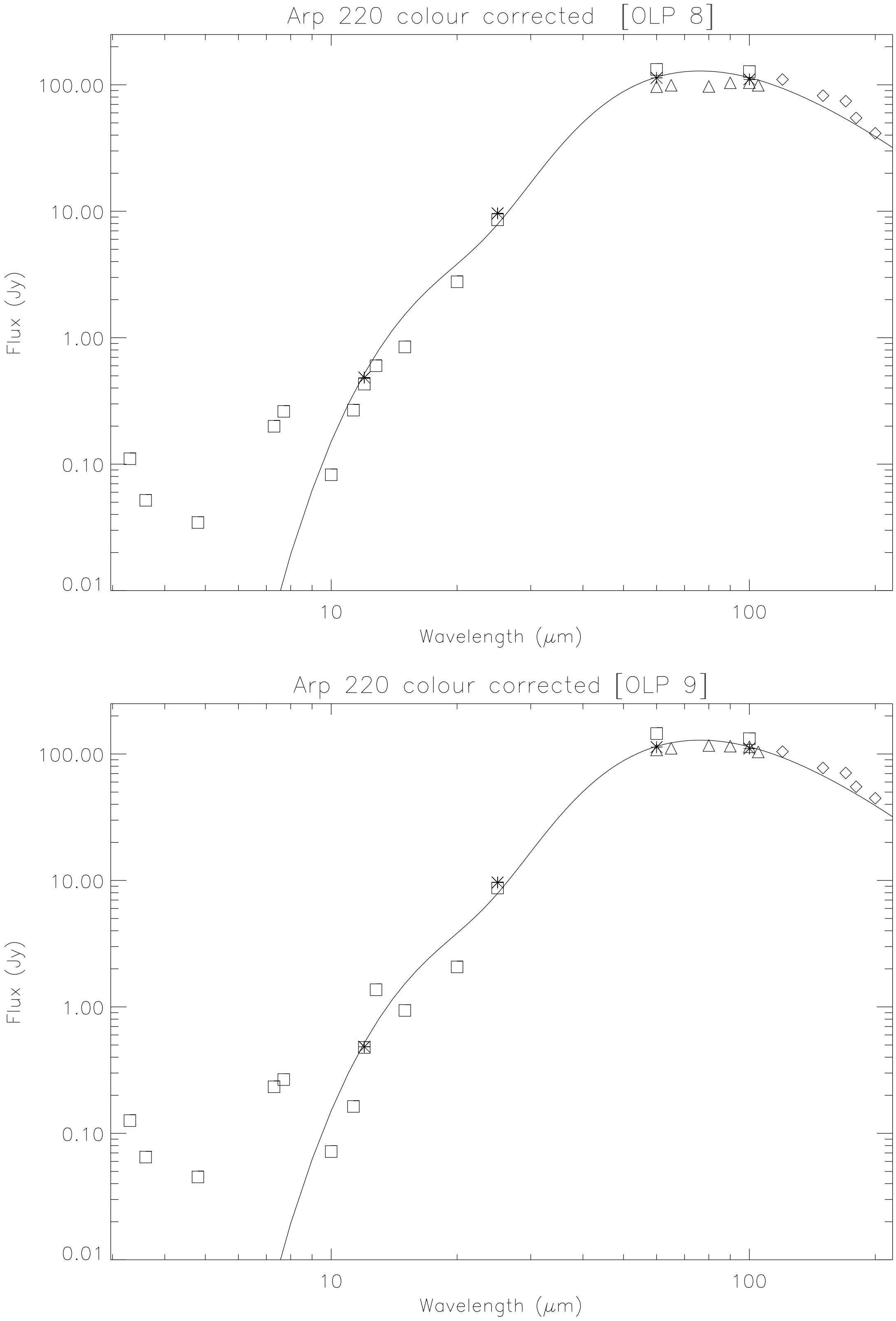

Figure 8.58: Comparison of PHT-P and PHT-C photometry, using the full ISOPHOT filter set, with IRAS photometry and the model fit as described in [15]. Note that this model fit only serves as a guide for the eye to recognize more easily the changes between the two versions. It is not an absolute photometric reference. Color correction according to the model parameters, modified BBs $\propto \lambda^{-1}$ with T1 = 120 K and T2 = 47 K, has been applied . The meaning of the symbols is the following: solid line: model, asterisk: IRAS, square: PHT-P (P03 AOT), triangle: C100 (P22 AOT), diamond: C200 (P22 AOT).

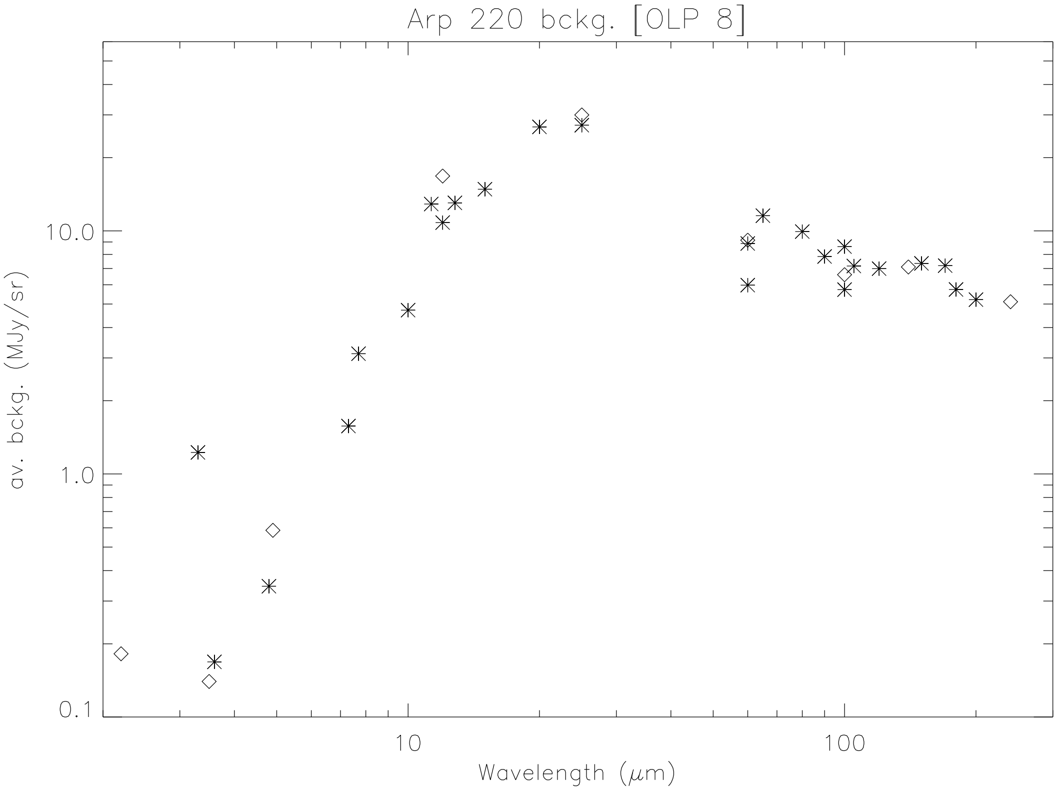

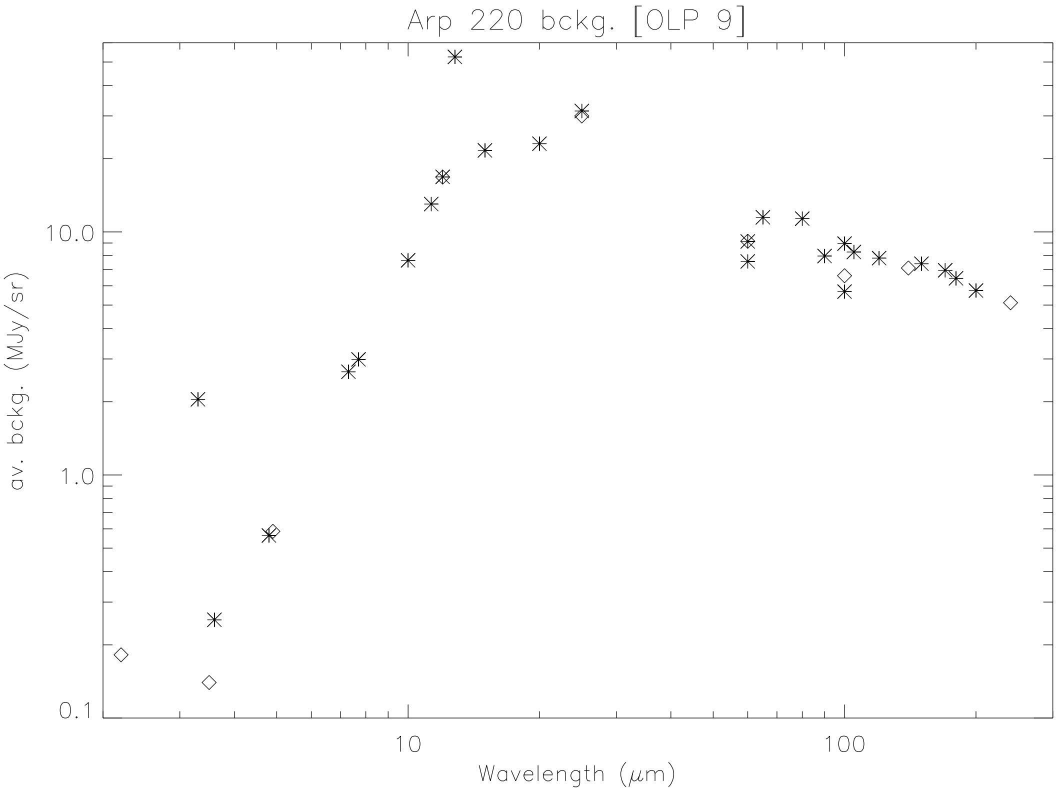

Figure 8.59: Comparison of PHT surface brightness photometry with COBE, both for OLP 8.6b1 and OLP 9.0b6. Asterisk: PHT-P and PHT-C photometry, diamond: COBE.

Evaluation Log

1) point source photometry of Arp 220 (not colour corrected)

Measurements:

PHT-P:	ppap47600414 (src+back)	FCS = 3.3, 25, 100 um
	ppae47600413 (back)	FCS = 3.3, 20, 100 um
PHT-C:	pcap47600416 (src+back)	FCS = 90, 170 um
	pcae47600415 (back)	FCS = 90, 170 um

Model: Sum of 2 modified bb, em. $\propto \lambda^{-1}$, T1 = 120 K, T2 = 47 K

Det	cwl (μm)	OLP 8	OLP 9	IRAS	Model	Δ (OLP 8)	Δ (OLP 9)
P1	3.3	0.110	0.126		-0.001	-15475.22	-17651.58
P1	3.6	0.052	0.065		-0.001	-8905.31	-11136.64
P1	4.8	0.035	0.045		-0.000	-50776.99	-66302.65
P1	7.3	0.199	0.233		0.009	2208.56	2601.82
P1	7.7	0.262	0.266		0.015	1669.48	1702.32
P1	10.0	0.082	0.072		0.151	-45.43	-52.50
P1	11.3	0.268	0.163		0.367	-27.05	-55.48
P1	12.0	0.430	0.478	0.484	0.519	-17.26	-8.03
P1	12.8	0.601	1.369		0.746	-19.44	83.47
P1	15.0	0.862	0.956		1.525	-43.48	-37.31
P2	20.0	2.717	2.031		3.827	-29.02	-46.93
P2	25.0	7.242	7.365	7.910	7.902	-8.35	-6.80
P3	60.0	126.798	138.928	103.800	114.880	10.37	20.93
C1	60.0	93.042	103.544	103.800	114.880	-19.01	-9.87
C1	65.0	92.523	103.301		122.541	-24.50	-15.70
C1	80.0	98.543	118.510		128.115	-23.08	-7.50
C1	90.0	101.134	112.382		122.723	-17.59	-8.43
P3	100.0	127.305	132.026	112.400	113.981	11.69	15.83
C1	100.0	105.380	115.721	112.400	113.981	-7.55	1.53
C1	105.0	99.406	104.062		109.033	-8.83	-4.56
C2	120.0	122.571	116.298		93.777	30.70	24.02
C2	150.0	87.091	82.277		67.225	29.55	22.39
C2	170.0	86.342	82.373		53.793	60.51	53.13
C2	180.0	59.597	59.993		48.236	23.56	24.37
C2	200.0	42.555	45.902		39.038	9.01	17.58

2) point source photometry of Arp 220 (colour corrected from 10 to 200 = μm)

Measurements:

PHT-P:	ppap47600414 (src+back)	FCS = 12, 25, 100 um
	ppae47600413 (back)	FCS = 12, 20, 100 um
PHT-C:	pcap47600416 (src+back)	FCS = 90, 170 um
	pcae47600415 (back)	FCS = 90, 170 um

Colour correction: according to model

Model: Sum of 2 modified bb, em. $\propto \lambda^{-1}$, T1 = 120 K, T2 = 47 K

Det	cwl (μm)	OLP 8	OLP 9	IRAS	Model	Δ (OLP 8)	Δ (OLP 9)
P1	3.3	0.110	0.126		-0.001	-15475.22	-17651.58
P1	3.6	0.052	0.065		-0.001	-8905.31	-11136.64
P1	4.8	0.035	0.045		-0.000	-50776.99	-66302.65
P1	7.3	0.199	0.233		0.009	2208.56	2601.82
P1	7.7	0.262	0.266		0.015	1669.48	1702.32
P1	10.0	0.082	0.072		0.151	-45.43	-52.50
P1	11.3	0.268	0.163		0.367	-27.05	-55.48
P1	12.0	0.430	0.478	0.484	0.519	-17.26	-8.03
P1	12.8	0.600	1.367		0.746	-19.60	83.10
P1	15.0	0.846	0.938		1.525	-44.54	-38.48
P2	20.0	2.769	2.070		3.827	-27.64	-45.90
P2	25.0	8.570	8.716	9.631	7.902	8.46	10.30
P3	60.0	132.357	145.019	113.300	114.880	15.21	26.23
C1	60.0	96.717	107.634	113.300	114.880	-15.81	-6.31
C1	65.0	99.273	110.838		122.541	-18.99	-9.55
C1	80.0	97.087	116.758		128.115	-24.22	-8.86
C1	90.0	103.727	115.263		122.723	-15.48	-6.08
P3	100.0	127.432	132.159	110.400	113.981	11.80	15.95
C1	100.0	103.925	114.123	110.400	113.981	-8.82	0.12
C1	105.0	99.109	103.751		109.033	-9.10	-4.84
C2	120.0	110.127	104.490		93.777	17.43	11.42
C2	150.0	82.084	77.547		67.225	22.10	15.35
C2	170.0	74.241	70.828		53.793	38.01	31.67
C2	180.0	54.727	55.090		48.236	13.46	14.21
C2	200.0	41.395	44.652		39.038	6.04	14.38

3) Surface brightness photometry of Arp 220 background

λ	OLP8 (MJy/sr)	OLP9 (MJy/sr)	COBE (MJy/sr)
3.3	1.23	2.05	
3.6	0.17	0.25	
4.8	0.35	0.56	
7.3	1.57	2.66	
7.7	3.12	2.99	
10.0	4.72	7.63	
11.3	12.89	13.02	
12.0	10.81	16.84	16.81
12.8	13.04	52.47	
15.0	14.83	21.64	
20.0	26.76	23.06	
25.0	27.21	31.44	29.99
60.0	5.98	7.56	9.15
100.0	5.73	5.68	6.60
60.0	8.87	9.13	9.15
65.0	11.54	11.48	
80.0	9.93	11.34	
90.0	7.84	7.96	
100.0	8.61	8.95	6.60
105.0	7.17	8.27	
120.0	6.99	7.80	
150.0	7.34	7.39	7.10
170.0	7.19	6.95	
180.0	5.74	6.44	
200.0	5.21	5.74	5.11

8.4.9 General Re-validation of PHT03 and PHT22 Staring Mode: The SED of NGC 6240 - Final Assessment

- authors: U. Klaas
- date: 15-May-2000
- SVP period 2

Motivation

TDTs 47600509(background, PHT-P), 47600510(NGC 6240, PHT-P), 47600511(background, PHT-C), 47600512(NGC 6240, PHT-C) is another one of the key OLP validation cases [1]. Like for Arp 220, the staring mode AOTs PHT-03 and PHT-22 in all PHT filters measure a galaxy SED which is steeply rising between 8 and 60 μm and gradually declining beyond 100 μm, hence has a very different shape than a stellar atmosphere SED. It can therefore be used for a check of the robustness of the relative filter-to-filter calibration and the color correction factors applied to modified Black Bodies in the temperature range 40 – 140 K. It is 3 times fainter than Arp 220 and does not reach possible upper boundary conditions with regard to the C100 fluxes like Arp 220. Its photometric properties are discussed in detail in "Infrared spectral energy distributions of the interacting galaxies Arp 244, NGC 6240 and Arp 220" [15].

Method

We compare the background subtracted flux values of both OLP V8.6 and OLP V9.0b6 results against the IRAS photometry and a model fit based on the OLP V6.x calibration.

Results

Fig. 8.60 shows the derived SED for NGC 6240. The model fit from [15] is plotted as a guide line to easier recognize the changes w.r.t. OLP V8.6. Note that this fit cannot serve as reference photometry.
We have color corrected the photometry w.r.t. modified blackbodies with emissivities $\propto \lambda^{-1}$ for the 12.8 to 200 μm range (for details, see part 2 of the evaluation log section). This color corrected SED is shown in Fig. 8.61.
We notice the following results:

- The good photometry for C100 and C200 yielding a relatively smooth SED in this range is confirmed. Also the P3 photometry matches here.
- There is now a good consistency with IRAS at 25 μm, while the 12 μm ISOPHOT flux is higher than the IRAS one. This indicates that the 20 μm flux is again too low, as for Arp 220. Again we find this positive flux excess of a factor of 2 for the 12.8 μm filter.

In Fig. 8.62 we plot the derived multi-filter surface brightness values in comparison with COBE photometry. Like for the background close to Arp 220, the PHT-P background photometry is very consistent with COBE/DIRBE, except for the 3.3, 12.8 and 20 μm filters. For C100 we see again the excess for the 65 and 80 μm filters, the one for the 100 and 105 μm filters is not noticable here. Again the C200 background surface brightness looks very smooth from filter to filter, the absolute values appear somewhat too high compared with COBE/DIRBE.

Conclusions

The second bright galaxy example, NGC 6240, confirms essential findings of the Arp 220 test case:

- The C100 and C200 photometry has a good quality in this flux range.

- There is a calibration problem with the 12.8 and 20 μm filters on the flux level $<$ a few Jy down to the background level. In the 12.8 μm filter too high fluxes (factor 2 for the source, factor > 3 for the background) and for the 20 μm filter too low fluxes are derived.
- There is also a calibration problem for the background level for the not so commonly used filters at 65 and 80 μm, showing a systematic surface brightness excess which is confirmed by other test cases.

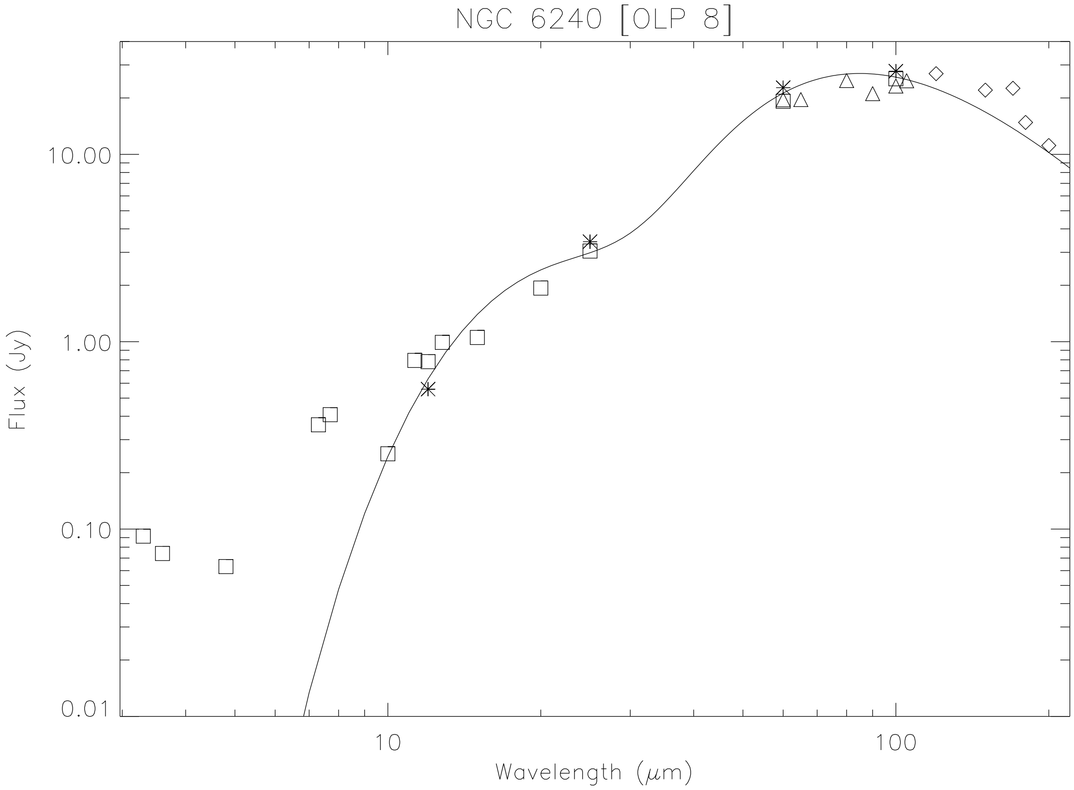

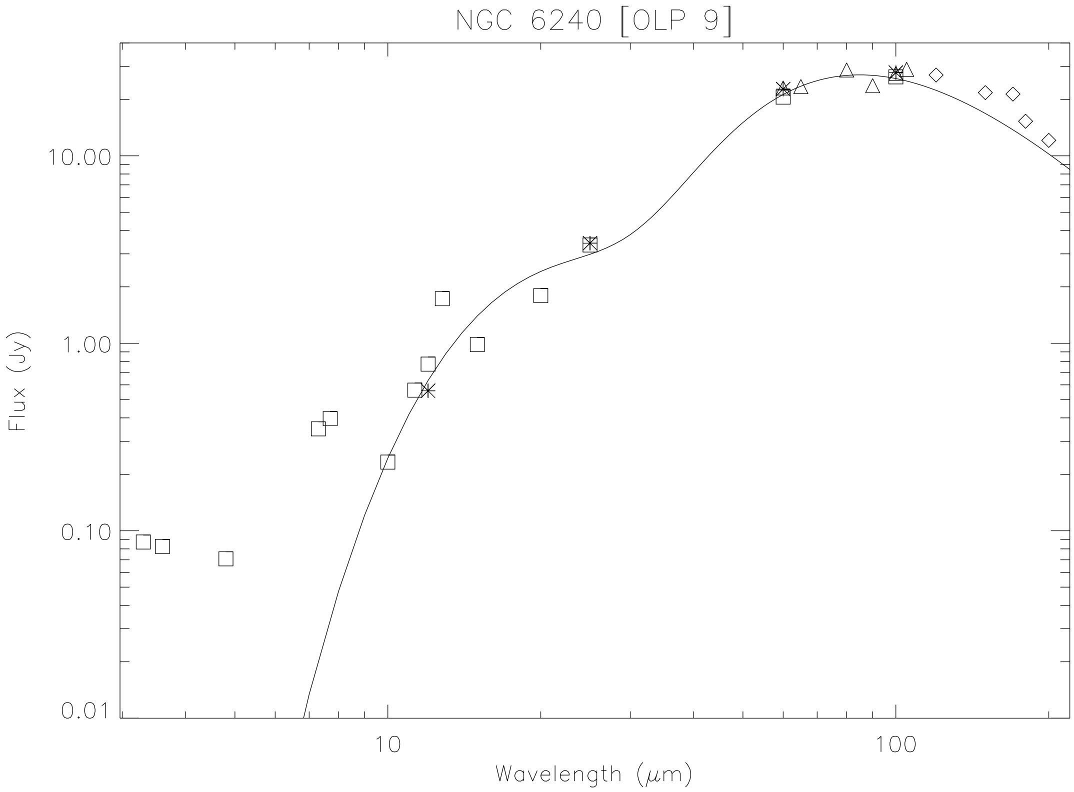

Figure 8.60: Comparison of PHT-P and PHT-C photometry, using the full ISOPHOT filter set, with IRAS photometry and the model fit as described in [15]. Note that this model fit only serves as a guide for the eye to recognize more easily the changes between the two versions. It is not an absolute photometric reference. No color correction has been applied. The meaning of the symbols is the following: solid line: model, asterisk: IRAS, square: PHT-P (P03 AOT), triangle: C100 (P22 AOT), diamond: C200 (P22 AOT).

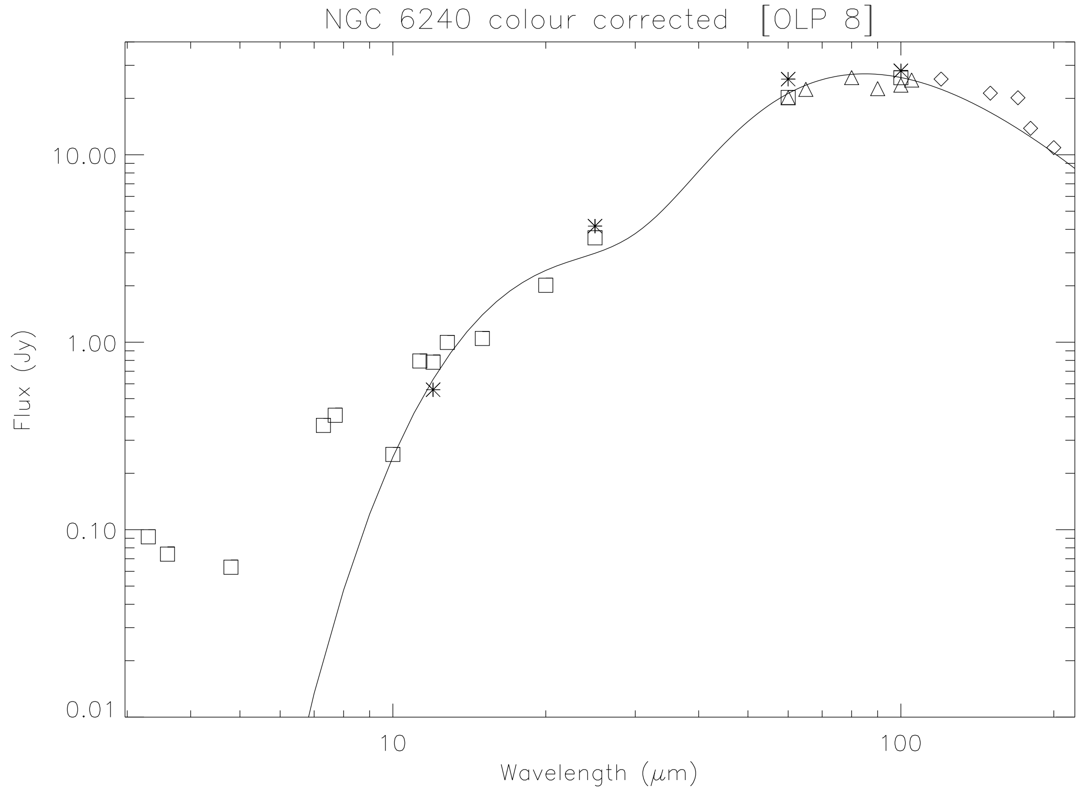

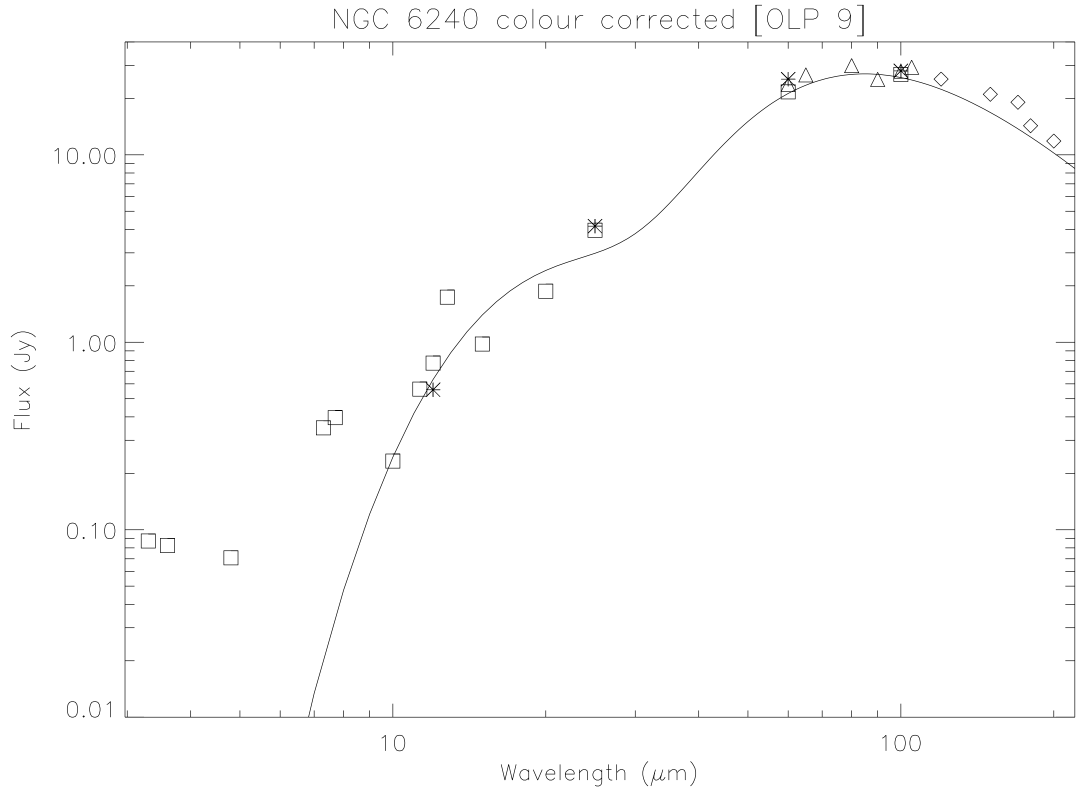

Figure 8.61: Comparison of PHT-P and PHT-C photometry, using the full ISOPHOT filter set, with IRAS photometry and the model fit as described in [15]. Note that this model fit only serves as a guide for the eye to recognize more easily the changes between the two versions. It is not an absolute photometric reference. Color correction according to the model parameters, modified BBs $\propto \lambda^{-1}$ with T1 = 140 K and T2 = 42 K, has been applied . The meaning of the symbols is the following: solid line: model, asterisk: IRAS, square: PHT-P (P03 AOT), triangle: C100 (P22 AOT), diamond: C200 (P22 AOT).

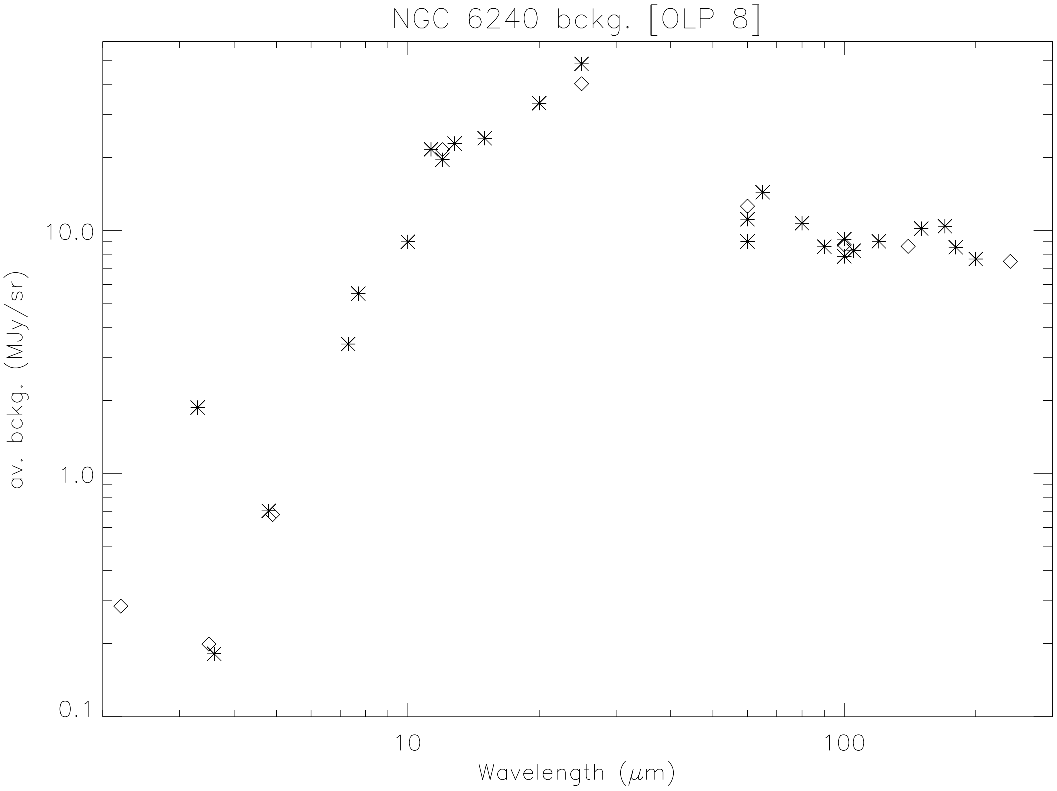

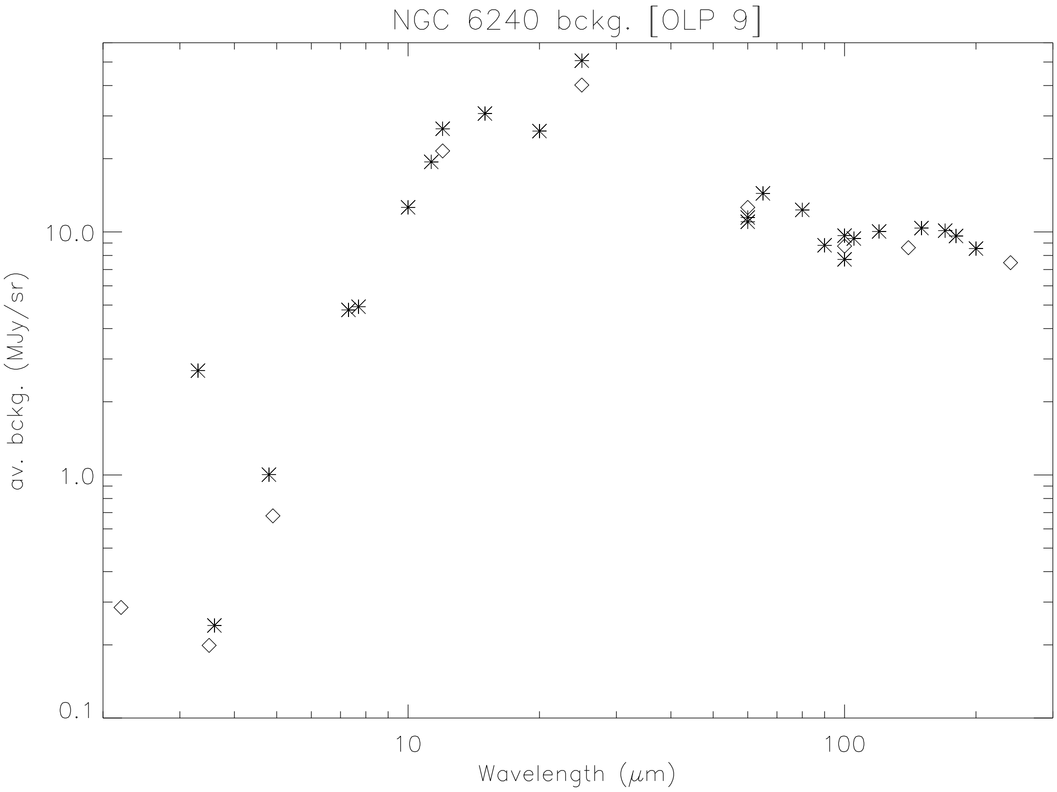

Figure 8.62: Comparison of PHT surface brightness photometry with COBE, both for OLP 8.6b1 and OLP 9.0b6. Asterisk: PHT-P and PHT-C photometry, diamond: COBE.

Evaluation Log

1) point source photometry of NGC 6240 (not colour corrected)

Measurements:			
PHT-P:	ppap47600510 (src+back)	FCS = 12, 25, 100 um	
	ppae47600509 (back)	FCS = 12, 20, 100 um	
PHT-C:	pcap47600512 (src+back)	FCS = 90, 170 um	
	pcae47600511 (back)	FCS = 90, 170 um	
Model:	Sum of 2 modified bb, em. $\propto \lambda^{-1}$, T1 = 140 K, T2 = 42 K		

Det	cwl (μm)	OLP 8	OLP 9	IRAS	Model	Δ (OLP 8)	Δ (OLP 9)
P1	3.3	0.092	0.087		-0.003	-2812.82	-2678.47
P1	3.6	0.074	0.082		-0.003	-2789.22	-3094.97
P1	4.8	0.063	0.071		-0.000	-24755.49	-27788.84
P1	7.3	0.360	0.349		0.024	1420.38	1375.15
P1	7.7	0.408	0.396		0.037	990.25	959.59
P1	10.0	0.252	0.232		0.244	3.31	-4.75
P1	11.3	0.794	0.562		0.482	64.69	16.55
P1	12.0	0.782	0.774	0.558	0.634	23.48	22.12
P1	12.8	0.991	1.730		0.830	19.43	108.38
P1	15.0	1.053	0.985		1.399	-24.70	-29.61
P2	20.0	1.932	1.797		2.417	-20.05	-25.65
P2	25.0	3.046	3.345	3.417	2.983	2.13	12.15
P3	60.0	19.204	20.576	22.680	21.233	-9.56	-3.09
C1	60.0	19.560	23.005	22.680	21.233	-7.88	8.35
C1	65.0	19.604	23.428		23.504	-16.60	-0.33
C1	80.0	24.762	28.704		26.842	-7.75	6.94
C1	90.0	21.099	23.668		26.852	-21.43	-11.86
P3	100.0	25.313	26.358	27.780	25.814	-1.94	2.11
C1	100.0	23.156	27.507	27.780	25.814	-10.30	6.56
C1	105.0	24.705	28.923		25.058	-1.41	15.43
C2	120.0	26.947	26.965		22.343	20.61	20.69
C2	150.0	22.025	21.736		16.814	30.99	29.27
C2	170.0	22.528	21.335		13.752	63.81	55.14
C2	180.0	14.806	15.290		12.442	19.00	22.90
C2	200.0	11.145	12.086		10.220	9.05	18.26

2) point source photometry of NGC 6240 (colour corrected from 12.8 to 200 μm)

Measurements:			
PHT-P:	ppap47600510 (src+back)	FCS = 12, 25, 100 um	
	ppae47600509 (back)	FCS = 12, 20, 100 um	
PHT-C:	pcap47600512 (src+back)	FCS = 90, 170 um	
	pcae47600511 (back)	FCS = 90, 170 um	

Colour correction: according to model

Model: Sum of 2 modified bb, em. $\propto \lambda^{-1}$, T1 = 140 K, T2 = 42 K

Det	cwl (μm)	OLP 8	OLP 9	IRAS	Model	Δ (OLP 8)	Δ (OLP 9)
P1	3.3	0.092	0.087		-0.003	-2812.82	-2678.47
P1	3.6	0.074	0.082		-0.003	-2789.22	-3094.97
P1	4.8	0.063	0.071		-0.000	-24755.49	-27788.84
P1	7.3	0.360	0.349		0.024	1420.38	1375.15
P1	7.7	0.408	0.396		0.037	990.25	959.59
P1	10.0	0.252	0.232		0.244	3.31	-4.75
P1	11.3	0.794	0.562		0.482	64.69	16.55
P1	12.0	0.782	0.774	0.558	0.634	23.48	22.12
P1	12.8	0.997	1.740		0.830	20.16	109.64
P1	15.0	1.047	0.979		1.399	-25.15	-30.03
P2	20.0	2.013	1.872		2.417	-16.72	-22.55
P2	25.0	3.605	3.958	4.162	2.983	20.86	32.72
P3	60.0	20.215	21.659	25.310	21.233	-4.80	2.01
C1	60.0	20.144	23.692	25.310	21.233	-5.13	11.58
C1	65.0	22.328	26.683		23.504	-5.01	13.52
C1	80.0	25.794	29.900		26.842	-3.91	11.39
C1	90.0	22.517	25.259		26.852	-16.14	-5.93
P3	100.0	25.777	26.841	28.030	25.814	-0.14	3.98
C1	100.0	23.509	27.926	28.030	25.814	-8.93	8.18
C1	105.0	25.030	29.304		25.058	-0.11	16.95
C2	120.0	25.326	25.343		22.343	13.35	13.43
C2	150.0	21.301	21.021		16.814	26.69	25.02
C2	170.0	20.132	19.066		13.752	46.39	38.64
C2	180.0	13.837	14.290		12.442	11.22	14.86
C2	200.0	10.915	11.837		10.220	6.81	15.83

3) Surface brightness photometry of NGC 6240 background

λ	OLP8 (MJy/sr)	OLP9 (MJy/sr)	COBE (MJy/sr)
3.3	1.87	2.69	
3.6	0.18	0.24	
4.8	0.70	1.00	
7.3	3.41	4.77	
7.7	5.50	4.92	
10.0	8.99	12.62	
11.3	21.58	19.41	
12.0	19.56	26.56	21.54
12.8	22.81	74.62	
15.0	23.99	30.68	
20.0	33.44	25.98	
25.0	48.51	50.62	40.18
60.0	9.02	11.01	12.61
100.0	7.83	7.70	8.74
60.0	11.14	11.46	12.61
65.0	14.38	14.40	
80.0	10.72	12.32	
90.0	8.58	8.81	
100.0	9.22	9.65	8.74
105.0	8.26	9.39	
120.0	9.03	10.04	
150.0	10.19	10.37	8.61
170.0	10.42	10.12	
180.0	8.54	9.62	
200.0	7.64	8.54	7.47

8.4.10 General Re-validation of PHT17/19 and PHT37/39 Sparse Map On-Off Mode: The SED of Arp 244 - Final Assessment

- authors: U. Klaas
- date: 15-May-2000
- SVP period 2

Motivation

The observations of Arp 244 complement the evaluation of galaxy SEDs, since the measurements were performed in sparse map off-on mode (PHT17/PHT19 for PHT-P observations and PHT37/PHT39 for PHT-C observations, respectively; note that the 25 μm observations failed due to R/T problems). Furthermore, the observations were performed in the Performance Verification Phase, so that the pre-rev. 94 FCS calibration is applied for the FIR detectors (C100 and C200). Since the object is extended, the 180 arcsec aperture was used for the PHT-P observations. This gives some feedback on the surface brightness calibration using the maximum aperture size with regard to the standard aperture for this filter. Also, the C200 sparse map elements have FCS calibrations in different filters so that they are test case for the check-out of SPR-3208 (sparse maps with different cal filters) implementation. The photometric properties of this object are discussed in detail in "Infrared spectral energy distributions of the interacting galaxies Arp 244, NGC 6240 and Arp 220" [15].

Method

We compare the background subtracted flux values of both OLP V8.6 and OLP V9.0b6 results against the IRAS photometry and a model fit based on the OLP V6.x calibration. As the source is extended, we do not use IRAS PSC or FSC photometry, but total fluxes as given in [29].

Results

Fig. 8.63 shows the derived SED for Arp 244. The model fit from [15] is plotted as a guide line to easier recognize the changes w.r.t. OLP V8.6. Note that this fit cannot serve as reference photometry.
We have color corrected the photometry w.r.t. modified blackbodies with emissivities $\propto \lambda^{-1}$ for the 12.8 to 200 μm range (for details, see part 2 of the evaluation log section). This color corrected SED is shown in Fig. 8.64.
We notice the following results:

- The C100 photometry gives by far too low fluxes, they have even drastically decreased with regard to OLP 8. At 60 μm only 1/3 of the IRAS flux is derived. Approximately the same factor is suggested for the 90 μm filter from the comparison of model fit with IRAS 100 mum phootmetry. We achieved a quite similar result with PIA batch processing, so that it does not seem to be related to the OLP processing. The FCS calibration filter is the 90 μm filter. For the C100 sparse map on-source, the SPD product PC1S06903806.FITS contains the following warning:

```
FILTER2 = 'C100_90_UM'         / Filter
 ...
CALFILT =                    8 / Filter for cal measurement
TRS1S2  =                    2 / Selected TRS for FCS1
POW1S2  =              2.45421 / Selected power for FCS1
POW1M2  =              2.45422 / Measured power for FCS1
CALPOW2 =             4.97E-14 / In-band power on detector for cal (Watts)
COMMENT ************************************************
COMMENT The selected FCS power was outside the calibrated range.
COMMENT ************************************************
```

That means the optical power by the FCS illumination is estimated a factor of 3 too low and hence the detector responsivity determined a factor of ~ 3 too high. The upper limt of the calibrated range is 1.93 mW, as can be seen from Table 2.1 in Sect. 2.1. It needs to be further investigated whether the extrapolation is optimal here.

- The C200 photometric points appear to be a bit too high with regard to IRAS photometry. Some caution is however necessary here, since beam size effects due to the extension of the object may play a role. The SPR-3208 implementation therefore gives results of the correct order.

In Fig. 8.65 we plot the derived multi-filter surface brightness values in comparison with COBE photometry. The PHT-P surface brightness photometry seems to be systematically below the COBE fluxes. Since for the Arp 220 background with a quite similar brightness the matching was quite good, this could indicate the order of a correction factor using the large 180 arcsec aperture, but clearly more statistics is needed here. The 60 mum background flux is derived too high and this accounts for part of the low source flux.

Conclusions

- For this pre-rev 94 test case we find that the C100 FCS calibration was outside the calibrated range. Consequently the source flux is a factor of $2.5 - 3$ too low, which might be due to a poor definition of the FCS extrapolation for the 90 μm filter.
- The SPR-3208 implementation seems to give correct results, although the C200 fluxes for OLP 9 are somewhat higher than for OLP 8 and match therefore less good with the IRAS 100 μm photometry, however this may be caused by some beam size effect due to the extension of the source.
- PHT-P surface brightness photometry (not validated yet) gives too low values compared with COBE/DIRBE. This seems to indicate the order of correction taking into account the effective solid angle ratio between the 180 arcsec aperture and the standard aperture for these filters (52 arcsec).
- The 60 μm surface brightness turns out to be a factor of 2 higher than the COBE/DIRBE value.

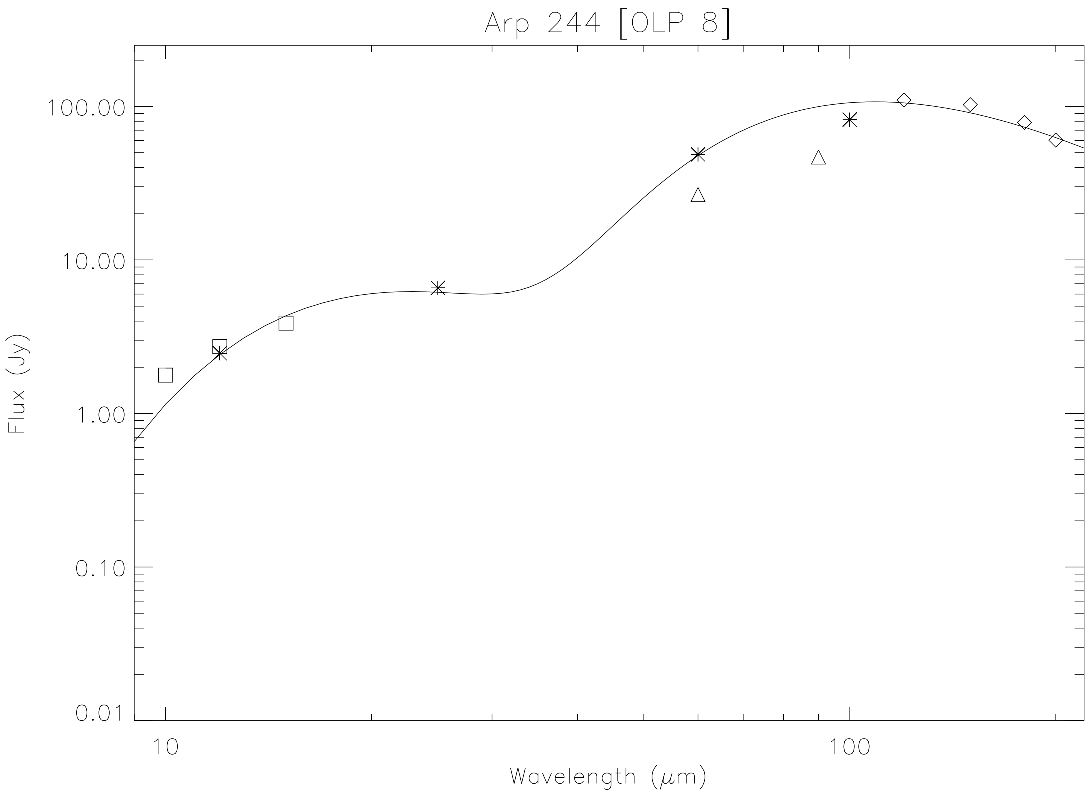

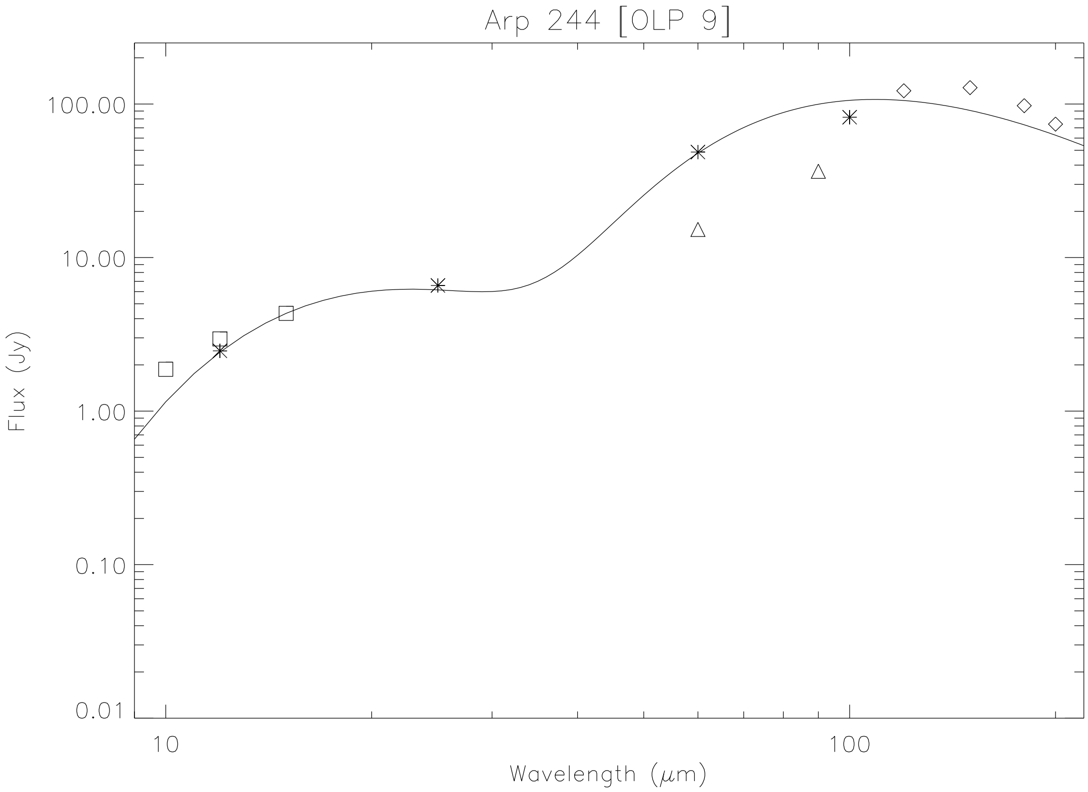

Figure 8.63: Comparison of PHT-P and PHT-C photometry with IRAS photometry and the model fit as described in [15]. Note that this model fit only serves as a guide for the eye to recognize more easily the changes between the two versions. It is not an absolute photometric reference. No color correction has been applied. The meaning of the symbols is the following: solid line: model, asterisk: IRAS, square: PHT-P (P03 AOT), triangle: C100 (P22 AOT), diamond: C200 (P22 AOT).

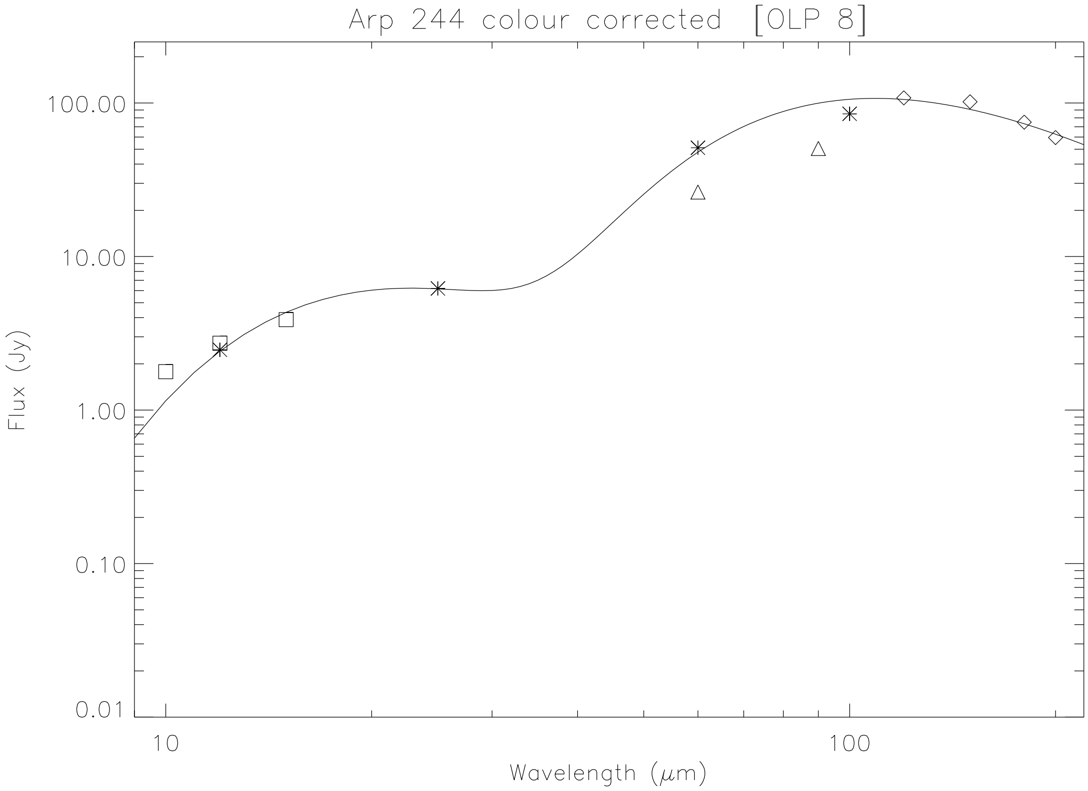

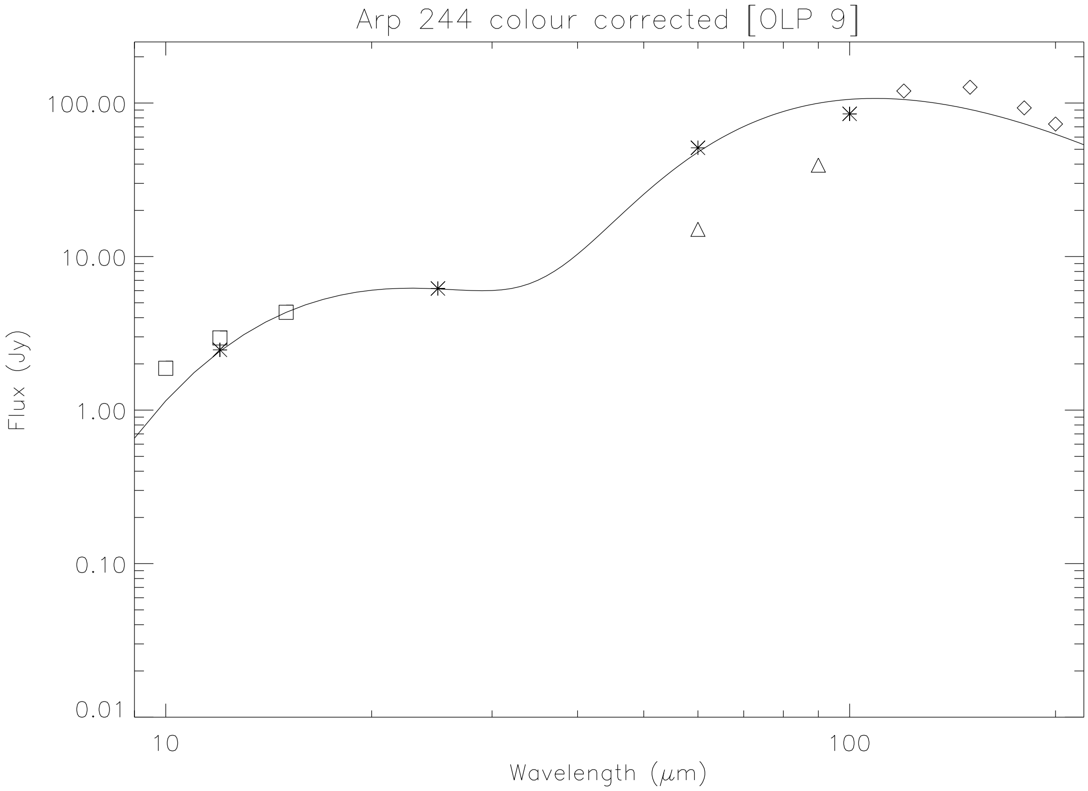

Figure 8.64: Comparison of PHT-P and PHT-C photometry with IRAS photometry and the model fit as described in [15]. Note that this model fit only serves as a guide for the eye to recognize more easily the changes between the two versions. It is not an absolute photometric reference. Color correction according to the model parameters, modified BBs $\propto \lambda^{-1}$ with T1 = 160 K and T2 = 33 K, has been applied. The meaning of the symbols is the following: solid line: model, asterisk: IRAS, square: PHT-P (P03 AOT), triangle: C100 (P22 AOT), diamond: C200 (P22 AOT).

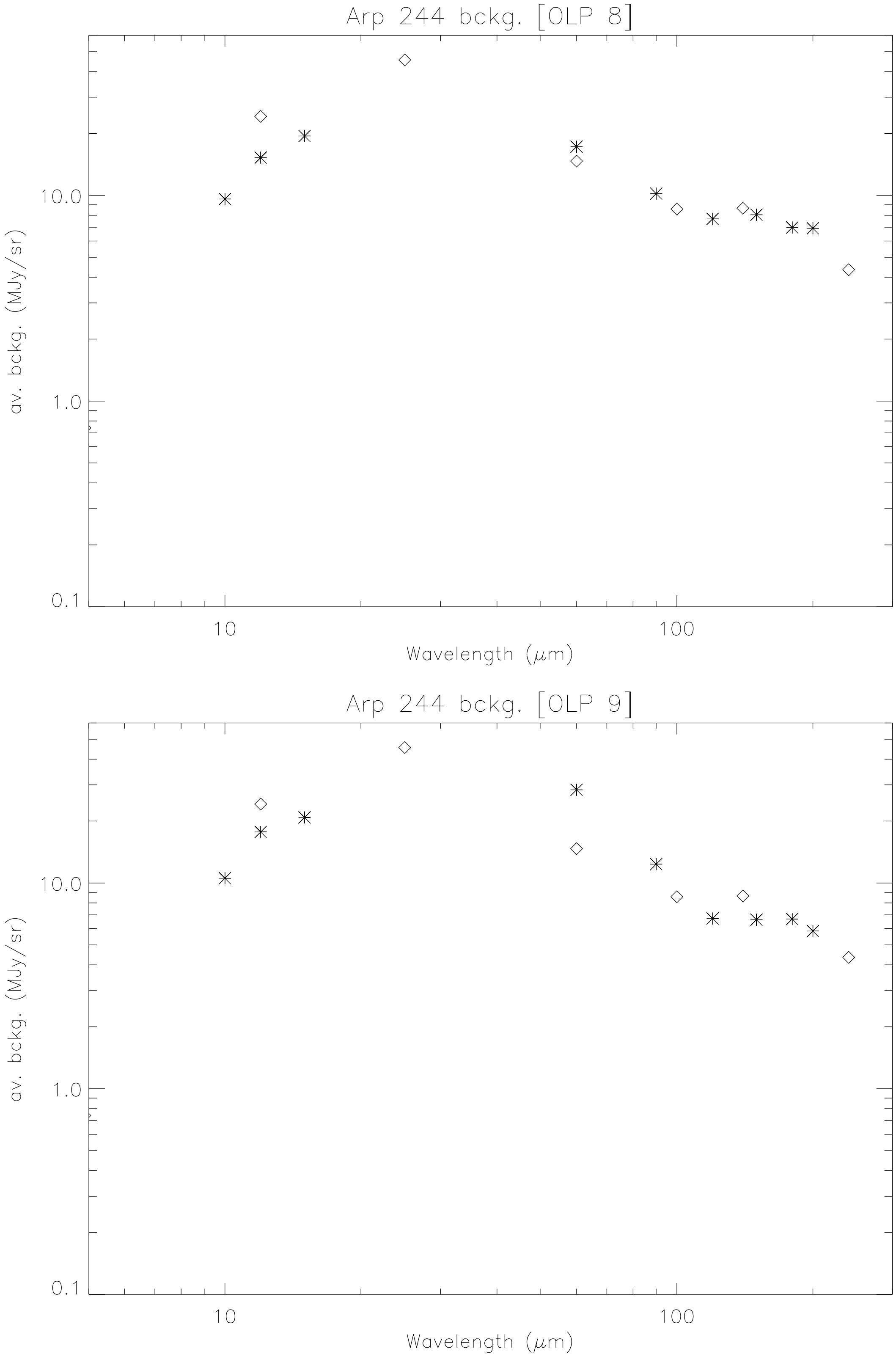

Figure 8.65: Comparison of PHT surface brightness photometry with COBE, both for OLP 8.6b1 and OLP 9.0b6. Asterisk: PHT-P and PHT-C photometry, diamond: COBE.

Evaluation Log

1) point source photometry of Arp 244 (not colour corrected)

Measurements:		
PHT-P:	ppap06903802 (P19 src+back)	FCS = 15 um
	ppae06903801 (P17 back)	FCS = 15 um
PHT-C:	pcap06903806 (P39 C100 src+back)	FCS = 90 um
	pcae06903805 (P37 C100 back)	FCS = 90 um
	pcap06903808 (P39 C200 src+back)	FCS = 150 um
	pcae06903807 (P37 C200 back)	FCS = 180 um

Model: Sum of 2 modified bb, em. $\propto \lambda^{-1}$, T1 = 160 K, T2 = 33 K

Det	cwl (μm)	OLP 8	OLP 9	IRAS	Model	Δ (OLP 8)	Δ (OLP 9)
P1	10.0	1.778	1.873		1.150	54.60	62.85
P1	12.0	2.723	2.952	2.470	2.420	12.52	21.97
P1	15.0	3.878	4.331		4.334	-10.52	-0.06
C1	60.0	26.659	15.248	48.680	47.813	-44.24	-68.11
C1	90.0	46.857	36.491		99.706	-53.00	-63.40
C2	120.0	109.886	121.987		105.397	4.26	15.74
C2	150.0	102.676	127.830		90.809	13.07	40.77
C2	180.0	78.634	97.579		73.181	7.45	33.34
C2	200.0	60.329	73.997		62.622	-3.66	18.16

2) point source photometry of Arp 244 (colour corrected from 12.8 to 200 μm)

Measurements:		
PHT-P:	ppap06903802 (P19 src+back)	FCS = 15 um
	ppae06903801 (P17 back)	FCS = 15 um
PHT-C:	pcap06903806 (P39 C100 src+back)	FCS = 90 um
	pcae06903805 (P37 C100 back)	FCS = 90 um
	pcap06903808 (P39 C200 src+back)	FCS = 150 um
	pcae06903807 (P37 C200 back)	FCS = 180 um

Colour correction: according to model

Model: Sum of 2 modified bb, em. $\propto \lambda^{-1}$, T1 = 160 K, T2 = 33 K

Det	cwl (μm)	OLP 8	OLP 9	IRAS	Model	Δ (OLP 8)	Δ (OLP 9)
P1	10.0	1.778	1.873		1.150	54.60	62.85
P1	12.0	2.723	2.952	2.470	2.420	12.52	21.97
P1	15.0	3.881	4.335		4.334	-10.43	0.04
C1	60.0	26.317	15.053	51.081	47.813	-44.96	-68.52
C1	90.0	50.574	39.386		99.706	-49.28	-60.50
C2	120.0	107.964	119.853		105.397	2.44	13.72
C2	150.0	101.851	126.803		90.809	12.16	39.64
C2	180.0	74.961	93.021		73.181	2.43	27.11
C2	200.0	59.537	73.025		62.622	-4.93	16.61

3) Surface brightness photometry of Arp 244 background

λ	OLP8 (MJy/sr)	OLP9 (MJy/sr)	COBE (MJy/sr)
10.0	9.60	10.54	
12.0	15.25	17.71	24.20
15.0	19.43	20.84	
60.0	17.24	28.38	14.68
90.0	10.20	12.34	
120.0	7.68	6.72	
150.0	8.05	6.63	8.65
180.0	6.98	6.68	
200.0	6.92	5.84	4.35

8.4.11 Re-validation of C200 Absolute Photometry: The SEDs of Ceres and Uranus - Final Assessment

- authors: U. Klaas
- date: 15-May-2000
- SVP period 2

Motivation

This is a check-out of the C200 absolute photometry mode for two bright sky standards, Ceres and Uranus.

Method

We compare the background subtracted, color corrected flux values of both OLP V8.6 and OLP V9.0b6 results against the model prediction by Lagerros for Ceres and Abbas for Uranus.

Results

Fig. 8.66 shows the results for Ceres and Fig. 8.67 the results for Uranus, respectively. With regard to OLP 8 we notice a somewhat smoother SED for Ceres, however the 200 μm point falls a bit lower now. The Uranus photometry has practically not changed.

Conclusions

- For the bright sources Uranus and Ceres C200 absolute photometry quality is maintained from OLP 8 to OLP 9. We notice a slight flux deficit in the 200 μm filter measurements.

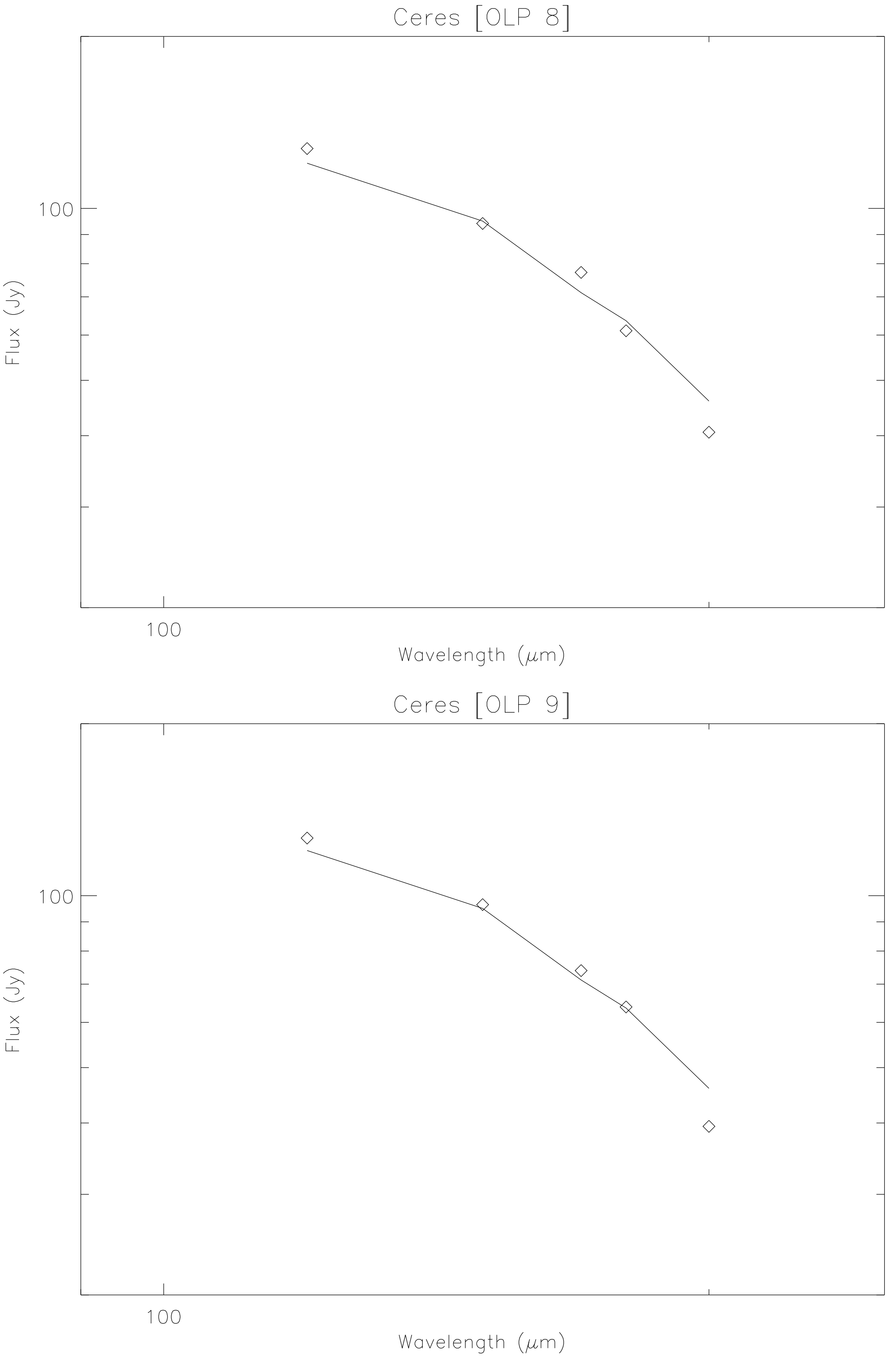

Figure 8.66: Comparison of C200 photometry of Ceres with the model thermophysical model by Lagerros for OLP 8.6b1 (upper panel) and OLP 9.0b6 (lower panel). All photometric points are color corrected for a 240 K BB. The meaning of the symbols is the following: solid line: Lagerros model, diamond: PHT-C200 (P25 AOT).

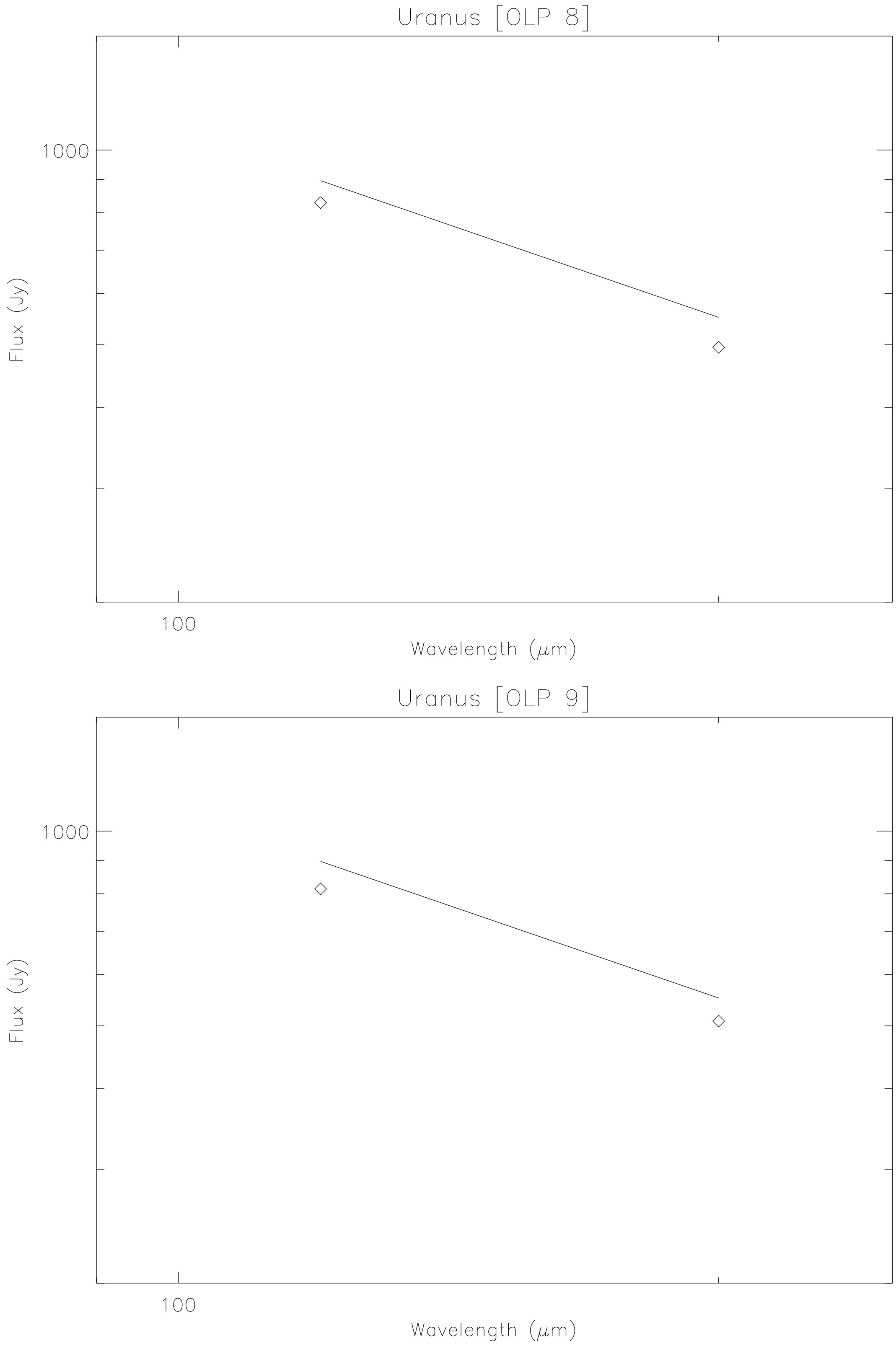

Figure 8.67: Comparison of C200 photometry of Uranus with the model provided by Abbas for OLP 8.6b1 (upper panel) and OLP 9.0b6 (lower panel). All photometric points are color corrected for a 60 K BB. The meaning of the symbols is the following: solid line: Abbas model, diamond: PHT-C200 (P25 AOT).

Evaluation Log

1) Absolute C200 Photometry of Ceres

Measurements:
PHT-C (120 um): pcap57901707 (src+back)
pcae57901606 (back)
PHT-C (170 um): pcap57902111 (src+back)
pcae57902010 (back)
PHT-C (200 um): pcap57901303 (src+back)
pcae57901302 (back)
PHT-C (150 um): pcap59402607 (src+back)
pcae59402506 (back)
PHT-C (180 um): pcap59402203 (src+back)
pcae59402102 (back)

Colour correction: black body, T = 240 K

Model: Lagerros

Det	cwl (μm)	OLP 8	OLP 9	Model	Δ (OLP 8)	Δ (OLP 9)
C2	120.0	127.281	126.149	119.960	6.10	5.16
C2	150.0	94.105	96.453	95.000	-0.94	1.53
C2	170.0	77.252	73.937	71.180	8.53	3.87
C2	180.0	61.055	63.859	63.570	-3.96	0.46
C2	200.0	40.563	39.458	45.990	-11.80	-14.20

2) Absolute C200 Photometry of Uranus

Measurements:
PHT-C (120 um): pcap55204907 (src+back)
pcae55204906 (back)
PHT-C (200 um): pcap55204703 (src+back)
pcae55204702 (back)

Colour correction: black body, T = 60
Model: Abbas

Det	cwl (μm)	OLP 8	OLP 9	Model	Δ (OLP 8)	Δ (OLP 9)
C2	120.0	829.006	813.865	897.600	-7.55	-9.33
C2	200.0	495.406	508.472	552.000	-10.11	-7.89

8.4.12 General Re-validation of PHT17/19 Sparse Map On-Off Mode: The SED of BS 5062 - Final Assessment

- authors: U. Klaas
- date: 19-December-2000
- SVP period 2 extended

Motivation

The sparse map observations of the star BS 5062 are an important check of the fix for SPR-3208 (sparse maps with different cal filters), because for the off-measurement the FCS calibration is in a different filter (4.8 μm) than for the on-measurement (3.6μm).

Method

We compare the background subtracted, color corrected flux values of both OLP V8.6b1 and OLP V9.0b6 results against the model prediction.

Results

Fig. 8.68 shows the PHT photometric data points in comparison with the model and IRAS photometry (color corrected). It can be seen that the OLP 8 photometry was completely useless due to the problem recorded in SPR-3208. However, the OLP 9 photometry is about a factor of 10 below the model expectation. Inspection of the SPD files shows the reason for that:

```
CALP1F2 = 'Both    '          / Cal used in SPD calculations
A0RI2   =            0.006886 / Reset interval correction offset, A0 (V/s)
A0RIU2  =            0.002526 / Unc. in reset interval cor. offset, A0 (V/s)
A1RI2   =            0.913772 / Reset interval correction slope, A1
A1RIU2  =            0.022913 / Unc. in reset interval cor. slope, A1
CALFILT =                   3 / Filter for cal measurement
TRS1S2  =                   1 / Selected TRS for FCS1
POW1S2  =             6.21490 / Selected power for FCS1
POW1M2  =             6.21490 / Measured power for FCS1
CALPOW2 =            2.56E-17 / In-band power on detector for cal (Watts)
COMMENT **************************************************
COMMENT The selected FCS power was outside the calibrated range.
COMMENT **************************************************
CALAP2  =                   1 / Aperture used for cal (CHW position)
CALPOL2 =                   4 / Polarizer used for cal (CHW position)
CALTYP2 =                   2 / Type of processing for cal measurement
RS1P1F2 =           38.268124 / Responsivity (A/W) for first cal measurement
RU1P1F2 =            8.697465 / Uncertainty in responsivity for first cal
RS2P1F2 =            0.655455 / Responsivity (A/W) for second cal measurement
RU2P1F2 =            0.006411 / Uncertainty in responsivity for second cal
RESPDEF =                   F / TRUE if default responsivity is used.
```

A check with Table 2.1 in the Caveat Section 2.1 shows that the selected FCS power for the 4.8 μm filter off-measurement of 6.2 mW is far below the lower limit of the calibrated FCS range in this filter of 12.36 mW. Presumably the combination of the lower quality FCS extrapolation and low signal levels (as reflected by the high uncertainty of 25 %) lead to an anomalously high responsivity value of 38.3 A/W (versus 1.1 A/W default responsivity). The interpolation between the "wrong" off-responsivity and the on-responsivity leads then to the too low fluxes, also for the background measurements, as shown in Fig. 8.69. This will be changed in OLP 10 and only actual FCS responsivities inside the calibrated range or default responsivities will be used. Using only the actual responsivity of the on-measurement leads to fluxes which are 40 to 60 % too high, which corresponds more or less to the ratio of default to actual response (1.1/0.655 = 1.68). The default responsivity would give accurate fluxes here. The usage of only the second responsivity value also restores the relative spectral shape between 3.6 and 4.8 μm.

Conclusions

- The fix for SPR-3208 works.
- For the specific test case a poor photometry is achieved due to the combination of a FCS measurement with heating power outside the calibrated range leading to an extremely high responsivity value and a FCS measurement with a heating power inside the calibrated range. It has been verified by the inspectin of many FCS measurements of this set-up that the resulting responsivities are always considerably higher than the default responsivity value. The usage of these FCS combinations will be prevented in the OLP 10 upgrade.

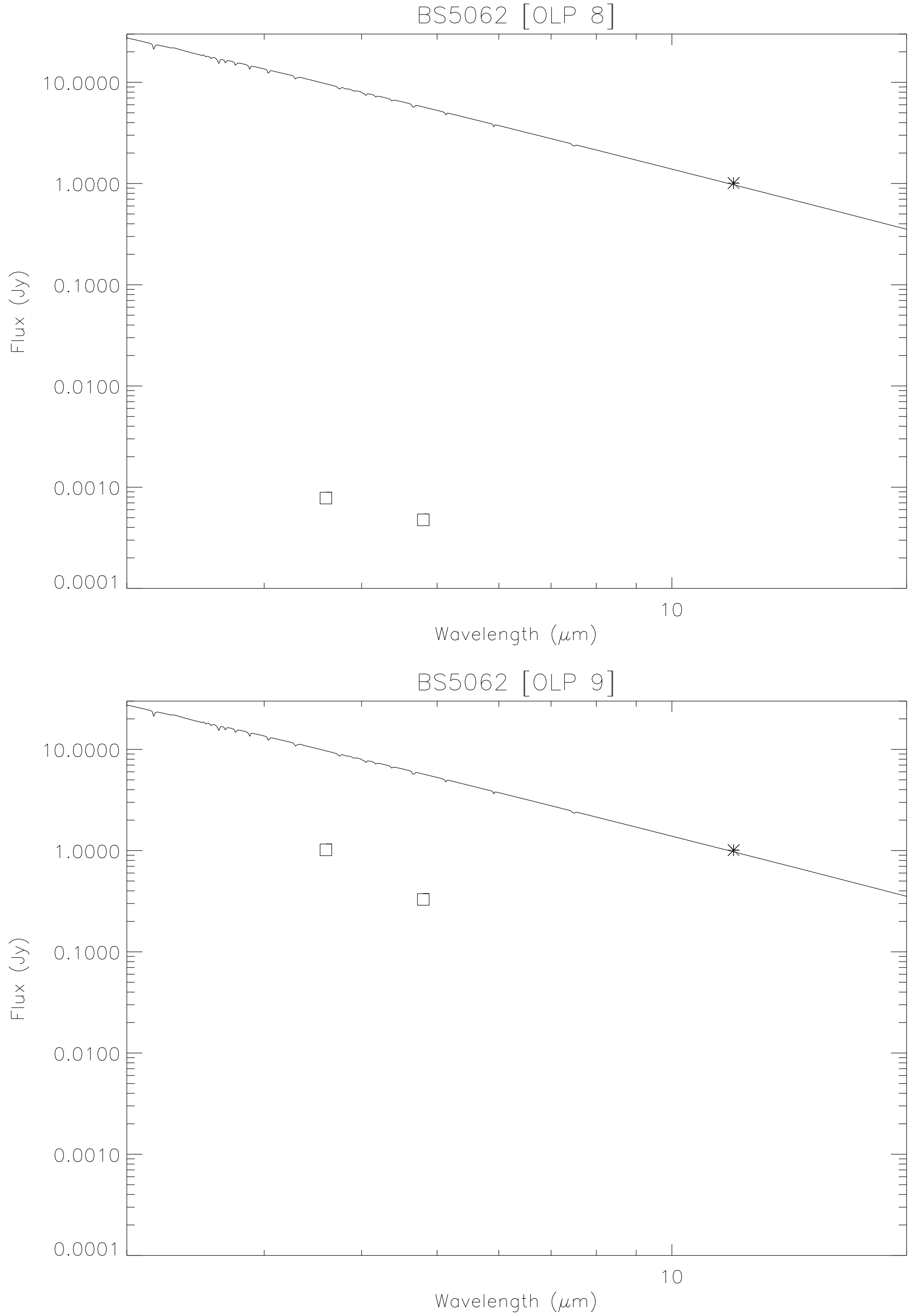

Figure 8.68: Comparison of PHT-P sparse map photometry with the model spectrum of BS 5062 provided by P. Hammersley and with IRAS photometry for OLP 8.6b1 (upper panel) and OLP 9.0b6 (lower panel). All photometric points are color corrected for a 8100 K BB. The meaning of the symbols is the following: solid line: model, asterisk: IRAS, square: PHT-P (P17/19 AOT).

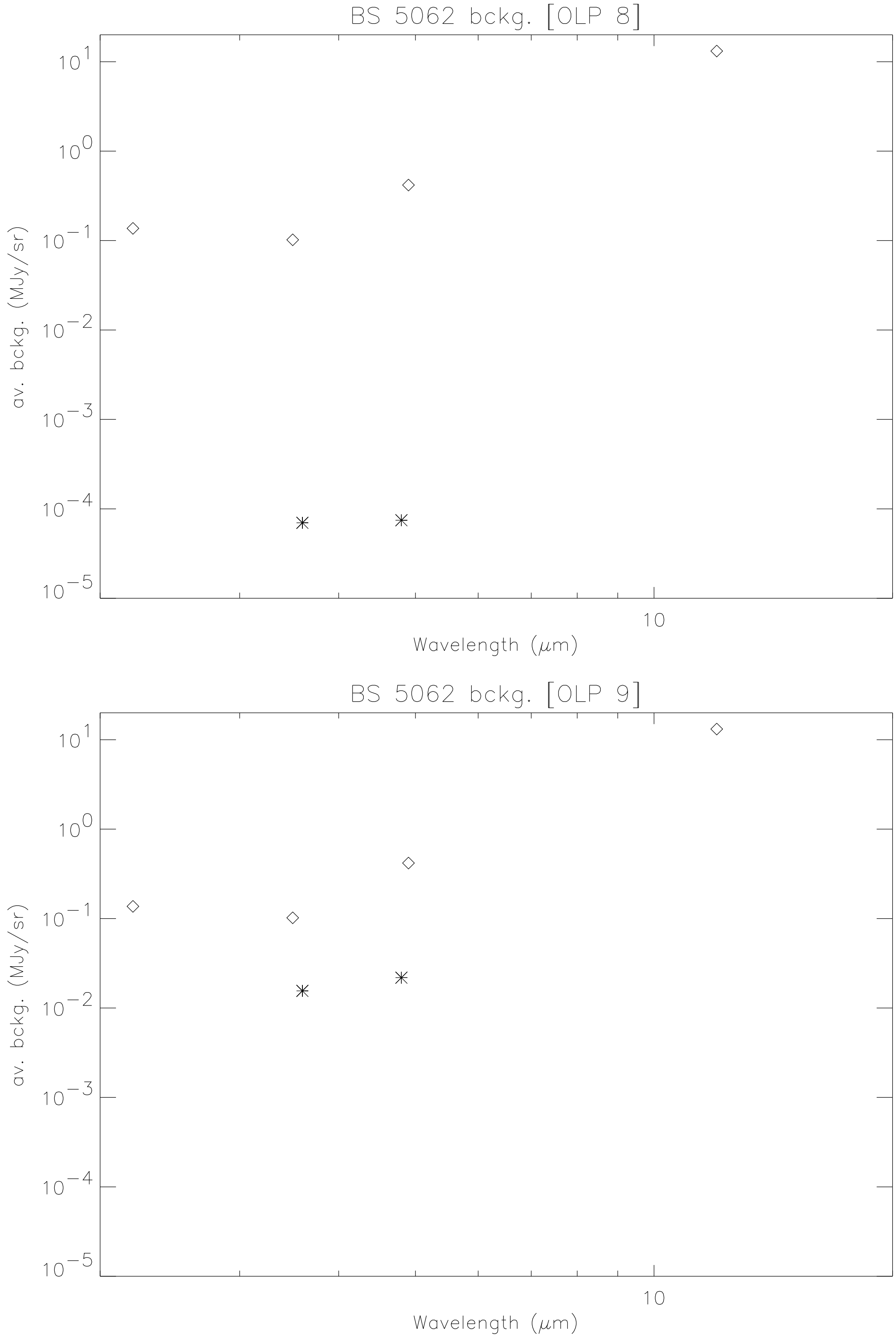

Figure 8.69: Comparison of PHT surface brightness photometry with COBE, both for OLP 8.6b1 and OLP 9.0b6. Asterisk: PHT-P photometry, diamond: COBE.

Evaluation Log

1) point source photometry of BS 5062

Measurements:

PHT-P:	ppap19500981 (P19 src+back)	FCS = 3.6 um
	ppae19500980 (P17 back)	FCS = 4.8 um

Colour correction: black body, T = 8087 K

Model: Hammersley

Det	cwl (μm)	OLP 8	OLP 9	IRAS	Model	Δ (OLP 8)	Δ (OLP 9)
P1	3.6	0.001	1.018		9.674	-99.99	-89.48
P1	4.8	0.000	0.329		5.705	-99.99	-94.23

2) Surface brightness photometry of BS 5062 background

λ	OLP8 (MJy/sr)	OLP9 (MJy/sr)	COBE (MJy/sr)
3.6	0.00	0.02	
4.8	0.00	0.02	

8.4.13 General Re-validation of PHT03 Multi-filter Staring Mode and PHT17/19 and PHT37/39 Sparse Map On-Off Mode: The SED of HR 337 - Final Assessment

- authors: U. Klaas
- date: 19-December-2000
- SVP period 2 extended

Motivation

For the calibration star HR 337 a small verification program of the reset interval correction calibration was worked out which was executed in form of sparse maps. Following the off-source pointing, the first on-source pointing is with the nominal reset interval length derived for the specified source flux. In the following two sparse map modules the reset interval length is either longer or shorter by factors two to four. The last sparse map module is again performed with the nominal reset interval length, in order to check for possible detector drifts. Ideally, the fluxes from all on-source modules should be the same. The sparse map sequences for P3, C100 and C200 are complemented by multi-filter on-off staring mode photometry of a general observer program.

Method

We compare the background subtracted, color corrected flux values of OLP V9.0b6/V9.01 against the model prediction.

Results

The multi-filter general observer program was executed in non-standard apertures (cf. Caveat Section 2.2; 13.8" versus 23" at $10\,\mu$m, 18" versus 52" at $15\,\mu$m and 23" versus 79" at $25\,\mu$m. The accuracy is not better than 40 to 50 %.
The P3 sparse map photometry gives accurate (5 % absolute and < 10 % relative filter-to-filter accuracy) and consistent results for all selected reset interval settings.
The C100 sparse map photometry gives systematically too high fluxes (10 - 40 % absolute, and 25 % relative filter-to-filter accuracy). No trend with the reset interval length can be recognized. This is a similar behaviour as for the slightly fainter star γ Dra (cf. Sect. 8.4.4).
The C200 sparse map photometry gives for the nominal reset interval setting a systematically too high flux of 60 %. It is similar for the factor of 2 longer rest interval setting. The very short reset interval of only 1/2 s shows a clear outlier, in particular, as the bracketing measurements with nominal reset interval length give reproducible results. Whether this indicates a possible problem with the C200 reset interval correction calibration (may be restricted to the small subset of the reset intervals considered here) cannot be decided on the basis of this one test case and needs further interactive analysis and alrger statistics.

Conclusions

- P1 and P2 multi-filter staring mode photometry in non-standard apertures gives accuracies of only 40 to 50 %, presumably mainly due to the non-linear aperture area scaling which is not taken into account in the current OLP processing.
- The small test data set on P3 reset interval correction gives good consistency (flux values are within 10 %) and good absolute (5 %) and relative filter-to-filter calibration.
- The small test data set on C100 reset interval correction shows some scatter which can, however, not be traced back to the systematic variation of the reset interval correction. There seems to be rather a upward drift in flux. The absolute levels are only as accurate as 10 to 40 % and the relative filter-to-filter accuracy is 25 %.
- The small test data set on C200 shows a systematic outlier of a rather short reset interval setting with regard to the considerably longer nominal reset interval settings.

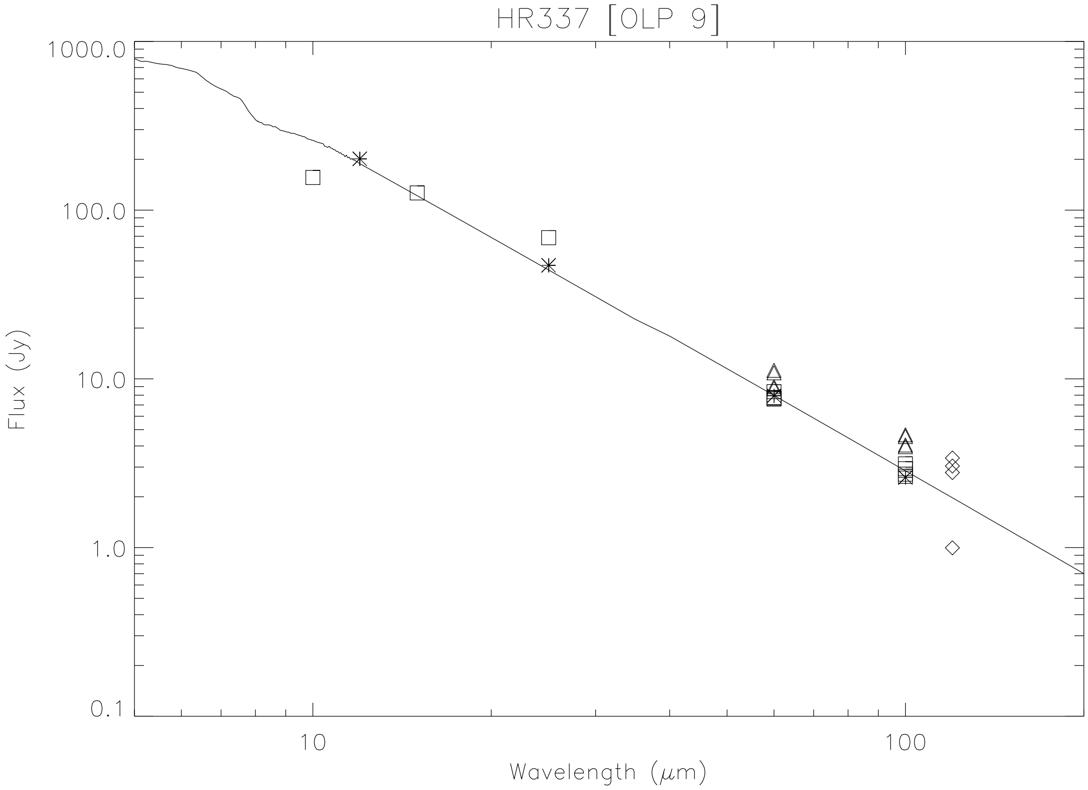

Figure 8.70: Comparison of PHT-P multi-filter staring mode and PHT-P and PHT-C sparse map photometry with the model spectrum of HR 337 provided by M. Cohen and with IRAS photometry for OLP 9.0b6/9.01. All photometric points are color corrected for a 3839 K BB. The meaning of the symbols is the following: solid line: model, asterisk: IRAS, square: PHT-P (P03,P17/19 AOTs), triangle: PHT-C100 (P37/39 AOT), diamond: PHT-C200 (P37/39 AOT).

Therefore some caveat about the C200 reset interval appropriate, although the inspection of the C200 reset interval correction coefficients did not show any obvious flaw. This has to be followed up by interactive processing.

Evaluation Log

1) point source photometry of HR 337

Measurements:

PHT-P1/P2:	ppap42301605 (P03 src+back)	FCS = 10,25 um
	ppap42301656 (P03 back)	FCS = 10,25 um
PHT-P3:	ppae80400601 (P17 back)	FCS = 60 um
	ppap80400602 (P18 src+back)	RI = 1/4s
	ppap80400603 (P18 src+back)	RI = 1/2s
	ppap80400604 (P18 src+back)	RI = 1/16s
	ppap80400605 (P19 src+back)	RI = 1/4s, FCS = 60um
PHT-C100:	pcae80400706 (P37 back)	FCS = 60 um
	pcap80400707 (P38 src+back)	RI = 1/4s
	pcap80400708 (P38 src+back)	RI = 1/2s
	pcap80400709 (P38 src+back)	RI = 1/16s
	pcap80400710 (P39 src+back)	RI = 1/4s, FCS = 60um
PHT-C200:	pcae80400811 (P37 back)	FCS = 120 um
	pcap80400812 (P38 src+back)	RI = 4s
	pcap80400813 (P38 src+back)	RI = 8s
	pcap80400814 (P38 src+back)	RI = 1/2s
	pcap80400815 (P39 src+back)	RI = 4s, FCS = 120um

Colour correction: black body, T = 3839 K

Model: Cohen

Det	cwl (μm)	OLP 8	OLP 9	IRAS	Model	Δ (OLP 8)	Δ (OLP 9)
P1	10.0	0.000	156.132		258.884	-100.00	-39.69
P1	15.0	0.000	126.426		121.759	-100.00	3.83
P2	25.0	0.000	68.664	47.057	44.169	-100.00	55.46
P3	60.0	0.000	8.395	7.924	7.972	-100.00	5.30
P3	100.0	0.000	3.131	2.603	2.851	-100.00	9.82
P3	60.0	0.000	7.591	7.924	7.972	-100.00	-4.77
P3	100.0	0.000	2.933	2.603	2.851	-100.00	2.88
P3	60.0	0.000	7.749	7.924	7.972	-100.00	-2.79
P3	100.0	0.000	2.724	2.603	2.851	-100.00	-4.44
P3	60.0	0.000	7.683	7.924	7.972	-100.00	-3.62
P3	100.0	0.000	2.644	2.603	2.851	-100.00	-7.26
C1	60.0	0.000	8.985	7.924	7.972	-100.00	12.71
C1	100.0	0.000	3.963	2.603	2.851	-100.00	38.99
C1	60.0	0.000	8.767	7.924	7.972	-100.00	9.97
C1	100.0	0.000	4.056	2.603	2.851	-100.00	42.27
C1	60.0	0.000	11.231	7.924	7.972	-100.00	40.88
C1	100.0	0.000	4.550	2.603	2.851	-100.00	59.59
C1	60.0	0.000	10.861	7.924	7.972	-100.00	36.24
C1	100.0	0.000	4.664	2.603	2.851	-100.00	63.60
C2	120.0	0.000	3.041		1.973	-100.00	54.13
C2	120.0	0.000	2.783		1.973	-100.00	41.05
C2	120.0	0.000	0.996		1.973	-100.00	-49.51
C2	120.0	0.000	3.394		1.973	-100.00	72.03

8.5 Revalidation of PHT-C Staring Mode Raster Maps

An overview of the test cases is outlined in Ref. [4], chapter 3.2, P22 mini-maps for photometry from mini-maps and chapter 4.1 for verification of flat-field accuracy and absolute surface brightness determination.

8.5.1 References to Calibration Analysis and Software Change Documentation

- calibration reports:
  - Linearization of ISOPHOT-P and -C detector signals in OLP8 [30]
- Software Problem Reports: SPRs 3214, 3215

8.5.2 Summary of Results

By a deeper investigation of photometry from mini-maps the following was found:

- Aperture photometry on PGAI map products gives reliable fluxes only for a rather limited flux range. These products should mainly be used for a check what can be seen in the maps (source detected, structures around ...)
- For reliable photometry over a wide flux range the PCAS products (photometry per raster point) should be used applying an evaluation method as outlined in Sect. 8.5.3.

The assessment of flat-field accuracies gives the following results:

- Qualitatively (appearance of residual flat-field patterns) and quantitatively (w.r.t. absolute surface brightness and standard deviation of average in flat sky areas) the OLP V9.0 is quite similar to the OLP V8.4.
- For C100 maps flat-field accuracies between 2.5 and 20 % were found. Maps with pixel overlap have typically 2.5 to 11 % accuracy, maps without any pixel overlap between 8 and 20 % accuracy.
- For C200 maps flat-filed accuracies between 2.5 and 15 % were found. Maps with pixel overlap have typically 2.5 to 5 %, maps without any pixel overlap between 6 and 15 % accuracy.
- In most cases the flat-field accuracy is limited by systematic array flat-field residuals, which can be recognized as systematic patterns. Improvement will be achieved by statistical flat-field procedures using the average 10%tiles for determination of the pixel variations in a map. These will be implemented with OLP V10.0. The expectation is that for C100 flat-field accuracies will be in the range 2.5 to 10 % and for C200 1.5 to 8 %, for all maps with more than 20 raster positions.

8.5.3 General Re-validation of Point Source Photometry from PHT22 Mini-Maps

- authors: Cs. Kiss, U. Klaas
- date: 17-May-2000
- SVP period 2

Motivation

The assessement of the calibration accuracy of mini-map photometry during the scientific validation of OLP V8.4 resulted in general accuracy numbers of not better than 40% [1]. On the other hand, photometry performed in absolute mode yielded a higher calibration accuracy. The purpose of this study is therefore also to find out what limited the accuracy of minimaps, a limitation of the calibration strategy or an impact by the evaluation used to derive source fluxes from mini-maps. We have selected mini-map observations as staring reference measurements for the chopped photometry validation. These observations, for which a large subset is performed on stars, are also used to verify the proper re-validation of point source photometry of the mini-map mode itself.

Method

For all mini-map observations of celestial standards with known reference fluxes we derive absolute calibration numbers with the reference photometry (as each mini-map observation has two FCS calibration measurement per filter, no relative filter-to-filter calibration values can be established from this assessment).
The absolute photometric accuracy was tested on a larger sample of objects for both C100 and C200 detectors. We have also investigated the homogeneity of the background on the same samples. We compare the results using aperture photometry on PGAI products and a new method developped to perform photometry using the *PCAS* products (PCASPHT, see **Appendix**).
We monitored the time-variation of the mini-map mode performance using the measurements of two stars, HR 7310 and HR 6705 to test the C100 and C200 mini-map reproducibility, respectively.

Results

C100 absolute photometric accuracy: In the OLP 8.4 re-validation of PHT22 mini-maps the reference fluxes were choosen for all stars according to black-body photospheric models which failed for several cases, since some of the sample stars were known showing the *Vega-phenomenon* (FIR excess caused probably by circumstellar matter). To avoid this, we used predictions taking into account the excess (usually from IRAS fluxes). In our sample, there are 6 stars of this kind (from 17). Table 8.5.3 and Fig. 8.71 present the results achieved by the two different methodes to derive fluxes. While aperture photometry on PGAI maps gives a moderate accuracy down to $\sim$0.5 Jy (accuracy within $\pm$ 30%), it usually fails for fainter objects. There is a clear trend seen in Fig. 8.71 for the PGAI fluxes that the fainter the star the higher the deviation towards higher fluxes. The background values seems to be fairly homogenous in all the cases. PCASPHT remains within the $\pm$ 20% accuracy range for the whole reference flux range, however the uncertainity of the derived flux is larger the fainter the star is. The only exception may be the star HR 6464 (HD 157325), observed at 90 μm, which shows a flux $\sim$40 % higher than the prediction. This might be caused by an overall higher uncertanity of the 90 μm calibration. On the other hand, the flux prediction for this star is based on a Rayleigh-Jeans extrapolation, since IRAS could observe the star at 60 μm at moderate flux quality, and only give an upper (cirrus confusion) limit at 100 μ. Therefore, the real 90 μ flux might be different from the predicted one. Predicted fluxes for Sirius (HD 48915 or HR 2491) were kindly provided by D. Backmann. Reference fluxes for all the other stars without known FIR excess were obtained according to Cohen (1996).

TDT number	target (HD #)	filter (μm)	color correction	pht. flux (PCAS)(Jy)	ref. flux (Jy)	accuracy (%)	R_σ (%)	R_S
61001139	142373	60	BB,10^4K	0.080 $\pm$ 0.010	0.064	24.5 $\pm$ 16.9	10.9	0.21
61001236	128167+	60	λ^{-1}BB,80K	0.104 $\pm$ 0.014	0.116	-10.3 $\pm$ 12.4	10.7	0.21
61002158	203280	60	BB,10^4K	0.210 $\pm$ 0.037	0.243	-13.4 $\pm$ 15.4	11.6	0.33
64700880	139664+	60	λ^{-1}BB,80K	0.522 $\pm$ 0.031	0.492	6.0 $\pm$ 6.2	8.8	0.49
69100108	12311	60	BB,10^4K	0.188 $\pm$ 0.013	0.178	5.6 $\pm$ 7.8	15.3	0.41
69301251	185395	60	BB,10^4K	0.062 $\pm$ 0.033	0.051	23.0 $\pm$ 66.0	9.7	0.15
69500449	185144	60	BB,10^4K	0.122 $\pm$ 0.017	0.055	26.4 $\pm$ 17.9	11.4	0.30
69700102	1581	60	BB,10^4K	0.098 $\pm$ 0.016	0.094	4.8 $\pm$ 17.3	7.7	0.23
70705603	48915	60	BB,10^4K	4.14 $\pm$ 0.167	4.130	1.0 $\pm$ 4.3	14.8	6.07
70705604	48915	100	BB,10^4K	1.421 $\pm$ 0.051	1.490	-4.6 $\pm$ 3.4	5.8	1.25
71500582	172167+	60	λ^{-1}BB,70K	7.708 $\pm$ 0.165	9.100	-15.3 $\pm$ 2.1	20.0	15.1
71800269	216956+	60	λ^{-1}BB,60K	9.888 $\pm$ 0.320	9.717	1.7 $\pm$ 3.2	16.1	15.1
72300260	203608+	60	λ^{-1}BB,80K	0.136 $\pm$ 0.019	0.148	-7.1 $\pm$ 13.1	9.2	0.27
72400584	187642	60	BB,10^4K	0.999 $\pm$ 0.031	1.050	-4.8 $\pm$ 2.9	10.2	1.25
74800404	180711	100	BB,10^4K	0.255 $\pm$ 0.023	0.208	17.9 $\pm$ 10.4	7.0	0.66
75701121	10700+	60	λ^{-1}BB,80K	0.420 $\pm$ 0.024	0.388	8.2 $\pm$ 6.3	8.5	0.61
78300465	157325	90	BB,10^4K	0.173 $\pm$ 0.017	0.123	41.0 $\pm$ 15.7	5.9	0.57

Table 8.12: Accuracy of OLP 8.6 mini-map PCAS photometry results for the C100 detector. The columns are: 1.) TDT number of the measurement; 2.) HD number of the target star. Objects marked by "+" are known as FIR excess stars; 3.) filter 4.) photometric flux derived from the PCAS files using the PCASPHT method (color corrected); 5.) color correction: BB denotes a black body spectral energy distribution with the temperature indicated. λ^{-1}BB denotes a modified black body spectrum with emissivity $\propto \lambda^{-1}$, also with the indicated temperature. The latter is applied for all the stars with known FIR excess. 6.) reference flux (in case the reference flux was derived from an IRAS measurement, the appropriate color correction was also performed); 7.) accuracy, calulated as $100\times((f_{ISO}-f_{ref})/f_{ref})$, where f_{ISO} is the derived color corrected flux and f_{ref} is the reference flux; 8.) R_σ: the ratio of the standard deviation of the background flux to the median background flux $\times$ 100; 9.) R_S: the ratio of the source flux to the median background flux.

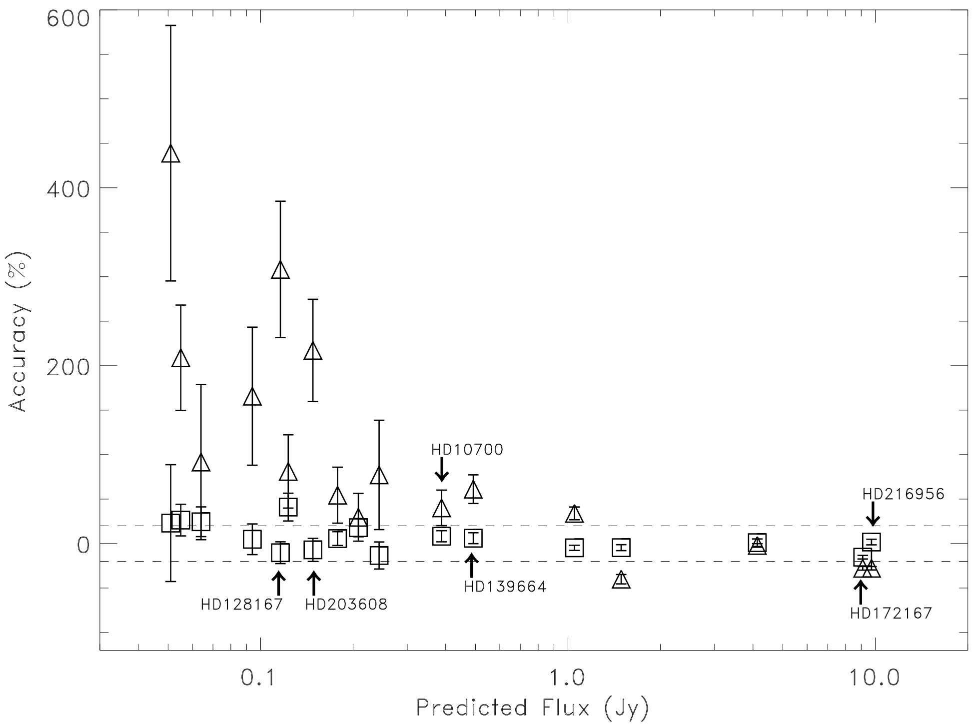

Figure 8.71: Absolute accuracy of the C100 mini-map results and comparison of the aperture photometry on PGAI maps (triangles) and the PCASPHT method using PCAS products (squares). Marked stars have known FIR excess.

TDT number	target	filter (μm)	color correction	pht. flux (PCAS)(Jy)	ref. flux (Jy)	accuracy (%)	R_σ (%)	R_S
55204704	Uranus	200	BB,60K	558.320 ± 32.805	511.130	9.2 ± 6.4	319.7	405.92
55204908	Uranus	120	BB,60K	810.166 ± 21.261	896.660	-9.6 ± 2.4	150.2	302.30
57901808	Ceres	120	BB,240K	116.616 ± 5.483	119.960	-2.8 ± 4.57	35.5	40.74
59402708	Ceres	150	BB,240K	87.400 ± 4.326	95.000	-8.0 ± 4.5	16.0	24.82
57902212	Ceres	170	BB,240K	57.603 ± 3.821	71.180	-19.1 ± 5.36	22.9	14.30
59402304	Ceres	180	BB,240K	66.092 ± 1.195	63.570	3.9 ± 1.9	27.2	28.17
57901404	Ceres	200	BB,240K	39.022 ± 3.232	45.990	-15.1 ± 7.0	40.9	23.56
65002103	HR 1654	150	BB,4000K	0.275 ± 0.022	0.254	8.6 ± 8.8	7.6	0.20
65002406	HR 1654	170	BB,4000K	0.193 ± 0.029	0.197	-2.2 ± 15.1	11.3	0.16
65002709	HR 1654	120	BB,4000K	0.350 ± 0.042	0.399	-12.3 ± 10.5	10.8	0.41

Table 8.13: Accuracy of OLP 8.6 mini-map photometry PCAS results for the C200 detector. The columns are: 1.) TDT number of the measurement; 2.) name of the target; 3.) filter; 4.) color correction. In the case of the C200 detector mini-map re-validation, we assumed black body (BB) specrtal energy distribution with the temperature indicated in this column for all the objects; 5.) photometric flux derived from the PCAS files using the PCASPHT method (color corrected); 6.) reference flux; 7.) accuracy, calulated as $100\times((f_{ISO}-f_{ref})/f_{ref})$, where f_{ISO} is the derived color corrected flux and f_{ref} is the reference flux; 8.) R_σ: the ratio of the standard deviation of the background flux to the median background flux × 100; 9.) R_S: the ratio of the source flux to the median background flux.

C200 absolute photometric accuracy: Comparison of fluxes from aperture photometry and PCASPHT show the superiority of the latter method even clearer than in the case of the C100 detector (see Table 8.5.3 and Fig. 8.72). Aperture photometry does not show accurate fluxes ($\leq$ 20%) anywhere in the whole flux range. The fluxes are excusively too low. The backgrounds are fairly homogenous in these cases, too. This is true even for the two Uranus measurements (TDT = 55204704 and 55204908), since the background is negligible here compared to the source flux. PCASPHT stays within the 20% range in the whole flux range, even for relatively faint objects. Reference fluxes were choosen according to Cohen (1996 and 1998).

Results of C100 monitoring of HR 7310: Measurements on the star HR 7310 (δ Dra) were repeated 23 times between rev. 500 and the end of the mission (rev. 875) with varying orbital phases. The results are presented in Table 8.5.3 and Fig. 8.73. The average deviation of the fluxes from the predicted one is +9±11 %. Since we have already tested the differences between aperture photometry and PCASPHT (see the previous paragraph), we used only PCASPHT (PCAS product) here. All these observations were performed using the 100 μm filter, and the used reference flux is 0.208 Jy (Cohen 1996). The two clear outliers on revs. 552 and 566 are due to Space Weather effects, since both observations were performed at the very end of the revolution.

Results of C200 monitoring of HR 6705: Observations of the star HR 6705 (γ Dra) were done 25 times at different orbital phases. The results are presented in Table 8.5.3 and Fig. 8.74. The average deviation of the fluxes from the predicted one is +14±7 %. Only PCAS files were used. The observations were performed using the 170 μm filter. The reference flux applied is 0.566 Jy (Cohen 1996).

Conclusions & Recommendations

- Aperture photometry of point sources in mini-maps using the PGAI images (aperture sized such that the total source intensity should be enclosed) yields an average accuracy of ∼ 30 % from the brightest stars down to ∼ 0.5 Jy and > 100 % below this limit in the case of the C100 detector. Using the same method, the C200 map results do not show the trend seen at C100 (see Fig. 8.71), but rather show in average a too low flux by ∼ –40 % compared to the reference. This high uncertainity in the case of both detectors can be traced back to the resampling and rotation of the original image while creating the PGAI images.

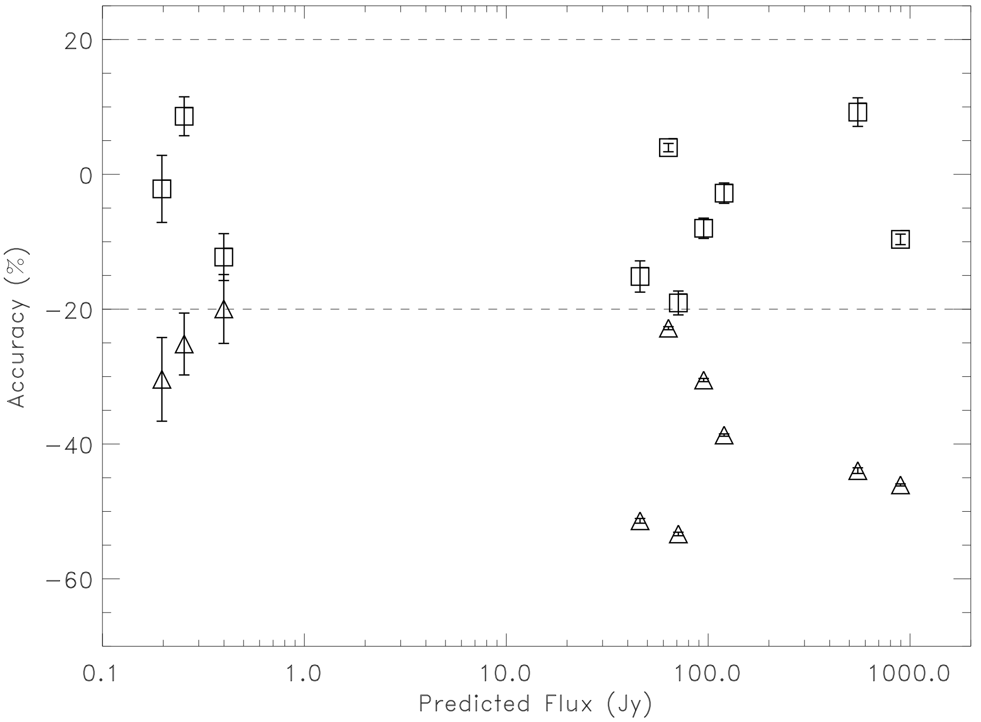

Figure 8.72: Absolute accuracy of the C200 mini-map results and comparison of the aperture photometry on PGAI maps (triangles) and the PCASPHT method using PCAS products (squares).

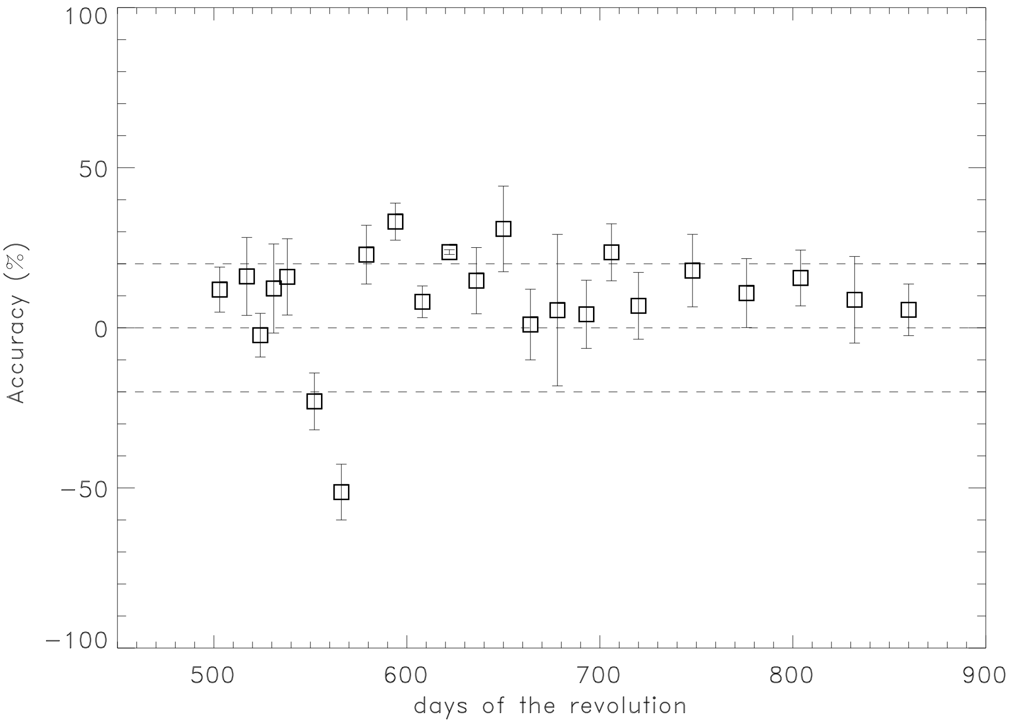

Figure 8.73: Results of the C100 detector monitoring by HR 7310.

HR 7310 100 μm			HR 6705 170 μm		
TDT number	photom. flux (Jy)	accuracy (%)	TDT number	photom. flux (Jy)	accuracy (%)
50301104	0.233 ± 0.044	11.94 ± 21.32	50303905	0.463 ± 0.031	-18.19 ± 5.53
51705004	0.241 ± 0.077	16.05 ± 36.87	51702505	0.484 ± 0.056	-14.41 ± 9.92
52402304	0.203 ± 0.043	-2.29 ± 20.66	52401505	0.453 ± 0.051	-19.92 ± 9.09
53101804	0.234 ± 0.088	12.28 ± 42.15	53102005	0.554 ± 0.069	-2.16 ± 12.25
53800704	0.241 ± 0.075	15.91 ± 36.08	53803705	0.462 ± 0.061	-18.43 ± 10.78
55206904	0.160 ± 0.056	-22.98 ± 26.90	55206105	0.422 ± 0.048	-25.47 ± 8.47
56602704	0.101 ± 0.055	-51.29 ± 26.41	56601805	0.446 ± 0.085	-21.23 ± 15.00
57900904	0.256 ± 0.058	22.86 ± 27.79	57903105	0.467 ± 0.068	-17.46 ± 12.04
59403704	0.277 ± 0.036	33.16 ± 17.52	59403105	0.452 ± 0.069	-20.12 ± 12.23
60801904	0.225 ± 0.031	8.13 ± 15.02	60801205	0.520 ± 0.063	-8.11 ± 11.11
62201704	0.257 ± 0.005	23.65 ± 2.23	62201305	0.492 ± 0.046	-13.00 ± 8.15
63601504	0.239 ± 0.065	14.73 ± 31.31	63601605	0.487 ± 0.052	-13.89 ± 9.18
65001304	0.272 ± 0.084	30.89 ± 40.51	65001005	0.486 ± 0.574	-14.05 ± 101.43
			66101501	0.513 ± 0.022	-9.29 ± 3.94
			66101702	0.423 ± 0.012	-25.25 ± 2.10
66400804	0.210 ± 0.070	1.03 ± 33.44	66400905	0.544 ± 0.058	-3.93 ± 10.17
67800604	0.219 ± 0.149	5.53 ± 71.67	67800705	0.529 ± 0.023	-6.50 ± 4.03
69300804	0.217 ± 0.067	4.22 ± 32.24	69301005	0.506 ± 0.016	-10.58 ± 2.91
70600604	0.257 ± 0.056	23.58 ± 26.97	70601005	0.491 ± 0.010	-13.20 ± 1.71
72000704	0.222 ± 0.066	6.87 ± 31.62	72000305	0.534 ± 0.035	-5.64 ± 6.23
74800404	0.245 ± 0.071	17.87 ± 34.31	74801305	0.485 ± 0.031	-14.31 ± 5.41
77600804	0.231 ± 0.068	10.84 ± 32.65	77602205	0.432 ± 0.026	-23.62 ± 4.53
80401304	0.240 ± 0.055	15.57 ± 26.39	80400905	0.494 ± 0.049	-12.75 ± 8.57
83200404	0.226 ± 0.085	8.76 ± 40.98	83200605	0.491 ± 0.128	-13.28 ± 22.65
86001604	0.220 ± 0.051	5.62 ± 24.44	86000505	0.519 ± 0.041	-8.38 ± 7.23

Table 8.14: Results of long-time monitoring of HR 7310 (left) and HR 6705 (right). The columns are: 1.) TDT number of the measurement; 2.) photometric flux derived from the PCAS files using the PCASPHT method (color corrected values); 3.) accuracy, calulated as $100\times((f_{ISO}-f_{ref})/f_{ref})$, where f_{ISO} is the derived color corrected flux and f_{ref} is the reference flux

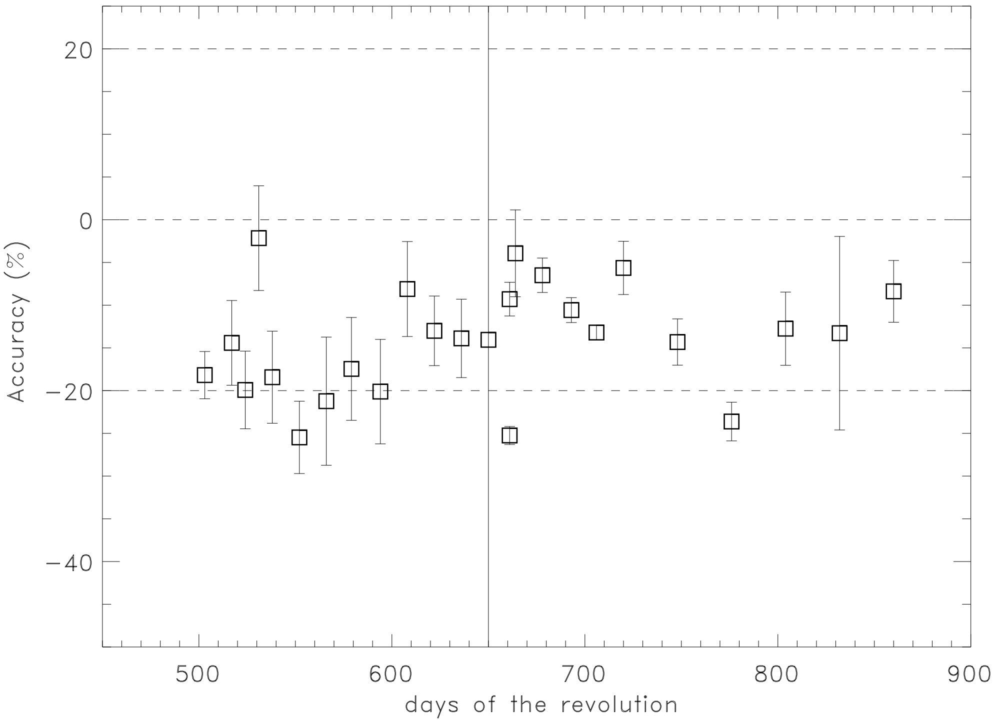

Figure 8.74: Results of the C200 detector monitoring by HR 6705.

- According to the tests, PCASPHT is stable for most objects in a wide flux range, and gives adequate accuracy (the typical absolute flux errors are < 20%).
- For accurate photometry from mini-maps we recommend to use PCAS products (original sampling) and the PCASPHT method for any kind of object, especially for the ones fainter than $\lesssim$0.5 Jy using the C100 detector. PCASPHT is superior for the whole flux range of the C200 detector. PGAI-images are good to investigate the background structure around the point source, the homogeneity of the background, the absolute background level, etc.
- Compared to the previous assessment of the mini-map mode photometry, the absolute photometric accuracy improved a lot, since a more accurate evaluation method was developed for both the C100 and C200 products with the PCASPHT method.

Appendix: the PCASPHT method

The PCASPHT method is based on the determination of fluxes for each individual pixel alone (the PCAS products contain the necessary data, for more detailed information about the PCAS structure see Laureijs et al. 1999). Each pixel at each raster position sees a certain amount of the flux of the central (point) source, plus the background assumed to be constant at all positions:

$$I_{ij} = f_{ij} \times I_j^S + I_j^{BG}$$

Here I_j^S is the total flux of the central source measured by the jth pixel, I_j^{BG} is the constant background flux, measured by the jth pixel, f_{ij} is the fraction of the central source flux on the jth pixel at the ith raster position and I_{ij} is the measured flux on the jth pixel at the ith raster position. f_{ij}-s are theoretically predicted for a given distance from the central source (Herbstmeier 1998). A general empirical re-establishment of f_{ij}-s was given by Laureijs (1999). We used the values from the latter one during the mini-map re-validation. As I_{ij}-s are the measured fluxes themselves, there are only two parameters to determine, I_j^S and I_j^{BG} for the jth pixel, which can be done by a simple line-fit using the f_{ij}-s and

I_{ij}-s. An example is presented in Fig.8.75. The medians of the resulting I_j^S-s and I_j^{BG}-s

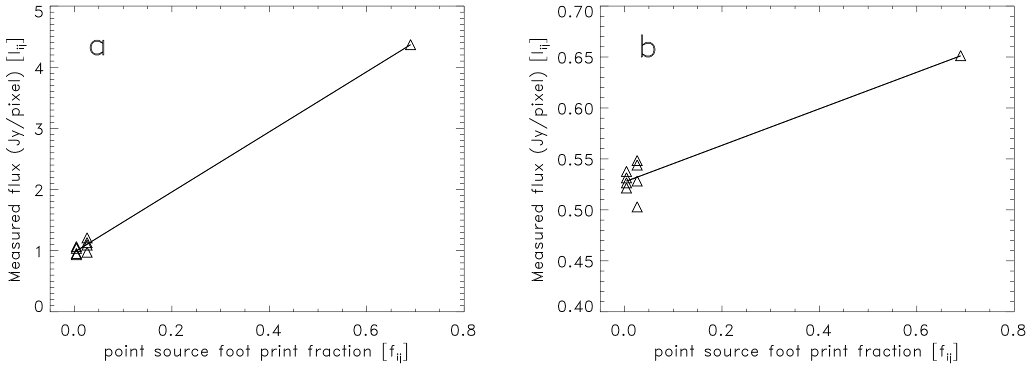

Figure 8.75: Examples of the I_{ij}–f_{ij} linear fit of the PCASPHT method. **a.)** for a bright star: Sirius (HD 48915), f_{ref}=4.13 Jy, TDT number = 70705603, pixel # 5; **b.)** for a faint star: HD 128167, f_{ref}=0.116 Jy, TDT number = 61001236, pixel # 5.

yield the final source- and background flux values. It should be noticed that for the C100 evaluations we had to take into account, that two stars from our sample, Vega (HD 172167) and Fomalhaut (HD 216956) are not point-sources for the C100 detector, since their 60 μm radiation mostly emerges from the circumstellar disk, which is extended (approximated by 22″ and 27″ width Gaussians, respectively, see Walker et al. 1999). Therefore we had to modify the f_{ij}-s accordingly (convolution of the point source foot print with an appropriate Gaussian). Examples of the modified f_{ij}-s are presented in Table 8.15.

source	$f(0)$	$f(46)$	$f(46\sqrt{2})$	$f(92)$
point source	0.6625	0.0429	0.0087	0.0044
22″ Gaussian (Vega)	0.5687	0.0580	0.0128	0.0037
27″ Gaussian (Fomalhaut)	0.5076	0.0691	0.0155	0.0037

Table 8.15: Example of original and modified values of the point source flux footprint fractions of the C100 detector array (60 μm filter). $f(0)$, $f(46)$, $f(46\sqrt{2})$ and $f(92)$ denote the footprint fractions in a distance of 0, 46, $46\sqrt{2}$ and 92″ from the center of the source, respectively. The original point source footprint fractions were choosen according to Herbstmeier (1998).

References

- Backmann,D. 2000, private comm.
- Cohen,M. et al. 1996, AJ 115, 1671
- Cohen,M. et al. 1998, AJ 117, 2274
- Herbstmeier,U., 1998, "ISOPHOT Footprint Tables Explanatory Supplement"
- Laureijs,R.J., Klaas,U., Richards,P.J. and Schulz,B. 1999, *ISOPHOT Data Users Manual,* Version 4.1 (SAI/95-220/Dc)
- Laureijs,R.J., 1999, "Point spread function fractions realted to the ISOPHOT C100 and C200 arrays", ISO Data Center, Villafranca
- Walker,H., Heinrichsen,I., Klaas,U. and Sylvester,R.J. 1999, in the proceedings of the Conference *"The Universe as seen by ISO"* , ESA SP-427, p.425

8.5.4 General Re-validation of Point Source Photometry from PHT22 Mini-Maps: The SED of HR 7980 - Final Assessment

- authors: U. Klaas
- date: 19-December-2000
- SVP period 2 extended

Motivation

For HR 7980 there exist mini-maps in all C100 filters and in three out of five C200 filters (120 to 170 μm). Therefore, the relative filter-to-filter calibration accuracy can be checked for this case.

Method

We compare the background subtracted, color corrected flux values of OLP V9.01 results against the model prediction.

Results

Fig. 8.76 displays the photometric results extracted from the mini-map PCAS product in the same way as described in the previous Sect. 8.5.3. The C100 photometry is as accurate as 10 % for all filters, except the 105 μm one. The C200 photometry is better than 25 %. In comparison with the IRAS photometry, one can see that the IRAS 100 μm FSC flux is suffering from cirrus confusion.

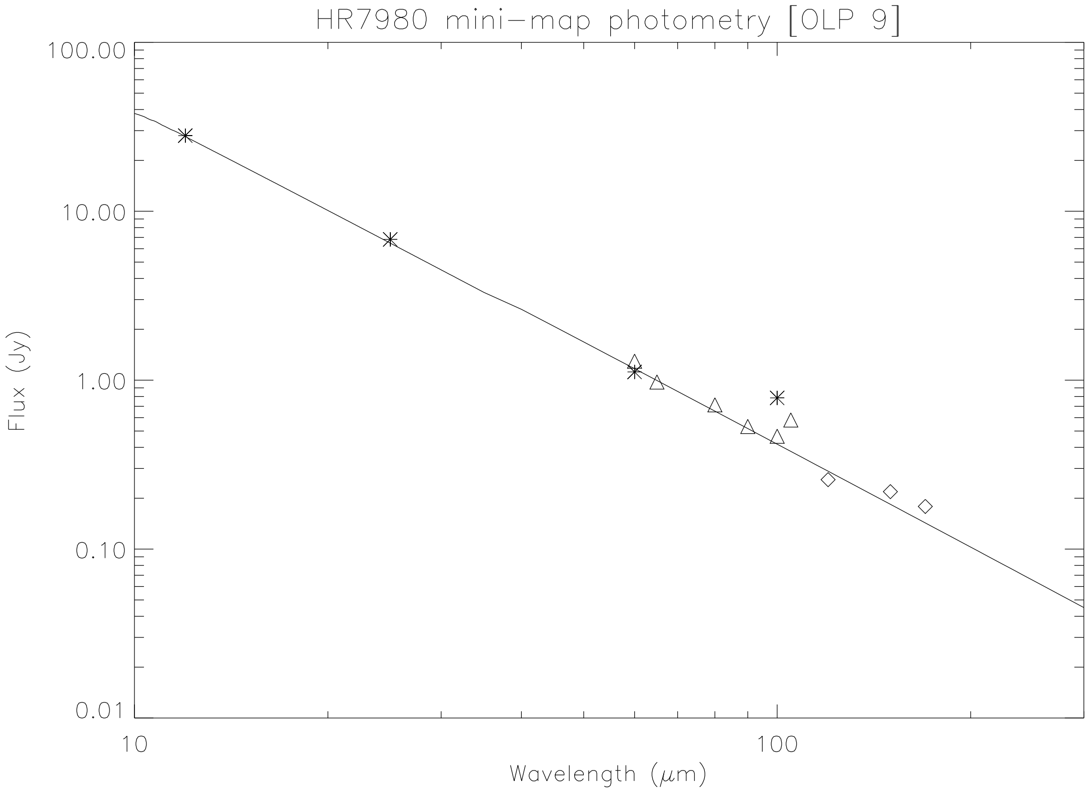

Figure 8.76: Comparison of PHT-C mini-map photometry with the model spectrum (plus extension out to 300 μm) of HR 7980 provided by M. Cohen and with IRAS photometry for OLP 9.01. All photometric points are color corrected for a 3850 K BB. The meaning of the symbols is the following: solid line: model, asterisk: IRAS, triangle: PHT-C100 (P22 AOT), diamond: PHT-C200 (P22 AOT).

Conclusions

- This test case shows that the good absolute photometric accuracy found for PCAS products holds for all C100 filters, except the $105\,\mu$m one and for three out of five C200 filters.

Evaluation Log

1) point source photometry of HR 7980 from mini-maps

Measurements:

PHT-C100:	pcas72701415 (P22 minimap)	FCS = 60 um
	pcas72701412 (P22 minimap)	FCS = 65 um
	pcas72701409 (P22 minimap)	FCS = 80 um
	pcas72701418 (P22 minimap)	FCS = 90 um
	pcas72701406 (P22 minimap)	FCS = 100 um
	pcas72701403 (P22 minimap)	FCS = 105 um
PHT-C200:	pcas73401709 (P22 minimap)	FCS = 120 um
	pcas73401603 (P22 minimap)	FCS = 150 um
	pcas73401706 (P22 minimap)	FCS = 170 um

Colour correction: black body, T = 3850 K

Model: Cohen

Det	cwl (μm)	OLP 8	OLP 9	IRAS	Model	Δ (OLP 8)	Δ (OLP 9)
C1	60.0	0.000	1.295	1.118	1.169	-100.00	10.80
C1	65.0	0.000	0.975		0.995	-100.00	-2.02
C1	80.0	0.000	0.714		0.655	-100.00	8.96
C1	90.0	0.000	0.532		0.517	-100.00	2.81
C1	100.0	0.000	0.466	0.785	0.418	-100.00	11.40
C1	105.0	0.000	0.581		0.379	-100.00	53.41
C2	120.0	0.000	0.258		0.289	-100.00	-10.96
C2	150.0	0.000	0.219		0.184	-100.00	18.78
C2	170.0	0.000	0.179		0.143	-100.00	25.07

8.5.5 Flat-field Accuracies of C100 Maps

- authors: U. Klaas
- date: 13-November-2000
- SVP period 2 extended

Motivation

As part of the scientific revalidation of staring raster maps the current flat-field accuracy is determined. At the moment the flat-field correction is performed as part of the FCS calibration taking into account the actual response of the individual pixels to the illumination by the FCS and interpolating between the two bracketing FCS measurements. This cannot correct for non-linear temporal detector drifts. The flat-field correction has to take into account a non-homogenous FCS illumination over the array (FCS illumination matrix). This is averaged and does not take into account possible systematic effects with heating power of the FCS. The responsivity matrix of the array is determined by rastering point source standards which are centered on each pixel, so that the bulk of the intensity is collected inside the central area of the pixel. For a flat sky, when the full pixel area and its spatial sensitivity is essential, there may be systematic variations due to slightly different solid angles among the pixels. There may be systematic additive offsets among the pixels as indicated by statistical flat-field assessment. Therefore, it is expected, that for faint surface brightness systematic flat-field effects should be seen much stronger than for bright surface brightness. Also the raster step size and final oversampling is expected to play a role, since several pixels are averaged or not.

Method

For OLP 8.4b3 we used the SKYVIEW program to determine the areas for the flat-field accuracy measurement on the preselected maps. The areas were defined drawing a polygon (rectangle). Afterwards a statistics on the defined area was performed determining the mean and standard deviation of the surface brightness. The flat-field accuracy was defined as the ratio of the standard deviation and the mean. It was checked that the minimum flux value is not undefined (equivalent to -1). The vertex points used for OLP 8.4b3 were stored and the SKYVIEW program was run in an automatic batch command sequence on the OLP 9.0b6 data.

Results

In Table 8.16 we give an overview on the selected maps with regard to selected filter and raster parameters. In Table 8.17 we compare the results of OLP 9.0b6 with those from OLP 8.4b3. We note, that overall, the results from both versions are very similar. For most cases the absolute surface brightness derived by OLP 9.0b6 is somewhat higher; considering all cases there is a slight net improvement in flat-field accuracy. However, the systematic patterns are still clearly visible in the OLP 9.0b6 products.

Conclusions

- Qualitatively (appearance of systematic flat-field structure) and quantitatively the results of OLP 9.0b6 are very similar to those of OLP 8.4b3. In general the absolute surface brightness is slightly higher and there is a slight net improvement considering all cases (for individual cases OLP 9.0b6 data may give slightly less good accuracies). The systematic patterns which occurred for OLP 8.4b3 results are still clearly visible.
- In general the achieved flat-field accuracy of C100 maps is better than $\pm$ 20 % (standard deviation of the mean background flux).
- There is some trend that with increasing absolute surface brightness better flat-field accuracies are found.
- The flat-field accuracy is limited by systematic instrumental flat-field residuals of the C100 array.

Table 8.16: Filter and raster parameters of C100 maps used for flat-field accuracy assessment.

OLP product name	**filter** (μm)	**raster parameters** **MxN**	**dMxdN** (arcsec)	**over samp ling**	**aligned with S/C-Y**
PGAI19002101	60	5x5	135x135	N	Y
PGAI08900102	60	7x7	130x130	N	Y
PGAI85001219	60	3x3	120x120	(Y)	Y
PGAI29902250	60	5x5	110x110	(Y)	Y
PGAI30301380	60	5x5	110x110	(Y)	Y
PGAI68300807	60	19x19	92x92	Y	Y
PGAI84403913	60	10x10	69x69	Y	Y
PGAI69801101	60	9x12	69x69	Y	Y
PGAI70401550	60	9x11	37x35	Y	N
PGAI35100809	90	12x12	135x135	N	Y
PGAI58200903	90	9x9	135x135	N	Y
PGAI19201091	90	10x20	130x130	N	Y
PGAI86901244	90	9x9	130x130	N	Y
PGAI41502788	90	12x12	130x130	N	Y
PGAI09000606	90	5x5	130x130	N	Y
PGAI08901904	90	3x3	130x130	N	Y
PGAI40100614	90	13x19	138x92	Y	Y
PGAI87001338	90	9x18	130x65	Y	Y
PGAI16701405	90	11x21	130x65	Y	Y
PGAI57501902	90	8x8	92x92	Y	Y
PGAI52700514	90	5x10	90x90	Y	N
PGAI60002009	90	16x16	87x87	Y	Y
PGAI50000124	90	20x20	75x138	Y	Y
PGAI50100273	90	20x20	75x130	Y	Y
PGAI20701079	90	5x5	75x75	Y	N
PGAI20800709	90	18x18	69x69	Y	Y
PGAI86800640	90	18x9	65x130	Y	Y
PGAI10101158	100	7x7	135x135	N	Y
PGAI79401149	100	4x4	135x135	N	Y
PGAI31000626	100	7x7	135x135	N	Y
PGAI44900714	100	20x20	135x135	N	Y
PGAI15601578	100	7x10	135x92	Y	Y
PGAI27600420	100	7x10	135x90	Y	Y
PGAI71901220	100	10x14	135x90	Y	Y
PGAI33401134	100	5x7	135x90	Y	Y

- The flat-field accuracy is significantly improved when there is overlap of individual pixels. Then the flat-field residuals are averaged out. The best results are observed, if the raster step size is less equal than half of the array size in both directions, resulting in half a pixel displacement in the centre of the map; then accuracies between 2.5 and 11 % are achieved.
- The flat-field residuals can be time dependent and only show up in part of the map.

Table 8.17: C100 flat-field accuracies. For some products several areas have been examined. Some products show a variable flat-field accuracy, they are characterized by the best, the worst and an average value.

OLP product name	no.	OLP8.4b3 surface brightness ($MJy\,sr^{-1}$)	OLP8.4b3 flat-field accuracy (%)	OLP9.0b6 surface brightness ($MJy\,sr^{-1}$)	OLP9.0b6 flat-field accuracy (%)
PGAI19002101		6.8	19.6	7.8	14.6
PGAI08900102		9.5	14.6	10.1	14.7
PGAI85001219		18.9	15.5	18.5	16.2
PGAI29902250		9.8	10.5	9.7	10.3
PGAI30301380		40.7	7.4	40.6	7.8
PGAI68300807		21.0	11.7	21.1	10.7
PGAI84403913		23.7	5.7	24.7	5.5
PGAI69801101		104.4	4.2	104.2	4.2
PGAI70401550		10.0	5.0	10.1	6.1
PGAI35100809		5.1	9.6	5.2	9.4
PGAI58200903		7.8	41.0	8.0	40.0
PGAI19201091	best	4.2	8.8	4.3	8.2
	worst	4.7	32.7	4.8	31.7
	average	4.7	20.4	4.8	19.7
PGAI86901244		5.2	12.6	5.3	12.8
PGAI41502788	best	7.9	4.8	8.0	4.8
	worst	8.4	8.7	8.5	9.0
	average	8.2	7.7	8.3	7.8
PGAI09000606		11.9	13.4	12.7	9.8
PGAI08901904		15.5	16.5	16.5	12.0
PGAI40100614	1	13.8	6.5	14.3	5.7
	2	13.7	6.3	14.3	5.9
PGAI87001338	best	4.9	7.1	5.0	7.8
	worst	5.8	20.0	5.8	19.1
	average	5.3	13.8	5.3	13.6
PGAI16701405	1	15.2	8.4	16.7	6.9
	2	15.5	7.7	17.1	6.7
PGAI57501902	best	11.7	3.9	12.3	4.0
	worst	12.5	5.5	13.1	6.0
	average	12.1	5.8	12.7	6.1
PGAI52700514		4.4	4.6	4.5	4.4
PGAI60002009		6.4	5.4	6.5	5.7
PGAI50000124	best	4.4	7.1	4.5	7.0
	worst	5.8	13.7	5.9	13.5
	average	4.7	13.2	4.8	13.1
PGAI50100273	1	5.5	6.2	5.6	5.9
	2	5.8	6.0	5.9	5.5
PGAI20701079		22.0	3.3	22.6	2.7
PGAI20800709	1	5.8	3.3	5.9	3.5
	2	5.8	3.6	5.9	3.9
PGAI86800640		5.4	5.8	5.5	5.9
PGAI10101158		27.5	13.8	28.7	12.0
PGAI79401149		44.7	8.0	45.8	7.9
PGAI31000626		136.9	7.7	139.9	8.1
PGAI44900714		116.6	13.3	114.3	12.7
PGAI15601578		12.6	18.0	13.3	15.0
PGAI27600420		14.2	9.8	14.9	9.8
PGAI71901220		16.1	4.4	16.8	4.8
PGAI33401134		27.9	10.3	28.8	9.9

8.5.6 Flat-field Accuracies of C200 Maps

- authors: U. Klaas
- date: 13-November-2000
- SVP period 2 extended

Motivation

As part of the scientific revalidation of staring raster maps the current flat-field accuracy is determined. At the moment the flat-field correction is performed as part of the FCS calibration taking into account the actual response of the individual pixels to the illumination by the FCS and interpolating between the two bracketing FCS measurements. This cannot correct for non-linear temporal detector drifts. The flat-field correction has to take into account a non-homogenous FCS illumination over the array (FCS illumination matrix). This is averaged and does not take into account possible systematic effects with heating power of the FCS. The responsivity matrix of the array is determined by rastering point source standards which are centered on each pixel, so that the bulk of the intensity is collected inside the central area of the pixel. For a flat sky, when the full pixel area and its spatial sensitivity is essential, there may be systematic variations due to slightly different solid angles among the pixels. There may be systematic additive offsets among the pixels as indicated by statistical flat-field assessment. Therefore, it is expected, that for faint surface brightness systematic flat-field effects should be seen much stronger than for bright surface brightness. Also the raster step size and final oversampling is expected to play a role, since several pixels are averaged or not.

Method

For OLP 8.4b3 we used the SKYVIEW program to determine the areas for the flat-field accuracy measurement on the preselected maps. The areas were defined drawing a polygon (rectangle). Afterwards a statistics on the defined area was performed determining the mean and standard deviation of the surface brightness. The flat-field accuracy was defined as the ratio of the standard deviation and the mean. It was checked that the minimum flux value is not undefined (equivalent to -1). The vertex points used for OLP 8.4b3 were stored and the SKYVIEW program was run in an automatic batch command sequence on the OLP 9.0b6 data.

Results

In Table 8.18 we give an overview on the selected maps with regard to selected filter and raster parameters. In Table 8.19 we compare the results of OLP 9.0b6 with those from OLP 8.4b3. We note, that overall, the results from both versions are very similar. For most cases the absolute surface brightness derived by OLP 9.0b6 is somewhat lower; considering all cases there is a slight net improvement in flat-field accuracy. However, the systematic patterns are still clearly visible in the OLP 9.0b6 products.

Conclusions

- Qualitatively (appearance of systematic flat-field structure) and quantitatively the results of OLP 9.0b6 are very similar to those of OLP 8.4b3. In general the absolute surface brightness is slightly lower and there is a slight net improvement considering all cases (for individual cases OLP 9.0b6 data give slightly less good accuracies for about half of all cases). The systematic patterns which occurred for OLP 8.4b3 results are still clearly visible.
- In general the achieved flat-field accuracy of C200 maps is better than $\pm$ 15 % (standard deviation of the mean background flux).
- A slight dependence on the absolute surface brightness is found with better flat-field accuracies for higher surface brightness.

Table 8.18: Filter and raster parameters of C200 maps used for flat-field accuracy assessment.

OLP product name	**filter** (μm)	**raster parameters** **MxN**	**dMxdN** (arcsec)	**over samp ling**	**aligned with S/C-Y**
PGAI56200110	150	32x4	180x180	N	N
PGAI56201814	150	20x4	92x92	Y	N
PGAI08900103	170	5x5	180x180	N	Y
PGAI25601309	170	7x4	180x180	N	N
PGAI79400434	170	13x13	96x96	Y	Y
PGAI59300101	170	19x19	92x92	Y	Y
PGAI19800208	170	27x14	46x92	Y	Y
PGAI21001305	170	27x14	46x92	Y	Y
PGAI79900733	170	12x5	46x92	Y	Y
PGAI33600108	180	12x4	180x180	N	N
PGAI33600705	180	12x4	180x180	N	N
PGAI35100907	180	9x9	180x180	N	Y
PGAI16701206	180	8x16	180x90	Y	Y
PGAI52700412	180	5x10	90x90	Y	N
PGAI85001037	180	15x15	90x90	Y	N
PGAI78200101	200	23x23	180x180	N	Y
PGAI36803005	200	10x10	180x180	N	Y
PGAI39602313	200	10x10	180x180	N	Y
PGAI26101401	200	13x13	180x180	N	Y
PGAI33401133	200	8x8	180x180	N	Y
PGAI86101801	200	14x6	180x180	N	N
PGAI15601577	200	5x10	180x90	Y	Y
PGAI33300559	200	10x20	180x90	Y	Y
PGAI10101157	200	5x10	180x90	Y	Y
PGAI31000625	200	5x10	180x90	Y	Y
PGAI26701013	200	15x30	180x90	Y	Y
PGAI40900802	200	11x6	90x180	Y	Y
PGAI28001303	200	11x6	90x180	Y	Y

- The flat-field accuracy is limited by systematic instrumental flat-field residuals of the C200 array. These are filter dependent.
- The flat-field accuracy is significantly improved when there is overlap of individual pixels. Then the flat-field residuals are averaged out. The best results are observed, if the raster step size is less equal than the pixel size in both directions; then accuracies between 2.5 and 5 % are achieved.

Table 8.19: C200 flat-field accuracies. For some products several areas have been examined.

OLP product name	no.	OLP8.4b3 surface brightness $(\mathrm{MJy\,sr^{-1}})$	OLP8.4b3 flat-field accuracy (%)	OLP9.0b6 surface brightness $(\mathrm{MJy\,sr^{-1}})$	OLP9.0b6 flat-field accuracy (%)
PGAI56200110		3.4	8.6	3.0	9.7
PGAI56201814		22.2	4.8	21.8	5.0
PGAI08900103		5.1	10.8	4.8	10.2
PGAI25601309	1	10.3	8.3	9.9	6.3
	2	10.2	7.7	9.9	5.8
	3	10.4	7.6	10.0	5.8
	4	10.6	7.3	10.3	5.6
	5	10.8	7.4	10.4	5.8
PGAI79400434		3.1	4.0	2.9	4.0
PGAI59300101		3.3	3.1	3.2	3.0
PGAI19800208		3.1	2.4	2.9	2.4
PGAI21001305		3.4	3.2	3.2	3.2
PGAI79900733	1	5.2	3.2	4.9	3.4
	2	5.4	2.4	5.1	2.3
PGAI33600108		2.7	13.0	2.2	13.0
PGAI33600705	1	4.7	6.1	3.8	6.8
	2	4.7	6.1	3.9	6.8
	3	4.8	6.0	3.9	7.8
PGAI35100907		4.1	12.5	3.4	13.2
PGAI16701206	1	9.2	4.3	9.3	3.7
	2	11.4	21.8	11.6	20.9
PGAI52700412		3.0	3.9	2.6	3.7
PGAI85001037		7.4	3.1	7.2	2.7
PGAI78200101		2.3	22.3	2.2	18.9
PGAI36803005		14.8	10.0	14.7	8.5
PGAI39602313		29.1	9.5	28.5	8.7
PGAI26101401		37.6	7.0	38.5	7.1
PGAI33401133	1	40.0	11.4	40.9	11.7
	2	51.3	14.3	53.0	14.6
PGAI86101801		158.0	11.0	157.2	11.7
PGAI15601577		8.6	16.3	7.9	12.7
PGAI33300559		18.4	7.6	18.9	7.8
PGAI10101157		49.3	6.4	47.4	6.6
PGAI31000625		180.2	4.5	180.4	4.6
PGAI26701013		184.2	14.2	184.0	14.1
PGAI40900802		6.6	3.6	6.8	3.7
PGAI28001303		10.0	5.1	10.5	3.9

Chapter 9

Validation of Chopped Photometry during SVP2

9.1 Validation of Chopped Photometry Test Cases with Quasi-simultaneous Staring Mode References and Reproducibility Checks

An overview of the test cases is outlined in Ref. [4], chapter 5.1.

9.1.1 References to Calibration Analysis and Software Change Documentation

- calibration reports:
  - Analysis of Chopped ISOPHOT Measurements [19]
- Software Change Requests: none
- Software Problem Reports: SPR 3213, 3216

9.1.2 Summary of Results

- P1 chopped photometry has been significantly improved to a level that most test cases show satisfying accuracies. There are still a few individual cases for which interactive processing gives signifcantly different results than the OLP processing (usually better accuracy). Also multi-filter cases are still an issue for investigation. In general P1 chopped processing looks very promising.
- P2 chopped photometry processing produces in general too high fluxes ($> 50\,\%$). There also significant discrepancies with PIA results are found. This needs to be clarified before any statement on the quality of the calibration can be made.
- For P3 chopped photometry the fluxes are in general too low, from acceptable $20\,\%$ up to $70\,\%$
- For C100 a major fraction of the test cases gives reasonable results. There seems to be still some fine-tuning with regard to the chopper frequency dependence necessary. For test cases with fluxes below 100 mJy the effect of cirrus confusion on the final accuracy needs to be considered. Multi-filter test cases show similar patterns as in the C100 staring mode background cases.
- Despite the strong flux discrepancies for P2 and P3, we could verify for all 4 detectors P1, P2, P3 and C100 an excellent reproducibility of the results of $15\,\%$ or better (both for differential source flux and surface brightness).
- The derived surface brightness values for the off-beams show sometimes a significant discrepancy with COBE/DIRBE photometry.

- For C200 the case looks different. There is no reproducibility of the monitoring results, which can be attributed to small scale background gradients (for C200 there is always only one off-position) and partly due to cirrus confusion ($1\,\sigma = 45\,\mathrm{mJy}$ for $5\,\mathrm{MJy\,sr^{-1}}$ background).

- For the brighter C200 test cases reasonable accuarcies are achieved. despite the fact that in general the surface brightness of the off-beam is quite consistent with COBE/DIRBE, the differential source fluxes show an unexpected scatter.

- On the basis of the results listed above the processing and calibration quality has not yet progressed enough to declare the chopped modes scientifically valid. However, we note promising improvements.

9.1.3 Validation of PHT03 and PHT22 Chopped Mode: The SED of IRAS 03068-5346 - Final Assessment

- authors: U. Klaas
- date: 29-June-2000
- SVP period 2

Motivation

Like for validation of staring mode observations The measurements on the IR galaxy IRAS 03068-5346 were designed to check out the processing of multi-filter chopped mode for all PHT-P and PHT-C filters. For reference photometry in nodding mode was taken for some filters and IRAS photometry is available.

Method

We compare the background subtracted flux values of both OLP V8.6b1 and OLP V9.0b6 results against the IRAS photometry and the ISOPHOT nodding mode photometry. Furthermore, we compare the derived background surface brightness with COBE/DIRBE photometry.

Results

Fig. 9.1 shows the derived SED for IRAS 03068-5346. In comparison to OLP V8, the P1 photometry has been considerably improved, due to the fix of SPR-3373. We note, however, still very low fluxes for the 12 and 15 μm filters. The P2 photometry is now signal corrected, the correction appears to be too strong, the 20 μm /25 μm flux ratio does not correspond to the SED shape. C100 60 and 100 μm photometry, as well as P3 60 μm photometry is quite consistent with IRAS photometry (for the color correction performed), within 15 %. The remaining C100 filters show a pattern which reminds very strongly of the background SED shapes for staring measurements, cf. e.g. Figs. 8.45, 8.50 and 8.51. The pattern of the C200 photometric points looks unchanged, however the fluxes are higher now and the 120 μm flux is consistent with the 100 μm flux; 170, 180 and 200 mum fluxes do not appear to be consistent among each other.
Fig. 9.2 shows the derived sky background SED at the position of IRAS 03068-5346 (not color corrected). We see a similar behaviour as for staring mode measurements. The P1 and P2 fluxes match COBE/DIRBE photometry quite well, except for the 12.8 (too high) and 20 μm (too low) filters. P3 and C100 60 μm surface brightness values match COBE/DIRBE photometry quite well, the same is true for P3 100 μm and the C200 photometry. Surprisingly, the C100 100 μm surface brightness is twice as high as COBE/DIRBE, despite the good differential source flux quality for this filter. Also the 65 μm surface brightness drops off significantly.
In general it appears, as if the utilization of the chopped FCS measurements for determination of the absolute flux background works reasonably well. For C100, there may be some correlation between the quality of the background surface brightness determination and the resulting differential source flux, however, this could not be verified on a one by one base. For C200, this does not seem to be the case at all.

Conclusions

- P1 chopped photometry has been significantly improved by the fix of SPR-3373 affecting the relative filter-to-filter calibration. There is still the open point, why the processing of the 12 and 15 μm filter measurements fails to produce reasonable fluxes. This is in contrary to the PIA behaviour.
- P2 chopped photometry still shows some inconsistency, in particular with regard to the relative filter-to-filter calibration of the 20 and 25 μm filters. The differential source fluxes appear too high now. Again, this behaviour is in contrast to the PIA behaviour.
- P3 chopped photometry is relatively consistent with IRAS.

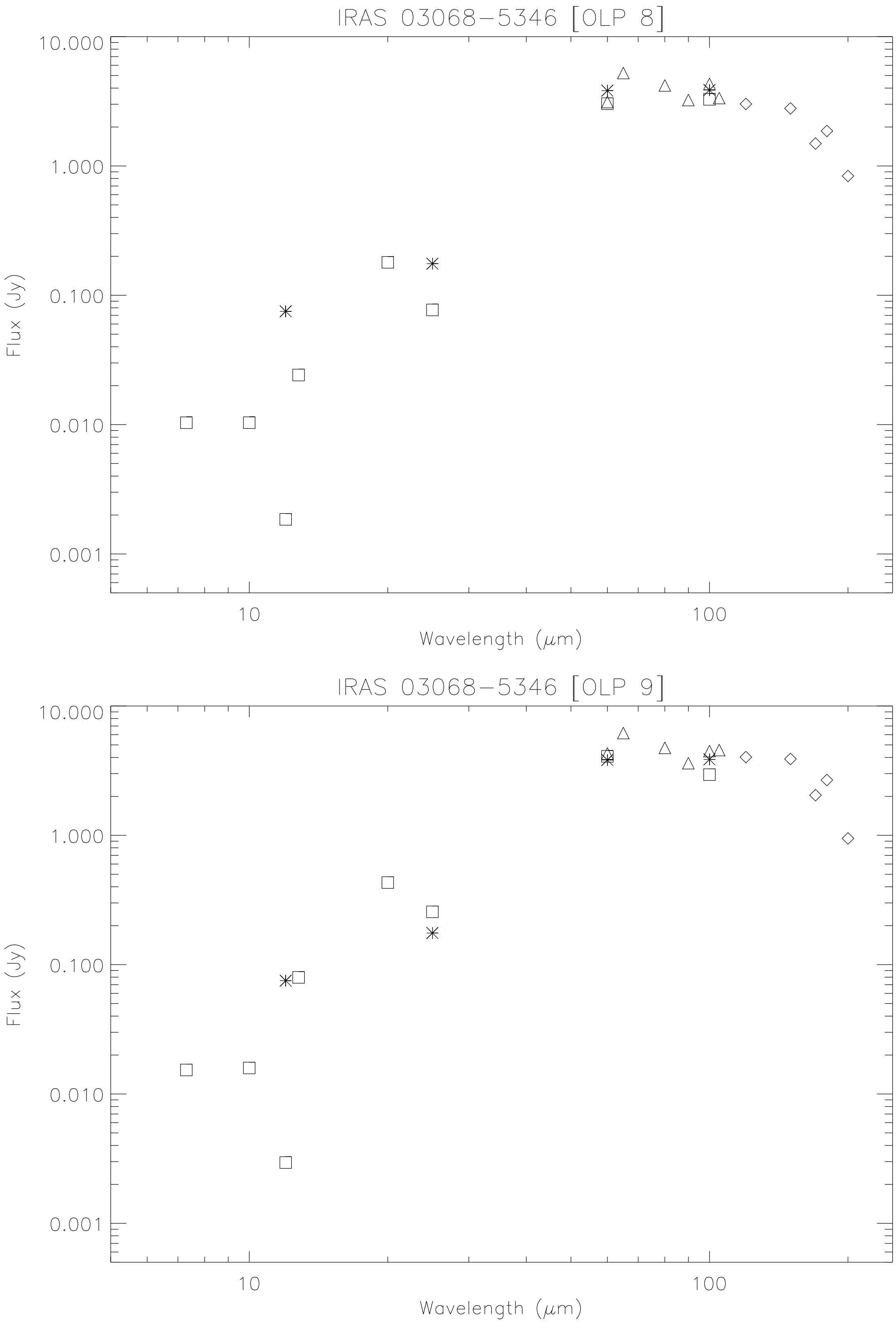

Figure 9.1: Comparison of PHT-P and PHT-C chopped photometry, using the full ISOPHOT filter set, with IRAS photometry both for OLP 8.6b1 (upper panel) and OLP 9.0b6 (lower panel). Color correction has been applied (modified BBs $\propto \lambda^{-2}$ with T1 = 140 K and T2 = 40 K). The meaning of the symbols is the following: asterisk: IRAS, square: PHT-P (P03 AOT), triangle: C100 (P22 AOT), diamond: C200 (P22 AOT).

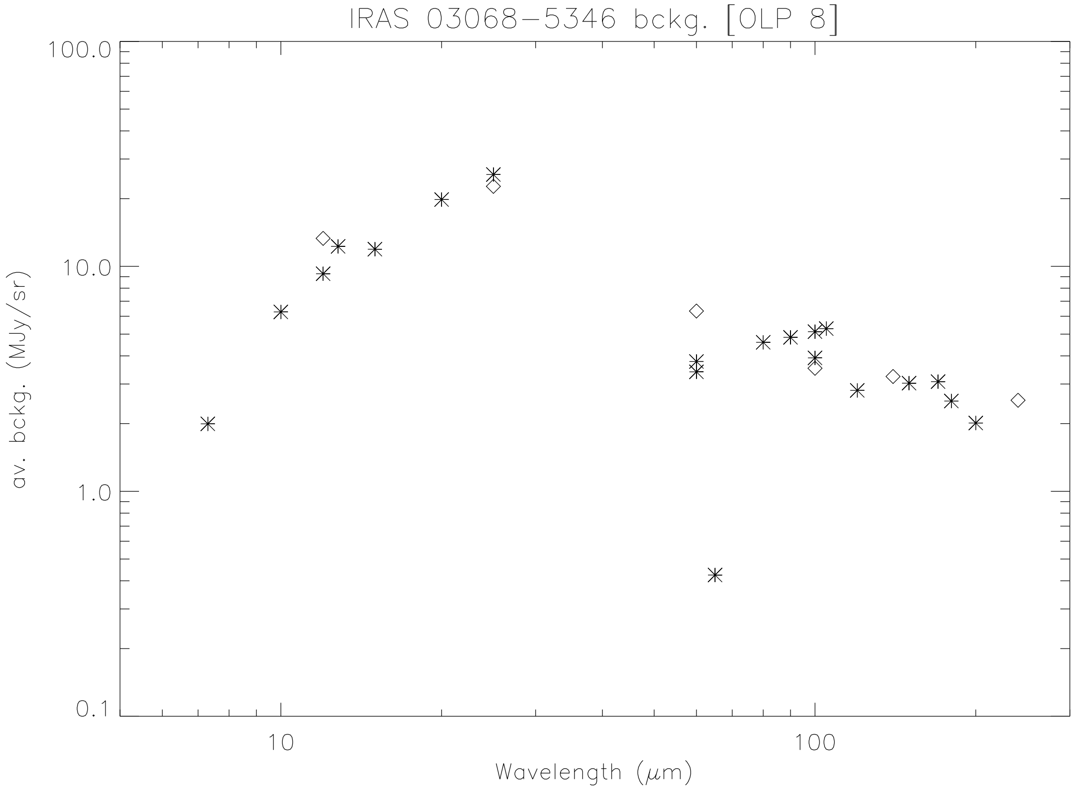

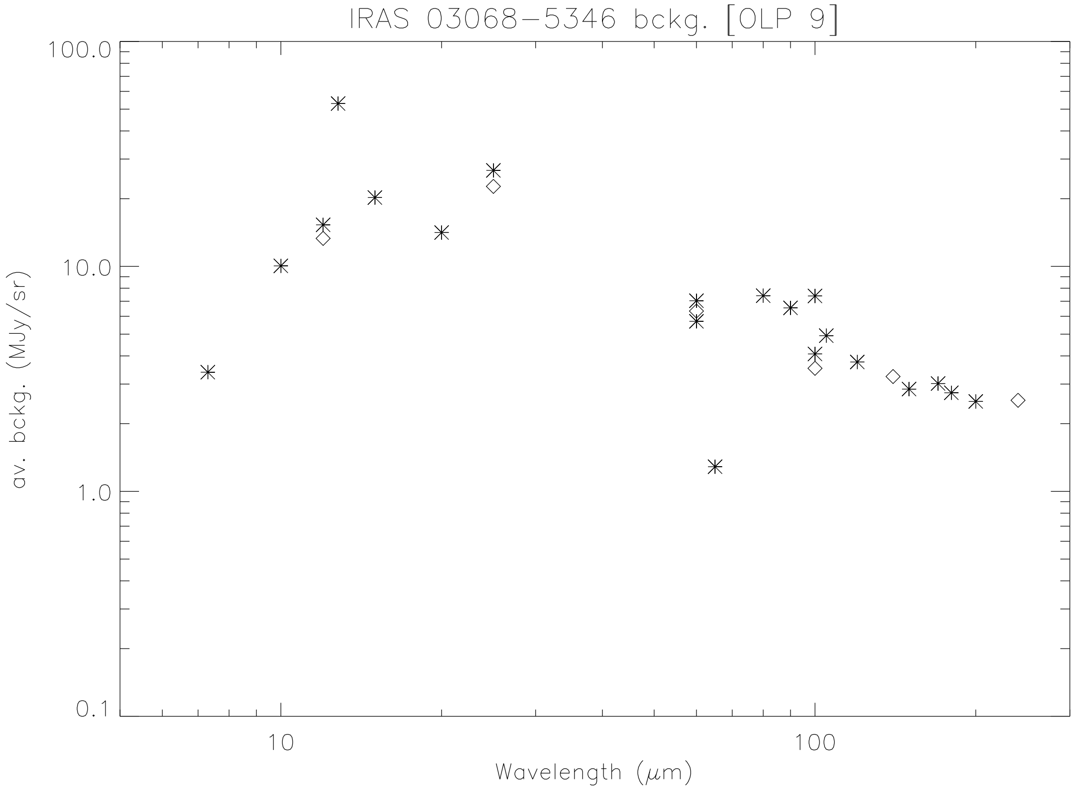

Figure 9.2: Comparison of surface brightness from chopped PHT photometry of the background beam for IRAS 03068-5346 with COBE, both for OLP 8.6b1 (upper panel) and OLP 9.0b6. Asterisk: PHT-P and PHT-C photometry, diamond: COBE.

- C100 60 and 100 μm chopped photometry is consistent with IRAS within 15 % (for the assumed flux model and applied color correction factors). For the other filters there appear a step-like pattern, which reminds of the behaviour of multi-filter surface brightness photometry in staring mode.

- C200 chopped photometry shows now increased fluxes, however the invidual filters do not reflect a smooth SED.
- PHT-P surface brightness photometry is well matched with COBE/DIRBE photometry, indicating that the utilization of the chopped FCS measurements works fine. An exception are the 12.8 and 20 μm filter measurements which stick out in the same way as for staring mode background measurements.
- For C100 the surface brightness consistency with COBE/DIRBE is only good for the 60 μm filter. Again there is a similar behaviour as for staring mode measurements, with the exception that the 65 μ filter measurement shows a significant drop off instead of showing a high positive excess.
- Like for staring measurements the C200 surface brightness values reflect a smooth SED and match quite well with the COBE/DIRBE photometry. Therefore, it is a bit surprising that the derived differential source fluxes vary so much, since the absolute calibration seems to work quite well here.
- For C100, there might be some correlation between the quality of the surface brightness (representative for the absolute calibration by FCS) and the quality of the differential source flux. However, this could not be verified one by one.

Evaluation Log

1) Chopped Point Source Photometry

Measurements:

PHT-P1:	ppap81101701	FCS = 12 um
PHT-P2:	ppap81101701	FCS = 25 um
PHT-P3:	ppap81101802	FCS = 100 um
PHT-C1:	pcap81101906	FCS = 90 um
PHT-C2:	pcap81102008	FCS = 170 um

Colour correction: mod. bb, em.=2, T1 = 140 K (P1, P2), T2 = 40 K (P3, C1, C2)

Det	cwl (μm)	OLP 8	OLP 9	IRAS
P1	7.3	0.010	0.015	
P1	10.0	0.010	0.016	
P1	12.0	0.002	0.003	0.075
P1	12.8	0.024	0.080	
P1	15.0	0.000	0.000	
P2	20.0	0.180	0.431	
P2	25.0	0.077	0.256	0.176
P3	60.0	3.031	4.079	3.822
C1	60.0	3.120	4.288	3.822
C1	65.0	5.231	6.178	
C1	80.0	4.195	4.744	
C1	90.0	3.234	3.609	
P3	100.0	3.273	2.944	3.862
C1	100.0	4.307	4.480	3.862
C1	105.0	3.351	4.563	
C2	120.0	3.014	4.023	
C2	150.0	2.788	3.891	
C2	170.0	1.490	2.043	
C2	180.0	1.864	2.674	
C2	200.0	0.836	0.946	

2) Background photometry from off-source beam

Det	λ	OLP8 (MJy/sr)	OLP9 (MJy/sr)	COBE (MJy/sr)
P1	7.3	2.00	3.39	
P1	10.0	6.27	10.06	
P1	12.0	9.27	15.31	13.32
P1	12.8	12.26	52.97	
P1	15.0	11.92	20.24	
P2	20.0	19.81	14.15	
P2	25.0	25.60	26.72	22.69
P3	60.0	3.40	5.70	6.33
C1	60.0	3.78	7.04	6.33
C1	65.0	0.42	1.29	
C1	80.0	4.59	7.41	
C1	90.0	4.84	6.54	
P3	100.0	3.92	4.08	3.52
C1	100.0	5.12	7.39	3.52
C1	105.0	5.29	4.92	
C2	120.0	2.81	3.76	
C2	150.0	3.03	2.85	3.24
C2	170.0	3.07	3.02	
C2	180.0	2.52	2.74	
C2	200.0	2.01	2.51	2.54

9.1.4 Comparison of Chopped and Staring Mode Photometry of Standard Stars from the Empirical Signal Correction Calibration Program

- authors: U. Klaas
- date: 28-July-2000
- SVP period 2

Motivation

A large calibration program had been set up to establish the empirical signal loss correction factors in chopped measurements from a comparison of chopped and nodding/staring photometry in the same instrumental set-up, on the same source and on the same revolution (as one block of measurements, to minimize differences in detector responsivities.) We have selected a few of these measurements to verify the end product of the chopped photometric calibration, as produced by OLP. This does not only include the signal correction, but also the signal derivation itself and the flux calibration using the chopped FCS measurement. We have selected test cases with more than one filter per detector in order to see the relative wavelength behaviour of the correction.

Method

All targets are standard stars for which flux models are available. In all cases ISOPHOT reference photometry, either in simple staring mode or in nodding technique are available. This allows to determine the absolute accuracy w.r.t. the model and in case of a discrepancy to cross-check how the consolidated staring mode photometry behaves. This last check is not done in this version of the report.

Results

Fig. 9.3 shows the chopped P1 photometry on HR 6817. With regard to OLP 8 the accuracy has slightly decreased, but is still within 10 % of the model flux for the 3.6 and 7.3 μm filters, it is completely off for the 3.3 μm filter for the same reason as explained in the OLP 8.4 Report [1]. Also the resulting surface brightness values in the off-beam are a bit farther away from the COBE/DIRBE photometry than last time (cf. Fig. 9.4).
Fig. 9.5 shows the chopped photometry on HR 6132. The 20 and 25 μm photometry was performed both with a 120 and a 180 arcsec aperture size. While OLP 8 gave good photometry (< 15 %) for the smaller aperture and less good photometry for the 180 arcsec aperture, the OLP9 gives now consistent fluxes for both apertures, but 50 % too high for 20 μm and a factor of 2 too high at 25 μm. This confirms the general trend found for P2 chopped photometry in OLP 9. The consistency of the surface brightness in the off-beam is not good either (cf. Fig. 9.6) and the relative ratio of 20/25 surface brightness looks too steep. This is similar to the finding for staring mode background surface brightness in OLP 9.
Fig. 9.7 shows the chopped P3 photometry on HR 1457. With regard to OLP 8 the photometry has slightly improved and shows now an accuracy of better than 20 %. On the other hand, the 60 μm surface brightness in the off-beam is around a factor of 2 higher than COBE/DIRBE (cf. Fig. 9.8).
Fig. 9.9 shows the chopped C200 photometry on HR 5340. With regard to OLP 8 the accuracy has decreased, in particular for the 120 mum filter, in which the FCS calibration is performed. Here only an absolute accuracy of 40 % is achieved. With regard to the model flux, the 180 mum filter gives an accuracy of 20 %, however the relative calibration with regard to the 120 μm filter and the SED shape has decreased to 60 %. The off-beam surface brightness (cf. Fig. 9.10) looks slightly more consistent with COBE/DIRBE.

Conclusions

- The accuracy of chopped P1 photometry on HR 6817 is better than 10 % (not considering the 3.3 μm measurement).

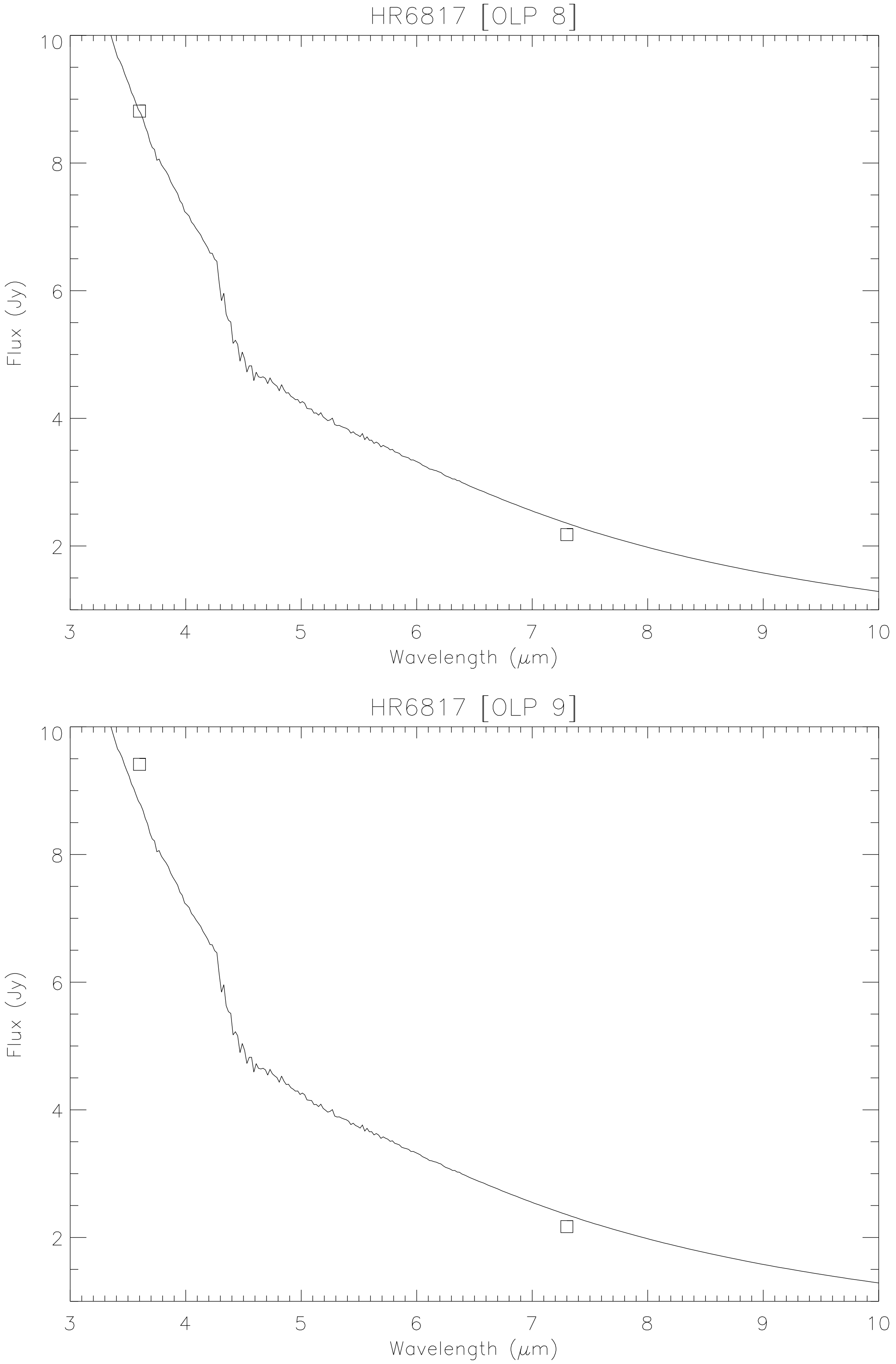

Figure 9.3: Comparison of PHT-P1 chopped photometry with the model spectrum of HR 6817, provided by P. Hammersley, for OLP 8.6b1 (upper panel) and OLP 9.01 (lower panel). The meaning of the symbols is the following: solid line: model, square: PHT-P1.

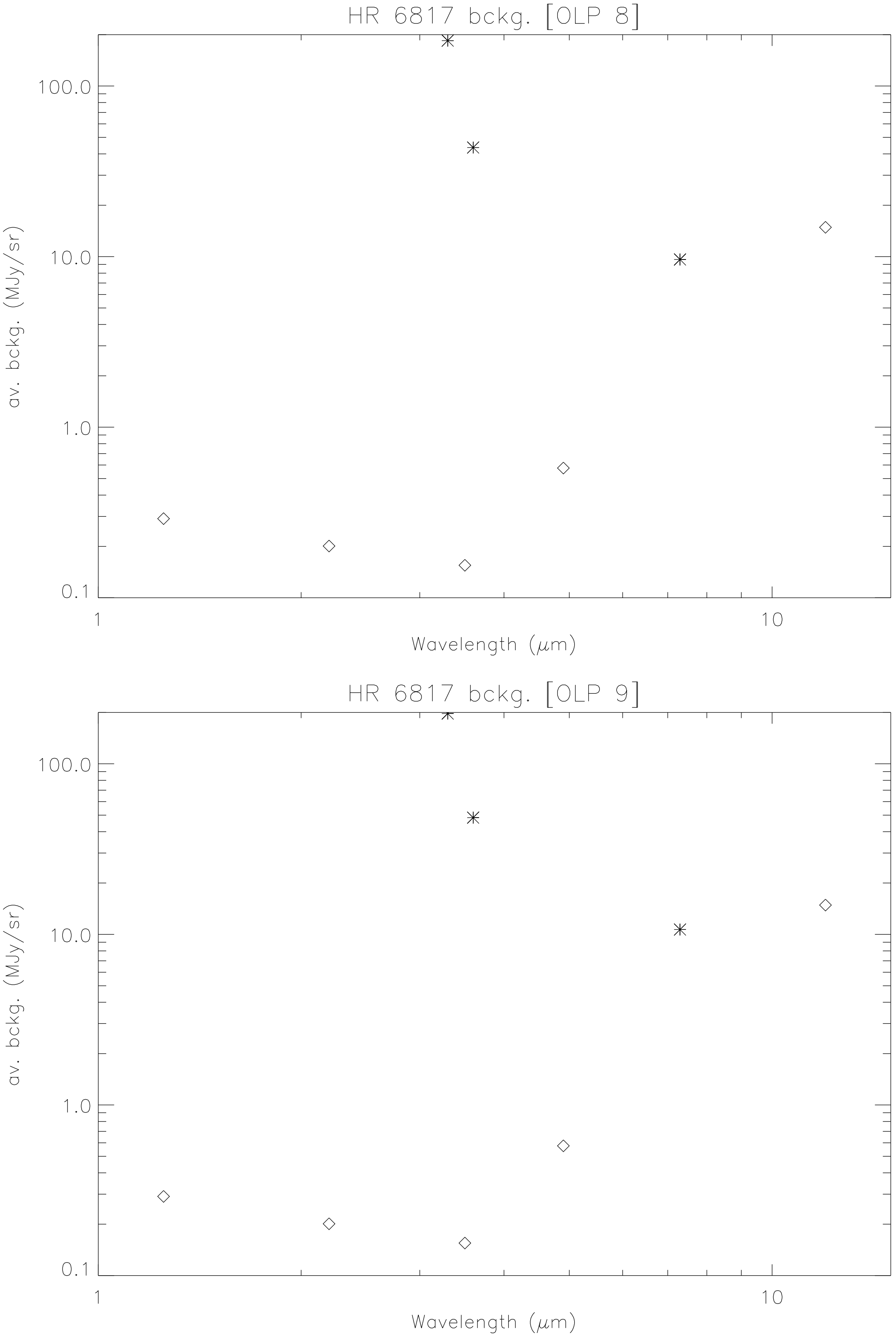

Figure 9.4: Comparison of surface brightness from chopped PHT photometry of the background beam for HR 6817 with COBE, both for OLP 8.6b1 (upper panel) and OLP 9.01. Asterisk: PHT-P and PHT-C photometry, diamond: COBE.

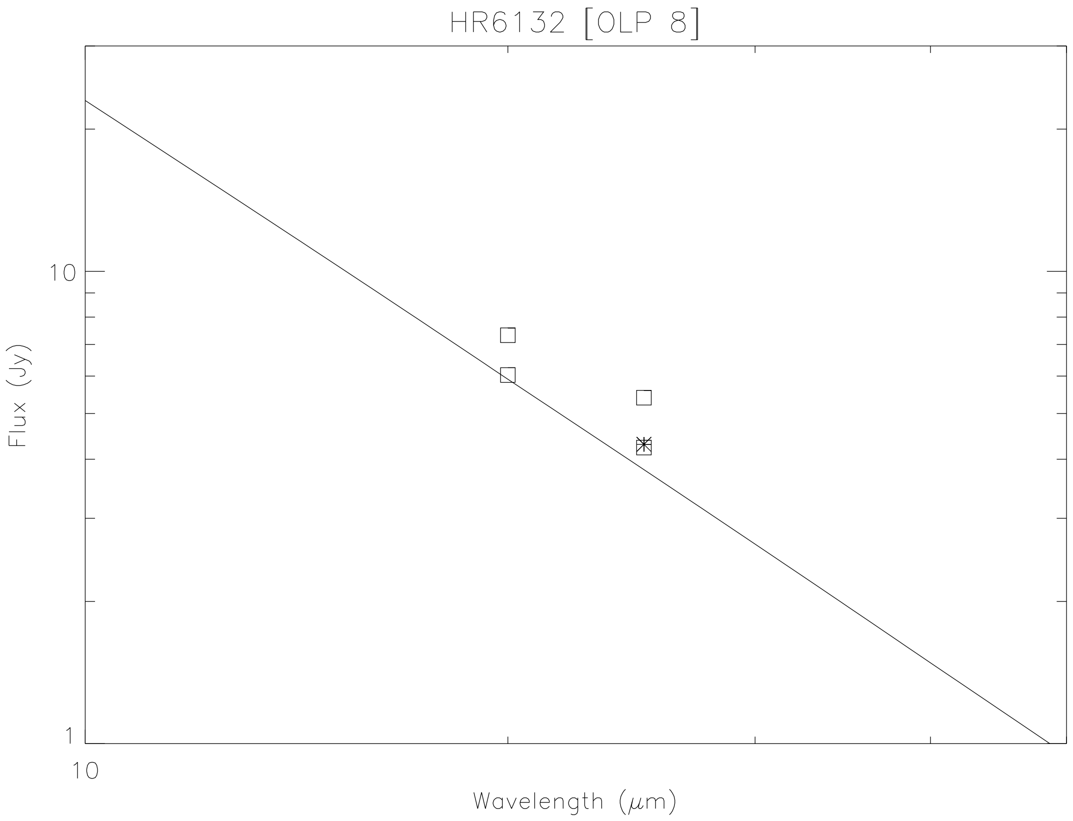

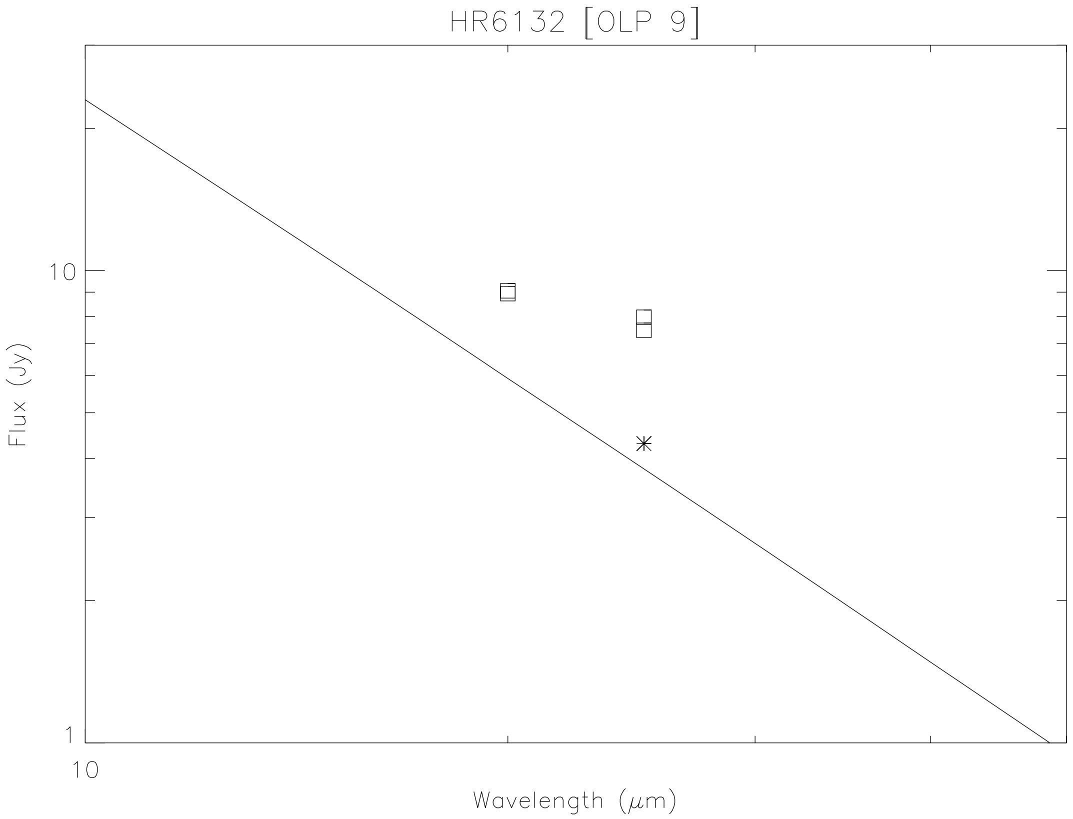

Figure 9.5: Comparison of PHT-P2 chopped photometry with the model spectrum of HR 6132, provided by P. Hammersley, for OLP 8.6b1 (upper panel) and OLP 9.01 (lower panel). The meaning of the symbols is the following: solid line: model, square: PHT-P2, asterisk: IRAS. Only the results with the 120 arcsec aperture are shown.

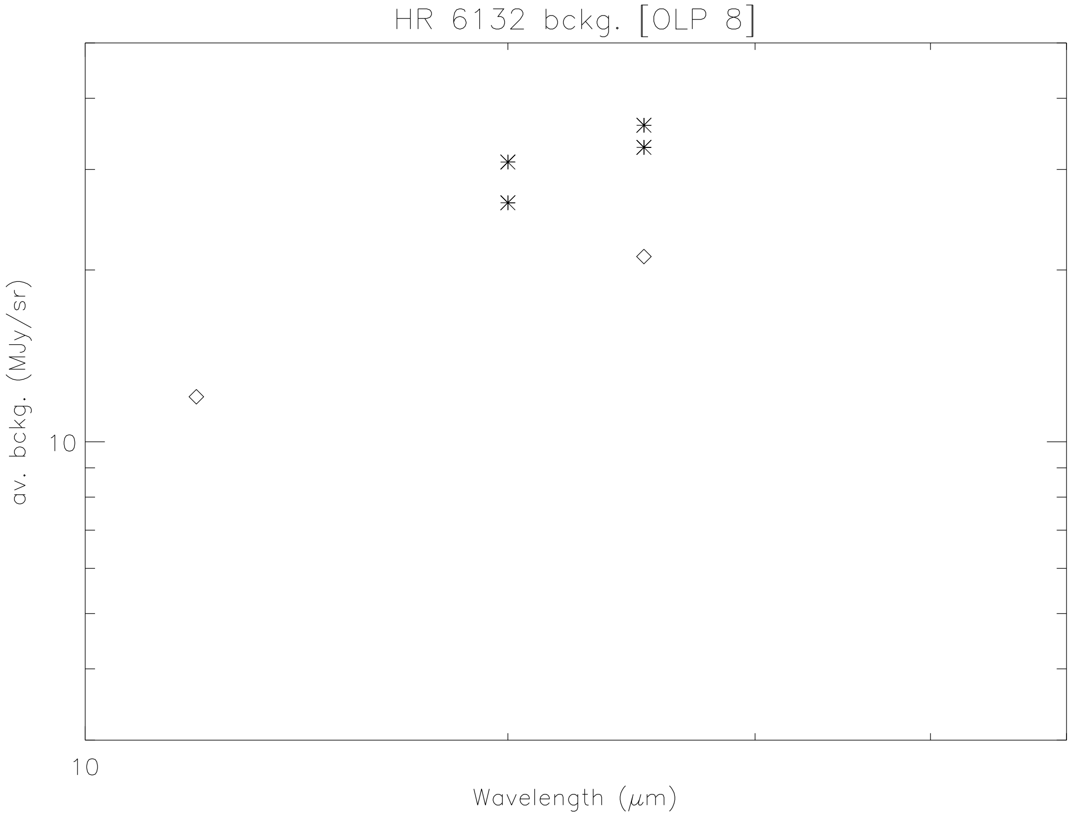

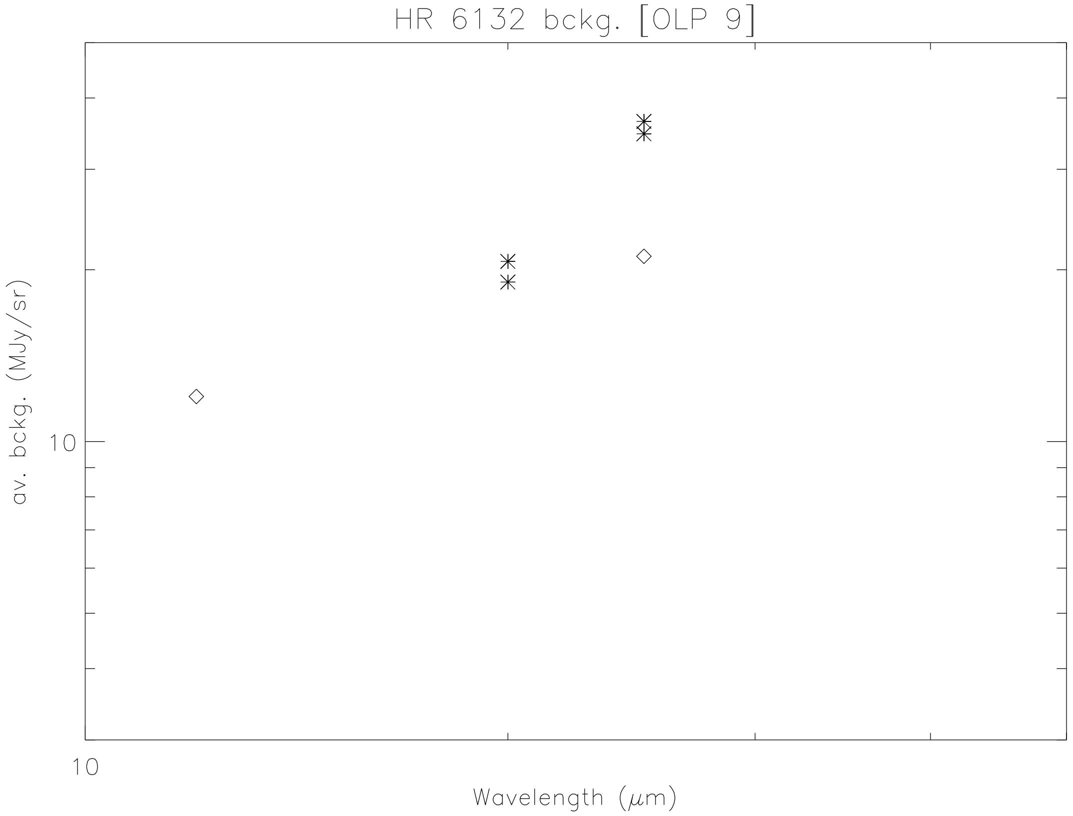

Figure 9.6: Comparison of surface brightness from chopped PHT photometry of the background beam for HR 6132 with COBE, both for OLP 8.6b1 (upper panel) and OLP 9.01. Asterisk: PHT-P and PHT-C photometry, diamond: COBE.

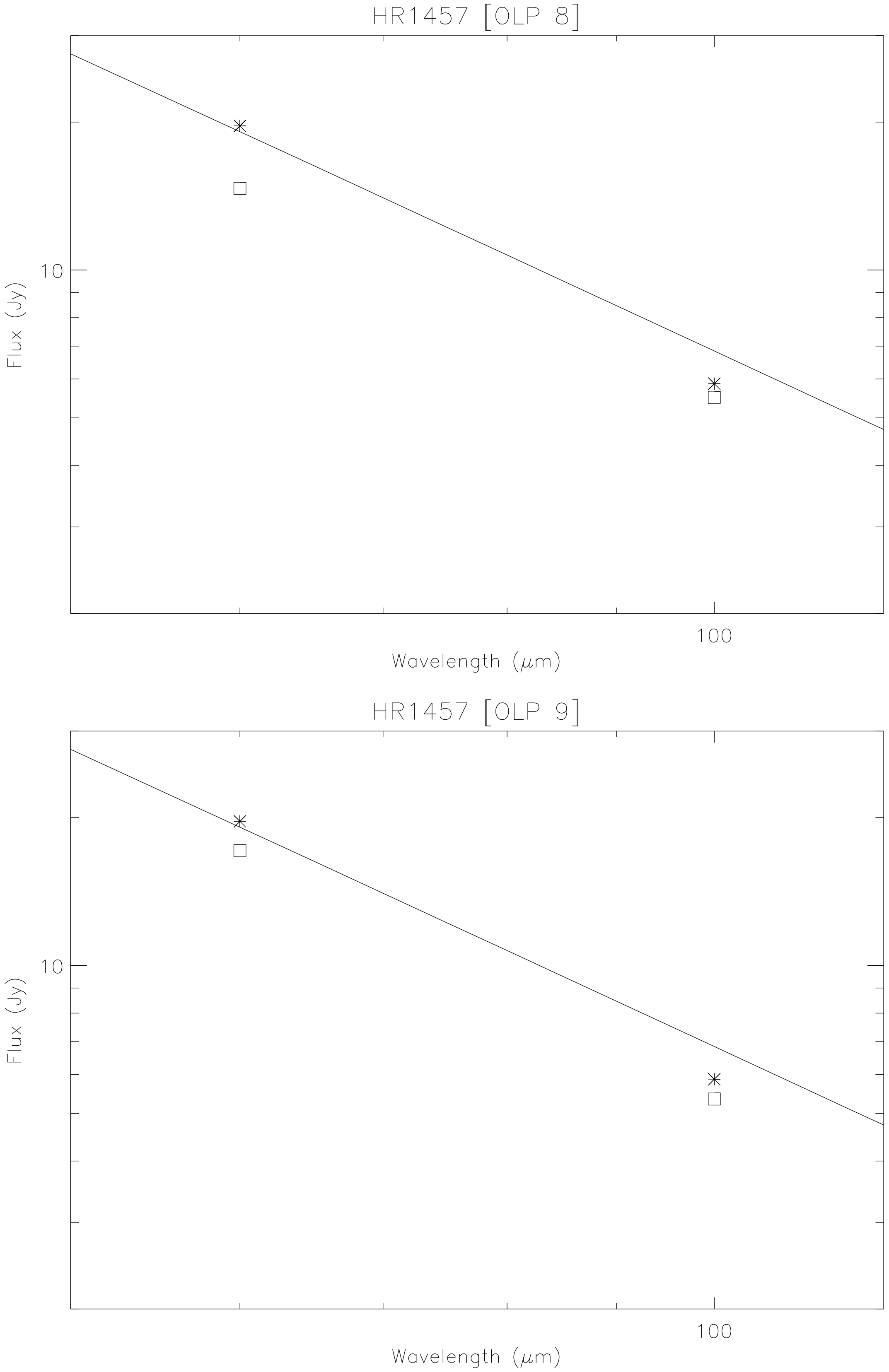

Figure 9.7: Comparison of PHT-P3 chopped photometry with the model spectrum of HR 1457, provided by M. Cohen, for OLP 8.6b1 (upper panel) and OLP 9.01 (lower panel). The meaning of the symbols is the following: solid line: model, square: PHT-P3, asterisk: IRAS.

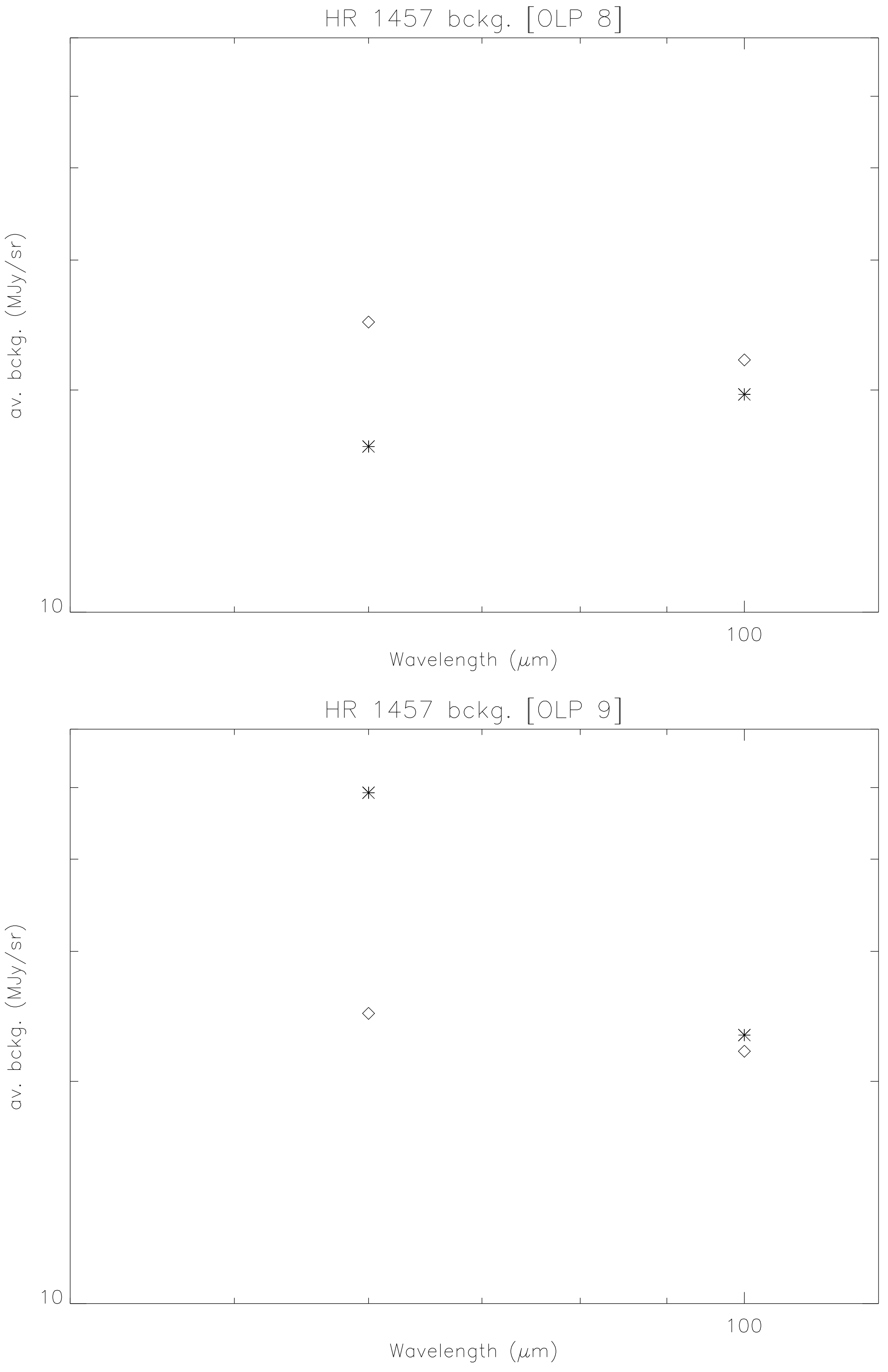

Figure 9.8: Comparison of surface brightness from chopped PHT photometry of the background beam for HR 1457 with COBE, both for OLP 8.6b1 (upper panel) and OLP 9.01. Asterisk: PHT-P and PHT-C photometry, diamond: COBE.

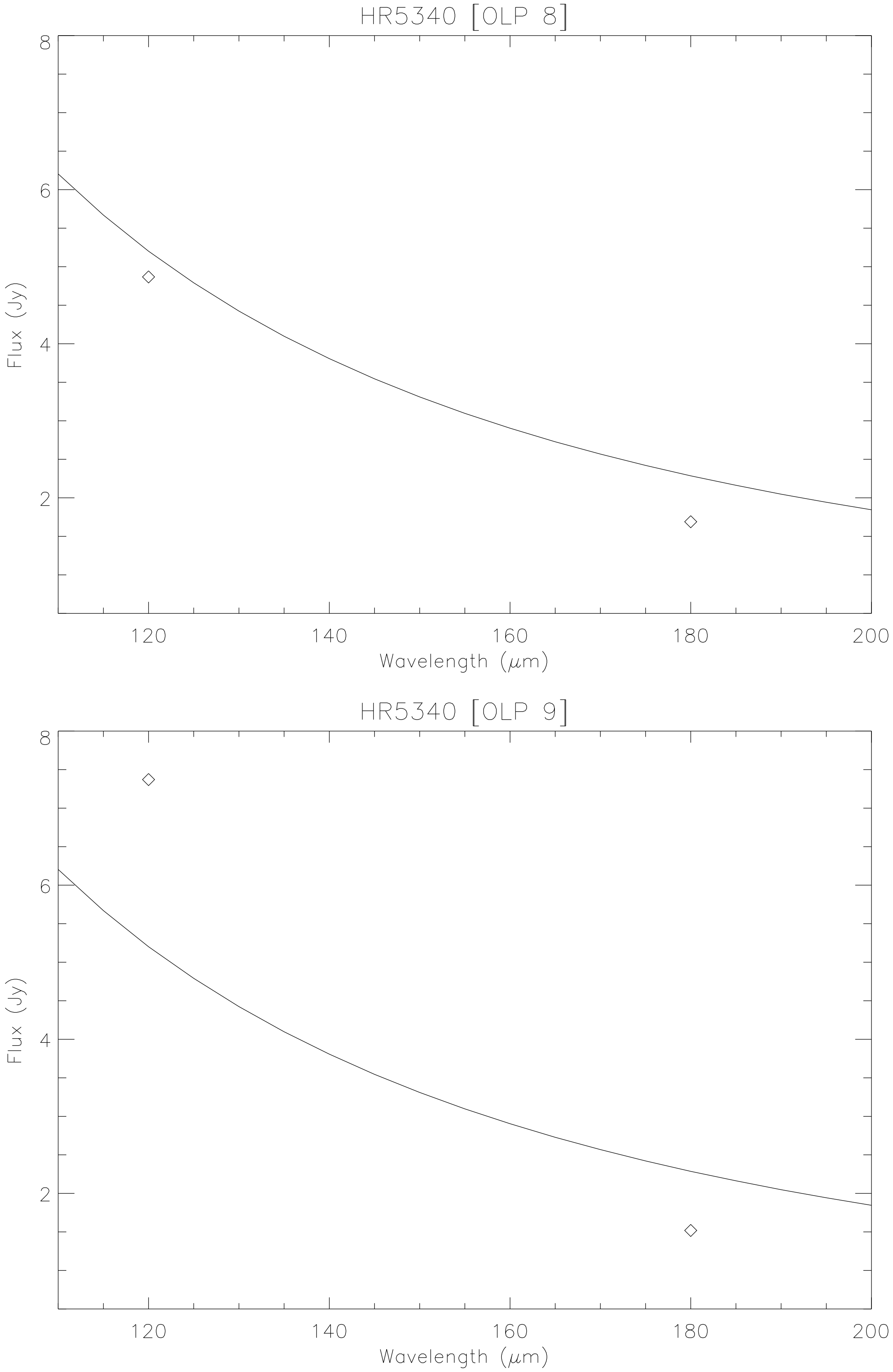

Figure 9.9: Comparison of PHT-C200 chopped photometry with the model spectrum of HR 5340, provided by M. Cohen, for OLP 8.6b1 (upper panel) and OLP 9.01 (lower panel). The meaning of the symbols is the following: solid line: model, diamond: PHT-C200.

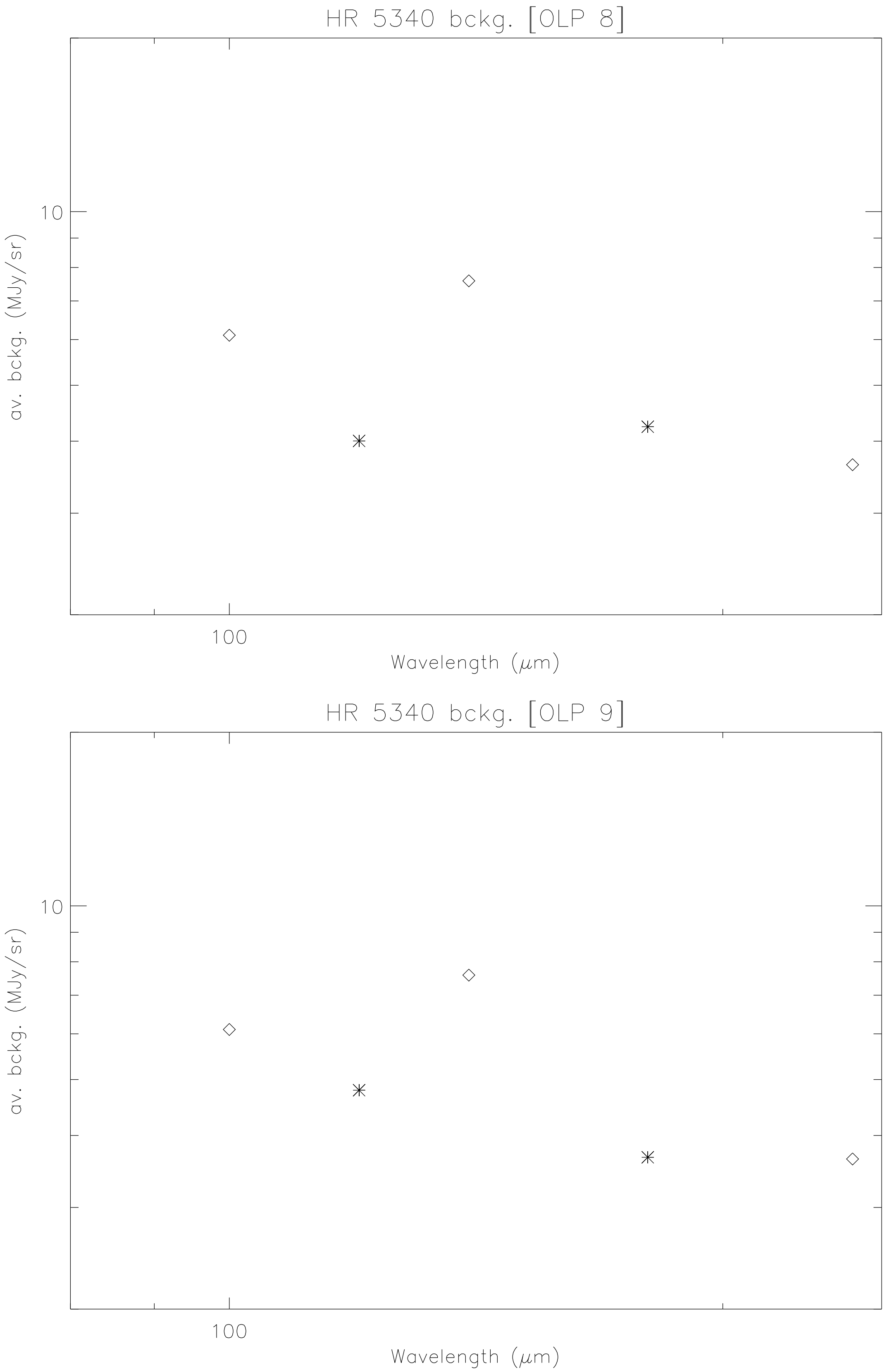

Figure 9.10: Comparison of surface brightness from chopped PHT photometry of the background beam for HR 5340 with COBE, both for OLP 8.6b1 (upper panel) and OLP 9.01. Asterisk: PHT-P and PHT-C photometry, diamond: COBE.

- Fluxes from chopped P2 photometry of HR 6132 are 50 % to a factor of 2 too high, in accordance with the results from other P2 test cases.
- Fluxes from chopped P3 photometry of HR 1457 are now within 20 % of the model flux, however the surface brightness of the off-beam in the 60 μm measurement is a factor of 2 higher than suggested by COBE/DIRBE, while the 100 μm surface brightness is consistent with COBE/DIRBE.
- The accuracy of chopped C200 photometry on HR 5340 is 40 % absolute and 60 % relative.

Evaluation Log

1) HR 6817

a) Chopped point source photomtery

Measurements:
PHT-P1: ppap78300901
PHT-P1: ppap78301005
PHT-P1: ppap78301107

Colour correction: black body, T = 5000 K

Model: Hammersley

Det	cwl (μm)	OLP 8	OLP 9	Model	Δ (OLP 8)	Δ (OLP 9)
P1	3.3	68.346	72.052	10.251	566.73	602.88
P1	3.6	8.813	9.412	8.809	0.05	6.84
P1	7.3	2.179	2.170	2.358	-7.61	-7.97

b) Background photometry from off-source beam

Det	λ	OLP8 (MJy/sr)	OLP9 (MJy/sr)	COBE (MJy/sr)
P1	3.3	184.59	197.05	
P1	3.6	43.61	48.35	
P1	7.3	9.62	10.67	

2) HR 6132

a) Chopped point source photomtery

Measurements:
PHT-P2: ppap76901902
PHT-P2b: ppap76902011
PHT-P2: ppap76902106
PHT-P2b: ppap76902216

Colour correction: black body, T = 5000 K

Model: Hammersley

Det	cwl (μm)	OLP 8	OLP 9	IRAS	Model	Δ (OLP 8)	Δ (OLP 9)
P2	20.0	6.031	8.935		5.909	2.06	51.22
P2b	20.0	7.322	9.060		5.909	23.91	53.33
P2	25.0	4.234	7.473	4.301	3.803	11.35	96.51
P2b	25.0	5.400	7.964	4.301	3.803	42.00	109.43

b) Background photometry from off-source beam

Det	λ	OLP8 (MJy/sr)	OLP9 (MJy/sr)	COBE (MJy/sr)
P2	20.0	30.92	20.68	
P2b	20.0	26.24	19.03	
P2	25.0	35.87	36.39	21.11
P2b	25.0	32.80	34.61	21.11

3) HR 1457

a) Chopped point source photomtery

Measurements:
PHT-P3 : ppap86101202
PHT-P3 : ppap86101306

Colour correction: black body, T = 4000 K

Model: Cohen

Det	cwl (μm)	OLP 8	OLP 9	IRAS	Model	Δ (OLP 8)	Δ (OLP 9)
P3	60.0	14.664	17.126	19.650	19.120	-23.30	-10.43
P3	100.0	5.507	5.348	5.870	6.842	-19.51	-21.84

b) Background photometry from off-source beam

Det	λ	OLP8 (MJy/sr)	OLP9 (MJy/sr)	COBE (MJy/sr)
P3	60.0	16.77	49.21	24.72
P3	100.0	19.73	23.11	21.97

4) HR 5340

a) Chopped point source photomtery

Measurements:
PHT-C2: pcap62900722 FCS = 120 um

Colour correction: black body, T = 4000 K

Model: Cohen

Det	cwl (μm)	OLP 8	OLP 9	Model	Δ (OLP 8)	Δ (OLP 9)
C2	120.0	4.868	7.380	5.201	-6.41	41.90
C2	180.0	1.690	1.835	2.286	-26.08	-19.74

b) Background photometry from off-source beam

Det	λ	OLP8 (MJy/sr)	OLP9 (MJy/sr)	COBE (MJy/sr)
C2	120.0	4.00	4.99	
C2	180.0	4.24	4.82	

9.1.5 Chopped Photometric Results for the Faint Point Source Detection Limit Program

- authors: U. Klaas
- Date: 28-July-2000
- SVP period 2

Motivation

In order to determine the optimal observing strategies for faint point sources a dedicated engineering program had been performed. This resulted in recommendations for the most sensitive and photometrically accurate faint source observation modes [27]. This program was largely done using AOTs so that the resulting OLP fluxes can be checked for their accuracies.

Method

Both chopped and staring (sparse map, nodding mode was not yet available at that time) mode OLP 7 and OLP 8 results are compared with each other. All targets are faint standard stars for which M. Cohen has provided extensions of the SED out to 300 μm, so that comparison with the model prediction is possible.

Results

Fig. 9.11 shows the 90 μm photometry for the star IRC+60228. The IRAS FSC gives for 100 μm only an upper limit. With regard to OLP 8 the model flux is further approached, however the measured flux is yet 70 % above. The cirrus confusion noise for this wavelength and a background of 5 MJy sr^{-1} is calculated as $1\,\sigma = 6.6$ mJy, so that the remaining offset is of the order of $9\,\sigma$. The consistency with the COBE/DIRBE background looks slightly worse than for OLP 8 (cf. Fig. 9.12).
For HR 5981 there exists 60 μm photomery both for P3 and C100. While the P3 photometry gives a too small flux (slight decrease w.r.t. OLP 8), the C100 photometry gives a very accurate result, see Fig. 9.13. The $1\,\sigma$ cirrus confusion noise for a background surface brightness of 6 MJy sr^{-1} is 4.4 mJy. For the background surface brightness (cf. Fig. 9.14), the P3 flux is now more consistent with COBE/DIRBE than for OLP 8, while C100 is less consistent, in contrary to the trend found for the differential flux accuracy.

Conclusions

- P3 chopped photometry of a star of the faint source detection limit program gives a too low flux, indicating some deficit in the signal correction.
- C100 chopped photometry of the stars of the faint source has been improved, but shows still a significant offset in one case. Part of it could be explained by cirrus confusion noise which allowed for IRAS to determine only an upper limit at 100 μm.

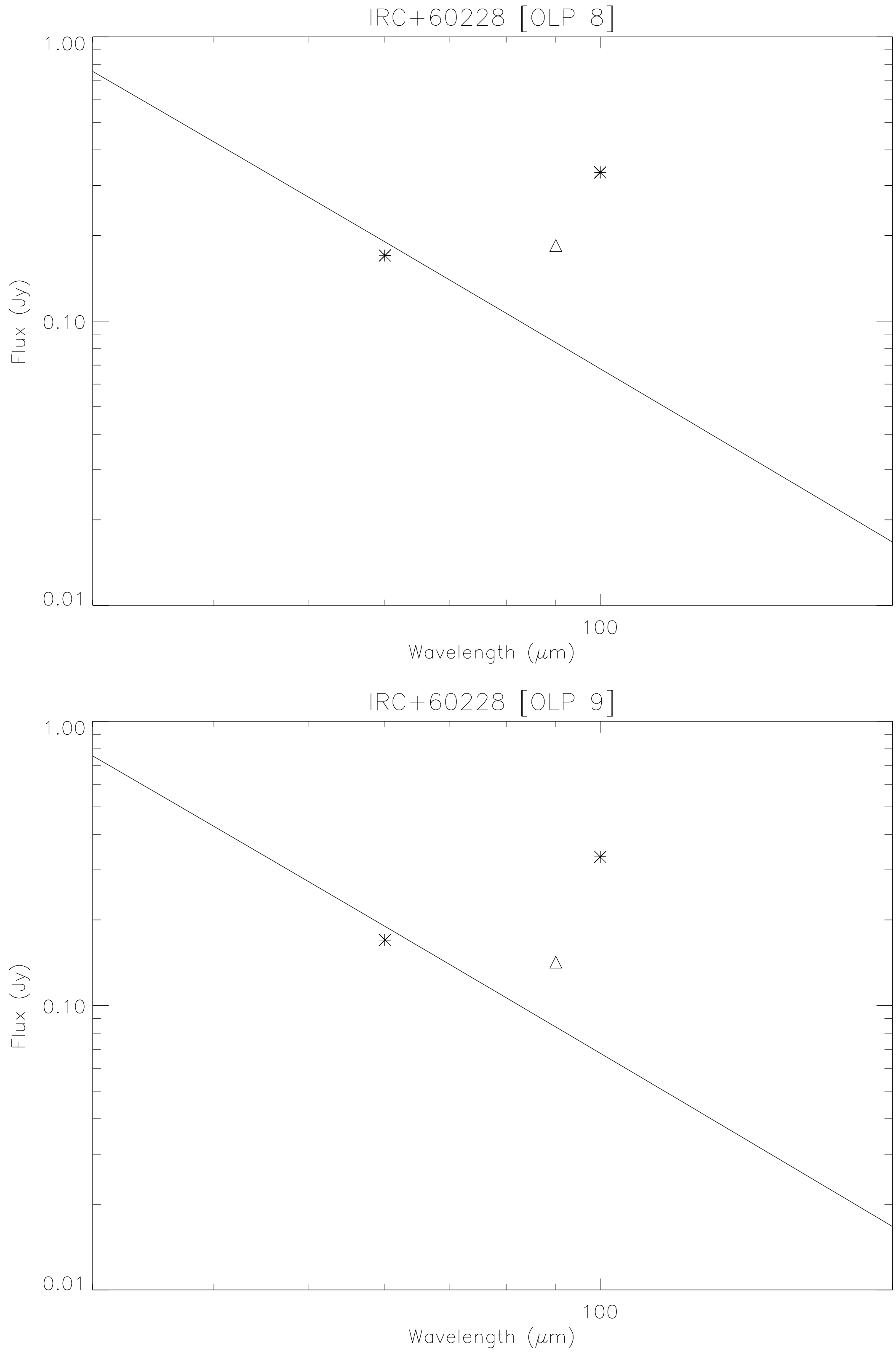

Figure 9.11: Comparison of PHT-C100 chopped photometry with the model spectrum of IRC+60228, provided by M. Cohen, for OLP 8.6b1 (upper panel) and OLP 9.01 (lower panel). The meaning of the symbols is the following: solid line: model, asterisk: IRAS, triangle: PHT-C100.

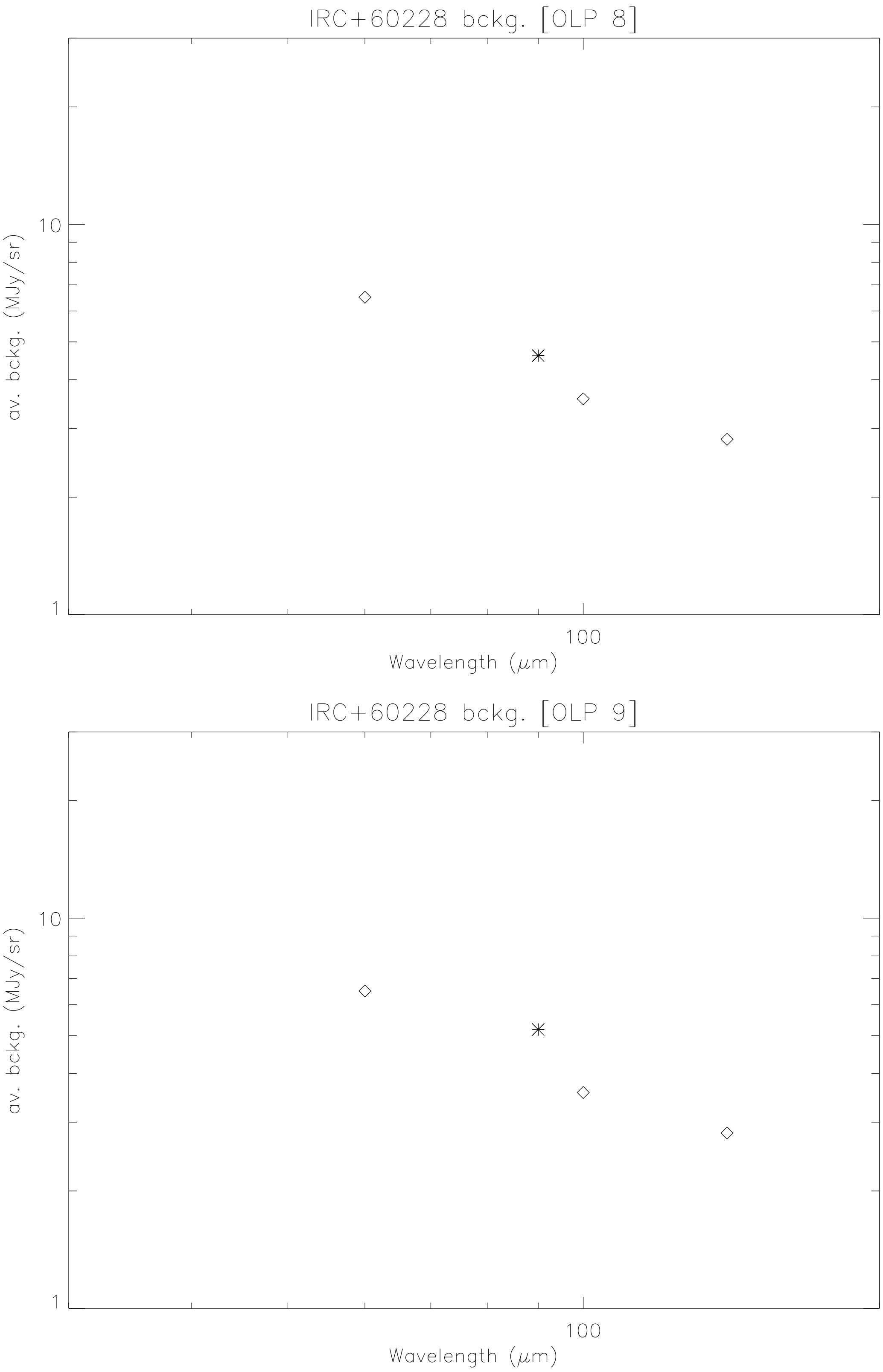

Figure 9.12: Comparison of surface brightness from chopped PHT photometry of the background beam for IRC+60228 with COBE, both for OLP 8.6b1 (upper panel) and OLP 9.01. Asterisk: PHT-C photometry, diamond: COBE.

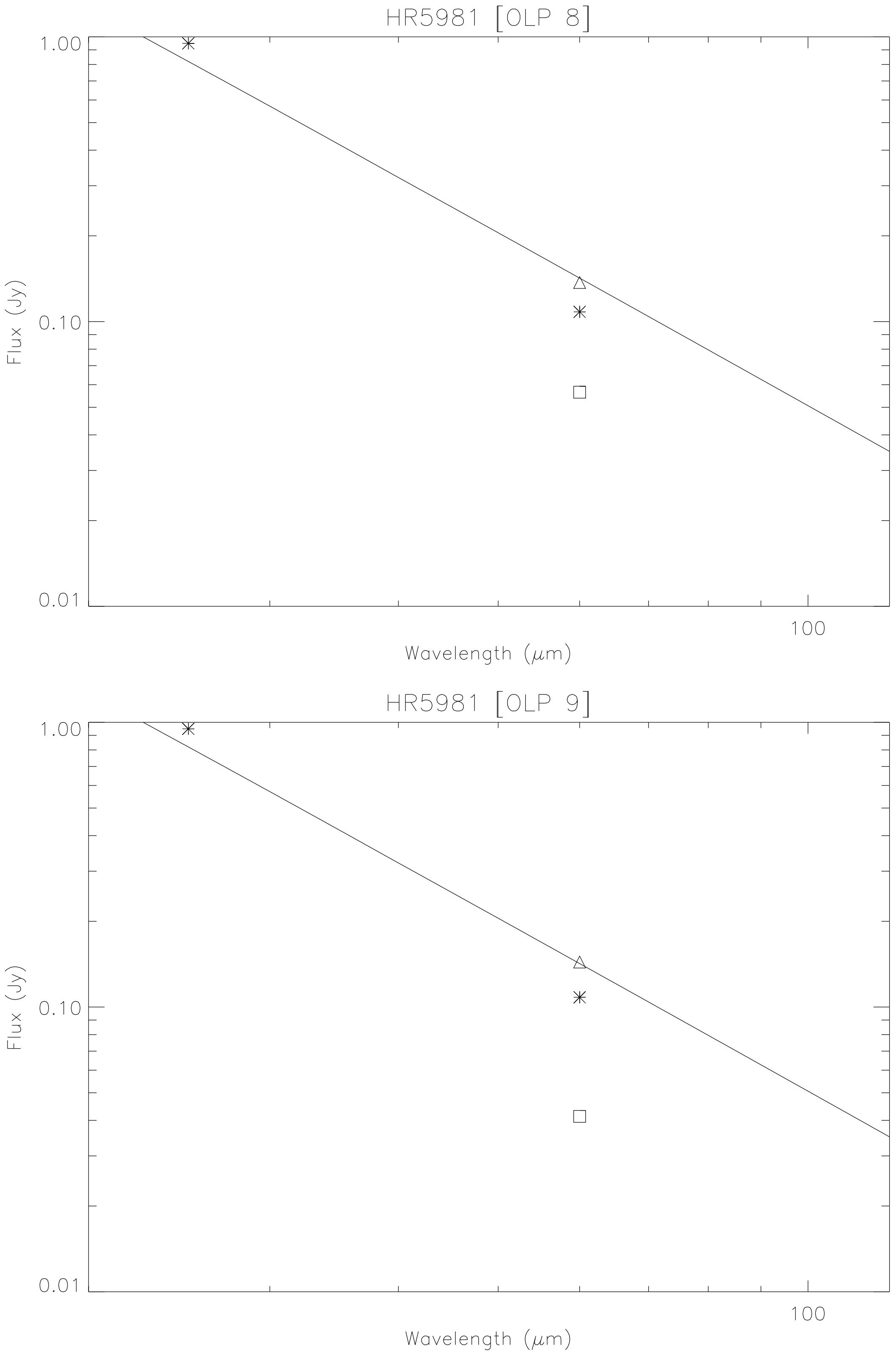

Figure 9.13: Comparison of PHT-P3 and -C100 chopped photometry with the model spectrum of HR 5981, provided by M. Cohen, for OLP 8.6b1 (upper panel) and OLP 9.01 (lower panel). The meaning of the symbols is the following: solid line: model, asterisk: IRAS, square: PHT-P, triangle: PHT-C100.

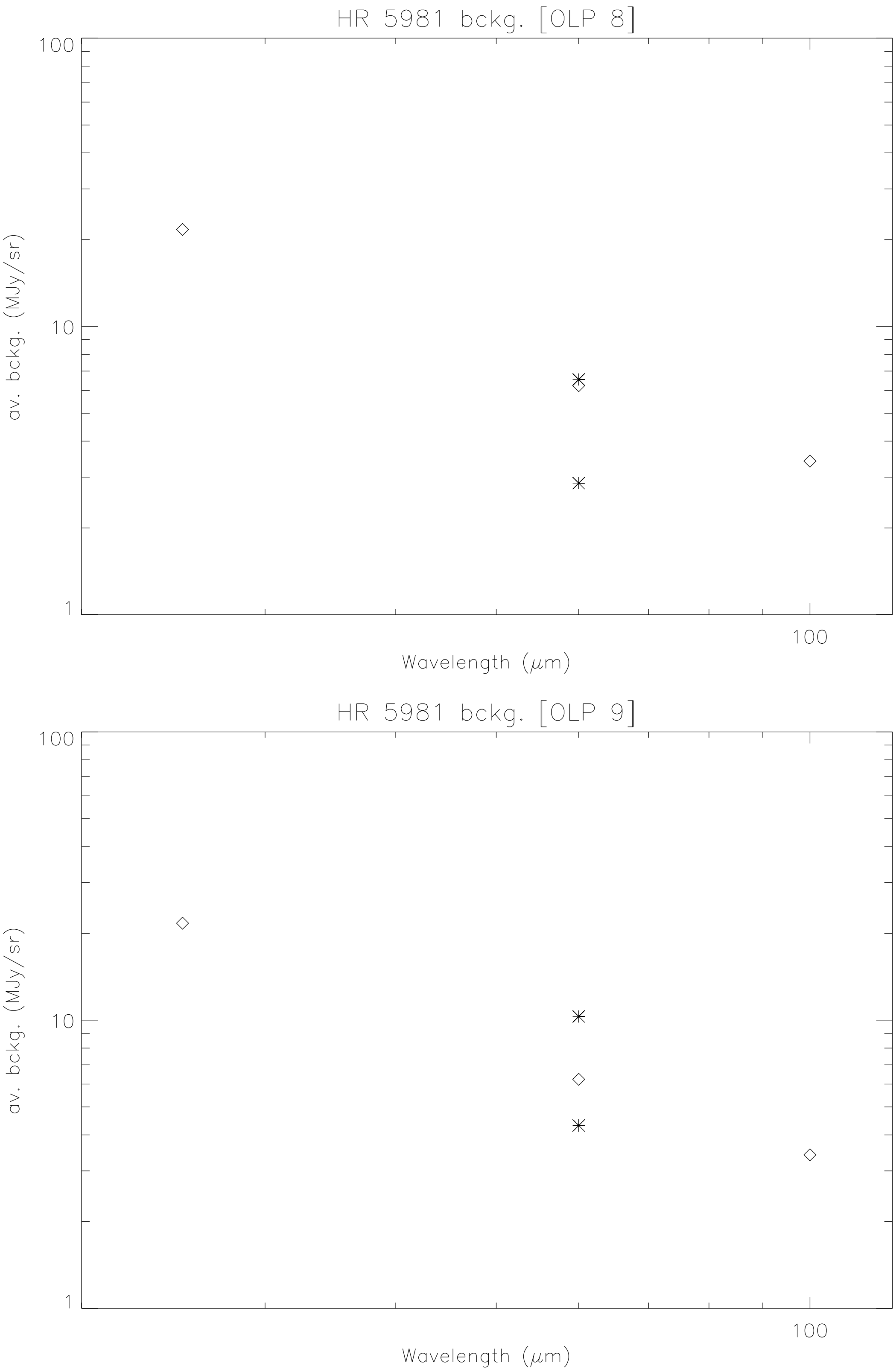

Figure 9.14: Comparison of surface brightness from chopped PHT photometry of the background beam for HR 5981 with COBE, both for OLP 8.6b1 (upper panel) and OLP 9.01. Asterisk: PHT-P and PHT-C photometry, diamond: COBE.

Evaluation Log

1) IRC 60228

a) Chopped point source photomtery

Measurements:
PHT-C1 : pcap25202408 FCS = 90 um

Colour correction: black body, T = 3898 K

Model: Cohen

Det	cwl (μm)	OLP 8	OLP 9	IRAS	Model	Δ (OLP 8)	Δ (OLP 9)
C1	90.0	0.185	0.142		0.084	119.50	69.02

b) Background photometry from off-source beam

Det	λ	OLP8 (MJy/sr)	OLP9 (MJy/sr)	COBE (MJy/sr)
C1	90.0	4.61	5.18	

2) HR 5981

a) Chopped point source photomtery

Measurements:
PHT-P3 : ppap39200626 FCS = 60 um
PHT-C1 : pcap39200413 FCS = 60 um

Colour correction: black body, T = 4048 K

Model: Hammersley

Det	cwl (μm)	OLP 8	OLP 9	IRAS	Model	Δ (OLP 8)	Δ (OLP 9)
P3	60.0	0.056	0.041	0.108	0.142	-60.24	-70.94
C1	60.0	0.137	0.144	0.108	0.142	-3.48	1.25

b) Background photometry from off-source beam

Det	λ	OLP8 (MJy/sr)	OLP9 (MJy/sr)	COBE (MJy/sr)
P3	60.0	2.86	4.31	6.23
C1	60.0	6.55	10.30	6.23

9.1.6 Chopped Photometry of Stars Observed by the MFAINT and CFAINT Programs

- authors: U. Klaas
- date: 28-June-2000
- SVP period 2

Motivation

The faint stars observed repeatedly by the monitoring program MFAINT have also been observed several times in chopped mode by the program CFAINT. MFAINT used the most recommended observation modes (nodding for P1, P2, and P3 and mini-map for C100 and C200). We compare here the results of the measurement set performed on revolution 748. The result of the measurement of HR 5986 is reported in Sect. 9.3.3. With regard to the reproducibility cf. Sect. 9.1.7.

Method

Both colour corrected nodding and chopped photometry are compared with each other and against the model predictions by Cohen or Hammersley. We compare also the flux values of OLP V8.6b1 and OLP V9.0b10/V9.01. Furthermore, we compare the derived background surface brightness with COBE/DIRBE photometry.

Results

Fig. 9.15 shows an improvement for chopped P1 photometry for OLP 9 which is now within the 25 % range. This is corrobotated by a monitoring sequence as described in Sect. 9.1.7.
For HR 7310, as shown in Fig. 9.16 the 25 μm photometric point is now too high. This is a common finding for P2 25 μm for OLP 9. Also the C100 photometry is not as good as it was for OLP 8. The fluxes are systematically higher than the model. On the other hand the background brightness of the off-beams seem to be more consistent with COBE/DIRBE. The same is tue for P3, here the differential source flux is too small.
For HR 6705 there exist two C100 chopped multi-filter series, the one denoted "b" is with a two times faster chopper frequency (0.5 Hz vs. 0.25 Hz). Both sequences reflect now the SED shape, the faster chopped sequence corresponds very well with the model, the slowly chopped sequence has on average too high fluxes by 20 %. Both measurements were performed at the same time so that background offsets cannot be the reason for the discrepancy. The relative C100 filter-to-filter calibration for this chopped observation is better than 20 %. The low 170 μm flux is explained by the monitoring sequence as described in Sect. 9.1.7. The surface brightness in the off-beam is a factor of two higher than indicated by COBE/DIRBE. This could be caused by additional local background emission. The relative shape of the background SED appears highly artificial and reminds of the pattern found for backgrounds derived from staring mode observations.

Conclusions

- The test case on HD 172323 shows a clear improvement in P1 chopped photometry accuracy.
- The accuracy of P2 chopped photometry is worse for the OLP 9 for the test case HR 7310. This case confirms the general trend.
- For C100 chopped photometry we have the following finding: For the fast chopping with 0.5 Hz on HR 6705 a very good accuracy of 5 % absolute is achieved. For the slower chopping (0.25 Hz on HR 6705 and 0.0625 Hz on HR 7310) fluxes are too high by 20 - 60 %. The relative filter-to-filter calibration reflecting the SED shape is 15 - 30 %.
- The C200 chopped photometry result can be better understood in the context of a monitoring sequence.

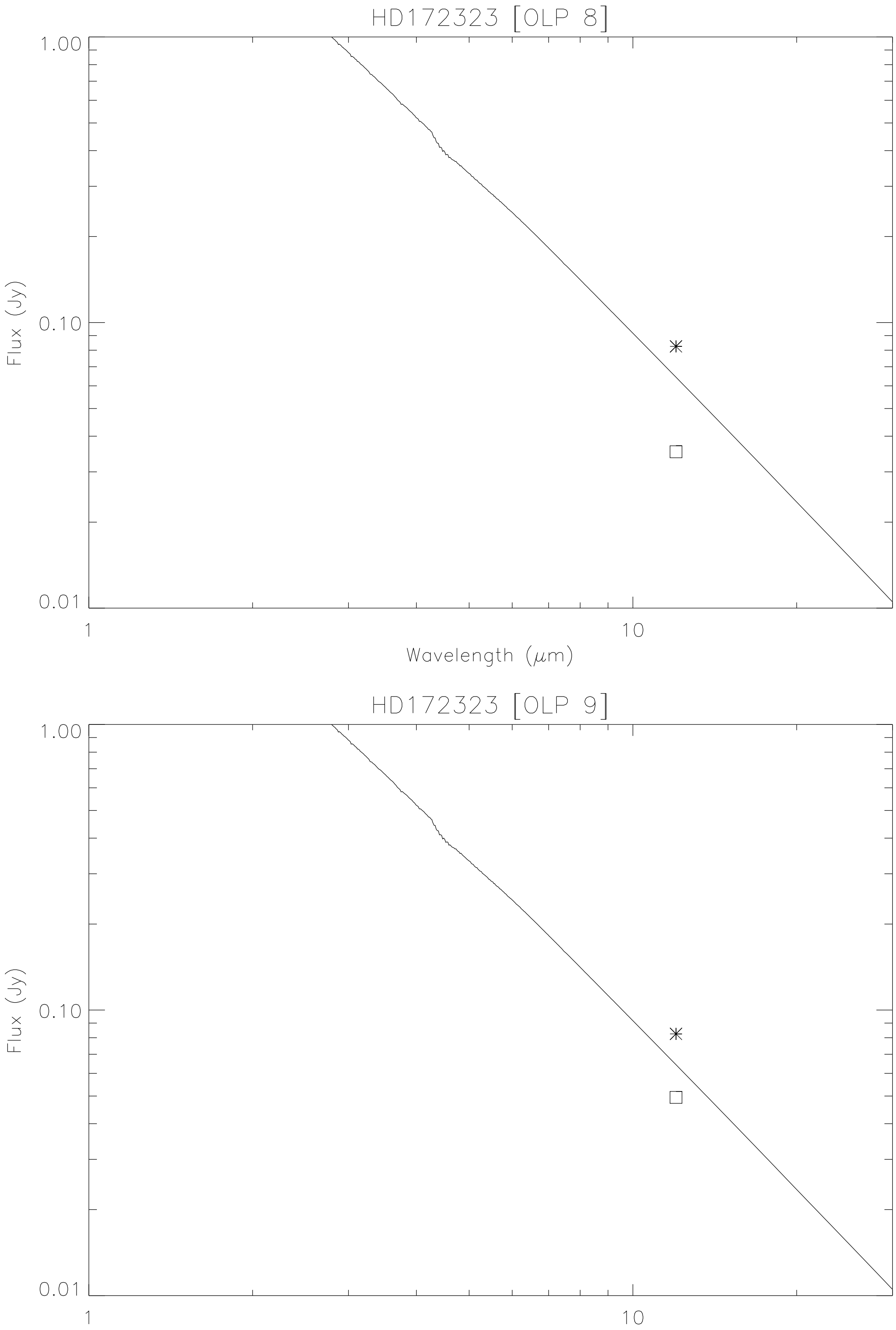

Figure 9.15: Comparison of PHT-P1 chopped photometry with the model spectrum of HD 172323, provided by P. Hammersley, for OLP 8.6b1 (upper panel) and OLP 9.0b10 (lower panel). The meaning of the symbols is the following: solid line: model, asterisk: IRAS, square: PHT-P.

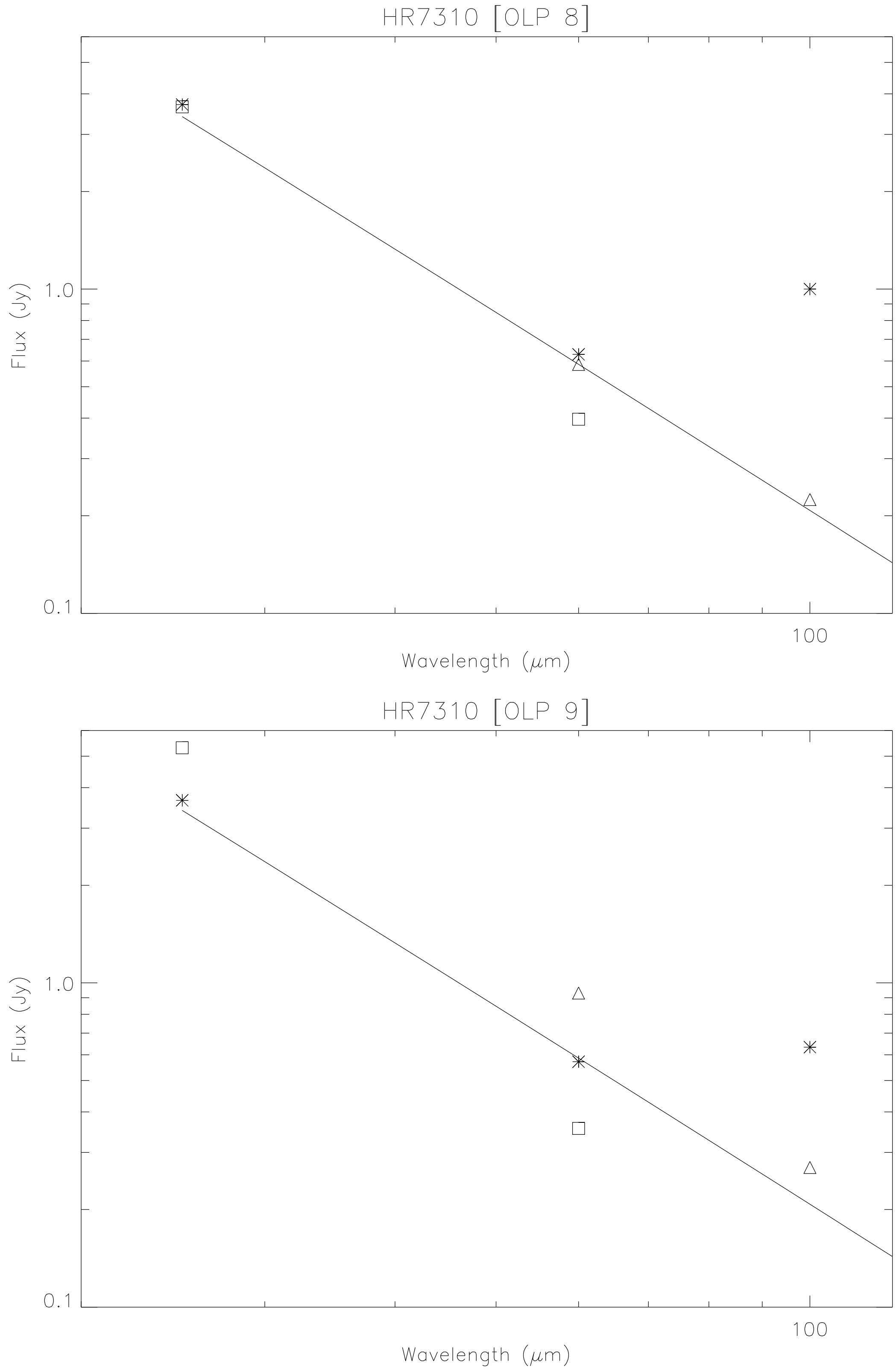

Figure 9.16: Comparison of PHT-P2, -P3 and -C100 chopped photometry with the model spectrum of HR 7310, provided by M. Cohen, for OLP 8.6b1 (upper panel) and OLP 9.0b10/9.01 (lower panel). The meaning of the symbols is the following: solid line: model, asterisk: IRAS (100 μm: upper limit), square: PHT-P, triangle: PHT-C100.

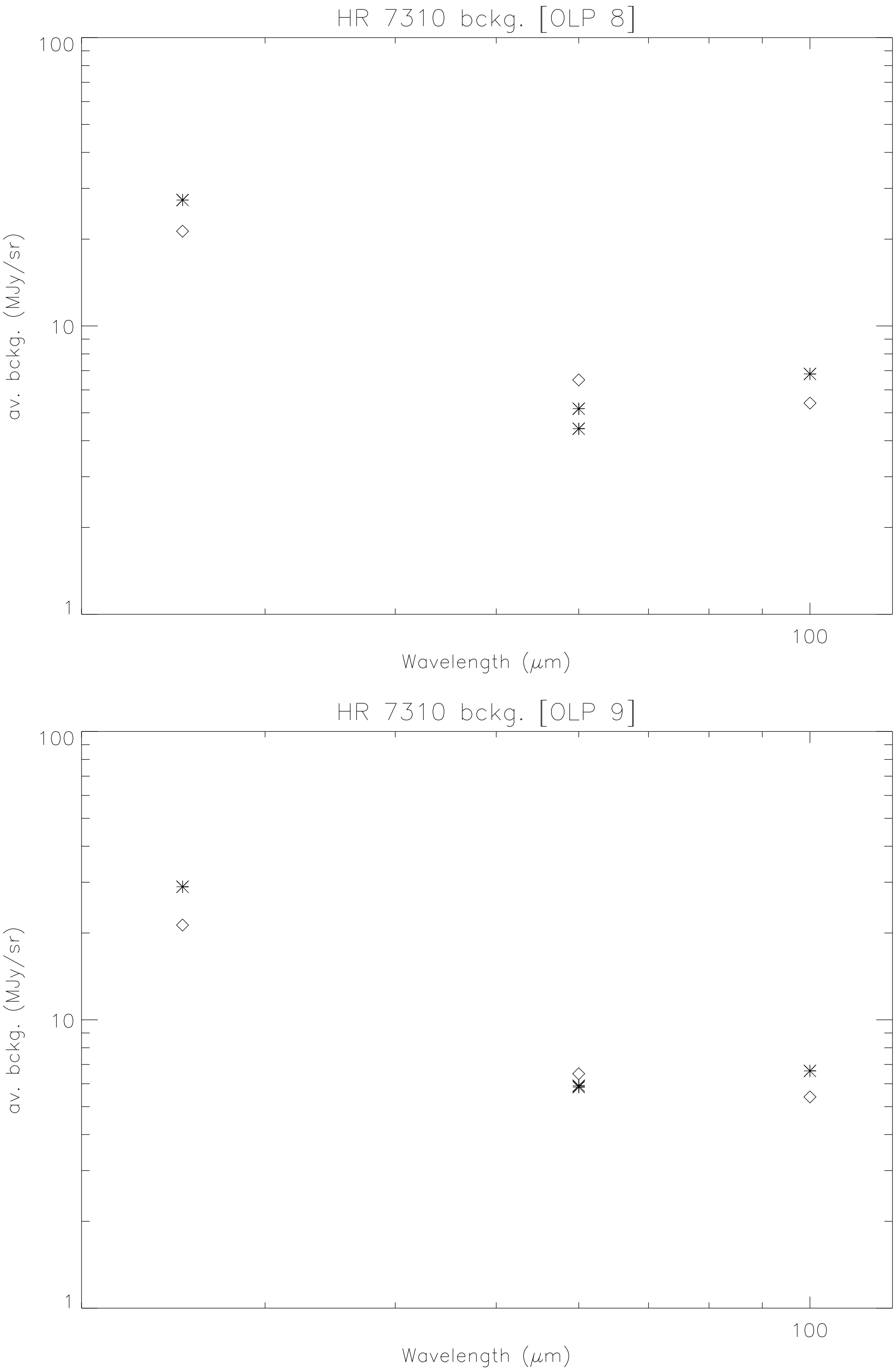

Figure 9.17: Comparison of surface brightness from chopped PHT photometry of the background beam for HR 7310 with COBE, both for OLP 8.6b1 (upper panel) and OLP 9.0b10/9.01. Asterisk: PHT-P and PHT-C photometry, diamond: COBE.

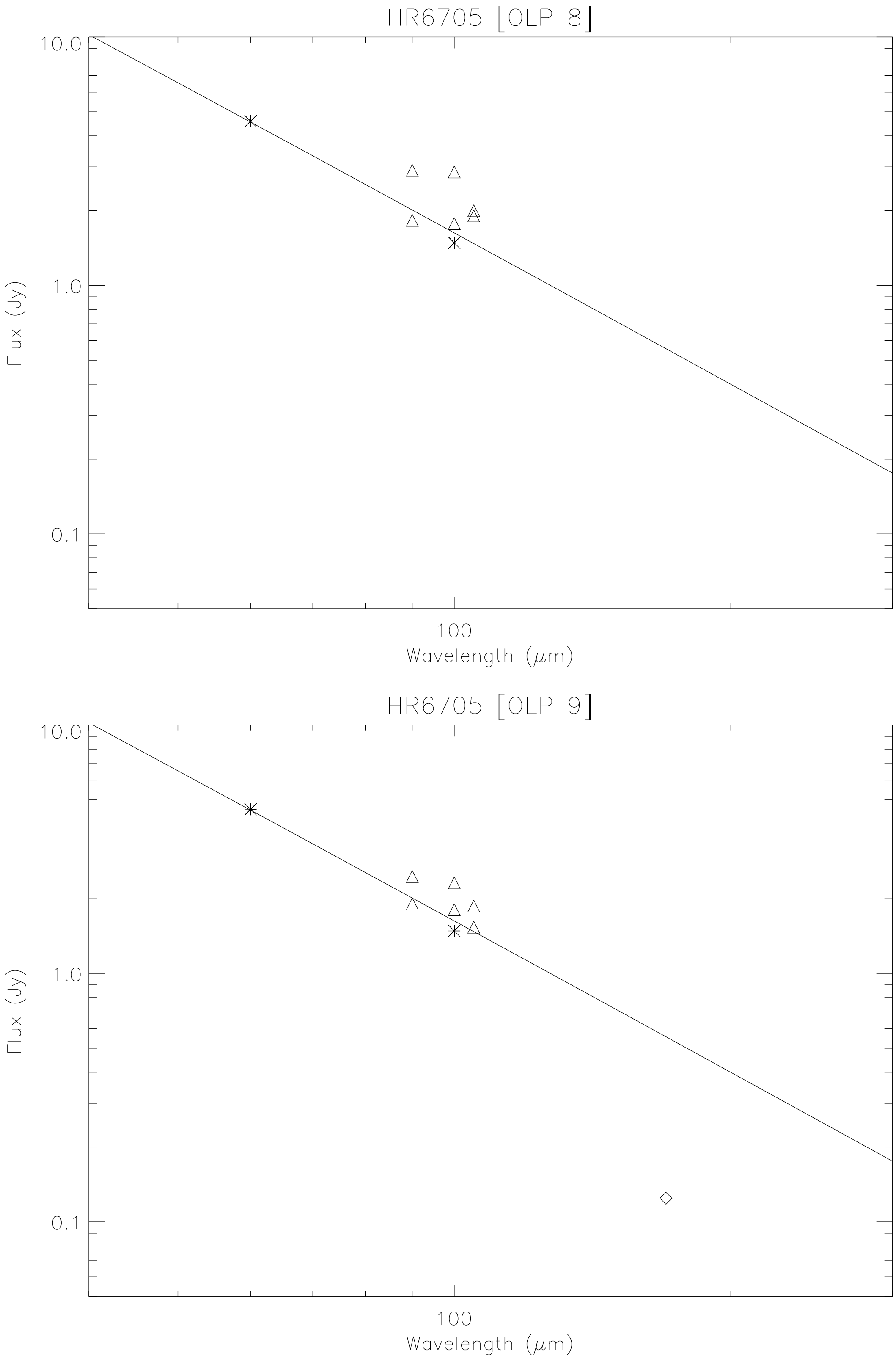

Figure 9.18: Comparison of PHT-C100 and -C200 chopped photometry with the model spectrum of HR 6705 (γ Dra), provided by M. Cohen, for OLP 8.6b1 (upper panel) and OLP 9.0b10 (lower panel). The meaning of the symbols is the following: solid line: model, asterisk: IRAS, triangle: PHT-C100, diamond: PHT-C200.

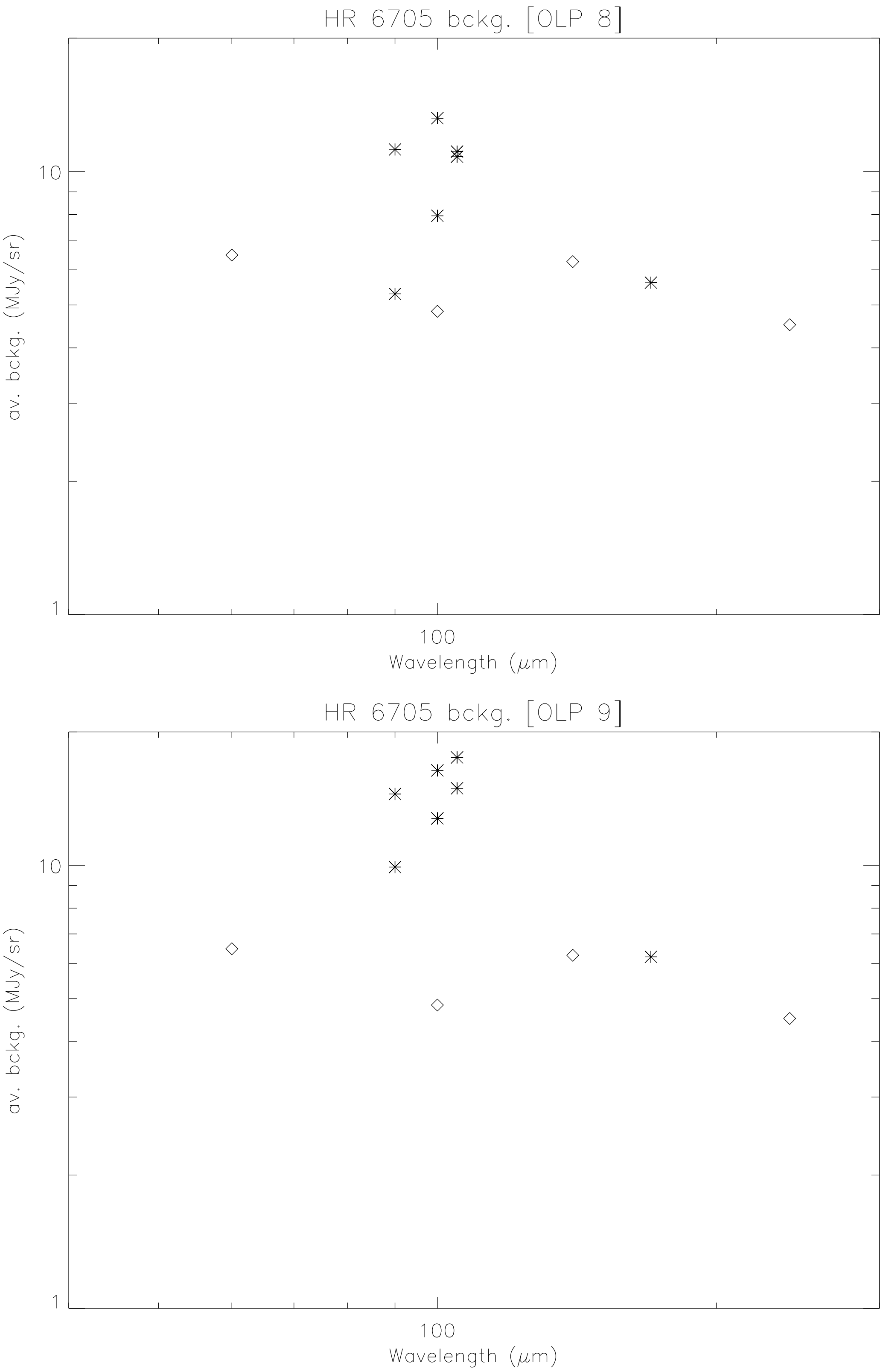

Figure 9.19: Comparison of surface brightness from chopped PHT photometry of the background beam for HR 6705 with COBE, both for OLP 8.6b1 (upper panel) and OLP 9.0b10. Asterisk: PHT-C photometry, diamond: COBE.

Evaluation Log

1) HR 7310

a) Chopped point source photomtery

Measurements:
PHT-P2 : ppap74800610 FCS = 25 um
PHT-P3 : ppap74800303 FCS = 60 um
PHT-C1 : pcap74800505 FCS = 60 um

Colour correction: black body, T = 4852 K

Model: Cohen

Det	cwl (μm)	OLP 8	OLP 9	IRAS	Model	Δ (OLP 8)	Δ (OLP 9)
P2	25.0	3.648	5.309	3.656	3.403	7.20	56.00
P3	60.0	0.397	0.356	0.571	0.586	-32.29	-39.29
C1	60.0	0.586	0.931	0.571	0.586	-0.03	58.76
C1	100.0	0.224	0.270	0.634	0.208	8.02	29.83

b) Background photometry from off-source beam

Det	λ	OLP8 (MJy/sr)	OLP9 (MJy/sr)	COBE (MJy/sr)
P2	25.0	27.33	28.94	21.31
P3	60.0	4.40	5.84	6.50
C1	60.0	5.16	5.90	6.50
C1	100.0	6.82	6.65	5.40

2) HD 172323

a) Chopped point source photomtery

Measurements:
PHT-P1 : ppap74800801 FCS = 12 um

Colour correction: black body, T = 5719 K

Model: Hammersley

Det	cwl (μm)	OLP 8	OLP 9	IRAS	Model	Δ (OLP 8)	Δ (OLP 9)
P1	12.0	0.035	0.049	0.118	0.064	-45.20	-23.15

b) Background photometry from off-source beam

Det	λ	OLP8 (MJy/sr)	OLP9 (MJy/sr)	COBE (MJy/sr)
P1	12.0	10.32	15.06	12.05

3) HR 6705

a) Chopped point source photomtery

Measurements:
PHT-C1 (a): pcap67100803 FCS = 90 um
PHT-C1 (b): pcap67100912 FCS = 90 um
PHT-C2 : pcap74801212 FCS = 170 um

Colour correction: black body, T = 4000 K

Model: Cohen

Det	cwl (μm)	OLP 8	OLP 9	IRAS	Model	Δ (OLP 8)	Δ (OLP 9)
C1	90.0	2.904	2.457		2.012	44.32	22.10
C1	100.0	2.862	2.316	1.483	1.627	75.93	42.35
C1	105.0	1.999	1.868		1.474	35.59	26.71
C1b	90.0	1.828	1.905		2.012	-9.14	-5.31
C1b	100.0	1.774	1.806	1.483	1.627	9.04	10.98
C1b	105.0	1.904	1.536		1.474	29.20	4.19
C2	170.0	-0.001	0.124		0.556	-100.20	-77.62

b) Background photometry from off-source beam

Det	λ	OLP8 (MJy/sr)	OLP9 (MJy/sr)	COBE (MJy/sr)
C1	90.0	5.30	9.91	
C1b	90.0	11.22	14.48	
C1	100.0	7.95	12.76	4.84
C1b	100.0	13.20	16.37	4.84
C1	105.0	10.81	14.92	
C1b	105.0	11.09	17.51	
C2	170.0	5.61	6.21	

9.1.7 Reproducibility Assessment of Chopped Mode Photometry from CFAINT Program

- authors: U. Klaas
- date: 28-June-2000
- SVP period 2

Motivation

We evaluate here a data set which was obtained for establishing the reproducibility of the chopped photometry mode. This data set helps to investigate the stability of the chopped mode processing. For P1 (12 μm), P3 (60 μm), C100 (100 μm) and C200 (170 μm) the measurement was repeated 6 times, for P2 (25 μm) only 3 times for technical reasons.

Method

We compare the differential source flux against the model prediction by Cohen or Hammersley and the surface brightness of the off-beam against COBE/DIRBE photometry (from weekly maps). This is done for OLP V9.0b10.

Results

Fig. 9.20 shows the reproducibility for P1 on the star HD 172323. The source flux agrees with the model prediction within 25 %. Also the surface brightness of the off-beam is consistent with COBE/DIRBE within 25 %, but the flux is always higher. There is no parallel trend in the scatter of differential flux and off-beam surface brightness. The average flux is 0.056 Jy $\pm$ 0.008 Jy, giving a 1 σ reproducibility accuracy of 14 %. For the off-beam we get 15.4 MJy sr^{-1} $\pm$ 0.8 MJy sr^{-1}, giving a 1 σ reproducibility accuracy of 5 %.
Fig. 9.21 shows the reproducibility for P2 on the star HR 5986. The resulting source flux is between 40 and 55 % higher than the model flux. The surface brightness of the off-beam is also systemtically higher than the COBE/DIRBE photometry. There is some correlation between the differential on-source and the off-source flux. Therefore, a scaling of the responsivity could improve the source flux accuracy. However, we checked in the SPD products the ratio actual/default responsivity: For two cases it is 1.2 and for one case 1.0. In order to decrease the flux the responsivity should be higher by 40 to 50 %. This is not a reasonable assumption. The average flux is 0.763 Jy $\pm$ 0.035 Jy, giving a 1 σ reproducibility accuracy of 5 %. For the off-beam we get 27.7 MJy sr^{-1} $\pm$ 1.0 MJy sr^{-1}, giving a 1 σ reproducibility accuracy of 4 %.
Fig. 9.22 shows the reproducibility for P3 on the star HR 7310. The resulting source flux is between 30 and 45 % lower than the model flux. There is some systematic trend in the source flux. During the monitoring period the focal plane rotated by 127 deg. However, the background flux in the off-beam is not anti-correlated with the resulting source flux, so that the measurement itself cannot confirm that structure in the background impacts on the resulting source flux. The background flux is relatively consistent with COBE/DIRBE. The average flux is 0.378 Jy $\pm$ 0.039 Jy, giving a 1 σ reproducibility accuracy of 10 %. For the off-beam we get 6.0 MJy sr^{-1} $\pm$ 0.1 MJy sr^{-1}, giving a 1 σ reproducibility accuracy of 1.5 %.
Fig. 9.23 shows the reproducibility for C100 again on the star HR 7310, but this time in the 100 μm filter where the star is 2.8 times fainter. The resulting on-source fluxes correspond with the model to better than 30 %. The off-beam surface brightness shows some scatter which is not correlated to the trend of the resulting source flux. For three off-source measurements there is a good consistency with COBE/DIRBE. The average flux is 0.238 Jy $\pm$ 0.030 Jy, giving a 1 σ reproducibility accuracy of 13 %. For the off-beam we get 6.7 MJy sr^{-1} $\pm$ 0.9 MJy sr^{-1}, giving a 1 σ reproducibility accuracy of 13 %.
Fig. 9.24 shows a remarkable strong trend. In the first measurement the resulting source flux is a factor 4.5 less than the model flux. For the second and third measurement the flux is within 20 % of the model flux. For the last three measurements the flux is a factor of 1.6 greater than the model flux. On the other hand the background flux decreases rather smoothly from 6.21 to 5.29 MJy sr^{-1}. A surface brightness of 6 MJy sr^{-1} corresponds to 6 Jy total flux in the 4 C200 pixels. A variation by 1 MJy sr^{-1}, i.e. 15 %, leads to 0.9 Jy variation

in flux in the C200 array which is approximately the order of variation of the differential flux. The focal plane rotates by 128 deg between first and last measurement, so that background variations could account for this trend. Cirrus confusion noise for the background brightness of 6 MJy sr^{-1} is estimated to be $1\,\sigma = 0.06$ Jy so that some background gradient with imposed cirrus fluctuation could cause this strong trend.

Conclusions

- For P1, P2, P3 and C100 we find a relative good reproducibility of chopped photometry. For the differential source flux the $1\,\sigma$ reproducibility is 14, 5, 10 and 13 %, respectively determined from 6 (3 for P2) measurements taken over a period of 126 revolutions. For the surface brightness of the off-beam the $1\,\sigma$ reproducibility is 5, 4, 1.5 and 13 %, respectively.

- For C200 we find a strong trend with a variation of the differential source flux by a factor of 7.5. This trend may be explained by small scale gradients in the background (on a 3 arcmin step), partially caused by cirrus, when the chop direction rotates with time relative to the sky N-direction (by 128 deg between the first and the last measurement).

- With regard to absolute accuracy of the differential source flux, satisfying results are achieved for P1 ($<$ 25 %) and C100 ($<$ 30 %). For P2 the derived fluxes are systematically too high (40 - 55 %), and for P3 systematically too low (30 - 45 %). For C200 no number can be given due to the strong trend.

- With regard to absolute accuracy of the background surface brightness in the off-beam good consistency with COBE/DIRBE is achieved for P1, P3 and partially C100. For P2 the derived surface brightness is significantly higher than COBE/DIRBE. For C200 the ISOPHOT surface brightness is in general lower than COBE/DIRBE, however the COBE/DIRBE 140 μm surface brightness shows a large scatter, while the ISOPHOT surface brightness displays a smooth behaviour.

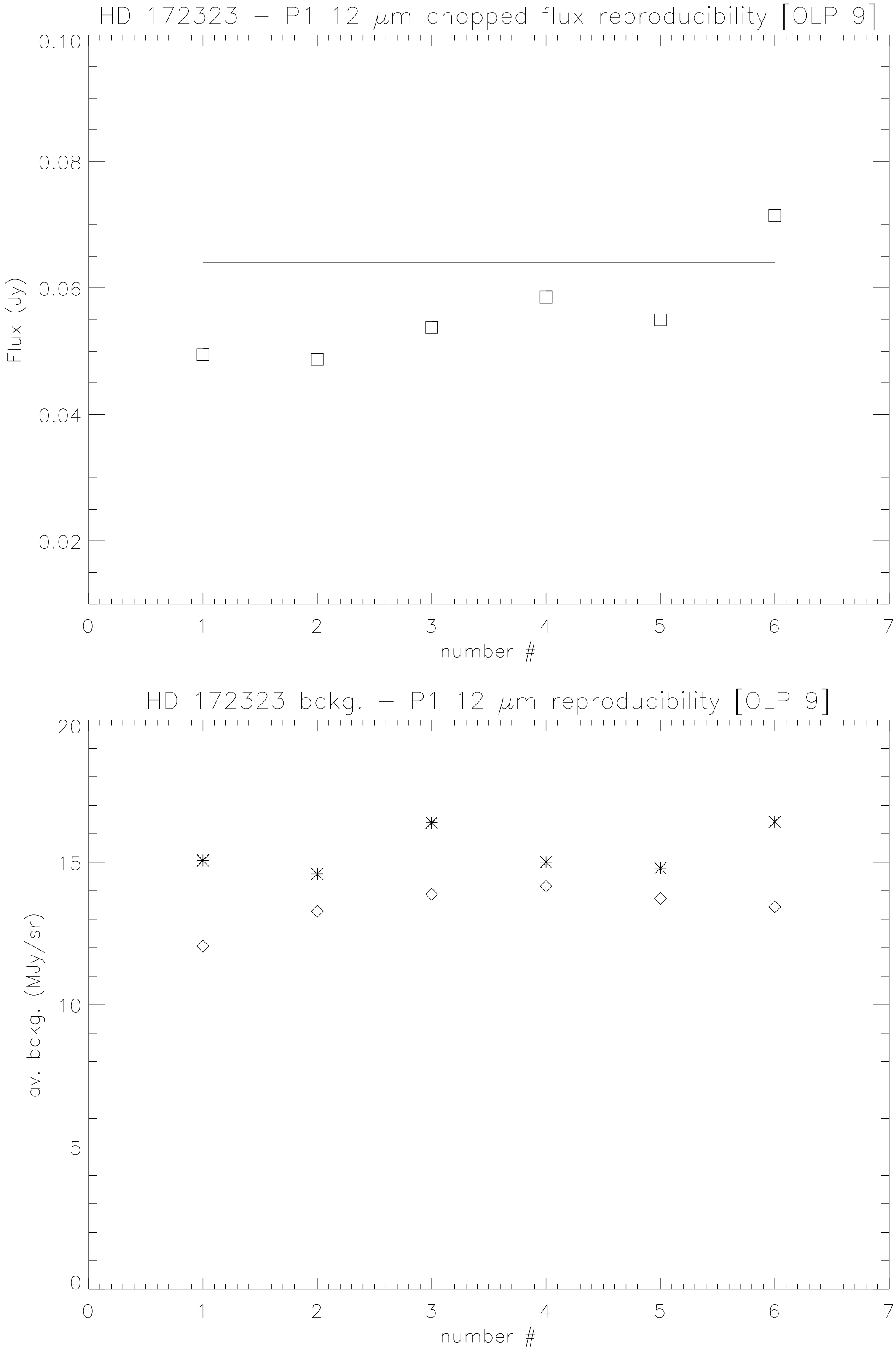

Figure 9.20: Reproducibility of P1 chopped photometry processed with OLP 9.0b10 with regard to point source flux derivation and background flux derivation from the off-source beam. The point source fluxes (upper panel) are compared with the flux value of the model of HD 172323, provided by P. Hammersley. The meaning of the symbols is the following: solid line: model flux at $12\,\mu$m, square: background subtracted ISOPHOT flux (for info on the revolution refer to the section evaluation log). The background fluxes (lower panel) are compared with COBE/DIRBE weekly photometry. The meaning of the symbols is the following: diamond: COBE/DIRBE photometry, asterisk: ISOPHOT background flux.

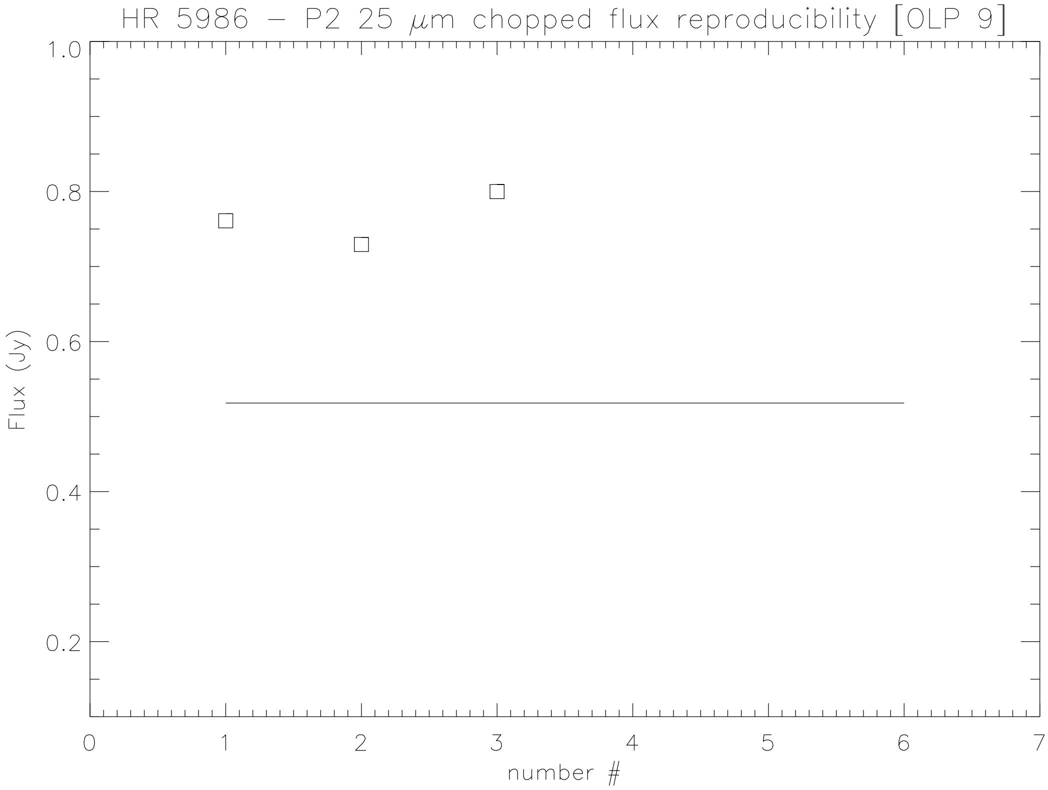

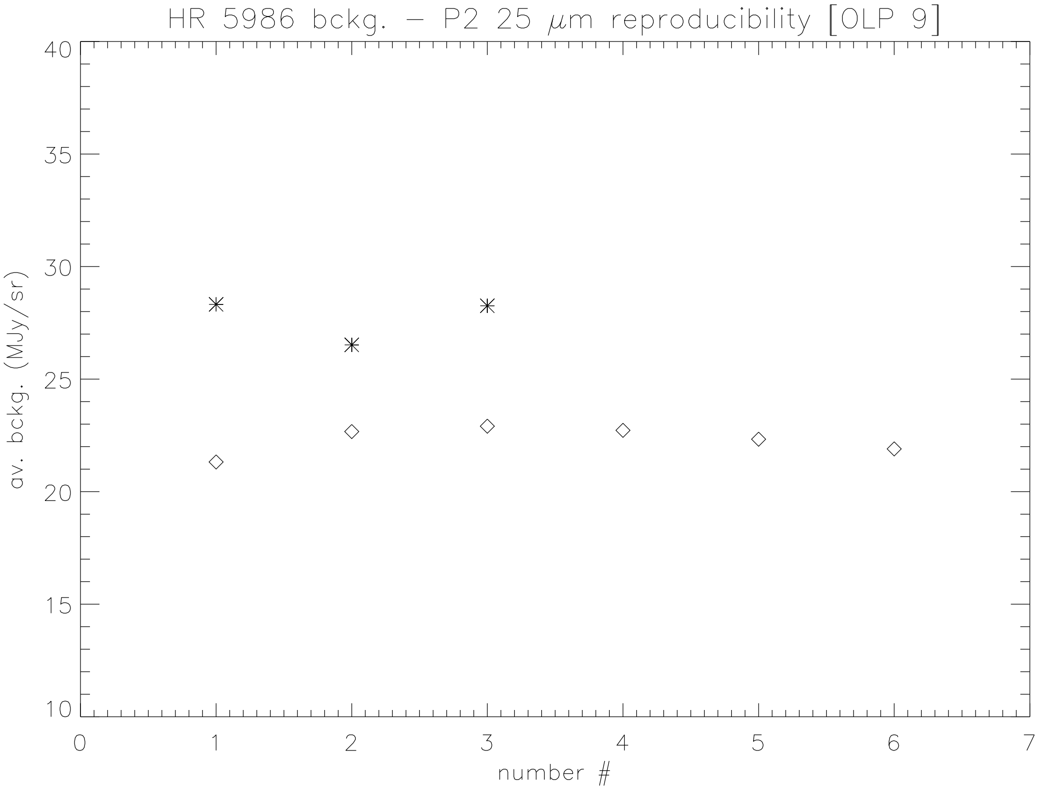

Figure 9.21: Reproducibility of P2 chopped photometry processed with OLP 9.0b10 with regard to point source flux derivation and background flux derivation from the off-source beam. The point source fluxes (upper panel) are compared with the flux value of the model of HR 5986, provided by P. Hammersley. The meaning of the symbols is the following: solid line: model flux at $25\,\mu$m, square: background subtracted ISOPHOT flux (for info on the revolution refer to the section evalutaion log). The background fluxes (lower panel) are compared with COBE/DIRBE weekly photometry. The meaning of the symbols is the following: diamond: COBE/DIRBE photometry, asterisk: ISOPHOT background flux.

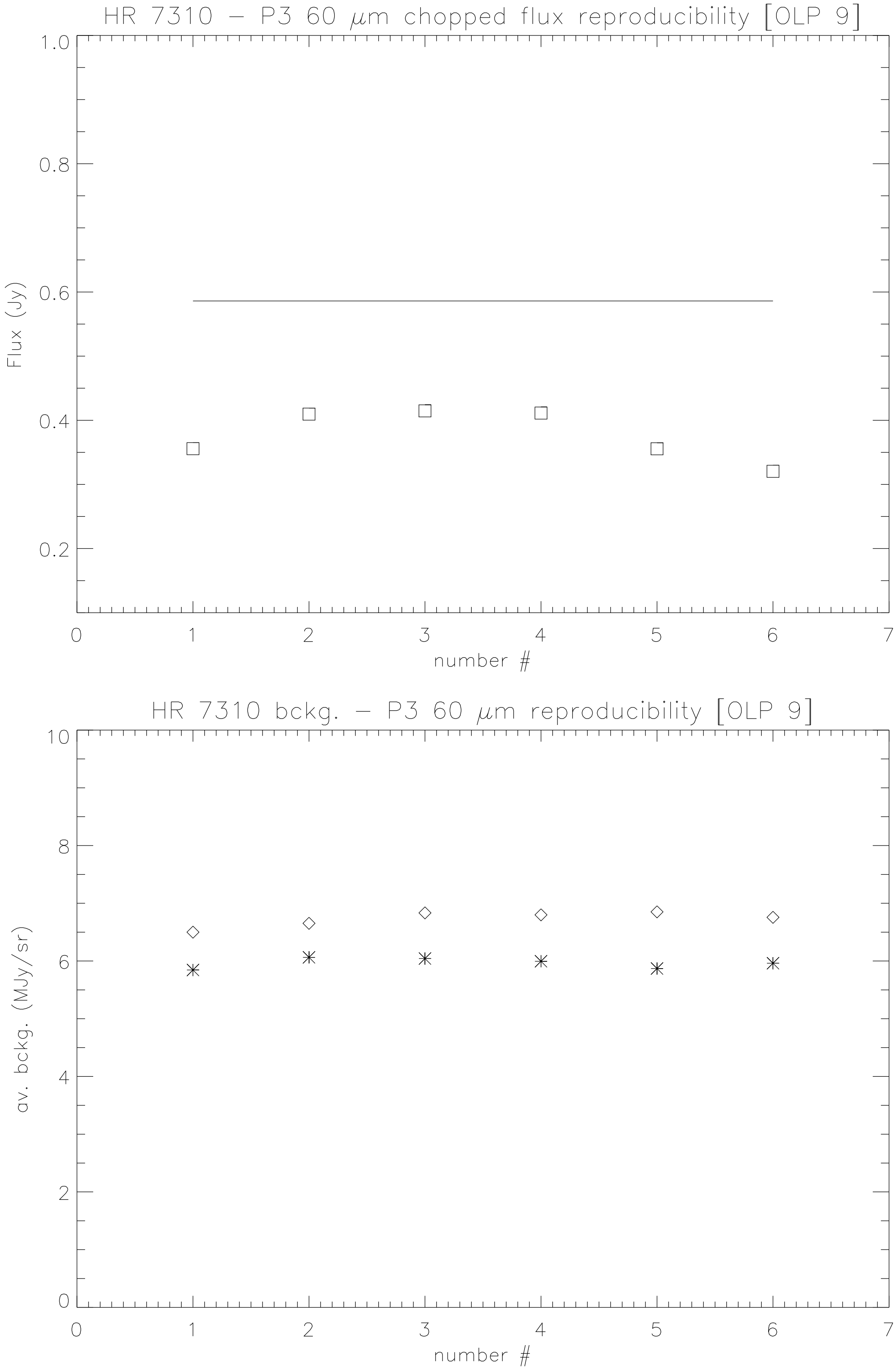

Figure 9.22: Reproducibility of P3 chopped photometry processed with OLP 9.0b10 with regard to point source flux derivation and background flux derivation from the off-source beam. The point source fluxes (upper panel) are compared with the flux value of the model of HR 7310, provided by M. Cohen. The meaning of the symbols is the following: solid line: model flux at $60\,\mu$m, square: background subtracted ISOPHOT flux (for info on the revolution refer to the section evalutaion log). The background fluxes (lower panel) are compared with COBE/DIRBE weekly photometry. The meaning of the symbols is the following: diamond: COBE/DIRBE photometry, asterisk: ISOPHOT background flux.

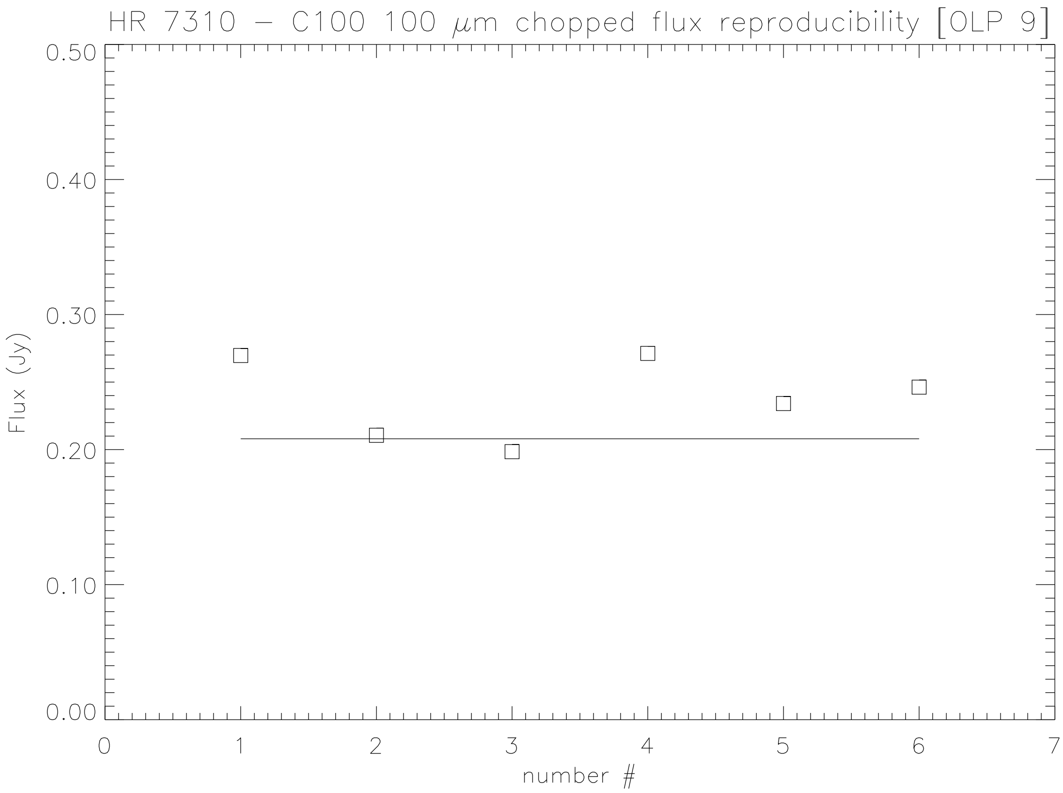

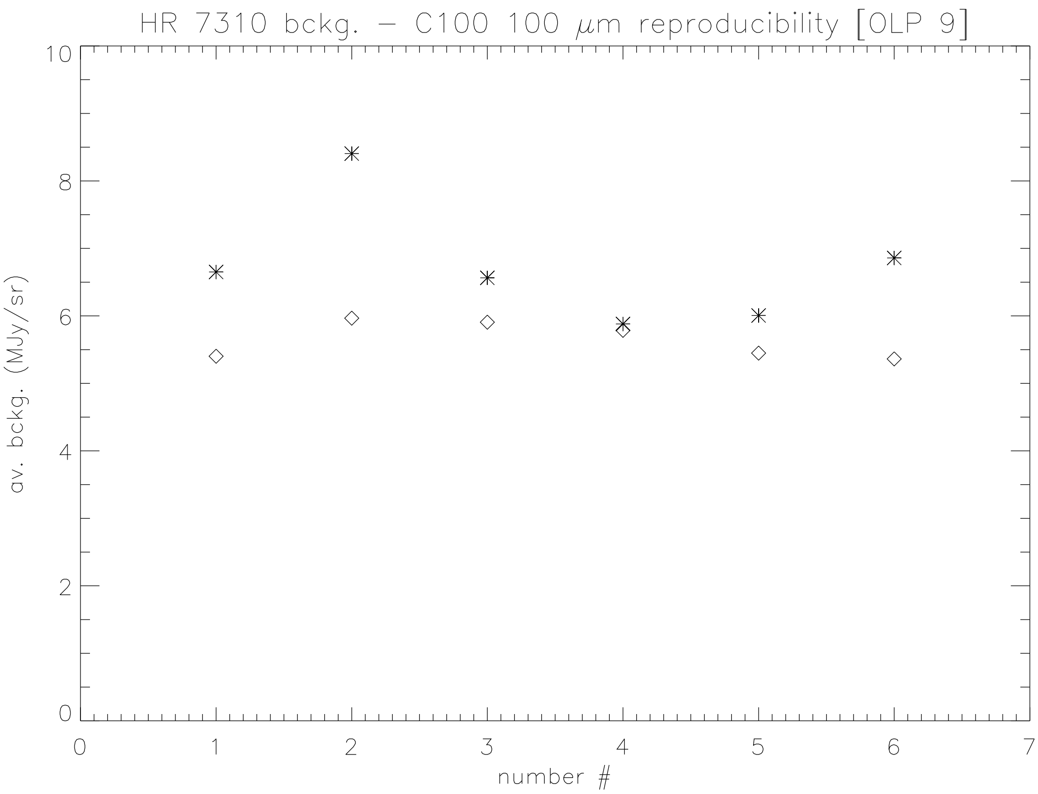

Figure 9.23: Reproducibility of C100 chopped photometry processed with OLP 9.0b10 with regard to point source flux derivation and background flux derivation from the off-source beam. The point source fluxes (upper panel) are compared with the flux value of the model of HR 7310, provided by M. Cohen. The meaning of the symbols is the following: solid line: model flux at $100\,\mu$m, square: background subtracted ISOPHOT flux (for info on the revolution refer to the section evalutaion log). The background fluxes (lower panel) are compared with COBE/DIRBE weekly photometry. The meaning of the symbols is the following: diamond: COBE/DIRBE photometry, asterisk: ISOPHOT background flux.

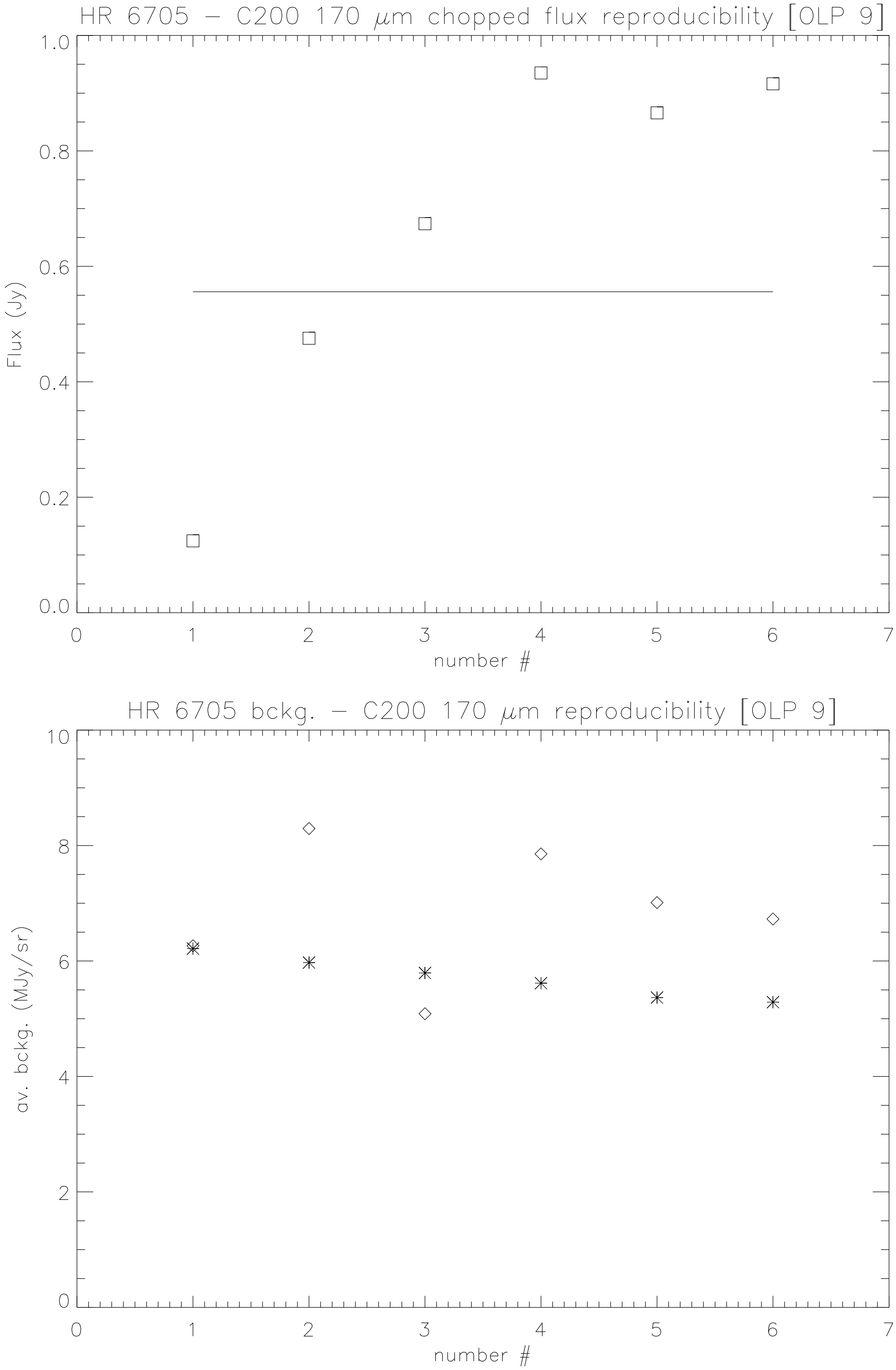

Figure 9.24: Reproducibility of C200 chopped photometry processed with OLP 9.0b10 with regard to point source flux derivation and background flux derivation from the off-source beam. The point source fluxes (upper panel) are compared with the flux value of the model of HR 6705, provided by M. Cohen. The meaning of the symbols is the following: solid line: model flux at 170 μm, square: background subtracted ISOPHOT flux (for info on the revolution refer to the section evaluation log). The background fluxes (lower panel) are compared with COBE/DIRBE weekly photometry. The meaning of the symbols is the following: diamond: COBE/DIRBE photometry, asterisk: ISOPHOT background flux.

Evaluation Log

1) HD 172323, P1

a) Chopped point source photometry

Measurements:
PHT-P1 : ppap74800801 FCS = 12 um
PHT-P1 : ppap76201302 FCS = 12 um
PHT-P1 : ppap79000801 FCS = 12 um
PHT-P1 : ppap81801801 FCS = 12 um
PHT-P1 : ppap84601901 FCS = 12 um
PHT-P1 : ppap87400601 FCS = 12 um

Colour correction: black body, T = 5719 K

Model: Hammersley

Det	cwl (μm)	OLP 8	OLP 9	IRAS	Model	Δ (OLP 8)	Δ (OLP 9)
P1	12.0	0.000	0.049	0.083	0.064	-100.00	-23.15
P1	12.0	0.000	0.049	0.083	0.064	-100.00	-24.33
P1	12.0	0.000	0.054	0.083	0.064	-100.00	-16.48
P1	12.0	0.000	0.059	0.083	0.064	-100.00	-8.99
P1	12.0	0.000	0.055	0.083	0.064	-100.00	-14.62
P1	12.0	0.000	0.071	0.083	0.064	-100.00	10.98

b) Background photometry from off-source beam

Det	λ	OLP8 (MJy/sr)	OLP9 (MJy/sr)	COBE (MJy/sr)
P1	12.0	0.00	15.06	12.05
P1	12.0	0.00	14.59	13.28
P1	12.0	0.00	16.39	13.88
P1	12.0	0.00	15.00	14.15
P1	12.0	0.00	14.79	13.73
P1	12.0	0.00	16.42	13.43

2) HR 5986, P2

a) Chopped point source photometry

Measurements:
PHT-P2 : ppap74801002 FCS = 25 um
PHT-P2 : ppap76201104 FCS = 25 um
PHT-P2 : ppap79000502 FCS = 25 um

Colour correction: black body, T = 6084 K

Model: Hammersley

Det	cwl (μm)	OLP 8	OLP 9	IRAS	Model	Δ (OLP 8)	Δ (OLP 9)
P2	25.0	0.000	0.761	0.527	0.518	-100.00	46.77
P2	25.0	0.000	0.729	0.527	0.518	-100.00	40.68
P2	25.0	0.000	0.800	0.527	0.518	-100.00	54.26
P2	25.0	0.000	0.000	0.527	0.518	-100.00	-100.00
P2	25.0	0.000	0.000	0.527	0.518	-100.00	-100.00
P2	25.0	0.000	0.000	0.527	0.518	-100.00	-100.00

b) Background photometry from off-source beam

Det	λ	OLP8 (MJy/sr)	OLP9 (MJy/sr)	COBE (MJy/sr)
P2	25.0	0.00	28.32	21.32
P2	25.0	0.00	26.52	22.67
P2	25.0	0.00	28.26	22.91
P2	25.0	0.00	0.00	22.73
P2	25.0	0.00	0.00	22.33
P2	25.0	0.00	0.00	21.90

3) HR 7310, P3

a) Chopped point source photomtery

Measurements:
PHT-P3 : ppap74800303 FCS = 60 um
PHT-P3 : ppap76201506 FCS = 60 um
PHT-P3 : ppap79000903 FCS = 60 um
PHT-P3 : ppap81802103 FCS = 60 um
PHT-P3 : ppap84602003 FCS = 60 um
PHT-P3 : ppap87400503 FCS = 60 um

Colour correction: black body, T = 4852 K

Model: Cohen

Det	cwl (μm)	OLP 8	OLP 9	IRAS	Model	Δ (OLP 8)	Δ (OLP 9)
P3	60.0	0.000	0.356	0.571	0.586	-100.00	-39.29
P3	60.0	0.000	0.410	0.571	0.586	-100.00	-30.11
P3	60.0	0.000	0.415	0.571	0.586	-100.00	-29.26
P3	60.0	0.000	0.411	0.571	0.586	-100.00	-29.84
P3	60.0	0.000	0.356	0.571	0.586	-100.00	-39.33
P3	60.0	0.000	0.321	0.571	0.586	-100.00	-45.31

b) Background photometry from off-source beam

Det	λ	OLP8 (MJy/sr)	OLP9 (MJy/sr)	COBE (MJy/sr)
P3	60.0	0.00	5.84	6.50
P3	60.0	0.00	6.06	6.65
P3	60.0	0.00	6.04	6.83
P3	60.0	0.00	6.00	6.80
P3	60.0	0.00	5.87	6.85
P3	60.0	0.00	5.96	6.76

4) HR 7310, C100

a) Chopped point source photomtery

Measurements:
PHT-C100 : pcap74800505 FCS = 100 um
PHT-C100 : pcap76201508 FCS = 100 um
PHT-C100 : pcap79000904 FCS = 100 um
PHT-C100 : pcap81802104 FCS = 100 um
PHT-C100 : pcap84602004 FCS = 100 um
PHT-C100 : pcap87400504 FCS = 100 um

Colour correction: black body, T = 4852 K

Model: Cohen

Det	cwl (μm)	OLP 8	OLP 9	IRAS	Model	Δ (OLP 8)	Δ (OLP 9)
C1	100.0	0.000	0.270	0.634	0.208	-100.00	29.83
C1	100.0	0.000	0.211	0.634	0.208	-100.00	1.40
C1	100.0	0.000	0.198	0.634	0.208	-100.00	-4.44
C1	100.0	0.000	0.271	0.634	0.208	-100.00	30.60
C1	100.0	0.000	0.234	0.634	0.208	-100.00	12.72
C1	100.0	0.000	0.246	0.634	0.208	-100.00	18.56

b) Background photometry from off-source beam

Det	λ	OLP8 (MJy/sr)	OLP9 (MJy/sr)	COBE (MJy/sr)
C1	100.0	0.00	6.65	5.40
C1	100.0	0.00	8.40	5.97
C1	100.0	0.00	6.56	5.91
C1	100.0	0.00	5.88	5.79
C1	100.0	0.00	6.01	5.45
C1	100.0	0.00	6.86	5.36

5) HR 6705, C200

a) Chopped point source photometry

Measurements:		
PHT-C200 :	pcap74801212	FCS = 170 um
PHT-C200 :	pcap76201014	FCS = 170 um
PHT-C200 :	pcap79000605	FCS = 170 um
PHT-C200 :	pcap81800705	FCS = 170 um
PHT-C200 :	pcap84600805	FCS = 170 um
PHT-C200 :	pcap87400705	FCS = 170 um

Colour correction: black body, T = 4000 K

Model: Cohen

Det	cwl (μm)	OLP 8	OLP 9	IRAS	Model	Δ (OLP 8)	Δ (OLP 9)
C2	170.0	0.000	0.124		0.556	-100.00	-77.62
C2	170.0	0.000	0.475		0.556	-100.00	-14.54
C2	170.0	0.000	0.674		0.556	-100.00	21.14
C2	170.0	0.000	0.935		0.556	-100.00	68.07
C2	170.0	0.000	0.866		0.556	-100.00	55.64
C2	170.0	0.000	0.916		0.556	-100.00	64.70

b) Background photometry from off-source beam

Det	λ	OLP8 (MJy/sr)	OLP9 (MJy/sr)	COBE (MJy/sr)
C2	170.0	0.00	6.21	6.26
C2	170.0	0.00	5.97	8.29
C2	170.0	0.00	5.79	5.09
C2	170.0	0.00	5.62	7.86
C2	170.0	0.00	5.37	7.01
C2	170.0	0.00	5.29	6.73

9.2 Validation of Chopped Photometry Test Cases with Staring Mode References on other Revolutions

An overview of the test cases is outlined in Ref. [4], chapter 5.2.

9.2.1 References to Calibration Analysis and Software Change Documentation

- calibration reports:
  - Analysis of Chopped ISOPHOT Measurements [19]
- Software Change Requests: none
- Software Problem Reports: SPR 3213, 3216

9.2.2 Summary of Results

- The test case 08900789 demonstrates that observations with read-out data reduction can be handled now and SPR-3209 has been fixed.
- For P2 and P3 we find improvement in the fluxes resulting in relative good consistency with staring mode observations.
- C100 and C200 photometry display a strange behaviour which needs further investigation. The PIA gives pratically identical results (except that the 200 μm point fits better to the neighbouring data points).

9.2.3 Validation of PHT03 and PHT22 Chopped Mode: The FIR Excess SED of Vega - Final Assessment

- authors: U. Klaas
- data: 28-July-2000
- SVP period 2

Motivation

We investigate here observations of a general observer's program for which photometry using Interactive Analysis has been published, cf. Ref. [14]. In addition, IRAS photometry at 25, 60, and 100 μm is available.

Method

We compare the color corrected source flux values of both OLP V8.6b1 and OLP V9.01 with model fluxes, IRAS photometry and the photometry derived in [14] (called HWK photometry in the following).
The color correction was dependent on the relative contribution by the stellar photosphere and the IR disc, and hence on the wavelength. We followed the description as given in Ref.[14]:

- from 60 to 100 μm the SED behaves like an 80 K modified BB, $\varepsilon \propto \nu$
- from 20 to 25 μm the SED is a mixture of a 10000 K BB and an 80 K modified BB with a ratio 2:1.

Results

Fig. 9.25 shows the results of the chopped photometry. We note that P2 and P3 results have been improved with regard to OLP 8. At 25 μm now an infrared excess with regard to the photospheric model is found. With regard to the staring mode observation on rev. 85 (cf. Fig. 8.54 in Sect. 8.4.7 the 25 μm flux appears to be still abit too low, while the P3 fluxes are in reasonable agreement. Also with the new calibration and processing the starnge shape of the resulting SED by C100 and C200 with a steep fall-off of the C100 fluxes from 60 to 100 μm and the strong step upwards in flux towards the C200 range did not disappear. In contrary, the step is higher, since the C200 SED part has become more oblique. One improvement in the C100 data processing can be reported nevertheless: the 90 μm point of TDT 08900789 which was previously not processed due to data reduction in the read-outs is now properly processed from the technical aspect, confirms however the unphysical trend in the C100 part of the SED. The surface brightness values of the C100 off-beams indicate a problem with the calibration, too, since they are far above COBE/DIRBE (cf. Fig. 9.26). The C200 off-beam surface brightness SED looks rather smooth and consistent with COBE/DIRBE which makes the scatter in the differential source fluxes hard to understand.

Conclusions

- The P2 photometry has been improved for this target, though the comparison with staring mode photometry on the same revolution indicates that the flux is derived still somewhat too low. Also the derived surface brightness in the off-beam is not consistent with COBE/DIRBE photometry.
- The P3 photometry shows a good performance, indicating that for brighter sources the flux deficits found in the previous chapters disappear.
- The 90 μm photometry of TDT 08900789 demonstrates that SPR-3209 has been properly fixed.
- The C100 photomery displays a strange behaviour with a steep flux fall-off towards longer wavelengths. This was already observed for earlier OLP versions and the reason for this is not yet understood. Also the C100 surface brightness photometry of the off-beam is very discrepant from COBE/DIRBE.

- While the C200 surface brightness of the off-beam shows now a smooth behaviour which is also very consistent with COBE/DIRBE, the C200 part of the SED appears to be too oblique and does not fit with the IRAS and P3 photometry any more. Furthermore the data points show a relatively large scatter.

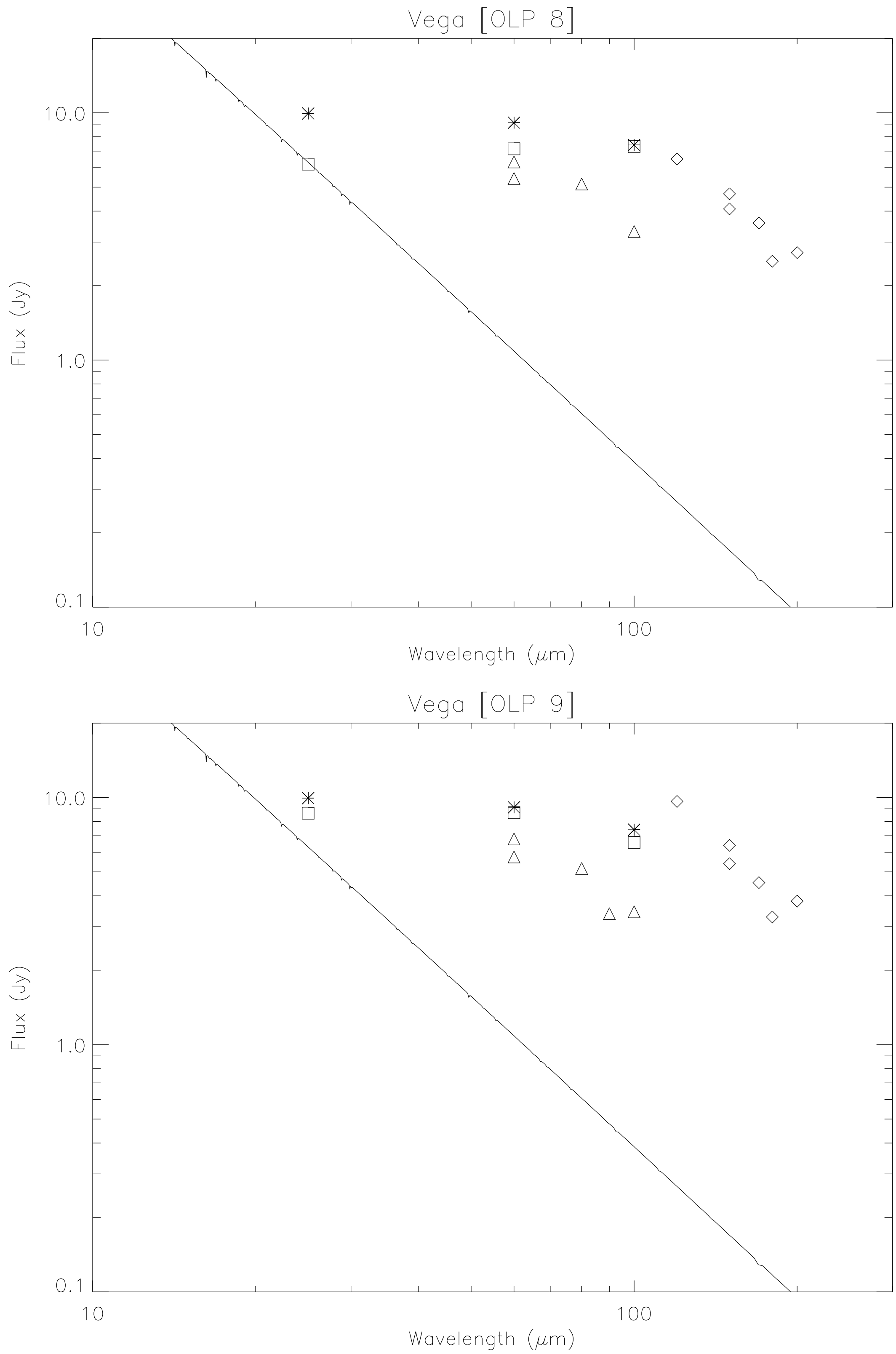

Figure 9.25: Comparison of PHT-P and PHT-C chopped photometry with the photospheric model of Vega by M. Cohen and with IRAS photometry both for OLP 8.6b1 (upper panel) and OLP 9.01 (lower panel). Color correction has been applied according to the description in the method section. The meaning of the symbols is the following: solid line: photospheric model, asterisk: IRAS, square: PHT-P (P03 AOT), triangle: C100 (P22 AOT), diamond: C200 (P22 AOT).

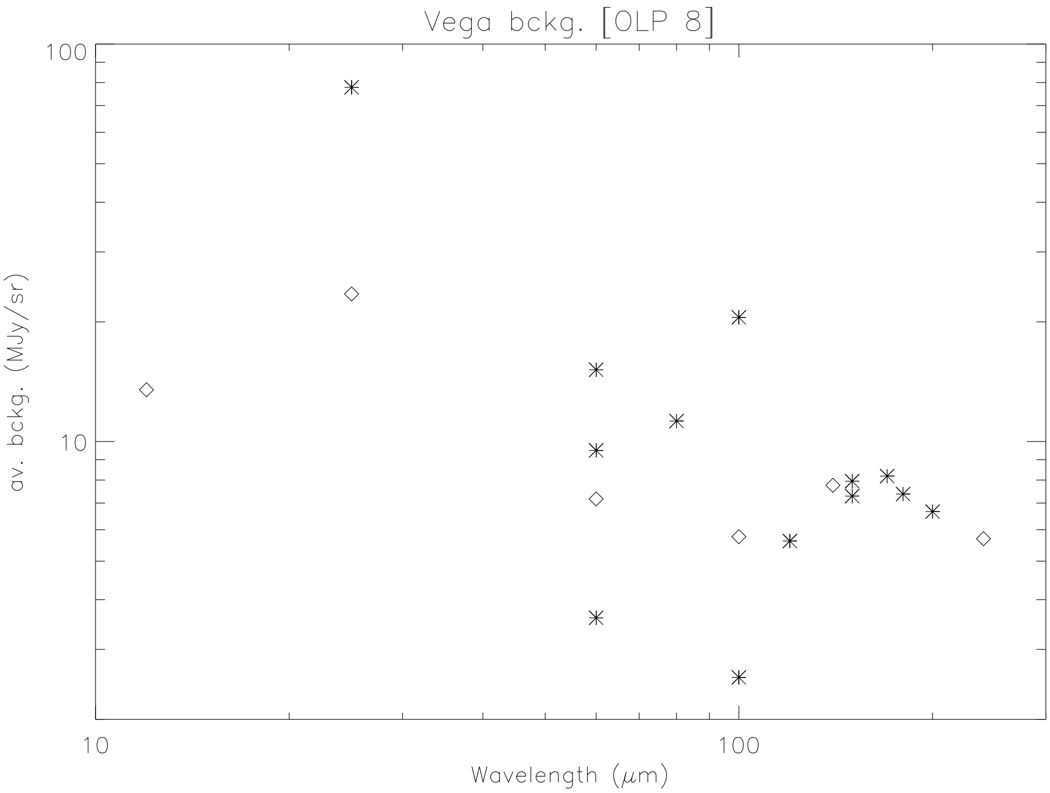

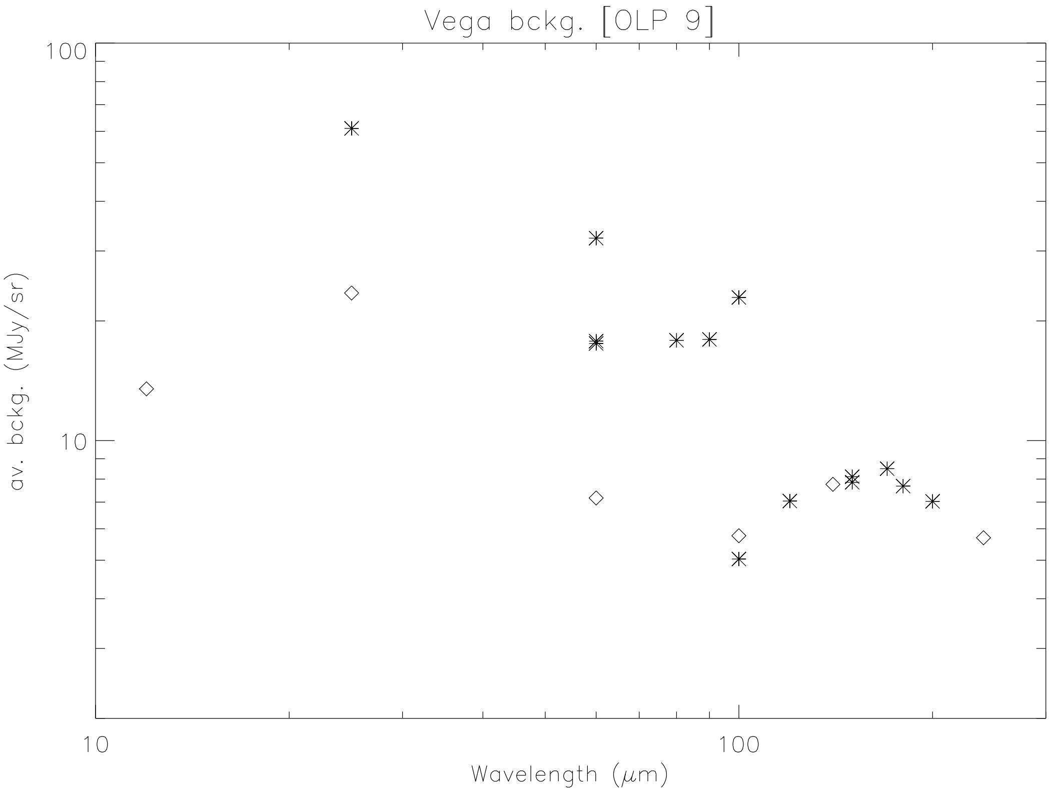

Figure 9.26: Comparison of surface brightness from chopped PHT photometry of the background beam for Vega with COBE, both for OLP 8.6b1 (upper panel) and OLP 9.01 (lower panel). Asterisk: PHT-P and PHT-C photometry, diamond: COBE.

Evaluation Log

1) Chopped Point Source Photometry

Measurements:		
PHT-P:	ppap08900788	FCS = 25 um
	ppap08500241	FCS = 100 um
PHT-C:	pcap08900789	FCS = 90 um
	pcap08900790	FCS = 150 um
	pcap10601101	FCS = 60, 170 um

Colour correction: mixture of 10000 K BB & 80 K modified (em.=1) BB
see text for details

Model: Cohen

Det	cwl (μm)	OLP 8	OLP 9	IRAS	Model	Δ (OLP 8)	Δ (OLP 9)
P2	25.0	6.198	8.636	9.938	6.301	-1.62	37.06
P3	60.0	7.148	8.678	9.121	1.087	557.80	698.66
P3	100.0	7.303	6.573	7.408	0.387	1789.46	1600.66
C1	60.0	6.328	5.744	9.121	1.087	482.32	428.60
C1	90.0	0.000	3.389		0.478	-100.00	608.72
C2	150.0	4.083	5.392		0.169	2308.96	3081.46
C2	180.0	2.510	3.285		0.117	2044.53	2706.84
C1	60.0	5.419	6.793	9.121	1.087	398.71	525.12
C1	80.0	5.150	5.163		0.607	748.72	750.87
C1	100.0	3.308	3.448	7.408	0.387	755.74	791.97
C2	120.0	6.502	9.637		0.267	2336.06	3510.43
C2	150.0	4.701	6.407		0.169	2673.57	3680.42
C2	170.0	3.582	4.523		0.129	2685.60	3417.64
C2	200.0	2.718	3.806		0.094	2789.38	3945.92

Note: The Δs do not give calibration accuracies here!

2) Background photometry from off-source beam

Det	λ	OLP8 (MJy/sr)	OLP9 (MJy/sr)	COBE (MJy/sr)
P2	25.0	77.83	61.02	23.51
P3	60.0	3.60	17.79	7.17
C1	60.0	9.50	17.55	7.17
C1	60.0	15.15	32.30	7.17
C1	80.0	11.26	17.88	
C1	90.0	0.00	17.97	
P3	100.0	2.55	5.04	5.76
C1	100.0	20.53	22.91	5.76
C2	120.0	5.62	7.04	
C2	150.0	7.95	8.11	7.76
C2	150.0	7.29	7.85	7.76
C2	170.0	8.18	8.49	
C2	180.0	7.37	7.68	
C2	200.0	6.66	7.03	5.69

9.3 Validation of Chopped Observations of Known Sources

This section refers to observations of sources with known SEDs, mainly celestial standards. An overview of the test cases is outlined in Ref. [4], chapter 5.3.

9.3.1 References to Calibration Analysis and Software Change Documentation

- calibration reports:
  - Analysis of Chopped ISOPHOT Measurements [19]
- Software Change Requests: none
- Software Problem Reports: SPR 3213, 3216

9.3.2 Summary of Results

The results by the test case analysis performed in this chapter confirm several findings of previous chapters and show a few additional systematics:

- The general good accuracy of P1 chopped photometry. In one multi-filter test case a potential problem with the relative filter-to-filter calibration accuracy was indicated.
- For P2 additonal cases confirming the commonly resulting overcorrection of P2 fluxes were found. There is one exception yielding a good accuracy with OLP 9.
- For C100 chopped photometry in multi-filter mode some systematics in the resulting deviations from the model fluxes were found: $60\,\mu$m fluxes are in general higher and less accurate than the OLP 8 ones, while the longer wavelength and relatively calibrated filter measurements are closer to the model. This relative filter issue should be investigated in more detail. Some impact on the results may come here from cirrus contamination (all IRAS $100\,\mu$m references are upper limits only).
- For C200 no quantitative results could be derived, since the expected source fluxes were always below the C200 detection limits and significant contamination by cirrus confusion is likely to play a role.

9.3.3 Validation of PHT03 and PHT22 Chopped Mode: The SEDs of Stars with Known Fluxes - Final Assessment

- authors: U. Klaas
- date: 16-May-2000
- SVP period 2

Motivation

We investigate here the results of chopped photometry for several stars, namely HR 5447, BS 5062, HR 5304, HR 5914 and HR 5986, for which model fluxes are available.

Method

We compare the background subtracted flux values of both OLP V8.6b1 and OLP V9.0b10/V9.01 results against the models by Cohen and Hammersley and IRAS photometry. Furthermore, we compare the derived background surface brightness with COBE/DIRBE photometry.

Results

Fig. 9.27 shows the results for HR 5447. The C100 and C200 photometry was performed twice, the first time on rev. 89 (i.e. pre-rev.94 FCS calibration) and the second time on rev. 269. For the P2 chopped photometry this is another test case which confirms that OLP 9 overestimates the fluxes now considerably. Both 60 μm flux values are close to the IRAS FSC value, but approximately a factor 2 - 2.5 above the model expectation. At 100 μm the IRAS FSC flux is clearly cirrus confusion limited. The ISOPHOT photometry at 90 μm goes deeper, but very discrepant fluxes are found from the two observations. The orientation of the chop on the sky was 277 deg vs. 93 deg, i.e. a rotation of 184 deg. Since for the C100 observations triangular chopping was applied, the same background positions were seen in both measurements, and hence the scatter is due to internal measurement uncertainty. For C200 the model fluxes are far below the detection limit of ISOPHOT and the measurement makes only sense, if an infrared excess was expected. Fig. 9.28 shows the average surface brightness from the off-beams. The COBE/DIRBE photometry has yet to be retrieved.
Fig. 9.29 shows the results for BS 5062. The P1 7.3 μm photometry is excellent, while the 12 μm point which is calibrated relative to it is far off now. The P2 photometry provides another case to show that the fluxes are determined too high for 25 μm. The OLP 9 C100 photometry is improved: the 60 μm flux is closer to the model than IRAS, while the 90 μm flux goes off, but is still considerably lower than the IRAS 100 μm upper limit. For the background of 4 MJy sr^{-1} a 1 σ cirrus confusion noise of 7 mJy is predicted, so the 90 μm photometric points can be very much affected by cirrus confusion. The comparison with COBE/DIRBE (Fig. 9.30) shows that also the 12 μm surface brightness is inconsistent. With the improvement of the differential fluxes of the C100 photometry, also the surface brightness values obtained for the off-beams are more consistent with COBE/DIRBE now.
HR 5304 is another example of a faint star with fluxes below 100 mJy in the C100 range. Fig. 9.31 shows the results. For OLP 9 the 60 μm flux is farther off the model, while the 100 μm flux comes very close to the model flux in absolute level (relative 78 %, but absolute 12 mJy). Since the calibration is in the 60 μm filter, the resulting SED is rather oblique w.r.t. the model SED. The comparison of the off-beam surface brightness photometry (Fig. 9.32) does not show much change from OLP 8 to OLP 9.
Fig. 9.33 shows the photometry for HR 5914. For this star OLP 8 gave a too low flux for the 25 μm chopped photometry. With the general trend that with OLP 9 P2 chopped photometry fluxes are higher, this is one of the exceptions, where OLP 9 gives now an accurate photometry. For C100 photometry the fluxes were close to the model reference with OLP 8. For OLP 9 the accuracy has been decreased and a similar phenomenon as for other test cases shows up: the 60 μm flux point falls now considerably higher and the 60 to 90 μm SED is oblique w.r.t. the model (the 90 μm flux is still quite close to the model flux in terms of absolute level). C200 photometry is also available. However, the fluxes come out negative as shown in the table in the evaluation log. The model fluxes are far below the detection limit of ISOPHOT C200 and the measurement makes only sense, if an infrared

excess was expected.For a background surface brightness of $4\,\mathrm{MJy\,sr^{-1}}$ the cirrus confusion noise at 150 and 180 μm is estimated to have a $1\,\sigma$ of 24 and 37 mJy, respectively. Therefore, cirrus fluctuations contribute significantly to the measurement uncertainty and can mimic negative flux results in the measurement. For the background surface brightness values we find the trend that they are more consistent with COBE/DIRBE for the version for which also the differential flux is closer to the reference (C200 surface brightness values were not determined for OLP 8 products). The 180 μm surface brightness appears not to follow the general shape of the background SED.
Fig. 9.35 shows the results for HR 5986, one of the monitoring stars for chopped P2 photometry, cf. Sect. 9.1.7. There are alos 2 P1 measurements in the 12 μm filter available (for OLP 8 only 1 was investigated). They confirm the generally good accuracy of the chopped P1 photometry. The P2 measurement is one of the monitoring measurements from rev. 748. The C100 photometry reflects a commonly found trend between OLP 8 and OLP 9 results: the 60 μm flux is now derived far too high, while the 100 μm flux is now closer to the model. In this multi-filter measurement again the FCS calibration is performed in the 60 μm filter, the 100 μm filter being relatively calibrated to it and yielding the oblique shape of the measured SED w.r.t. the model SED. The comparison of surface brightness photometry from the off-beams with COBE/DIRBE photometry indicates a somewhat better consistency (without any proper color correction yet!) for OLP 8.

Conclusions

- For P1 the test cases confirm the generally good accuracy achieved with chopped photometry. Only one multi-filter case (BS 5062) indicates a potential calibration problem for the relatively calibrated filter.
- For P2 we investigated three additional test cases: 2 confirmed the generally found trend that the OLP 9 fluxes are too high, while 1 gives now a good consistency with the model with the flux having been too low for the previous version.
- For C100 we investigated two different multi-filter cases:
  - For 2 sources the combination 60 and 100 μm filter with the FCS measurement in the 60 μm filter was performed. Both show the same trend, that with OLP 9 the 60 mum flux is much farther off to higher fluxes than for OLP 8, while the 100 μm flux comes closer to the model, yielding a measured SED which is oblique w.r.t. the model SED.
  - For 3 sources the combination 60 and 90 mum filter, for one source twice. There, for two cases a flat SED results with the 90 μm filter point too high, while the other two cases resemble the behaviour 60/100 μm.

  One has to put a caveat that these are all relatively faint sources and cirrus confusion is not completely neglible, in particular since for 4 sources IRAS 100 μm photometry presents only upper limits (the fifth source is even fainter). However, some internal inconsistency of the ISOPHOT measurements on HR 5447 point to a still underlying calibration inconsistency.
- For two test cases (HR 5447 & HR 5914) C200 photometry had been performed. However, in both cases the expected source fluxes are below the ISOPHOT C200 detection limits. The resulting fluxces are either far above the model reference (in relative terms) or negative, being consistent with a significant contamination by cirrus. Therefore, no quantitative numbers can be derived here.

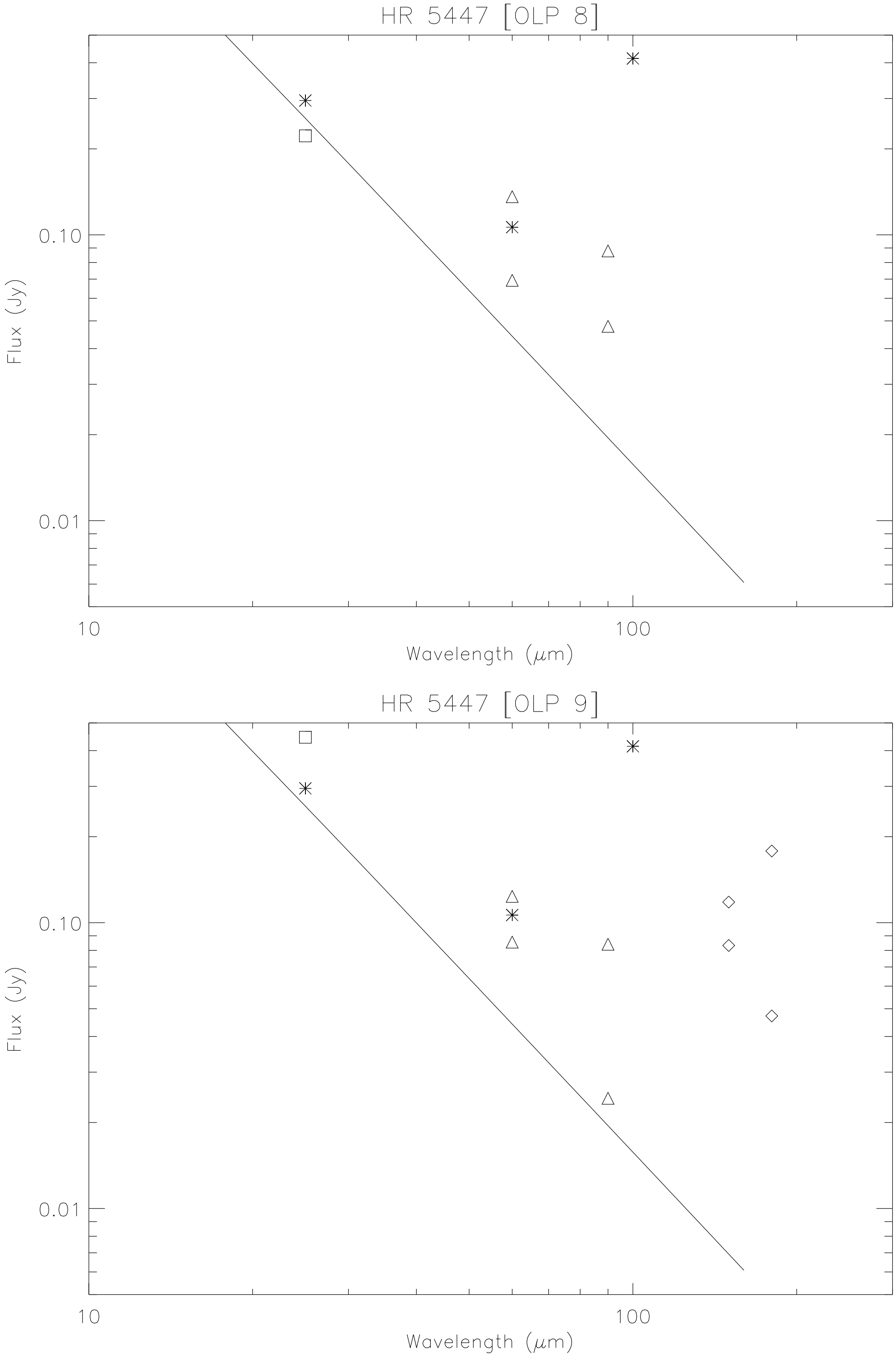

Figure 9.27: Comparison of PHT-P and PHT-C chopped photometry with the model by Hammersley and IRAS photometry both for OLP 8.6b1 (upper panel, no C200 photometry) and OLP 9.01 (lower panel). The meaning of the symbols is the following: solid line: model, asterisk: IRAS, square: PHT-P (P03 AOT), triangle: C100 (P22 AOT), diamond: C200 (P22 AOT).

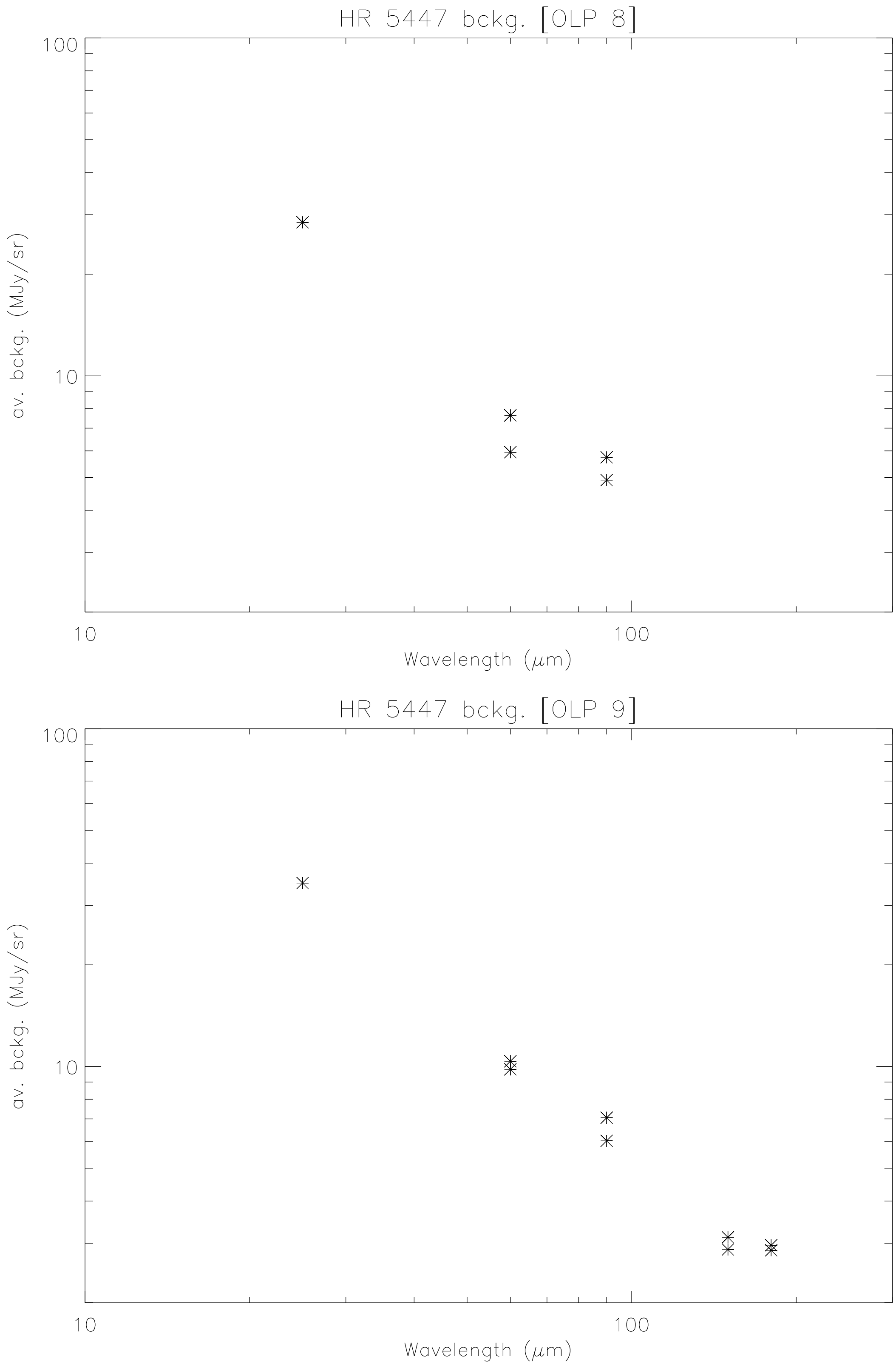

Figure 9.28: Surface brightness from chopped PHT photometry of the background beam for HR 5447, both for OLP 8.6b1 (upper panel) and OLP 9.01. Asterisk: PHT-P and PHT-C photometry.

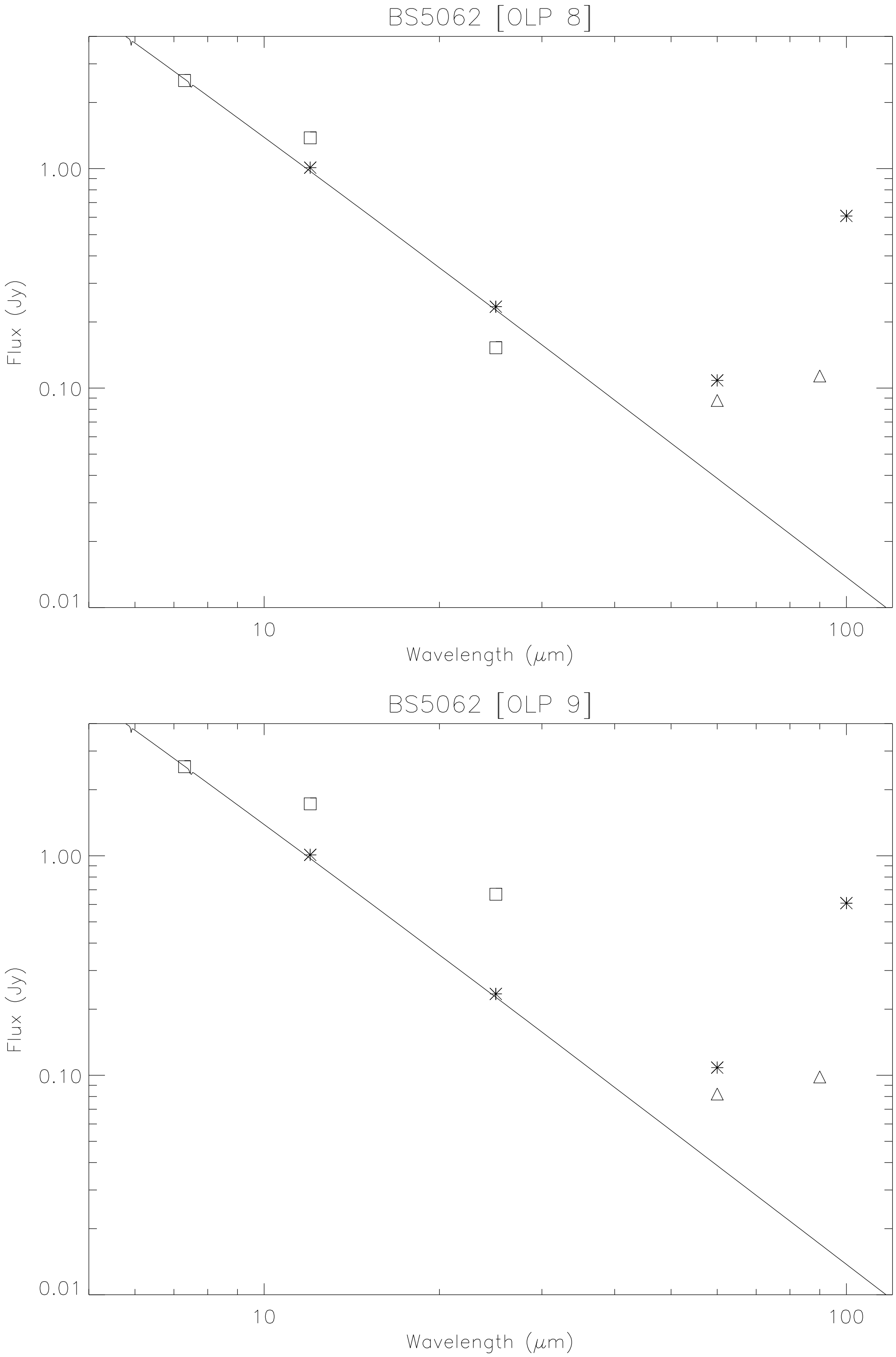

Figure 9.29: Comparison of PHT-P and PHT-C chopped photometry with the model by Hammersley and IRAS photometry both for OLP 8.6b1 (upper panel) and OLP 9.0b10 (lower panel). The meaning of the symbols is the following: solid line: model, asterisk: IRAS, square: PHT-P (P03 AOT), triangle: C100 (P22 AOT).

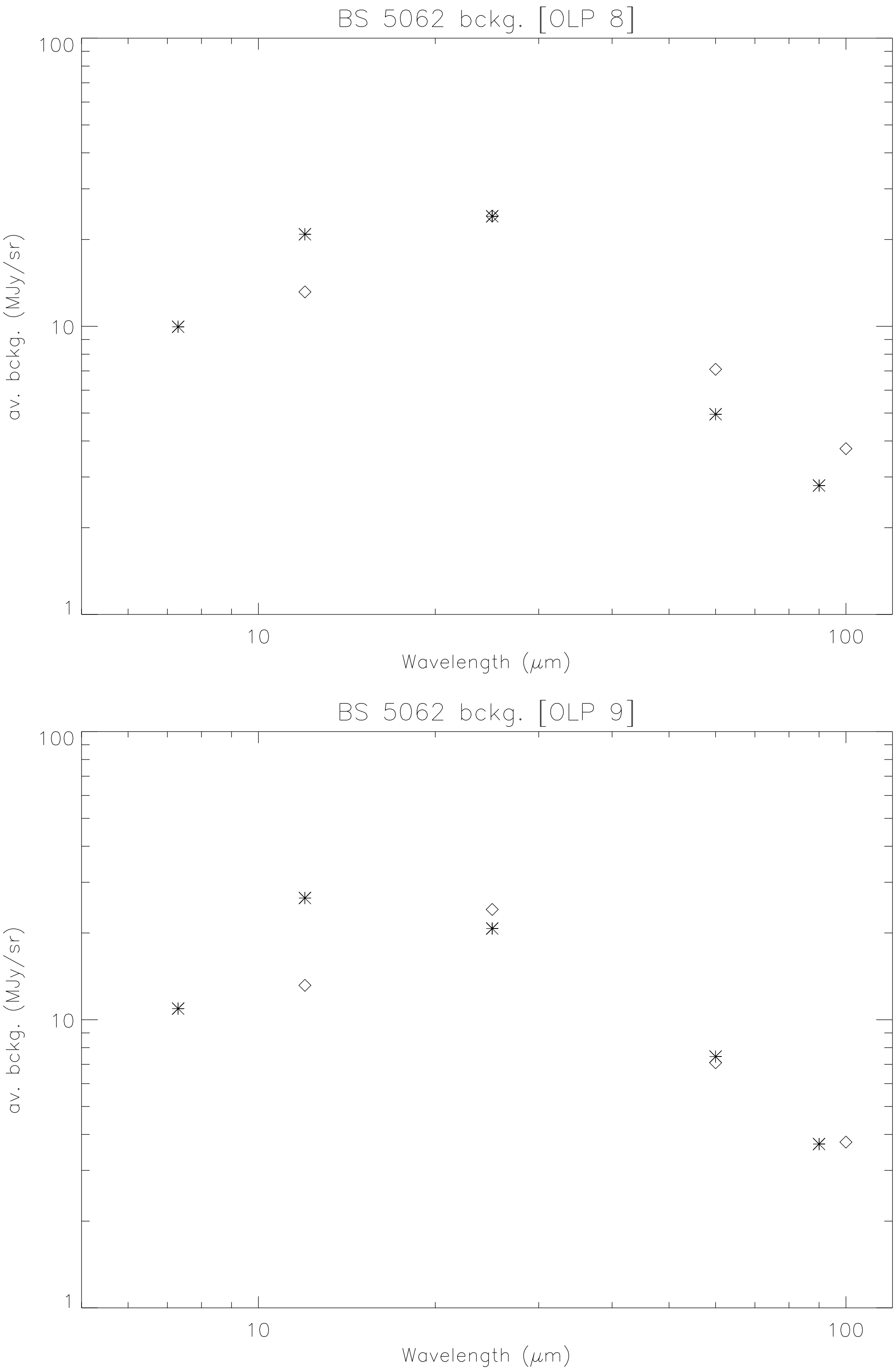

Figure 9.30: Comparison of surface brightness from chopped PHT photometry of the background beam for BS 5062 with COBE, both for OLP 8.6b1 (upper panel) and OLP 9.0b10. Asterisk: PHT-P and PHT-C photometry, diamond: COBE.

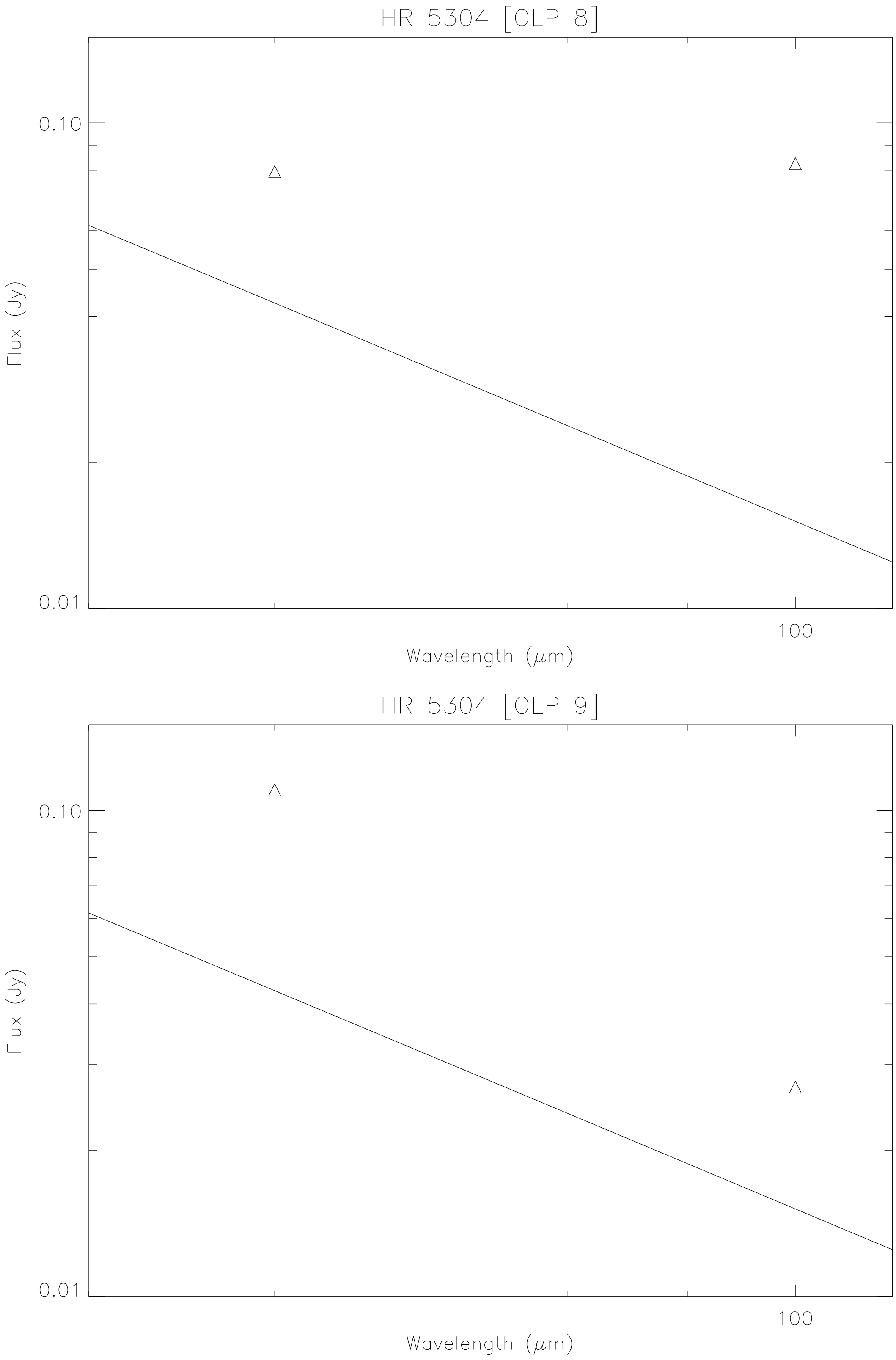

Figure 9.31: Comparison of PHT-C chopped photometry with the model by Cohen both for OLP 8.6b1 (upper panel) and OLP 9.01 (lower panel). The meaning of the symbols is the following: solid line: model, triangle: C100 (P22 AOT).

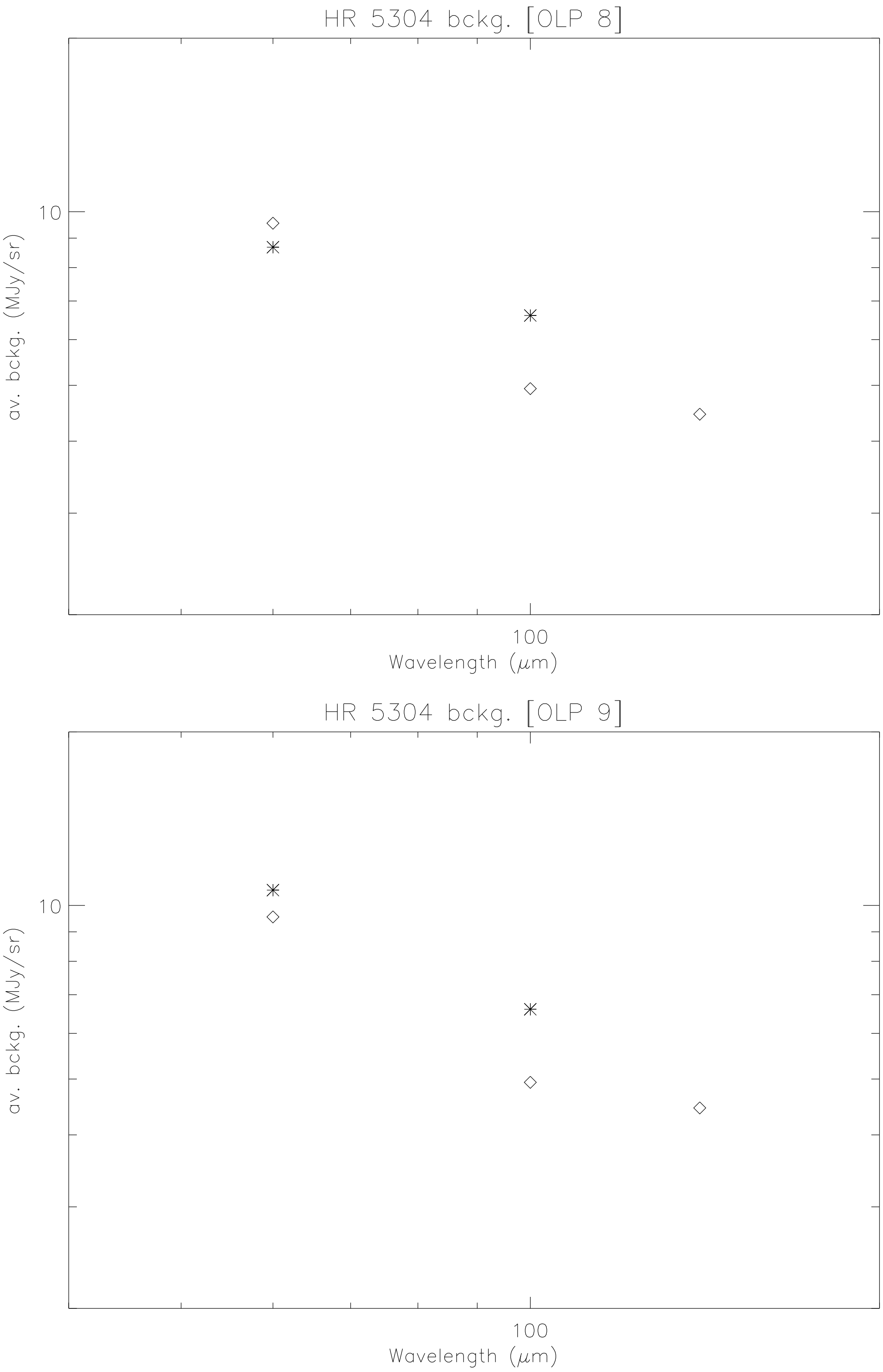

Figure 9.32: Comparison of surface brightness from chopped PHT photometry of the background beam for HR 5304 with COBE, both for OLP 8.6b1 (upper panel) and OLP 9.01. Asterisk: PHT-C photometry, diamond: COBE.

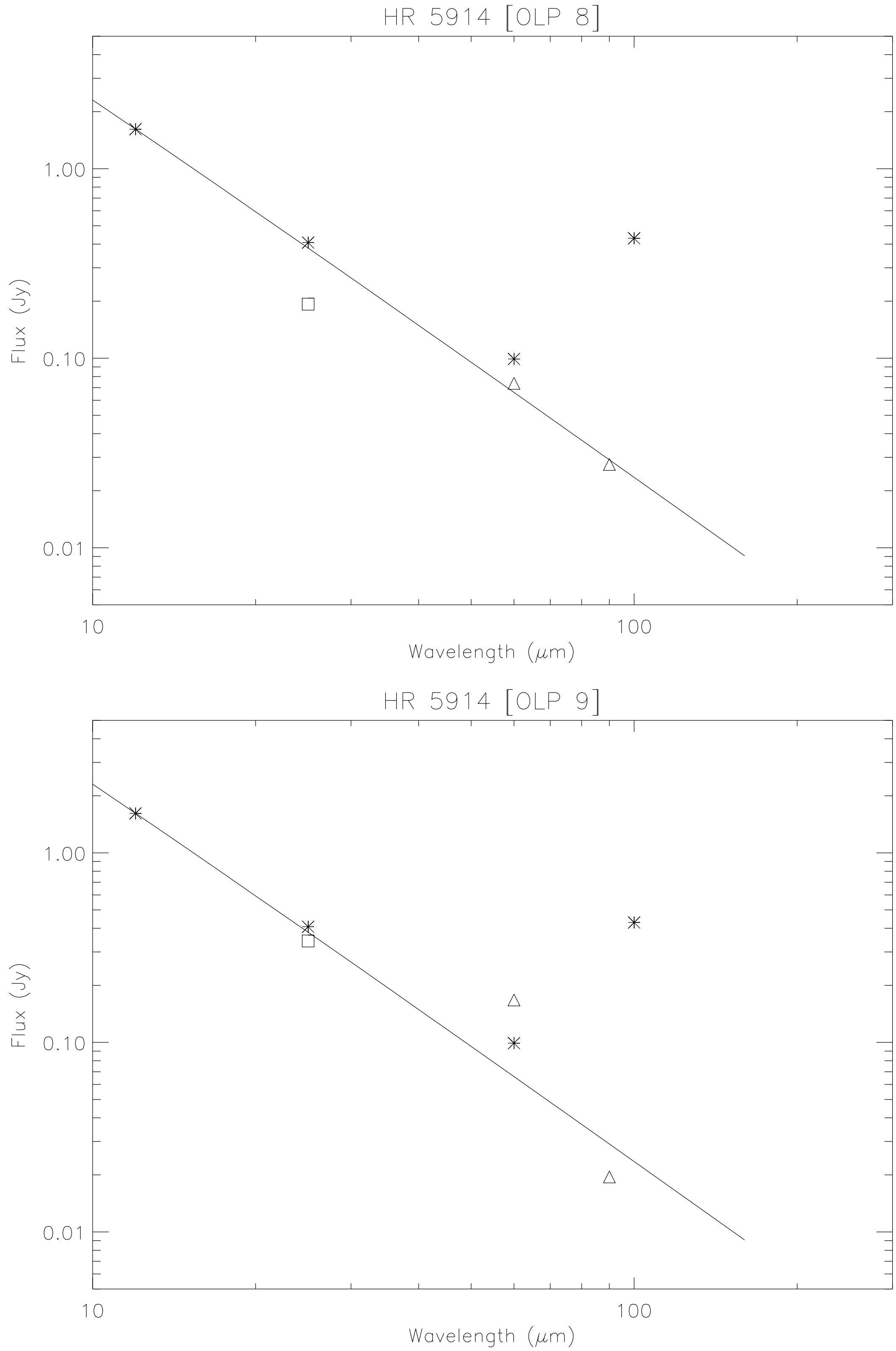

Figure 9.33: Comparison of PHT-P and PHT-C chopped photometry with the model by Cohen and IRAS photometry both for OLP 8.6b1 (upper panel) and OLP 9.01 (lower panel). The meaning of the symbols is the following: solid line: model, asterisk: IRAS, square: PHT-P (P03 AOT),triangle: C100 (P22 AOT). The C200 chopped photometry gives negative source fluxes, see text.

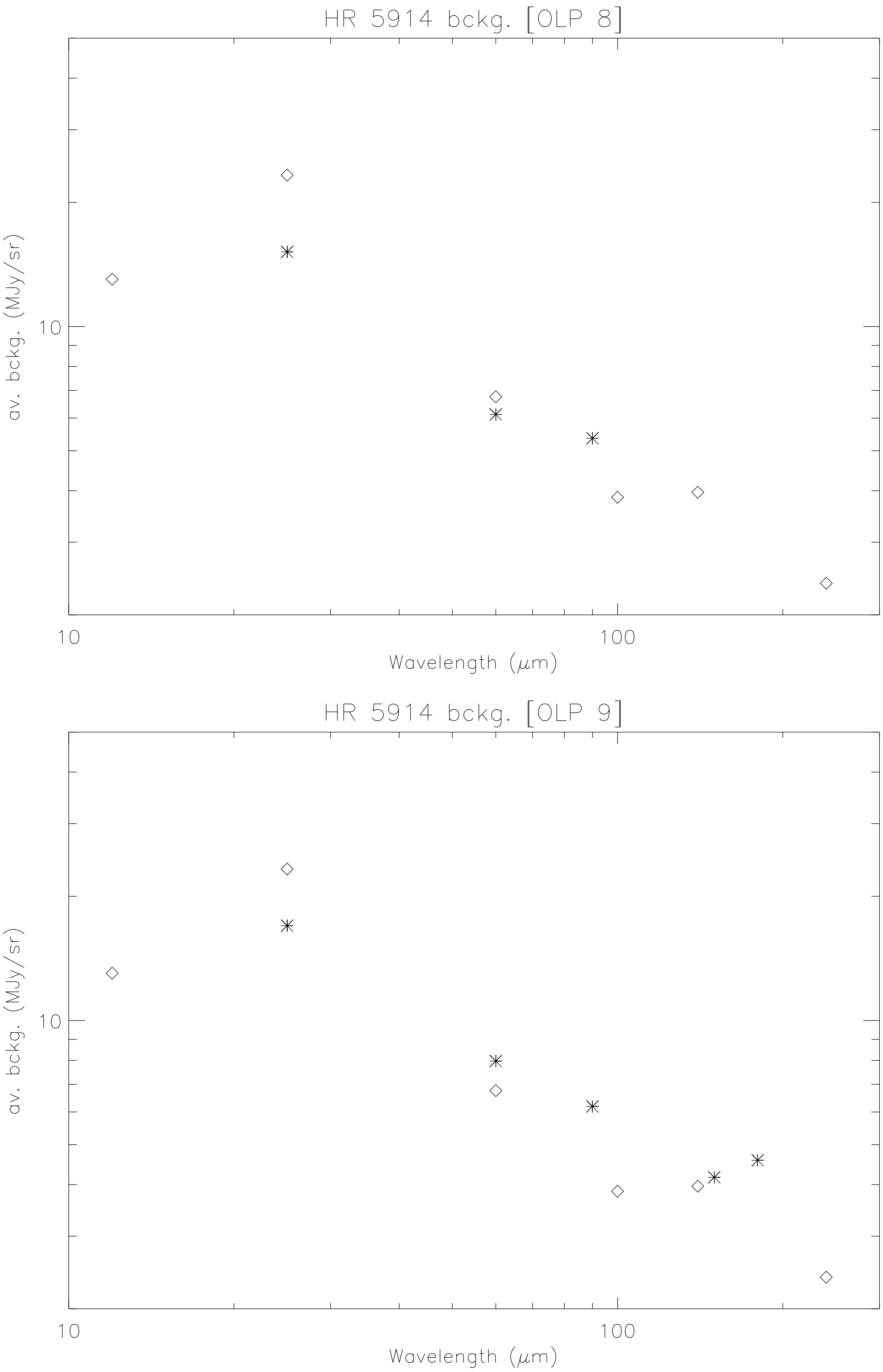

Figure 9.34: Comparison of surface brightness from chopped PHT photometry of the background beam for HR 5914 with COBE, both for OLP 8.6b1 (upper panel) and OLP 9.01. Asterisk: PHT-P and PHT-C photometry, diamond: COBE.

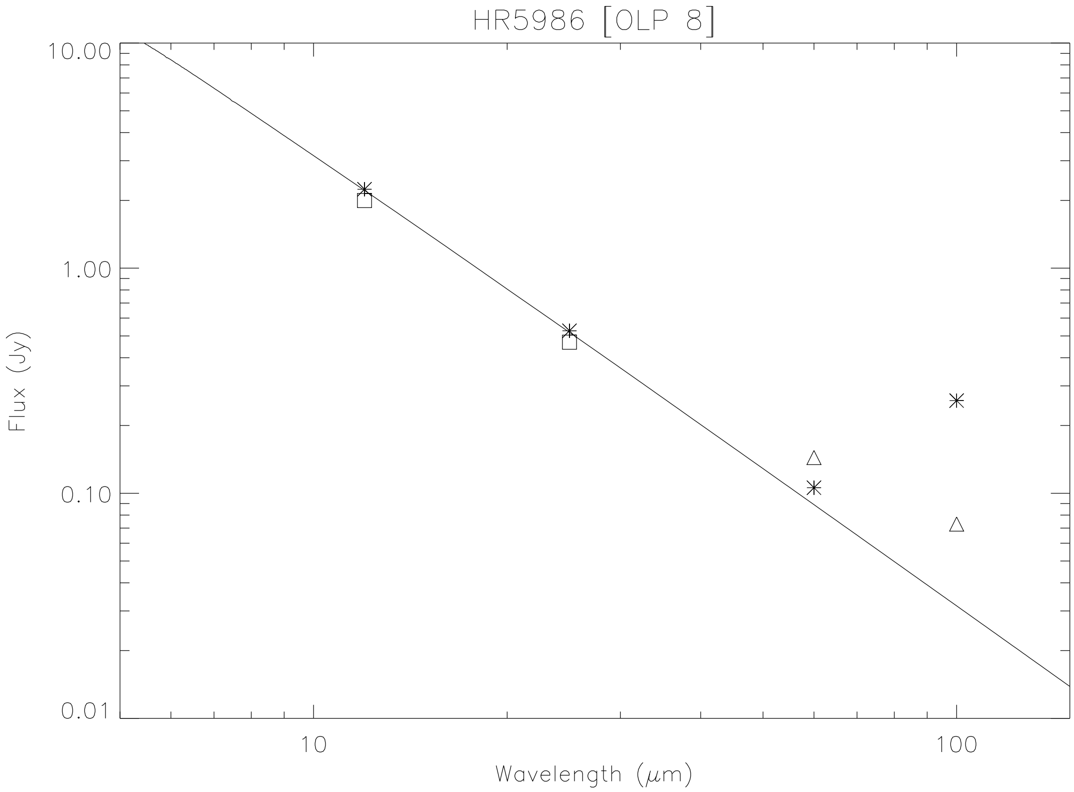

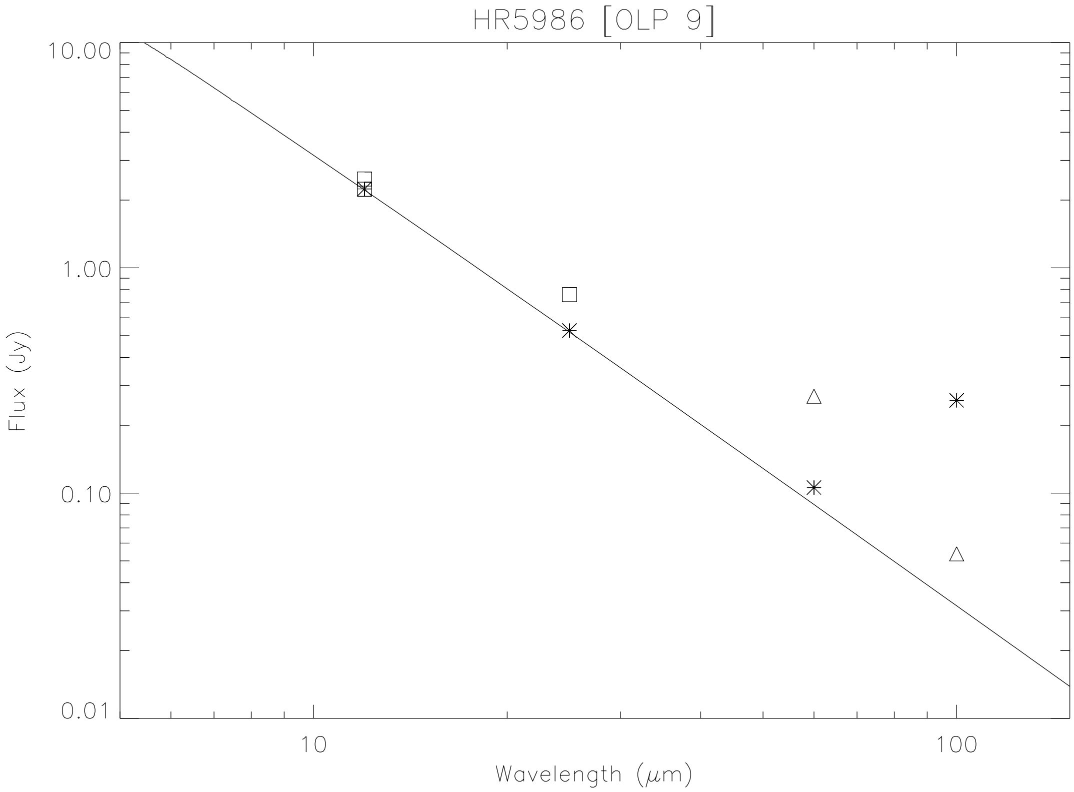

Figure 9.35: Comparison of PHT-P and PHT-C chopped photometry with the model by Hammersley and IRAS photometry both for OLP 8.6b1 (upper panel) and OLP 9.01 (lower panel). The meaning of the symbols is the following: solid line: model, asterisk: IRAS, square: PHT-P (P03 AOT), triangle: C100 (P22 AOT).

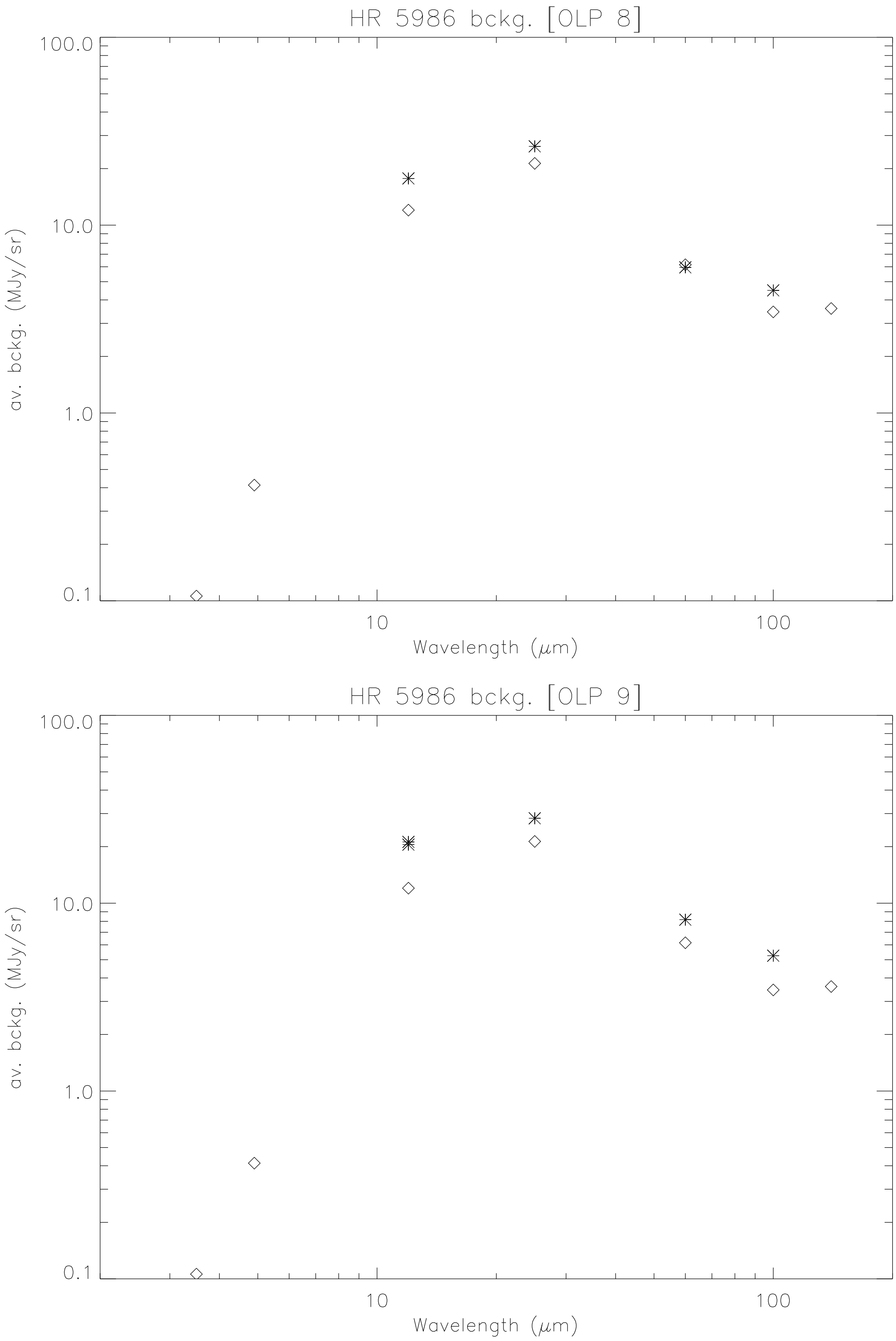

Figure 9.36: Comparison of surface brightness from chopped PHT photometry of the background beam for HR 5986 with COBE, both for OLP 8.6b1 (upper panel) and OLP 9.01. Asterisk: PHT-P and PHT-C photometry, diamond: COBE.

Evaluation Log

1) HR 5447

a) Chopped point source photometry

Measurements:

PHT-P :	PPAP26900346	FCS = 25 um
PHT-C100:	PCAP08900847	FCS = 90 um
	PCAP26900347	FCS = 90 um (b)
PHT-C200:	PCAP08900848	FCS = 180 um
	PCAP26900348	FCS = 180 um (b)

Colour correction: black body, T = 6687 K

Model: Cohen

Det	cwl (μm)	OLP 8	OLP 9	IRAS	Model	Δ (OLP 8)	Δ (OLP 9)
P2	25.0	0.222	0.446	0.295	0.256	-13.15	74.25
C1	60.0	0.136	0.086	0.106*	0.044	207.81	93.55
C1b	60.0	0.069	0.124	0.106*	0.044	56.92	179.76
C1	90.0	0.088	0.024		0.019	350.86	24.68
C1b	90.0	0.048	0.084		0.019	145.58	331.27
C2	150.0	0.000	0.083		0.007	-100.00	1101.43
C2b	150.0	0.000	0.118		0.007	-100.00	1604.49
C2	180.0	0.000	0.178		0.005	-100.00	3842.62
C2b	180.0	0.000	0.047		0.005	-100.00	944.18

* upper limit

b) Background photometry from off-source beam

Det	λ	OLP8 (MJy/sr)	OLP9 (MJy/sr)	COBE (MJy/sr)
P2	25.0	28.47	34.93	
C1	60.0	5.94	10.37	
C1b	60.0	7.64	9.81	
C1	90.0	4.91	7.06	
C1b	90.0	5.74	6.03	
C2	150.0	0.00	2.87	
C2b	150.0	0.00	3.12	
C2	180.0	0.00	2.86	
C2b	180.0	0.00	2.96	

2) BS 5062

a) Chopped point source photometry

Measurements:
PHT-P: ppap19500982 FCS = 7.3, 25 um
PHT-C: pcap19500983 FCS = 90 um

Colour correction: black body, T = 8087 K

Model: Hammersley

Det	cwl (μm)	OLP 8	OLP 9	IRAS	Model	Δ (OLP 8)	Δ (OLP 9)
P1	7.3	2.517	2.545		2.559	-1.62	-0.54
P1	12.0	1.380	1.724	1.010	0.972	42.05	77.44
P2	25.0	0.153	0.668	0.235	0.227	-32.66	194.76
C1	60.0	0.088	0.082	0.108	0.039	126.40	111.86
C1	90.0	0.114	0.098		0.017	566.02	476.38

b) Background photometry from off-source beam

Det	λ	OLP8 (MJy/sr)	OLP9 (MJy/sr)	COBE (MJy/sr)
P1	7.3	9.96	10.93	
P1	12.0	20.87	26.45	13.16
P2	25.0	24.08	20.73	24.14
C1	60.0	4.95	7.45	7.09
C1	90.0	2.80	3.70	

3) HR 5304

a) Chopped point source photometry

Measurements:
PHT-C: PCAP24602245 FCS = 60 um

Colour correction: black body, T = 6143 K

Model: Cohen

Det	cwl (μm)	OLP 8	OLP 9	IRAS	Model	Δ (OLP 8)	Δ (OLP 9)
C1	60.0	0.079	0.110		0.043	86.35	159.11
C1	100.0	0.082	0.027		0.015	444.48	78.09

b) Background photometry from off-source beam

Det	λ	OLP8 (MJy/sr)	OLP9 (MJy/sr)	COBE (MJy/sr)
C1	60.0	8.68	10.63	9.55
C1	100.0	6.61	6.61	4.93

4) HR 5914

a) Chopped point source photometry

Measurements:
PHT-P: PPAP28100658 FCS = 25 um
PHT-C: PCAP28100659 FCS = 90 um
PCAP28100660 FCS = 180 um

Colour correction: black body, T = 5676 K

Model: Cohen

Det	cwl (μm)	OLP 8	OLP 9	IRAS	Model	Δ (OLP 8)	Δ (OLP 9)
P2	25.0	0.193	0.343	0.408	0.381	-49.40	-10.12
C1	60.0	0.074	0.167	0.099	0.066	11.72	153.79
C1	90.0	0.028	0.020		0.029	-5.48	-32.96
C2	150.0	0.000	-0.387		0.010	-100.00	-3844.62
C2	180.0	0.000	-0.740		0.007	-100.00	-11085.50

b) Background photometry from off-source beam

Det	λ	OLP8 (MJy/sr)	OLP9 (MJy/sr)	COBE (MJy/sr)
P2	25.0	15.17	16.97	23.28
C1	60.0	6.12	7.97	6.76
C1	90.0	5.36	6.19	
C2	150.0	0.00	4.17	3.96
C2	180.0	0.00	4.58	

5) HR 5986

a) Chopped point source photometry

Measurements:

PHT-P1 :	ppap74801108	FCS = 12 um
	ppap76201110	FCS = 12 um
PHT-P2 :	ppap74801002	FCS = 25 um
PHT-C1 :	pcap27702221	FCS = 60 um

Colour correction: black body, T = 6084 K

Model: Hammersley

Det	cwl (μm)	OLP 8	OLP 9	IRAS	Model	Δ (OLP 8)	Δ (OLP 9)
P1	12.0	1.997	2.234	2.242	2.216	-9.89	0.85
P1b	12.0	0.000	2.481	2.242	2.216	-100.00	11.96
P2	25.0	0.469	0.761	0.527	0.518	-9.56	46.77
C1	60.0	0.144	0.269	0.106	0.089	61.92	202.72
C1	100.0	0.073	0.054	0.258*	0.032	130.92	69.95

* upper limit

b) Background photometry from off-source beam

Det	λ	OLP8 (MJy/sr)	OLP9 (MJy/sr)	COBE (MJy/sr)
P1	12.0	17.73	20.50	12.02
P1b	12.0	0.00	21.19	12.02
P2	25.0	26.27	28.32	21.32
C1	60.0	5.96	8.17	6.16
C1	100.0	4.49	5.25	3.45

Chapter 10

Conclusions and Outlook

The Scientific Validation of the OLP 9.0 version has demonstrated and achieved the following:

- The successful implementation of the dynamic spectra response calibration for staring mode PHT-S measurements boosting the absolute and relative calibration accuracies of the corresponding OLP products considerably.
- Further consolidation with improved photometric accuracy for staring mode observations, including faint source photometry from mini-maps.
- More detailed assessment of the photometric accuracy of absolute and multi-filter staring modes.
- Further consolidation of the correction for non-linearity of signals due to flux dependence of detector responsivity.
- Upgraded FCS power tables.
- Further progress in chopped photometry calibration:
  - processing of measurements with read-out data reduction;
  - consistent reletive filter-to-filter calibration;
  - verification of absolute surface brightness levels of off-beams using the chopped FCS measurement;
  - verification of the reproducibility of the chopped photometry calibration.

For the final OLP Version 10.0, to be validated during the first quarter of 2001, the following items are confirmed for inclusion:

- Inclusion of a two-threshold deglitching algorithm to cope with glitch tails in staring mode observations.
- Further consolidation of the staring mode photometry accuracy by further refinement of the signal linearization and FCS power calibration files.
- The interpolation in time between the responsivity values of two bracketting FCS measurements will be removed, because it was found that it cannot appropriately correct for detector drifts. Instead the simple average of the responsivity will be given, provided both measurements are inside the calibrated FCS range. Otherwise, only the one with the FCS heating power inside the calibrated range will be used. In the same way, for all measurements, regardless whether single pointing with one FCS measurement or raster pointing with two FCS measurements, default responsivities will be applied, if the FCS heating power should be found to lie outside the calibrated range for the respective filter. Investigation of a large number of FCS measurements has shown that the application of the default responsivity yields more accurate results for these cases.

- Improvement of the flat-field accuracy of P22 raster maps with greater equal 20 raster points by a statistical flat-field method and their scientific re-validation.
- The scientific quality assessment of the chopped observing modes of the multi-filter photometry AOTs, both for PHT–P (P03) and PHT–C (P22) with improved signal correction and chopper offset calibration.
- The installation of a more efficient glitch removal and improvement of the flat-field accuracy of P32 oversampled maps and their scientific quality assessment.
- The introduction of a processing to determine a background subtracted source flux normalized to the flux in the 180 arcsec aperture for suitable multi-aperture photometry (P04) measurements to determine a relative source profile and their scientific quality assessment.
- The scientific quality assessment of surface brightnesses from aperture photometry (P03, P05, P17/18/19).
- The provision of better interfaces to the overall ISO Data Archive structure, e.g. by calculating the on-source positions for rectangular chopped measurements and using world coordinates for mapping products.

A basic schedule is outlined in Table 10.1.

Table 10.1: Schedule for PHT OLP 10.0 Upgrades

OLP 10.0 software and calibration file delivery (1)	11-Dec-2000
OLP 10.0 scientific validation period I	05-Jan - 25-Jan-2001
OLP 10.0 software and calibration file upgrades delivery (2)	25-Jan-2001
OLP 10.0 scientific validation period II	13-Feb - 05-Mar-2001
OLP 10.0 software and calibration file upgrades final delivery (3)	05-Mar-2001
Release of OLP 10.0	12-Mar-2001
Version 1 of ISOPHOT OLP 10.0 Scientific Validation Report	30-Mar-2001
Version 5.0 of ISOPHOT Calibration Accuracies (adapted to OLP 10)	May 2001

Bibliography

[1] U. Klaas, M. Radovich, K. Wilke and P. Richards, "Report on the PHT Scientific Validation for OLP Version 8.4", SAI/1999-041/Rp, Version 2.0, 10-March-2000.

[2] R.J. Laureijs, U. Klaas, P.J. Richards and B. Schulz, "ISO Data User Manual (IDUM)", SAI/95-220/Dc, Version 4.0, October 1998

[3] R.J. Laureijs and U. Klaas, "ISOPHOT Error Budgets", SAI/98-091/Dc, Version 1.0, 21-April-1999 (DERIVE_SPD Processing Steps)

[4] U. Klaas, "Plan for the PHT Scientific (Re-)Validation of PHT OLP Version 9.0", SAI/2000-006/Dc, Version 1.0, 11-February-2000

[5] J. Acosta, "Dynamic Calibration for ISOPHOT-S", IAC / IDC PHT internal calibration report, 03-August-1999

[6] K. Sellgren, L.J. Allamandola, J.D. Bregman, et al., "Emission Features in the 4-13 Micron Spectra of the Reflection Nebulae NGC 7023 and NGC 2023", ApJ 299, 416, 1985

[7] D. Cesarsky, J. Lequeux, A. Abergel, et al., "Infrared Spectrophotometry of M17 with ISOCAM", A&A 315, L305, 1996

[8] P.F. Roche, D.K. Aitken, C.H. Smith and M.J. Ward, "An Atlas of Mid-infrared Spectra of Galaxy Nuclei", MNRAS 248, 606, 1991

[9] J. Acosta-Pulido, "Calibration of ISOPHOT-S Chopped Measurements", IDC PHT Internal Calibration Report, 08-March-1999

[10] R.J. Laureijs, "Point Spread Function Fractions Related to the ISOPHOT C100 and C200 Arrays", IDC PHT Internal Calibration Report, Version 1.0, 29-June-1999

[11] P.L. Hammersley, M. Jourdain De Muizon, M.F. Kessler, P. Bouchet, R.D. Joseph, H. Habing, A. Salama, L. Metcalfe, "Infrared standards for ISO. I. A new calibration of mid infrared photometry", A&AS 128, 207, 1998

[12] P.F. Roche, D.A. Allen, D.K. Aitken, "Symbiotic stars: spectrophotometry at 3-4 and 8-13 um", MNRAS 204, 1009, 1983

[13] C.H. Smith, D.K. Aitken, P.F. Roche, C.M. Wright, "Mid-infrared spectroscopy of galactic novae", MNRAS 277, 259, 1995

[14] I. Heinrichsen, H.J. Walker, and U. Klaas, "Infrared Mapping of the Dust Disc around Vega", MNRAS 293, L78, 1998

[15] U. Klaas, M. Haas, I. Heinrichsen, B. Schulz, "Infrared spectral energy distributions of the interacting galaxies Arp 244, NGC 6240 and Arp 220", 1997, A&A 325, L21

[16] L. Verstraete, J.L. Puget, E. Falgarone, S. Drapatz, C.M. Wright, R. Timmermann, "SWS Spectroscopy of Small Grain Features across the M17-Southwest Photodissociation Front", 1996, A&A 315, L337

[17] D. Cesarsky, J. Lequeux, A. Abergel, M. Perault, E. Palazzi, S. Madden, D. Tran, "Infrared Spectrophotometry of M17 with ISOCAM", 1996, A&A 315, L309

[18] B. Schulz & S. Huth, "Explanatory Supplement for FCS Monitoring Observations", Draft 2.0, 20-June-97 and related diagrams

[19] P. Ábrahám, M. Radovich, L. Schmidtobreick, U. Klaas, T. Kranz, "Analysis of Chopped ISOPHOT Measurements", Version 1.0, PHT/MPIA Calibration Report, 24-November-1999

[20] N. Ginestet, J.M. Carquillat, C. Jaschek, "Spectral classifications in the near infrared of stars with composite spectra", 1999, A&A Supp 134, 473

[21] C.K. Mitrou, J.G. Doyle, M. Mathioudakis, E. Antonopoulou, "The emission of the RS CVn binaries in the IRAS passbands", 1996, A&A Supp 115, 61

[22] C.L. Perry, E.H. Olsen, D.L. Crawford, "A catalog of bright uvbybeta standard stars", 1987, PASP 99, 1184

[23] K. Mattila, D. Lemke, L.K. Haikala, R.J. Laureijs, A. Léger, K. Lehtinen, Ch. Leinert, and P.G. Mezger, "Spectrophotometry of UIR bands in the diffuse emission of the galactic disk", 1996, A&A 315, L353

[24] T. Onaka, and the IRTS team, "IRTS observations of the unidentified infrared bands in the diffuse Galactic light", 1997, Diffuse Infrared Radiation and the IRTS, H. Okuda, T. Matsumoto, and T.L. Roellig (eds.), ASP Conference Series, Vol. 124, 170

[25] I. Heinrichsen, H.J. Walker, U. Klaas, R.J. Sylvester, and D. Lemke, "An infrared image of the dust disc around β Pic", 1999, MNRAS 304, 589

[26] U. Klaas, J.A. Acosta–Pulido, P. Ábrahám, H.O. Castañeda, L. Cornwall, F. Garzon, P. Hammersley, I. Heinrichsen, U. Kinkel, D. Lemke, J. Schubert, and M. Wells, "ISOPHOT-S: Capabilities and Calibration", Proc. First ISO Workshop on Analytical Spectroscopy, p. 113, ESA SP-419, December 1997

[27] U. Klaas, P. Ábrahám, M. Haas, U. Herbstmeier, and R.J. Laureijs, "General ISOPHOT Observing Strategies for Faint Sources", SAI/97-013/Wb, Version 1.3, 28-February-1997

[28] P. Ábrahám, U. Klaas, M. Haas, U. Herbstmeier, M. Linden, and D. Lemke, "Detection Limit and Observing Strategy for Very Faint Point Sources: Test Observations with P3, C100, and C200", Version 2.0, PHT/MPIA Calibration Report, 29-April-1997

[29] B.T. Soifer, L. Boehmer, G. Neugebauer, D.B. Sanders, "The *IRAS* Bright Galaxy Sample. IV. Complete *IRAS* Observations", 1989 AJ 98, 766

[30] B. Schulz, Linearization of ISOPHOT-P and C detector signals in OLP8", IDC PHT Internal Calibration Report, Version 1.0, 29-Sep-1999

[31] T. Müller & J.S.V. Lagerros, "Asteroids as far-infrared photometric standards for ISOPHOT", 1998, A&A 338, 340

[32] U. Herbstmeier, P. Abraham, D. Lemke, R.J. Laureijs, U. Klaas, K. Mattila, Ch. Leinert, Ch. Surace, M. Kunkel, "Small-scale structures in the far-infrared background", 1998, A&A 332, 739

[33] C. Gabriel, M. Haas, I. Heinrichsen, and W.-M. Tai, "The ISOPHOT Interactive Analysis - PIA User's Manual", 2000 (for PIA V9.0)

[34] D.K. Aitken & P.F. Roche, "8–13 μm spectroscopy of compact planetary nebulae and emission line objects", 1982, MNRAS 200, 217

[35] P.F. Roche, D.K. Aitken, & B. Whitmore, "8–13 μm spectral observations of eight moderately extended planetary nebulae", 1983, MNRAS 204, 101

[36] P.F. Roche & D.K. Aitken, "The infrared spectral properties of planetary nebulae", 1986, MNRAS 221, 63

[37] S.R. Pottash, A. Preite–Martinez, F.M. Olnon, Mo Jing–Er, S. Kingma, "IRAS spectra of planetary nebulae. III", A&A 161, 363, 1986